Binder Characterization and Evaluation

Volume 3: Physical Characterization

David A. Anderson
Donald W. Christensen
Hussain U. Bahia
Raj Dongre
M.G. Sharma
Charles E. Antle
Pennsylvania State University
University Park, Pennsylvania

Joe Button
Texas Transportation Institute
Texas A&M University
College Station, Texas

Acknowledgments

Dr. Andrea Chow, formerly of Stanford Research International, was responsible for dynamic shear and dielectrics studies during the first year of the program.

Contents

List of Figures

List of Tables

Abstract

The research results in this report concern the characterization of physical properties of asphalt binders and the development of test procedures for aging and adhesion. Asphalt binders were shown to be linear viscoelastic materials at expected pavement strains. Test methods and models describing rheological behavior were developed with the assumption of linear behavior. A mathematical model that contains parameters that can be used to relate physical and chemical parameters was developed. The test methods and models allow the stiffness of asphalt binders to be characterized as a function of loading time and temperature with the dynamic shear rheometer at intermediate to upper pavement surface temperatures and with a newly developed bending beam rheometer at low temperatures, where thermal cracking is important. To characterize fracture properties, the project developed a direct tension test, in which failure strain, stress, and energy are determined as functions of loading time and temperature. Limited work on fatigue properties at low temperatures successfully related them to tensile properties. A new phenomenon, low-temperature physical hardening, was identified during the project. This phenomenon results in increased stiffness of the binder when it is held at a constant temperature at room temperature or below. The blister test for quantitative measurement of adhesion between asphalt binder and aggregate surfaces was found to be impractical. The investigation of various factors, including film thickness, aging temperature, the effect of oxygen versus air, and the effect of mineral surfaces, led to a new aging procedure for simulating in-service oxidative hardening of asphalt binders, which was adopted as part of the new SHRP binder specification.

Binder Characterization and Evaluation

Related Reports

Executive Summary

Research studies conducted at the Pennsylvania State University to characterize the physical properties of asphalt binders are reported in this volume. There were two main objectives in these studies: to develop rational methods for characterizing the fundamental physical properties of asphalt binders and to develop methods that could be used to condition the asphalt binders to simulate field aging and moisture damage. The physical property characterization studies were intended for two purposes: to provide the information needed to develop fundamental, performance-related specifications for asphalt binders and to develop the parameters needed to develop relationships between the physical and chemical properties of asphalt cement. In this work, asphalt cement was considered as a linear viscoelastic material. This assumption, which was based on testing done early in the project, greatly simplifies the characterization and modeling of the physical behavior (rheology or stiffness) of asphalt binders. Test methods that were developed were intended to be equally applicable to plain or modified asphalt cements, collectively called asphalt binders.

In order to provide a means for mathematically characterizing the stiffness of asphalt binders so that quantitative relationships between field performance and chemical properties could be developed, it was necessary to develop a quantitative (mathematical) model that characterizes the stiffness of asphalt binders. The work of earlier researchers was reviewed and, based on their work, a new model was developed that characterizes the stiffness of asphalt binders as a function of loading time and temperature. This model assumes that asphalt cements reach a unique value of stiffness at very low temperatures and reach Newtonian behavior at high temperatures. With these limiting stiffness properties, the stiffness of the binder at intermediate temperatures can then be defined in terms of the shape of the stiffness curve (rate of change with temperature or time of loading) and the location of the stiffness curve with respect to temperature or time of loading. The resulting model requires three parameters: a location parameter that indicates the hardness of the asphalt, a shape parameter that indicates the time dependency of the asphalt, and a temperature dependency parameter that indicates the temperature dependency of the asphalt. The original intention was to use this model as a specification tool and to specify the asphalt binders in accordance with parameters derived from the model using measurements at only two test temperatures. However, as the SHRP asphalt program developed, the research team was directed to develop a specification that would include both plain and modified asphalt cement. As a result, it was necessary to abandon the rheological model as a specification tool and to adopt a philosophy in which the specification values are obtained at temperatures that relate specifically to each asphalt grade. Nonetheless, the parameters in the rheological model are

of value in understanding the behavior of asphalt cement and in relating physical properties to chemical properties.

The dynamic shear rheometer was selected as one of the primary test devices for characterizing asphalt binders and was studied extensively in order to determine testing protocols and the equipment limitations. The dynamic shear rheometer using parallel plate geometry was found acceptable for measuring the stiffness of asphalt binders in the temperature range where the dynamic modulus varies from approximately 10 MPa (1.45 lb/in.^{2}) to 1 kPa (0.145 lb/in.^{2}). A linear response region for asphalt binders in this stiffness range was determined and was subsequently incorporated into the SHRP binder specification. The bending beam rheometer was developed in order to obtain reliable stiffness measurements at low temperatures where the stiffness of asphalt binders is greater than 10 MPa and where the compliance of the dynamic shear rheometer can otherwise lead to errors in the test measurements. The bending beam rheometer is based on a simple flexural creep test in which a beam of asphalt binder is loaded at its midpoint for 240 s. It was shown that the stiffness values obtained with the dynamic shear rheometer and the bending beam rheometer can be related to each other using linear viscoelasticity. Together, the dynamic shear rheometer and the bending beam rheometer are sufficient to completely define the rheological properties of asphalt binders in the time and temperature region of interest for specification and research purposes. By combining the bending beam and dynamic shear data, asphalt binders were shown to be thermorheologically simple and it was demonstrated that time-temperature superposition is valid. Time-temperature superposition was subsequently used to establish rheological master curves, allowing the asphalt binder to be described over a wide range of loading times and test temperatures. A simple ball indentation test was also evaluated as a test method for characterizing asphalt binders. Reasonable correlation between the indentation test and the dynamic shear and bending beam rheometer were observed; however, the indentation test resulted in nonlinear strains, requiring a much more sophisticated analysis than the linear viscoelastic analysis used for the dynamic shear and bending beam test results.

During the initial work with the bending beam rheometer, it was noticed that when specimens were stored at low temperatures for an extended period of time, the stiffness increased. This led to the identification of low-temperature physical hardening, the result of time-dependent volume changes in the binder when it is stored at low temperatures. This phenomenon is well known for other organic-amorphous materials but, prior to this study, had not been described for asphalt cements. The degree of physical hardening depends on the asphalt source, isothermal aging temperature, and time of storage. The presence of low-temperature physical hardening demonstrates that asphalt cements, when cooled to low temperatures, do not reach thermodynamic equilibrium instantly and instead undergo slow isothermal volume changes that may continue for long periods of time. Limited data available during the project indicate that the low-temperature physical hardening also affects the failure properties, causing a decrease in the failure strain as physical hardening proceeds. Based on results available during the project, it also appears that there is a relationship between wax content and the degree of low-temperature physical hardening.

Very little fundamental work has been done on the fatigue and fracture properties of asphalt cements. After a thorough review of the literature, it was decided to develop a direct tension

4

test as a specification-type test. The results of the direct tension test were to be related to fracture mechanics parameters in order to enhance the validity of the direct tension test as a specification-type test. Resources limited the development of the fracture mechanics testing and the correlation with the direct tension test results. In addition to the direct tension testing, limited fatigue testing at low temperature was also accomplished. The fatigue testing clearly demonstrated that the energy dissipated per cycle of loading is related to the number of cycles to failure. This result is in agreement with work done by other SHRP researchers in the mixture area and was used as one of the justifications for the fatigue criteria used in the development of the specification. Neither fatigue nor fracture mechanics testing was considered a viable option for specification development. Consequently, considerable effort was spent in the development of a specification-type direct tension test for asphalt binders. With this test, the strain, stress, and energy at failure can be reliably determined. At low temperatures, asphalt binders typically undergo a rather sudden transition from ductile to brittle behavior within a relatively small temperature range, typically 6° to 12°C. It was demonstrated that master curves for failure strain, failure stress, and failure energy can be determined using time-temperature shift factors obtained from rheological (stiffness) data. In other words, the time-temperature dependency of the fracture properties is similar to the time-temperature dependency rheological (stiffness) properties. The direct tension test procedure was further developed as part of this study to adopt it to specification use. The test procedures include a unique set of grips for aligning the specimen, a noncontact extensometer for measuring specimen deformation, and silicone rubber molds for preparing the test specimen.

The aging studies completed during this project were focused primarily on long-term, in-service oxidative aging. The current thin film oven test, ASTM D 1754, and rolling thin film oven test, ASTM D 2872, are used by most agencies to simulate the hardening that occurs during mixing and laydown. Consideration was given to the validation of these test procedures or to the development of a new test procedure for the volatilization and oxidative aging that occur during the mixing and laydown process. However, there were insufficient resources within the project to study short-term aging, and the primary focus during the project was therefore placed on long-term oxidative aging. After considering several test methods, the pressurized aging test, which has been used previously by other researchers, was adopted for study. Initially, the test procedure was based on pressurizing test samples with pure oxygen for 6 days at the maximum pavement temperature. This was found to be impractical because of safety problems associated with pure oxygen and the time required to conduct the test. As a consequence, air was subsequently used at temperatures ranging from 90° to 110°C for 20 hours. A number of variables were studied in an extensive set of experiments during the development of the pressure aging vessel (PAV) test. These variables included the thickness of the film during the aging process, the effect of commingling asphalts from different sources during a test, temperature variability within the aging vessel, and the effect of replenishing the air supply during the test. Asphalt cements from different sources were compared after pressure aging and the sensitivity of the test to asphalt source was verified. Samples recovered from the field after as many as 12 years of service were then compared to PAV-aged samples.

After examining the rheological properties of unaged, field-aged, and PAV-aged materials, it was concluded that the specification for fatigue and thermal cracking should be

based on PAV-aged material. The rheological and chemical properties of the laboratory-aged and the field-aged examples were highly comparable, thereby validating the choice of the pressure aging test as a specification test. The aging process causes significant changes in the rheology of the asphalt cement that cannot be described by a simple aging index. Further, the aging process also changes the failure characteristics of asphalt binders. As a consequence, the specification criteria for fatigue and low-temperature cracking were based on material aged in the pressure aging vessel. Limited testing accomplished with several asphalt-mineral filler systems showed, unexpectedly, that the mineral surface does not affect the oxidative aging process.

A number of additional test procedures were evaluated as part of this study. The Brookfield rotational viscometer was investigated as a replacement for the capillary tube viscometers at mixing and compaction temperatures. Techniques for obtaining a continuous viscosity-temperature curve were investigated; however, it was concluded that significant changes in equipment design would be necessary in order to make such measurements. Instead, the Brookfield viscometer was adopted as a specification test for evaluating the pumpability characteristics of both plain and modified binders. An adherometer (blister test) was evaluated for quantitatively measuring the adhesion between asphalt cement and mineral aggregate surface in the presence of water. The test procedure proved to be very cumbersome and time-consuming, and serious concerns were raised by the research team with respect to the representative nature of the mineral aggregate surface used in the test. A freshly sawn surface is necessary in order to conduct the test and such a surface is not representative of stockpile aggregate. As a consequence, the blister test was not pursued as a specification or research test.

Two other test procedures, dielectric testing and ultrasound testing, were pursued as rapid techniques for estimating rheological properties. Ultrasound proved unsatisfactory because the time of response under the ultrasound wave is very short compared to the relaxation time of the asphalt cement. As a consequence, the ultrasound technique responds primarily to the glassy stiffness which is common to all asphalts; therefore, ultrasound is not sensitive to differences between different asphalt cements. The dielectric technique proved encouraging, although not as a specification tool. The dielectric measurements did discriminate between different asphalt sources and the dielectric properties were significantly affected by aging. Measurements obtained at low frequencies were more discriminating than measurements obtained at higher frequencies. Attempts were made to use dielectric measurements as a measure of aggregate asphalt interaction; however, the dielectric properties of the aggregate overwhelmed those of the asphalt cement and this technique was considered unsuitable for studying asphalt-aggregate interactions.

In summary, the products of this research were new and improved test methods for asphalt binders that determine fundamental, performance-related properties. The dynamic shear rheometer was selected for measuring the stiffness of asphalt binders at intermediate to high pavement temperatures, and the bending beam rheometer was selected for measuring properties at low pavement temperatures. Together these two devices are capable of measuring the stiffness (rheological properties) of asphalt binders within the range of temperature and loading times required for the new SHRP asphalt binder specification, for relating thermal and physical properties, and for further research studies. The direct tension

test was also developed and recommended for use in the specification as an indicator of low-temperature performance. The rheological model that was developed during the project forms the basis for developing rational relationships between the chemical and physical properties of asphalt binders. An accelerated pressurized aging test was developed to simulate long-term, in-service oxidative aging. The test was validated by comparing samples of material aged in the laboratory and recovered from the field. Low-temperature physical hardening was identified and characterized.

1

Linear Viscoelastic Model

There are many important reasons for developing a mathematical model or expression to explicitly describe the linear viscoelastic (LVE) response of asphalt cements:

- Since the mechanical response of asphalt cement, like other viscoelastic materials, is a continuous function of time and temperature, an infinite number of loading conditions and responses constitute its overall behavior. By expressing this behavior with a mathematical model, the responses can be reduced to a limited number of variables.

- By mathematically modeling the LVE response and reducing the characterization to a few rational variables, relating the rheological behavior to chemical compositional parameters is simpler, more efficient, and more rational. This approach is in contrast to correlating individual response variables, obtained under arbitrary loading conditions, to chemical variables.

- In some situations, it is necessary to know the response of an asphalt cement at loading frequencies (or times) and temperatures different from those for which directly measured data are available. Mathematical models allow such calculations to be made directly and quickly in a repeatable fashion.

- In many approximate conversions from one viscoelastic function to another, numerical methods are used that require data at specific frequency or time intervals, which may not be the same as those used for the measurement. Using mathematical models simplifies the application of such approximate conversions.

- Through the use of mathematical models, the testing needed to control various performance-related properties can be simplified. For example, the finding that, over a limited temperature range, the shift factors for plain asphalts at temperatures below about 0°C (32°F) could be approximated by a simple logarithmic relationship, allowed a simplified testing scheme in which a creep test is performed for only 2 minutes at a temperature 10°C (18°F) above the expected

minimum pavement temperature. Using this common shift factor allows the creep compliance after 2 hours loading time to be approximated by the compliance measured after 60 seconds loading time.

- In order to predict the mechanical behavior of paving mixtures within the context of a rational microstructural model, the behavior of the binder must be described under a broad range of conditions—a task accomplished efficiently through the use of mathematical models.

- In order to effectively model pavement response and predict pavement performance, it is necessary to accurately predict the stress-strain response of the binder over a wide range of temperatures, loading times, and stresses or strains. This prediction can only be realistically made with the use of reasonably accurate mathematical models of the binder's viscoelastic behavior.

The purpose of this chapter is to describe the LVE model developed for modeling asphalt cement during the A-002A research project. The following sections present some background concerning the nature of viscoelasticity and its significance in the study of asphalt cements and related paving binders. Then, a section is presented in which several previously proposed LVE models for asphalt cement are described. The next portion of the chapter describes in some detail the model developed during the A-002A project. Finally, some conclusions and recommendations are made concerning the mathematical modeling of the LVE behavior of asphalt cement. The model was developed for plain asphalt cements and should be applied with caution to modified asphalt cement.

Linear Viscoelastic Theory

Stress and Strain

In order to predict the engineering performance of any material, it is necessary to understand its stress-strain behavior. To determine how a given material will respond to an applied load, laboratory tests must be performed and analyzed, and the results summarized in a form that is readily applicable to engineering design methods. To characterize the stress-strain behavior of materials in the laboratory, the simplest test methods are uniaxial (extensional) tests and shear tests. Such tests may be conducted under controlled stress or controlled strain conditions. The resulting response may then be stated in various ways, depending on the response of the material. Materials for which the stress-strain behavior is linear, and largely independent of time and temperature, can be effectively characterized by the elastic (Young's) modulus. Newtonian fluids, on the other hand, can be characterized through the coefficient of viscosity. Materials such as asphalt cement, which exhibit aspects of both elastic and viscous behavior, are called viscoelastic, and must be characterized with test methods and analytical techniques that account for the time (or rate) of loading and the loading temperature.

In predicting the response of a material or system under realistic loading conditions, three-dimensional analyses must generally be used. These analyses require that, in addition to the uniaxial or shear response, additional properties such as the bulk response or Poisson's ratio be characterized. A detailed explanation of constitutive relationships for viscoelastic materials is beyond the scope of this report. However, in the interest of completeness, some reference is made to the bulk response and Poisson's ratio, since these parameters are needed when solving stress-strain problems in three dimensions and are also required in relating various stress-strain parameters, as described later in this report.

Elasticity, Viscosity, and Viscoelasticity

One of the simplest tests for characterizing the stress-strain response of a material is the creep test. In this test, a load of constant magnitude is applied to a material at time t_o; at time t_i, the load is removed. The inherent differences between elastic, viscous, and viscoelastic behavior are readily apparent in such a test, as is shown in figure 1.1.[1]

An elastic material, when loaded in creep, will immediately deform to a constant strain. When the load is removed, the material will immediately return to its initial shape. A viscous material, on the other hand, will deform at a constant rate when the load is applied at t_o, and will continue to deform at that rate until the load is removed, at which point there is no further deflection or recovery. Elastic and viscous responses under creep (constant stress) loading are shown schematically in (a) and (b) of figure 1.1.

A viscoelastic material, as shown in figure 1.1 (c), has both elastic and viscous components of response. When loaded in creep, there is an immediate deformation, corresponding to the elastic response, followed by a gradual time-dependent deformation. This time-dependent deformation may further be divided into a purely viscous component and a delayed elastic component. Upon removing the load at t_i, the viscous flow ceases, and none of this deformation is recovered. The delayed elastic deformation is, however, recovered, but not immediately as with purely elastic deformation. Instead, once the load is removed, the delayed elastic deformation is slowly recovered, at a decreasing rate, as is shown in part (c) of figure 1.1.

The description of elastic, viscous, and viscoelastic response given above is for a linear response; that is, the deformation at any time and temperature is directly proportional to the applied load. Nonlinear response, especially for viscoelastic materials, is extremely difficult to characterize in the laboratory and to model in practical engineering problems. Fortunately, linear methods of characterization and analysis are generally more than adequate for engineering design problems. Analysis of the test data collected during this project indicates that asphalt binders, including both plain and most modified asphalt cements, can effectively be treated as LVE materials under loading conditions likely to be encountered in a pavement under traffic and thermal loads. For this reason and because the primary motivation for characterizing the stress-strain response of asphalt cement was to provide

---

[1]All figures and tables referenced in this chapter appear at the end of the chapter.

parameters suitable for specific purposes, the model development was, of necessity, limited to linear response.

Creep Compliance and Stiffness Modulus

A commonly used test for determining the viscoelastic properties of viscoelastic materials, including asphalt cement, is the creep test. During a creep test, a constant load is applied to a specimen, and the resulting deflection is monitored as a function of time. In analyzing the data from a creep test on asphalt cement, use is generally made of the stiffness modulus, which is defined as

$$S(t) = \sigma_0 / \epsilon(t) \qquad (1.1)$$

where

$$
\begin{aligned}
S(t) &= \text{time-dependent stiffness modulus, Pa} \\
t &= \text{loading time, s} \\
\sigma_0 &= \text{applied constant uniaxial stress, Pa, and} \\
\epsilon(t) &= \text{resulting uniaxial strain at time t, m/m.}
\end{aligned}
$$

Note that stiffness is a uniaxial property, relating uniaxial, or extensional, strain and stress. The stiffness modulus is simply the inverse of the uniaxial creep compliance, $D(t)$. A related function is the shear creep compliance, $J(t)$, which is directly related to both the stiffness and the uniaxial creep compliance. Methods for introconverting shear and uniaxial functions are discussed below. Among rheologists and in the literature of viscoelastic theory, the term "creep compliance" is in standard usage for characterizing the creep response; the term "stiffness modulus" was originally coined by Van der Poel (1954) and is widely used among asphalt technologists. The term stiffness was retained to provide continuity with the traditional literature.

A typical plot of creep stiffness versus time for an asphalt cement is shown in figure 1.2 on a log-log scale. At very short loading times, the creep stiffness approaches a limiting value, called the glassy modulus, that has a value close to 3 MPa for all asphalt cements. This constant value for the glassy modulus results from the stiffness of the carbon-carbon backbone of which asphalt cement molecules are largely formed. Many polymers, which are also largely composed of carbon molecules, have a similar value for the glassy modulus. As the loading time increases, the modulus decreases at an increasing rate until the slope on a log-log scale approaches negative one. At this point, asphalt cement behaves as a simple Newtonian fluid, and the rate of deformation is directly proportional to the applied stress. For this reason, an asymptote drawn through this portion of the creep stiffness curve is called the viscous asymptote. If a horizontal asymptote is drawn through the glassy modulus to the point of intersection with the viscous asymptote, the log-log slope of the creep curve at this point will always be close to 0.5. The term "crossover time," t_c, is used within this report to denote this characteristic parameter of the creep stiffness curve. Similar constructions have been used by other asphalt researchers to model the rheological behavior of asphalt cement.

12

Dynamic Mechanical Analysis

In dynamic mechanical analysis, a sinusoidal strain is applied to a specimen and the resulting stress is monitored as a function of frequency. This testing is termed "strain controlled" and has been more commonly used than stress-controlled dynamic mechanical analysis, in which a sinusoidally varying stress is applied and the strain response is measured. The dynamic mechanical properties are directly related to the creep properties, but in a mathematically complex way. Both characterizations give a complete indication of the viscoelastic properties of the material tested. Both the complex modulus and the stiffness modulus are simply indicators of the resistance of an asphalt cement to deformation under a given set of loading conditions.

The primary response in dynamic testing is the complex dynamic modulus, which is computed in strain-controlled testing using the following equation:

$$G^*(\omega) = |\tau(\omega)| / |\gamma(\omega)| \tag{1.2}$$

where

$G^*(\omega)$ = complex dynamic shear modulus at frequency ω, Pa
$|\tau(\omega)|$ = absolute magnitude of the dynamic shear stress response, Pa, and
$|\gamma(\omega)|$ = absolute magnitude of the applied dynamic shear strain, m/m.

As can be seen from the variables used in equation 1.2, the dynamic complex moduli are normally measured and reported in terms of shear response. The phase angle, δ, indicates the lag in the stress response compared with the applied strain. For purely elastic materials, the phase angle will be zero, whereas for purely viscous materials, the phase angle will be 90°. Thus, the phase angle is important in describing the viscoelastic properties of a material such as asphalt cement.

In reporting the results of dynamic mechanical testing, three other parameters are often used: the storage modulus $G'(\omega)$; the loss modulus $G''(\omega)$; and the loss tangent, or tan δ (pronounced "tan delta"). These parameters are directly related to the complex modulus and the phase angle and can be computed through the following series of relatively simple equations.

For the calculation of the storage modulus from the complex modulus and phase angle:

$$G''(\omega) = G^*(\omega) \cos \delta \tag{1.3}$$

where

$G'(\omega)$ = dynamic storage modulus at frequency ω, Pa, and
$G^*(\omega)$ = dynamic complex modulus at frequency ω, Pa.

For the calculation of the loss modulus from the complex modulus and phase angle:

$$G''(\omega) = G^*(\omega) \sin \delta \qquad\qquad (1.4)$$

where

$\qquad$ $G''(\omega) =$ $\quad$ dynamic loss modulus (in Pa) at frequency ω,

and the other variables are as defined above for equation 1.3. Tan delta, or the loss tangent, is calculated simply as the tangent of the phase angle, or, alternatively, as the ratio of the loss to the storage moduli: $\tan \delta = G''(\omega)/G'(\omega)$. The various relationships among the complex, storage, and loss moduli, and the phase angle, are effectively visualized through the vector representation, as shown schematically in figure 1.3.

The storage modulus, $G'(\omega)$, represents the in-phase component of the complex modulus, while the loss modulus, $G''(\omega)$, represents the out-of-phase component of the complex modulus. These terms are sometimes misinterpreted as the elastic and viscous moduli; in reality, the elastic component of the response only represents part of the storage modulus, and the viscous response only part of the loss modulus. In addition to the elastic and viscous response, most real viscoelastic materials exhibit a significant amount of delayed elastic response that is time-dependent but completely recoverable. In interpreting the storage and loss moduli, it should be kept in mind that both these parameters reflect a portion of the delayed elastic response. Therefore, they cannot be strictly interpreted as elastic and viscous moduli and are properly referred to as the storage and loss moduli.

In a master curve of dynamic mechanical data, one or more of the viscoelastic functions are plotted against frequency. In a particularly useful plot used by many researchers, the complex shear modulus, $G^*(\omega)$, and the phase angle δ are plotted against frequency on a log-log scale. Such a plot, in this case for SHRP asphalt AAB-1, is shown as figure 1.4. At high frequencies, the complex shear modulus approaches a limiting value, which is the glassy modulus in shear. It is about one-third the glassy extensional stiffness modulus, or about 1 GPa. At low frequencies, the slope of the log-log plot of complex modulus versus frequency approaches 1:1, which signifies that viscous flow has been reached, and that the asphalt is behaving as a Newtonian fluid. At intermediate frequencies, the behavior of the asphalt changes gradually from that of a simple fluid to a glassy solid. In this intermediate region, centered around the intersection of the glassy and viscous asymptotes, much of the deformation will be of the delayed elastic type. The master curve of complex modulus versus frequency is essentially a mirror image of the master stiffness curve, although there is a slight shifting downward because of differences in shear and extensional moduli. The crossover frequency ω_c, which is the frequency at which tan delta equals one, is the inverse of the crossover time when the frequency, ω, is expressed in Hertz or cycles per second.

Examining the behavior of the phase angle as a function of frequency, the general shape is sigmoidal. The phase angle at very low frequencies approaches 90 degrees, and at very high frequencies the phase angle approaches 0 degrees. At the crossover frequency, the phase angle is approximately equal to 45 degrees. The phase angle in dynamic testing is directly proportional to the log-log slope of the creep stiffness curve at time $1/\omega$ when the frequency is expressed in Hertz; this conversion can be used in comparing dynamic and creep data.

14

Introconversion of Viscoelastic Functions

Because the different viscoelastic moduli can be estimated from different types of mechanical tests, and because these different functions are needed in modeling the behavior of asphalt cement under different loading conditions, it is useful to be able to convert from one viscoelastic function to another. In general, exact closed-form equations for the introconversion of viscoelastic functions for real materials do not exist, and numerical methods or approximate equations must be used. This latter approach is more practical, and is the one recommended in this report.

In the simplest and most common method for converting shear moduli to uniaxial or extensional moduli, asphalt cement is assumed to be incompressible and thus to have a Poisson's ratio of 0.5. This assumption leads to the following approximate equation relating extensional stiffness and shear stiffness:

$$E^*(\omega) = 3\, G^*(\omega) \tag{1.5}$$

where

$E^*(\omega)$ = uniaxial or extensional complex modulus at frequency ω, Pa, and

$G^*(\omega)$ = shear complex modulus at frequency ω, Pa.

The uniaxial or extensional creep compliance, D(t), can similarly be calculated from the shear creep compliance, J(t), by dividing by a factor of three. Similar conversions can be made between other shear and extensional moduli and compliances, remembering that when Poisson's ratio is 0.5, the uniaxial moduli will always be three times the corresponding shear moduli, and uniaxial compliances will always be one-third the corresponding shear compliance. Although this method for converting shear to uniaxial properties is only approximate, it is in most cases sufficiently accurate for engineering calculations.

The other major conversion frequently needed is between the creep stiffness and the dynamic complex modulus. Van der Poel (1954), in defining stiffness, indicated that it can be treated as either the inverse of the creep compliance at loading time t, or the uniaxial dynamic modulus at loading frequency 1/t, which is based on the simplest and most direct approximation between the creep compliance and the dynamic complex modulus:

$$G^*(\omega) \approx 1 / J(t) \tag{1.6}$$
$$t \rightarrow 1/\omega$$

where

$G^*(\omega)$ = shear dynamic complex modulus at frequency ω, Pa, and

$J(t)$ = shear creep compliance at time t, Pa.

In other words, the shear compliance, $J(t)$, obtained at time t_i is approximately equal numerically to the complex shear modulus $G^*(\omega)$ at a frequency ωc where $t_i = 1/\omega_i$

expressed in H_2. More rigorous approximate introconversions are discussed by Ninomiya and Ferry (1959) and Tschoegl (1989).

Time-Temperature Superposition

One of the primary analytical techniques used in analyzing the dynamic mechanical data for the SHRP asphalts involved construction of master curves for the dynamic complex modulus and phase angle. In constructing such master curves, the time-temperature superposition principle, or method of reduced variables, is used. In constructing a master curve using time-temperature superposition, dynamic data are first collected over a range of temperatures and frequencies. A standard reference temperature must then be selected; 25°C (77°F) or 0°C (32°F) is often used. In this study 25°C was used as the reference temperature for constructing master curves. The data at all other temperatures are then shifted with respect to time until the curves merge into a single smooth function. The shifting may be done based on any of the viscoelastic functions; if time-temperature superposition is valid, the other viscoelastic functions will all form continuous functions after shifting.

The amount of shifting required at each temperature to form the master curve is of special importance, and is called the shift factor, a(T). A plot of log a(T) versus temperature is generally prepared in conjunction with the master curve. This type of plot gives a visual indication of how the properties of a viscoelastic material change with temperature. A schematic representing the basic process involved in constructing a master curve is shown in figure 1.5. The time or frequency scale used in a master curve is referred to as reduced time or reduced frequency.

Literature Review: Empirical Modeling of Linear Viscoelastic Behavior

Van der Poel's Nomograph

In the mid-1950s Van der Poel (1954) developed a nomograph that could be used to estimate stiffness over a wide range of temperatures and loading times for a variety of bitumens. This nomograph used ring-and-ball softening-point temperature and the penetration index as input parameters. Unfortunately, the precise mathematical functions used by Van der Poel in developing the nomograph were never described in any publication. He did, however, describe in broad terms the theory behind this method of predicting rheological properties from routine test data. Van der Poel assumed a more or less hyperbolic shape for stiffness as a function of time. The shape of the master curve is estimated from the penetration index, which is calculated from the penetration at a specified temperature (usually 25°C (77°F)) and the ring-and-ball softening-point temperature. Although not discussed by Van der Poel in detail, it must be assumed that time-temperature superposition was used in the construction of the nomograph, so that there is some assumed function for describing the shift factors as a function of temperature. The nomograph was developed to give stiffness at a temperature relative to the softening point at any arbitrary loading time. Van der Poel's nomograph has

16

been widely used in pavement design and by various researchers in asphalt technology (Boannaure 1977; Heukelom 1966).

As part of this research project, Van der Poel's nomograph was analyzed in terms of the mathematical models presented within this report. A full set of master curves was developed from the nomograph, with accompanying shift factors, for various values of the penetration index (PI). Several of these master curves are shown in figure 1.6. Shift factors for different values of PI are shown in figure 1.7.

Several researchers have attempted to modify Van der Poel's nomograph, including McLeod (1972) and Heukelom (1966). These latter modifications were largely minor and only cosmetic, although the suggestion of using viscosity and "base temperature" rather than the ring-and-ball softening-point temperature significantly deviates from Van der Poel's approach. An analysis of these revised nomographs gave results similar to those described above. However, space and time prevent a detailed comparison and discussion of the precise differences and similarities of the various versions of Van der Poel's nomograph. It was found that they all suffer from more or less the same shortcomings, and their use should be avoided if other, more rational and accurate methods of characterization are available. Discrepancies between stiffness values measured as part of this study and those estimated with the nomographs tend to be more pronounced at lower temperatures and longer loading times.

Jongepier and Kuilman's Model

Various researchers have used explicit mathematical models to characterize master curves of stiffness or a complex modulus for asphalt cement. Jongepier and Kuilman (1969) suggested that the relaxation spectra for asphalt cements are approximately log normal in shape and derived models for various rheological functions based on this assumption. Unfortunately, use of this model requires the application of integral equations and/or transforms, which can only be solved using numerical methods. Additionally, evidence gathered during the course of this research has indicated that the relaxation spectra of asphalt, although close to a log normal distribution at long relaxation times, significantly deviate from a log normal distribution at shorter loading times.

Jongepier and Kuilman's model is expressed mathematically using a relatively complex set of equations. First, the reduced frequency is replaced by the dimensionless frequency parameter ω_r:

$$\omega_r = \omega \eta_0 / G_g \qquad (1.7)$$

where

ω_r = reduced frequency, rad/s;
η_0 = the steady-state (Newtonian) viscosity, Pa^{-1}; and
G_g = the glassy modulus, Pa.

The relaxation spectrum, H(τ), is expressed mathematically as a log normal distribution:

$$H(\tau) = \frac{G_g}{\beta \sqrt{\pi}} \exp-\{\frac{\ln \tau/\tau_m}{\beta}\}^2 \qquad (1.8)$$

where

$$
\begin{aligned}
H(\tau) &= \text{the relaxation spectrum distribution;} \\
\beta &= \text{the scale parameter for the log normal distribution} \\
&= 1.414\ \sigma\ \text{(standard deviation);} \\
G_g &= \text{the glassy modulus, Pa;} \\
\tau &= \text{relaxation time, s; and} \\
\tau_m &= \text{the exponential of the mean of the natural logarithims of the relaxation} \\
&\quad \text{times.}
\end{aligned}
$$

In order to describe the storage and loss moduli mathematically, the following transformations are first applied to the reduced frequency:

$$u = \ln \omega_r \tau \quad \text{and} \quad x = (2/\beta^2) \ln \omega_r \qquad (1.9)$$

The storage modulus is given as follows:

$$G'(x) = \frac{G_g}{\beta \sqrt{\pi}} \exp -\{\frac{\beta(x-1/2)}{2}\}^2\ x \int_0^\infty \exp -(\frac{u}{\beta})^2\ \frac{\cosh(x+1/2)u}{\cosh u}\ du \qquad (1.10)$$

The loss modulus is given by a similar equation:

$$G'(x) = \frac{G_g}{\beta \sqrt{\pi}} \exp -\{\frac{\beta(x-1/2)}{2}\}^2\ x \int_0^\infty \exp -(\frac{u}{\beta})^2\ \frac{\cosh(x-1/2)u}{\cosh u}\ du \qquad (1.11)$$

where the variables are as described for equations 1.7 through 1.9. As previously discussed, the loss tangent, or tan delta, is simply the ratio of the loss to the storage modulus (Jongepier and Kuilman 1969).

In application, Jongepier and Kuilman (1969) numerically integrated equations 1.10 and 1.11 for a range of β values, producing a set of master curves for complex modulus and phase angle. These master curves were then compared to experimental data, and values for the various parameters were selected for a best fit. Jongepier and Kuilman reported that values predicted from this model fit the observed data to within the experimental error, but that the

accuracy of the model was not as good for asphalts with large β-values as for asphalts with small β-values. This finding was attributed to practical problems in measuring the viscoelastic properties of such asphalts, which tend to be quite rubbery in behavior.

In characterizing the temperature dependence, or shift factors, of asphalt cement, Jongepier and Kuilman relied upon the Williams-Landel-Ferry (WLF) (1955) equation:

$$\log \; a(T) \; = \; \frac{-C_1(T-T_R)}{C_2+(T-T_R)} \qquad (1.12)$$

where

$\quad$ a(T) $\; = \;$ the shift factor at temperature T

$\qquad = \quad \eta_0(T)/\eta_0(T_R)$, $\eta_0(T)$ being the Newtonian viscosity at temperature T, and $\eta_0(T_R)$ being the Newtonian viscosity at the reference temperature, T_R, and

$\quad C_1, \; C_2 \; = \;$ empirically determined coefficients.

Jongepier and Kuilman (1969) pointed out that for the coefficients C_1 and C_2 to be interpreted radionally, the reference temperature must be chosen so as to have some physical meaning. This step was done by fitting their viscosity data to the Vogel equation:

$$\log \eta \; = \; A \; + \; B/(T \; - \; T_0) \qquad (1.13)$$

where

$\qquad \eta \; = \;$ viscosity, and

$\quad A, \; B, \; T_0 \; = \;$ empirical constants.

In the Vogel equation, the parameter B should correspond to the product $C_1 \times C_2$ in the WLF equation. Jongepier and Kuilman found that for paving-grade asphalts, the parameter B varied from about 600 to 1,000, and T_0 varied from about $-80°$ to $-40°C$ (-112 to $-40°F$). The values for asphalts with high β-values were, however, found to differ substantially from these ranges. For paving-grade asphalts, the range of values in B correspond closely to the value of 900 for the universal coefficients ($C_1 = 8.86$ and $C_2 = 101.6$).

The Jongepier and Kuilman model appears to be reasonably accurate and rigorous in its treatment of the LVE properties of asphalt cement. However, Brodnyan and co-workers (1960) found relaxation spectrum that appeared to be highly skewed on a log-log scale, suggesting that the relaxation times are not log-normally distributed, as discussed by Dickinson and Witt (1974). These latter researchers proposed a hyperbolic model more consistent with the observed relaxation spectra; this model is discussed in some detail in the following section.

An additional shortcoming of Jongepier and Kuilman's model, from a practical standpoint, is the mathematical complexity of its formulation. Although the expression of the moduli in terms of integral equations is theoretically sound, the approach prohibits use of the model for the simple calculations needed for routine practical applications in paving technology. Additionally, no details concerning the precise determination of the model parameters were presented by Jongepier and Kuilman.

Dobson's Model

Dobson (1969, 1972) developed a mathematical model for describing the master curve, based upon empirical relationships between the phase angle and the modulus for paving-grade asphalts. The equation he developed, unfortunately, was for transformed frequency in terms of a complex function of transformed modulus. That is, his equation does not express modulus in terms of frequency, but the reverse. Furthermore, this equation cannot be rearranged to solve explicitly for modulus. Dobson presented his results in terms of a universal master curve; the intent, apparently, was to characterize asphalts by graphical comparison with this master curve.

The fundamental assumption of Dobson's model, which was based on empirical observations of dynamic mechanical data on a range of paving-grade asphalts, is that the log-log slope of the complex modulus with respect to the loading frequency is a function of the loss tangent and the width of the relaxation spectrum:

$$\frac{dy}{dx} = \frac{t}{(1+t)(1-0.01t)} \tag{1.14}$$

where

$$
\begin{aligned}
y &= \log\left(\,|\,G^*(\omega)\,|\,/G_g\right), \\
G^*(\omega) &= \text{the complex modulus at frequency } \omega, \\
G_g &= \text{the glassy modulus,} \\
x &= \log\left(\eta_0\omega a(T)/G_g\right), \\
\eta_0 &= \text{the steady-state or Newtonian viscosity,} \\
a(T) &= \text{the shift factor at temperature } T \text{ relative to the reference temperature, and} \\
t &= \tan\delta \text{ (the loss tangent).}
\end{aligned}
$$

Additionally, Dobson (1972) observed a linear relationship between the loss tangent and the complex modulus, as expressed in the following equation:

$$\log\left(1 + t\right) = -by \tag{1.15}$$

20

where b is a parameter proportional to the width of the relaxation spectrum, and y is as defined above. Equations 1.14 and 1.15 can be mathematically combined to give Dobson's equation for relating reduced frequency and complex modulus:

$$\log \omega_r = \log G_r - \frac{1}{b} \left[\log(1 - G_r^b) + \frac{20.5 - G_r^{-b}}{230.3} \right] \tag{1.16}$$

where

$$\omega_r = \eta_0 \omega a(T)/G_g, \text{ and}$$
$$G_g = |G^*(\omega)| / G_g.$$

Like Jongepier and Kuilman (1969), Dobson used the WLF equation to characterize the temperature dependency of asphalt cement. Dobson found that a single set of coefficients could be used to fit the shift factor data for a range of asphalt cements, but that different coefficients were needed for low temperatures and high temperatures:

$$\log a(T) = \frac{-12.5(T - T_s)}{142.5 + T - T_s} \tag{1.17}$$

where, at temperature *above* T_s

$a(T)$ = the shift factor at temperature T *relative to* T_s, and
T_s = an empirical standard reference temperature; $T < T_s$.

$$\log a(T) = \frac{-8.86(T - T_s)}{101.6 + T - T_s} \tag{1.18}$$

where, at temperature *above* T_s

$a(T)$ = the shift factor at temperature T *relative to* T_s, and
T_s = an empirical standard reference temperature; $T > T_s$.

For equation 1.18, the coefficients C_1 and C_2 have the "universal values" suggested by Ferry (1980). Dobson did not report estimated values for T_s, but suggested that T_s is about 64°C (147°F) above the glass transition temperature where T_g is presumably determined from dilatometric measurements.

It is difficult to assess the accuracy of Dobson's model, since little comparison of measured and predicted moduli and phase angles was made in his papers. Additionally, the failure to express modulus as an explicit function of reduced frequency is a serious drawback, as is the lack of a well-defined procedure for determining the constants in his equation for the modulus. However, Dobson's method for characterizing the temperature dependency appears to be reasonably accurate and, additionally, he presents a practical means for applying this part of his model to rheological data on asphalt cement.

Dickinson and Witt's Model

Dickinson and Witt (1974) developed a model in which the master curve of complex modulus is mathematically treated as a hyperbola. Several parameters can be calculated from the master curve using statistical methods that then characterize the master curve. The equation proposed for describing the variation in the complex modulus with frequency is given in the following equation:

$$\log |G_r^*(\omega)| = 0.5 \{\log \omega_r - [(\log \omega_r)^2 + (2\beta)^2]^{0.5}\} \tag{1.19}$$

where

$$
\begin{aligned}
|G_r^*(\omega)| &= \text{the relative complex modulus at frequency } \omega \\
&= |G^*(\omega)|/G_g, \\
\omega_r &= \omega \eta_0 a(T)/G_g, \\
\eta_0 &= \text{the Newtonian viscosity,} \\
a(T) &= \text{the shift factor at temperature } T \text{ relative to the selected reference} \\
&\quad \text{temperature, and} \\
\beta &= \text{a "shear susceptibility" parameter, which is defined as the distance on a} \\
&\quad \text{log-log scale between the glassy modulus and the modulus at } \omega_r = 1.
\end{aligned}
$$

Dickinson and Witt proposed the following, similar equation for calculating the phase angle:

$$\delta(\omega) = \delta' + 0.25 (\pi - 2\delta') \{\log \omega_r - [(\log \omega_r)^2 + (2\beta)^2]^{-0.5}\} \tag{1.20}$$

where

$$
\begin{aligned}
\delta(\omega) &= \text{the phase angle at frequency } \omega, \text{ and} \\
\delta' &= \text{the limiting phase angle at infinite frequency,}
\end{aligned}
$$

and the other variables are as defined above for the previous equation.

The procedure suggested by Dickinson and Witt for determining the coefficients of these equations involved an initial estimate of β and δ' by performing a linear regression on a linear version of the equation for the complex plane:

$$\log |G_r^*| = -\beta \left[\frac{2(\delta - \delta')}{(\pi - 2\delta)} \right]^{1/2}$$

(1.21)

where the variables are as defined in equations 1.19 and 1.20 above. Note: Constants are estimated by rewriting equation 1.21 and regressing 1 of G_r^* versus $(\delta - \delta^1)/(\pi - 2\delta)$. Dickinson and Witt recommend that an iterative procedure then be used to determine final values for G_g, β, and η_0, which involves successive linear regressions on alternate linear forms of equation 1.19. However, with the advent of powerful microcomputers and various statistical packages, direct determination of the model coefficients using nonlinear least squares methods is probably more efficient. Dickinson and Witt used the equations developed by Dobson to describe temperature dependence in characterizing the shift factors for their asphalt cements. These equations were presented earlier (equations 1.16 and 1.17).

Dickinson and Witt reported the standard error of fit for G*(ω) using their model to be no more than 0.025 on a log scale, corresponding to a maximum error of about 10 percent. The accuracy in terms of the phase angle was not reported, although plots presented in their paper indicated that the accuracy was comparable to the experimental error in determining the phase angles. As mentioned previously, Dickinson and Witt found that the relaxation spectra for the asphalt cements studied were somewhat skewed, rather than symmetrical, as would occur if the distribution of relaxation times were log normal, as suggested by Jongepier and Kuilman.

In general, the above model appears to be somewhat simpler than either Jongepier and Kuilman's or Dobson's, and of similar or better accuracy. However, Dickinson and Witt found a strong relationship between G_g and β for their model. Additionally, the reported values of log G_g ranged from 8 to 9.6 Pa, which is considerably different from the more or less constant value of 9 Pa reported by other researchers (Van der Poel 1954; Pink et al. 1980). This fact suggests that there is some inaccuracy in both the glassy modulus and β parameters determined from their model; a similar error should be expected in the estimated value of the Newtonian viscosity.

Other Studies

DeBats et al. (1983) evaluated various models for predicting the dynamic mechanical properties of asphalt cements. They found that the Jongepier and Kuilman model fit observed rheological data much better than the Dickinson and Witt model.

Maccarone (1987) studied the dynamic mechanical properties of a large number of asphalt cements recovered from sprayed seal coats in Australia. He concluded that Dickinson and Witt's model fit the observed data quite well, and was in fact suitable for describing the dynamic mechanical response of paving-grade asphalts. Maccarone reported typical standard errors of fit for Dickinson and Witt's model of from about 0.004 to 0.008 on a log scale, corresponding to maximum errors of only a few percentage points. Maccarone also

evaluated Dobson's equations for describing the temperature dependence of asphalt cements, and found that for the weathered asphalts studied, the WLF equation with Dobson's coefficients overpredicted the shift factors at temperatures below about 20°C (68°F). Maccarone suggested that the coefficients for use in the WLF equation are approximately the same for most paving asphalts and have average values of $C_1 = 23$ and $C_2 = 230$.

Linear Viscoelastic Model Developed during A-002A Research

Determination of Range of Linear Behavior

Since the characterization of the SHRP core asphalts as reported in this phase of the research program was intended for the LVE case only, it was necessary to determine the range of linear behavior for each asphalt. This step was done by performing strain sweeps at selected temperatures, typically 15°, 35°, and 60°C (59°, 95°, and 140°F). During a strain sweep, a specimen is mounted in the rheometer, allowed to equilibrate at the selected test temperature, and subjected to a gradually increasing sinusoidal strain at a given frequency. In this case, the frequency used was 10 rad/s. The strain is allowed to increase until the measured modulus decreased to about 30 percent of its highest observed value, which ensured that the sweep was carried out well into the nonlinear region. In analyzing the strain sweep data for the SHRP asphalts, it was found that there was rarely a clear distinction between the linear and nonlinear regions, but that with increasing strain levels, the modulus would decrease at an ever-increasing rate. The linear strain limit was therefore somewhat arbitrarily established as the strain at which the storage modulus decreased to 95 percent of its maximum value. All strain sweeps were replicated on separate samples of asphalt. Because this testing had to be completed before further characterization, and because performing only a few strain sweeps is relatively quick, replicate testing was generally done only a few days later.

In using the data from these strain sweeps, the linear strain limit was plotted versus temperature, and a line or curve drawn through the data points. Generally, the LVE strain limit increases with temperature. Appropriate strains for testing could then be read from this plot. The dynamic mechanical analysis of the SHRP asphalts was done at strains that were in general 50 to 75 percent of this estimated LVE limit. In testing with the torsion bar at low temperatures, it was not necessary to perform strain sweeps. In this testing, the strains used are exceedingly small, generally between 0.01 and 0.5 percent, therefore ensuring linearity. A plot of the LVE strain limit as a function of complex modulus for the eight SHRP asphalts (tank) is shown in figure 1.8. There is a clear relationship between the complex modulus and the linear strain limit; this relationship is apparently similar for a wide range of asphalt cements. This information was used later in the study to develop the standard test specification method for the dynamic mechanical analysis of asphalt cements.

Characteristic Parameters of the Master Curve

In reviewing the literature on the LVE properties of asphalt cement, and in analyzing the dynamic mechanical data gathered to date on the SHRP asphalts, it has become clear that four primary parameters are needed to fully characterize the LVE properties of any asphalt cement:

- *The glassy moduli, G^*_g*—the value that the complex modulus or stiffness modulus approaches at low temperatures and high frequencies or short loading times; the glassy modulus is normally very close to 1 GPa in shear loading for most asphalt cements and a single value of 1 GPa may be assumed for most purposes.

- *The steady-state viscosity, η_o*—the steady-state, or Newtonian viscosity. In dynamic testing, it is approximated as the limit of the dynamic viscosity, η^*, as the phase angle approaches 90°. The 45° line that the dynamic master curve approaches at low frequencies is often referred to as the viscous asymptote. It is indicative of the steady-state viscosity, and the value of η_o is asphalt specific.

- *The crossover frequency, ω, or crossover time, t_c*—the frequency at a given temperature where tan delta is 1. At this point, the storage and loss moduli are equal. For most asphalt cements, the crossover frequency is nearly equal to the point at which the viscous asymptote intersects the glassy modulus. The crossover frequency can be thought of as a hardness parameter that indicates the general consistency of a given asphalt at the selected temperature and is asphalt specific. The crossover frequency is the reciprocal of the crossover time,
  $t_c = 1/\omega_c$.

- *The rheological index, R*—the difference between the glassy modulus, G_g, and the dynamic complex modulus at the crossover frequency, $G^*(\omega_c)$. The rheological index is directly proportional to the width of the relaxation spectrum and indicates rheologic type. R is not a measure of temperature but reflects the change in modulus with frequency or leading time and therefore is a measure of the shear-rate dependency of asphalt cement. R is asphalt specific.

The diagram of a typical dynamic master curve shown in figure 1.9 illustrates the meaning of these parameters.

Although a single set of these four parameters is adequate to describe the time dependence of most asphalt cements under a wide range of loading conditions, it has been found that as viscous flow is approached, irregularities occur in the behavior of most asphalt cements. These irregularities require that a second set of parameters be defined in order to describe the viscoelastic behavior at long loading times or high temperatures. Fortunately, it has been found that the rheological index in this case can be assumed to be constant at 0.81. Because of mathematical constraints concerning the continuity of the master curve, only a single parameter is needed to describe the viscoelastic behavior as viscous flow is approached. A more suitable way of expressing this parameter is a phase angle, δ_v, above which the second

set of parameters applies. The values for all these secondary parameters can be derived from the primary set of LVE parameters and δ_v.

The parameters for the master curve, as described above, are meant to be clearly definable characteristic parameters, as opposed to statistically determined parameters that may or may not truly reflect the mechanical properties of the asphalt. Therefore, specific procedures must be used to determine these parameters from experimental data.

The glassy modulus can be *estimated* by plotting the measured complex modulus as a function of the phase angle for values of the phase angle less than about 10. The intercept on such a plot is the glassy modulus. A plot showing this construction is given as figure 1.10, for SHRP core asphalt AAB-1 (tank); the intercept at $\delta = 0$ is the glassy modulus. Regression techniques can be used to provide a standard, reproducible estimate of the glassy modulus. If data at low phase angles are unavailable, the glassy modulus can be assumed to be 1 GPa for most practical purposes. The extensional glassy stiffness, $S_g(t)$, is equal to $G^*_g/(1+\delta_v)$.

A similar construction at a given temperature is used to estimate the steady-state viscosity from dynamic data. A plot of complex viscosity versus $(1-\delta/90°)$ is prepared, and the intercept, at $(1-\delta/90°) = 0°$, represents the estimated steady-state viscosity. In constructing this type of plot, data should be used only for phase angles greater than approximately 70°. If regression methods are used, the plot may be rendered more linear by plotting η^* against the quantity $(1-\delta/90°)$ raised to the 1.5 power. A typical plot of η^* as a function of $(1-\delta/90)^{1.5}$ for asphalt AAB-1 (tank) is shown in figure 1.11.

The crossover frequency can be estimated by plotting the log of the reduced frequency versus log tan δ. For values of tan δ between about 0.5 and 2, this plot is normally nearly linear. It is easy to determine the crossover frequency, either graphically or statistically, as the frequency at which tan δ is equal to one (log tan $\delta = 0$). Figure 1.12 is a plot of log frequency versus log tan δ for asphalt AAB-1 (tank).

An estimation of the rheological index is done in a manner similar to that of determining the crossover frequency. In this case, log (log G*) is plotted versus log tan δ for values of tan delta between about 0.5 and 2. The value of the transformed complex modulus at tan $\delta = 1$ is converted to log G* by taking its antilog (base 10), giving the log of the crossover modulus, log $G^*(\omega_c)$. The rheological index is calculated by subtracting the log of the crossover modulus from the log of the glassy modulus. A plot of log (log G*) versus log tan δ is given as figure 1.13, which is again for asphalt AAB-1 (tank).

Linear Viscoelastic Parameters for the SHRP Asphalts

The calculations described above were performed on the master curves generated for the SHRP core asphalts, tank, thin film oven test (TFOT) and pressure aging vessel (PAV) residue, and for the Materials Research Library (MRL) asphalts. These LVE parameters for the core asphalts are summarized in table 1.1. The crossover frequency and the steady-state

viscosity are always dependent upon the reference temperature. In table 1.1, the values for these parameters were found by using the defining temperature, T_d, as the reference point because it represents a point of approximate rheological equivalence (equal free volume). (Note: In table 1.1 the reference is not 25°C (77°F), but the defining temperature, T_d, which is asphalt specific.) As discussed in chapter 2, the use of T_d as the reference temperature simplifies the calculation of various rheological functions using the appropriate equations. Estimation of the LVE parameters was done individually for each of the two replicates, which allowed the calculation of precision estimates, based on the 95 percent confidence interval determined by pooling error terms over all asphalts. It is apparent from table 1.1 that the LVE parameters are quite different for the various asphalts, and clearly differentiate not only among the various asphalts but also between the aging treatments. These LVE parameters represent a unique, rational, and efficient description of the LVE behavior of a given asphalt cement.

Mathematical Model for Describing the Master Curve

The complex mechanical behavior of viscoelastic materials such as asphalt cement is a result of the interaction of both time and temperature dependence. In the mathematical modeling of the LVE behavior of asphalt cement, these effects must be treated separately. This fact was recognized by early researchers such as Saal and Labout (1958) who used precisely the terminology suggested here: time dependency and temperature dependency. Time dependency is reflected in the location (t_c or ω_c) and shape (R) of the master curve; temperature dependency is indicated by the plot of log $a(T)$ versus temperature. Temperature dependency as reflected in the shift factors should not be confused with temperature susceptibility; temperature susceptibility is an empirical concept based on the change of consistency or hardness of an asphalt with temperature. Temperature dependency is a fundamental concept that indicates how the relaxation processes within a given asphalt cement change with temperature.

A review of the various models asphalt researchers have proposed in order to describe the time dependency was presented above; a brief comparison and evaluation of these models is now in order. Van der Poel, in the construction of his nomograph (Van der Poel 1954), undoubtedly used mathematical models for the master curve. Unfortunately, these models were never published or explicitly described in the literature. Jongepier and Kuilman (1969) assumed that the relaxation spectrum for all asphalt cements followed a log normal distribution, and used integral equations to describe the various viscoelastic functions in terms of the relaxation spectrum. Dickinson and Witt (1974) proposed a hyperbolic model for the master curve. All these models, although reasonably accurate, have shortcomings. Van der Poel's nomograph is inherently limited by its use of empirical consistency measurements, such as penetration. Additionally, because of the current availability of powerful hand calculators and personal computers, it is no longer necessary or even desirable to work with graphical calculation systems, and the original mathematical formulation of Van der Poel's nomograph is not available. The model of Jongepier and Kuilman is more fundamental and its formulation is explicitly available. However, the use of integral equations makes practical calculations with this model impossible. The model of Dickinson

and Witt is more practical than Jongepier and Kuilman's log normal model, but has other shortcomings. Specifically, the glassy modulus and viscosity in this model are determined statistically, and, in many cases, are grossly overestimated when compared with the rigorously determined values. Additionally, the mathematics of this model are such that useful manipulation of the various equations is difficult, thus making engineering calculations cumbersome.

During SHRP A-002A research, various mathematical models were used to characterize the master curve; many were abandoned for reasons such as those given above. However, a model was developed that was rigorous in its treatment of the master curve, reasonably accurate, and mathematically simple enough to allow direct engineering calculations. This model is presented below as a series of equations for the primary dynamic viscoelastic functions.

For the complex modulus, the following mathematical function can be used:

$$G^*(\omega) = G_g[1+(\omega_c/\omega)^{(\log 2)/R}] - R/(\log 2) \tag{1.22}$$

where

$$
\begin{array}{ll}
G^*(\omega) = & \text{complex dynamic modulus, in Pa, at frequency } \omega, \text{ rad/s;} \\
G_g = & \text{glassy modulus, typically 1 GPa;} \\
\omega_c = & \text{the crossover frequency, rad/s; and} \\
R = & \text{the rheological index.}
\end{array}
$$

For the phase angle, δ, the following related equation applies:

$$\delta(\omega) = 90/[1+(\omega/\omega_o)^{(\log 2)/R}] \tag{1.23}$$

where

$$\delta(\omega) = \text{the phase angle, in degrees, at frequency } \omega, \text{ rad/s, and}$$

the other variables are as defined above in equation 1.22. Equations 1.22 and 1.23 can be combined and algebraically manipulated to show that the rheological index, R, is given by the following equation:

$$R = (\log 2) \log[G^*(\omega)/G_g] / \log(1 - \delta/90) \tag{1.24}$$

where the variables are as previously defined. This equation is quite useful when the value of the rheological index is desired, but not for data covering the region where tan $\delta = 1$ is not available or is impossible to obtain with the test methods at hand. In using this equation to calculate R, the glassy modulus can generally be assumed to be 1 GPa in shear or 3 GPa in extension or flexure. Equation 1.24 is quite accurate within the region where the phase angle is between about $10°$ and $70°$; however, the best results are obtained near the crossover point, where $\delta = 45°$.

28

The mathematical model described above can be used over a wide range of temperatures and frequencies that extend well into the glassy region. However, as viscous flow is approached at high temperatures and/or long loading times, this model often does not generate results consistent with measured values of complex modulus or phase angle. As viscous flow is approached, the suggested way to deal with such anomalies is to calculate a second set of parameter values for the secondary region in which R can be assumed to be 0.81. The equations can then be manipulated to generate a series of equations from which the LVE parameter values for the secondary viscoelastic region will be calculated.

The most important of these calculations is for the determination of δ_v, which divides the primary and secondary regions:

$$\delta_v = 90 \; (\eta_{ss}\omega_c/G_g)^{\log 2/(R-0.81)} \tag{1.25}$$

where

δ_v = transition phase angle, degrees;
η_{ss} = the steady-state viscosity, Pa·s;
ω_c = the crossover frequency, rad/s;
G_g = the glassy modulus, Pa; and
R = the rheological index.

From equation 1.25, it is clear that the value of G_g/ω_c must be equal to or less than the value of the steady-state viscosity, η_{ss}, which is always the case for unmodified asphalt cements. If the value of these parameters is equal, it means that the same LVE parameters apply throughout the entire region of behavior. This phenomenon will sometimes occur in asphalts having very high asphaltene contents. Once δ_v is known, it can be used in conjunction with the primary LVE parameters to estimate the appropriate values for the viscous flow region.

For estimating G_{gv},

$$G_{gv} = G_g[90/(90-\delta_v)]^{0.81-R/\log 2} \tag{1.26}$$

where

G_{gv} = the limiting modulus in the viscous flow region;
G_g = the glassy modulus, in Pa;
δ_v = the transition phase angle, in degrees; and
R = the rheological index.

For estimating ω_{cv},

$$\omega_{cv} = \omega_c[(90-\delta_v)/\delta_v]^{R/\log 2 - 0.81} \tag{1.27}$$

where

ω_{cv} = the location parameter, in rad/s, for the viscous flow region;

ω_c = the crossover frequency, rad/s,;
δ_v = the transition phase angle, degrees; and
R = the rheological index.

These two parameters, G_{gv} and ω_{cv}, can be used in conjunction with the standard value of R in the viscous flow region (0.81) to generate all viscoelastic functions at high temperatures and/or low frequencies. The primary set of parameters should be used when the phase angle is below δ_v, the secondary parameters (for viscous flow), when the phase angle is above δ_v. In many cases it is tedious to first estimate the phase angle, compare it with δ_v, and then determine if the proper set of parameters has been used. Therefore, a fourth parameter, the transition frequency ω_v, is useful:

$$\omega_v = \omega_c[(90-\delta_v)/\delta_v]^{R/\log 2} \qquad (1.28)$$

where

ω_v = the transition frequency, rad/s;
ω_c = the crossover frequency, rad/s;
δ_v = the transition phase angle, degrees; and
R = the rheological index.

When estimating the modulus or phase angle from the LVE parameters, it is first necessary to check whether the loading frequency is above or below ω_v. If the loading frequency is above ω_v, the primary LVE parameters are used. If the loading frequency is below ω_v, the values for the viscous flow region are used.

Although the division of the master curve into two regions with two sets of parameters may seem unnecessarily complicated, it has been found that this method is the only way to achieve reasonable accuracy in mathematical modeling while still maintaining the use of the explicit parameters that characterize the master curve. In practice, the primary parameters are of more interest and can be applied with confidence to temperatures up to about 45°C (113°F) under typical traffic loading times. At higher temperatures, the only property that is of practical interest is the steady-state viscosity, which is one of the explicit parameters from the master curve. Therefore, in practical applications, it is generally not necessary to use the parameters for the viscous flow region. These parameters were developed and presented here in the interest of completeness. In research and detailed pavement modeling applications, it may also be desirable to have a comprehensive and accurate model for the LVE behavior of asphalt cement.

The procedures described above for determining the characteristic parameters for the master curve and for determining the secondary LVE parameters for the viscous flow region were applied to the SHRP core asphalts. The proposed LVE model typically fits the measured data to within about 15 percent, which is lower than the experimental error, given the measurement techniques, especially temperature control, that were used early in this study.

Mathematical Functions for Describing the Temperature Dependence of Asphalt Cement

Data gathered on the eight SHRP core asphalt cements, including those aged with different treatments, indicate that the temperature dependence of the viscoelastic behavior of asphalt cement, as indicated by the shift factors determined from construction of the master curve, can be represented by two equations. The first of these equations, the WLF equation (Williams and others 1955), is used *above* the defining temperature, T_d, and *within* the Newtonian region:

$$\log a(T)_d = -C_1(T-T_d)/(C_2+T-T_d) \tag{1.29}$$

where

$$
\begin{aligned}
a(T)_d &= \text{the shift factor relative to the defining temperature, } T_d; \\
C_1, C_2 &= \text{empirically determined constants;} \\
T &= \text{the selected temperature, in °C or °K; and} \\
T_d &= \text{the defining temperature, in °C or °K, which is a characteristic parameter} \\
&\quad \text{for each asphalt cement.}
\end{aligned}
$$

An Arhennius function is used to describe the shift factors as a function of temperature *below* the defining temperature and within the Newtonian region:

$$\log a(T)_d = 2.303 \, E_a/R \, (1/T - 1/T_d) \tag{1.30}$$

where

$$
\begin{aligned}
E_a &= \text{the activation energy for flow below } T_d; \\
R &= \text{the ideal gas constant, 8.34 J/mol-°K;}
\end{aligned}
$$

and the other variables are as defined for equation 1.29. In analyzing the shift factor data for the SHRP asphalts, it has been found that the values of C_1 and C_2 for use in the WLF equation can be fixed for all asphalts to 19 and 92, respectively. The activation energy for flow below T_d, E_a, can similarly be fixed to 261 kJ/mol. This calculation greatly simplifies the characterization of the temperature dependence of asphalt cements, reducing this aspect of the viscoelastic behavior to a single parameter, T_d. When this step is done, equations 1.29 and 1.30 are functions of T and T_d.

When a full dynamic characterization has been performed, nonlinear least squares analyses can be used to determine the value of T_d, using equation 1.30, with the suggested constant values for the various coefficients. The shift factors for the SHRP core asphalts under all aging treatments were analyzed in this way, resulting in the defining temperature values given in table 1.1 above. The precision of determining T_d in this way is ± 3°C (± 5.4°F), based on pooled variances and a 95 percent confidence interval. An illustration of the similarity of the function describing the shift factors for the SHRP core asphalt cements is

shown in figure 1.14, in which the shift factors for the eight SHRP core asphalts under all aging treatments normalized with respect to T_d are plotted.

Rheological Protocols

It is sometimes necessary to interrelate various rheological functions. The purpose of this section is to describe the interrelationships among the rheological functions characterized by the various tests used during the A-002A project, to characterize the properties of pavement binders, and to semiquantitatively define the effect on these test data of variations in the primary operational parameters.

Interrelation of Viscoelastic Test Data and Functions

There are three commonly used test methods of determining viscoelastic functions: (1) creep, (2) stress relaxation, and (3) dynamic mechanical analysis. Each of these methods provides complete information on the LVE behavior of a selected material, but in different forms. There are theoretically exact introconversions among these functions, but the mathematics of these exact interrelations involve either integral equations or transforms (Laplace or Fourier) that in general can only be attacked numerically. There are, however, many approximate introconversions that are discussed in chapter 2 of this volume. In addition to the three common loading modes of determining viscoelastic response, tests may be carried out using either shear or extensional/flexural loading. There are, of course, reasonably accurate means of converting shear data to extensional or flexural data, and vice versa.

Given the three common loading modes (creep, stress relaxation, dynamic testing) and the two general geometries (shear and extension/flexure), there are six commonly used viscoelastic functions:

- Creep compliance in shear, $J(t)$
- Creep compliance in extension or flexure, $D(t)$
- Relaxation modulus in shear, $G(t)$
- Relaxation modulus in extension or flexure, $E(t)$
- Dynamic complex modulus in shear, $G^*(\omega)$
- Dynamic complex modulus in extension or flexure, $E^*(\omega)$

In dynamic mechanical analysis, a parameter frequently referred to is the phase angle, δ. Alternatively, rheologists often refer to "tan delta" or the loss tangent, which in both cases refers to the tangent of the phase angle. The phase angle in mechanical testing indicates the phase lag between the mechanical input and the resulting response. For a perfectly elastic material, the phase angle is zero; for a Newtonian fluid, the phase angle is 90 degrees. Various other viscoelastic functions can be defined through the complex modulus and the phase angle:

- Storage modulus in shear, $G' = G^* \cos \delta$
- Storage modulus in extension or flexure, $E' = E^* \cos \delta$
- Loss modulus in shear, $G'' = G^* \sin \delta$
- Loss modulus in extension or flexure, $E'' = E^* \sin \delta$
- Dynamic complex compliance in shear, $J^* = 1/G^*$
- Dynamic complex compliance in extension or flexure, $D^* = 1/E^*$
- Storage compliance in shear, $J' = \cos \delta / G^*$
- Storage compliance in extension or flexure, $D' = \cos \delta / E^*$
- Loss compliance in shear, $J'' = \sin \delta / G^*$
- Loss compliance in extension or flexure, $D'' = \sin \delta / G^*$
- Dynamic viscosity in shear, $\eta^* = G^*/\omega$

The assumption here that extensional and flexural moduli are equivalent is not a rigorous one; this assumption will only be true if the extensional properties of a material are equivalent in tension and compression. For many materials, this assumption is only true at strains of less than a few percent. Fortunately, for asphalt cement, flexural tests, such as the bending beam, can only be performed when the asphalt is in a rigid state, and the strains are for this reason practically limited to about one percent or less. This result should create equivalent or nearly equivalent moduli in tension, compression, and flexure.

Asphalt technologists frequently make use of the term "stiffness," $S(t)$. Stiffness was originally coined by Van der Poel (1954), and is most correctly defined as the inverse of the extensional creep compliance:

$$S(t) = 1/D(t) \tag{1.31}$$

However, the following approximate relationship is often inferred in the use of the term "stiffness" in asphalt rheology:

$$S(t) \approx E^*(\omega) \tag{1.32}$$
$$t \rightarrow 1/\omega$$

That is, the stiffness modulus at time t is approximately equal to the extensional complex modulus at frequency $\omega = 1/t$. To provide an indication of the error involved in this approximation, for a single Maxwell element with a spring of unit stiffness and a relaxation time τ of one, $S(t) = 1/D(t) = 0.500$, while $1/E^*(1/t) = 0.707$. The error, in this case, is 41 percent. This value, however, represents approximately the maximum possible error for this approximation. For paving grade binders the error will usually be much less, typically less than 20 percent.

The basis for the approximate relationship between the stiffness modulus and the complex modulus is a more generalized relationship between creep compliance and dynamic modulus; in shear loading,

$$J(t) = 1/G^*(\omega) \tag{1.33}$$
$$t \rightarrow 1/\omega$$

33

or in extension/flexure,

$$D(t) = 1/E^*(\omega)$$
$$t \to 1/\omega$$

(1.34)

These approximations are of similar accuracy to the previous equation (1.32) that relates $S(t)$ and $E^*(\omega)$. More accurate approximate introconversions have been given by various authors. Among the most commonly used are those developed by Ninomiya and Ferry (1959). As an example, the approximate formula below is suggested for calculating the relaxation modulus in shear, $G(t)$, from the dynamic storage (G') and loss (G'') moduli:

$$G(t) = G'(\omega) - 0.40\ G''(0.40\omega) + 0.014\ G''(10\omega)$$
$$t \to 1/\omega$$

(1.35)

In introconverting shear and extensional properties, a rigorous treatment requires the knowledge of the shear moduli, and one other function, such as Poisson's ratio (μ) or the bulk modulus, K. Most commonly in asphalt technology, incompressibility is assumed (μ = 0.5). The relationship between the shear and extensional relaxation modulus is then:

$$E(t) = 2(1+\mu)\ G(t) = 3\ G(t)$$

(1.36)

Similarly, the dynamic modulus in extension is approximately three times the dynamic modulus in shear. This relationship holds for the storage and loss moduli also. For compliance, a similar approximate relationship exists:

$$D(t) = J(t) / [2(1+\mu)] = J(t) / 3$$

(1.37)

This relationship, along with the previously defined concept of stiffness, leads to approximate formulas for the stiffness modulus, as defined by Van der Poel (1954), in terms of the shear compliance and dynamic modulus:

$$S(t) = 3 / J(t)$$

(1.38)

$$S(t) = 3\ G^*(\omega)$$
$$t \to 1/\omega$$

There is an almost infinite variety of approximate relationships among the various viscoelastic functions. The above discussion is intended only to present a few of the more commonly used relationships of asphalt technology. The interested reader should refer to papers and references in which such interrelationships are discussed in greater detail (Ninomiya and Ferry 1959; Ferry 1980; Tschoegl 1989).

In regard to the suggested specification tests, the following comments can be made concerning the relationships among the test data produced by each method. The results of dynamic shear testing are more commonly reported in terms of the complex modulus in shear (G^*) and the phase angle. The bending beam rheometer, on the other hand, produces data in

the form of extensional creep compliance, which is inverted to give a stiffness modulus. From the above discussion it should be apparent that the flexural stiffness at time t from the bending beam rheometer should be approximately equal to three times the dynamic shear modulus when the frequency, given in Hertz, equals $1/t$.

Conclusions and Recommendations on the Linear Viscoelastic Modeling of Pavement Binders

A reasonably accurate, relatively simple model for characterizing and predicting the LVE behavior of asphalt cement and other paving binders is essential in order to understand the behavior of such materials, characterize and specify them efficiently, and predict their performance in paving applications with acceptable accuracy. Although more theoretically rigorous than linear models, nonlinear models require such large amounts of testing as to be impractical for routinely specifying asphalt cements. Additionally, the response of most paving binders under conditions that are apt to occur in a paving mixture in situ would appear to be largely linear under a wide range of conditions.

LVE models for asphalt cement have been proposed by various other researchers. Most of these models are reasonably accurate, although not well suited for routine engineering use. Some also show evidence of systematic bias in the model parameters when compared with the actual, physically determinable values for the parameters.

The LVE model developed by the A-002A research team for asphalt cement and related binders is fairly accurate and complete, and is mathematically simply, using parameters. By using a LVE model having only a few parameters, it is possible to rapidly characterize an asphalt cement using limited testing with the degree of accuracy necessary for engineering design purposes. Additionally, the LVE model parameters have specific physical meanings, which allow them to be used in the development of rational physico-chemical property relationships. The model parameters can be used to estimate the rheological response under various critical conditions associated with the major mechanisms of pavement distress.

applied stress τ

(a) elastic response γ

(b) viscous response γ

(c) viscoelastic response γ
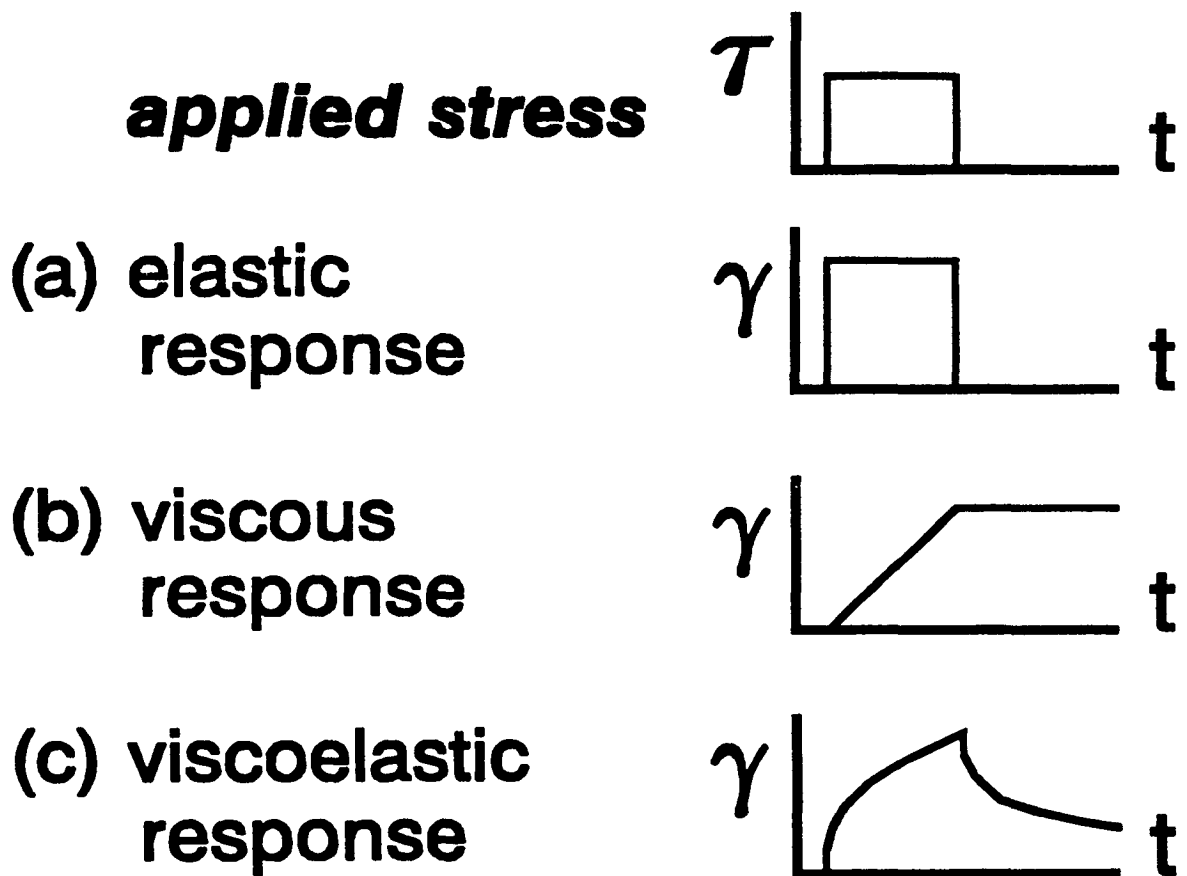
Figure 1.1   Idealized Response of Elastic, Viscous, and Viscoelastic Materials under Constant Stress Loading
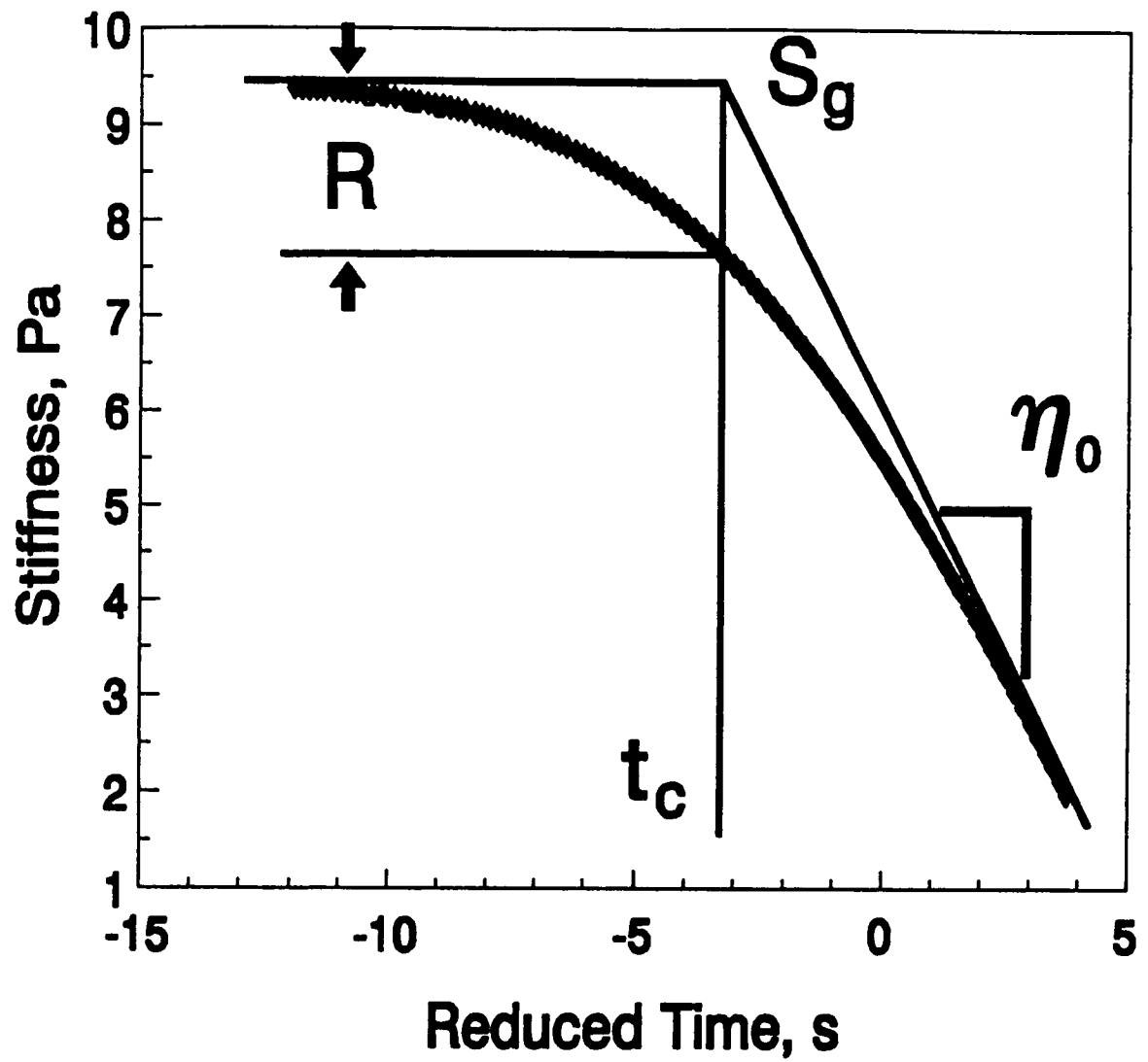
Figure 1.2   Typical Plot of Log Creep Stiffness versus Log Time for Asphalt Cement
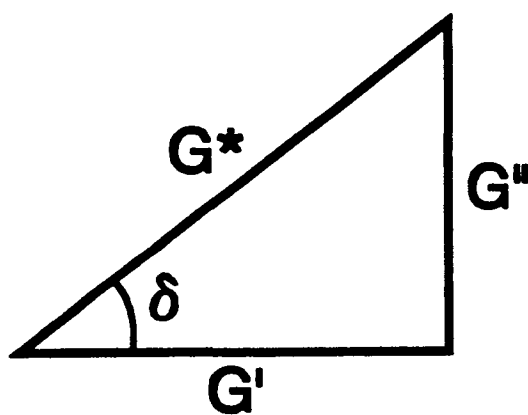
$$G' = G^* \cos \delta$$

$$G'' = G^* \sin \delta$$

$$G^* = \sqrt{G'^2 + G''^2}$$

Figure 1.3   Relationship among Complex Modulus (G*), Storage Modulus (G'), Loss Modulus (G"), and the Phase Angle (δ), as Shown through the Trigonometry of a Right Triangle
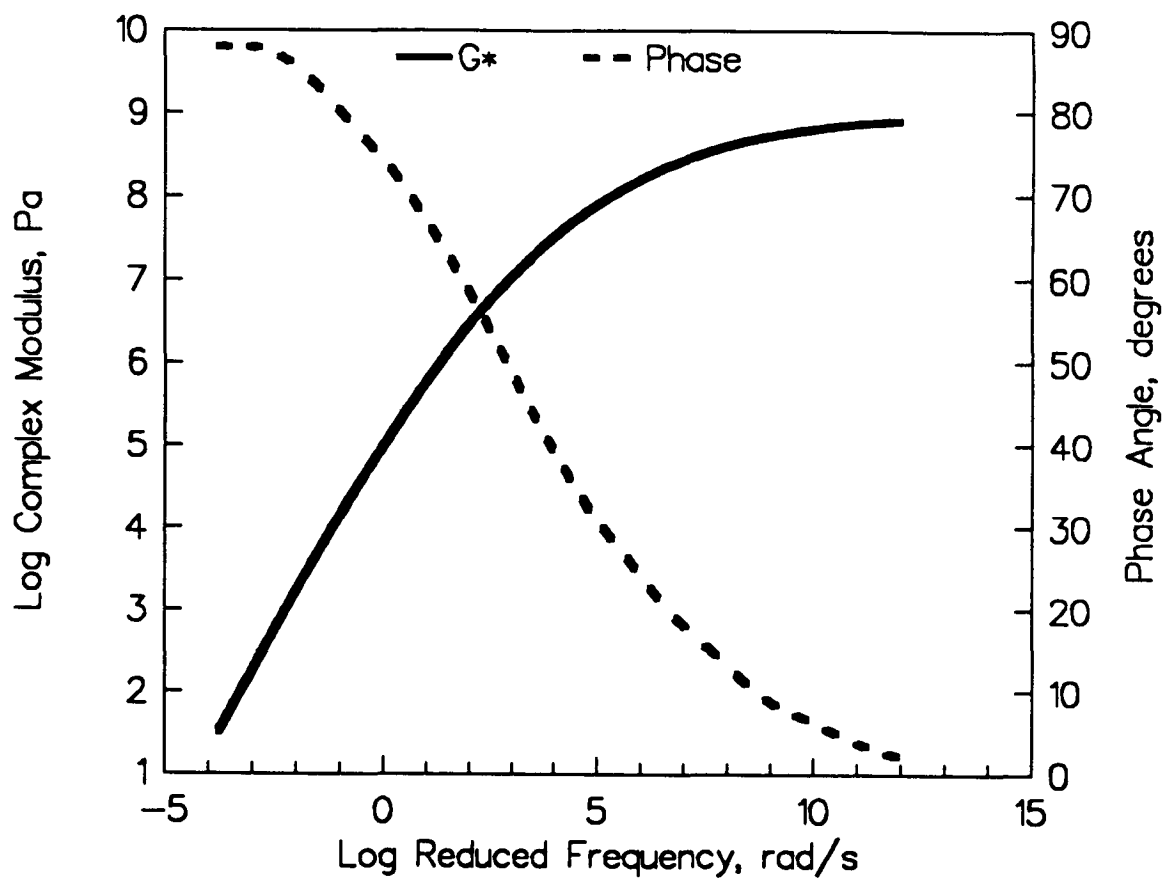
Figure 1.4 Complex Modulus and Phase Angle versus Frequency for Asphalt AAB-1 (Tank)
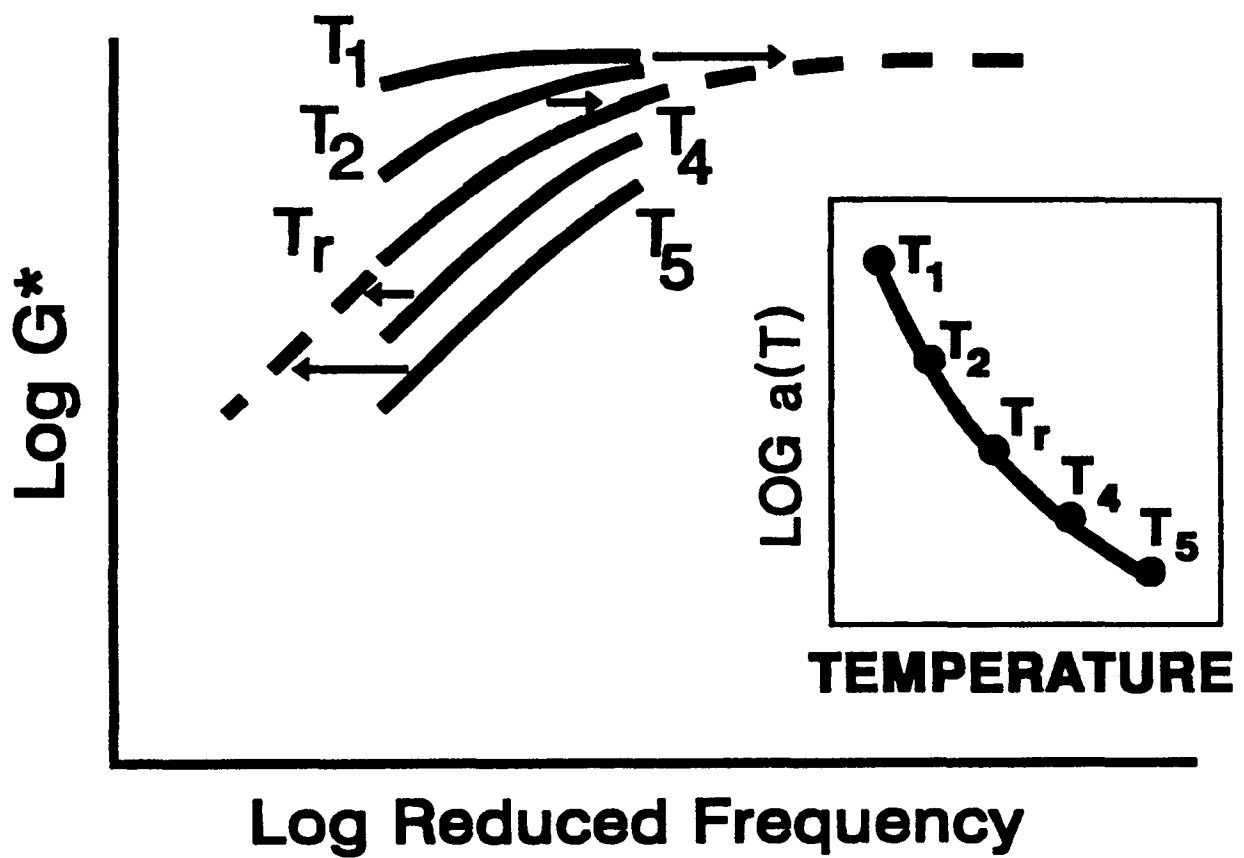
Figure 1.5   Use of Time-Temperature Superposition in Construction of a Master
Curve of Complex Modulus versus Frequency
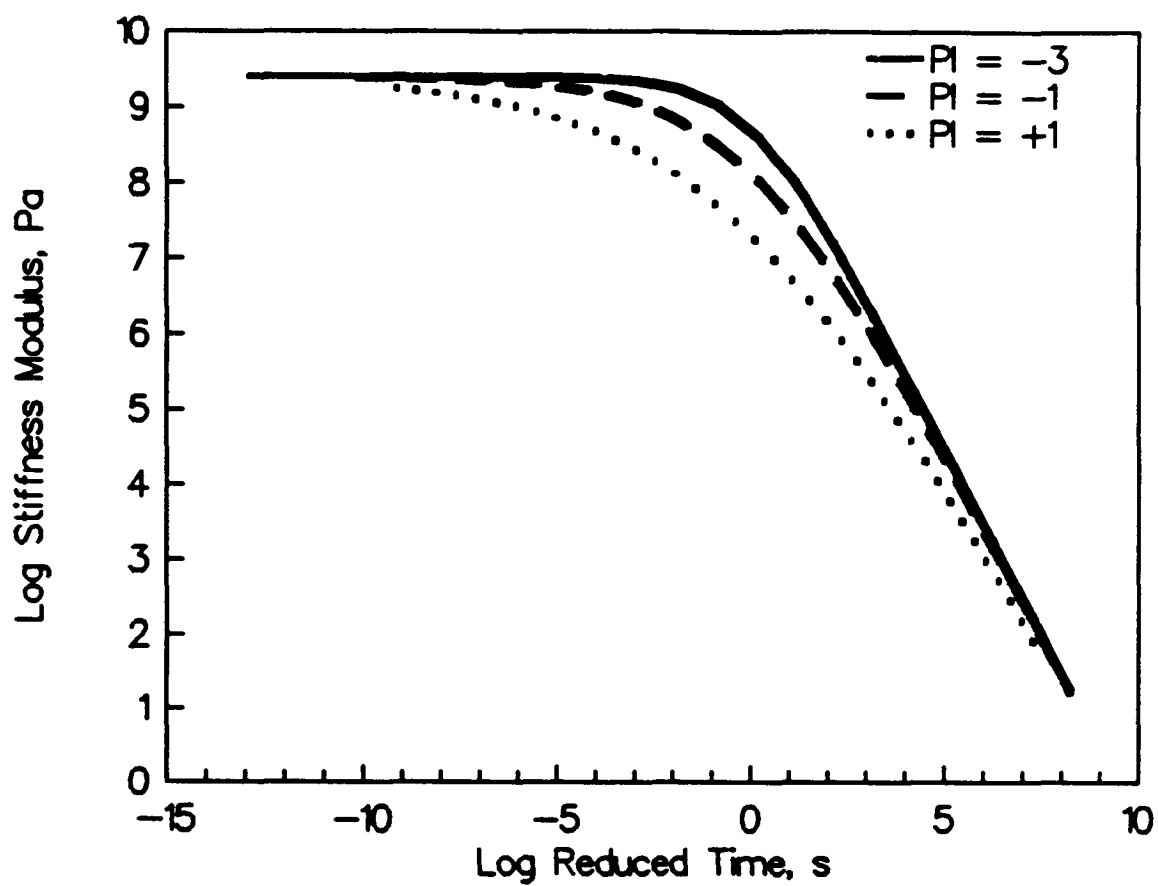
Figure 1.6   Master Curves Developed from Van der Poel's Nomograph, for Different
Values of the Penetration Index
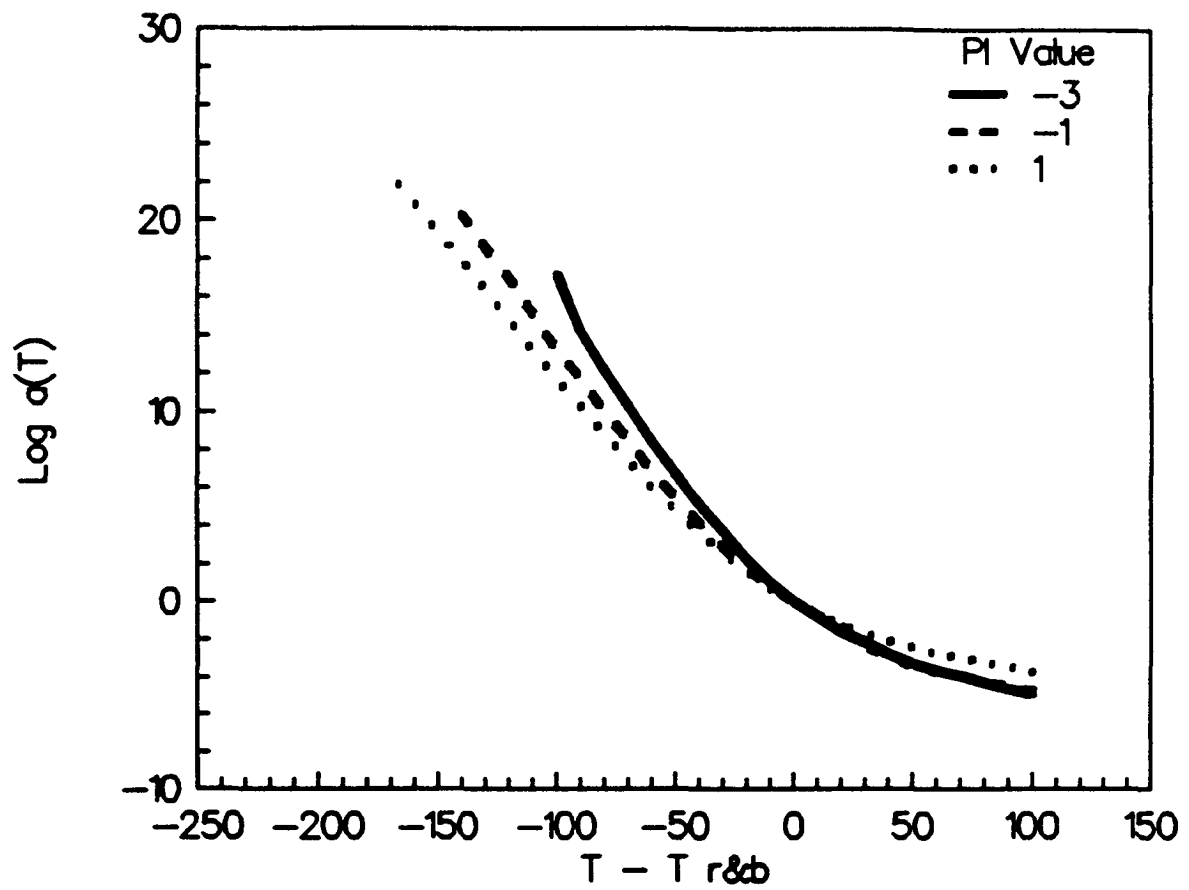
Figure 1.7   **Shift Factors Developed from Van der Poel's Nomograph, for Different Values of the Penetration Index**
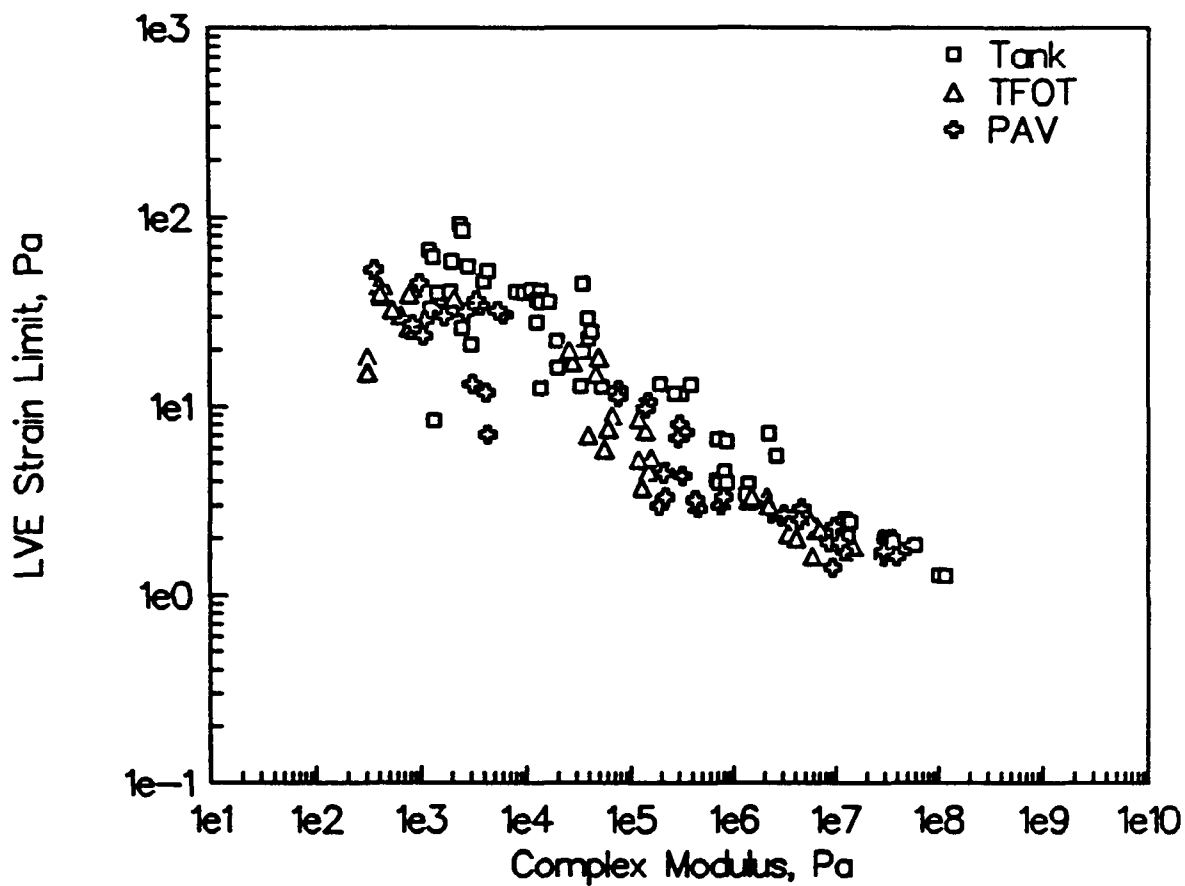
Figure 1.8   Linear Viscoelastic Strain Limit as a Function of Complex Modulus for Core Asphalts (Tank, TFOT, and PAV/60°C (140°F) and 144 hrs)
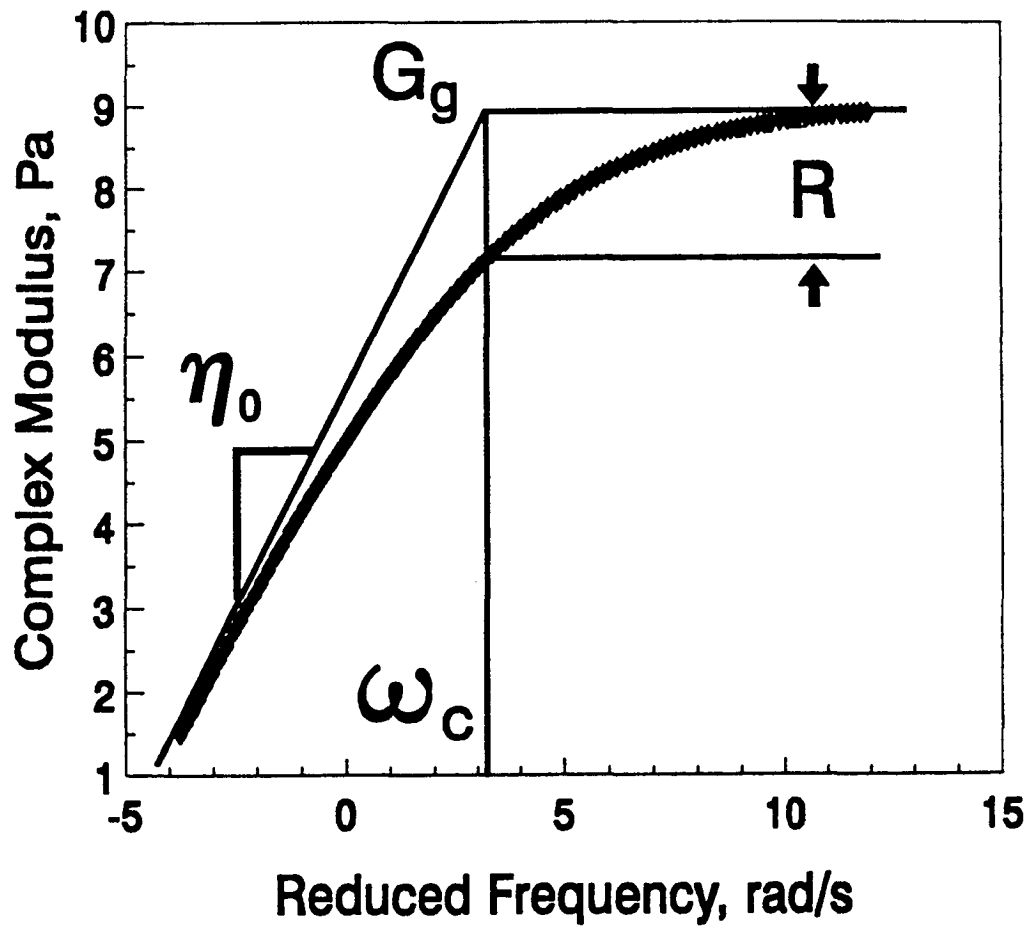
Figure 1.9   Typical Dynamic Master Curve for Asphalt Cement, with Important
            Parameters Described
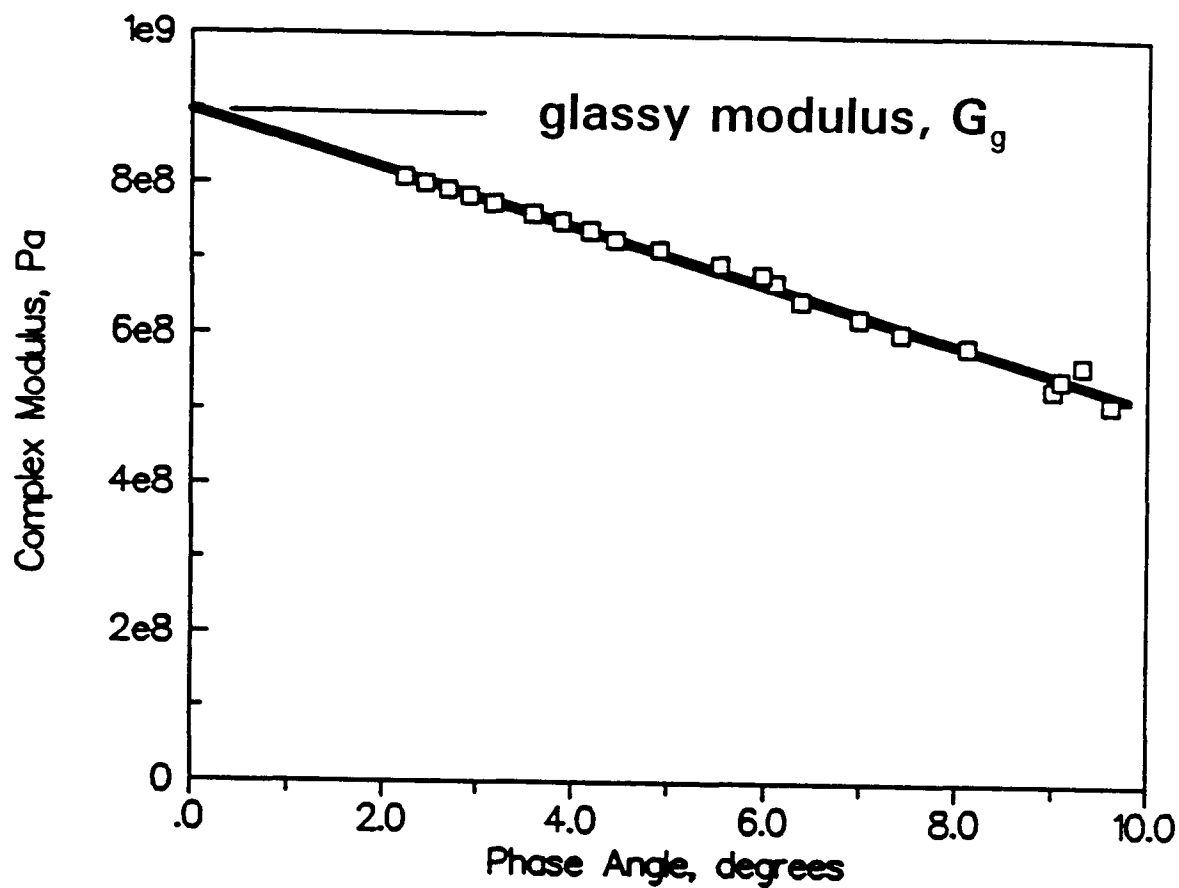
Figure 1.10 Determination of the Glassy Modulus G_g from Dynamic Data at Low-Temperature by Plotting Complex Modulus versus Phase Angle (Asphalt AAB-1, Tank)
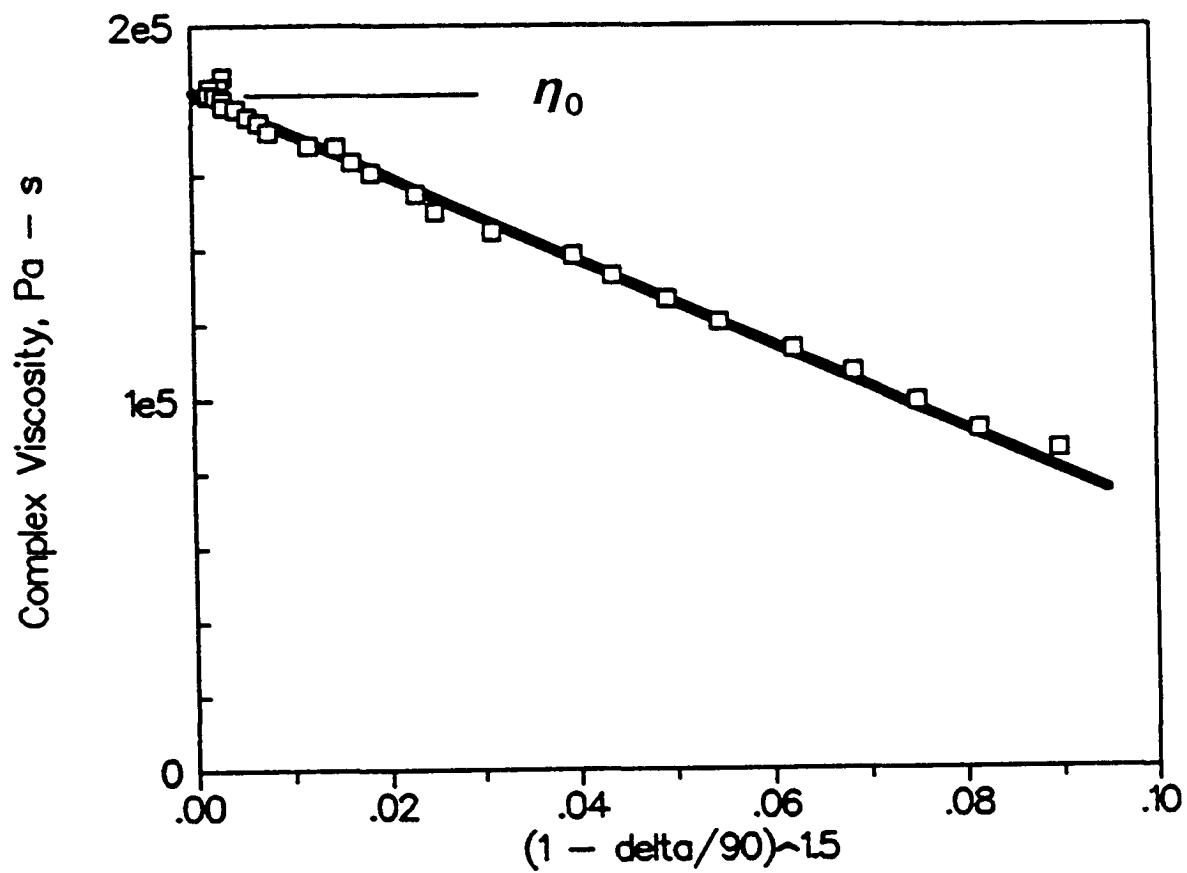
Figure 1.11 Determination of the Steady-State Viscosity η_0 from Dynamic Data, by Plotting η^* versus Transformed Phase Angle (Asphalt AAB-1, Tank)
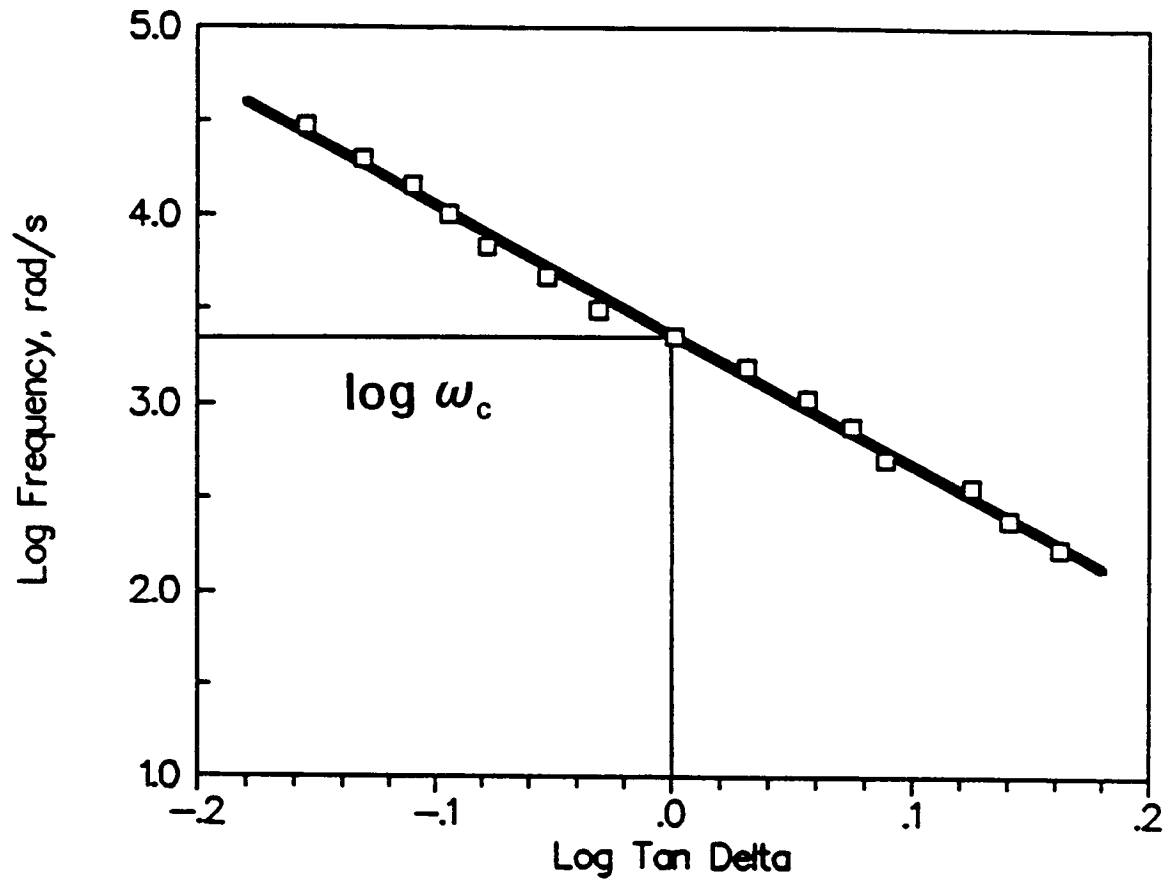
Figure 1.12 Determination of the Crossover Frequency ω_c from Dynamic Data, by Plotting Frequency versus Loss Tangent (Asphalt AAB-1, Tank)
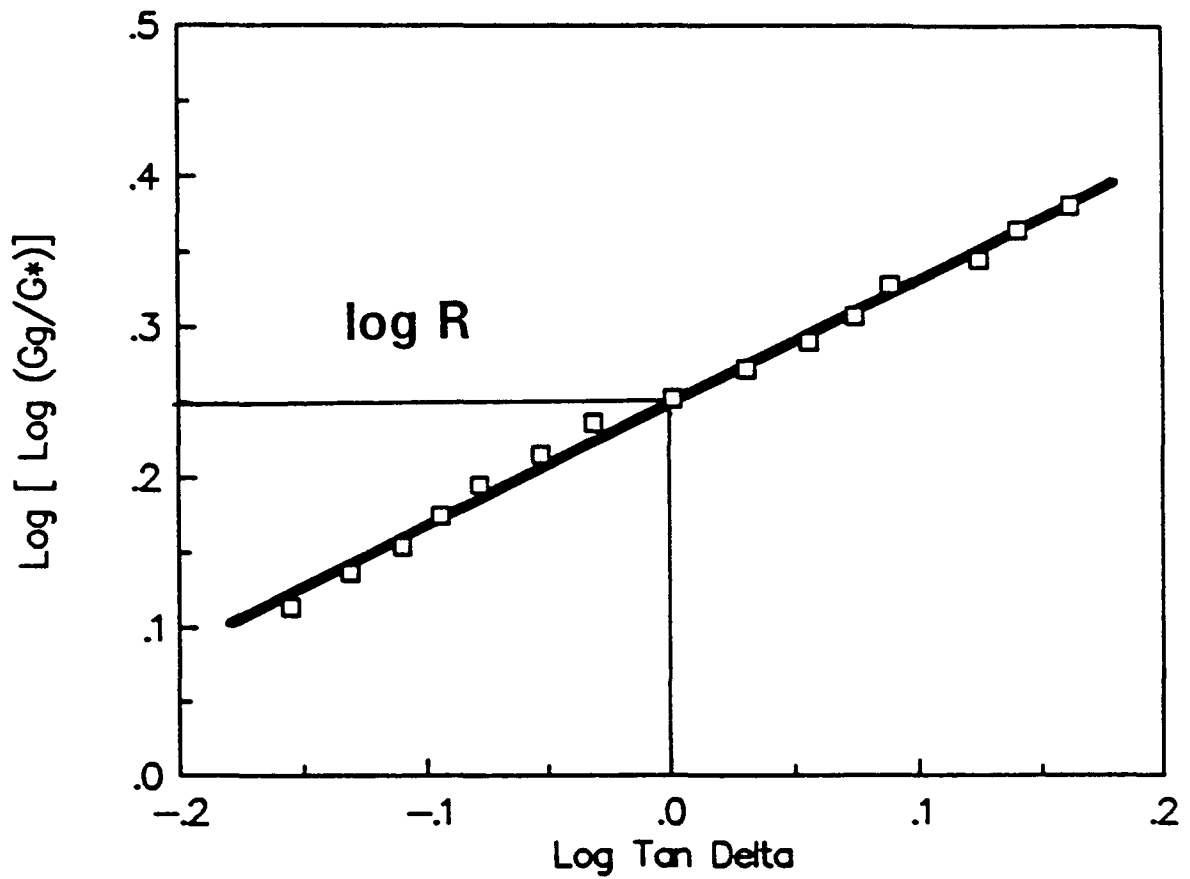
Figure 1.13 Determination of G* at the Crossover Frequency, by Plotting G* versus Tan Delta, and Calculation of R (Asphalt AAB-1, Tank)
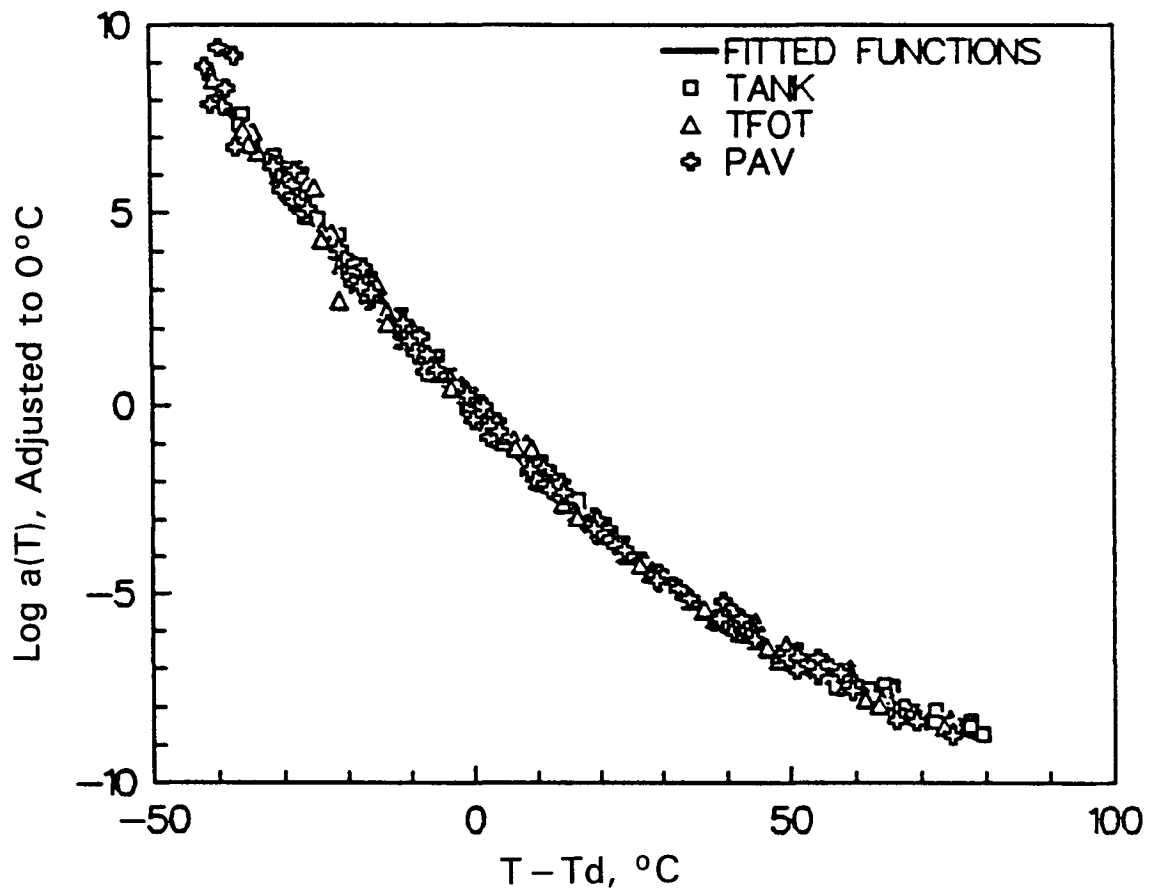
Figure 1.14 Shift Factors as a Function of Temperature for SHRP Core Asphalts (Tank, TFOT, and PAV/60°C (140°F) and 144 hrs)

Table 1.1 Linear Viscoelastic Model Parameters for SHRP Core Asphalts (Tank, TFOT, and PAV/60°C and 144 hrs)

Asphalt	Treatment	Rep.	T_d °C	Log G_g Pa	Log ω_o rad/s	R	Log ω_v rad/s	Log G_{gv} Pa	Log ω_{ov} Pa
AAA-1	Tank	1	−20.4	8.98	−2.13	1.49	−10.60	5.12	−5.97
AAA-1	Tank	2	−18.2	8.99	−1.92	1.51	−8.38	5.95	−4.91
		Avg.:	−19.3	8.99	−2.03	1.50	−9.49	5.54	−5.44
AAB-1	Tank	1	−13.0	8.95	−2.16	1.73	−5.32	6.95	−3.84
AAB-1	Tank	2	−10.1	8.94	−1.77	1.78	−4.96	6.86	−3.51
		Avg.:	−11.6	8.95	−1.97	1.76	−5.14	6.90	−3.67
AAC-1	Tank	1	−3.9	9.00	−0.87	1.63	−3.79	7.24	−2.33
AAC-1	Tank	2	−7.1	8.94	−1.46	1.63	−4.10	7.28	−2.78
		Avg.:	−5.5	8.97	−1.16	1.63	−3.95	7.26	−2.56
AAD-1	Tank	1	−17.7	9.01	−2.10	1.67	−8.04	5.87	−5.14
AAD-1	Tank	2	−16.4	9.07	−1.92	1.65	N/A	N/A	N/A
		Avg.:	−17.1	9.04	−2.01	1.66	−9.68	5.09	−5.92
AAF-1	Tank	1	−8.7	8.92	−2.36	1.58	−3.51	7.83	−2.92
AAF-1	Tank	2	−5.2	8.99	−1.78	1.61	−3.05	7.84	−2.41
		Avg.:	−7.0	8.96	−2.07	1.60	−3.28	7.83	−2.67
AAG-1	Tank	1	−2.2	8.95	−1.13	1.26	−1.13	8.51	−1.13
AAG-1	Tank	2	−5.6	8.94	−1.72	1.23	−1.76	8.52	−1.74
		Avg.:	−3.9	8.94	−1.43	1.24	−1.44	8.51	−1.43
AAK-1	Tank	1	−13.5	9.00	−2.18	1.62	N/A	N/A	N/A
AAK-1	Tank	2	−15.9	8.96	−2.48	1.58	N/A	N/A	N/A
		Avg.:	−14.7	8.98	−2.33	1.60	N/A	N/A	N/A
AAM-1	Tank	1	2.5	8.90	−0.98	1.94	−3.43	6.91	−2.40
AAM-1	Tank	2	−0.5	8.85	−1.53	1.92	−4.28	6.76	−3.11
		Avg.:	1.0	8.88	−1.26	1.93	−3.85	6.84	−2.76
Pooled 95%		C.I.:	± 3.0	± .08	± .48	± .10	± .77	± .27	± .52

Table 1.1 Linear Viscoelastic Model Parameters for SHRP Core Asphalts (Tank, TFOT, and PAV/60°C and 144 hrs) (continued)

Asphalt	Treatment	Rep.	T_d °C	Log G_g Pa	Log ω_o rad/s	R	Log ω_v rad/s	Log G_{gv} Pa	Log ω_{ov} Pa
AAA-1	Tank	1	−20.4	8.98	−2.13	1.49	−10.60	5.12	−5.97
AAA-1	Tank	2	−18.2	8.99	−1.92	1.51	−8.38	5.95	−4.91
		Avg.:	−19.3	8.99	−2.03	1.50	−9.49	5.54	−5.44
AAB-1	Tank	1	−13.0	8.95	−2.16	1.73	−5.32	6.95	−3.84
AAB-1	Tank	2	−10.1	8.94	−1.77	1.78	−4.96	6.86	−3.51
		Avg.:	−11.6	8.95	−1.97	1.76	−5.14	6.90	−3.67
AAC-1	Tank	1	−3.9	9.00	−0.87	1.63	−3.79	7.24	−2.33
AAC-1	Tank	2	−7.1	8.94	−1.46	1.63	−4.10	7.28	−2.78
		Avg.:	−5.5	8.97	−1.16	1.63	−3.95	7.26	−2.56
AAD-1	Tank	1	−17.7	9.01	−2.10	1.67	−8.04	5.87	−5.14
AAD-1	Tank	2	−16.4	9.07	−1.92	1.65	N/A	N/A	N/A
		Avg.:	−17.1	9.04	−2.01	1.66	−9.68	5.09	−5.92
AAF-1	Tank	1	−8.7	8.92	−2.36	1.58	−3.51	7.83	−2.92
AAF-1	Tank	2	−5.2	8.99	−1.78	1.61	−3.05	7.84	−2.41
		Avg.:	−7.0	8.96	−2.07	1.60	−3.28	7.83	−2.67
AAG-1	Tank	1	−2.2	8.95	−1.13	1.26	−1.13	8.51	−1.13
AAG-1	Tank	2	−5.6	8.94	−1.72	1.23	−1.76	8.52	−1.74
		Avg.:	−3.9	8.94	−1.43	1.24	−1.44	8.51	−1.43
AAK-1	Tank	1	−13.5	9.00	−2.18	1.62	N/A	N/A	N/A
AAK-1	Tank	2	−15.9	8.96	−2.48	1.58	N/A	N/A	N/A
		Avg.:	−14.7	8.98	−2.33	1.60	N/A	N/A	N/A
AAM-1	Tank	1	2.5	8.90	−0.98	1.94	−3.43	6.91	−2.40
AAM-1	Tank	2	−0.5	8.85	−1.53	1.92	−4.28	6.76	−3.11
		Avg.:	1.0	8.88	−1.26	1.93	−3.85	6.84	−2.76
Pooled 95%	C.I.:		± 3.0	± .08	± .48	± .10	± .77	± .27	± .52

51

Table 1.1   Linear Viscoelastic Model Parameters for SHRP Core Asphalts (Tank, TFOT, and PAV/60°C and 144 hrs) (continued)

Asphalt	Treatment	Rep.	T_d °C	Log G_g Pa	Log ω_o rad/s	R	Log ω_v rad/s	Log G_{gv} Pa	Log ω_{ov} Pa
AAA-1	TFOT	1	−15.4	9.00	−2.13	1.75	−8.46	5.51	−5.51
AAA-1	TFOT	2	−13.2	9.03	−1.84	1.76	−8.19	5.51	−5.26
		Avg.:	−14.3	9.01	−1.98	1.75	−8.32	5.51	−5.38
AAB-1	TFOT	1	−3.4	9.06	−1.76	2.13	−4.81	6.58	−3.64
AAB-1	TFOT	2	−7.3	8.94	−2.27	2.00	−5.54	6.53	−4.21
		Avg.:	−5.3	9.00	−2.02	2.06	−5.17	6.55	−3.93
AAC-1	TFOT	1	−3.0	8.90	−1.73	1.80	−4.48	6.97	−3.24
AAC-1	TFOT	2	−4.6	8.89	−2.06	1.81	−4.90	6.91	−3.62
		Avg.:	−3.8	8.90	−1.89	1.80	−4.69	6.94	−3.43
AAD-1	TFOT	1	−10.5	9.13	−1.82	1.93	−11.67	3.37	−7.53
AAD-1	TFOT	2	−16.1	8.86	−2.68	1.66	N/A	N/A	N/A
		Avg.:	−13.3	8.99	−2.25	1.80	−13.24	2.95	−8.27
AAF-1	TFOT	1	0.8	8.94	−1.77	1.80	−3.77	7.30	−2.87
AAF-1	TFOT	2	−3.6	8.94	−2.40	1.75	−4.61	7.28	−3.58
		Avg.:	−1.4	8.94	−2.08	1.77	−4.19	7.29	−3.23
AAG-1	TFOT	1	−0.1	8.96	−1.31	1.35	−1.74	8.33	−1.48
AAG-1	TFOT	2	1.7	8.95	−1.11	1.35	−1.72	8.29	−1.35
		Avg.:	0.8	8.96	−1.21	1.35	−1.73	8.31	−1.42
AAK-1	TFOT	1	−9.1	9.04	−2.39	1.81	N/A	N/A	N/A
AAK-1	TFOT	2	−9.5	9.02	−2.38	1.79	N/A	N/A	N/A
		Avg.:	−9.3	9.03	−2.39	1.80	N/A	N/A	N/A
AAM-1	TFOT	1	4.5	8.83	−1.49	2.15	−4.11	6.50	−3.12
AAM-1	TFOT	2	5.1	8.91	−1.53	2.27	−4.25	6.40	−3.28
		Avg.:	4.8	8.87	−1.51	2.21	−4.18	6.45	−3.20
Pooled 95%	C.I.:		± 3.0	± .08	± .48	± .10	± .77	± .27	± .52

Table 1.1 **Linear Viscoelastic Model Parameters for SHRP Core Asphalts (Tank, TFOT, and PAV/60°C and 144 hrs)** (continued)

Asphalt	Treatment	Rep.	T_d °C	Log G_g Pa	Log ω_o rad/s	R	Log ω_v rad/s	Log G_{gv} Pa	Log ω_{ov} Pa
AAA-1	PAV	1	−14.2	8.92	−2.91	1.95	−7.78	5.82	−5.75
AAA-1	PAV	2	−14.8	8.80	−2.99	1.86	−8.41	5.57	−6.04
		Avg.:	−14.5	8.86	−2.95	1.90	−8.09	5.70	−5.90
AAB-1	PAV	1	−4.4	8.98	−2.65	2.17	−5.67	6.47	−4.53
AAB-1	PAV	2	−7.6	8.92	−3.09	2.09	−6.40	6.36	−5.11
		Avg.:	−6.0	8.95	−2.87	2.13	−6.03	6.41	−4.82
AAC-1	PAV	1	2.2	9.01	−1.82	2.11	−4.47	6.72	−3.45
AAC-1	PAV	2	4.8	8.99	−1.35	2.09	−4.04	6.71	−2.99
		Avg.:	3.5	9.00	−1.58	2.10	−4.26	6.72	−3.22
AAD-1	PAV	1	−10.9	9.00	−2.86	2.04	−10.51	4.27	−7.47
AAD-1	PAV	2	−6.6	9.09	−2.21	2.10	−10.70	3.77	−7.42
		Avg.:	−8.7	9.05	−2.54	2.07	−10.61	4.02	−7.45
AAF-1	PAV	1	3.4	9.01	−2.48	2.04	−4.23	7.18	−3.53
AAF-1	PAV	2	7.0	8.96	−1.96	2.00	−3.66	7.19	−2.96
		Avg.:	5.2	8.99	−2.22	2.02	−3.94	7.19	−3.25
AAG-1	PAV	1	2.5	8.94	−1.79	1.48	−2.28	8.15	−2.01
AAG-1	PAV	2	3.0	8.86	−1.70	1.40	−2.13	8.18	−1.88
		Avg.:	2.7	8.90	−1.74	1.44	−2.21	8.16	−1.95
AAK-1	PAV	1	−10.1	8.96	−3.17	1.94	−12.28	3.61	−8.46
AAK-1	PAV	2	−8.4	8.96	−3.02	1.94	−13.08	3.08	−8.86
		Avg.:	−9.2	8.96	−3.10	1.94	−12.68	3.34	−8.66
AAM-1	PAV	1	4.0	8.86	−3.07	2.74	−4.47	6.39	−4.06
AAM-1	PAV	2	8.0	8.90	−2.15	2.47	−5.31	5.96	−4.27
		Avg.:	6.0	8.88	−2.61	2.61	−4.89	6.17	−4.16
Pooled 95%	C.I.:		± 3.0	± .08	± .48	± .10	± .77	± .27	± .52

References

Boannaure, F., Gest, G., Gravois, A., and Uge, P. 1977. "A New Method of Predicting the Stiffness of Asphalt Paving Mixtures," *Proceedings of the Association of Asphalt Paving Technologists*, vol. 46, pp. 64–100.

Brodnyan, J.G., Gaskins, F.H., Philippoff, W., and Thelen, E. 1960. "The Rheology of Asphalt. III. Dynamic Mechanical Properties of Asphalt," *Transactions of the Society of Rheology*, vol. 4, pp. 279–296.

De Bats, F.Th., Raadsen, J., and Snel, M.C. 1983. "Characterization of Linear and Non-Linear Rheologic Properties of Bitumen," *Symposium RILEM*, p. 219.

Dickinson, E.J., and Witt, H.P. 1974. "The Dynamic Shear Modulus of Paving Asphalts as a Function of Frequency," *Transactions of the Society of Rheology*, vol. 18, no. 4, pp. 591–606.

Dobson, G.R. 1969. "The Dynamic Mechanical Properties of Bitumen," *Proceedings of the Association of Asphalt Paving Technologists*, vol. 38, p. 123.

Dobson, G.R. 1972. "On the Development of Rational Specifications for the Rheological Properties of Bitumens," *Journal of the Institute of Petroleum*, vol. 58, no. 559, pp. 14–24.

Ferry, J.D. 1980. *Viscoelastic Properties of Polymers*. New York: John Wiley & Sons.

Heukelom, W. 1966. "Observations on the Rheology and Fracture of Bitumens and Asphalt Mixes," *Proceedings of the Association of Asphalt Paving Technologists*, vol. 36, pp. 359–397.

Jongepier, R., and Kuilman, B. 1969. "Characteristics of the Rheology of Bitumens," *Proceedings of the Association of Asphalt Paving Technologists*, vol. 38, pp. 98–122.

Maccarone, S. 1987. "Rheological Properties of Weathered Asphalts Extracted from Sprayed Seals Nearing Distress Conditions," *Proceedings of the Association of Asphalt Paving Technologists*, vol. 56, pp. 654–687.

McLeod, N.W. 1972. "A 4-Year Survey of Low Temperature Transverse Pavement Cracking on Three Ontario Test Roads," *Proceedings of Association of Asphalt Paving Technologists*, vol. 41, pp. 424–493.

Ninomiya, K., and Ferry, J.D. 1959. "Some Approximate Equations Useful in the Phenomenological Treatment of Linear Viscoelastic Data," *Journal of Colloid Science*, vol. 14, pp. 36–48.

Pink, H.S., Merz, R.E., and Bosniak, D.S. 1980. "Asphalt Rheology: Experimental Determination of Dynamic Moduli at Low Temperature," *Proceedings of the Association of Asphalt Paving Technologists*, vol. 49, p. 64.

Saal, R.N.J., and Labout, J.W.A. 1958. "Rheological Properties of Asphalts," in *Rheology: Theory and Applications*, vol. II, F.R. Eirich, ed. New York: Academic Press, chap. 9.

Tschoegl, N.W. 1989. *The Phenomenological Theory of Linear Viscoelastic Behavior*. Berlin: Springer-Verlag.

Van der Poel, C. 1954. "A General System Describing the Viscoelastic Properties of Bitumens and its Relation to Routine Test Data," *Journal of Applied Chemistry*, vol. 4, p. 221.

Williams, M.L., Landel, R.F., and Ferry, J.D. 1955. "The Temperature Dependence of Relaxation Mechanisms in Amorphous Polymers and Other Glass-forming Liquids," *Journal of the American Chemical Society*, vol. 77, pp. 3701–3706.

2

Rheological Measurements

The word *rheology* is derived from the Greek word *rheo*, which translates literally as "to flow." The stiffness of asphalt binders is time dependent—they flow with time—and consequently asphalt binders are classified as rheological materials. The properties of rheological materials are also temperature dependent; consequently, both the time of loading and the temperature of loading must be considered when characterizing the flow properties of rheological materials such as asphalt cement binders.

In keeping with the tradition established by asphalt technologists, the modulus that relates stress to strain is referred to as the stiffness modulus, or simply stiffness, $S(T,t)$, where T indicates temperature dependency and t indicates time dependency. The stiffness of asphalt cement varies tremendously over its application and service temperature range. At low temperatures, where asphalt binders behave as elastic solids, their stiffness values approach 5×10^9 Pa (30,000 lb/in.^{2}), whereas at the upper range of service temperatures their stiffness values may be only 1 kPa (0.15 lb/in.^{2}). Coefficients of viscosity for asphalt cement binders may range from 0.1 mPa·s (1 mpoise) at the upper range of service temperatures to 1 Pa·s (1 poise) at mixing and compaction temperatures. The stiffness values of asphalt binders are much more temperature dependent than other organic construction materials, which makes the selection of testing equipment particularly challenging. Asphalt cements are approximately 20 times more temperature dependent than many polymeric materials.

The testing equipment and protocols developed during the project served a dual purpose—to provide fundamental physical properties that could be used to develop relationships between physical and chemical properties and to provide test methods and criteria for developing a performance-related specification. At the outset of the project, the research team recognized the need for characterizing the low-temperature stiffness of asphalt cement binders and developed the bending beam rheometer for this purpose. Dynamic shear measurements were originally envisioned as primarily serving the need for generating the sophisticated rheological data required to develop relationships between physical and chemical properties. As low-cost, specification-type dynamic shear rheometers became available, they were

adopted for specification use. Early in the project, it was not expected that the dynamic shear rheometers could be adapted to routine specification applications.

Before it became obvious that low-cost, specification-type dynamic shear devices would become commercially available, an indentation test was investigated as a low-cost, specification-type rheometer. This device was abandoned when it became apparent that the low-cost, specification-type constant stress rheometers could be used for specification testing. In an attempt to provide a low-cost device that could measure permanent strain resulting from repeated loading, the plastic deformation device was investigated. Because it was not judged practical as a specification device, and because its further development was beyond the resources of the project, such development was discontinued.

The rheological measurements obtained at Penn State University with the bending beam rheometer, the dynamic shear rheometer, the indentation device, and the permanent deformation device are described in this chapter. The majority of the rheological data were obtained with the bending beam rheometer and the dynamic shear rheometer because these devices were adopted for specification purposes. The other two devices were not adopted for specification use and are described only briefly at the end of the chapter.

Dynamic Shear Rheometer

The dynamic shear rheometer (DSR) used to conduct dynamic mechanical analysis (DMA) is perhaps misnamed. Dynamic forces are not considered; the word "dynamic" refers to the manner in which the stresses or strains applied to the test specimen vary with time. In the DSR the shear stresses and strains vary with time from positive to negative in a sinusoidal fashion. The variation may be rather slow, requiring 100 seconds per cycle, or quite rapid, such that as many as 100 cycles of alternating positive and negative shear stress and strain are applied per second. The DSR provides stress-strain moduli at different rates of loading, expressed in terms of frequency, and at different test temperatures. Shear strains or stresses may be applied to test specimens in the DSR by mounting the test specimens between plates or twisting beams of material in torsion.

Dynamic Mechanical Rheometer Test Program

Dynamic mechanical analysis was performed on the Materials Research Library (MRL) asphalts using a Rheometrics Mechanical Spectrometer, model RMS-803. This device applies sinusoidal angular deflections to specimens of various geometries and sizes. In the linear viscoelastic (LVE) characterization of the MRL asphalts, two geometries were used: parallel plates and torsion bar. The two specimen geometries used in the dynamic mechanical analysis of the MRL asphalts are shown schematically in figure 2.1.[1] At temperatures from approximately 5° to 35°C (41° to 95°F), 8-mm (0.31-in.)-diameter parallel plates were used in performing the dynamic testing. At temperatures above 35°C

---

[1]All figures and tables referenced in this chapter appear at the end of the chapter.

(95°F), 25-mm (0.98-in.)-diameter plates were used. At temperatures of 5°C (41°F) and below, the torsion bar geometry was used with the RMS-803.

The Rheometrics Mechanical Spectrometer is a fully automated testing system that automatically acquires and reduces the data to engineering units. Data acquired include:

- Applied maximum peak-to-peak strain as a function of time

- Resulting maximum peak-to-peak torque as a function of time

- The temperature of the lower plate (parallel plates) or oven (torsion bar)

The spectrometer contains appropriate computer software to compute and report the following:

- Complex modulus, the maximum peak-to-peak stress divided by the maximum peak-to-peak strain

- The phase angle between the applied strain and the resulting stress

The data analysis is based on standard equations for analyzing the response of the given geometry. The analysis is performed using a personal computer that is integral with the testing system, and is supplied with proprietary software for data acquisition and analysis. The data for each test are analyzed and stored on floppy discs for further reference. These data may be exported to other software, such as commercial spreadsheet software or statistics software, for further analysis and presentation.

Dynamic Shear Rheometry Operational Parameters

Specimen Preparation

Two geometries were used for the dynamic mechanical testing: parallel plates and torsion bar. A silicone rubber mold was used to cast small pellets of material that were subsequently placed between the parallel plates. This technique facilitated the division of sample material when replicate test specimens were required, without the necessity for reheating the sample container. This technique also minimized the trimming that was required.

To facilitate clamping and enhance repeatability, steel end inserts were used for the torsion bar testing. The inserts were placed in the torsion bar molds, and the hot asphalt cement was then poured into the mold between the inserts. The procedures for the parallel plates and torsion bar testing are described in detail in volume 4, chapter 3 of this report.

Control of Specimen Dimensions and Gap Corrections

The specimen dimensions, regardless of the type of test used, must be carefully controlled to ensure maximum accuracy of test data. The sensitivity of test results to variations in specimen dimensions varies with test geometry. For parallel plate geometry, the dynamic modulus is proportional to the gap, and inversely proportional to the fourth power of the radius. To limit errors caused by variation in the dimensions of the specimen to 3 percent or less, the radius of a 25-mm (0.98-in.)-diameter specimen must be controlled to within about $\pm$ 0.8 percent, or 0.1 mm (4×10^{-3} in.). Similarly, the gap must be measured to an accuracy of $\pm$ 0.03 mm (1.2×10^{-3} in.). Similar calculations can be performed for the torsion bar geometry. Specific recommendations for controlling the dimensions during specification testing are given in volume 4 of this report.

Specimen Preparation and Hardening

Care must be taken to ensure representative samples and to avoid unnecessary heating and shrinking during handling. Specific recommendations for specimen handling and storage are given in volume 4 of this report.

Selection of Plate Size

It was found during early testing of the MRL asphalts that using the 8-mm- (0.31-in.-) diameter parallel plate geometry at temperatures where G* is greater than approximately 5°C (41°F) produced substantial compliance errors in the data generated by the mechanical spectrometer, because of the extremely high stiffness of the asphalt under dynamic loading at low temperatures. For harder asphalts, particularly the pressure aging vessel (PAV) residue, the specific geometries used at each test temperature had to be varied. For example, in testing extremely hard field-aged (recovered) asphalts, the torsion bar geometry was used for temperatures as high as 25°C (77°F).

The approximate temperature and modulus ranges for which each of the various geometries were used are given in table 2.1, which also lists approximate strain ranges for each case. As reflected in table 2.1, the proper choice of plate size or specimen geometry is not dictated by the temperature of the test specimen, but by the stiffness of the test specimen. Based on the work conducted on the RMS 803, 8-mm (0.31-in.) parallel plates should be used when the complex modulus ranges from 1×10^5 Pa (14.5 lb/in.^{2}) to 1×10^7 Pa (1450 lb/in.^{2}); 25-mm (0.98-in.) parallel plates should be used when the complex modulus ranges from 1×10^3 Pa (0.145 lb/in.^{2}) to 1×10^5 Pa (14.5 lb/in.^{2}); and 50-mm (1.97-in.) parallel plates should be used when the complex modulus is less than 1×10^3 Pa (0.145 lb/in.^{2}). When the complex modulus is greater than 1×10^7 Pa (1,450 lb/in.^{2}), the torsion bar or bending beam rheometer should be used.

Thus, the useful temperature range for the 25-mm- (0.98-in.-) diameter parallel plates is much lower for a softer grade of asphalt than for one of the harder grades. Similarly, the

25-mm- (0.98-in.-) diameter plates can be used at a much lower temperature for a tank asphalt than for the same asphalt after pressure or extended field aging. The recommended temperature ranges given above are valid for the RMS 803 used by the researchers. These ranges may vary for other instruments.

Temperature Control

Many of the commercial rheological testing devices available today were designed primarily for use with polymers, foodstuffs such as cheese, and other materials, many of which exhibit changes of modulus or viscosity with a temperature of less than a percent per °C. Under such a situation, temperature control of ± 2°C (± 3.6°F) would be adequate for maintaining suitable repeatability of test data. Unfortunately, asphalt cement and related materials are much more sensitive to changes in temperature. A change in temperature of 1°C (1.8°F) can, for example, result in a modulus change of up to 25 percent for some asphalts. This type of change is shown in figure 2.2, in which the percentage change in $G*$ per °C is plotted versus $G*$ at 10 rad/s.

Over most of the range of interest in paving applications, the rate of change of $G*$ with respect to temperature ranges from 15 to 25 percent/°C (8 to 14 percent/°F). Because of the extreme temperature dependency of asphalt cements, it is necessary to control the temperature for the rheological testing of asphalts to a much finer degree than for most other viscoelastic materials. To limit the contribution of temperature variations to the coefficient of variation of the modulus to about 2.5 percent, the temperature of the specimen during rheological testing should be controlled with an accuracy of *at least* ± 0.2°C (± 0.36°F). Failure to obtain this level of temperature control will result in high variability, especially between different laboratories and devices, rendering the resulting data useless for specification purposes. Temperature control to ± 0.1°C was recommended for specification testing (volume 4, chapter 3).

Linear Viscoelastic Region Defined

A linear viscoelastsic representation of the flow properties of the asphalt cement was used throughout most of the research; the specifications were also based on an LVE representation. Therefore, it is important to define the range of linear behavior. Within the linear region, the modulus is independent of stress or strain. This independency can be ascertained by applying a varying (increasing) strain to the sample and observing the resulting stress or modulus. This procedure is often referred to as a strain sweep. For the purposes of this project, the upper limit of the linear region was defined as the point at which the modulus decreased to 95 percent of the initial modulus. A typical strain sweep, with a definition of the linear region, is shown in figure 2.3.

During the dynamic shear testing of the MRL asphalts, a large number of strain sweeps were done to determine the region of linear behavior. Briefly, during a strain sweep, the shear strain that a specimen is subjected to is gradually increased until a significant decrease in the

modulus is observed. This type of testing was replicated at various temperatures on all core asphalts and a large number of extended MRL asphalts. When the LVE limit is plotted against a complex modulus, a reasonable relationship is seen, in which the linear limit increases with decreasing modulus. This plot was presented earlier as figure 1.8, and is reproduced below as figure 2.4.

Care must be taken when extrapolating the linear region as shown in figure 2.4 to other types of rheological testing. The shear strains and stresses in the parallel plate geometry are not uniform. Therefore, the overall effect of nonlinearity on the resulting test data is not easy to analyze, and would probably be different if, for instance, cone-and-plate geometry were used rather than parallel plate geometry. Apparent nonlinearity can also occur from secondary flow patterns (flow vortices within the specimen) and edge effects, which are also geometry dependent. Additionally, it is quite possible that the degree of nonlinear response for asphalt cement may depend on the degree of restraint during testing. A significantly larger gap or aspect ratio, for instance, could increase or decrease the degree of nonlinearity. Therefore, the linear region, as determined above, should only be applied to dynamic shear testing using parallel plate geometries with gaps of 1 to 2 mm (0.04 to 0.08 in.). For other test geometries, these data can only be used as a rough guideline. The determination of the linear region should be performed prior to characterization when other test methods are used.

Another important nonlinear effect results when strains used during testing become too large. This type of nonlinearity is referred to as geometric nonlinearity as opposed to material nonlinearity. In the theory of elasticity and viscoelasticity, the assumption of small strains is generally made to simplify the required analyses. The theoretical reason for this assumption is beyond the scope of this report. It is necessary to use the approximation $\theta \approx \sin \theta$ in the analysis of strains. The error involved in this approximation is about 4 percent at 50 percent shear strain, and 19 percent at 100 percent shear strain. Therefore, shear strains above approximately 50 percent should be avoided during dynamic shear testing because geometric nonlinearity will result. It should be noted that when performing steady-state viscosity measurements, this limitation does not apply. The limitation is necessary when characterizing the time-dependent modulus or compliance.

DSR Test Results

Frequency Sweeps

In testing the MRL asphalts (core plus extended) in the unaged and thin film oven test (TFOT ASTM D2872)-aged conditions, frequency sweeps were performed with frequencies ranging from 0.1 to 100 rad/s. These tests were performed using parallel plate or torsion bar geometry at temperatures of $-35°$, $-25°$, $-15°$, $-5°$, $5°$, $15°$, $25°$, $35°$, $45°$, and $60°C$ ($-31°$, $-13°$, $5°$, $23°$, $41°$, $59°$, $77°$, $95°$, $113°$, and $140°F$). All frequency sweeps were replicated, on specimens prepared from separate sample tins, and at least a few weeks apart. This method ensured as much independence in the replicate test data as practical. The eight core asphalts were tested after aging for 144 hours at $60°C$ ($140°F$) and 20 hours at $100°C$ ($212°F$) using the above protocol. The remaining asphalts, including the second

62

grade of many of the MRL asphalts, were tested after aging for 20 hours at 100°C (212°F) using a reduced protocol that consisted of frequency sweeps as described above, but at five temperatures.

Prior to performing these frequency sweeps, strain sweeps were performed at selected temperatures to determine the maximum strain that could be used while maintaining linear behavior. All the frequency sweep testing was done at strains well below this linear limit, thus ensuring LVE behavior during the dynamic testing.

Isochronal Plots

An isochronal plot is simply a plot of a viscoelastic function versus temperature. For the SHRP testing, complex modulus and phase angle were used at a frequency of 10 rad/s. This frequency was used because it corresponds to a loading time of 0.1 second, which is a standard time for laboratory testing and is meant to simulate traffic loading. The selected viscoelastic function(s) are then plotted against temperature, as shown in figure 2.5, in which the complex moduli for SHRP asphalts AAA-1, AAG-1, and AAM-1 (tank) are plotted versus temperature. It is clear from this plot that of these three asphalts, asphalt AAA-1 is the softest at all temperatures. At high temperatures, asphalts AAG-1 and AAM-1 are similar in hardness, but at low temperatures, asphalt AAG-1 is considerably harder than AAM-1. These curves demonstrate the need to characterize the asphalt binder at the temperature and time of loading that is representative of in-service conditions. For example, viscosity rankings at 60°C (140°F) can be very misleading if compares with mixture resilient modulus rankings at 25°C (77°F). As shown in the figures, the viscosity ranking at the higher temperature may be reversed at the lower temperature. The disparities can be even greater when the results, such as those at 60°C (140°F), of the viscosity data are extrapolated to low-temperature thermal shrinking cracking temperatures.

Master Curves and Shift Factors

In constructing the master curves for the asphalts tested, the dynamic mechanical data were shifted on the basis of the complex dynamic modulus, $G^*(\omega)$. In general, this shift esulted in fairly smooth functions for the other viscoelastic functions: the phase angle, the storage modulus, and the loss modulus. Shifted and unshifted complex modulus data for asphalt AAD-1 (tank) are shown in figure 2.6 as an example. Data at several temperatures have been omitted from this figure for clarity. As a comparison, the master curve for storage and loss moduli, shifted using factors derived from the analysis based on complex modulus, are shown in figure 2.7. The shift factors associated with the master curves shown in figure 2.6 and figure 2.7 are given in figure 2.8.

The master curves shown for asphalt AAD-1 are fairly typical. There is some misalignment in the shifted data but overall, smooth curves are generated. Additionally, the shift factors shown in figure 2.8 are smooth and appear typical for many viscoelastic polymers (Ferry 1980). Therefore, on this basis the time-temperature superposition can be concluded to be a

valid analytical method for asphalt cement. However, as discussed below, there are some limitations to this method of analysis, and it should be applied with caution.

Dynamic master curves and shift functions for the MRL asphalts after all aging treatments are shown in an appendix at the end of this report. The master curves in this appendix show complex modulus and tan delta as a function of reduced frequency. The master curves for the core asphalts shown in these appendices are based on replicate measurements done at 10 temperatures, ranging from $-35°$ to $60°C$ ($-31°$ to $140°F$). To complement the dynamic shear data, the asphalts were also tested at low temperatures using the bending beam rheometer described later in this chapter. Thus, the master curves are based on dynamic shear data and either torsion bar or bending beam data.

Anomalies in Time-Temperature Shift Factors

In analyzing the dynamic mechanical data for the MRL asphalts, it was found that in many cases the various dynamic functions could not be shifted to form a set of perfectly smooth, continuous curves. This finding indicates that time-temperature superposition, although a useful approximate concept for the analysis of rheological data on asphalt cements, is not rigorously applicable in all cases. As an example, figure 2.9 is provided, which shows complex modulus as a function of tan delta for asphalt AAD-1 (tank). This figure was generated using the shift function developed by shifting the complex modulus. If time-temperature superposition were perfectly valid, this plot would show a smooth, continuous curve, except for minor deviations that might be expected from a slight increase in the glassy modulus with temperature, and experimental error. However, examination of figure 2.9 reveals that there are breaks in the curve, particularly at temperatures between about $15°$ and $60°C$ ($59°$ to $140°F$).

There are three possible explanations for the failure of strict applicability of the time-temperature superposition principle to asphalt cement. The first explanation is that the density of a network of secondary forces in asphalt cement changes with temperature, causing a change in the equilibrium modulus and therefore a vertical shift. Similar phenomena have been observed in methacrylate polymers (Ferry 1980).

The second explanation revolves around the dispersed polar fluid model for asphalt chemical structure proposed by Christensen and Anderson (1991). In this explanation the apparent vertical shift is not really a vertical shift at all, but is actually a small change in the width of the relaxation spectrum with temperature. This change occurs because of changes with temperature of the mutual solubility of the various chemical compound types present in asphalt cement. At low temperatures, the mutual solubility is decreased, so that strongly polar molecules tend to associate more with other strongly polar molecules; weakly polar or nonpolar molecules also tend to associate more strongly with one another. This pphenomenon results in a wider distribution of relaxation times and an increase in the spectrum width. At high temperatures, the mutual solubility improves, so that dissimilar molecules tend to associate more strongly, resulting in a reduction in extreme relaxation times and a narrowing of the relaxation spectrum. These changes in the relaxation spectrum

width are consistent with the observed minor failure of time-temperature superposition, and are difficult to differentiate from a vertical shift effect. More research is needed to fully explain this phenomenon.

The third explanation is attributed to the presence of wax crystallites that have melting point temperatures in the range of 25° to 60°C (77° to 140°F). The molecular structure of the wax is ill defined with varying chain length and branching, which suggests a broad melting point range and could explain the broad temperature effect as opposed to a sudden change in viscoelastic properties if the wax is uniform in composition (Bahia and Anderson 1992).

To more fully quantify the time-temperature anomaly, the master curves were prepared by first shifting the data on the basis of the phase angle, and then applying a vertical shift to smooth the master curves. The vertical shifts normalized for a reference temperature are similar to all core asphalts as shown in figure 2.10. In general, there is a pronounced vertical shift in the temperature region of from about 0° to 45°C (32° to 113°F), much larger than would be expected from temperature and density effects alone. This vertical shift was quantified using an Arrhenius function, so that an activation energy could be calculated for the process and compared with other physicochemical data. It was felt that the melting/crystallization of wax could be the primary cause for the anomaly. To evaluate this hypothesis, figure 2.11 was constructed. In this figure the activation energy for the vertical shift is plotted against wax content, as reported by SHRP. There appears to be only a weak relationship between these parameters, suggesting that wax melting/crystallization might only be one of several factors active in causing the observed anomaly.

Although the anomalies in the time-temperature superposition are not large, they indicate that the time-temperature superposition principle should be considered an approximate means of analyzing viscoelastic data for asphalt cement. This procedure is certainly useful for a general characterization of the time dependence of asphalt cement, and has been used by the authors of this report and other researchers in developing mathematical models for the rheological behavior of paving-grade asphalts (Jongepier and Kuilman 1969).

Flexural Creep

Asphalt binders at low temperatures are viscoelastic liquids with mechanical behavior similar to that of amorphous polymers. Because of the high stiffness (10^7 to 10^8 Pa (1,500 to 150,000 lb/in.^{2})) of asphalts at low temperatures, the techniques that have been developed over the years to measure their properties at moderate and high temperatures are not suitable for low temperatures. Most of the high- to intermediate-temperature testing techniques were designed to test fluid-like materials where stiffness is somewhat less than 1 kPa (0.15 lb/in.^{2}). The main problem with the use of these devices for asphalts at low temperatures is that, because of the high stiffness, the deformations are very small and therefore cannot be accurately measured or reproduced.

The bending beam, or flexural beam, rheometer was developed to measure stiffness values at low temperatures where stiffness values are typically greater than 10^7 Pa (1,500 lb/in.^{2}). By

molding a prismatic beam of asphalt binder and testing it in three-point bending, accurately measured deflections can be produced without the need for excessively high loads and without stressing the material to its ultimate strength. In this section, the newly refined bending beam rheometer, which was developed for the SHRP project, is briefly described and the procedure used to collect low-temperature rheological measurements on the asphalts is then reviewed.

Description of Bending Beam Rheometer

Based on a critical review of techniques used to characterize low-temperature rheology of asphalts and similar polymeric materials, the concept of using a prismatic beam specimen loaded in three-point bending was selected (Andersen et al. 1990). The technique developed was based mainly on the guidelines of the ASTM D790 Standard Test Method for measuring flexural properties of plastics and other elastomers (ASTM 1991). The prototype of the bending beam device developed as part of the project proved that the system is relatively simple to use and gives reliable measurements of low-temperature creep stiffness.

The rheometer is made up of the loading frame unit, a temperature-controlled bath, and a data acquisition system that uses a personal computer. The device shown in figure 2.12 consists of a loading frame, specimen supports, air bearing-pneumatic piston loading unit, and loading shaft. The deflection is measured by a high-precision linear variable differential transformer (LVDT); the load applied is measured by a load cell. A pneumatic control panel and an electronics control unit control the pressure system and the electronic system, respectively.

Test data, which include deflection of the asphalt beam (measured by the vertical translation of the loading shaft), load on the beam, and time and temperature of loading, are acquired by the personal computer through a digital/analog acquisition board. The board interfaces with signal conditioning units in the electronics panel, connected to both the LVDT and the load cell. All testing and data acquisition control parameters are selected and entered through user-friendly menus. The program is written to display on-line plotting of load and deflection during testing, perform calculations of stiffness values at selected loading times, and display the results together with input parameters at the end of each test.

For a mechanical testing technique to be reliable and accurate, two important factors need to be considered: (1) the stress-strain distribution within the test specimen should be well defined so that it can be accurately represented, and (2) the preparation of the specimen should not result in excessive residual stresses or deformations. Unlike many other materials that can be simply cut or machined to prepare specimens, asphalt cement specimens have to be molded by heating to a fluid state, poured into molds, and then cooled to be tested.

66

Calculation of Creep Stiffness

It was decided that to simplify the stress analysis and the molding operation for the bending beam rheometer, a simply supported beam would be used. To select the dimensions, a set of criteria was established:

- Simplify the stress analysis required to determine the modulus—To achieve reliable estimates of the actual stress distribution, the dimensions were selected to meet the requirements for applying the elementary Bernoulli-Euler theory of bending (Timoshenko and Goodier 1981; Agural and Fenster 1981). The dimensions were also selected in accordance with those recommended for testing the flexural properties of plastics and other thermosets given by ASTM Standard D790.

- Minimize the amount of test material—It is important to minimize the amount of material required to produce the test specimens when working with aged or recovered material.

- Maximize dimensions for test repeatability—The dimensions of the specimen should be large enough to keep the effect of dimensional variability to a minimum and to give an acceptable level of load resolution. The specimen size should, however, be small enough to allow for acceptable deflection resolution.

- Ensure that the specimens can be handled without damage—The specimen should not be fragile because of its small dimensions; it should be large enough so that it can be handled easily.

- Minimize the effects of physical hardening—The specimen configuration and testing protocol must be such that thermal history can be closely controlled and such that the specimen is not restrained during thermal cooling.

With a testing span of 102 mm (4 in.), the dimensions selected for the specimen result in a span-to-depth ratio of 16 to 1, and a depth-to-width ratio of 1 to 2. The selected geometry, which meets the requirements for using the elementary bending theory, requires approximately 12 g of asphalt when material wasted during pouring and trimming is considered. A net specimen weight of approximately 10 g was considered acceptable.

Calculation of Modulus from Test Data

Using the elementary bending theory, the deflection for a prismatic beam of an elastic material in a three-point loading mode is maximum at the center of the span and can be calculated using the following formula:

$$\delta = PL^3/48EI \tag{2.1}$$

where

δ = deflection of beam at midspan
P = load applied, N (lb)
L = span length, mm (in.)
E = modulus of elasticity, Pa (lb/in.²)
I = moment of inertia of section = bh³/12, mm⁴

With a span-to-depth ratio of 16 to 1, the effects of shear can be neglected.

According to the elastic-viscoelastic correspondence principle (Flugge 1975), the stress distribution in a viscoelastic beam is the same as that in an elastic beam under the same load. Further, the strains and displacements depend on time and are derived from displacements of the elastic problem by replacing E with $1/D(t)$ (Flugge 1975). Since, as explained earlier, $1/D(t)$ is equivalent to $S(t)$, rearranging the elastic solution results in the following formula:

$$1/D(t) = S(t) = PL^3/4bh^3\delta(t) \tag{2.2}$$

where

$D(t)$ = extensional creep compliance
$S(t)$ = time-dependent flexural creep stiffness
$\delta(t)$ = time-dependent deflection of beam
P = constant load
b = width of beam
h = depth of beam

The maximum tensile/compressive bending stress, σ, and strain, ϵ, can be calculated as follows:

$$\sigma = 3PL/2bh^2 \tag{2.3}$$

$$\epsilon = 6\delta(t)h/L^2 \tag{2.4}$$

where σ and $\epsilon(t)$ are the bending stress and strain, respectively, at the upper and lower faces of the beam. Using the above equations, a deflection of 2.5 mm (0.1 in.) at the midspan, which is the maximum recommended deflection, will result in a maximum tensile/compressive strain of 0.92 percent. The deflection-to-depth ratio will be 1 to 2.5, and the deflection-to-span ratio will be 1 to 40. The maximum recommended deflection is within the limits for small strain criteria for which a simple bending theory is valid; geometric nonlinearity does not need to be considered.

68

To illustrate stiffness values compared with the selected dimensions, for a load of 100 g (0.2205 lb), stiffness values range between 32.2 MPa (4,516 lb/in.^{2}) at the maximum recommended deflection of 2.5 mm (0.1 in.), and 31,000 MPa (450,000 lb/in.^{2}), at a deflection of 0.025 mm (0.001 in.).

Data Acquisition

Deflection data acquired with the data acquisition system are first digitized and stored in the computer as a function of loading time. The deflection and load data are then selected at loading times of 8, 16, 30, 60, 120, and 240 seconds, and stiffness is calculated at these times. Least squares regression is then used to fit a second-order polynomial to the data using the logarithm of the stiffness as the independent variable and the logarithm of time as the dependent variable. From the fitted polynomial, the stiffness and slope of the logarithm of stiffness versus logarithm of time curve, $d[\log S(t)]/d[\log t]$, is calculated from the polynomial at 8, 16, 30, 60, and 120 seconds. It is important that the curve-fitting be performed on the transformed variables to avoid biasing the calculations toward the longer loading times.

Molding Technique and Specimen Preparation Procedure

It is difficult to mold asphalt cements because they adhere strongly to almost all solid materials and, in particular, to metals. The first technique used to prepare test specimens was to pour hot asphalt into aluminum molds. To isolate the asphalt material from the aluminum mold, high-density polyethylene strips 0.1-mm (4 × 10^{-3} in.) thick were used to cover the inner sides of the mold. The mold consists of two side bars, a base bar, two end pieces, and three polyethylene strips. The mold is assembled using two o-rings around the end portions, as shown in figure 2.13. The aluminum bars are covered with the polyethylene strips from the inside, the asphalt is then poured into the mold, and the assembly is cooled to room temperature. For demolding, the specimen and the mold are cooled to the test temperature, the aluminum sides are removed, and the specimen is left with the polyethylene sheets. The sheets, which are flexible, can then be easily peeled off the asphalt specimen. This technique was useful because the aluminum bars greatly improved the dimensional stability during pouring and cooling, and the thin plastic sheets could be peeled off without causing any distortion to the specimen.

Because molding the test specimen is the most time-consuming step in the testing process, an alternative molding technique was sought. At this time, a new molding technique is under development. In this technique, a female silicone rubber mold is covered with a Plexiglas™ plate and the asphalt binder is poured in the cavity between the plate and the mold. This technique shows promise of being more rapid, eliminates the need for trimming, and results in more uniformly dimensioned beams.

Bending Beam Rheometer (BBR) Testing Program

Once the prototype of the Bending Beam Rheometer (BBR) was constructed, an experiment was designed to evaluate its repeatability. The experiment included the eight core asphalts, and the testing was done at four different temperatures. The testing temperatures selected were $-35°$, $-25°$, $-15°$, and $-5°C$ ($-31°$, $-13°$, $5°$, and $23°F$). The asphalts were tested in the unaged condition, after aging according to the standard thin film oven test procedure (ASTM D2872), and after aging according to the initial pressure aging vessel procedure, 6 days at $60°C$ ($140°F$). For each combination of asphalt source-test temperature-aging condition, two independent replicate tests were conducted. Loading times from 4 to 240 seconds were selected. This range of loading times was selected as the minimum needed to sufficiently perform the time-temperature superposition; the 240-second loading time provided sufficient overlap between the creep curves at the selected temperatures to give reliable shift factors and the testing time.

During the initial course of the testing program, the physical hardening phenomenon was observed (see chapter 3), and, as a result, the isothermal time was added as a control factor in the bending beam rheometer evaluation. Physical hardening is a process in which the rheological properties of an asphalt cement change because of free volume collapse when subjected to temperatures below about $0°C$ ($32°F$) for an extended time. The collapse of free volume causes a rheological change equivalent to a lowering of temperature, resulting in an increase in stiffness modulus. The effect is more pronounced at lower temperatures, and tends to increase at a decreasing rate with continued isothermal conditioning. Over a few hours at $-15°C$ ($5°F$), increases in stiffness modulus of 30 to 50 percent are common. Physical hardening is addressed in detail in chapter 3 of this report.

The testing was extended to include five isothermal ages ranging between 30 minutes and 96 hours. A standard procedure was selected in which the test specimens were tested after 2 hours of conditioning at the test temperature. This time was selected as a compromise that allowed the testing to be completed within a reasonable period but yet did not allow the testing to occur within a short conditioning time when the stiffness changes rapidly with time.

Analysis of the results of this first experiment led to a standard testing procedure to characterize the remaining SHRP asphalts. A temperature of $-15°C$ ($5°F$) and two loading times, 30 minutes and 2 hours, were selected. The unaged and the TFOT-aged asphalts were tested with the standard TFOT procedure. By the time the PAV procedure was finalized and the asphalts were aged, the new SHRP specification resulted in adjustment to the testing schedule. The testing of the PAV-aged material was done at different temperatures to define the temperature at which the creep stiffness, after 60 seconds of loading time, is equal to or less than 200 MPa ($29,000$ lb/in.^{2}). All 32 SHRP asphalts were tested, after aging with the final recommended PAV procedure (20 hours at $100°C$ ($212°F$)), according to the latter schedule. The results presented in the next sections are samples of that testing program and are meant to emphasize the main findings from the rheological characterization done with the bending beam rheometer.

Temperature Dependency of Creep Response

A typical example of creep response measured using the bending beam rheometer, at five different temperatures, is shown in figure 2.14 for asphalt AAM-1. A load of 100 g (.2205 lb) was used in these tests, and the deformation was measured over a 4 minutes. At these temperatures, which are in the vicinity of the glass transition temperature, a significant amount of creep can be observed. *Significant creep occurs at and below the glass transition temperature.* The data reflect the sensitivity of asphalt stiffness to temperature, even within this low-temperature range. At a loading time of 240 seconds, the deflection at $-5°C$ (23°F) is 40 times the deflection at $-35°C$ ($-31°F$). To deal with such large differences in stiffness, and to apply the time-temperature superposition principle, it is necessary to plot the logarithm of stiffness versus the logarithm of loading time as shown in figure 2.15. By selecting a reference temperature, for example $-15°C$ (5°F), and shifting the curves to a master curve at $-15°C$ (5°F), a master curve can be constructed, as shown in figure 2.16a.

Temperature shift factors for the stiffness data are developed in the same manner as they are for the DSR data. The shift function shown follows a simple linear relationship with temperature within the range of testing temperatures. An important observation is the interaction of loading time and temperature. In figure 2.14, an infinite number of temperature susceptibility parameters can be clearly defined. For example, if a loading time of 2 seconds is selected, the ratio of stiffness at $-35°C$ ($-31°F$) to the stiffness at $-5°C$ (23°F) is approximately 10, and if a loading time of 240 seconds is selected, the ratio will be about 40. As the loading time increases, the "temperature susceptibility" ratio increases. The increase with loading time will depend on the shape of the master curve, which is a property of the type of asphalt, and on the temperature levels. This fact explains why a single temperature-susceptibility parameter is not useful; temperature dependency is best described with the shift function as depicted in figure 2.16b.

To compare the temperature shift functions of the studied asphalts, the shift factors for all eight asphalts are shown in figure 2.17. Data in the figure indicate that a simple linear relationship holds for all asphalts. The figure also depicts the similarity of shift factors for all asphalts within the range of testing. The slopes of the shift functions vary between 0.173 log(s)/°C to 0.199 log(s)/°C (0.096 to 0.11 log (s)/°F). The validity of the linear relation is reflected in the high correlation coefficients that were obtained. The minimum R^2 was 99.84 percent and the maximum standard error of estimate was 0.087 log(s)/°C (0.048 log(s)/°F), which can be translated to less than 0.56°C (1°F). The average slope when all shift factors are considered is -0.183 log(s)/°C (0.1 log(s)/°F). The 95 percent confidence interval of the common shift estimate is $\pm$ 0.31 log(s)/°C (0.17 log(s)/°F), which is equivalent to approximately $\pm$ 1.7°C (3°F). These results indicate that asphalts are fairly similar in their temperature dependency at low temperatures. The commonality of the shift function at low temperatures was confirmed for more than 30 different asphalts using the dynamic shear rheometer as described in the previous chapter.

Using the temperature shift functions of figure 2.17, the master curves for the eight asphalts were constructed using time-temperature superposition. The fitted curves are shown in figure 2.18, which depicts the master curves at a reference temperature of $-15°C$ (5°F) and at an

isothermal age of 2 hours. Since the same shift function can be used for all asphalts, the relative position of the master curves in figure 2.18 will remain approximately the same at all temperatures. Unlike the temperature shift functions, the master curves in figure 2.18 indicate that asphalts are different with regard to loading-time dependency.

Bending Beam Rheometer Repeatability

One of the most important criteria for a successful measuring device is its precision. To test the precision of the bending beam rheometer, two replications of the stiffness measurements for the eight core asphalts were considered. Other variables in the analysis included

- Unaged and aged specimens with TFOT procedure

- Isothermal ages of 2, 6, 24, and 96 hours

- Test temperatures of $-15°$ and $-25°$C ($5°$ and $-13°$F), and

- Loading times of 15, 30, 60, and 240 seconds

The data set consisted of 1,256 measurements—two independent replications in 628 cells. To measure the size of experimental error, the standard deviation was usually used. However, because of the wide range in measured stiffness values, it was more appropriate to use the coefficient of variation. Furthermore, the coefficient of variation was expected to depend on stiffness level because the LVDT has a certain level of resolution; the lower the deflections, the higher the expected experimental noise. To solve this problem, the stiffness values were divided in sets that represent different ranges of stiffness values. The range in measured values included in the analysis was between 16.5 MPa and 1.85 gPa (2,400 and 268,000 lb/in.^{2}). The ranges were selected so that an approximately equal number of measurements were contained in each range. The stiffness ranges selected, the number of replicate measurements, and the results of the statistical analysis are summarized in table 2.2. The coefficients of variation were obtained by calculating the average of the sample means and standard deviations for the paired replicates in each of these stiffness intervals.

Because of the large number of paired replicates used to provide the estimate of the pure experimental error variance, the estimates of the coefficient of variation can be considered very accurate. However, it is important to recognize that the analysis here represents a measure of the variability in a well-controlled setting, in one laboratory, with a well-trained operator. The values of the coefficients of variation shown in table 2.2 are very low, and they show a trend with the stiffness interval; the higher the stiffness mean the higher the coefficient of variation. The variability levels reported reflect experimental error involved in not only the testing operation but also the variation, caused by specimen preparation procedure, temperature control, and variability because of isothermal age control.

To study the source of variability and investigate whether it is a function of any of the variables studied, the coefficients of variation as a function of loading time and isothermal age are plotted in figures 2.19 and 2.20. These two factors were selected because the

72

loading time is related to the stability of the signal measured from the LVDT and the load cell, and the isothermal age is a property of the material that was observed to significantly affect response, particularly at early ages. In both figures, the variability is clearly a function of the stiffness interval: the lower the stiffness, the more precise the measurements. The loading time does not show strong effect; shorter isothermal ages show somewhat more variability than longer ages. In all cases, however, the coefficients of variation, obtained from this relatively limited experiment, are well within acceptable limits.

Permanent Deformation

The rutting potential of asphalt mixes in the field is related to the permanent deformation characteristics of the asphalt binder in the mix. Since asphalts are rheological in nature, the permanent deformation properties are directly related to the irrecoverable part of viscoelastic deformation. The magnitude of the irrecoverable deformation is a function of temperature. At low temperatures, permanent deformation is generally a small percentage of the total deformation.

A repeated deformation test was developed to determine the permanent deformation parameters of asphalt under repeated shear stresses (0.1-second loading time and 0.9-second unloading time) and to subsequently correlate these parameters to rheological properties obtained from the dynamic shear rheometer. Permanent deformation parameters of four core asphalts and four polymer-modified asphalts were studied for 40° and 60°C (104° and 140°F), and are discussed below.

Description of Equipment

The permanent deformation behavior of asphalts was studied using a specially developed apparatus, a schematic of which is shown in figure 2.21. To conduct a test, asphalt cement in a fluid state is poured into a cylindrical cup 18.8 mm (0.75 in.) in internal diameter and 50 mm (2 in.) in length and one cup is then placed in a thermal chamber whose temperature can be set at a desired temperature, between 40° and 103°C (−40° and 217°F), using a precision digital temperature controller. The material contained in the cup is subjected to repeated shear stress by means of a cylindrical plunger with a spherical tip. The repeated shear stresses are produced by loading the shaft through a pneumatic cylinder (Bellofram). The flow of air in the Bellofram is controlled by a solenoid valve that is operated by an electronic signal generator. The cyclic force imposed on the plunger is measured by a load cell, and the deformation of the plunger is measured by two LVDTs.

Test Program and Results

Plastic deformation properties of four core asphalts, AAA-1, AAF-1, AAG-1, and AAM-1, and four polymer modified asphalts, MA-1, MA-2, MA-3, and MA-4, were studied at two temperatures, 40° and 60°C (104° and 140°F). The tests were conducted by subjecting

asphalt cement contained in the cup (see figure 2.21) to repeated pulses of 0.1-second loading and 0.9-second unloading (or a frequency of 1 Hz). The force amplitude as well as the resulting motion of the plunger were measured by a load cell and two linear variable differential transformers, respectively. All the asphalts tested were subjected to load amplitudes of 40 g (0.02 lb). Figures 2.22 and 2.23 show the typical data in terms of vertical displacement of the plunger versus the total number of cycles plotted on a log-log scale.

Theoretical Consideration

An analysis was developed to reduce the test results into a useful permanent deformation parameter, as given by the following equation:

$$\gamma_p = \frac{1}{\eta_n} = \frac{KL_n v}{P} \tag{2.5}$$

where

$$
\begin{array}{ll}
\gamma_p & = \text{permanent deformation parameter} \\
\eta_n & = \text{viscosity coefficient associated with permanent deformation behavior (a} \\
& \quad \text{function of number of cycles)} \\
P & = \text{load amplitude} \\
v & = \text{velocity of plunger during each load pulse} \\
L_n & = \text{length of the plunger in contact with asphalt (a function of number of} \\
& \quad \text{cycles)} \\
K & = \text{constant of the apparatus}
\end{array}
$$

or

$$K = 2\pi \ \frac{2\pi(r_a^2 - r_i^2)}{(r_a^2 + r_i^2) \ln\dfrac{r_a}{r_i} - (r_a^2 - r_i^2) \ln\dfrac{r_a}{r_i} \ln\dfrac{r_a}{r_i}} \tag{2.6}$$

where

$$
\begin{array}{ll}
r_a & = \text{inner radius of the cup} \\
r_i & = \text{radius of the plunger}
\end{array}
$$

Analysis of Results

Using the above equations, the experimental data were analyzed and the permanent deformation parameter, γ_p, as a function of the total number of cycles (N) was obtained for all the eight asphalts tested. Figure 2.24 shows the log-log plot of the permanent deformation parameter versus the cumulative cycle of loading for the core asphalt AAG-1. Similar curves for all eight asphalts tested are shown in figures 2.25 and 2.26 for 40°C (104°F) and 60°C (140°F), respectively.

Discussion of Results

The analysis for permanent deformation characteristics was developed on the assumption that the material response is linear. However, the cumulative permanent deformation, which equals the sum of permanent deformations in each cycle, represents the mechanical damage because of repeated application of load. The cumulative permanent deformation is found to be nonlinear, and is found to fit a power law function with the cycles of loading. The permanent deformation parameter of asphalt is important in determining the rutting in asphalt pavements at elevated temperatures.

Indentation Tests

The purpose of this test method was to develop an alternative, inexpensive, and easy-to-perform method for determining the rheological properties of asphalts. An indentation technique was used for this purpose, and the results were compared to the rheological properties obtained from the dynamic shear rheometer.

Rheological properties of eight core asphalts were studied for a temperature range of $-30°$ to $5°C$ ($-22°$ to $41°F$), and master stress relaxation modulus curves were obtained. Rheological behavior in the nonlinear range was studied. Rheological behavior in the nonlinear range is characterized by a single nonlinear hereditary integral of the Volterra type.

Description of Equipment

Rheological properties of asphalts were studied by performing stress relaxation experiments using a screw-driven universal testing machine (Toyo Manufacturing Company) that was adapted to perform indentation tests. A schematic of the apparatus is shown in figure 2.27. Asphalt was heated to a temperature of 135°C (275°F) until it became fluid and was then poured into a cylindrical cup (60 mm (0.79 in.) in diameter and 20 mm (2.4 in.) in height) with an exposed planar surface. To conduct the test, a cylindrical rod with a spherical tip is pressed against the free surface of the asphalt binder. The cylindrical rod is connected to the top frame of the universal machine. The vertical displacement of the indenter is measured by an LVDT. The whole assembly is placed in a thermal cabinet. The desired temperature

can be maintained in the thermal cabinet with an accuracy of $\pm$ 0.1°C ($\pm$ 0.2°F) using a digital temperature controller.

Test Method

The test protocol included the following. Immediately after the material was poured into the cylindrical cup, the material was allowed to cool to room temperature. Subsequently, the cylindrical cup with the material in it was placed in the thermal cabinet and quenched to the temperature at which the properties were to be measured. The sample was maintained at this temperature for about half an hour and subsequently tested.

The rheological properties of asphalt were measured by observing the relaxation of load with time using a preselected vertical deformation of the indentor as it was pressed down in the material. Specific displacements for which the stress relaxation was observed are 0.10, 0.15, and 0.30 mm (0.004, 0.006, and 0.012 in.). The above tests were conducted at various temperatures, ranging from -30° to 10°C (-22° to 50°F) at intervals of 5°C (9°F). Figure 2.28 shows the typical load versus time curves obtained from stress relaxation tests for asphalt AAK-1.

Theoretical Considerations

Indentation Problem (Linear Viscoelastic Medium)

The contact problem of a spherical indentor pressed against a LVE half space was solved to obtain the vertical load for a given deformation history as follows:

$$P(t) = \frac{16\sqrt{r_1}}{3} \int_0^t G(t-t_1) \frac{d[\alpha(t)]^{3/2}}{dt_1} dt_1 \qquad (2.7)$$

where

$$
\begin{aligned}
P(t) \quad &= \quad \text{load} \\
r_1 \quad &= \quad \text{radius of the indenter at the surface of the asphalt at time } t_1 \\
G(t) \quad &= \quad \text{stress relaxation modulus function} \\
\alpha(t) \quad &= \quad \text{displacement at time } t
\end{aligned}
$$

For a step function vertical displacement $\alpha = \alpha_o H(t)$, the above equation reduces to

$$P(t) = 16\frac{\sqrt{r_1}}{3} G(t)\alpha_o^{3/2} \qquad (2.8)$$

Nonlinear Viscoelastic Solution

A finite element model for the prediction of stress field and contact pressure in a nonlinear viscoelastic medium subjected to indentation by a spherical indentor was developed. This model, in conjunction with a material parameter identification model, was used to back calculate the parameters of the following nonlinear hereditary integral:

$$S_{ij} = \int_0^t m(t-t_1)h(I)C^{-1}dt_1 \qquad (2.9)$$

$$m(t-t_1) = \frac{dG(t-t_1)}{dt_1}$$

where

$$
\begin{aligned}
S_{ij} &= \quad \text{deviatoric stress tensor} \\
G(t) &= \quad \text{shear relaxation modulus function} \\
h(I) &= \quad \text{the damage function } I = \beta I_1 + (1 - \beta)I_2 \\
I_1 \text{ and } I_2 &= \quad \text{the first and second strain invariants respectively } \alpha \text{ and } \beta \text{ are} \\
&\qquad \text{constants} \\
C^{-1} &= \quad \text{strain tensor} \\
t &= \quad \text{time}
\end{aligned}
$$

Results

Using equation 2.8 above, the experimental data were reduced and the relaxation modulus versus time curves were obtained. Figure 2.29 shows the relaxation modulus versus time curves for asphalt AAK-1 tested at various temperatures. Using the time-temperature shift hypothesis, master stress relaxation modulus curves were obtained for all the eight core neat asphalts and are shown in figure 2.30. In figure 2.31 the master curve for AAK-1 obtained from the indentation test is compared with that obtained from the master complex shear modulus curves obtained from the dynamic shear rheometer.

For higher magnitudes of strain, stress relaxation data were found to be nonlinear viscoelastic. Using the nonlinear hereditary integral equation (equation 2.9) in the material

parameter identification model, the relaxation modulus function, G(t), and the damage function, h(I), were evaluated. Figure 2.32 shows the comparison of load versus time curves predicted by using the developed model with the experimental data. Some limited number of double-step relaxation tests were conducted to determine whether the developed nonlinear viscoelastic model predicts the double-step response. Figure 2.33 shows the comparison between the new nonlinear model predictions and the experimental data. The same figure illustrates the prediction from the Bernstein, Kearsley, Zapas (BKZ) theory (Bernstein et al. 1963). The new nonlinear viscoelastic model predicts the behavior better than the BKZ theory. In figure 2.34 a typical damage function curve for AAK-1 asphalt is given.

Introconversion of Dynamic Data and Flexural Creep Data

Although complete implementation of the proposed specification test is beyond the scope of this project, it may become necessary during implementation and other research studies to introconvert specification-type data between dynamic shear testing and flexural creep testing. Therefore, the following method is presented as a relatively simple but highly accurate method of simple shifting and introconversion of specification-type data from dynamic shear testing to the equivalent creep stiffness at a specified loading time.

The first step in this process is to convert the complex shear modulus into creep stiffness, which is the inverse of extensional creep compliance. For simplicity, it is assumed that asphalt cement in the modulus range of interest is incompressible, so that Poisson's ratio is 0.5. Thus, the extensional stiffness or modulus will be three times the shear stiffness or modulus. Also, an approximate introconversion between dynamic shear and creep compliance must be applied. Ninomiya and Ferry (1959) proposed an equation for the approximate introconversion of dynamic mechanical data to creep compliance:

$$J(t) \approx J'(\omega) + 0.40\, J''(0.40) - 0.014\, J''(10\omega) \qquad (2.10)$$

$$t \to 1/\omega$$

where

$$
\begin{aligned}
J(t) &= \text{creep compliance at time } t,\ 1/\text{Pa} \\
J'(\omega) &= \text{storage compliance at frequency } \omega,\ 1/\text{Pa} \\
J''(0.40) &= \text{loss compliance at frequency } 0.40,\ 1/\text{Pa} \\
J''(10\omega) &= \text{loss compliance at frequency } 10\omega,\ 1/\text{Pa}
\end{aligned}
$$

This equation is quite accurate but requires data at three specific frequencies (ω, 0.4ω, and 10ω) for the computation of the creep compliance. As an expeditious alternative, an empirical equation was developed as part of the study, which agrees with Ninomiya and Ferry's approximation to within 3 percent for paving grade asphalt binders at low to intermediate temperatures. This technique requires only the complex modulus and phase angle for the introconversion:

$$S(t) = 1/D(t) \approx 3 \ G^*(\omega)/[1 + 0.2 \sin (2\delta)] \qquad (2.11)$$

$$t \rightarrow 1/\omega$$

where

$S(t)$	=	creep stiffness at time t, Pa
$D(t)$	=	extensional creep compliance at time t, 1/Pa
$G^*(\omega)$	=	complex modulus at frequency ω, Pa
δ	=	phase angle at frequency ω, degrees

Note that equation 2.11 is in terms of creep stiffness, which is the inverse of the extensional creep compliance; hence, the factor of 3 in converting from shear to extensional modulus. As an example of the accuracy of this simple formula, figure 2.35 is provided, in which creep stiffness estimated from Ninomiya and Ferry's approximation is compared with creep stiffness estimated from equation 2.11, for three hypothetical asphalt binders having widely different rheological behaviors. The agreement is nearly exact in all cases. Because of the empirical nature of equation 2.11, it is not recommended for use when the stiffness is less than (about 10^5 Pa) (14.5 lb/in.^{2}), especially for modified binders, without further verification.

Since the creep stiffness in the proposed specification is based on creep data at 60 seconds, it may be desirable to shift dynamic data in an approximate way to account for differences in effective loading times. This shift can be done by assuming an Arhennius function for the shifts at low temperatures, with a constant activation energy of 250 kJ/mol. The resulting expression can be rearranged to give the equivalent temperature for some other loading time:

$$T_2 \approx \{ \ 2.303 \ R \ [\log (t_2/t_1)] \ / \ 250{,}000 + 1/(T_1+273) \ \}^{-1} - 273 \qquad (2.12)$$

where

T_2	=	equivalent temperature at desired loading time, °C
R	=	ideal gas constant, 8.31 J/°K-mol
t_2	=	desired loading time, s
t_1	=	actual loading time, s
	=	$1/\omega$ when introconverting dynamic test data to creep stiffness
T_1	=	actual test temperature, °C

In order to introconvert dynamic shear data to equivalent creep stiffness at a selected loading time, equation 2.11 is first applied, giving the equivalent creep stiffness at the actual test temperature at time $1/\omega$ (ω in rad/s). Then, the equivalent temperature at the selected loading time is calculated using equation 2.12. As an example, dynamic shear data at 0.1 rad/s at temperatures of $-25°$, $-15°$, $-5°$, and $5°C$ ($-13°$, $5°$, $23°$, and $41°F$) was introconverted to creep stiffness at both 15 and 240 seconds, and compared with creep

stiffness measured with the bending beam (2-hour conditioning time). In figure 2.36, measured creep stiffness and values estimated from dynamic data for asphalt AAA-1 (tank) are compared; in figure 2.37, the same comparison is made for asphalt AAM-1 (TFOT residue). The agreement is quite good, within about 20 percent, for all cases.

Although the results presented above would seem to verify the proposed introconversion and shifting procedure, care must be taken in comparing dynamic data gathered using a typical rheometer, and creep stiffness measured using the bending beam rheometer. In the former test, the thermal history is difficult to control precisely; the data here were gathered after rapid cooling to $-35°C$ ($-31°F$), equilibrating for about 20 minutes, testing using a frequency sweep, and then increasing the temperature by $10°C$ ($18°F$) and repeating the equilibration and testing. The thermal treatment in the bending beam data consisted of quenching to the desired test temperature, and then conditioning isothermally for 2 hours. Because of physical hardening, it might be expected that the two treatments would result in substantially different properties. Apparently, the two thermal treatments, though quite different, produce similar rheological states. In application to specifications, it will be necessary to study in more detail the precise correspondence between the thermal treatments typically used in testing with a dynamic shear rheometer and those used in the bending beam rheometer.

To illustrate the importance of controlling thermal history in comparing rheological data at low temperatures, figure 2.38 has been constructed. In this figure, dynamic data gathered at $-5°C$ ($23°F$) for asphalt AAM-1 (tank) has been converted to creep stiffness using equation 2.11, and shifted to a reference temperature of $-15°C$ ($5°F$), using an Arhennius shift with an activation energy of 250 kJ/mol. These data are then compared with creep stiffness data measured with the bending beam rheometer at $-15°C$ ($5°F$), after 30 minutes and 2 hours of isothermal conditioning. As expected, the data for a conditioning time of 2 hours agree very well with the estimates based on dynamic data. However, the bending beam data for a conditioning time of 30 minutes is significantly below the stiffness estimated from the dynamic data.

In specification testing, where introconversion from dynamic data to creep stiffness is desired, the problem of shifting the data to another time and temperature is somewhat different than the problem stated above. In the first example, the problem was to determine an equivalent temperature for a desired loading time, given the testing temperature and loading time. In this case, the problem is to determine the desired test temperature, given the equivalent (specification) temperature, desired loading time, and test frequency. In this case, the following equation can be used to determine the test temperature for comparison at given equivalent conditions for creep stiffness:

$$T_d \approx \{ 1/(273 + T_s) - 2.303 \, R \, [\log (t_s \omega)] \, / \, 250{,}000) \}^{-1} - 273 \qquad (2.13)$$

where

$$T_d = \text{test temperature for dynamic testing at frequency } \omega, \, °C$$
$$T_s = \text{specified temperature for creep testing, } °C$$
$$R = \text{ideal gas constant, 8.31 J/°K-mol}$$

80

t_s =   specified creep loading time, s

ω =   dynamic testing frequency, rad/s

The dynamic test is then run at the calculated temperature, T_d, at the selected frequency, ω. Equation 2.12 is used to estimate the creep stiffness at the specified temperature, T_s, and the specified loading time, t_s. The m value (d log D/d log t) at the specified conditions, in this case, is simply estimated as $\delta/90$, where the phase angle, δ, is in degrees.

More generalized and elaborate schemes are possible for estimating creep stiffness from dynamic data. However, such schemes will generally be complex and involve empirical modeling and various assumptions. The scheme suggested above is relatively simple, direct, and accurate, and is based only on the assumption of a constant flow activation energy for all asphalts at low temperatures, which is substantially supported by the research performed during this project. This scheme is, I believe, the best method for estimating creep stiffness from dynamic data for specification purposes, although additional work is needed to establish thermal conditioning for dynamic testing equivalent to the specified isothermal aging time of 1 hour for flexural creep tests.

Summary and Conclusions

The eight core asphalts were characterized with the dynamic shear rheometer using 25-mm and 8-mm parallel plates and torsion bar geometry. Frequency sweeps were obtained at different temperatures, and time-temperature superposition was used to obtain master curves. Time-temperature superposition was shown to be valid; however, certain anomalies were observed in the time-temperature shift factors. These were not completely explained but were tentatively related to wax content. The Williams-Landers-Ferry (WLF) equation is valid in the intermediate or viscoelastic region; however, an Arrhenius function is necessary to describe the time-temperature dependency in the low temperature region, below the glass transition temperature, and in the high-temperature Newtonian region.

A bending beam rheometer was developed to measure the stiffness of asphalt cement at low temperatures where the stiffness values are typically greater than 100 MPa. The bending beam rheometer is based upon the creep response of a simple beam supported at its ends and loaded at its midpoint with a constant load. Excellent repeatability was demonstrated with the bending beam rheometer, resulting in a test procedure that is suitable for specification purposes. The bending beam rheometer was also shown to be very useful for the study of physical hardening because the test specimens may be prepared and stored for various times before being tested. A ball indentation test was also developed and relaxation moduli were obtained for several of the core asphalts. Further development of the indentation test was discontinued because of limited project resources and the adoption of the dynamic shear and bending beam rheometers as specification tests.

Interconversation between the dynamic, flexural creep, and indentation test results was demonstrated through the use of various viscoelastic functions obtained from the literature. The results clearly showed that the rheological data obtained from the bending beam

rheometer, torsion bar geometry, and parallel plate geometry are interconvertable and can be used interchangeably in the development of master curves.

The importance of sample preparation techniques and temperature control were clearly shown and appropriate test protocols were developed. At the upper range of pavement surface temperatures molecular associations or steric hardening can affect the test results, and at low temperatures physical hardening can affect the test results. As a consequence, it is important to carefully control the thermal history of the test specimens prior to testing.

In conclusion:

1. The dynamic shear rheometer is an acceptable device for determining the specification properties of asphalt binders at the intermediate to upper range of pavement surface temperatures.

2. The bending beam rheometer is an acceptable device for obtaining the stiffness characteristics of asphalt binders at the minimum pavement temperature.

3. Time-temperature superposition is valid for asphalt cements.

4. Time-temperature shift factors are described by an Arrhenius equation below the glass transition temperature and in the Newtonian flow region. At the intermediate range of temperatures the WLF equation provides an adequate description of time-temperature shift factors.

5. The ball indentation test shows promise for characterizing the stiffness properties of asphalt binders but was not sufficiently developed during the project for specification use.

6. Data obtained with the bending beam rheometer, torsion bar geometry, and parallel plate geometry may be interconverted and used interchangeably in the development of master curves.
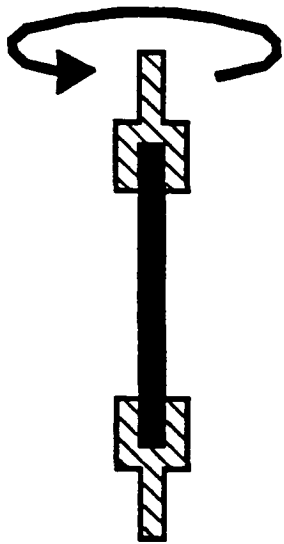
Rectangular Torsion
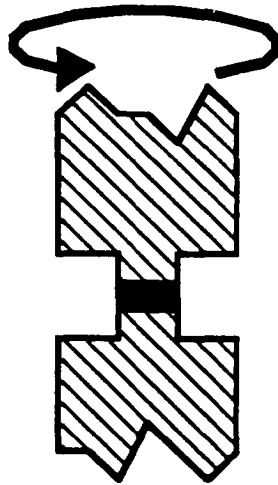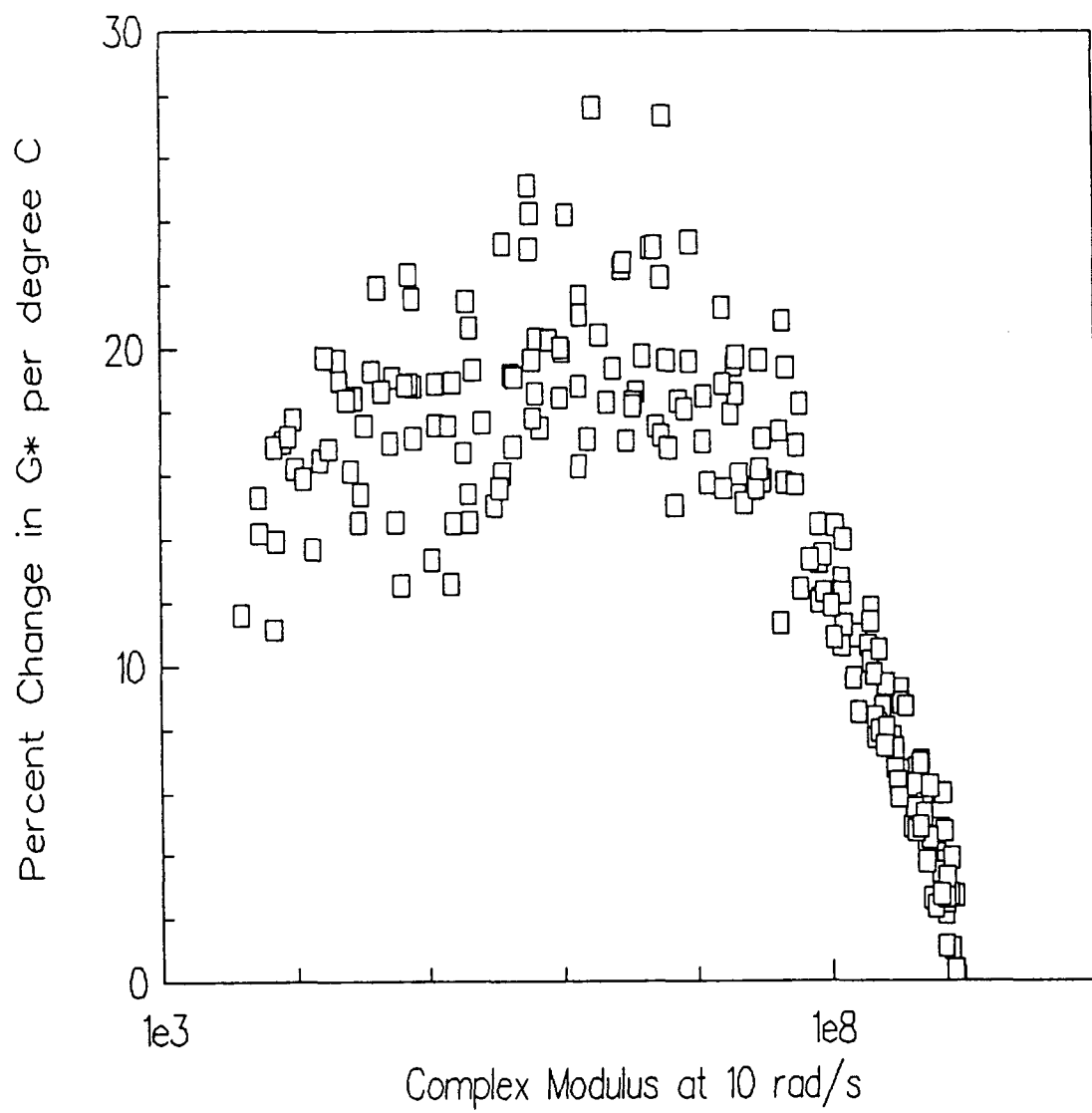
8 mm parallel plates
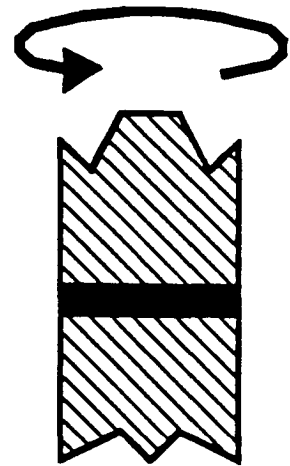
25 mm parallel plates

Figure 2.1   Parallel Plate and Torsion Bar Geometries Used for Dynamic Mechanical Analyses

Figure 2.2   **Change in Complex Modulus per Degree Celsius as a Function of Complex Modulus**
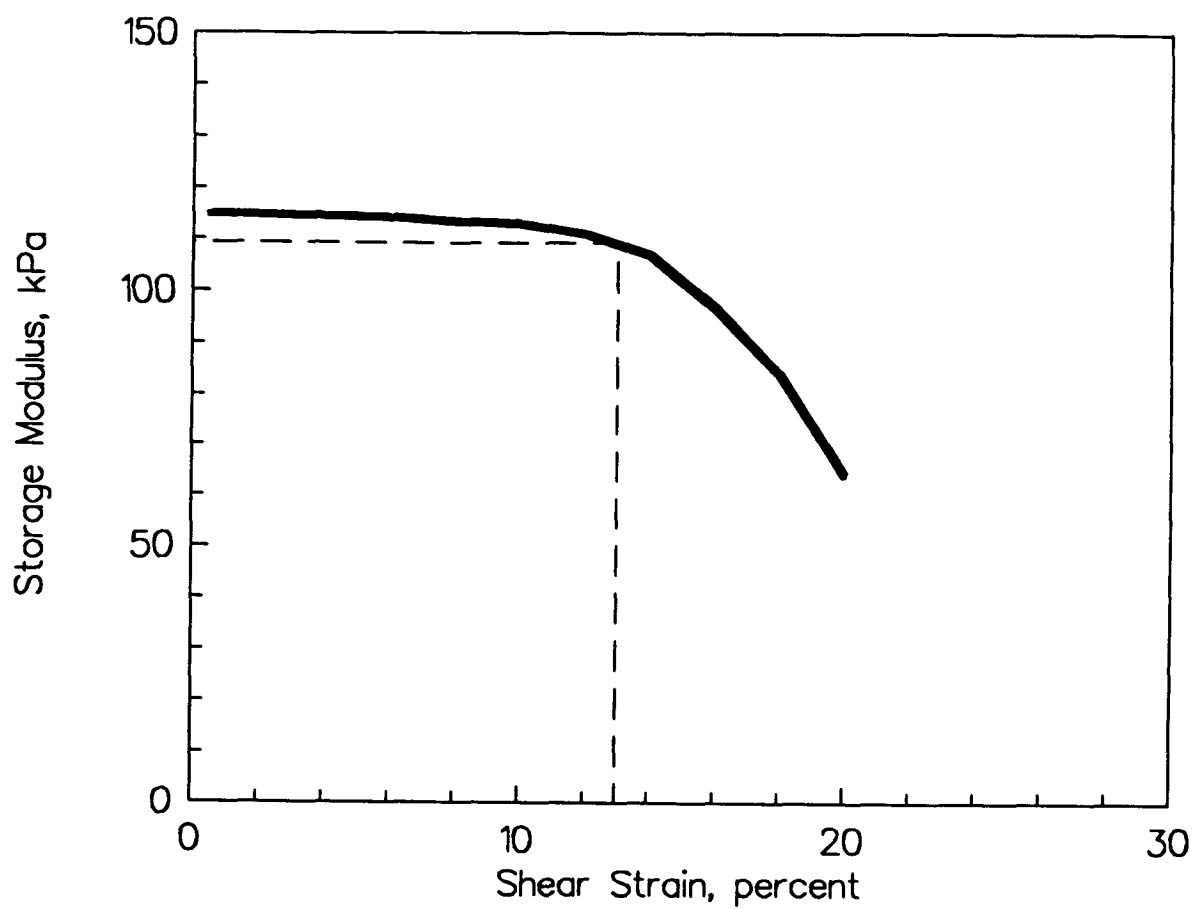
Figure 2.3 **Example of a Strain Sweep Test Used to Define the Linear Viscoelastic Limit for Dynamic Mechanical Testing of Asphalts**
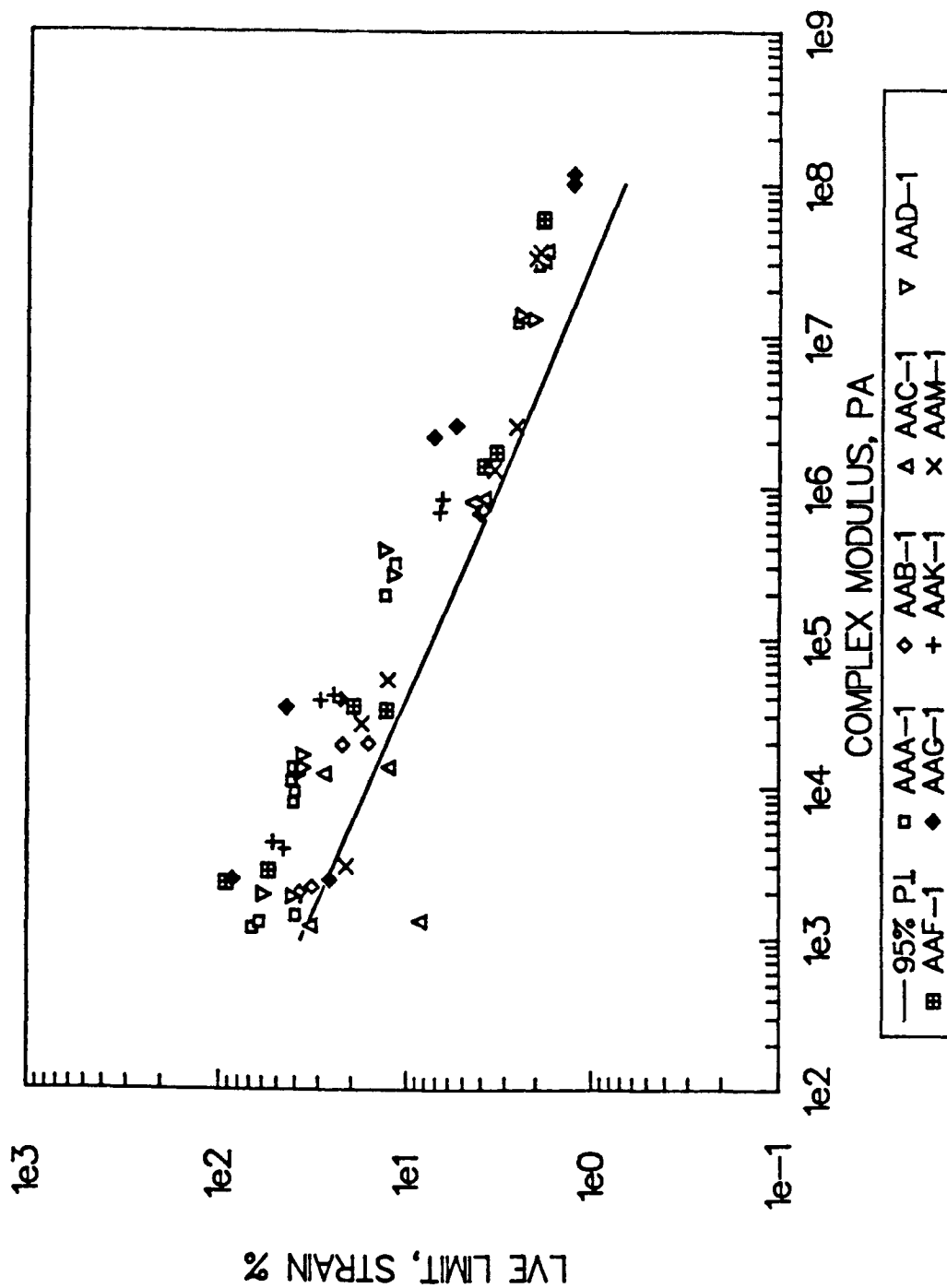
Figure 2.4 Linear Viscoelastic Limit as a Function of Complex Modulus for Core Asphalts
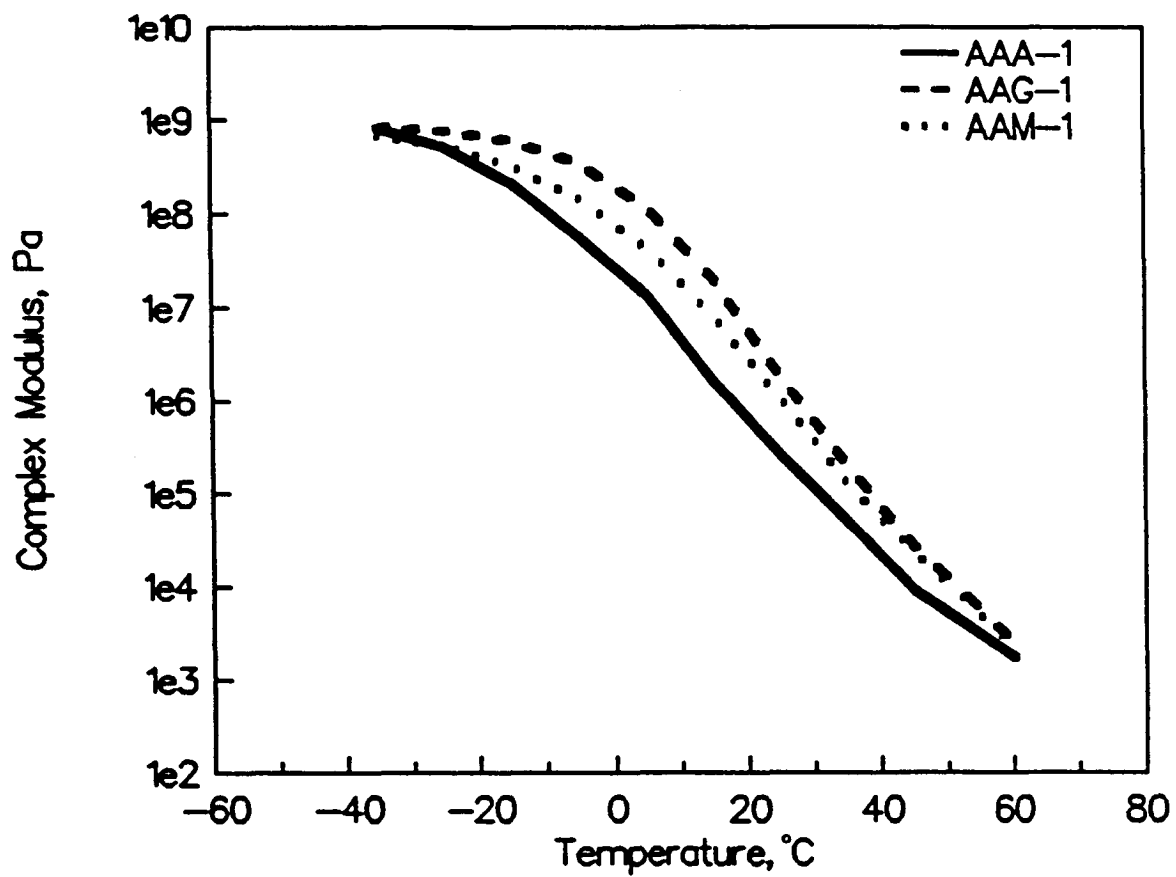
Figure 2.5   Isochronal Plots of Complex Modulus, G*, versus Temperature at 10 rad/s for Asphalts AAA-1, AAG-1, AAM-1 (Tank)
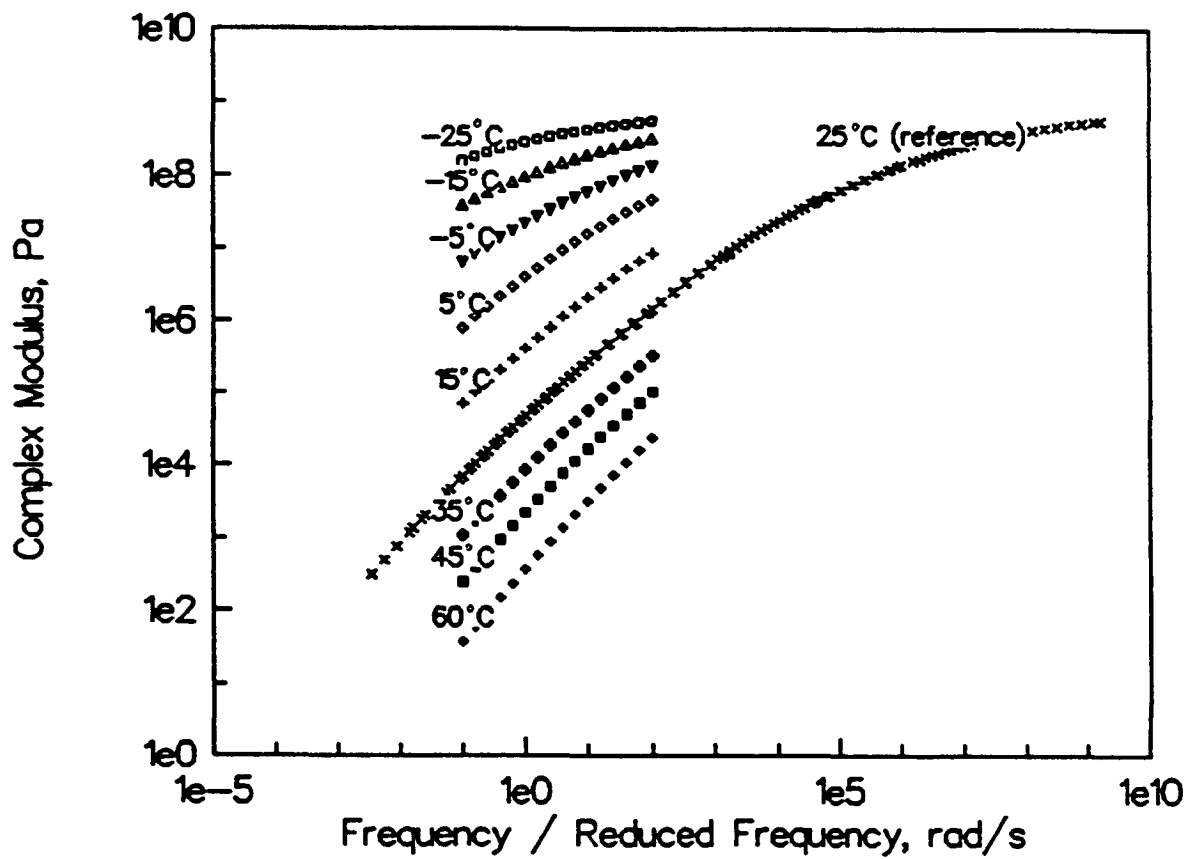
Figure 2.6 Unshifted and Shifted Complex Modulus versus Temperature for Asphalt AAD-1 (Tank)
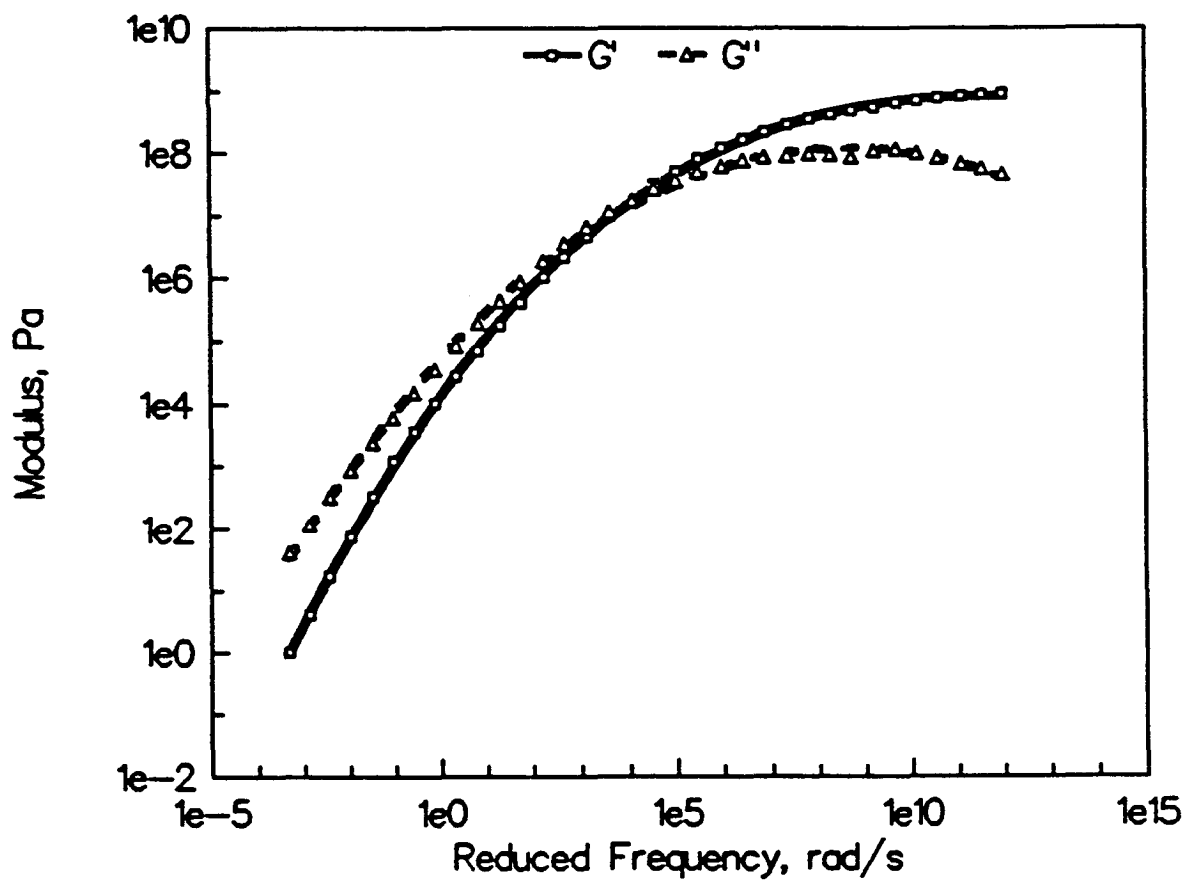
Figure 2.7 Master Curves for Storage and Loss Moduli, G′ and G″, for Asphalt AAD-1 (Tank)
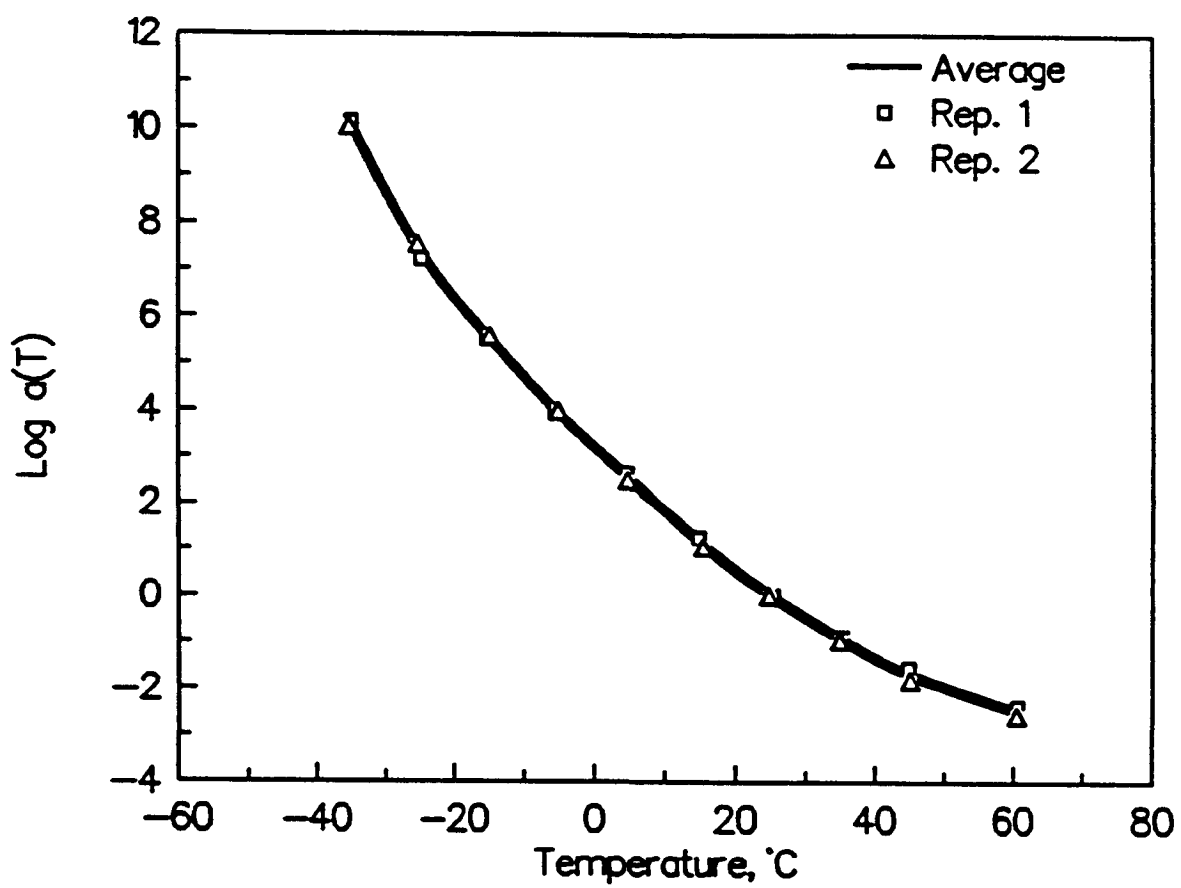
Figure 2.8   Temperature Shift Factors for Asphalt AAD-1 (Tank)
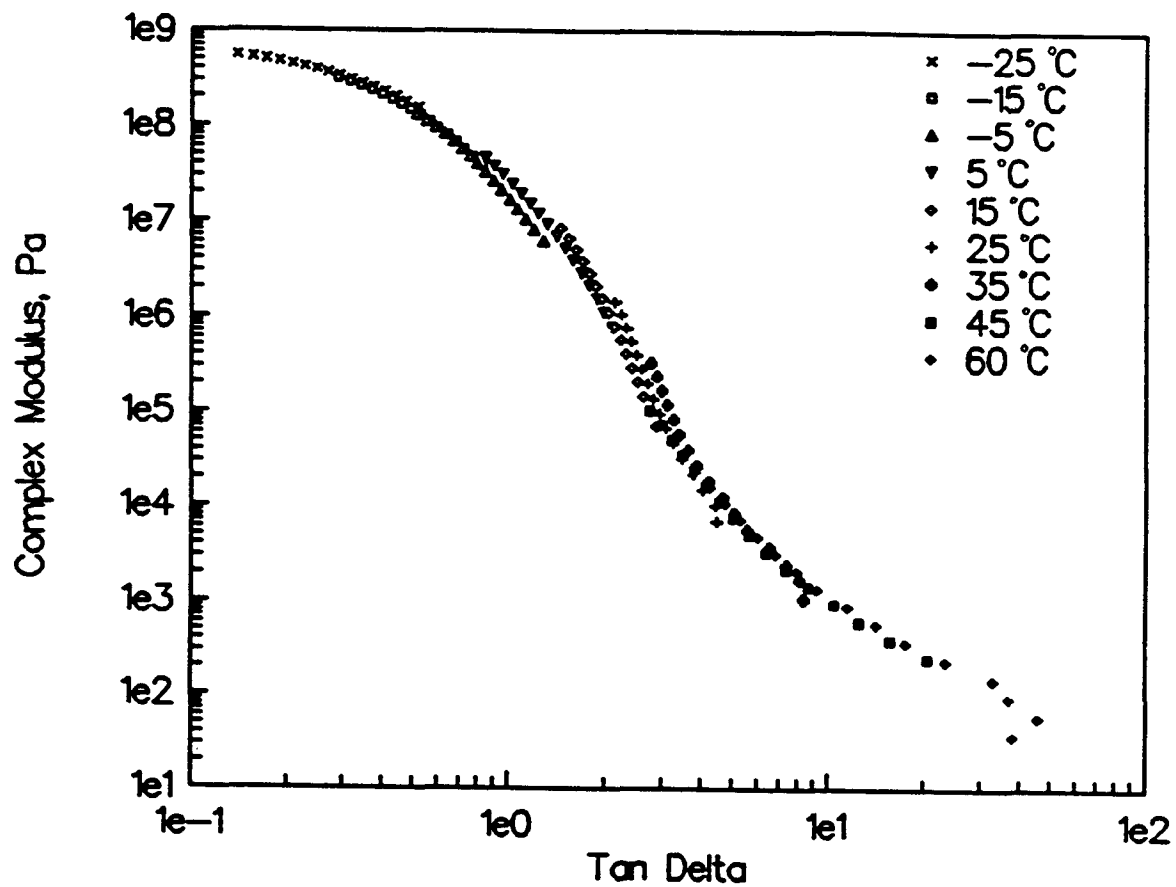
Figure 2.9   Complex Modulus versus Tan Delta for Asphalt AAD-1 (Tank)
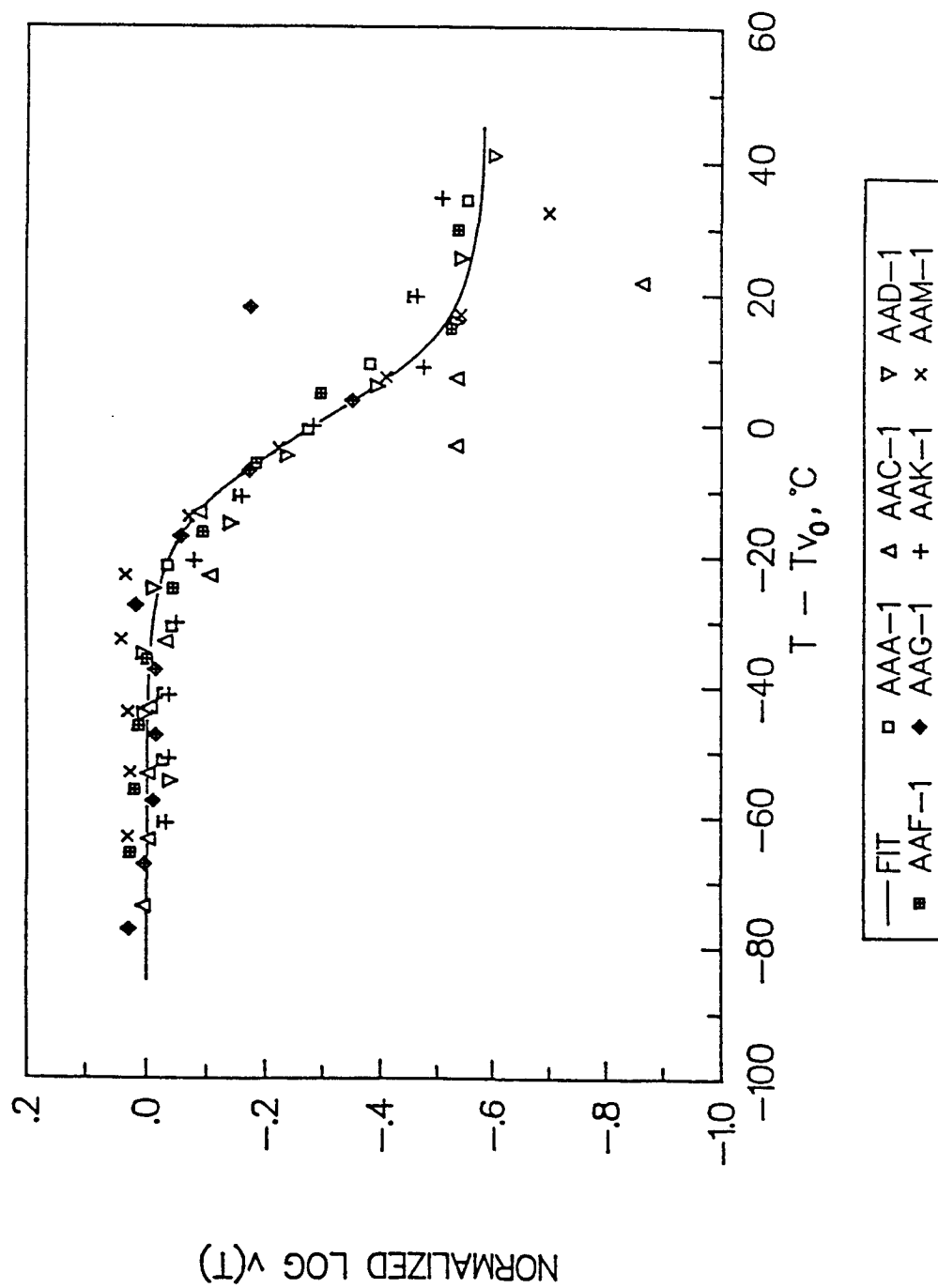
Figure 2.10 Normalized Log Vertical Shift Factors for Unaged Core Asphalts

92
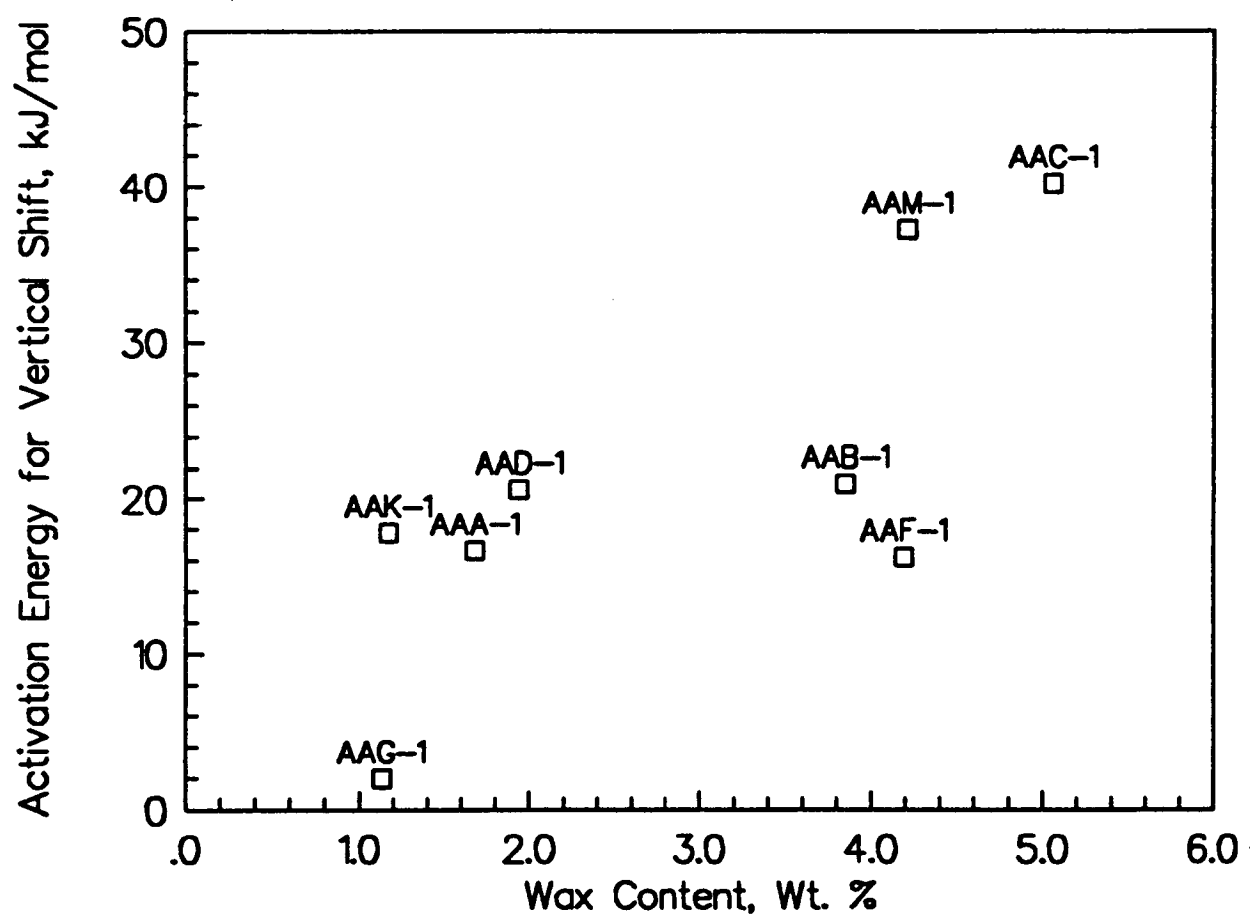
Figure 2.11 Correlation between Wax Content and Activation Energy for Vertical Shift of Core Asphalt
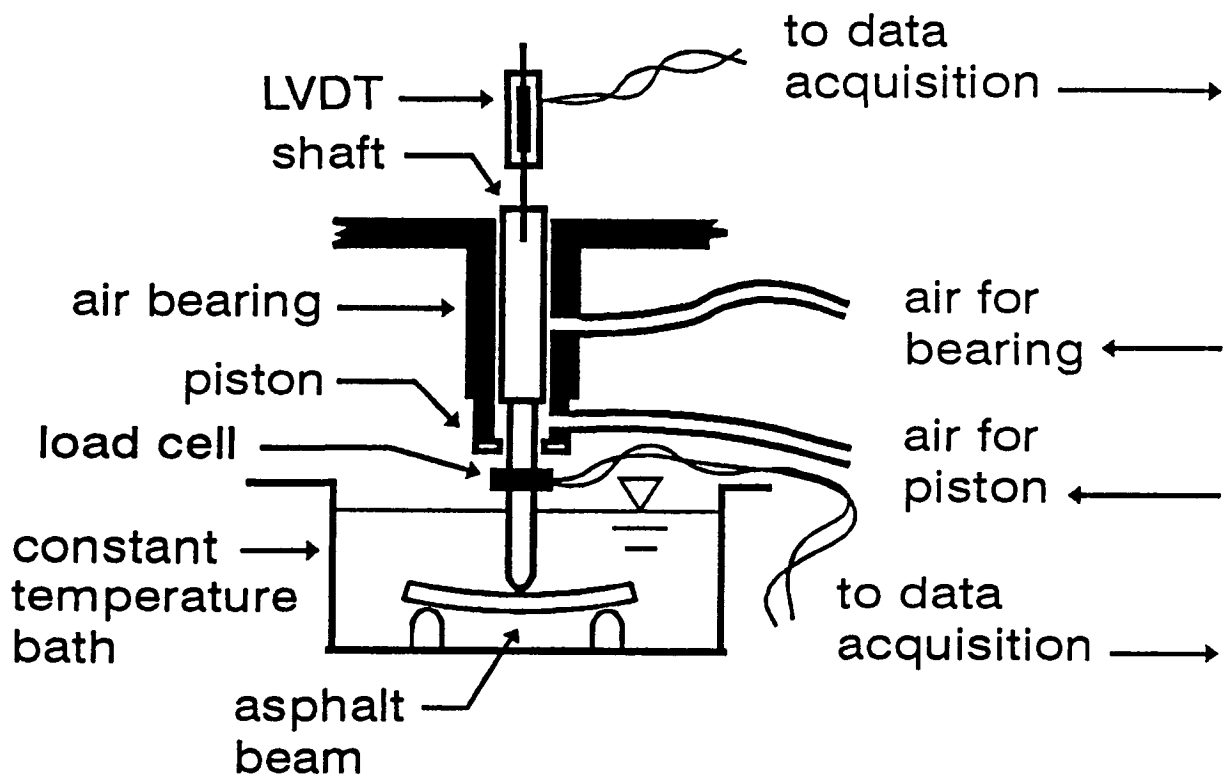
Figure 2.12 Bending Beam Rheometer, SHRP Test Method B-002

TOP VIEW

0.250

0.750

0.750 5.000 0.750

6.500

RUBBER
O-RING

SIDE VIEW

0.500

0.750

END VIEW

DWG NAME: SPECIMEN MOLD
MATERIAL: ALUMINUM
DIMENSIONS: INCHES
TOLERANCE: 0.001"
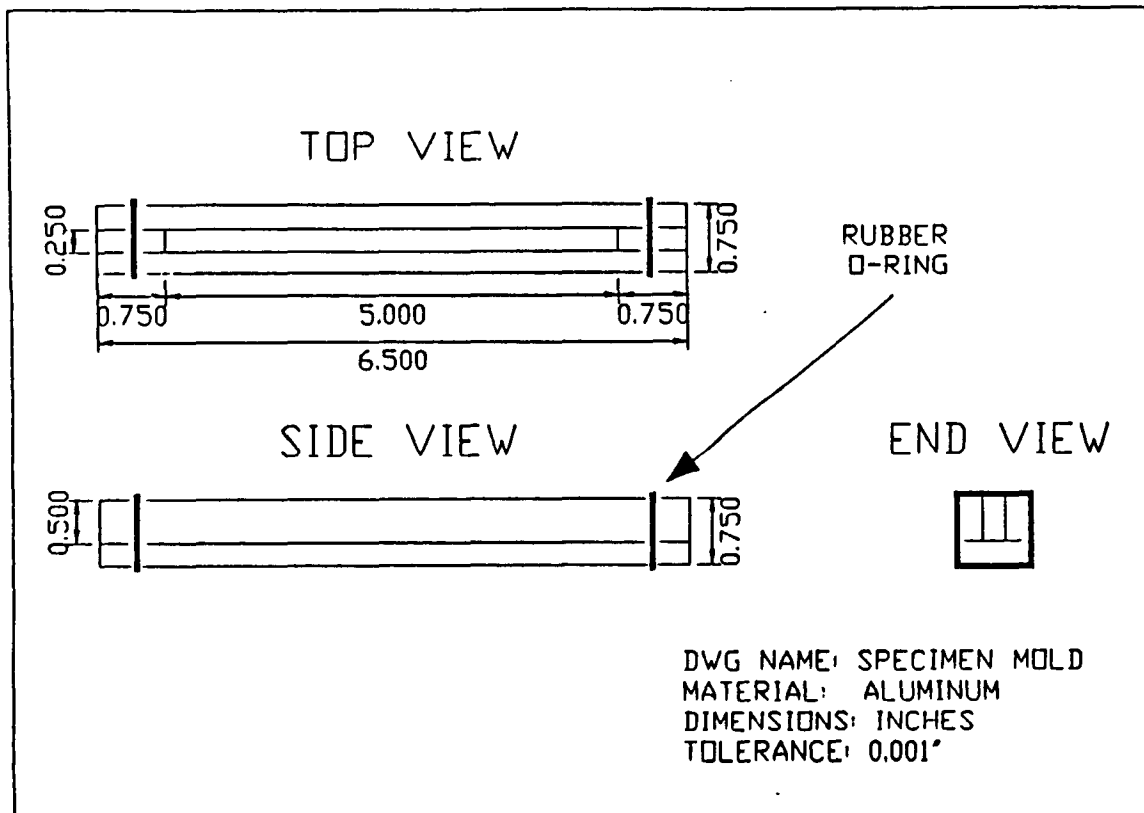
Figure 2.13   Aluminum Molds Used for Bending Beam Rheometer Test Specimens
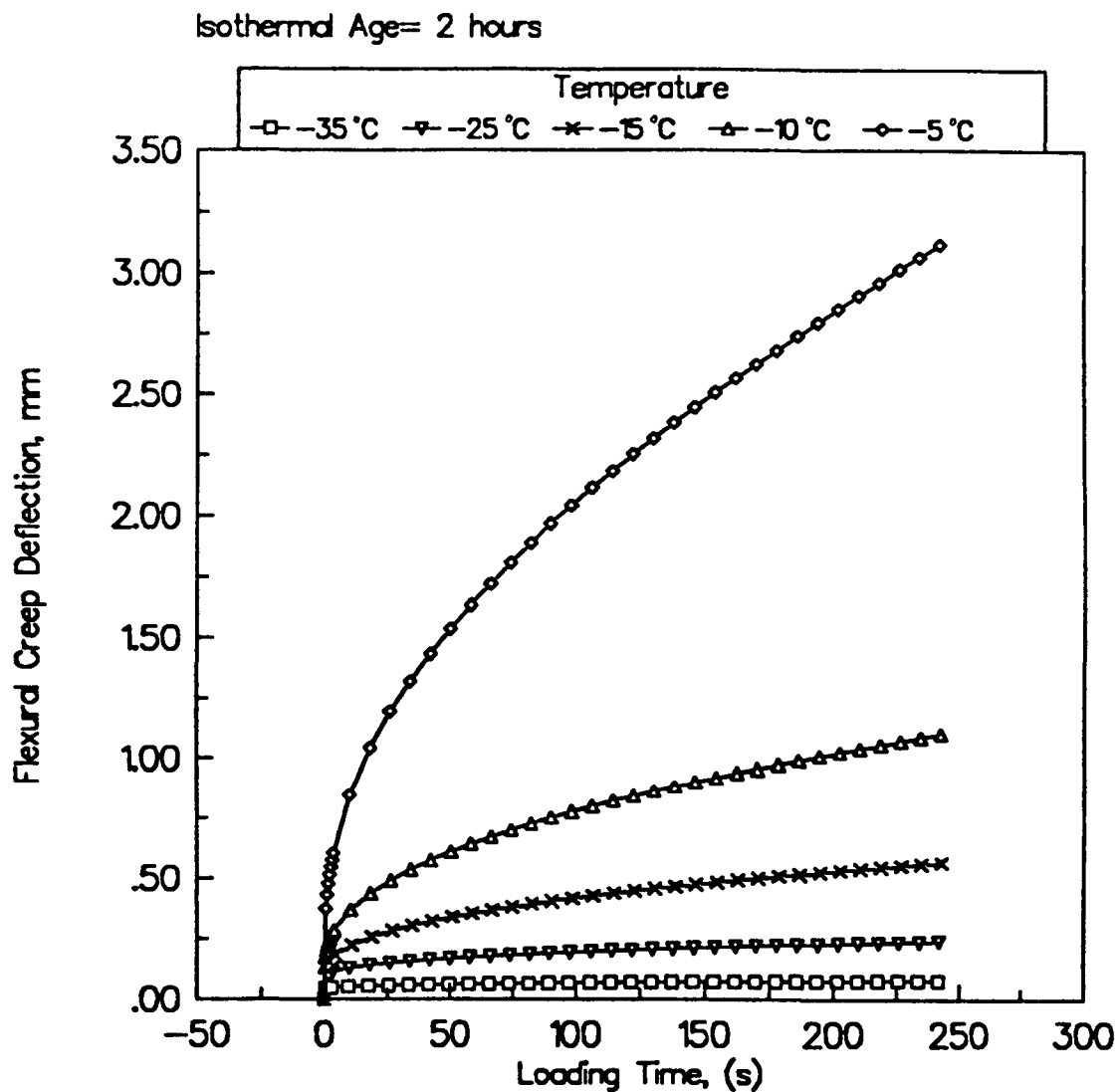
Figure 2.14 Creep Deflection Curves, Midpoint of Beam, for Asphalt AAM-1 at Five Temperatures
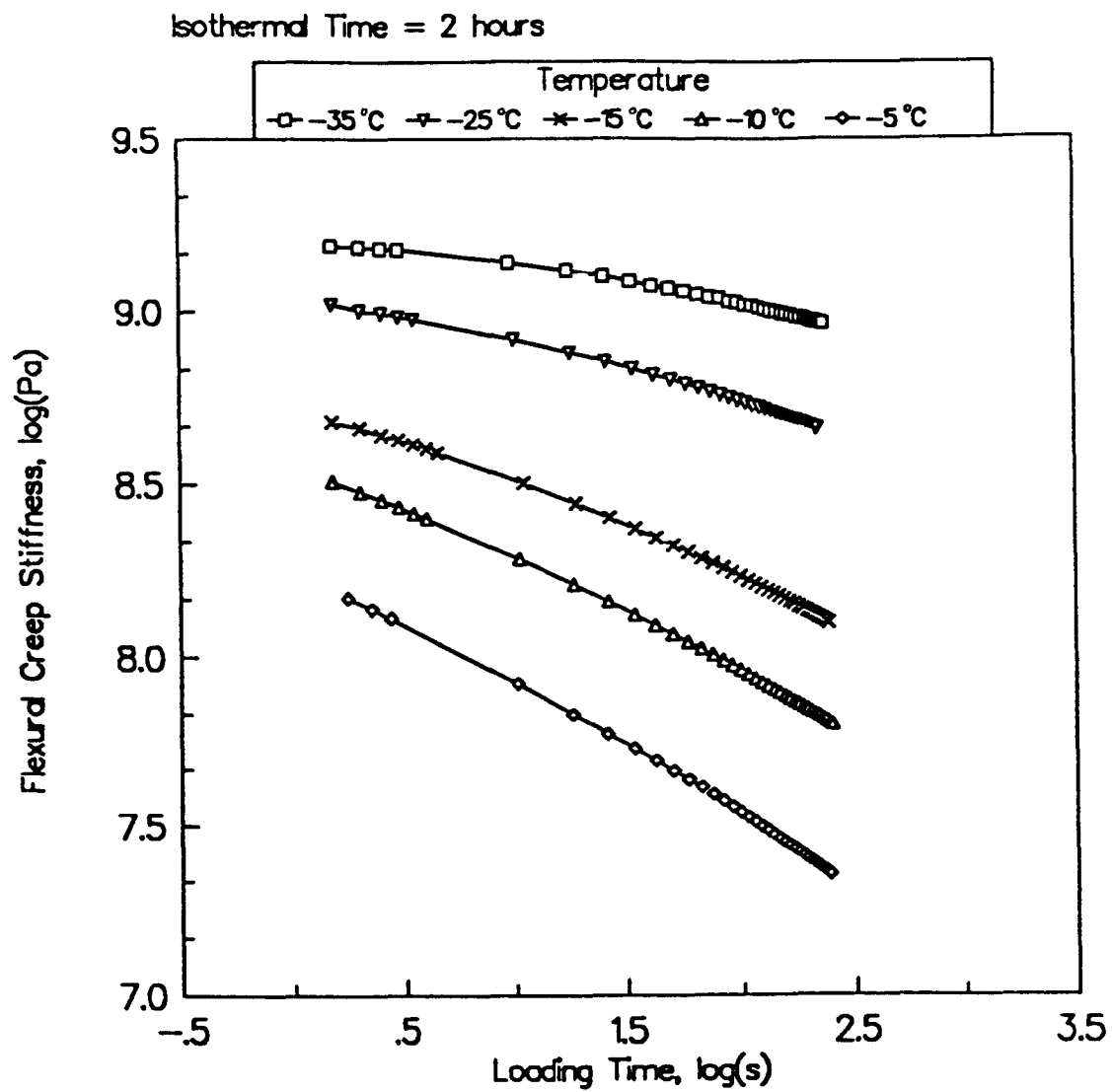
Figure 2.15 Creep Stiffness Curves at Five Temperatures, Asphalt AAM-1
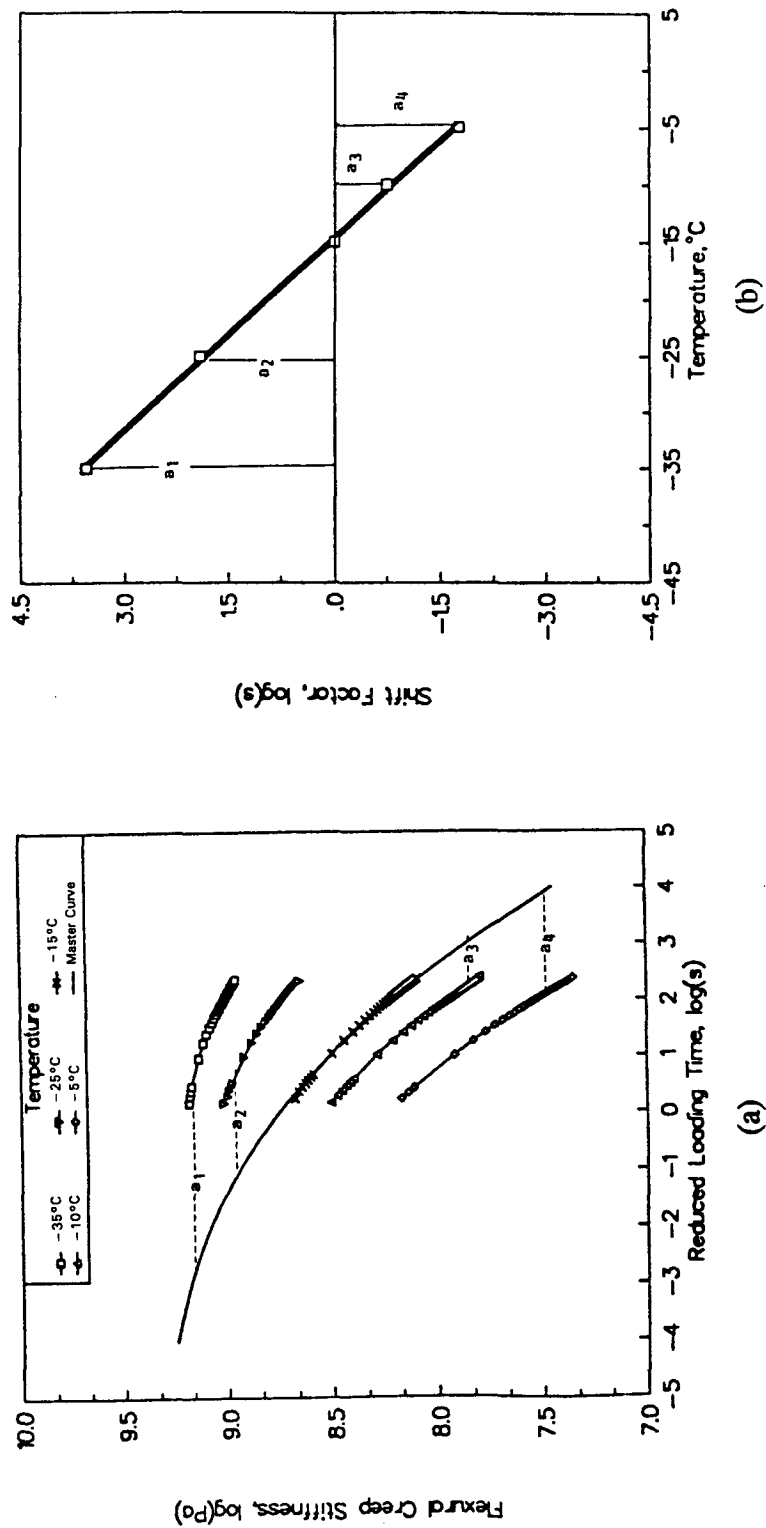
Figure 2.16   Time-Temperature Superposition Principle as Applied to Flexural Creep Data, Asphalt AAM-1

ISOTHERMAL AGE= 2 hours
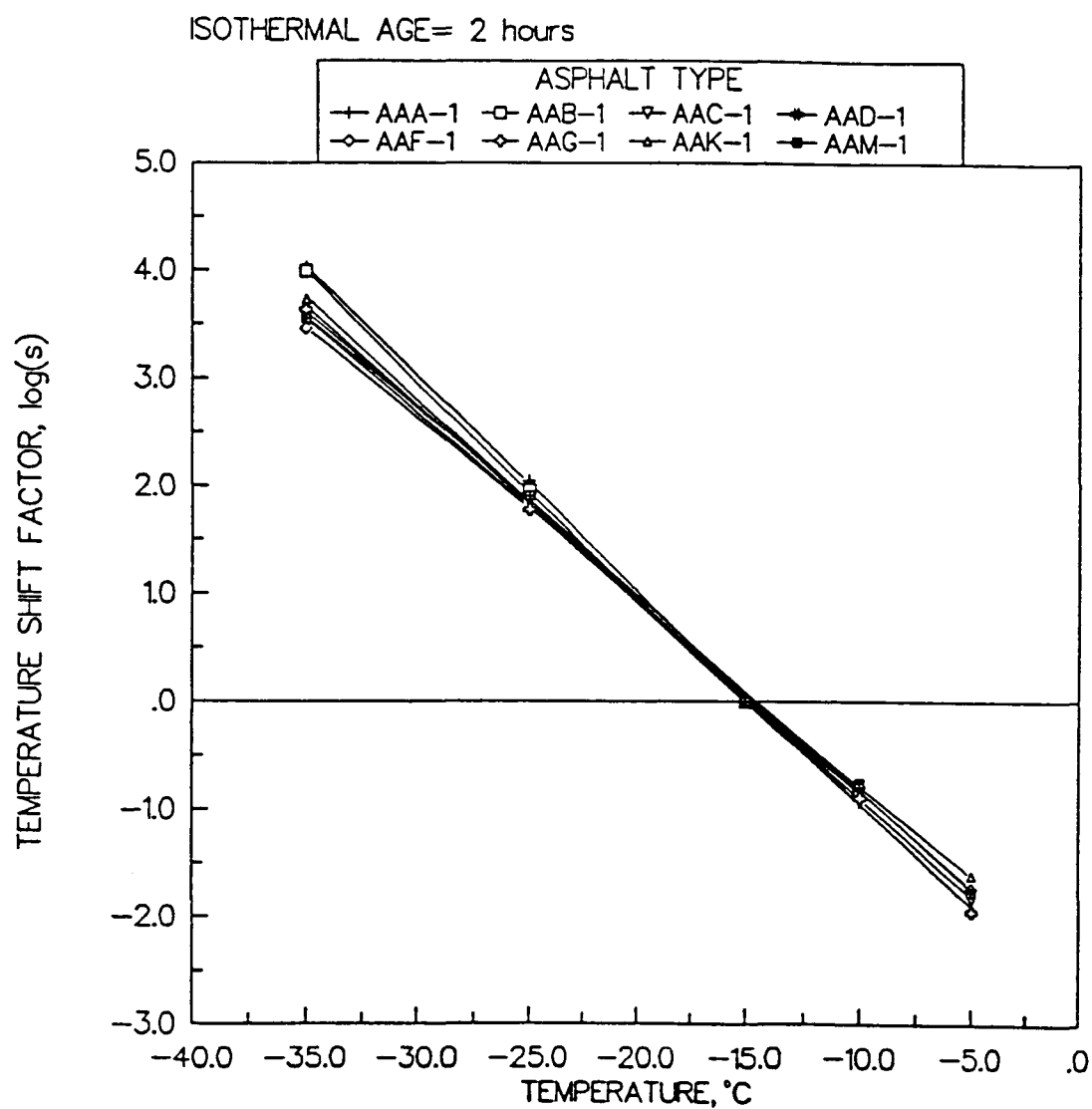
Figure 2.17   Temperature Shift Factors for Eight Asphalts Calculated Using Nonlinear
Regression at 2 hrs Isothermal Storage Time
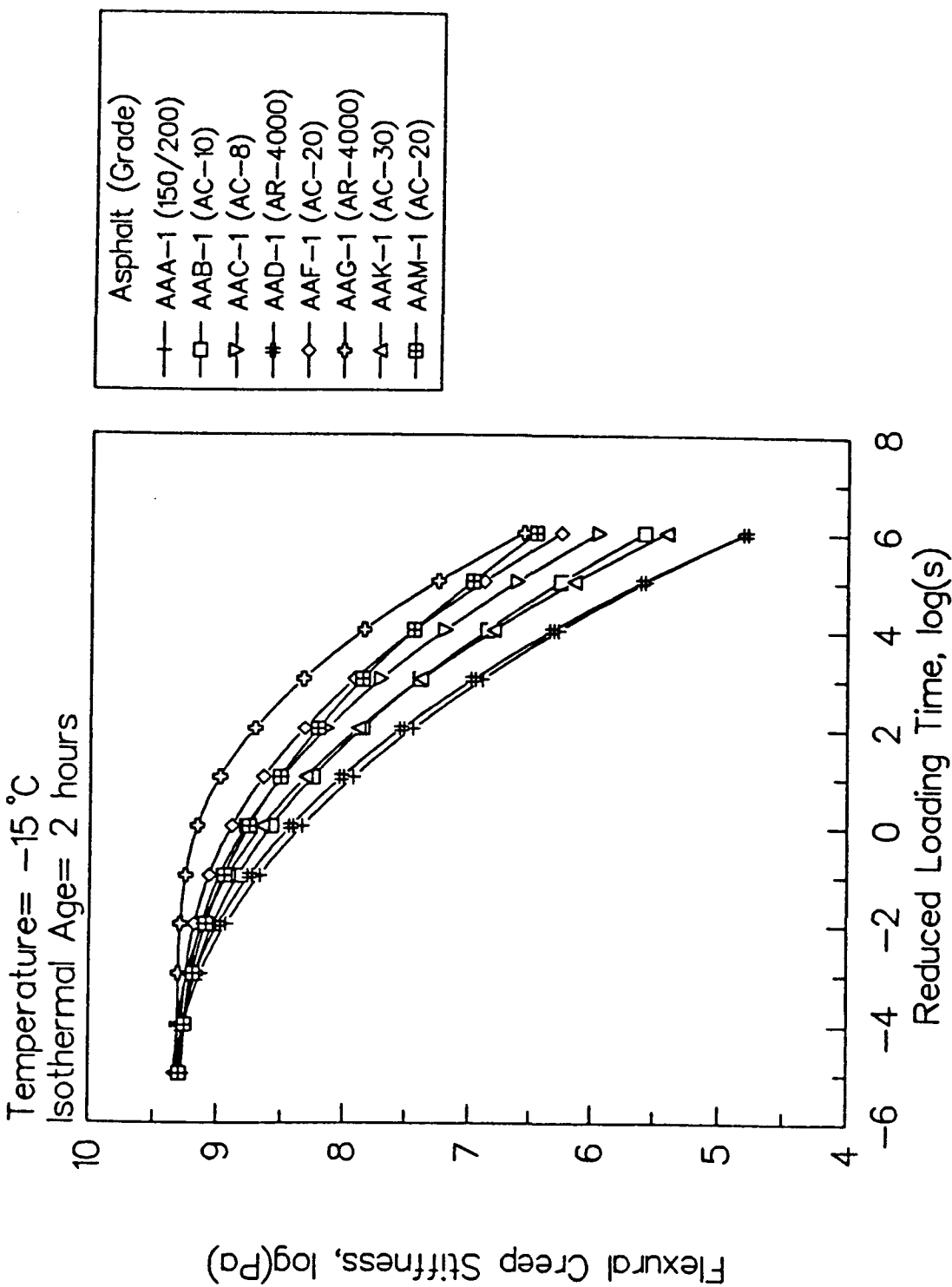
Figure 2.18 Flexural Creep Master Curves for Eight Asphalts at 2 hrs Isothermal Storage Time and 2 hrs Isothermal Loading Time
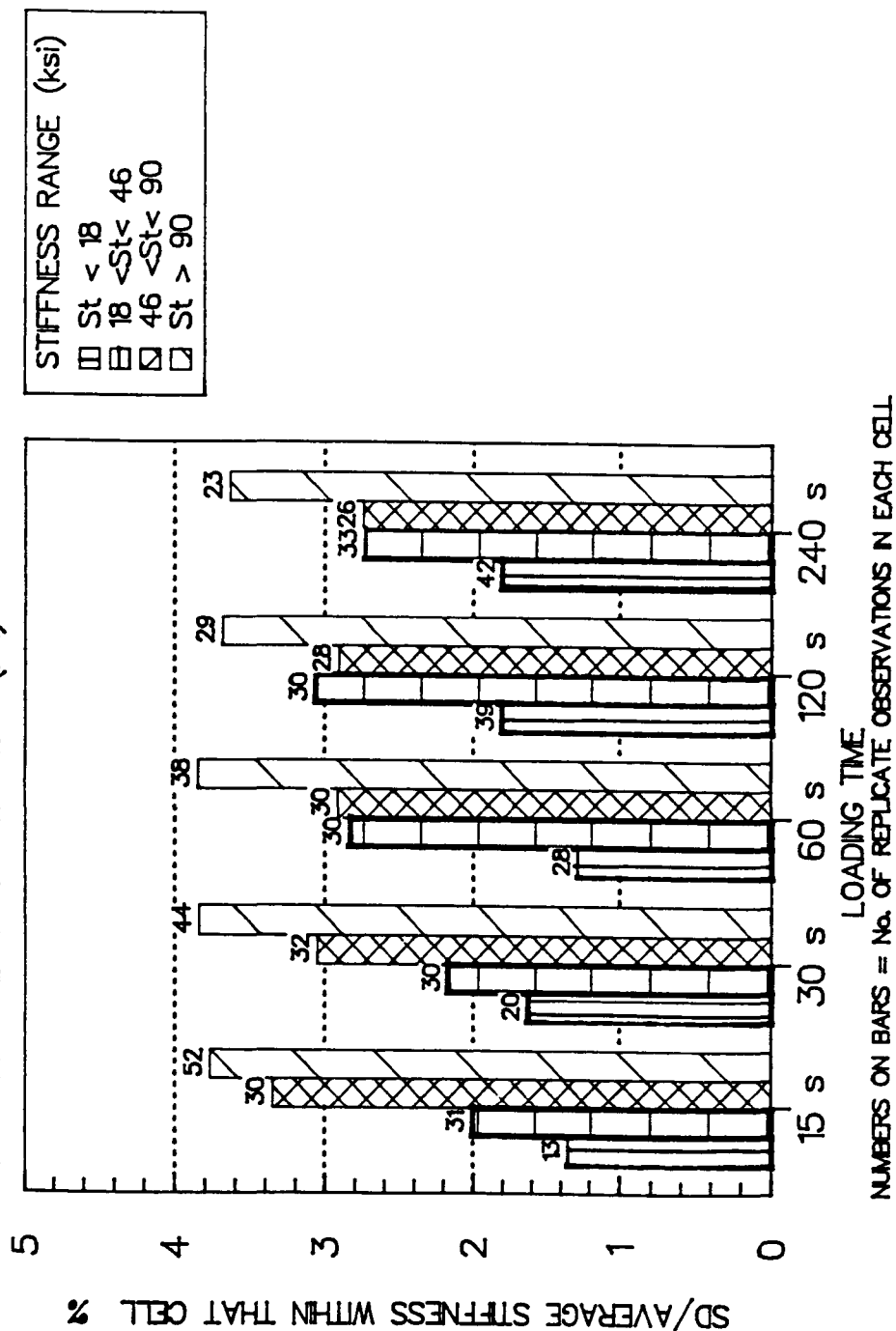
Figure 2.19 Within-Laboratory Repeatability of Bending Beam Rheometer Data at Different Loading Times
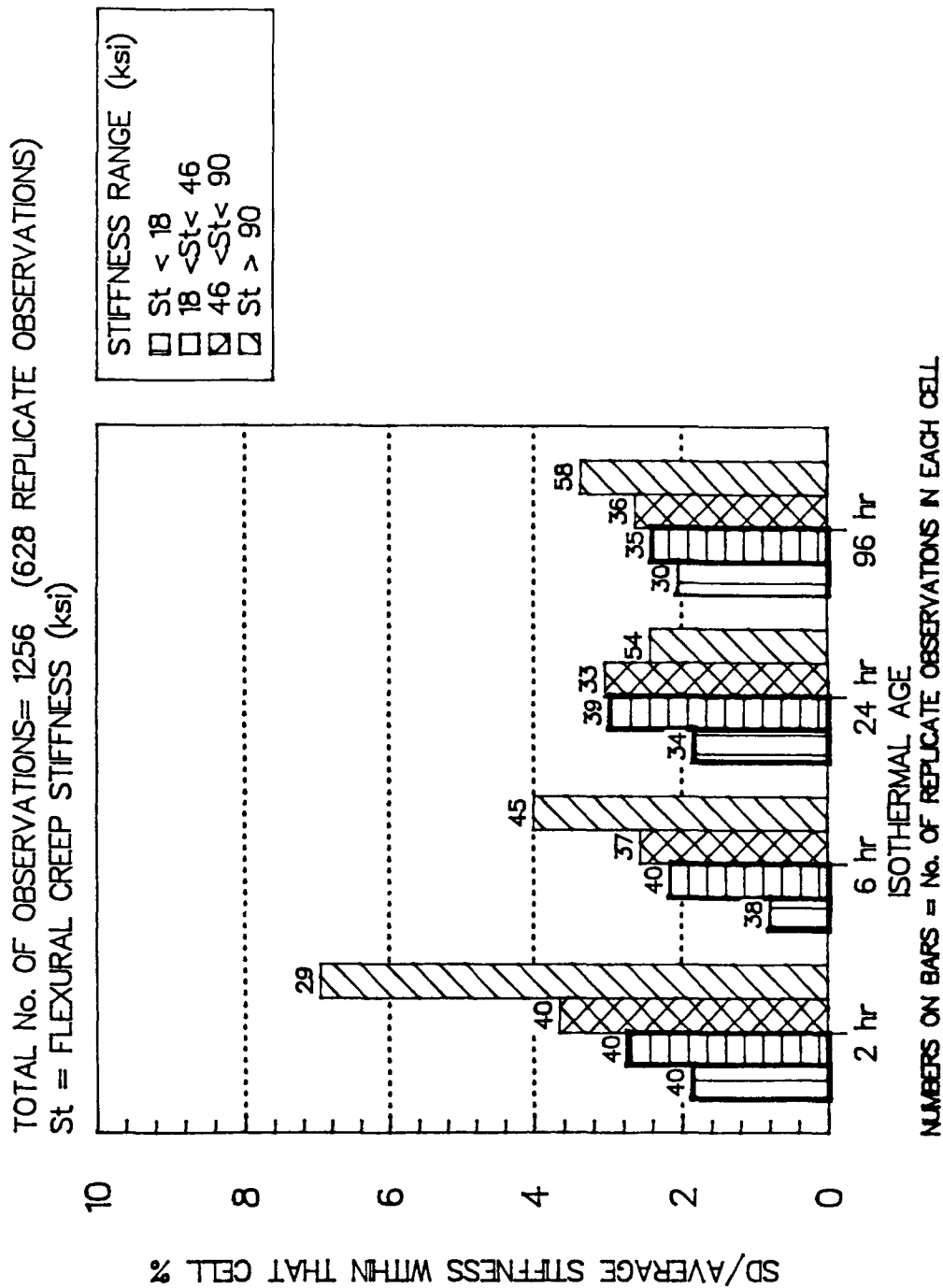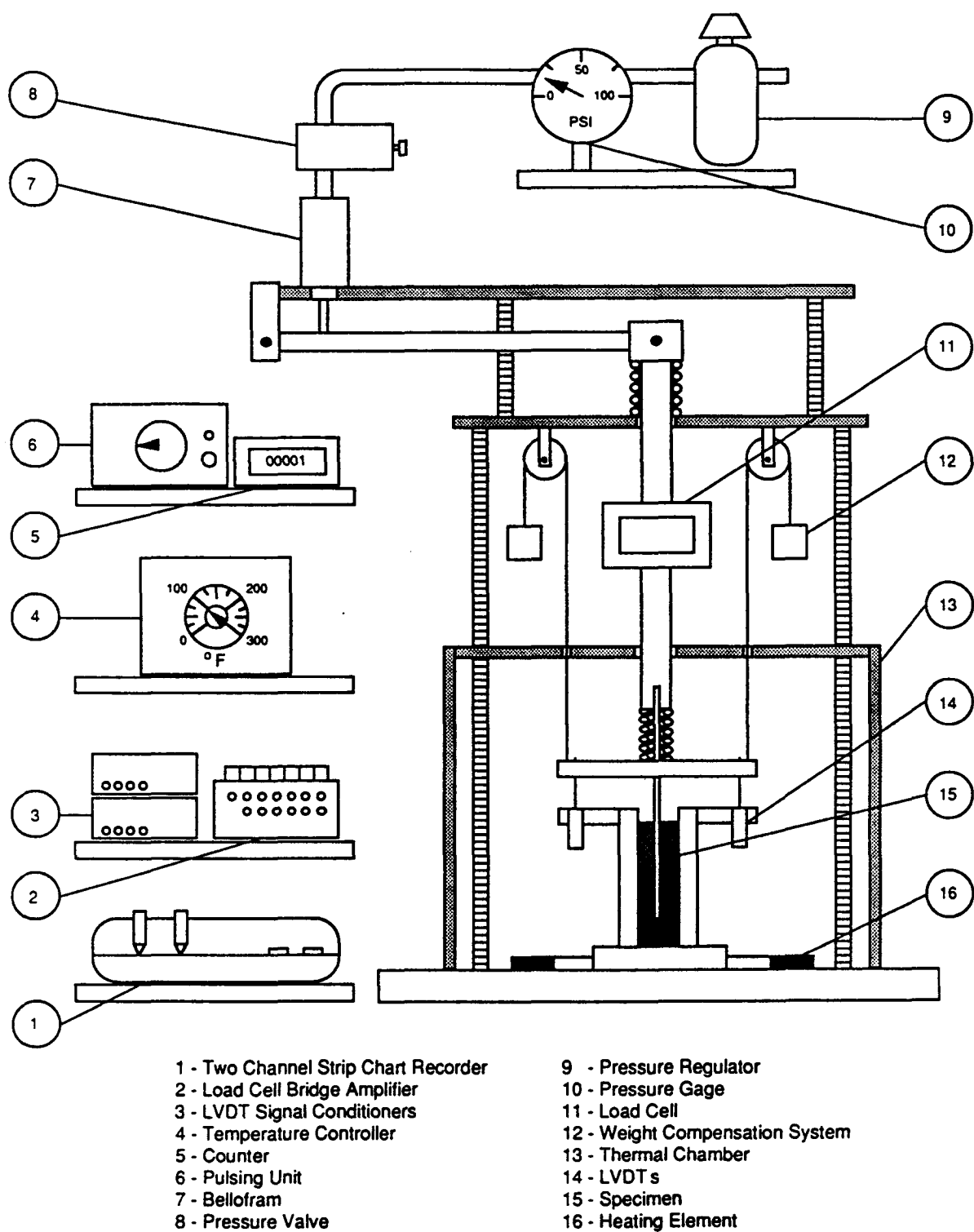
Figure 2.20   Within-Laboratory Repeatability of Bending Beam Rheometer Data at Different Isothermal Storage Times
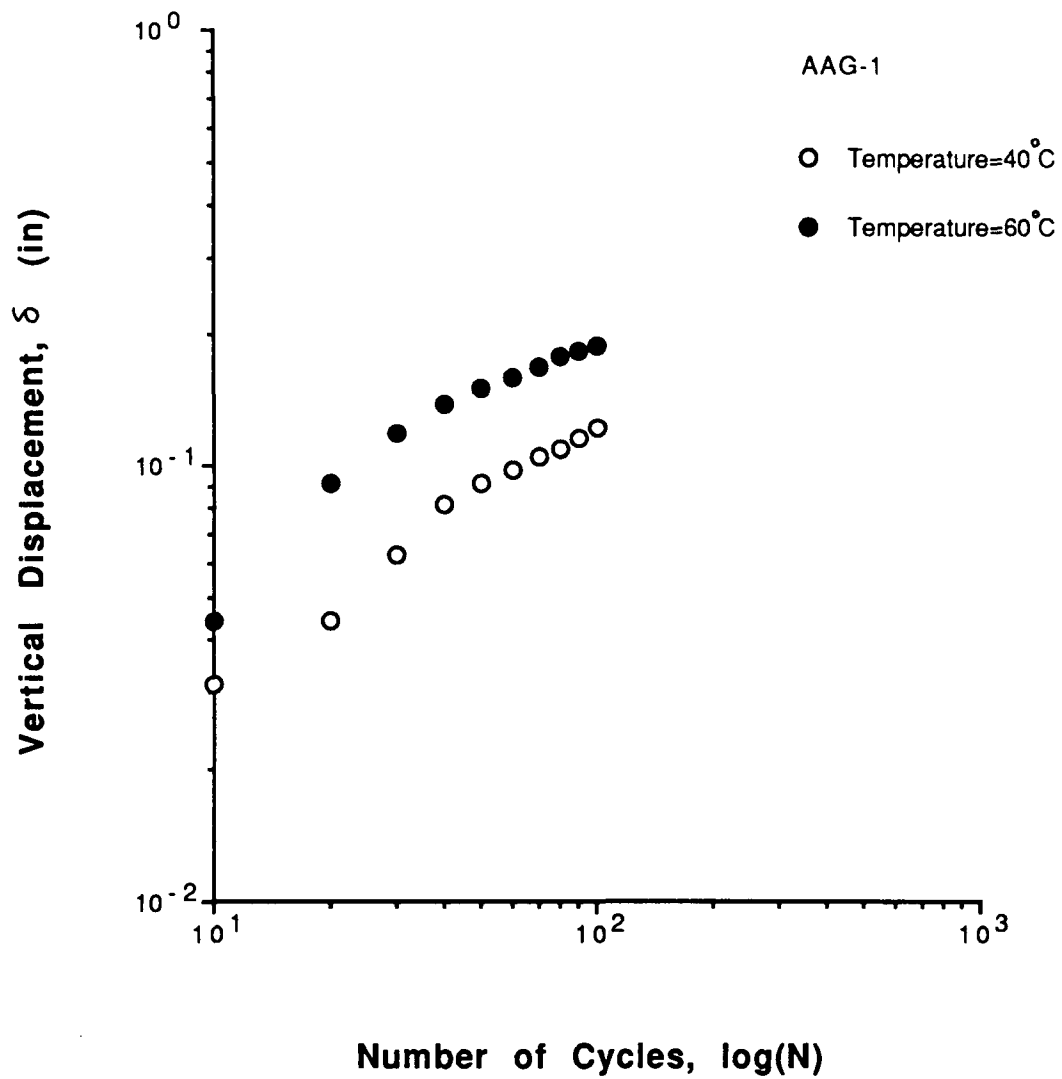
Figure 2.21   Permanent Deformation Apparatus

1 - Two Channel Strip Chart Recorder
2 - Load Cell Bridge Amplifier
3 - LVDT Signal Conditioners
4 - Temperature Controller
5 - Counter
6 - Pulsing Unit
7 - Bellofram
8 - Pressure Valve

9 - Pressure Regulator
10 - Pressure Gage
11 - Load Cell
12 - Weight Compensation System
13 - Thermal Chamber
14 - LVDT s
15 - Specimen
16 - Heating Element
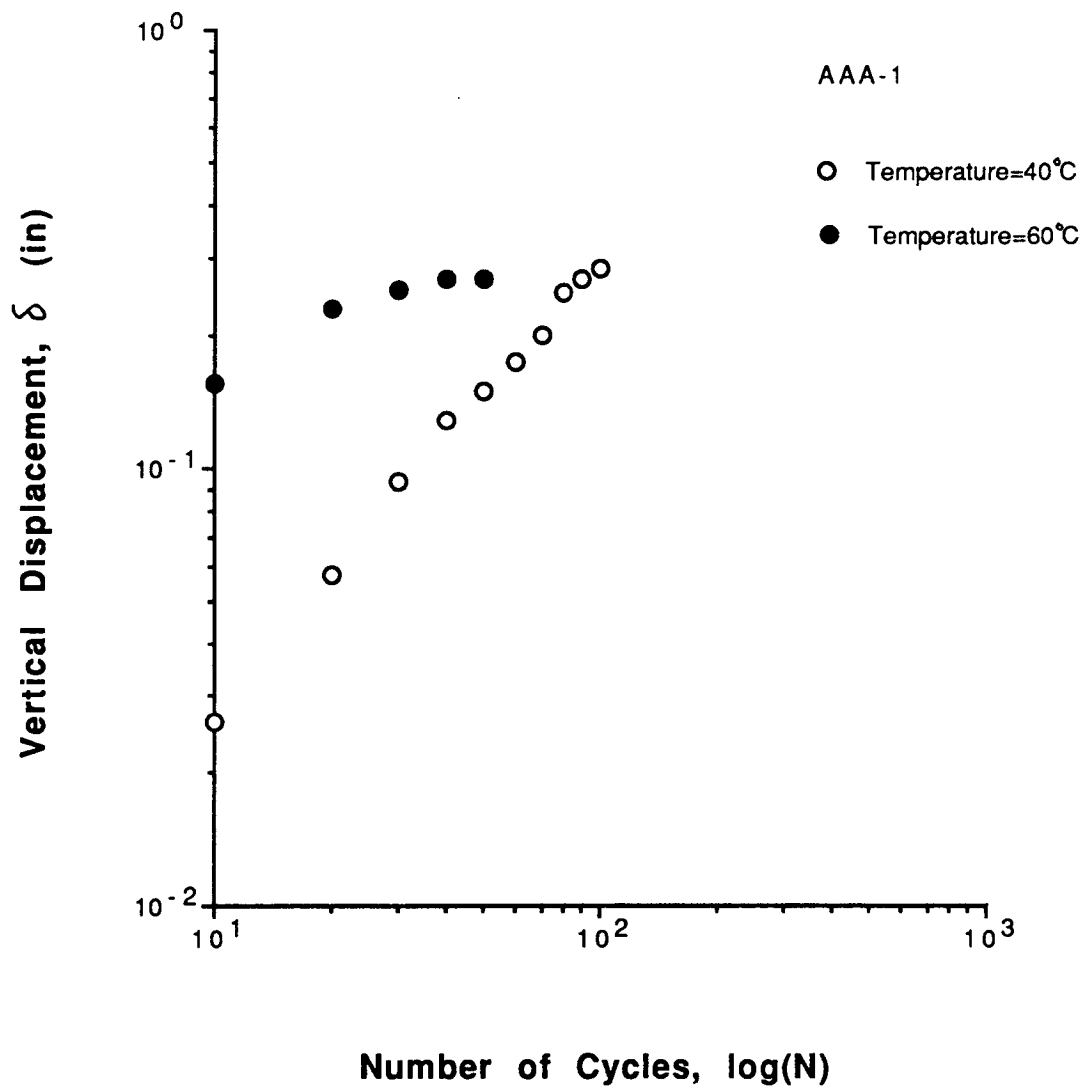
Figure 2.22   Vertical Displacement versus Number of Loading Cycles, Asphalt AAA-1

Figure 2.23   Vertical Displacement versus Number of Loading Cycles, Asphalt AAG-1
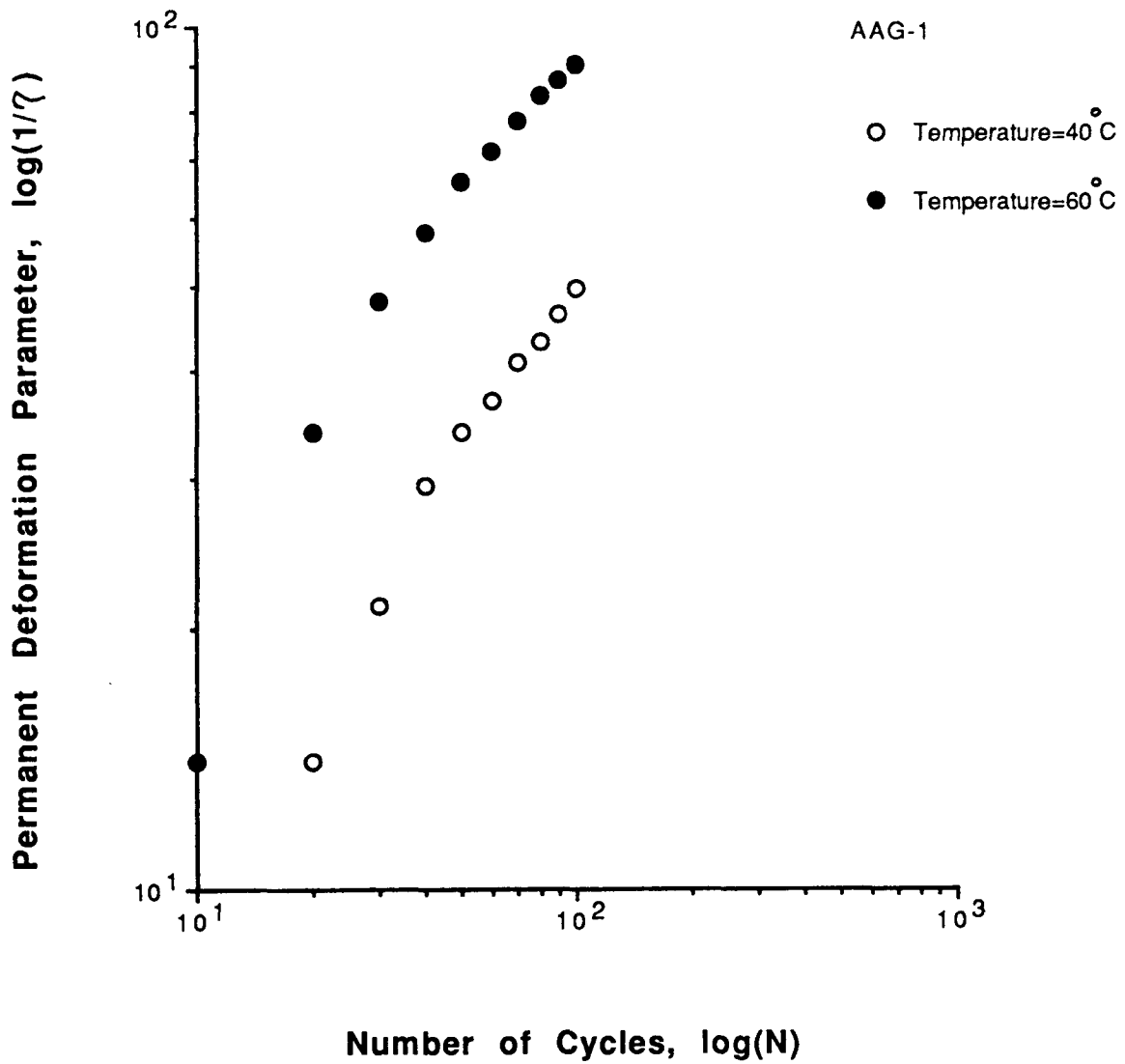
Figure 2.24   Permanent Deformation Parameter versus Number of Loading Cycles,
Asphalt AAG-1
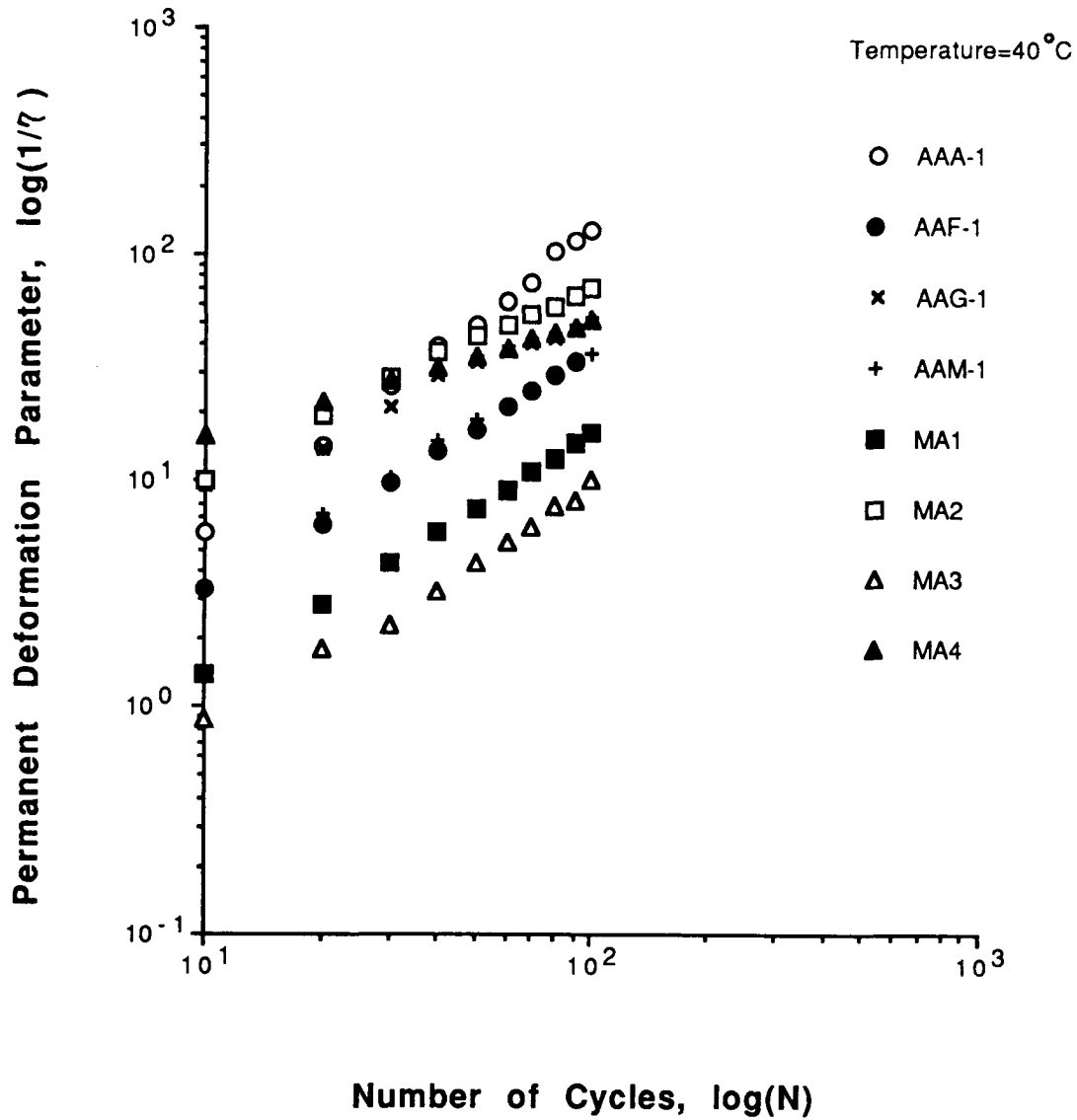
Figure 2.25 Permanent Deformation Parameter versus Number of Loading Cycles, Various Asphalts, 40°C

Plastic Deformation
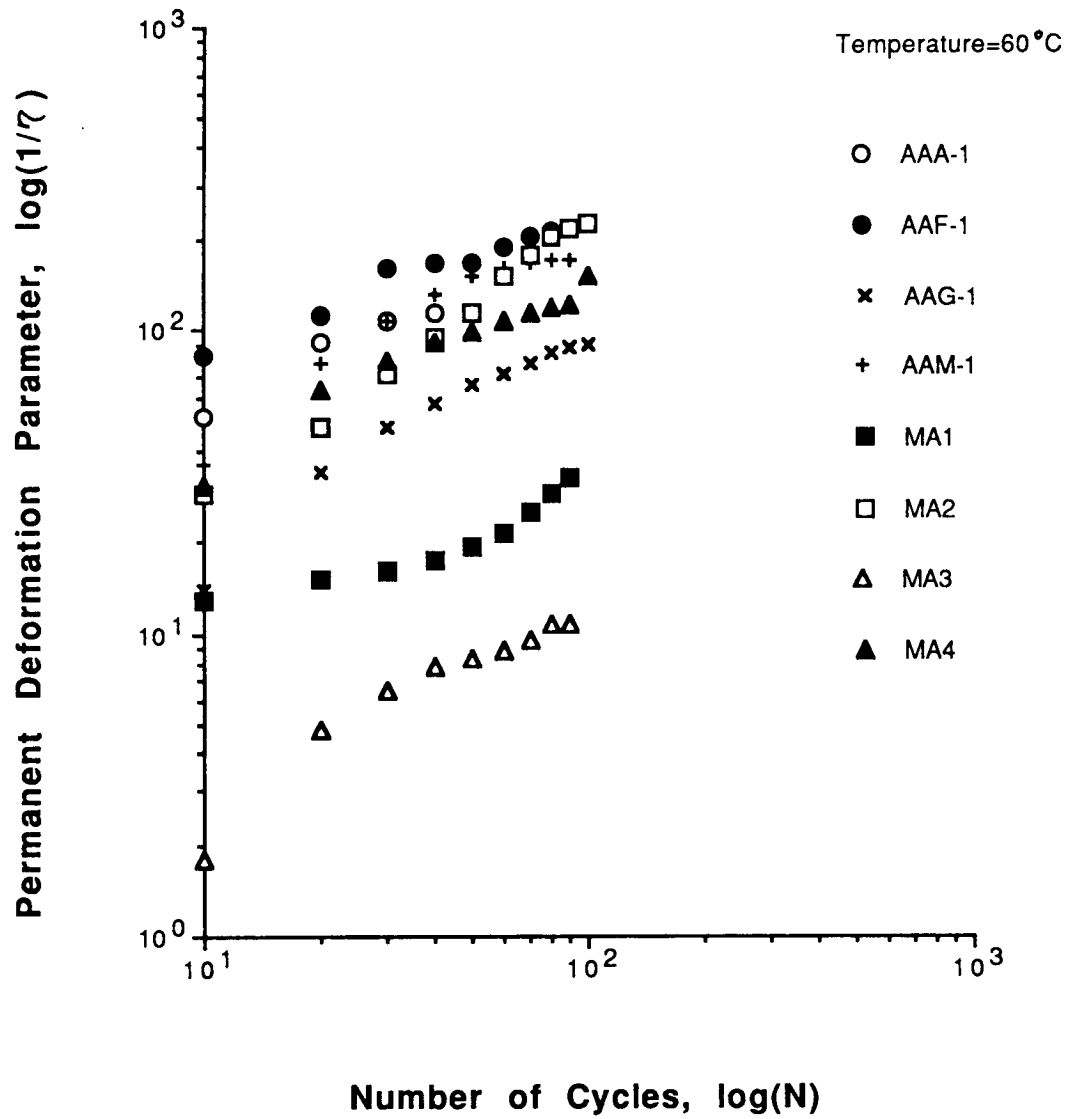
Figure 2.26   Permanent Deformation Parameter versus Number of Loading Cycles, Various Asphalts, 60°C
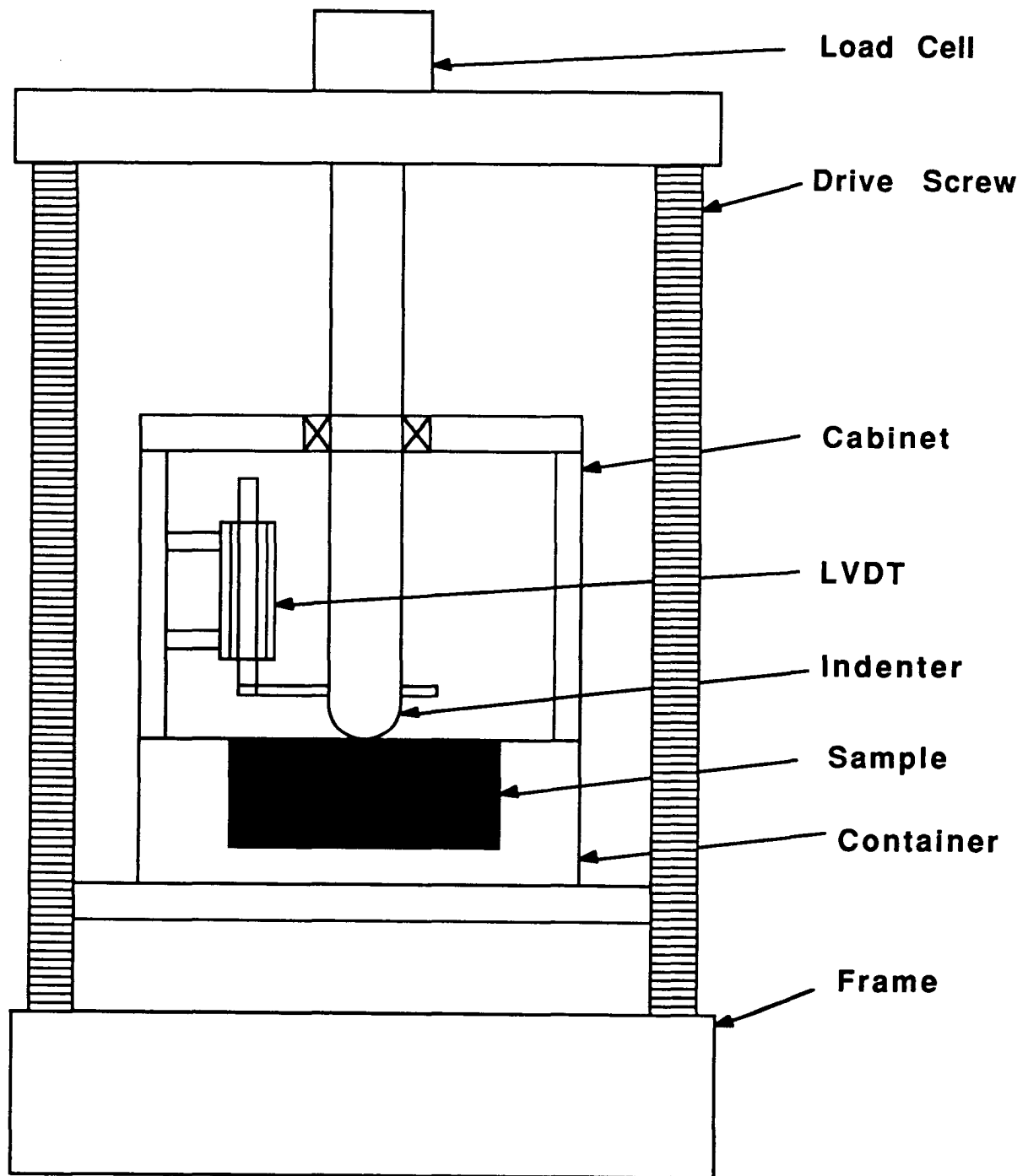
Figure 2.27   Indentation Test Apparatus
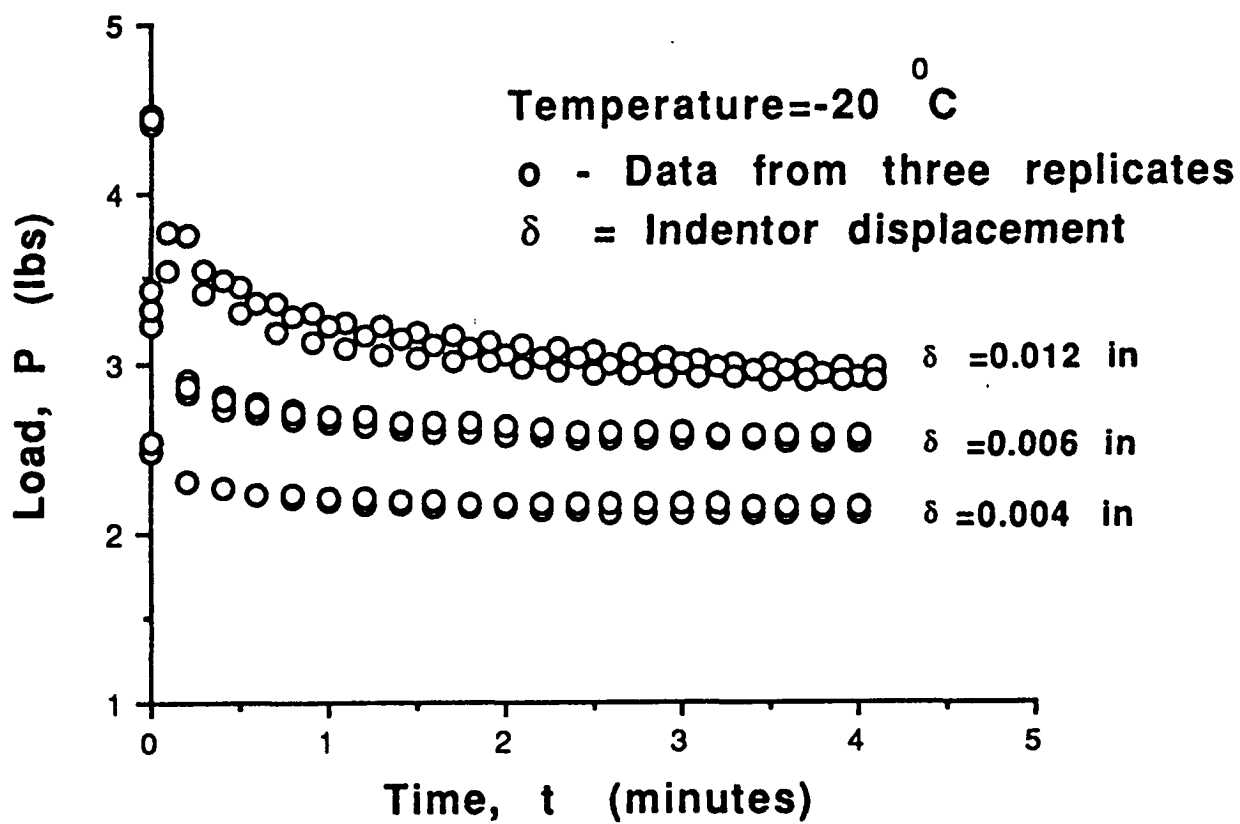
Figure 2.28   Indenter Load versus Time

Relaxation Modulus (AAK-1)
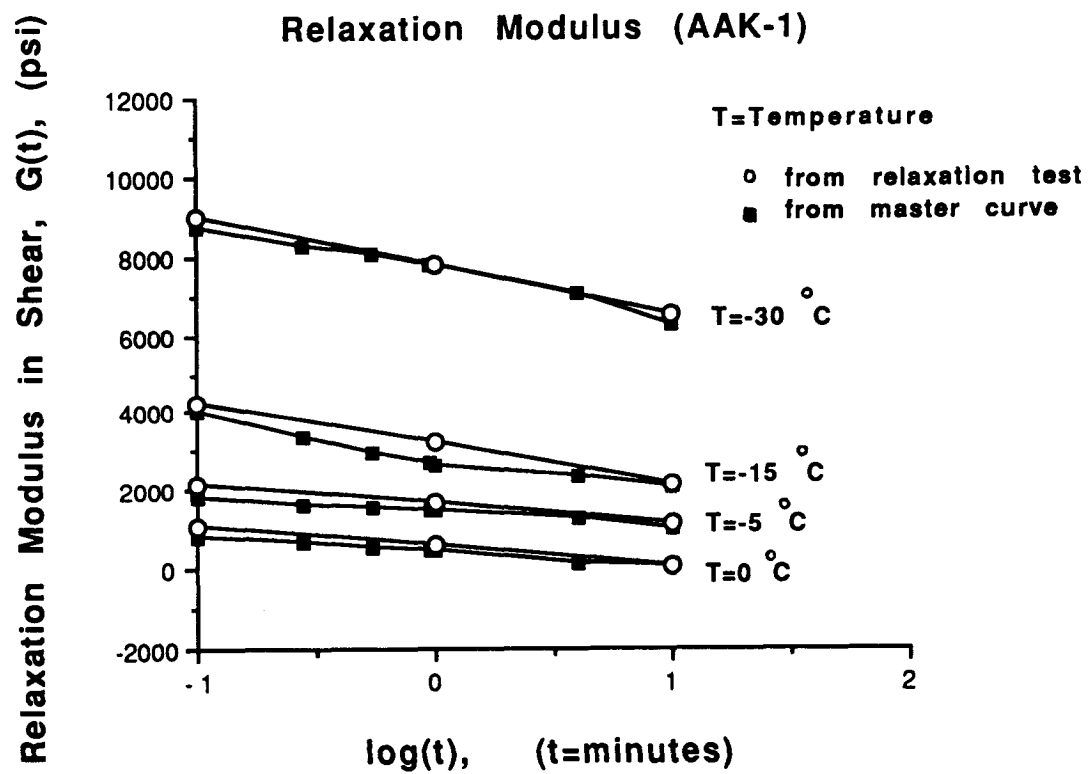
Figure 2.29   Shear Relaxation Modulus, G(t), at Different Temperatures, Asphalt
AAK-1
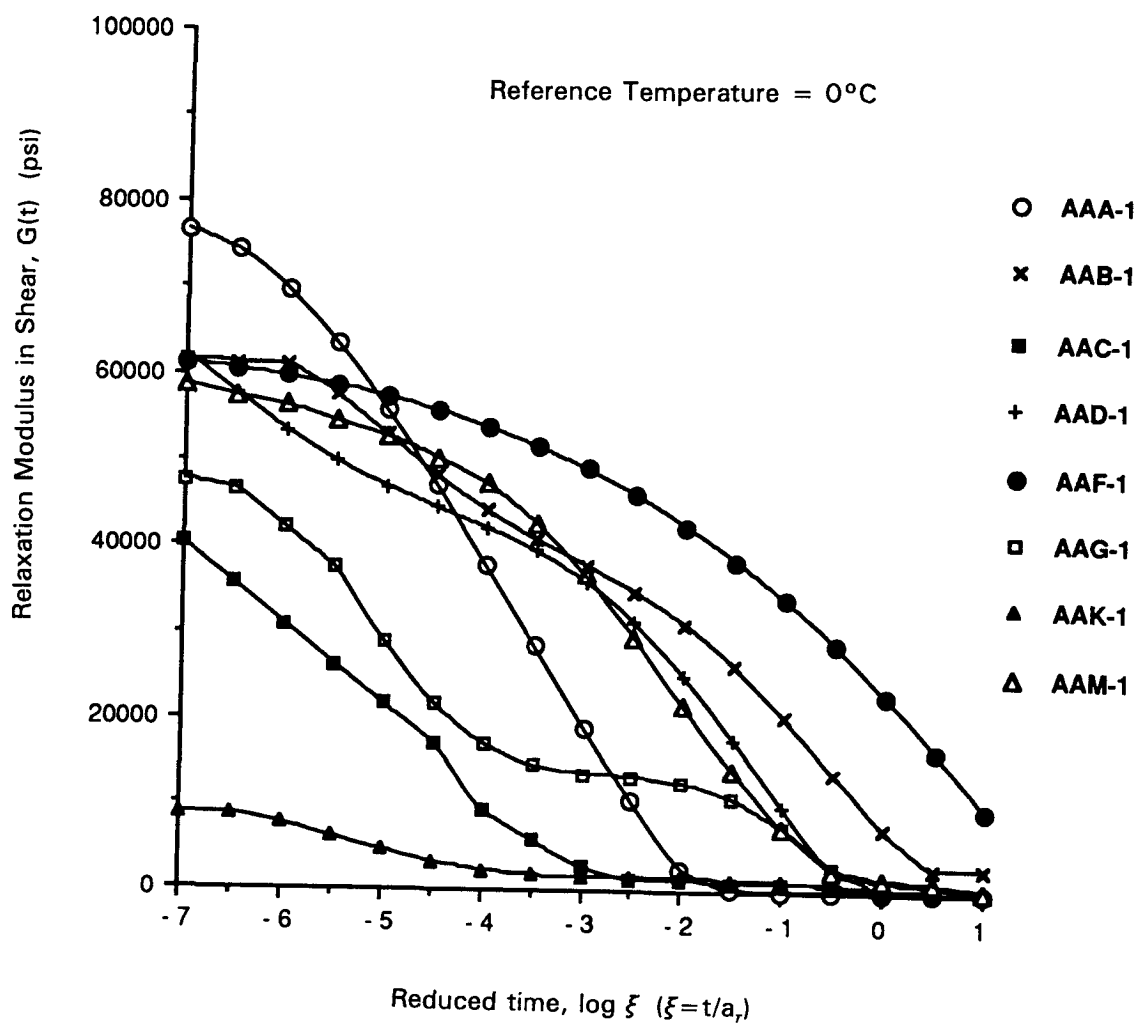
Figure 2.30   Shear Relaxation Modulus, G(t), at 0°C, Various Asphalts
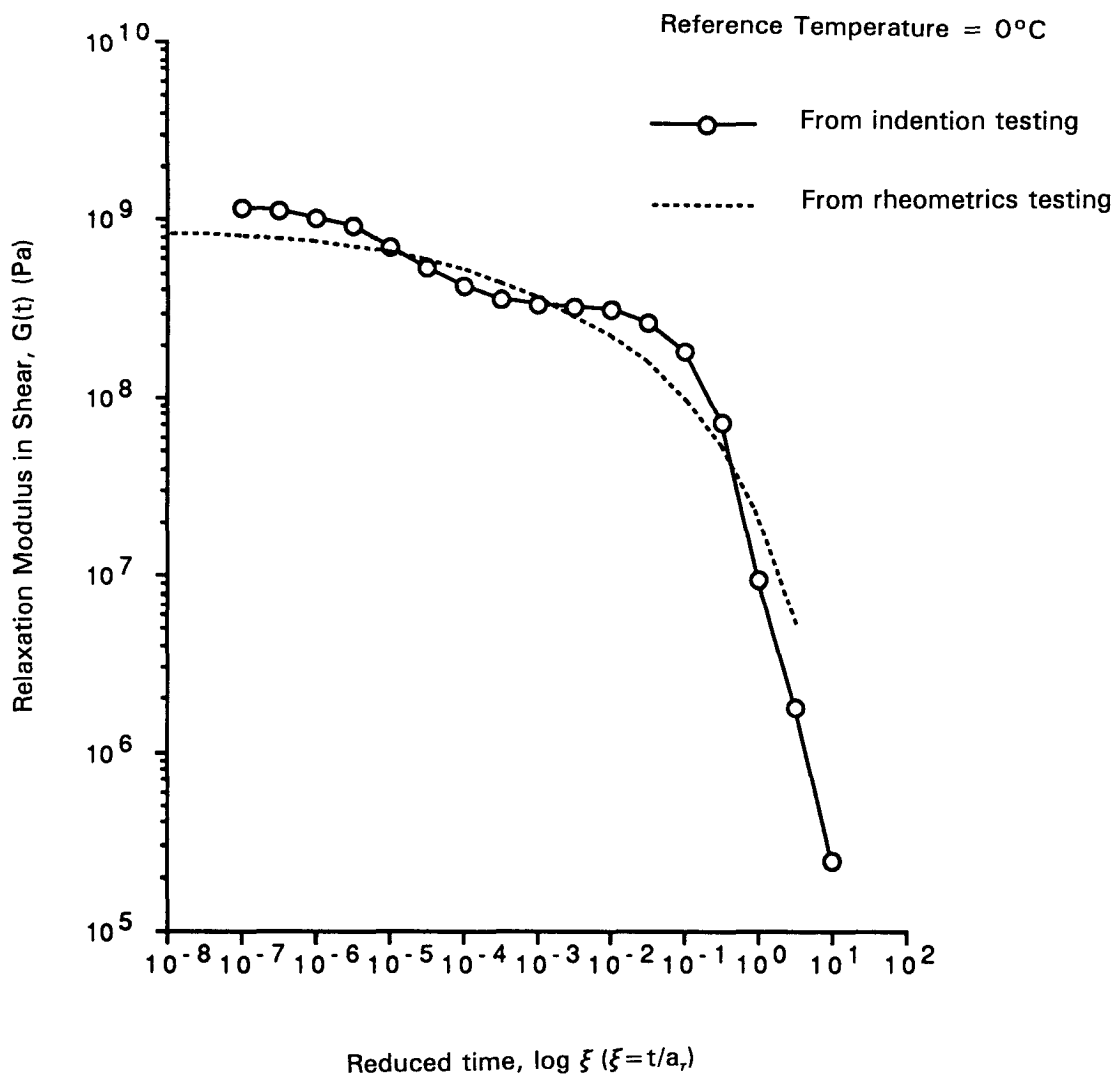
Figure 2.31   Comparison of Relaxation Modulus in Shear Based on Indentation and
Dynamic Shear Data, Reference Temperature 0°C
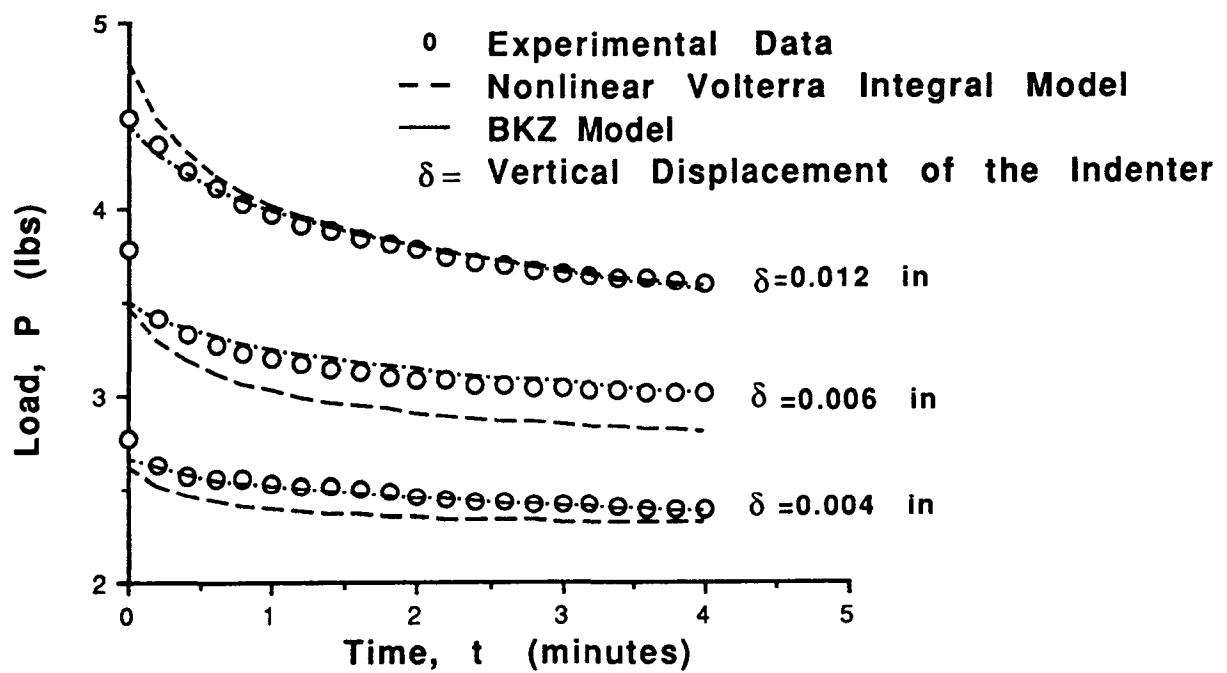
Figure 2.32 Comparison of Measured Indenter Load and Indenter Load Predicted by Nonlinear Volterra Integral and BKZ Model
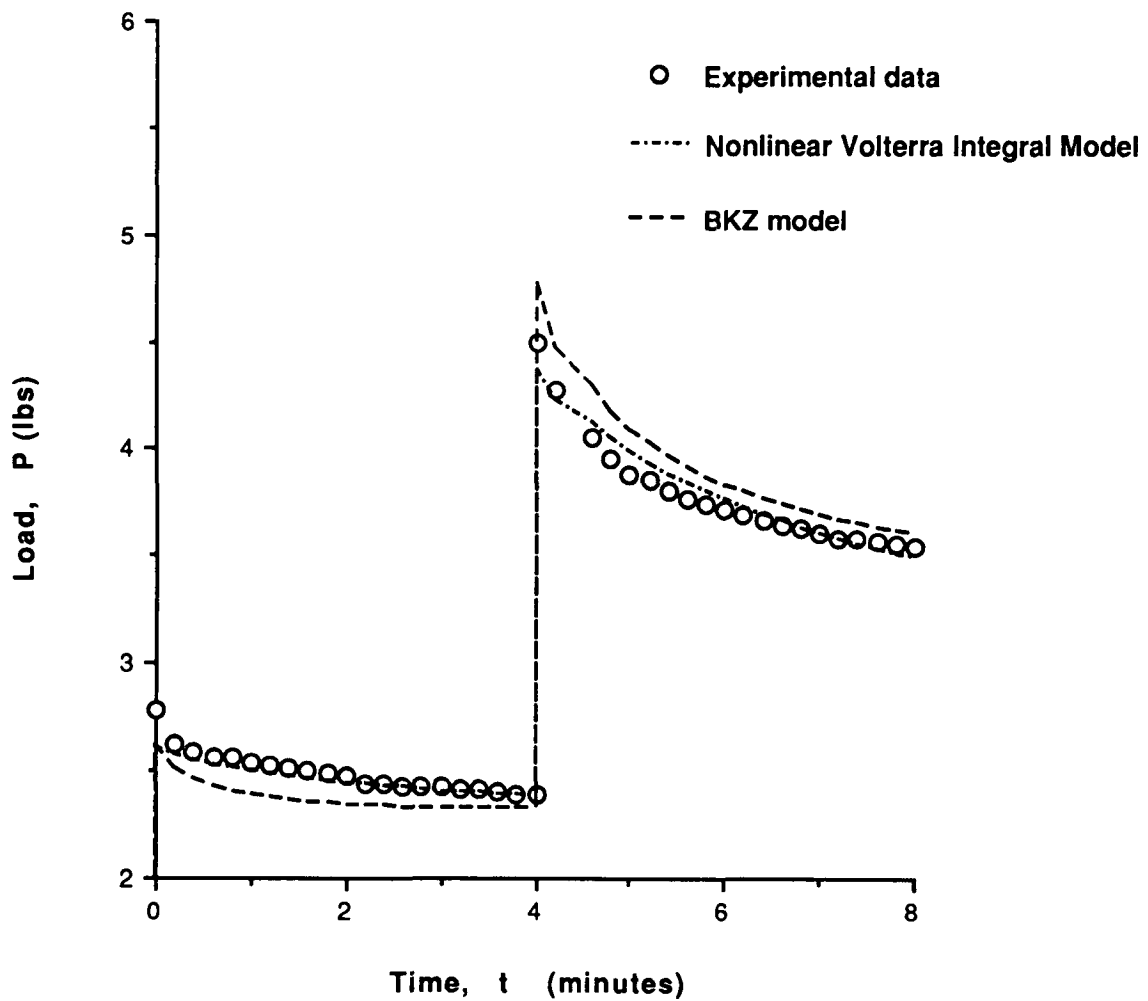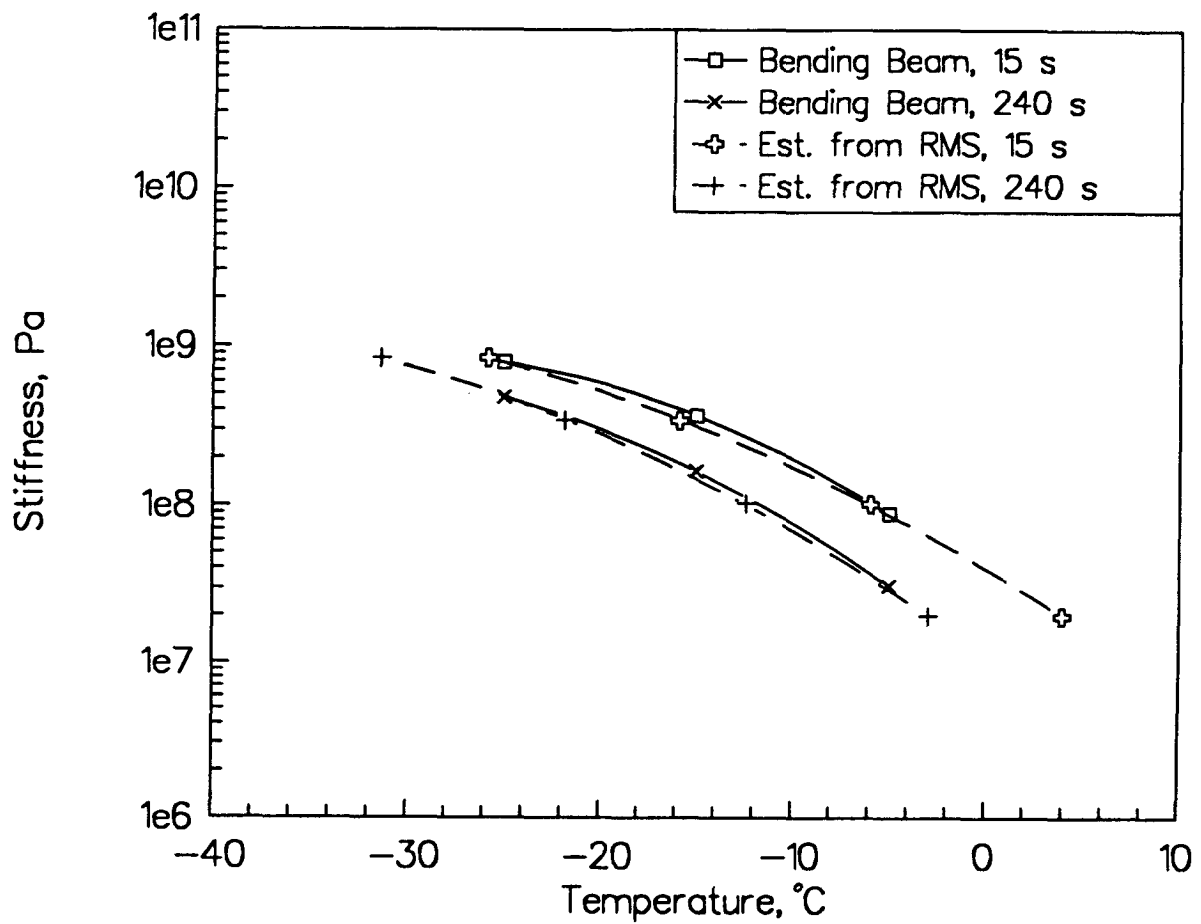
Figure 2.33   Comparison of Measured Indenter Load and Indenter Load Predicted by Nonlinear Volterra Integral and BKZ, Two-Step Loading
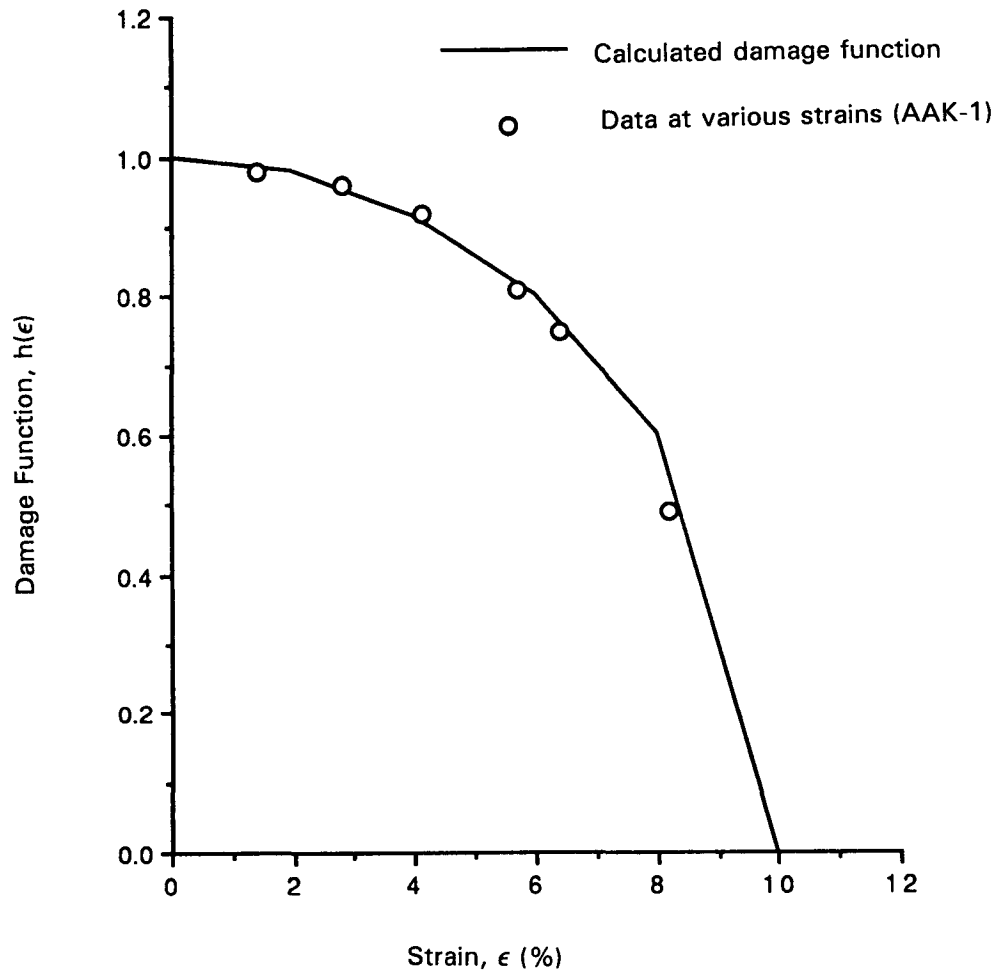
Figure 2.34   Damage Function as a Function of Strain, Asphalt AAK-1
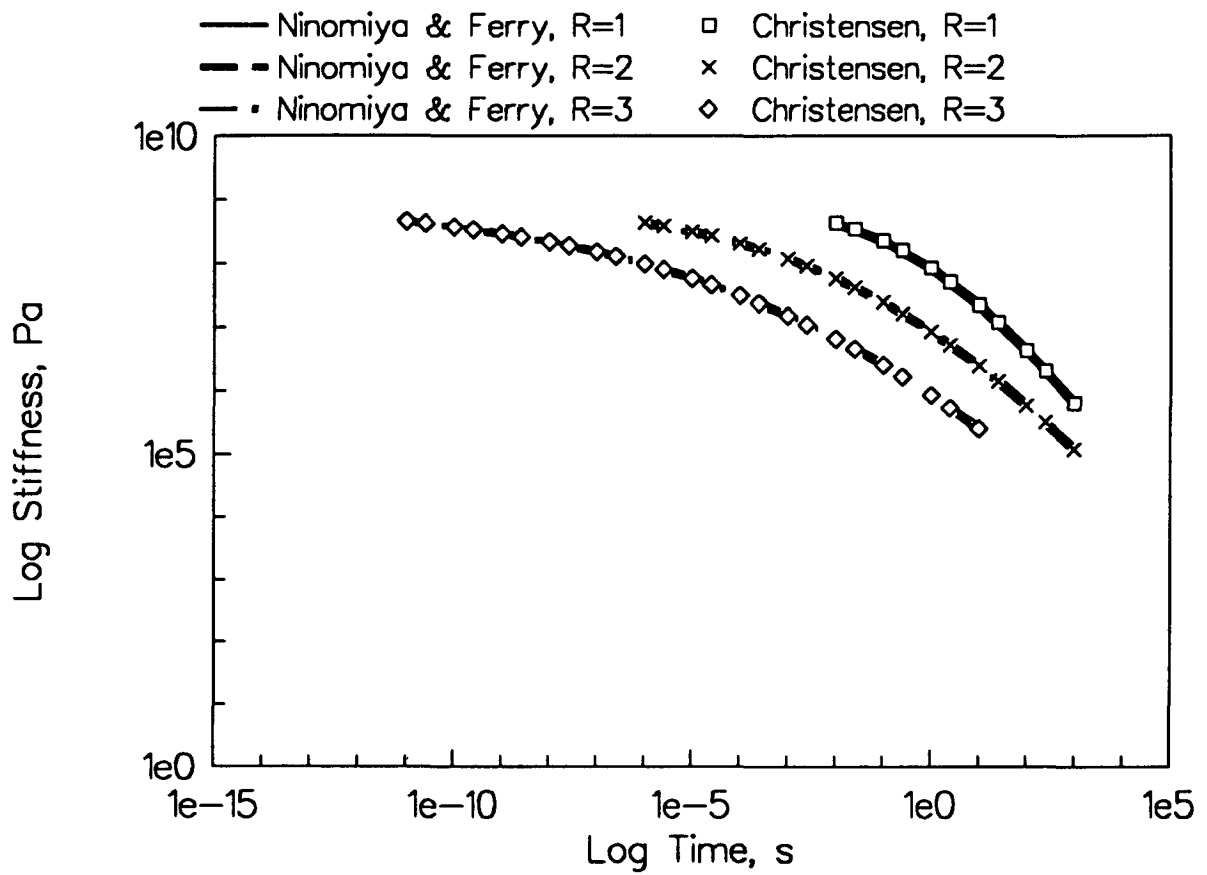
Figure 2.35 Creep Stiffness Estimated Using Ninomiya and Ferry's Approximation and Estimated from Equation 2.11

Figure 2.36 Creep Stiffness at 15 and 240 Seconds, Estimated from Dynamic Data and as Measured Using the Bending Beam Rheometer for Asphalt AAA-1 (Tank)
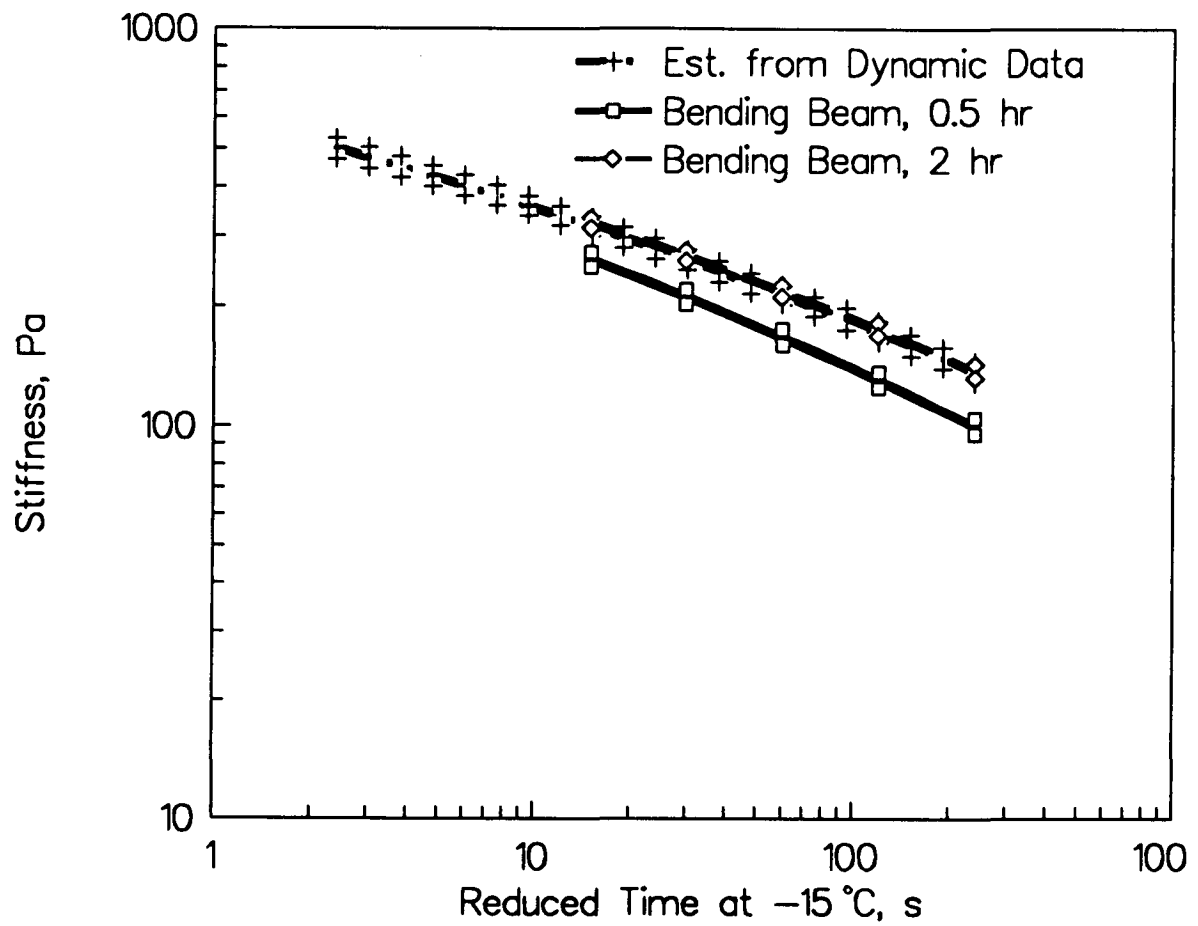
Figure 2.37 Creep Stiffness at 15 and 240 Seconds, Estimated from Dynamic Data and as Measured Using the Bending Rheometer for Asphalt AAM-1 (TFOT Residue)

119
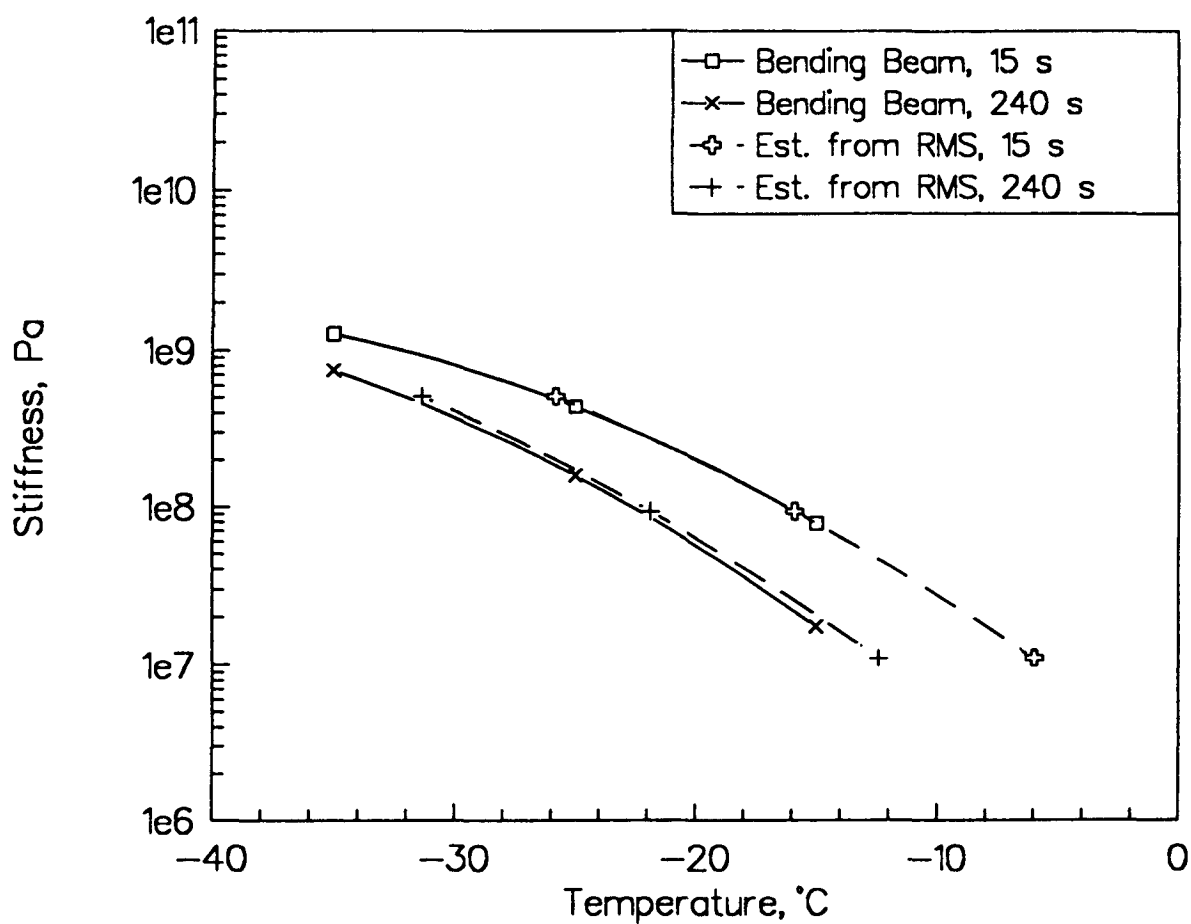
Figure 2.38 Creep Stiffness at −15°C, Estimated from Dynamic Data and as Measured Using the Bending Beam Rheometer for Asphalt AAM-1 (Tank)

Table 2.1   Approximate Temperature and Moduli Ranges for Geometries Used in Dynamic Mechanical Analysis of Asphalt Cement

Geometry	Typical Temperature Range, °C	Typical Modulus (G*) Range, Pa
Rectangular torsion bar	< 0	> 10^7
Parallel plates, 8-mm diameter	0 to 40	10^5 to 10^7
Parallel plates, 25-mm diameter	> 40	< 10^5

Table 2.2   Statistical Summary of Stiffness Repeatability for the Bending Beam Rheometer

Stiffness Range, MPa	Mean Stiffness, MPa	Number of Test Cells	Standard Deviation, MPa	Coefficient of Variation, percent
<0.124	71	142	1.16	1.6
0.124 to 320	211	154	5.47	2.6
320 to 620	457	146	13.7	3.0
>620	1,000	186	37.8	3.8

References

Anderson, D.A., Christensen, D.W., Dongre, R., Sharma, M.G., Runt, J., and Jordahl, P. 1990. *Asphalt Behavior at Low Service Temperatures*, FHWA-RD-88-078. McLean, Virginia: Federal Highway Administration.

Anderson, D.A., Christensen, D.W., and Bahia, H. 1992. "Physical Properties of Asphalt Cement and the Development of Performance-Related Specification," Preprint of the 204th American Chemical Society National Meeting, Division of Fuel Chemistry, vol. 37, nos. 3 and 4.

Bahia, H.U., and Anderson, D.A. 1992. "Physical Hardening of Asphalt Binders and Relation to Composition Parameters," Preprint of the 204th American Chemical Society National Meeting, Division of Fuel Chemistry, vol. 37, nos. 3 and 4.

Bernstein, B., Kearsley, E.A., and Zapas, L.J. 1963. "A Study of Stress Relaxation with Finite Strain," *Transaction of Society of Rheology*, vol. 7, p. 391–410.

Flugge, W. 1975. *Viscoelasticity*, 2nd ed. Berlin: Springer-Verlag.

Jongepier, R., and Kuilman, B. 1969. "Characterization of the Rheology of Bitumens," *Proceedings of the Association of Asphalt Paving Technologists*, vol. 38, p. 98.

Ninomiya, K., and Ferry, J.D. 1959. "Some Approximate Equations Useful in the Phenomenological Treatment of Linear Viscoelastic Data," *Journal of Colloid Science*, vol. 14, pp. 36–48.

Timoshenko, S.P., and Goodier, J.N. 1981. *Theory of Elasticity*. New York: McGraw-Hill.

Ugural, A.C., and Fenster, S.K. 1981. *Advance Strength and Applied Elasticity*. New York: Elsevier, chap. 5.

3

Low-Temperature Physical Hardening

Introduction

Before this study, the only well-documented reports of time-dependent, reversible hardening of asphalt binders was that of steric hardening, referred to within SHRP as molecular association. Steric hardening does not occur at very high temperatures because the buildup of the structure is destroyed by excess kinetic energy in the system, and does not take place at very low temperatures because the rate of association is considered slowed as a result of the high viscosity of the asphalt (Barth 1962; Brown and Sparks 1958; Petersen 1984; Traxler and Coombs 1937).

During measurement of low-temperature properties with the bending beam rheometer at Penn State University, it was clearly observed that asphalt cements undergo significant hardening at low temperatures close to or below the glass transition temperature. Further, the rate and magnitude of the physical hardening increases with decreasing temperature. An example of this hardening is shown for asphalt AAK-1 in figure 3.1.[1] The magnitude and rate of this hardening was observed to be relatively rapid and to have a significant influence on the measured rheological response. This type of hardening is believed to be similar to what is called physical aging in many amorphous solids (Struik 1978). To differentiate this phenomenon from oxidative aging, the term "physical hardening" was selected to describe this phenomenon in asphalt cement.

Physical hardening of asphalt cements has not been reported previously. A review of published research on the physical aging of other amorphous materials indicated that this phenomenon may significantly influence physical properties. Many studies have shown that mechanical properties measured without considering this phenomenon may lead to misleading conclusions and may not reflect material properties during service.

---

[1]All figures and tables referenced in this chapter appear at the end of the chapter.

Objectives of Research and Scope of Work

Physical hardening, as shown for other types of amorphous solids, may significantly change the mechanical as well as other properties of asphalt cements. Therefore, the investigation of the physical hardening phenomenon is essential for the accurate characterization of low-temperature rheology of asphalt cements, and it is important for understanding the response and performance of asphalt concrete pavements.

The main objectives of the investigation reported in this chapter were to

- Define in quantitative terms the effects of physical hardening on the flexural creep response within the linear viscoelastic (LVE) range;

- Define physical hardening rates as a function of asphalt composition, temperature level, and isothermal age;

- Investigate the effects of oxidative aging and interaction with mineral surfaces on the physical hardening trends of selected asphalt cements;

- Determine the relation between changes in the mechanical creep response and isothermal volume changes; and

- Conduct glass transition measurements to establish a relation between physical hardening and the glass transition behavior of asphalts.

The investigation concentrated on testing the eight core asphalts. Two types of testing techniques were used: the bending beam device to measure low-temperature creep response and specially designed dilatometric cells to measure isothermal volume changes and conduct glass transition measurements. The asphalts were tested after different oxidation treatments, and after mixing with two different types of mineral fillers. The testing temperatures covered the range of $-35°$ to $-5°C$ ($-31°$ to $23°F$), and the isothermal age typically varied between 30 minutes and 96 hours.

A comprehensive literature review of the physical hardening (physical aging) of other amorphous materials was first conducted. The literature review summarized in the next section was the departure point for conducting this study. Several experiments were designed to investigate the phenomenon and to understand the mechanism leading to physical hardening. The experimental work started with testing the physical hardening of unaged asphalts. The results were analyzed to define the effect of physical hardening on creep response and to identify factors affecting the hardening. Then, the oxidatively aged asphalts and filled systems were tested. After quantifying the effects of oxidative aging and interaction with mineral fillers on hardening, the volume measurement experiments were started. The volume measurements included isothermal volume changes and glass transition behavior. The results of these experiments were then used to establish relationships between volume changes and hardening as reflected in the creep measurements. Figure 3.2 depicts a flowchart that represents the work plan followed in this investigation.

124

Current State of Knowledge

The origin of the physical hardening phenomenon can best be explained by the free volume concept and the relationship between temperature and molecular mobility. The resistance to flow of liquids is a function of their molecular mobility. Therefore, flow properties of liquids are known to depend on temperature. To explain this dependency, researchers introduced the concept that mobility is a primary function of temperature. A large number of models were introduced to relate the viscosity of liquids to temperature (Doolittle 1951a). These models were, however, found by many researchers to be insufficient or too complicated to be effectively used (Doolittle 1951b). In the early 1950's, a new approach was introduced, which considered molecular mobility to depend on the relative volume of molecules present per unit of free space, i.e., "free volume." The idea was not new; it had been neglected for some time (Doolittle 1951b). The concept that molecular mobility, and therefore resistance to deformation, is a function of free volume laid the foundation for the free volume concept that is now widely accepted.

In the early 1950s Doolittle used the free volume concept to prove that if relative free volume rather than temperature were considered the primary variable controlling viscosity of liquids, satisfactory reproduction of the measured values might be obtained by the use of a relatively simple relationship (Doolittle 1951b; Doolittle and Doolittle 1957). A few years later Williams and his collaborators, studying the temperature dependence of relaxation mechanisms in amorphous polymers and other glass-forming liquids, proposed that the changes in relaxation times with temperature are not caused by thermal activation, but by thermal expansion (Williams et al. 1955). Using Doolittle's formula, which connects viscosity of fluids to free volume fraction, the authors could derive the WLF-equation, which is now widely used, to represent the temperature dependence of mechanical and other properties of numerous types of viscoelastic materials. Williams and his co-workers, in fact, concluded that the existence of a universal function for temperature dependence of different properties arises from the fact that the rates of all such processes depend on temperature primarily through their dependence on free volume. The physical basis of the free volume concept was explained using the molecular flow theory of Cohen and Turnbull (1959), which is based on the assumption that the motion of a molecule can occur only when a void exceeding some critical value is available for the molecule to move. Ferry (1980) indicated that if the translation friction coefficient introduced in the Cohen and Turnbull theory is assumed to have the same temperature dependence as that of the coefficient of viscosity, then relations proposed by Cohen and Turnbull can be reduced to viscosity-volume relations derived empirically by Doolittle (1951b).

The free volume concept has also been valuable in understanding the glass transition behavior of many types of materials. According to the free volume concept, the total volume per gram, V, of a material is considered to consist of the sum of free volume, V_f, and an occupied volume, V_o. The first is presented as holes in the order of molecular dimensions or smaller voids associated with packing irregularities, while the second includes not only the volume of molecules as represented by their van der Waals radii, but also the volume associated with vibrational motions. When a temperature change occurs, although both

volume portions change, the magnitude and rate of the change in occupied volume is very small; thus, free volume is the main contributor to volume change (Ferry 1980).

Based on the free volume concept, when an amorphous material is cooled from a high temperature far above its glass transition temperature (T_g), the molecular adjustments and therefore the collapse of free volume is rapid and of the same order of magnitude as the temperature drop. Within this region, the contraction is of a fluid-like character, α_f. As the temperature reaches T_g, however, the adjustments become slower, and if crystallization does not occur, a temperature is reached in which the collapse of free volume cannot occur within the experimental cooling time. The only residual contraction in this region is of a solid-like character, and the thermal coefficient of contraction (α_g) is only slightly larger than or equal to the occupied volume coefficient of contraction, α_o. To a first approximation, the structural state at $T_g(t)$ is frozen in, and because of the decrease in thermal energy, the structural state at temperatures below T_g deviates from the equilibrium state. Therefore, T_g is not an equilibrium transition in the thermodynamic sense; but it originates from kinetic limitations on the rates of internal adjustments occasioned by changes in temperature. For this reason, it is accepted that T_g is a function of the time scale of the volumetric experiment, and many scientists suggest that it cannot be considered a true second-order transition (Kauzmann 1948; McKenna 1988).

The consequences of the existence of such a metastable structural state near or below T_g is slow, time-dependent structural relaxation processes driven by the bias in internal energy, which induce changes in different material properties. These time-dependent changes are referred to as the physical aging or isothermal aging of amorphous materials.

Physical aging is not a new phenomenon; as early as 1921 Vogel reported on the large increase in viscosity and the temperature derivatives of viscosity in glasses at temperatures below T_g (Kovacs et al. 1963). Numerous works came later during the following decades, and a great variety of materials ranging from metals to foods were investigated (Struik 1978). All types of mechanical properties, electrical properties, and volume were characterized for changes with isothermal time. The results of these investigations proved that physical aging is a general phenomenon that is a basic feature of the glassy state. These investigations also proved that physical aging is an important phenomenon and its consequences, which will be reviewed in a later section, have vital implications on the behavior within the application conditions of many materials.

Paving-grade asphalts are viscoelastic materials that exhibit the glass transition behavior. They are among the very few materials whose physical aging characteristics have not yet been studied. They have been shown in numerous studies to exhibit glass transition behavior similar to many amorphous solids (Wada and Hirose 1960; Schmidt and Santucci 1966; Traxler and Schweyer 1936; Barrall et al. 1964; Schweyer 1974). The results of these studies give sufficient evidence that asphalt binders exhibit two thermal coefficients of expansion: a coefficient above T_g that is characteristic of a fluid-like material, and a coefficient below T_g, which is one-half to one-third the first and is characteristic of a glass-like material. The low value of the coefficient below T_g reflects the effect of reduced molecular mobility as the asphalt is cooled through the glass transition region. The reported

glass transition behavior of asphalt cements suggests that asphalts may undergo physical hardening similar to other types of amorphous solids.

Influence of Physical Hardening on Asphalt Rheology

To evaluate the influence of physical hardening on asphalt rheology, the bending beam rheometer was used to measure the changes in flexural creep response with storage at low temperatures. The creep tests were carried out at five different temperatures; $-35°$, $-25°$, $-15°$, $-10°$, and $-5°C$ ($-31°$, $-13°$, $5°$, $14°$, and $23°F$), and the storage times varied typically between 30 minutes and 96 hours. The temperatures were selected to cover the range that is normally encountered in the field. The storage times were selected mainly for practical purposes, but for some asphalts the storage continued much longer in order to investigate long-term hardening behavior. The experiments were designed to define the nature of the effect on rheological response and to investigate the roles that temperature level, isothermal time, and asphalt source play in the hardening phenomenon.

Hardening Shift Described

During the early tests the reduction in creep deflection was clearly not the same at all loading times. There was also a reduction in the creep rate. An example is shown in figure 3.3 for one of the study asphalts. The variation in stiffness ratio (aging index) with loading time indicates that a single ratio at a selected loading time is not suitable to represent the effect of hardening. It also indicates that a parameter that describes change in creep rate with storage time is needed.

For other materials, physical hardening has been found to influence rheological response, within the LVE range, in a manner similar to the influence of decreasing temperature. The influence could be defined by a one-dimensional shift of the rheological spectrum along the loading-time scale. The effect of hardening on asphalts tested in this study was found to comply with this behavior. The results for the study asphalts at the different temperatures were all found to comply with that behavior.

An example of the shift procedure is shown in figures 3.4 and 3.5 for asphalt AAF-1. Figure 3.4 depicts the unshifted creep curves; figure 3.5 depicts the shifted data. The data in the figures are for $-15°C$ ($5°F$) temperature and for several isothermal ages extending up to 4 months. Clearly, shifting the creep curves along the logarithmic loading time scale resulted in the formation of a single curve. Essentially, the superposition of the curves in figure 3.5 indicates that physical hardening does not affect the shape of the creep master curve. The constancy of the master curve shape, which is a reflection of the retardation spectrum, indicates that physical hardening increased all retardation times by the same amount. As more data were collected, the shift along the loading-time scale was further observed to give very good superposition of the creep curves for all types of asphalts and at the different test temperatures.

More was done to evaluate the suitability of using the shifting along the loading-time scale to describe hardening. The typical measured response was for only 240 seconds loading time, which may not have been long enough to test the validity of the shifting procedure. Therefore, creep tests were run for longer loading times to verify this behavior over a wider range of loading times. Figure 3.6 depicts creep tests of 3 hours loading time for one asphalt that was aged for only 30 minutes and for the same asphalt after being stored for 16 days at −15°C (5°F). The result of shifting the 2-hour-age response to superimpose the 16-day-age response is also shown in the figure. The results again proved that the shifting technique results in excellent superposition. Furthermore, statistical procedures were used to estimate the hardening shift factors and to evaluate the shifting procedure. The procedure followed was to define the shape of a reference creep master curve for each asphalt, and then allow the statistical routine to determine the least square estimates of the loading-time shifts required to superimpose the curves measured at different isothermal ages on the reference master curve. In other words, the statistical routine was used to fit all the measured data for each asphalt, to a single master curve by allowing only shifting along the loading time scale. The results for all study asphalts showed good fit, indicating the appropriateness of the procedure. Table 3.1 lists examples of the results obtained using the SAS package to estimate the isothermal time shifts. The isothermal time shifts of the eight study asphalts are shown at different temperatures and for different isothermal ages. The success of the procedure and the appropriateness of using the isothermal time shifts can be seen in the high adjusted R^2 values and the relatively small standard error of the estimated isothermal shifts.

The results of the above analyses were considered sufficient to prove the hypothesis that physical hardening of asphalt cements can be successfully defined by shift along the loading-time scale. No results were observed that indicate hardening causes any important changes in the shape of the creep master curve, or that a two-dimensional shifting is needed to describe the effect of hardening on the response. The results also suggest that since physical hardening affects the LVE creep response in the same manner as temperature, then hardening should be related to isothermal volume changes. This subject will be discussed further in a following section that presents results of the isothermal volume measurements.

The shift factors used to represent the effects of hardening, in order to differentiate them from temperature shift factors, will be called here the "isothermal time shifts," (a_{ti}), and they will be used to analyze the effects of the different controlled variables considered in the study.

Hardening Rates with Age and the Influence of Temperature Level

To successfully characterize the hardening behavior of any asphalt, two aspects had to be addressed: (1) the rate of hardening as a function of isothermal age (t_i) and (2) the effect of test temperature (T) on the hardening levels. The isothermal time shifts (a_{ti}), similarly to temperature shifts (a_T), have to be taken relative to some reference. Instead of a reference temperature, physical hardening is taken with reference to an isothermal reference age (time). In this study all hardening shift factors are taken relative to a t_i of 2 hours. This reference time was selected for experimental convenience. A shorter time is inappropriate because

hardening is rapid, response is sensitive to minor time variations, and a longer time is impractical.

Figure 3.7 depicts the isothermal shifts as a function of time for asphalt AAM-1 at five different temperatures. Clearly, the hardening is very fast at early ages but the rate decreases rapidly with age. This behavior, which was also observed for all other study asphalts, is similar to the behavior reported for other materials that exhibit similar types of hardening (Struik 1978). For those materials the convention has been to plot the isothermal shifts as a function of the logarithmic time scale. Using the same convention, a logarithmic plot of isothermal shifts is shown in figure 3.8. Unlike many other materials in which the rate of hardening has been observed to stay constant for a long aging time, the plots for the tested asphalt show that the rate decreases with logarithmic age, especially at higher temperatures. The plots also show that the hardening does not reach a limiting value within the time limits of the experiment.

The other important observation concerns the effect of isothermal storage temperature. The plots show that the hardening rates and levels are strong functions of temperature; the lower the temperature, the higher the rate of hardening.

The above observations were found to be true for all asphalts tested. This finding indicates that in order to adequately describe the physical hardening of paving grade asphalts, the hardening rates as a function of both temperature level and isothermal age have to be characterized.

The behavior of the asphalts show some deviations from the behavior of other materials as reported by several researchers. Struik (1978) and others have reported that the rate of hardening for a variety of materials is invariant with logarithmic isothermal age for very prolonged ages, and that the rates are approximately constant along a wide range of temperature levels. Struik also reported that the rate of hardening, as measured by the isothermal shift (log a_{ti}) divided by the logarithmic isothermal age, is close to unity. The anomalous behavior of asphalts may be explained here by the fact that the present measurements are made within the vicinity of the glass transition temperatures of the asphalt cements (values of T_g for asphalts are presented in a later section). Within the transition region, the rate of hardening for all materials has been found to be sensitive to temperature; the lower the temperature, the higher the hardening rate (Struik 1978).

The results indicate that within the temperature range covered, the rate of hardening is rapid at early isothermal ages but tends to decrease significantly with increasing age. The results also indicate that hardening trends are significantly affected by temperature level.

Influence of Asphalt Source

The study asphalts show wide differences in their compositional or chemical properties. For many other materials, previous work has shown that the nature of the material may play only a minor role in the kinetics of physical hardening (Struik 1978). The hardening behavior

observed for the study asphalts, however, indicates that asphalt cements vary widely in their hardening behavior and that hardening kinetics is a function of the source of the asphalt.

Figure 3.9 depicts the hardening rates as a function of isothermal age of the eight asphalts at −15°C (5°F). Clearly, there are significant differences between the asphalts. At this temperature asphalt AAM-1 shows the most hardening while AAG-1 shows the least hardening. If the chemical properties reported earlier in this report are examined, some interesting trends can be observed. For example, AAG-1 has one of the lowest molecular weights, while AAM-1 shows the highest value. Although some general trends were observed between certain compositional properties and the relative hardening rates of the asphalts, no single parameter could be found that is highly correlated with the relative hardening rates. The lack of a direct relation between the hardening trends and the compositional parameters is probably attributable to the complex nature of the molecular structure of asphalt cements, and to the difficulty of characterizing that structure with conventional chemical tests. The differences between asphalts were also found to stay significant at all other testing temperatures. Figures 3.10 and 3.11 depict the hardening rates at two other testing temperatures. The figures clearly indicate that hardening is highly asphalt specific at all temperatures, and that the hardening rates and levels for each asphalt are highly dependent on the temperature level.

Effect of Thermal History

As a newly observed phenomenon for asphalt cement, the effect of several specimen conditioning factors had to be studied to ensure that the testing procedure used did not result in some apparent behavior that did not reflect the true asphalt hardening. The factors selected included the effect of cooling rate, the effect of mechanical working, and the effect of the cooling liquid used in the refrigeration bath.

Effect of Cooling Rate

The cooling rate was important because in the field pavements do not cool instantaneously as do those used in this study. To investigate the effect, specimens were cooled from 25°C (77°F) to −15°C (5°F) at two different cooling rates—3°C (5.4°F) per hour and 10°C (18°F) per hour. After reaching the test temperature, the hardening measurements were taken at several isothermal ages. Figure 3.12 depicts the hardening of asphalt AAM-1 after the slow cooling treatment. Comparing the response of this specimen with that of a specimen that was quenched (see figure 3.1), two observations can be made. First, slow cooling affects only the early response. This effect is expected because the asphalt hardens while it is cooled. Second, the hardening rate proceeds at a rate similar to the quenched sample. The results of the slow cooling indicated that the observed hardening is not an artifact of the quenching operation. This finding agrees with results reported for other polymeric materials (Struik 1978).

130

Effect of Mechanical Working

It was also important to study the effect of mechanical working on the sample because the same specimens were repeatedly tested in this study. The concern was that the repeated testing, although limited to very small strains, might result in an apparent reduction of the hardening level. Also, asphalts in field pavements are subjected to continuous traffic; if mechanical working reduces this type of physical hardening, then this factor has to be evaluated. To evaluate the effect, two asphalt specimens were tested. The first was tested at certain isothermal ages while the specimen was kept unloaded between the tests. The second specimen, on the other hand, was continuously subjected to a repeated angular strain of 1 percent at a frequency of 1 rad/s. A dynamic mechanical analyzer (RMS 800) was used to run the tests using the parallel plate fixtures. The frequency of 1 rad/s was selected to simulate traffic loading. The comparison of the hardening shift factors is shown in figure 3.13. The results clearly indicate that physical hardening is not affected by such small-strain continuous mechanical working. Other testing was also done using the bending beam rheometer in which different specimens were tested at different isothermal ages and the hardening was compared with that of a repeatedly tested specimen. The results confirmed the finding that the effect of mechanical working within the small strain level is negligible.

Dry versus Wet Cooling

In order to evaluate the effect of the fluid used in the refrigeration bath, the hardening of a specimen cooled in the bath was compared with that of a specimen that was dry-cooled in a freezer at the same temperature. The procedure of testing was that the beam specimens were transferred from the dry freezing unit to the testing bath only at the time of testing. The results of the wet and dry storage hardening are shown in figure 3.14. The difference is negligible and therefore it was concluded that the fluid had not affected the hardening level.

Effect of Thermal Cycling

Thermal cycling effects were investigated in several limited experiments. The first was conducted to study the reversibility of hardening when heating to temperatures above the glass transition region. Four specimens of asphalt AAK-1 were poured and left to cool to room temperature. The specimens were then demolded and quenched to $-15\,°C$ ($5\,°F$) and tested after one hour in the testing bath. The specimens were then taken out, returned to the molds and stored in chambers maintained at four different temperatures—$40\,°$, $25\,°$, $10\,°$, and $-5\,°C$ ($104\,°$, $77\,°$, $50\,°$, and $23\,°F$). The demolding, quenching to $-15\,°C$ ($5\,°F$), and testing after one-hour storage at $-15\,°C$ ($5\,°F$) was repeated after 3 hours, 24 hours and 72 hours. The results are shown in figure 3.15; only the specimen stored at $-5\,°C$ ($23\,°F$) showed a steady increase in stiffness while the other specimens gave the same stiffness. After the 72-hour tests, the four specimens were left in the bath for an additional 48 hours and tested repeatedly at different intervals. All specimens showed an increase in stiffness, and after 48 hours all specimens showed approximately the same stiffness level. At that time (120 hours since the beginning of the experiment), the specimens were again taken out and transferred to

the chambers at the four storage temperatures. They were kept there for 72 hours, then taken out, brought back to −15°C (5°F) and tested after 1 hour at test temperature. All specimens, except for the one stored at −5°C (23°F), showed low stiffness values that were close to the unaged values. In other words, the hardening was lost. For the specimens stored at −5°C (23°F), the hardening was not lost and the stiffness stayed at the low temperature. The specimens were then left in the testing bath and tested repeatedly at different intervals for up to 72 additional hours. The specimens started a new hardening cycle and the stiffness increased continuously.

The results of the experiment as shown in figure 3.15 reflected the reversibility of the hardening when the asphalt is heated to certain temperatures. For all specimens, except the one stored at −5°C (23°F), the original properties were recovered after heating the specimen for only few hours. The specimen stored at −5°C (23°F) did not lose the hardening because it appears that this temperature is close to the glass transition region. Therefore, the hardening was maintained throughout the testing period of more than 12 days.

The reversibility of hardening was also checked in another experiment with another asphalt. Figure 3.16 includes the results in terms of hardening shift factor. In this experiment, asphalt AAM-1 was used and the temperatures included −25°, −15°, −5°, 10°, 25°, and 40°C (−13°, 5°, 23°, 50°, 77°, and 104°F). The testing this time was done at −5°C (23°F). The data in figure 3.16 clearly reveal that the specimens stored at −5°C (23°F) and lower did not lose the hardening, while the others showed the reversal cycle of hardening.

The third experiment was on the effect of cycling between temperatures below the glass transition temperatures. The objective was to explore whether asphalts exhibit the asymmetrical hardening behavior reported for other amorphous polymers. The thermal treatment followed was to quench the specimens to −35°C (−31°F) and measure the hardening for 120 hours. Then the specimen was rapidly heated to −15°C (5°F) and held there for another 96 days while the hardening being measured at the latter temperature. Figure 3.17 shows the results that indicate some interesting behavior. Although significant hardening was observed at −35°C (−31°F), when the specimen was heated to −15°C (5°F) it lost all the hardening. The response was similar to the response of a specimen cooled for the first time from room temperature. This behavior is not unique for asphalts. Similar behaviors are known for many materials that exhibit the hardening phenomenon. The explanation is related to the tendency toward accelerated recovery of equilibrium volume when the material is heated from temperatures far below the glass transition temperature. Several asphalts were tested for this behavior and the cycling was done for different temperature steps. The trends indicated that the degree of recovery depends on asphalt type, temperature difference, and proximity of temperature region of cycling to the glass transition zone.

Constructing Master Curves for Physical Hardening

In a previous section physical hardening was shown to be asphalt specific, to depend on the temperature at which the material is isothermally stored, and to have a rate that decreases

rapidly with isothermal time. From a practical point of view, it is difficult to test at all ages and all temperatures to obtain a generalized characterization of the hardening potential of an asphalt. Therefore, a model that involves few parameters and requires fewer tests is needed to predict hardening at different temperatures and ages. In this section concepts used to model the isothermal volume contraction of other materials are used to develop a simplified hardening model for asphalts. The model is based on the free volume concept and uses the method of reduced variables to construct isothermal shift master curves.

In the literature of glass-forming materials, many models have been developed to describe isothermal volume recovery (reduction with time) of a wide range of glasses. Although little work has been done to extend these models so as to estimate changes in mechanical response, the concepts on which the volume models were based are very useful in modeling the effect of hardening on mechanical response. One widely accepted model is the Kovacs, Aklonis, Hutchinson, Ramos (KAHR) model, which assumes that, under isobaric conditions volume recovery depends on two main factors: (1) temperature and (2) the departure of the material state from equilibrium (Kovacs et al. 1979). In the KAHR model these dependencies are expressed in a manner equivalent to the time-temperature superposition principle of viscoelastic theory—the method of reduced variable. The model is based on the following assumptions: (1) that there is a continuous distribution of retardation times involved in the isothermal volume reduction process; (2) that a change in temperature, or a change in the structural state, will change each retardation time by the same amount (the shape of the retardation time spectrum is not changed); and (3) that the amount of shift because of a change in temperature is independent of the change in structural state, i.e., the two effects are uncoupled.

Taking the above concepts into consideration, and assuming that the hardening shift is highly correlated with volume recovery, it was logical to hypothesize that the method of reduced variables should be appropriate to construct master curves for the isothermal shift factors. The master curves should combine the isothermal shift factors measured at different temperatures and reflect the change in hardening with reduced isothermal time.

The concept is explained in the schematic plots of figure 3.18. The creep curves are first shifted as shown in plot 3.18a to calculate the isothermal shift factors, $\log(a_{ti})$, at different temperatures. The isothermal shifts are then used to plot isothermal shift functions (as a function of isothermal age) for the different test temperatures, T_1 and T_2 in Plot 3.18b. The isothermal shift curves are then shifted along both scales to construct a hardening master curve as shown in Plot 3.18c. The hardening master curve together with the shift functions, β_E and a_T, can be used to predict the effect of isothermal hardening on response by defining the location of the creep curve at any selected isothermal age and any temperature, relative to the reference temperature and reference isothermal time.

An example of the isothermal shift curves at different temperatures for asphalt AAM-1 is shown in figure 3.7. The isothermal shifts in the figure were all obtained relative to the creep response at $-15\,^{\circ}C$ ($5\,^{\circ}F$) at an isothermal age of two hours. To construct master curves, the individual curves have to be shifted with respect to the isothermal shift scale (vertical axes in the figure), and the isothermal age scale (horizontal axes in the figure). The age shift reflects the effect of temperature; i.e., the rate of hardening at a temperature lower

than the reference temperature is equivalent to the rate of hardening at the reference temperature but at a shorter isothermal time. This situation is analogous to a mechanical creep test with the temperature as the stimulant instead of load in mechanical creep. To select age shift factors, it was assumed that the temperature shift factors calculated from mechanical creep are suitable to shift the data. The assumption is logical because the temperature shift factors should apply to all modes of loading including volumetric creep; the only difference here is that the loading mode used is thermal rather than mechanical. Using the temperature shift factors the hardening curves in figure 3.7 are shifted as shown in figure 3.19. To superimpose the hardening curves, the data need to be shifted along the isothermal shift scale (vertical scale in the figure). This shift is necessary to reflect the dependency of the hardening rate on the departure from thermodynamic equilibrium; in other words, it is dependent upon the departure from equilibrium as caused by the temperature jump that has been applied. This dependency is analogous to that in mechanical creep tests in which the deflection is normalized by dividing by the load applied and using the compliance to construct master curves. In the case of hardening the load, the temperature jump is used. To estimate the required equilibrium shifts, (β_E), a function that describes the master curve had to be chosen to represent the hardening master curve. Thinking in terms of volumetric creep, an exponential function describing a Voigt-Kelvin model was used. The relation used is as follows:

$$\log a_{ti} = \beta_E + \beta_o \{ \exp(\log(t_o)/\beta_1) - \exp(t_r/\beta_1) \} \qquad (3.1)$$

where

$a_{ti} =$ isothermal time shift factor relative to reference temperature and isothermal time

$\beta_E =$ equilibrium shift (shift along isothermal shift scale) as a function of temperature reflecting the initial departure from the thermodynamic equilibrium state. It also reflects the magnitude of the temperature change applied.

$\beta_o =$ regression constant equivalent to the spring constant (D) in a Voigt-Kelvin model constitutive equation.

$t_o =$ the reference isothermal age; in the present study it was always taken as 2 hours at $-15°C$ (5°F). The choice is arbitrary but it is in the middle range of temperatures chosen and it is the selected reference temperature for creep data reduction.

$\beta_1 =$ regression constant equivalent to the retardation time (η/D) in a Voigt-Kelvin model constitutive relation.

$t_r =$ $\log(t) + 0.183(T - T_o)$; this variable is the reduced isothermal age relative to the reference age t_o. (t) is the isothermal age at temperature T while T_o is the reference temperature (in the present case it is $-15°C$).

Nonlinear regression was used to fit the data to the exponential function and to estimate the equilibrium shifts for all eight study asphalts. The estimated vertical shifts are shown in figure 3.20 for the eight asphalts. It is interesting to see that the shifts for each asphalt produce a simple curve with respect to temperature. The simple continuous shift curves indicate that the procedure is rational and has certain merits. The goodness of fit, with allowance for equilibrium (vertical) shifts, was very high; the R-squared values and the

134

parameters of the function are listed in table 3.2. The fitted functions for two of the study asphalts are shown in figure 3.21. As shown in table 3.2, the functions include only two parameters, or in other words, only one retardation time for thermodynamic equilibrium volume recovery is considered. The fit looks good for all asphalts, indicating there is probably no need to consider a multiplicity of retardation times.

To develop a hardening prediction model, the equilibrium shift curves have to be modeled. The following exponential function was chosen to represent the shift curves:

$$\beta_E = C_o \{ \exp(T/C_1) - \exp(T_o/C_1) \}$$ (3.2)

where

C_o and C_1 = regression constants,
T = temperature of measurement, and
T_o = reference temperature.

A good fit was observed for the study asphalts. Introducing these shift functions into the statistical regression procedure resulted in new estimates of the shift function parameters (C_o and C_1), and the hardening function parameters (β_o and β_1). Although the model prediction was observed to be highly reliable, the parameters C_o and C_1 were very difficult to obtain. Therefore, a relation with other simply measured parameters was sought. Interestingly, the two parameters were found to be highly correlated with the hardening function parameters. C_o showed a linear correlation with β_o while C_1 showed a linear correlation with β_1. The linear correlation coefficients were estimated using the data for the eight asphalts with both replicates. The best estimates were found to be as follows:

$$C_o = 0.726*\beta_o, \text{ and}$$ (3.3)

$$C_1 = -6.211* \beta_1.$$

Using these correlations, the exponential prediction model was used again to get the best least square estimate of β_o and β_1. The results of this analysis are shown in table 3.3 for the eight study asphalts. Except for asphalt AAG-1, the R-squared values are all above 95%. For asphalt AAG-1, the isothermal time shift values are small, and there is a large variation between replicates. The large variation is believed to be the source of the reduced R-square value. The final form of the prediction model is as follows:

$$a_{ti} = \beta_E + \beta_o \{ \exp(\log(t_o)/\beta_1) - \exp(t_r/\beta_1) \},$$ (3.4)

$$\beta_E = C_o \{ \exp(T/C_1) - \exp(T_o/C_1) \}$$

where

t_r = $\log(t) + 0.183(T - T_o)$,
C_o = $0.726*\beta_o$, and
C_1 = $-6.211* \beta_1$.

All other variables are as defined before, and the final estimated parameters are listed in table 3.3. The fitted models were used to plot the hardening functions for the study asphalts in figure 3.22. The master curves in the figure are plotted for a reference temperature of $-15°C$ ($5°F$) and a reference isothermal time of two hours.

To investigate the accuracy of the prediction model, data for all asphalts were used to estimate the residuals and to look at the appropriateness of the regression model. Figures 3.23 through 3.27 depict the residual plots versus predicted hardening shift factors, isothermal time shifts, isothermal age, temperature of aging, and asphalt type, respectively. No systematic patterns of variation with any of the measured variables are apparent. Therefore, the model appears appropriate within the limits of data collected. The average residual value for each asphalt is listed in table 3.3 together with the standard deviation of the residuals.

The equivalent variation in terms of temperature is useful in order to give an idea about the prediction power of the developed model. As mentioned earlier, the average temperature shift for all asphalts is estimated at 0.183 log(s)/$°C$ (0.1 log(s)/$°F$) within the temperature range of the tests. Taking this into consideration, the maximum standard deviation of the residual is calculated to be within 0.75 $°C$ (1.4$°F$), a level of accuracy believed to be adequate for practical purposes.

The model is obviously a phenomenological model that is good within the limits of the experiment conducted. It certainly needs to be verified for additional asphalts before any generalizations can be made. However, it is useful in providing parameters that give a general characterization of the hardening behavior irrespective of the temperature level. The model includes only two parameters that need to be defined for each asphalt. The parameters can be obtained with reduced amount of testing which may involve only a few isothermal ages at one or two temperatures.

No attempts were made to define the best testing protocol to estimate the model parameters or to study the sensitivity of the parameters to testing conditions. However, the model is believed to serve as a starting point to model physical hardening of asphalt and as a model that can be used in a pavement response model. The other weakness of the model is that it does not include the behavior of thermal cycling which has been observed to be complicated for other materials. Certainly, more work should be done to modify this model and establish its reliability in predicting physical hardening.

Validation of Free Volume Collapse as the Hardening Mechanism

In an effort to explain the hardening phenomenon and investigate its mechanism, two types of volume measurement studies were conducted: (1) isothermal volume contraction measurements and (2) glass transition temperature, T_g, measurements. In the first, the volume contraction of an asphalt specimen was measured continuously with time at a constant temperature. In the second, the change of volume of an asphalt specimen as a result of

136

changing temperature at a constant rate was measured to obtain T_g and the thermal coefficients of expansion/contraction above and below T_g.

Volume Measuring System

In both studies, specimen disks of asphalt, 7.6 mm (0.3-inch) thick by 40.6 mm (1.6-inch) in diameter were used. The volume changes were measured using methanol-filled dilatometers equipped with high precision glass capillary bores. The isothermal volume measurements were made in the same circulating bath used for the bending beam measurements, while the T_g measurements were made in a specially designed controlled temperature bath.

The dilatometers consisted of an aluminum cell connected to a precision bore capillary tube which was open to the atmosphere at its top end. To ensure no air bubbles are entrapped in the dilatometers, the asphalt disk was placed in the cell, and the dilatometer was assembled, inside a container filled with specification grade methanol. After the assembly of each cell, the cell was checked to be tightly sealed by applying pressure using a syringe connected to the top end of the capillary tube through a plastic tube. The height of methanol in the capillary tube was observed and recorded to the nearest 0.5 mm (0.02 in.) in both types of measurements. Since volume measurements are known to be affected by many factors, several precautionary steps were taken to ensure accuracy and precision of the measurements. These precautions are discussed in the next two sections.

Isothermal Volume Measurements

After several exploratory tests, it was observed that isothermal volume measurements for the specimen size used are very small and sensitive to many external factors such as temperature level, barometric pressure and evaporation of the methanol. Therefore, several precautions were taken to ensure accuracy of the data collected. The capillary tubes used were high precision bore diameter that are usually used for construction of capillary viscometer. The tubes were all with bore diameter of 0.54 mm ($\pm$ 0.01 mm) (0.02 in. $\pm$ 0.0004 in.), and were checked thoroughly for uniformity of bore diameter with length. The temperature during the measurements was controlled through the circulating bath temperature controller, which has a control accuracy of $\pm$ 0.03°C (0.05°F) within the range of testing temperatures. To check for changes in capillary height due to methanol evaporation, water vapor condensation, or variation in barometric pressure, each series of tests included a reference cell identical to the cells charged with asphalt specimens but which contains an aluminum disk of the same dimensions as the asphalt disk. The height in the capillary tube of the reference cell was always recorded and any changes were taken into consideration when calculating the net volume contraction of the asphalt specimens. In addition, the isothermal volume changes were always done in four replicates to ensure that no artifacts had affected the measurements. Although after taking these precautions, the measurements showed good repeatability, the use of the reference cell, and running the measurements in four replicates was continued throughout the testing program.

T_g Measurements

The dilatometric cells were filled with specification grade methanol which has a thermal coefficient of volume change approximately double that of asphalts. Also the parts of the dilatometric cell will definitely contribute to the change in capillary height taken as the measure for asphalt specimen volume change. Therefore, it was necessary to accurately calibrate each cell used for T_g measurements of asphalts so that the net volume change of asphalt specimen can be accurately calculated. To achieve the required calibration, each dilatometric cell was charged with an aluminum disk identical in size with the asphalt specimen and the change in capillary height was measured with temperature change to obtain a calibration chart for each cell. Since the aluminum disk has a thermal coefficient of volume change that is approximately two orders of magnitude less than that of the asphalt, the calibration chart of each cell was considered to give the net change in volume due to changes of the volume of methanol and any changes in cell dimensions as the temperature is lowered, or raised, at the specified rate. By subtracting this volume change from the volume change obtained during testing the asphalt specimens, the net change in asphalt volume could be calculated.

The rate of temperature change selected for conducting the T_g measurements was always 1°C/min (1.8°F/min) during cooling and heating ramps. It is known that T_g measurements for asphalts and other amorphous polymers is a function of the time scale of the experiment (Schmidt and Santucci 1966, Jones et al. 1968; Ferry 1980). However, the variation of T_g with cooling rate has been reported to be very small and on the order of only 3°C (5.4°F) for a tenfold change in the cooling rate (Ferry 1980; Schmidt et al. 1965; McKenna 1988). For asphalt cements, cooling rates ranging from 2°C/min (3.6°F/min) to less than 0.1°C/min (0.18°F/min) have been used (Jones et al. 1968). For this study, a slow rate was desired to reduce any effects due to temperature lag between the surface and center of the asphalt sample. The rate of 1°C/min (1.8°F/min) was selected as the lowest practical rate that would provide a reasonable time schedule for the experiment.

To ensure very accurate temperature measurements, a high precision digital thermometer with readout capability of 0.1 °F was used. The temperature measurements were made using a type T immersion thermocouple calibrated with the digital thermometer according to procedures recommended by the National Institute of Standards and Technology. The thermocouple was placed in a methanol-filled dilatometric cell identical to cells used for the asphalt specimens. The temperature-sensitive tip of the thermocouple was placed in approximately the same position as the asphalt specimen. The temperature measurement cell was placed at the center of the testing bath.

For each asphalt, the volume-temperature measurements was started by a heating ramp from a temperature of around −80°C (−112°F) up to a temperature of around 30°C (86°F). The readings of capillary height and temperature were recorded every 4 minutes. After the heating ramp was completed, the specimen was left to equilibrate for 20 minutes. Then the cooling ramp was started. The same recording rate was followed during the cooling ramp. To estimate the experimental error, measurements were made in two independent replicates.

138

(Independent replication herein means that a different specimen was used employing a different dilatometric cell.)

Isothermal Volume Experiment

The main objective of the isothermal volume change experiment was to determine if low temperature hardening is associated with volumetric shrinkage. Time-dependent isothermal volume measurements are very difficult to obtain and have to be very precise because of the small volumes being measured (Ferry 1980; Kovacs 1958). After several preliminary tests, it was observed that the measuring system developed as part of this study is sufficiently sensitive to measure the isothermal volume shrinkage with a high degree of precision.

The experiment included two parts. In the first part, the isothermal volume changes for the eight asphalts at a single temperature were measured. Since the measurements were to be compared with hardening shifts (a_{ti}) from the creep measurements, -15 °C (5°F) was chosen as the isothermal test temperature. Except for the specimen configuration, the specimen preparation was identical to the preparation of beam specimens, and continuous measurements were obtained between 30 minutes and 24 hours. Figure 3.28 depicts examples of the isothermal volume change measured for three of the study asphalts. The variability of the measurements is within reasonable limits, and these results indicate that there are significant differences between the amount and rate of isothermal volume change for the different asphalts. The shapes of the curves were observed to be simple and approximated by simple functions. To be able to estimate the amount of volume change at specific isothermal times, a simple regression model was used to fit the data for each asphalt. A second order polynomial resulted in very good fit. The polynomial is not meant to model the behavior but to serve the purpose of averaging the replicate measurements and giving a simple equation to interpolate between the measured data points. Figure 3.29 gives the fitted polynomials for the eight study asphalts. The statistical summary of the fitted polynomials for the eight asphalts at -15°C (5°F) is presented in table 3.4.

To determine the correlation between the volume changes and the hardening shifts, the same test temperature, the same isothermal age, and the same reference age had to be used for both measures. The 30-minute isothermal time was selected for both types of measurements and the shifts (log a_{30}), and volume changes ($\triangle V_{30}$), were calculated relative to that isothermal time. The results are plotted in figure 3.30. The isothermal ages included in the plot are 2, 6, and 24 hours for each asphalt. The temperature is always -15°C (5°F). The correlation is very high; R-square adjusted is 93.9 percent. Considering the amount of experimental noise expected in such measurements, the correlation is considered very good and clearly indicates that the physical hardening being observed is highly correlated with isothermal volume contraction.

To show that the observed correlation between hardening shifts (a_{ti}) and isothermal volume measurements is not accidental but related to fundamental behavior of the material, the concept of free volume and the effect of temperature on free volume of the asphalt in general, can be used. It was shown in an earlier section that the influence of hardening

resembles the effect of temperature—a simple shift of creep master curves along the loading time scale. If this finding is true, then a relation should be found between the cubical coefficient of expansion of asphalts and the isothermal volume change results. The slope of the linear correlation curve shown in figure 3.30 is equal to 0.457 log(s)/mm³/g (0.0126 log(s)/in.³/lb). On the other hand, it has been observed here that for the study asphalts the average slope of the temperature-shift function (log a_T), below 0°C (32°F), is approximately 0.183 log(s)/°C (0.1 log(s)/°F). If the latter slope is divided by the correlation slope (0.457), the result is 0.403 mm³/g/°C (0.0062 in.³/lb/°F). Assuming the density of asphalt is 1.0 g/cm³ (0.036 lb/in.³), the latter number is equal to 0.000403 cm³/cm³/°C (2.2 x 10⁻⁴ in.³/in.³/°F), which is close to the value of cubical thermal coefficients of expansion measured in this study at temperatures below or close to T_g. Similar values of the expansion coefficient have also been reported in many previous studies.

The second part of the volume experiment was designed to measure the volume change at of two selected asphalts at different temperatures. The asphalts selected were AAM-1, which showed the maximum isothermal volume change, and AAD-1, which is one of the asphalts that showed the minimum volume change within 24 hours. The results for AAM-1 are shown in figure 3.31, while those for AAD-1 are shown in figure 3.32.

The plots depict the significant effect of temperature on the volume shrinkage and indicate that generally the volume reduction is slower at higher temperatures. This behavior is similar to the behavior observed for the isothermal time shifts in which the shifts were less for higher temperatures. This similarity confirms the direct relationship between hardening and collapse of free volume. In addition, the plots in figures 3.31 and 3.32 indicate two important points: for asphalt AAM-1 significant volume change can be seen even at 15°C (59°F), which was not expected considering that the specimen was cooled from only 25°C (77°F). The second observation is related to asphalt AAD-1 and shows that at −25°C (−13°F), the initial volume change rate is lower than that at −15°C (5°F) but higher for a longer time. The temperature effects on volume recovery were exploratory in nature, and unless more work is done, it will be hard to draw solid conclusions about how the rate and the ultimate volume recovery are affected by temperature level. However, the fact that isothermal volume recovery extends well above 0°C (32°F) warns that physical hardening of certain asphalts may not be limited to low temperatures but may extend to temperatures well above their glass transition temperature. Also, as will be discussed in the next section, the observation may indicate of the broad transition region and the early departure, on the temperature scale, of some asphalt cements from the thermodynamic equilibrium state.

Glass Transition Measurements

In this section the procedure for the analysis of the volume-temperature data collected is discussed followed by a presentation of the relationship between these measurements and the physical hardening phenomenon.

140

Estimation of Glass Transition Temperatures

One important finding from the literature review conducted for this study is that asphalt cements exhibit relatively wide glass transitional regions. Such transitional behavior makes the definition of the glass transition temperature, T_g, difficult and, in some cases, arbitrary (Jongepier and Kuilman 1969; Schweyer 1974). The common approach of obtaining the T_g value is to manually fit two tangents to the two ends of the measured volume-temperature relation and the temperature at which the tangents intersect is taken as the T_g value. The problem with this approach is that it is not statistically sound. When used in this study, it results in a high degree of uncertainty for two reasons: first the transition zones, as reflected by the curved part in the measurements, are very wide. This results in difficulty in selecting the appropriate tangents and in drawing them. The second reason is the experimental noise; the measurements that were taken in this study as well as in many previous studies are recorded manually, and there is always, no matter how efficient the temperature control system being used, some temperature fluctuation and some temperature lag. All these reasons produce some unavoidable experimental noise which makes it very difficult to select the appropriate tangents.

Recognizing all these problems, several statistical approaches were investigated to get a better definition of the glass transition temperature. Before discussing these approaches, some general comments on the nature of the data are necessary.

As described earlier, two independent replicates were tested for each asphalt. In each replicate the measurements were made by first cooling the specimen to low temperature, waiting for 30 minutes to ensure thermal equilibrium, then starting the measurements on a heating ramp. After reaching the highest temperature, the specimen is left to stabilize for 30 minutes and then a new set of measurements is taken on a cooling ramp. The rate of heating and cooling was fixed at approximately 1°C (1.8°F) per minute. The lowest temperature was selected to be approximately −80°C (−112°F), while the highest temperature reached was selected to be more than 30°C (86°F). The rate and the limiting temperatures were selected based on previous studies to cover the widest practical range suitable for obtaining T_g. The time intervals between preparing the specimens, cooling them, and starting the heating and cooling ramps were very tightly controlled to avoid any effects of isothermal volume changes which were observed to be rapid early during isothermal aging. Also, to minimize temperature lag problems, the temperature readings were taken using a thermocouple placed inside a cell identical to the measuring cells and at the center of the liquid bath.

To analyze the data, two procedures could be followed: (1) each independent replicate could be analyzed separately or (2) all data could be pooled and one estimation of T_g obtained. After reduction of all data, it was observed that the two replicates for each asphalt were very close and no separation was necessary. Examples of the data are shown in figure 3.33. The plot depicts how the two replicates are close and how the cooling ramp is close to the heating ramp. The latter is important to observe here because in several previous studies the T_g value was estimated by averaging the T_g value for the cooling ramp and the T_g value for the heating ramp. In this study the differences were minimized by taking the temperature

measurements inside a dilatometric cell instead of measuring the temperature of the liquid bath as commonly done. In addition, relatively slow rates of temperature change were chosen as compared to previous studies. As a result, it was decided that the data for each asphalt be pooled and a common estimation of T_g made for each asphalt.

Several different nonlinear regression procedures were used to estimate T_g. First, a bilinear function was fit which gave the least square estimates of two coefficients of expansion/contraction, one below T_g (α_g), and one above T_g (α_l), in addition to the T_g value. This procedure was the common approach of fitting two straight lines, the only difference being that a statistical routine was used to choose the slope of the lines and gave the best estimates of the parameters. The procedure gave very good results and the minimum R-squared adjusted was more than 99.5 percent. However, two problems were encountered: first, the estimates were found to be highly dependent on the initial value selected to run the statistical routine. The dependency was so important that for certain asphalts a variation of more than 10°C (50°F) could be observed when the starting value of T_g was changed. Such dependency was the result of nonsalability of the minimum sum of squares due to error. The second problem was the distribution of residuals (deviation of fitted values from measured values). A typical example for asphalt AAB-1 is shown in figure 3.34 which depicts that there is a definite pattern in the residual distribution versus temperature. The pattern clearly reflects the problem of trying to force a bilinear relation to a curved relation like the volume-temperature measurements being analyzed here.

The analysis of results from fitting the bilinear model led to the conclusion that the transition region is very wide and to get an appropriate fit, a model that accounts for the curvature had to be used. The following function, which is basically a hyperbolic function that allows the rotation of the asymptotes and the adjustment of the curvature between the asymptotes, was selected.

$$V = C + \alpha_g(T - T_g) + \ln\{[1+\exp((T - T_g)/R_o)]^{R_o \cdot \Delta\alpha}\} \tag{3.5}$$

where

$$
\begin{aligned}
V &= \text{specific volume change,} \\
C &= \text{an intercept; has no physical significance,} \\
\alpha_g &= \text{slope of lower asymptote,} \\
T &= \text{temperature in °C,} \\
R_o &= \text{a parameter representing the curvature between the asymptotes,} \\
\Delta\alpha &= \text{the difference between the slopes of the second and the first asymptotes.}
\end{aligned}
$$

As expected, the hyperbolic function gave a better fit. However, a new problem was observed with the standard error of the estimated parameters; for several asphalts the standard error of parameters estimated was larger than the estimate itself. Many trials were made to control the significance of the estimated values by working interactively with nonlinear regression and varying the initial selected values, but the trials did not prove

142

useful. The conclusion reached was that because of high intercorrelations, some parameters had to be fixed so that reliable estimates could be obtained.

The selection of parameters to be fixed relied on findings of previous studies and other results collected in this study. As discussed previously in the review chapter, several studies have indicated that the coefficient of expansion below T_g, α_g, is constant for all asphalts irrespective of their source or chemical composition. Also the results of thermorheological study in this work indicated that the eight study asphalts have very similar thermorheological behavior. Therefore, it was thought that it is justified to give a common α_g for all asphalts was justified. The common value was estimated using nonlinear regression and using the hyperbolic model. All asphalts were included in the data set with indicator variables to estimate other parameters for each asphalt individually. The results significantly improved but the standard errors for the estimated parameters were still unacceptable. However, two important observations could be seen in the results: the R-squared adjusted was not affected significantly, and the curvature parameter was significantly different for the different asphalts. Another trial was made giving a common parameter for the slope of the second asymptote ($\Delta\alpha + \alpha_g$) in addition to α_g. The results were much better and the standard errors were within acceptable limits. The estimated values of α_g and α_l were reasonable and agreed with values given in previous studies. The values of T_g were also reasonable and agreed with the expectation from mechanical measurements obtained in this as well as other studies performed on the study asphalts. However, other than some previous reports (Schmidt and Santucci 1966; Schmidt et. al. 1965; Jones et al. 1968), there are no justifications for why these slopes should be constant. Also, the rheological measurements at high temperatures do not support the assumption that α_l should be constant.

The above reasons led to the conclusion that although the results with the last approach was reasonable, the assumption of common values for the asymptotes was not well justified. Therefore, another procedure was used. The procedure was based on selecting individual values for the asymptotes for each asphalt which are used later to estimate the curvature and the T_g value using the hyperbolic model.

The asymptote slopes were selected by taking each of the replicate measurements and calculating the change in slope versus temperature using analytical differentiation of the second order. The slope was plotted versus temperature and the approximately linear region can be defined from such plots. An example of the slope plots is shown in figure 3.35. As may be seen, the plot has an S-shape with the relatively large jump at about $-25\,^\circ C$ ($-13\,^\circ F$) in the derivative value clearly delineating the linear region of the measurements. After selecting the cut-off temperatures, linear regression was used to estimate the slope of the relation. Not all asphalts showed such clear cuts in the derivative-temperature relations. In such cases, the first 6 data points at each end of the curve were considered to give the best estimate of the slope at each end of the measurement's set. Following this procedure, two values of α_g and two values of α_l were estimated for each asphalt using linear regression. The values were averaged and used as input for estimating T_g and the curvature, R, using the hyperbolic model. The results are shown in table 3.5 and although they may not be much different from the values estimated using the bilinear fit, the procedure used to estimate them is believed to be more realistic. The accuracy of the new estimates was ascertained by

comparing them with values reported in the literature and by comparing them with estimates obtained by different methods.

The coefficients of cubical expansion for the study asphalts are plotted in figure 3.36. The values of α_g, even with the independent estimation procedure, still varies within a narrow range. This finding is supported by previous studies and by the thermorheological measurements made in this study. In addition the range of the values (3.32 to 3.57 $\times$ 10^{-4} per °C (1.84 to 1.98 $\times$ 10^{-4} per °F)) agrees well with values reported in the literature. For example, Schmidt and Santucci (1966) tested more than 50 asphalts and reported a common value of 3.47 $\times$ 10^{-4} per °C (1.93 $\times$ 10^{-4} per °F).

The T_g values are highly correlated with values estimated from dynamic measurements using the WLF equation. The correlation between the values estimated using dilatometric measurements and those estimated using dynamic mechanical measurements is shown in figure 3.37. The R-squared is approximately 90 percent which is remarkable considering the difference between the two types of measurements and the expected experimental noise that are commonly encountered in glass transition temperatures.

The important finding drawn from the glass transition temperature experiment is the fact that estimation of the T_g value has to consider the wide transition region. Otherwise, it is difficult to interpret the data and obtain reliable estimates. The new approach of fitting a curvelinear relation to the volume-temperature relation proved here to be reliable and that may account for the widely transitional nature of the asphalts.

T_g Measurements and the Physical Hardening Phenomenon

Generally, it is accepted that physical hardening appears for many materials below their glass transition temperature because below that temperature the material starts deviating from thermodynamic equilibrium. At high temperatures, the volume-temperature line is considered the equilibrium line and many scientists believe that if this line is extended, the distance between the volume-temperature relation and this line reflects the deviation from thermodynamic equilibrium and therefore the amount of what may be called free volume. The concept is illustrated in figure 3.38 for one asphalt. As may be seen, because of the curvature involved in the fitted relation the point of deviation from thermodynamic equilibrium, for this asphalts, extends well beyond the T_g value and is approximately 20°C (68°F). The deviation of the measured response from the equilibrium line was called the non-equilibrium free volume and was used to relate the T_g measurements to the physical hardening behavior of the asphalts tested.

The non-equilibrium free volume as a function of temperature was estimated using the hyperbolic functions fitted for the eight study asphalts. The estimated deviation versus temperature is plotted in figure 3.39. It is interesting to observe that the nonequilibrium free volume extends well above the freezing temperature (0°C (32°F) for many asphalts.

144

To test for correlation, the free volume values at the temperatures of physical hardening testing, $-5°$, $-15°$, $-25°$, and $-35°C$ ($23°$, $5°$, $-13°$, and $-31°F$), were calculated and plotted versus the physical hardening shift values at the corresponding temperatures. The shifts used reflects the hardening occurring between 30 minutes and 96 hours. Although the 96-hour age by no means reflects the time required to reach equilibrium, the shift values should give some correlation with the nonequilibrium free volume values. The values are plotted in figure 3.40 that depicts a high correlation. The value of the correlation coefficient (R-squared) is 85.0 percent when all asphalts at the different temperatures are considered.

To our knowledge, no published study has attempted to find such a relation. The correlation observed is important because it puts in perspective the validity of the free volume concept in explaining the physical hardening phenomenon. It also confirms the necessityof considering the wide transition zone in interpreting volume-temperature relationships. The isothermal volume measurements made in this study and the relations found between physical hardening and volume-temperature measurements all point out the importance of understanding the effect of thermal history on the behavior of asphalts, and the understanding that asphalt behavior within the transition region is not stable and changes significantly with both time and temperature variations.

Effect of Physical Hardening on Failure Properties

It has been reported for other amorphous materials that the physical hardening influence on the small-strain–small-stress response of the material is different than the hardening influence on the tensile failure properties that mostly involve large strains or large stresses (Struik 1986). The explanation for the difference has been linked to the mechanism by which hardening occurs: applying a large tensile strain or stress involves an expansion mechanism, which tends to result in recovery of the free volume that collapsed during the isothermal storage that resulted in hardening. Obviously, not all free volume can be recovered, and the amount that can be recovered is expected to depend largely on the strength of the bonds developed after the hardening took place, and the failure strength of these bonds.

Because of the importance of this subject and its implications for characterization of failure properties, two asphalts—one with high potential for hardening (AAM-1) and one with low potential (AAA-1)—were tested in the direct tension test device after being stored in the testing chamber for two different isothermal times—1 hour and 24 hours. Because of the inherent variability of the failure properties, eight replicate specimens of each asphalt were tested at both isothermal times. Figures 3.41 and 3.42 depict the results for asphalts AAM-1 and AAA-1, respectively. Table 3.6 lists the failure properties.

The results indicated that the effect of hardening was significant for both asphalts. The failure stress after 24 hours was 26 percent higher for asphalt AAA-1 and 41 percent higher for asphalt AAM-1 when compared with the 1-hour values. The failure strains, although they showed high variability, were on average lower for the 24-hour treatment for both asphalts. The results indicated the same trend exists that was observed for the creep measurements and confirmed that as the storage time increases, the material becomes harder

and less tolerant of strain. The results were not sufficient to investigate whether the influence of hardening on failure properties is less or different than the influence on creep response. The results, however, clearly demonstrate the importance of controlling the thermal history of the specimen in order to get consistent repeatable results. More testing should be done to study this phenomenon and quantify the effects of hardening on failure properties.

Crystallizable Fraction (Wax) and Physical Hardening

Because physical hardening is observed at low temperatures and is completely reversible, it has been related to crystallization of waxes in asphalts by several researchers (Claudy et al. 1992). To investigate this recently proposed hypothesis, the physical hardening measured for 16 MRL asphalts was studied with respect to wax content with the use of differential scanning calorimetry (DSC).

Using a modified Shell method (SMS-1769) (Krom 1968), the wax contents of SHRP asphalts were measured for SHRP by researchers of INTEVEP-Venezuela. The wax contents and the melting points are listed in table 3.7 for 16 SHRP asphalts that have different chemical compositions and different low-temperature creep compliance properties. Figure 3.43 shows the correlation of the wax content and the hardening shift factor at $-15°C$ ($5°F$). The shift factors were obtained for each asphalt by measuring the isothermal shift factor needed to superimpose creep response measured after 30 minutes at $-15°C$ ($5°F$) on the creep response after 24 hours at $-15°C$ ($5°F$). There is a definitive relation between the wax content determined by the modified Shell method and the physical hardening, $R^2 > 70$ percent. What is surprising, however, is that the melting points of these asphalts are all above $30°C$ ($86°F$), while the hardening is observed only at temperatures below $-5°C$ ($23°F$).

Hardening Potential and Endothermic Peaks in Differential Scanning Calorimetry Thermograms

Differential scanning calorimetry (DSC) has been used by several asphalt researchers to determine glass and melting transition. In the early 1970s Noel and Corbett (1970) compared wax determinations by several traditional methods and indicated that variations as high as fivefold can be observed when these methods are used for the same asphalts. The authors stated that "the traditional concept of asphalt wax content is of questionable significance" (p. 267). However, they presented DSC thermograms that show clear endothermic peaks at moderate temperatures. The peaks were typical of crystallite melting transitions and therefore led the authors to conclude that asphalts contain waxes that are neither completely crystalline nor completely amorphous. They called the material crystallized fractions and offered a method for calculating them from DSC thermograms. Recently, this concept was used by other researchers in the United States and Europe, and relations between the crystallized fractions and physical properties were reported (Brule et al. 1990).

As part of another SHRP project, DSC measurements were conducted on eight of the asphalts used in this study (Harrison et al. 1992). Distinct endothermic peaks were observed for several of the asphalts in the temperature region of 0° and 90°C (32° and 194°F), and the enthalpies of these peaks were reported to an accuracy of ± 10 percent. Asphalts showing the most hardening and the most isothermal volume change also showed the largest endothermic peaks (figure 3.44). Although the temperatures at which these endothermic peaks occurred did not correlate well with the melting point temperatures of the waxes extracted from the corresponding asphalt, the peaks were within the same temperature range as the melting points, 30° to 90°C (86° to 194°F). In contrast, physical hardening as reported in earlier sections here was observed some 30°C (86°F) below the melting point temperatures and became more pronounced as the isothermal temperature decreased. Further, the physical hardening was completely destroyed by heating the asphalt to 25°C (77°F), well below the melting point of the wax.

Discussion of the Proposed Relation between Hardening and Wax

The above results leave no doubt that there is some connection between physical hardening at low temperatures and the amount of crystallizable or wax fractions in an asphalt. The isothermal volume measurements and the dilatometric T_g measurements, on the other hand, suggest that the hardening is caused by the time-dependent collapse of free volume below the glass transition temperature. Further, the creep compliance master curves do not indicate the presence of a crystallizable phase at low temperatures (Anderson et al. 1991). The master curves and the relaxation spectra are smooth and without the shape that suggests a second low-temperature phase. The only irregularity in the master curve, as mentioned in chapter 2 of this report, is in the region of the melting point temperatures where a vertical shift in the data is required to produce smooth master curves.

Ignoring the temperatures at which these two phenomena, physical hardening and crystallization, occur, the reason for the volume change could merely be crystallization. The maximum volume change measured for an isothermal time of 23.5 hours is 0.0025 ml/g for asphalt AAM-1. Considering the wax content of this asphalt, 4.21 percent, a 6-percent volume change in the wax would be sufficient to account for the 0.0025-ml/g volume change. Other studies indicate that a wax changes volume by 4 to 10 percent upon crystallization. Therefore, it is plausible that the crystallization of wax is the source of the low-temperature volume change. There are, however, a number of points that stand against this hypothesis:

- The large difference between the melting points of the waxes and the temperature at which the isothermal volume change is observed cannot be ignored. If dissolution of wax and the endothermic peaks are observed at high temperatures, why is hardening observed at much lower temperatures?

- Physical hardening and isothermal volume change continue for a long time (hardening is measured after 4 months for some asphalts). It is highly unlikely that crystallization continues for such a long time and continues to affect the creep compliance significantly.

- The effect of physical hardening on viscoelastic properties is analogous to the effect of temperature reduction on thermorheological-simple material. The rheological properties show no evidence of a second phase at the low temperatures but do seem to account for some orientation of the wax molecules in the region of the melting point temperatures.

- The rheological behavior of all SHRP asphalts is simple in that creep compliance master curves and the relaxation spectra show no sign of crystallization in the temperature region between $-35°$ and $60°C$ ($-31°F$ and $140°F$).

It is interesting that both the wax content and the degree of physical hardening appear to increase with the molecular weight of the neutral fraction.

Summary of Findings

In this investigation the low-temperature rheological and volumetric properties of eight different paving-grade asphalt cements were investigated. Each asphalt was tested to determine its creep behavior within the LVE response range. The dependency of the creep response on loading time, temperature, and isothermal age was characterized using the bending beam rheometer. The asphalts tested were found to exhibit low-temperature isothermal physical hardening. The physical hardening was defined in terms of the change in creep response as a function of isothermal time. The hardening behavior of the eight asphalts was characterized as a function of temperature, isothermal age, and asphalt source.

The study included isothermal volume measurements, which were used to relate the physical hardening phenomenon to isothermal volume contraction, and dilatometric glass transition measurements, which were used to study the nature of the glass transition behavior of asphalts and to establish a relationship between physical hardening and volume changes within the glass transition region.

The key findings from this study are summarized as follows:

- *Physical Hardening*—All tested asphalts were found to exhibit an increase in stiffness and a reduction in creep rate as a function of isothermal time. This phenomenon, which has not been reported before for asphalt cements, is herein referred to as physical hardening. The effect of hardening on the rheology of the asphalt binders was found to be reflected in the shifting of the retardation times spectrum without changing its shape—an effect similar to the effect of decreasing the test temperature. The amount of shift was called the isothermal time shift factor, a_{ti}, and was found to be a rapidly decreasing function of isothermal age.

- *Factors influencing physical hardening*—Asphalt source, temperature level, and isothermal age were investigated. Within the range of the covered conditions, physical hardening rates and levels were found to be highly asphalt specific. General trends indicate that the higher the average molecular weight, the longer the isothermal time

required to reach thermodynamic equilibrium. The hardening rates were also found to be highly dependent on temperature level. For all asphalts, hardening rate and level were inversely proportional to the isothermal temperature. The temperature dependency was attributed to the proximity of the glass transition region and the glass transition nature of the asphalts. The temperature dependency was also observed to be asphalt specific. The hardening rates decreased rapidly with isothermal time; however, the hardening was observed to continue for more than 4 months. Unlike many other amorphous materials, the hardening rates of the study asphalts were not found to be directly proportional to logarithmic isothermal time.

- *Hardening model*—A general engineering model was conceptualized that allows the prediction of hardening shift factors as a function of isothermal temperature and isothermal age. The model was developed after observing that hardening curves at different temperatures can be shifted and superimposed to construct hardening master curves. The model developed resembles a Voigt-Kelvin mechanical element with a single retardation time. Only two parameters are needed to describe the hardening behavior.

- *Isothermal volume shrinkage*—The hypothesis introduced in this study to explain physical hardening is that hardening is mainly caused by the time-dependent collapse of free volume at low temperatures. Isothermal volume changes measured in this study strongly supported that hypothesis. The correlation between isothermal volume change and hardening shift factors, measured at an equi-isothermal age, for the eight study asphalts was found to be in excess of 94 percent. The measured isothermal volume changes were used to estimate an average value for the coefficient of thermal expansion. This measurement was taken by calculating the change in temperature required to cause a temperature shift equivalent to the isothermal time shifts caused by the measured volume contractions. The estimated coefficient of thermal expansion agreed well with values measured in this study and reported in previous studies.

Time-dependent isothermal volume shrinkage is not limited to very low temperatures. For some asphalts, considerable isothermal shrinkage was measured well above the estimated glass transition temperatures for those asphalts.

- *Glass transition measurements*—Analysis of the glass transition measurements indicated that asphalt cements exhibit relatively wide transition regions, which for some asphalts extend well above 0°C (32°F). A statistical fitting procedure was used to estimate the glass transition temperatures. The procedure illustrated the complications that may arise from the common practice of estimating the glass transition temperature by fitting a bilinear function to the volume-temperature behavior. A simple hyperbolic function was used to fit the measurements and estimate the glass transition temperature, T_g, with allowance for the curvature in the volume-temperature relationship caused by the broad glass transition region of the asphalts.

Using the concept of nonequilibrium free volume, a linear relation between isothermal time shift factors and the amount of nonequilibrium free volume was found to have a

correlation coefficient of more than 85 percent. Given the inherent difficulty of glass transition measurements, the observed correlation strongly supports the hypothesis of a direct relationship between hardening and collapse of free volume.

The T_g values estimated from dilatometric measurements were found to show a linear correlation coefficient in excess of 90 percent with WLF reference temperatures estimated from dynamic rheological measurements. The dilatometric T_g values, however, were lower than the rheological reference temperatures by an average value of 5°C (9°F). The coefficient of thermal expansion below T_g, α_g, varied within a very narrow range, a finding that agrees with many previous studies. Above T_g, however, the value of α_l was asphalt specific. The values obtained for T_g, α_g, and α_l are well within the range of values previously reported for paving grade asphalts.

- *Effect of hardening on failure properties*: The limited data collected indicate that failure properties are significantly affected by the hardening phenomenon. More work, however, needs to be done to quantify the effects and compare them with the effects on small-strain creep response.

- *Relation to crystallizable fractions (wax)*—There appears to be a link between wax content and low-temperature physical hardening. The exact role that paraffinic-like molecules play in physical hardening is not known for certain at this time.

Conclusions

In this study, low-temperature rheological and volumetric properties of eight asphalts were investigated to test the hypothesis that asphalt cements, when cooled to low temperatures, exhibit isothermal changes, which lead to physical hardening. Factors that affect the amount and rate of hardening were identified and their effects were studied. Relationships between changes in rheological properties, caused by the isothermal physical hardening phenomenon, and volume changes as a function of isothermal age and temperature were established. Based on the analyses of the results, the following conclusions were drawn:

- The measured isothermal creep response and volume changes prove the hypothesis that asphalt cements, when cooled to low temperatures, do not reach thermodynamic equilibrium instantly. They instead undergo slow isothermal volume contraction that may continue for long periods. This volume contraction results in significant hardening. The hardening, being systematically reported for the first time, was herein referred to as low-temperature isothermal physical hardening.

- The high correlations between volume changes and hardening shift factors; the simplicity of the influence of hardening on creep response of the different asphalts; and the dependency of the hardening rates on temperature and age prove the hypothesis that physical hardening is caused by isothermal relaxation processes reflected in the collapse of free volume.

- The effect of hardening on creep response can be defined by a simple one-dimensional shift defined as isothermal time shift log a_{ti}.

150
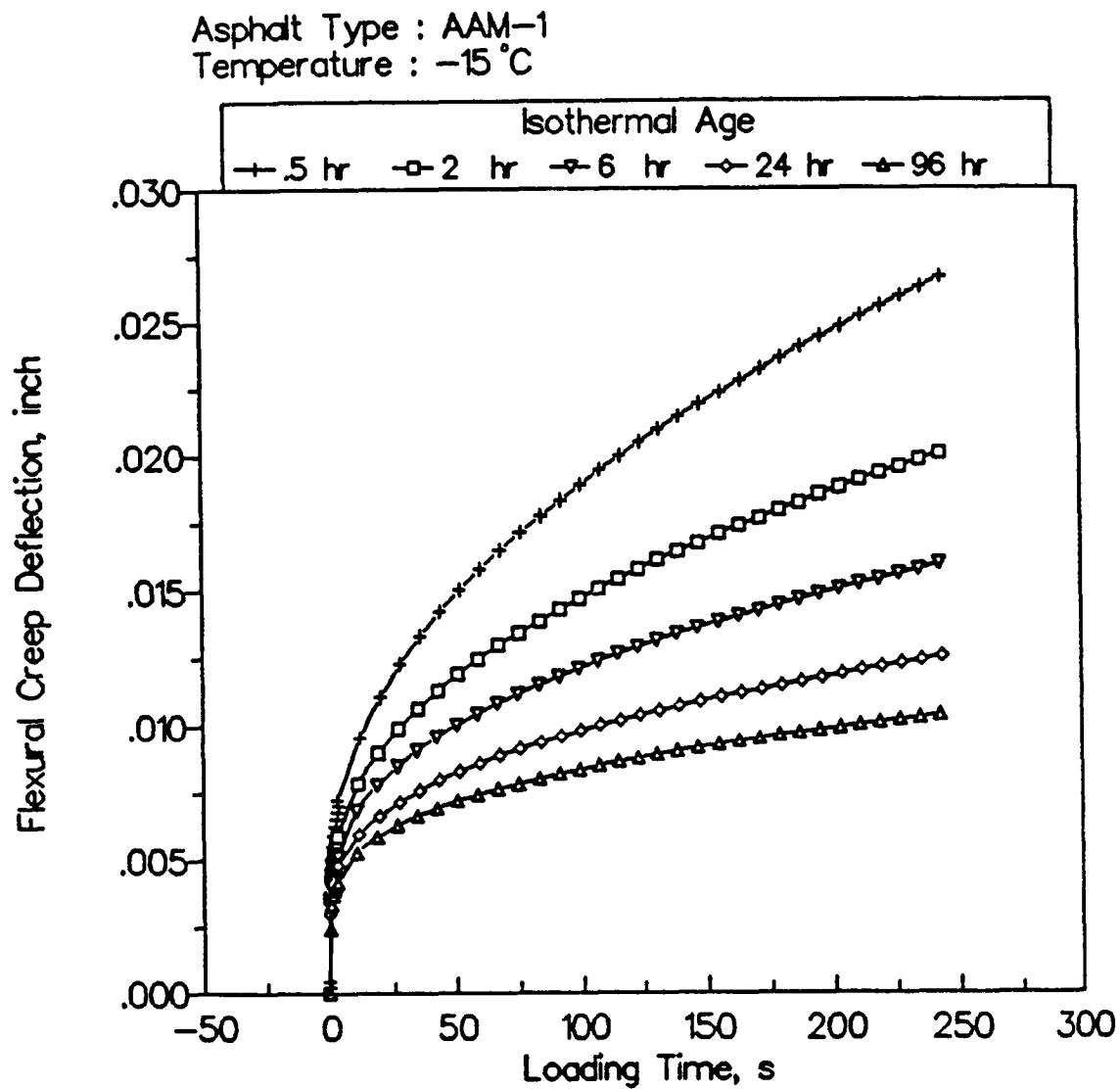
Figure 3.1   Change in Creep Stiffness with Storage Time at −15°C for Asphalt
AAK-1
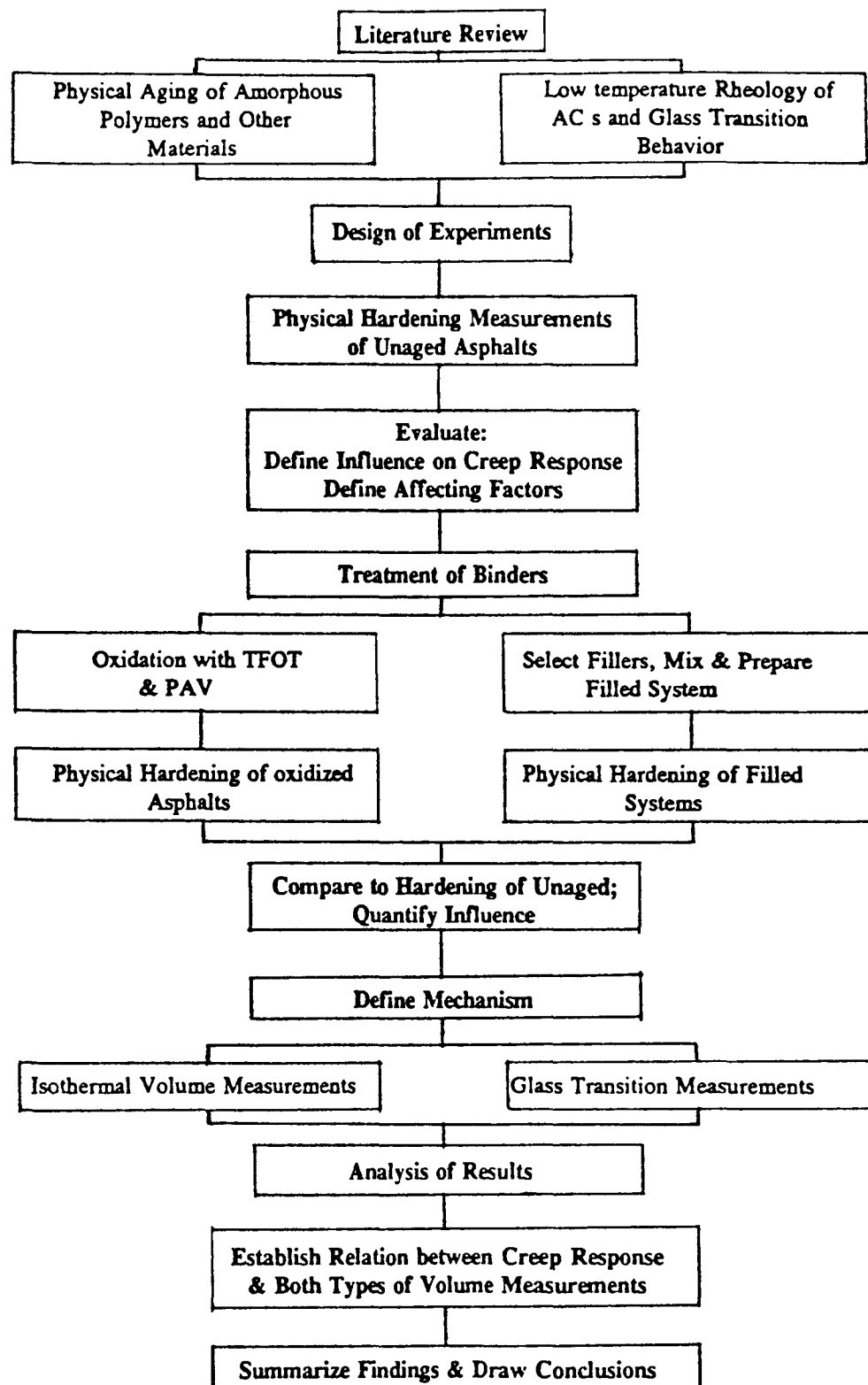
Figure 3.2   The Research Approach

152
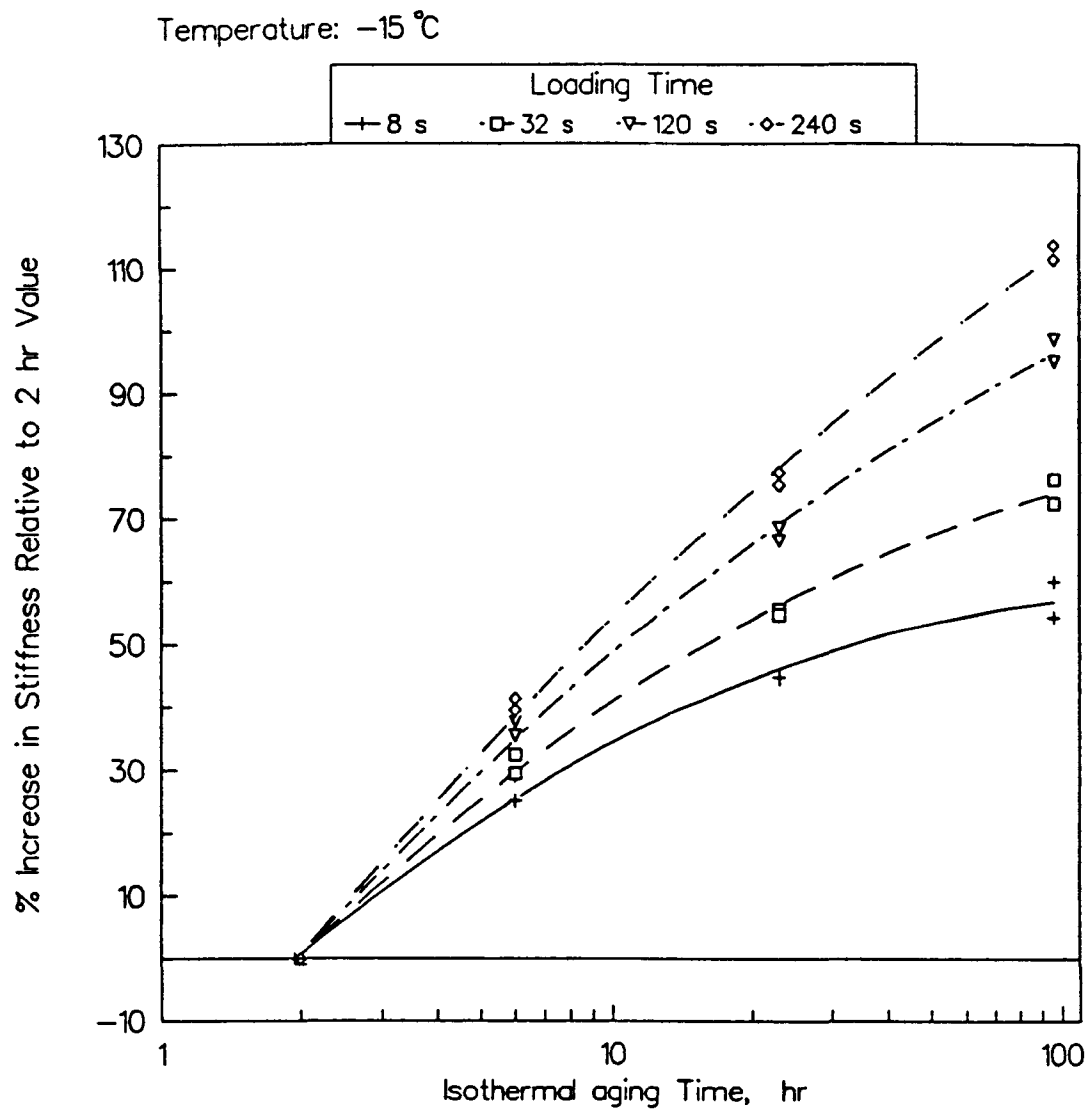
Figure 3.3 Typical Example of Measured Creep Response and Its Variation with Isothermal Age
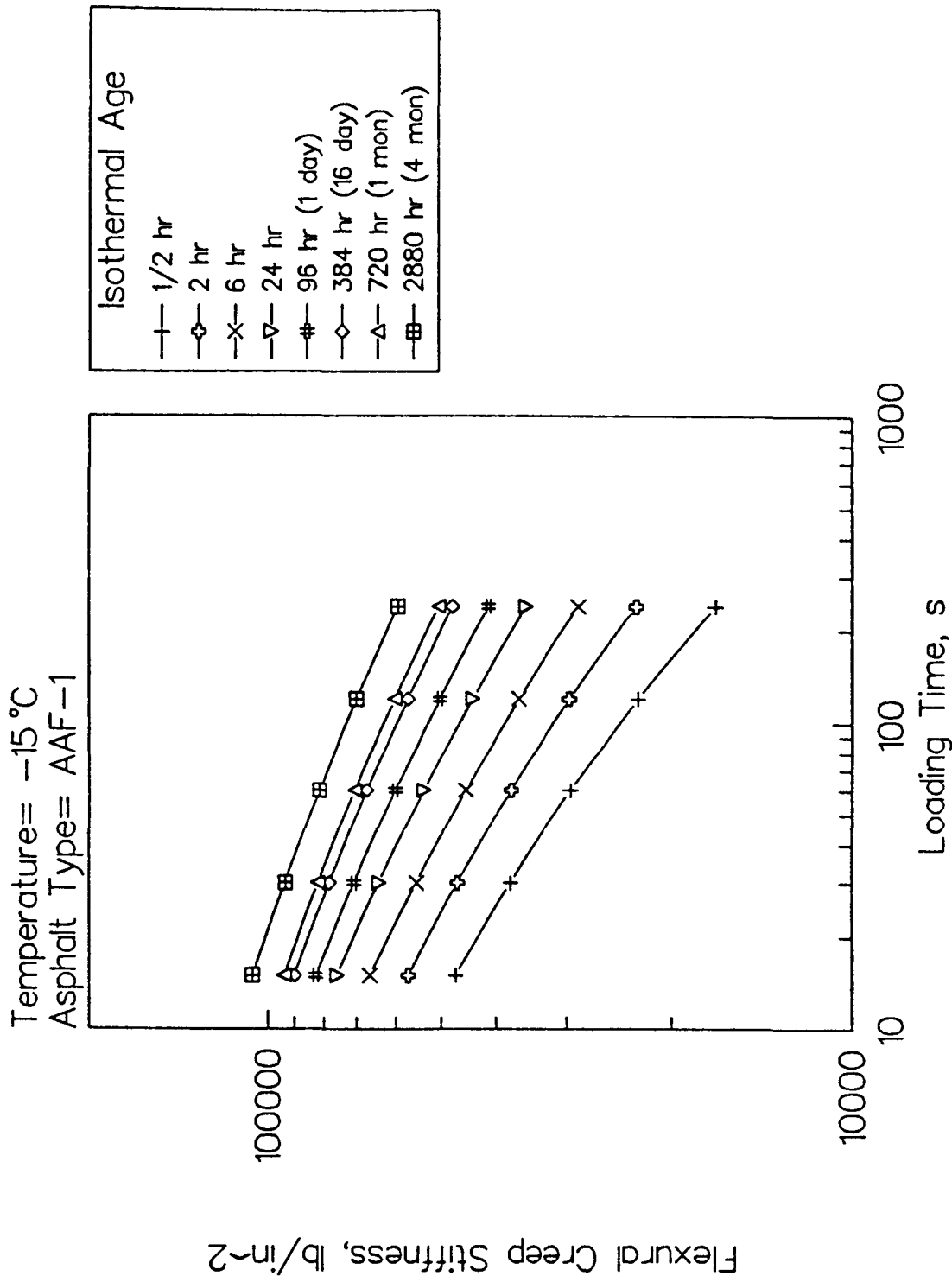
Figure 3.4 Typical Example of Influence of Physical Hardening on Creep Response of Asphalt Cements before Shifting

154
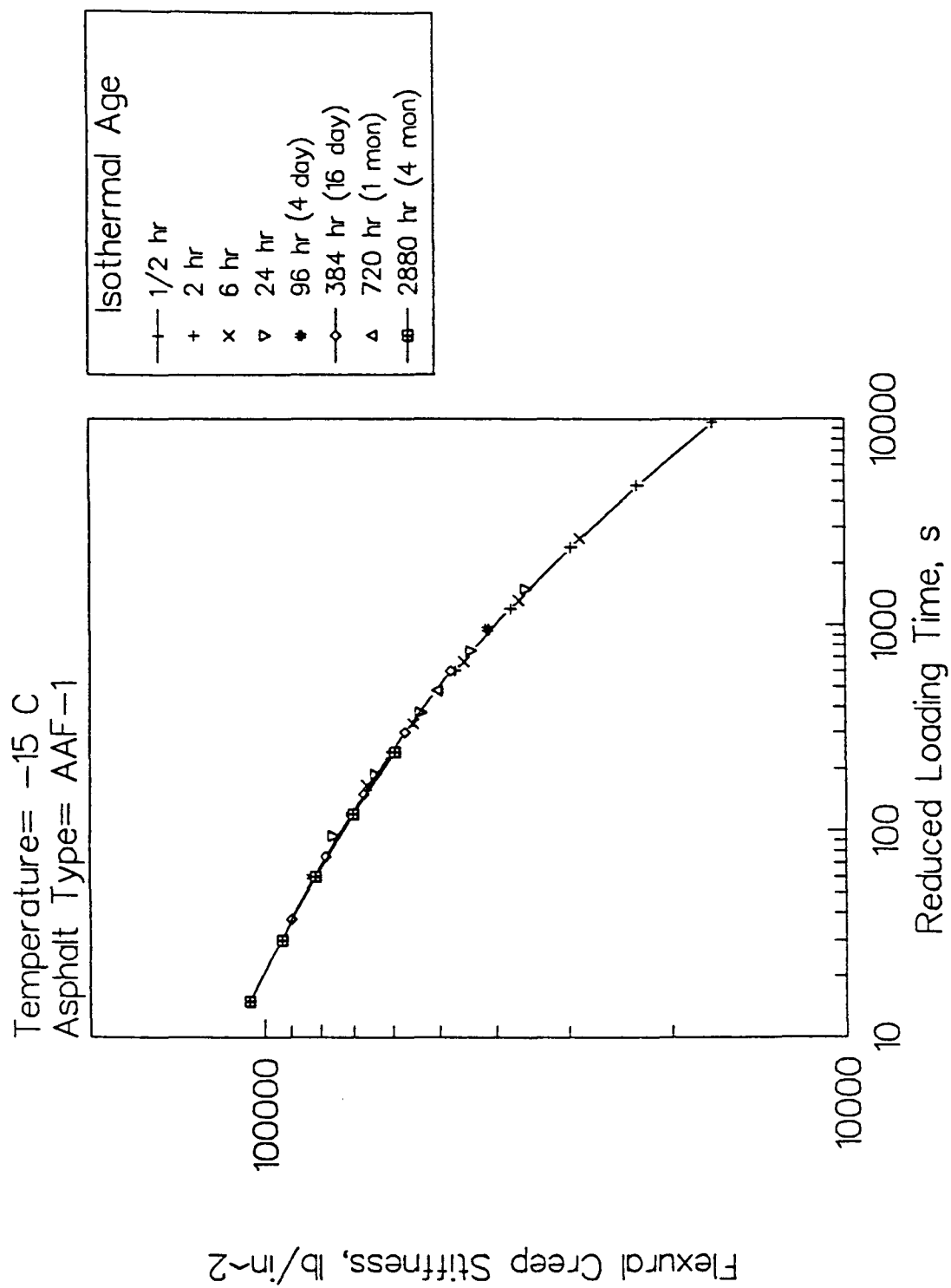
Figure 3.5 Overlap of Creep Curves after Shifting Because of Physical Hardening

155
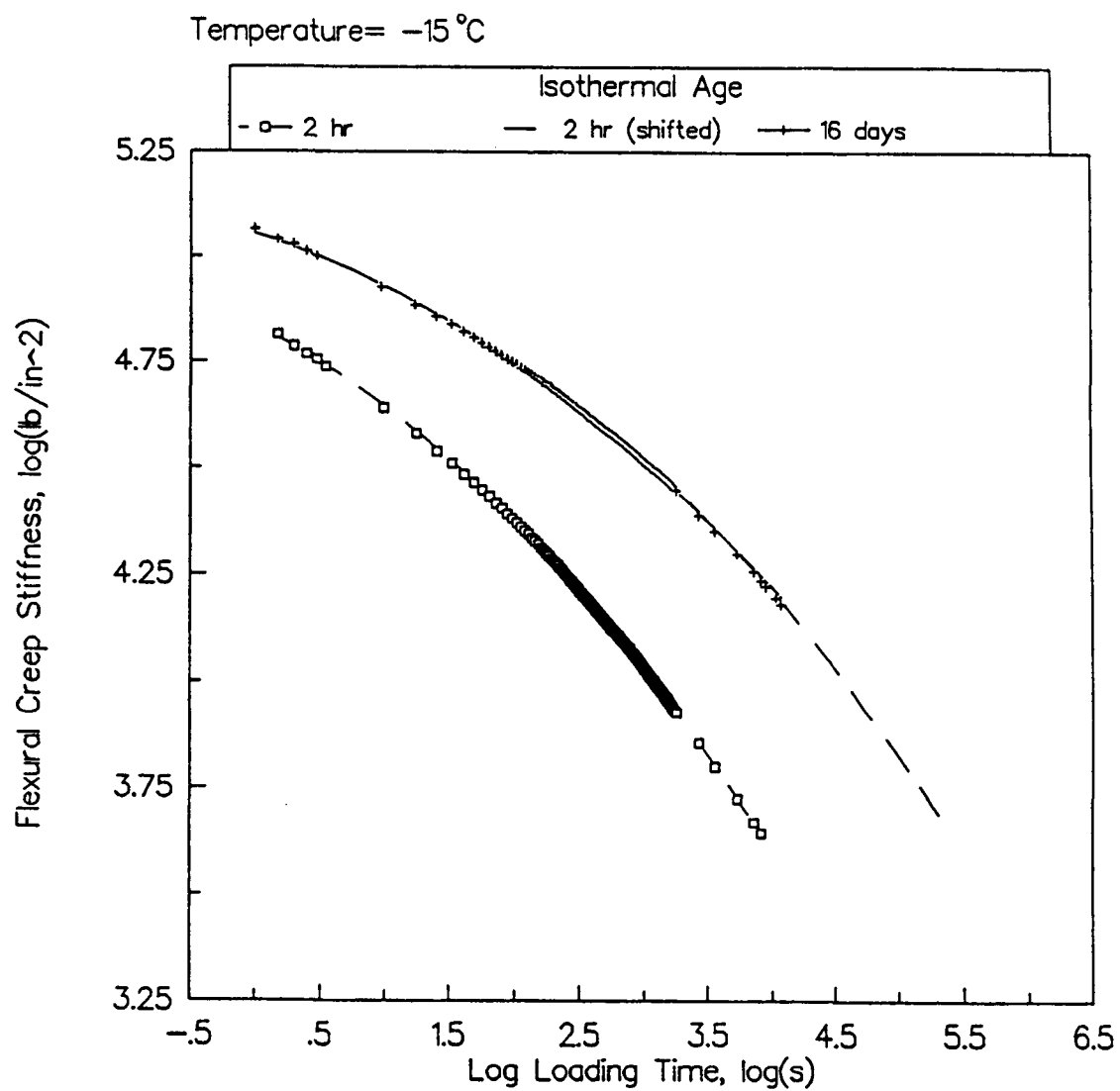
Figure 3.6   Log Time Creep Tests of Asphalt AAM-1 after Two Isothermal Ages
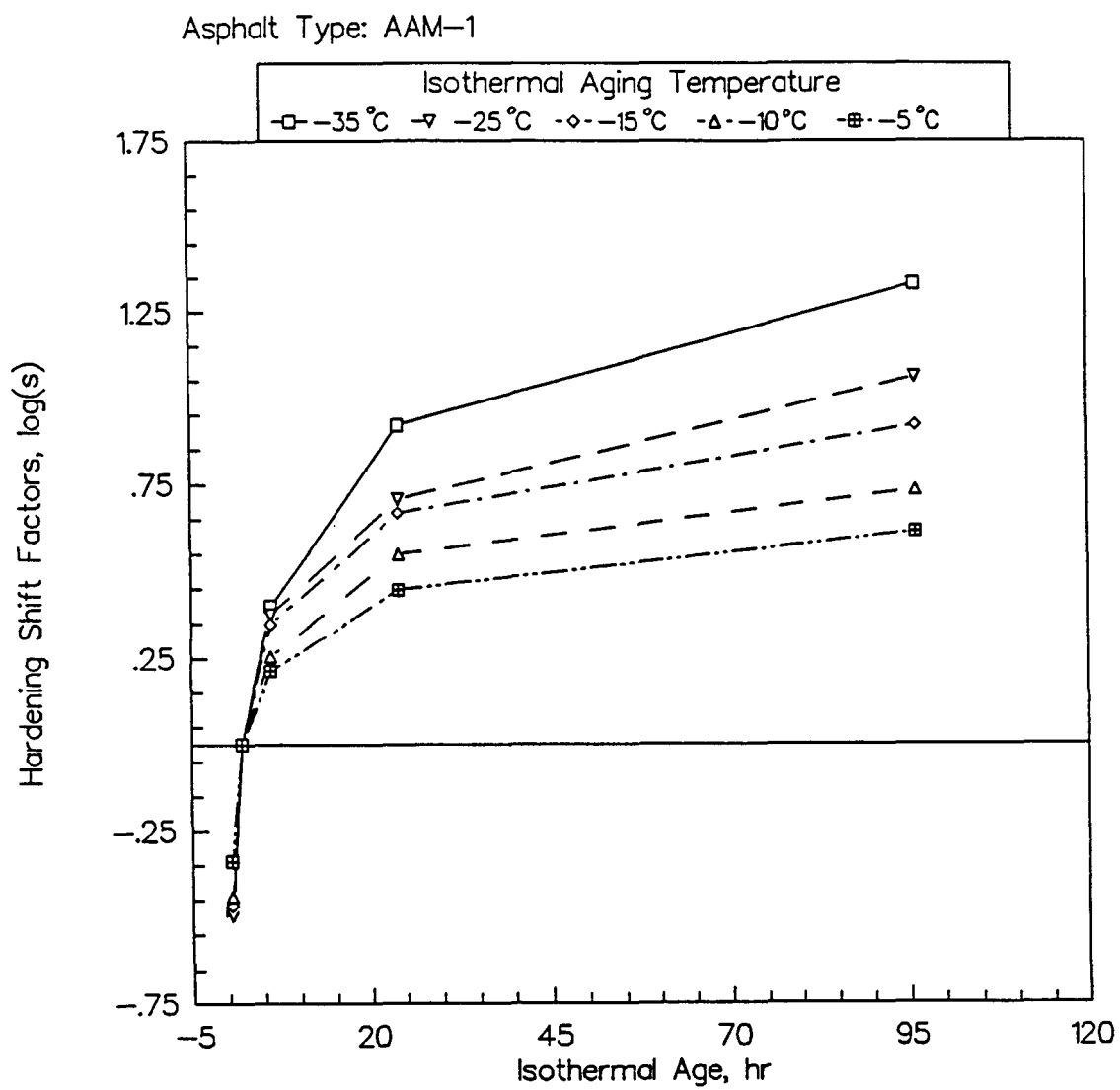
Figure 3.7 Isothermal Time Shift Functions of Asphalt AAM-1 at Different Temperatures
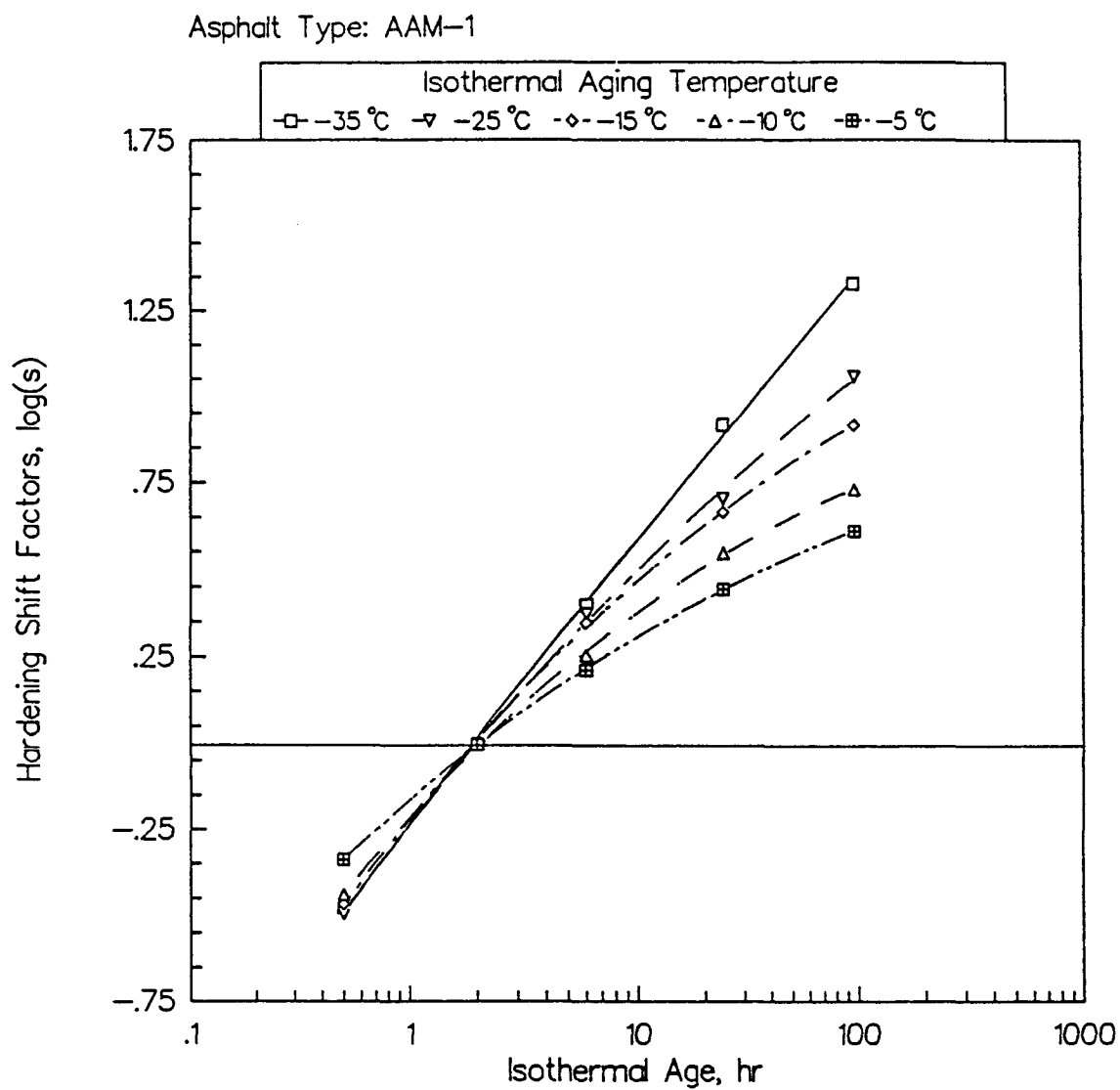
Figure 3.8 **Isothermal Time Shift Functions for Asphalt AAM-1 Plotted versus Logarithmic Isothermal Time**
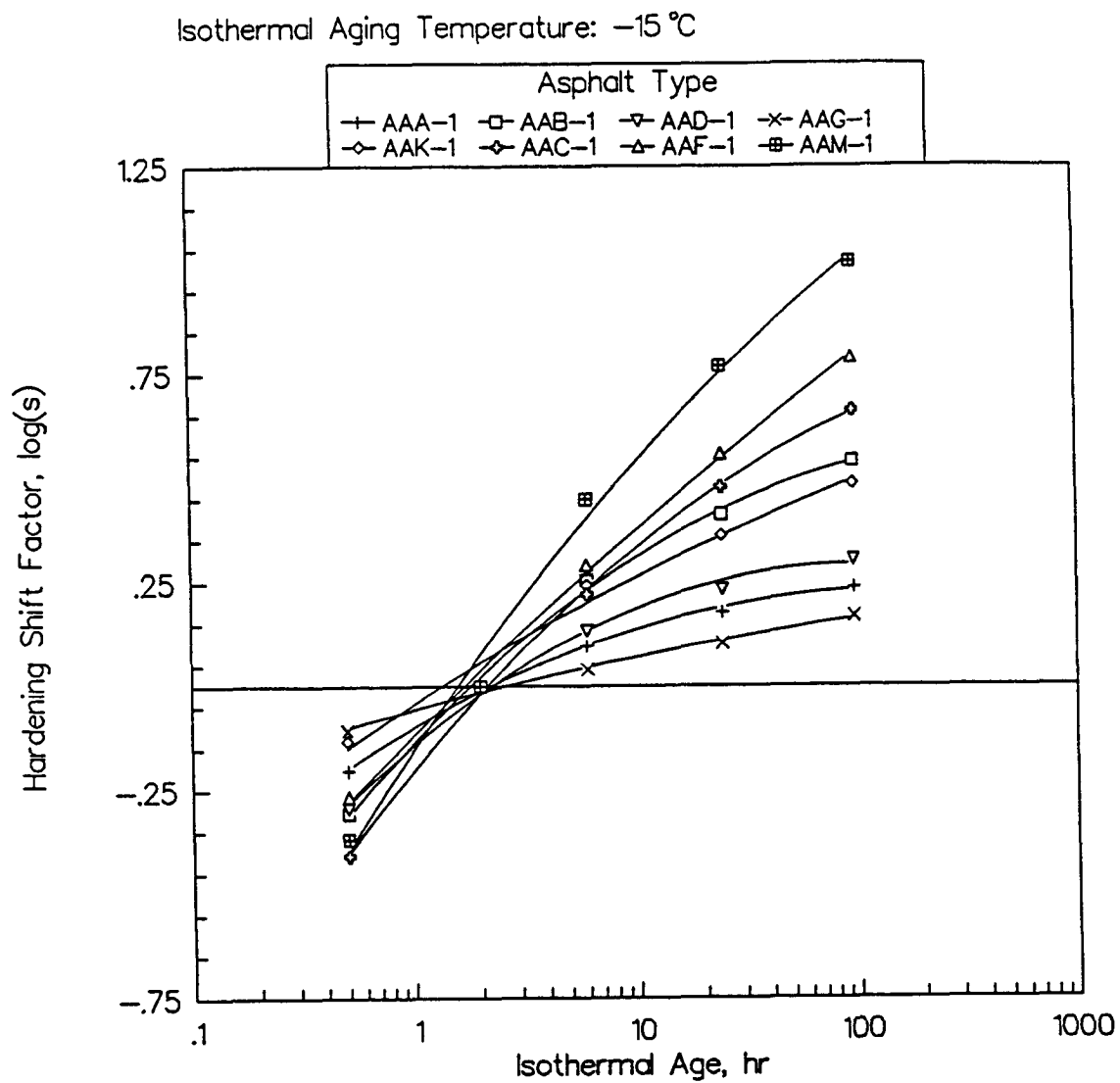
Figure 3.9   Isothermal Time Shift Functions of the Eight Study Asphalts at −15°C
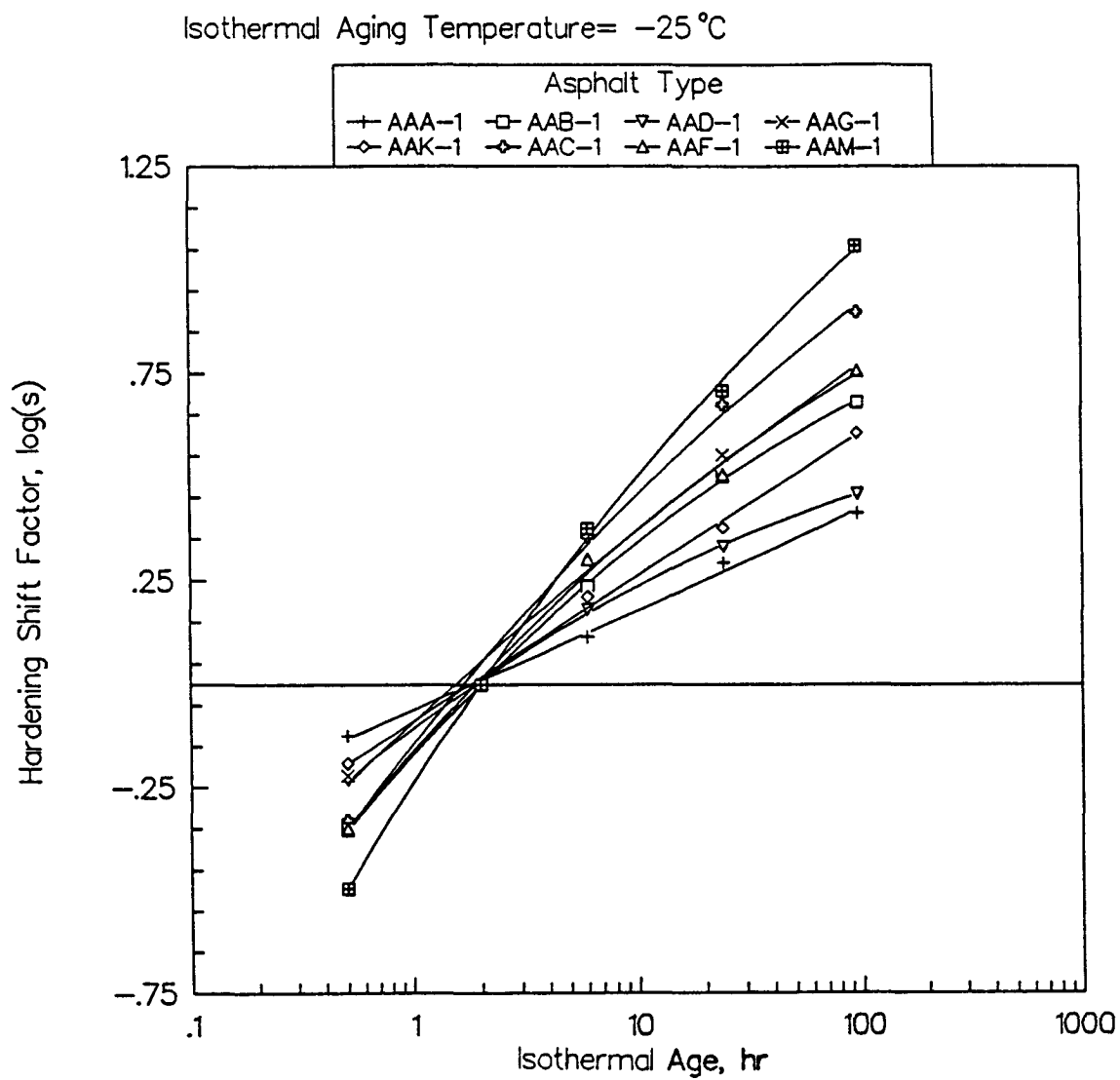
Figure 3.10   Isothermal Time Shift Functions of the Eight Study Asphalts at −25°C

160
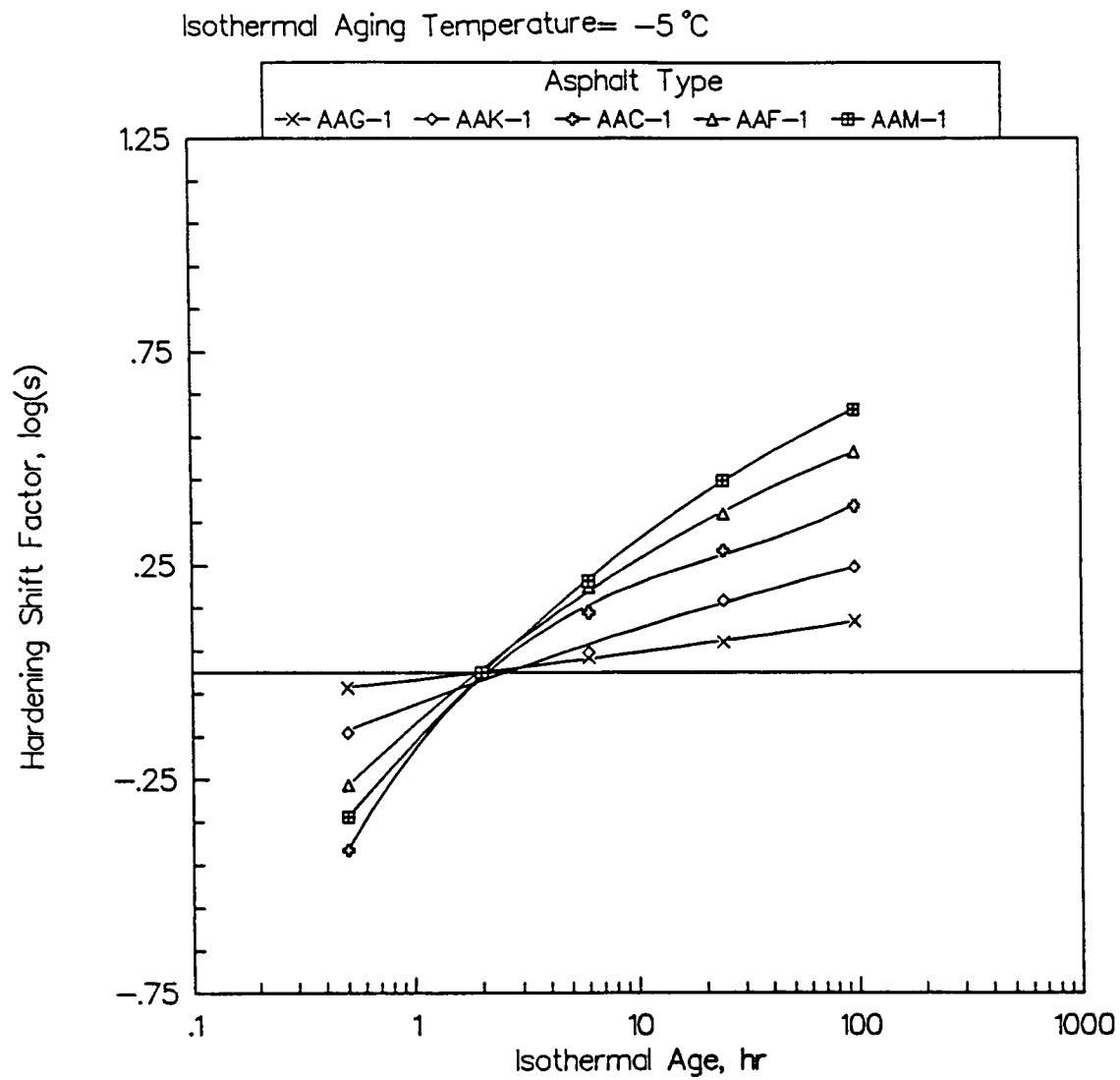
Figure 3.11   Isothermal Time Shift Functions of the Eight Study Asphalts at −5°C

THERMAL HISTORY EFFECTS
ASPHALT TYPE: AAM-1
RESPONSE MEASURED: FLEXURAL CREEP DEFLECTION
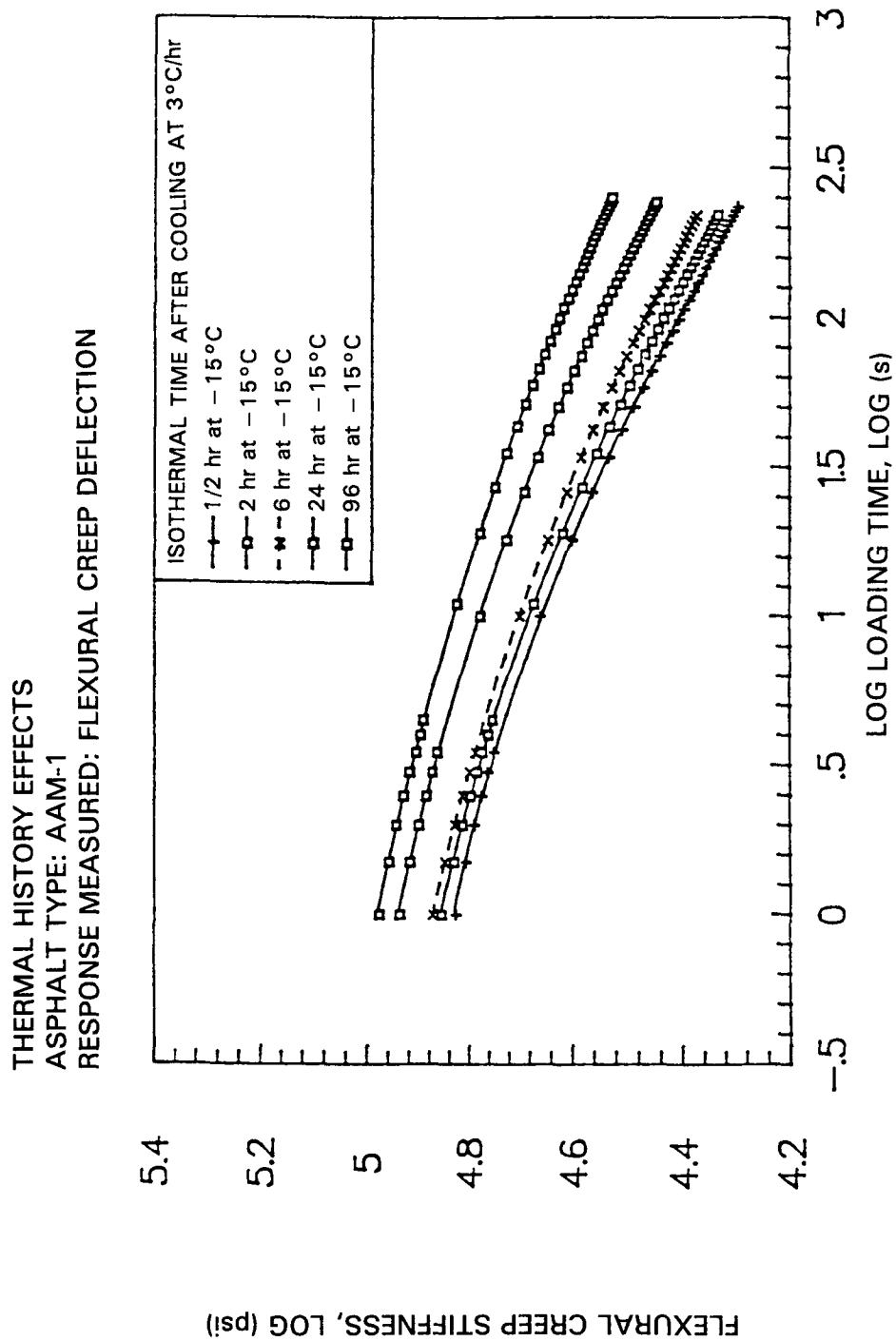
Figure 3.12 Physical Hardening of Asphalt AAM-1 after Cooling from 25°C to −15°C at the Rate of 3°C/hr

162
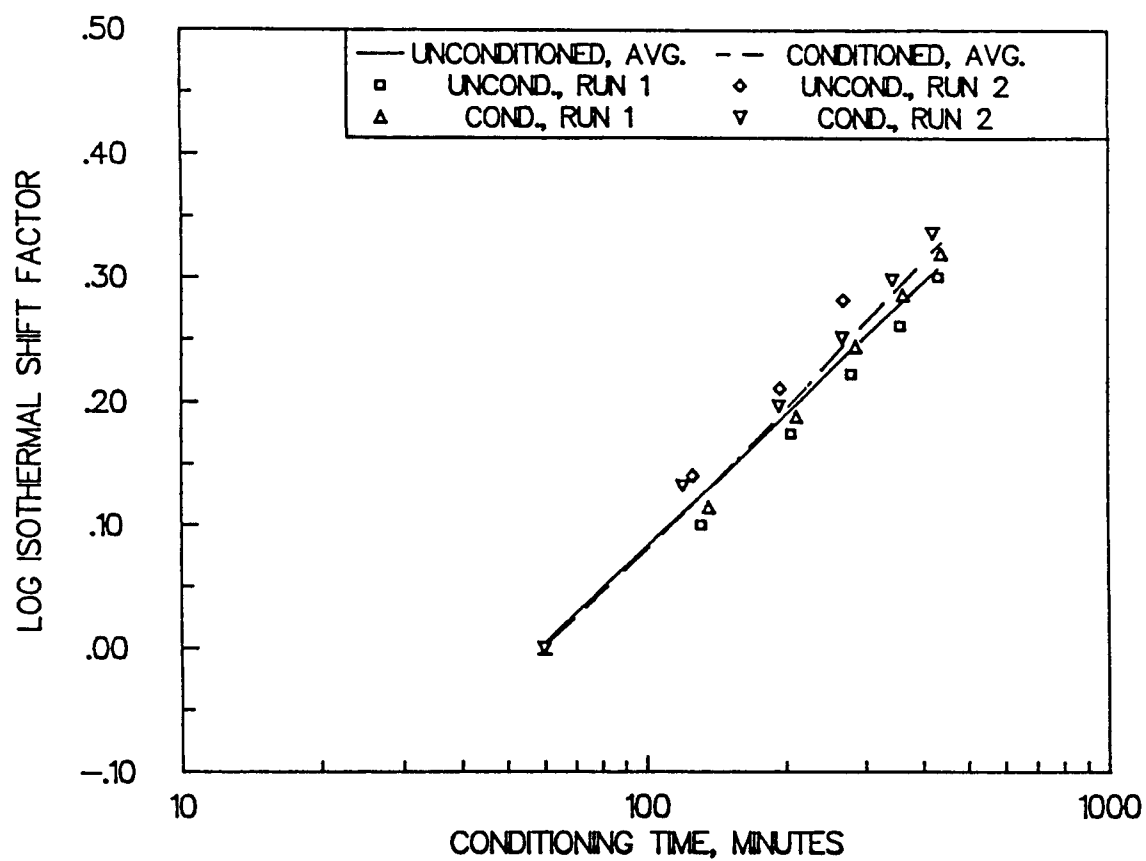
Figure 3.13   **Effect of Continuous Mechanical Working of Specimen on Physical Hardening of Asphalt AAM-1**

AC Type: AAK-1 Oxidized with TFOT
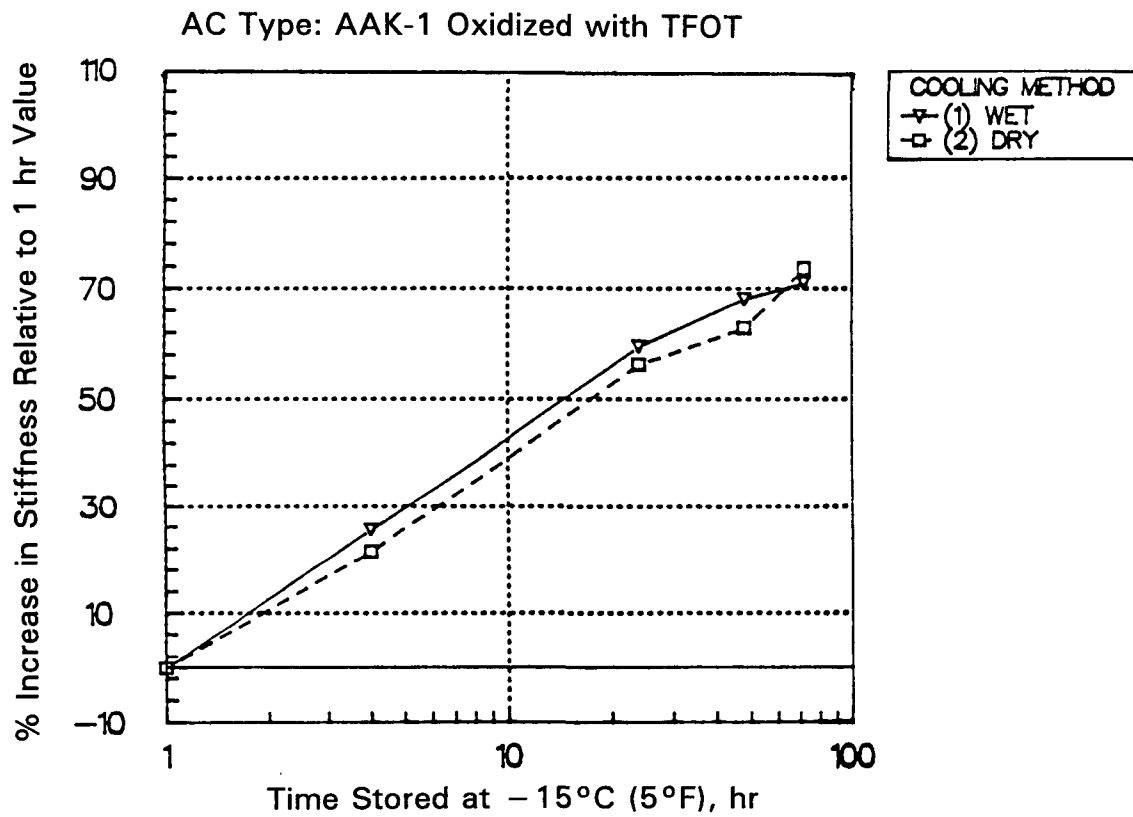
Figure 3.14 Comparison of Increase in Stiffness at 240 Seconds after Storage in Wet versus Dry Environment

164
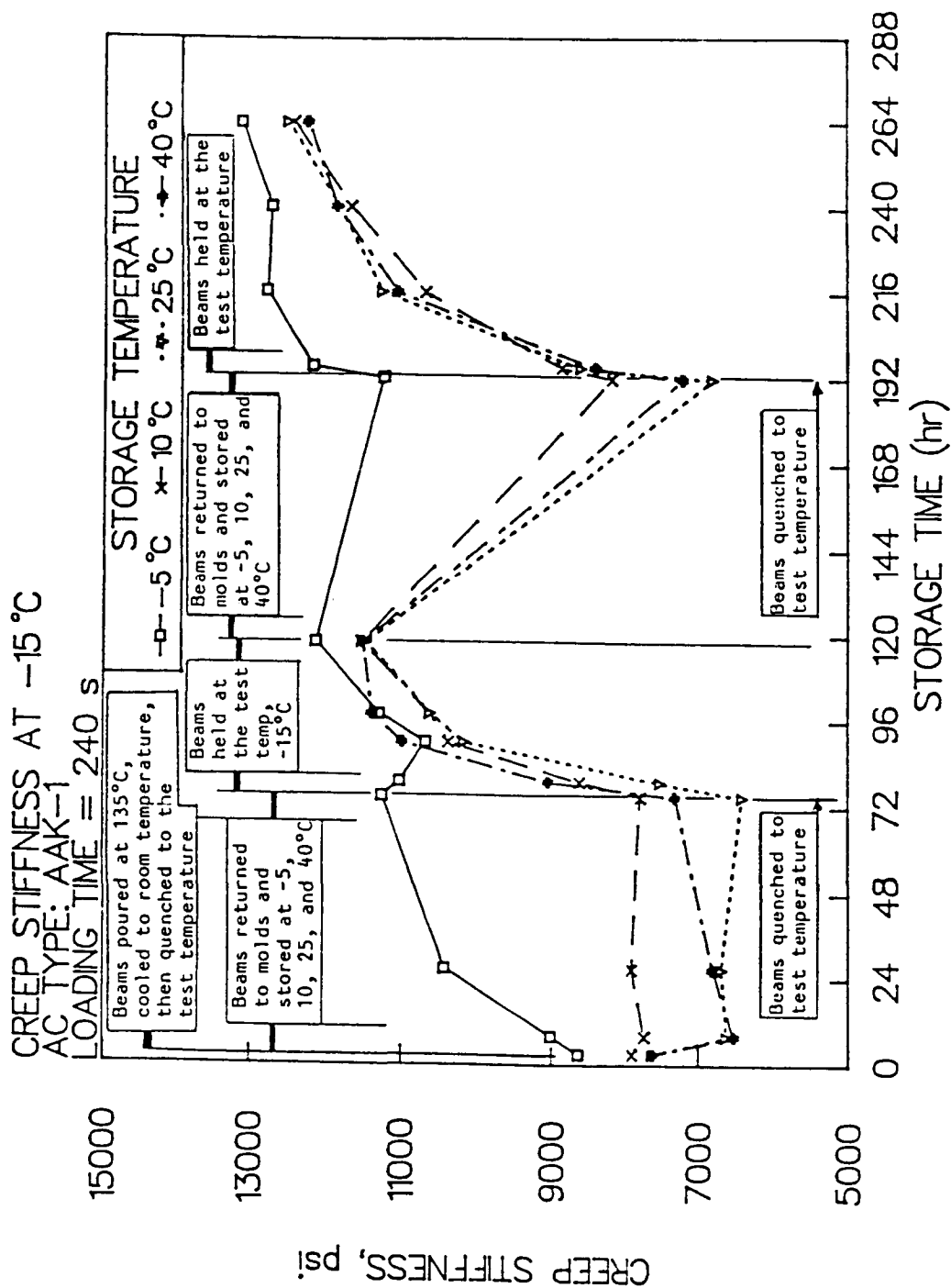
Figure 3.15   Effect of Thermal Cycling on Stiffness of Asphalt AAK-1
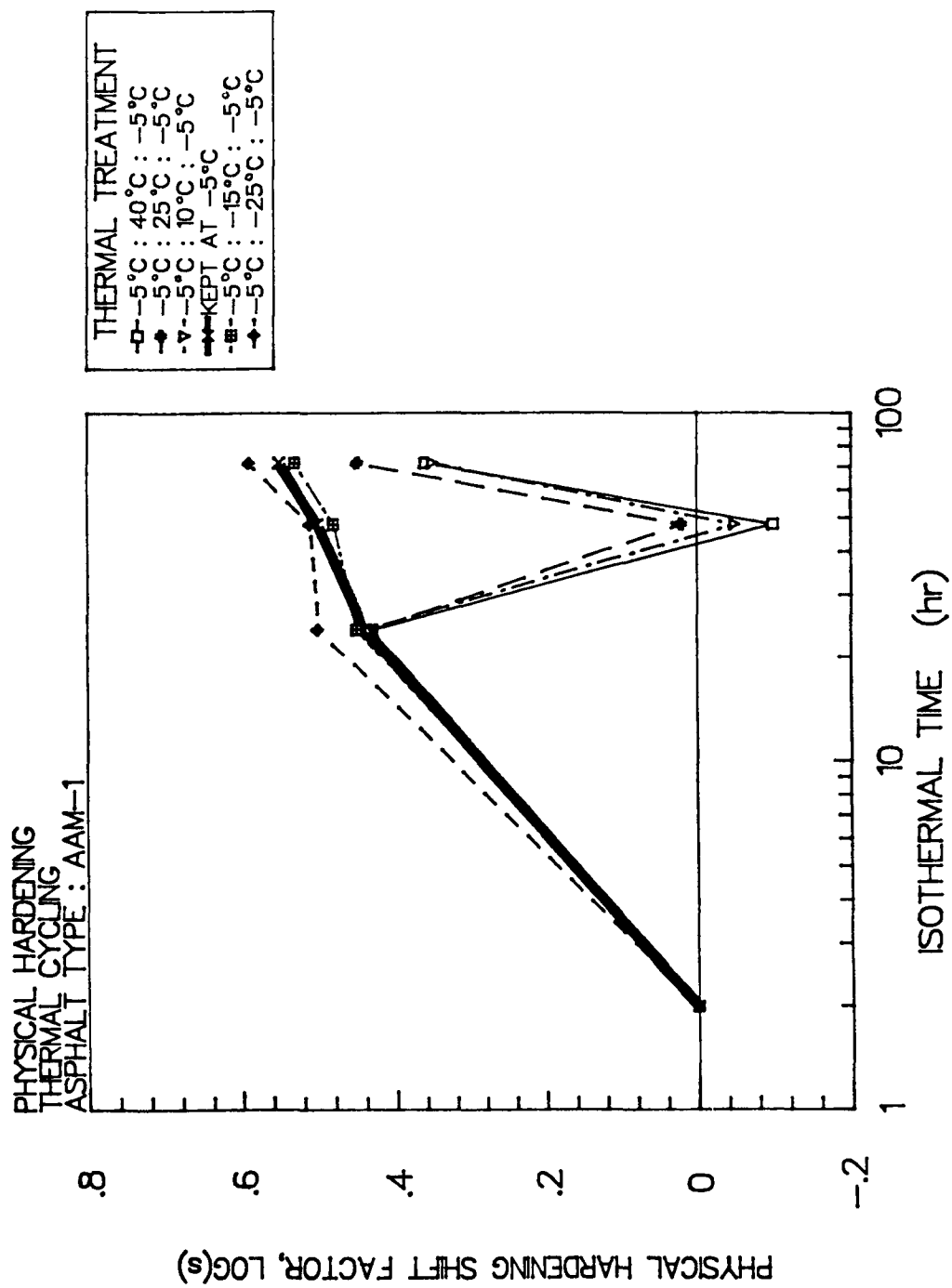
Figure 3.16 Reversibility of Physical Hardening in Terms of Shift Factors for Asphalt AAM-1
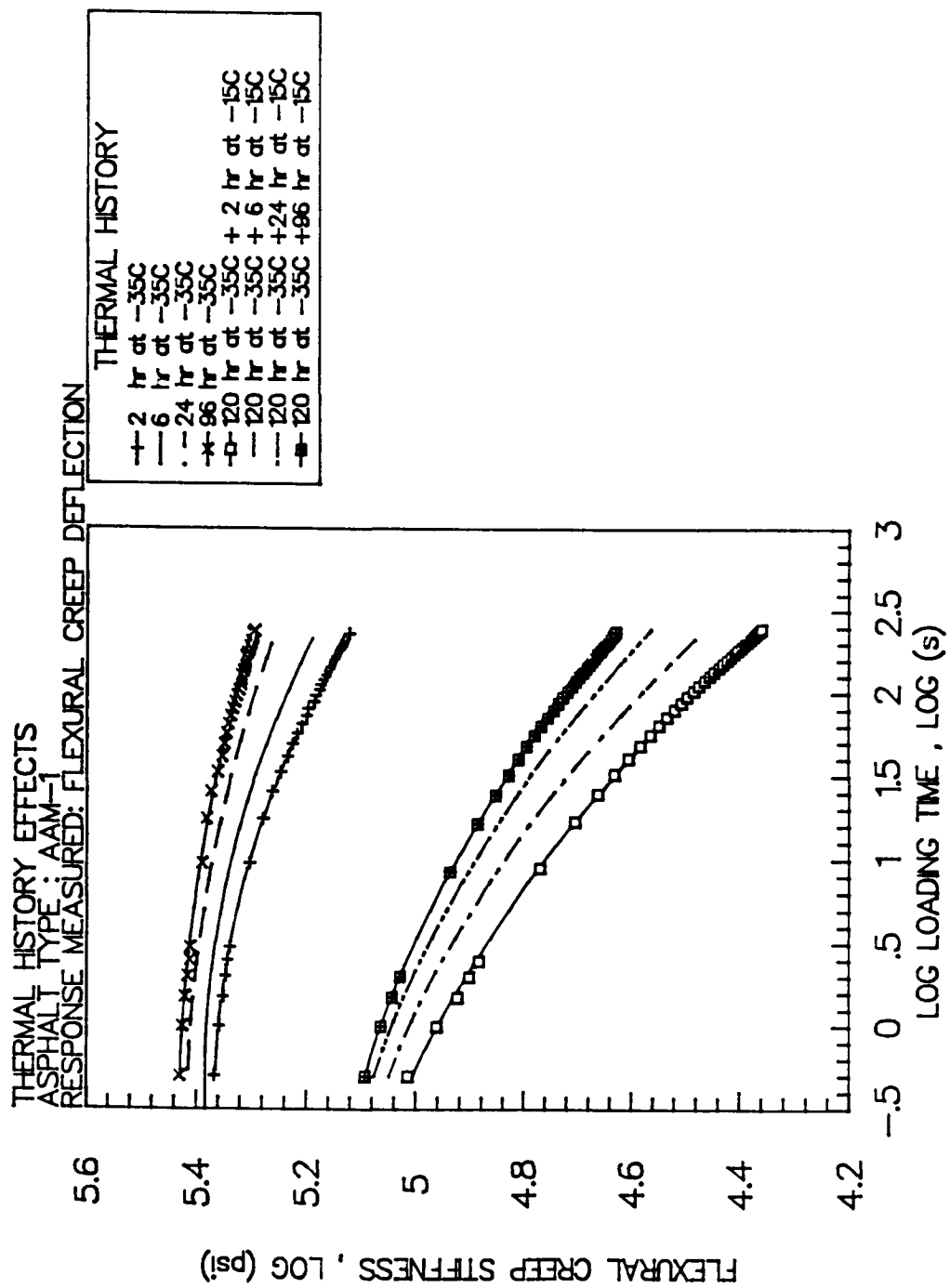
Figure 3.17 Reversiblity of Physical Hardening Because of Cycling below the Glass Transition Temperature

167
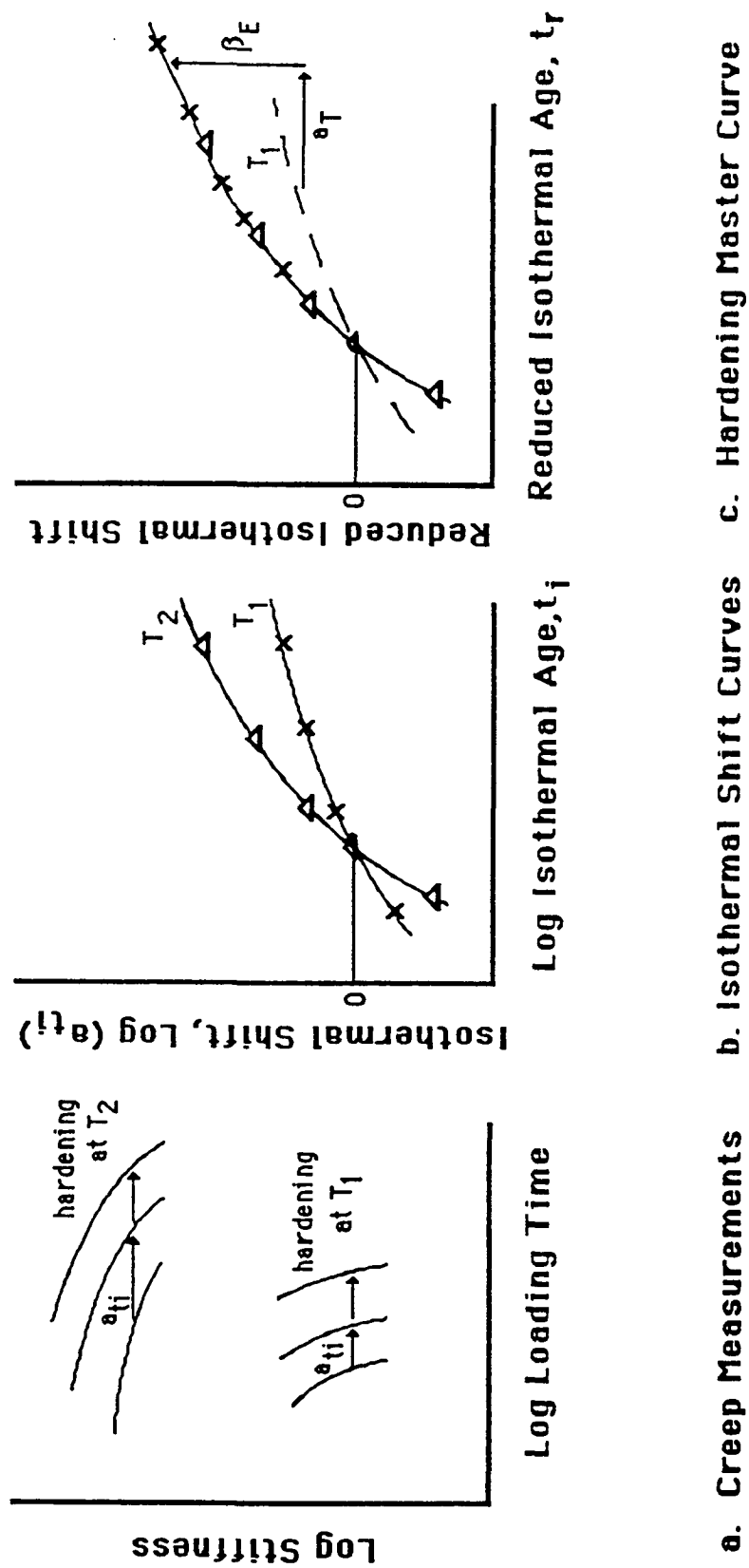
Figure 3.18   Schematic Plots Explaining the Concept of Constructing Master Curves for Physical Hardening
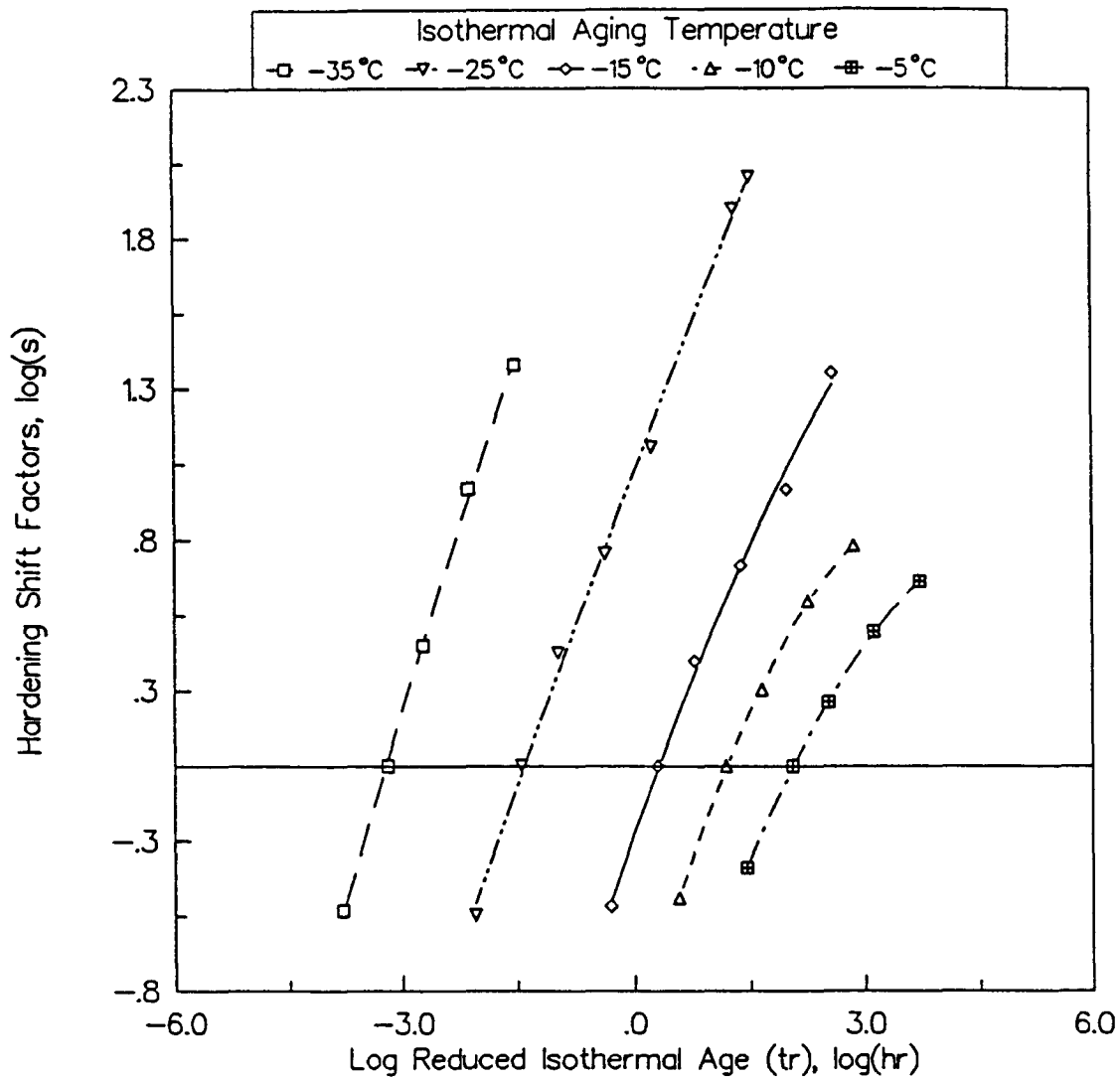
Figure 3.19   Shifting of Isothermal Shift Curves of Asphalt AAM-1 along the Isothermal Age Scale, Using Temperature Shift Factors, log(a$_T$)

Reference Isothermal Age: 2 hr
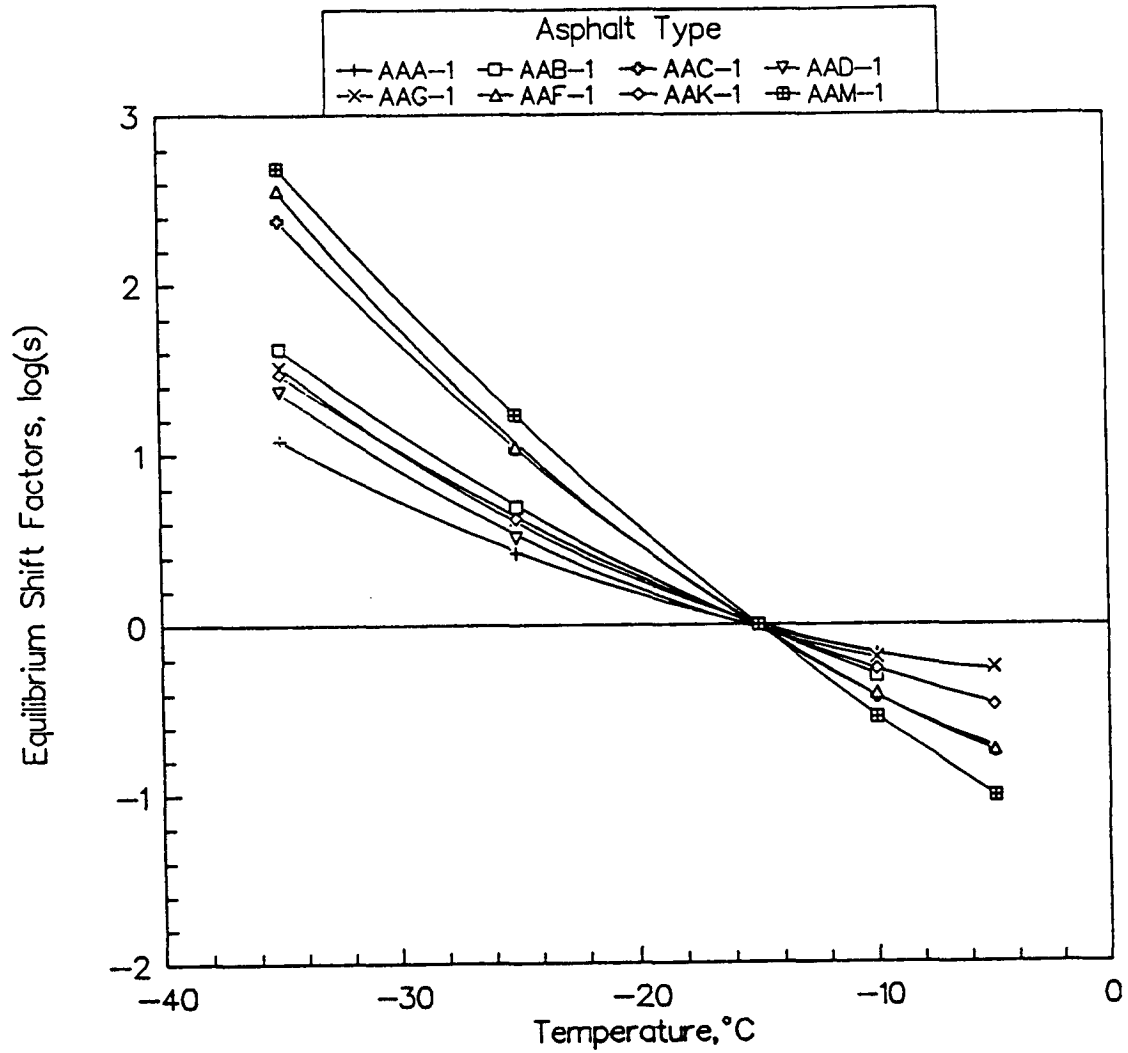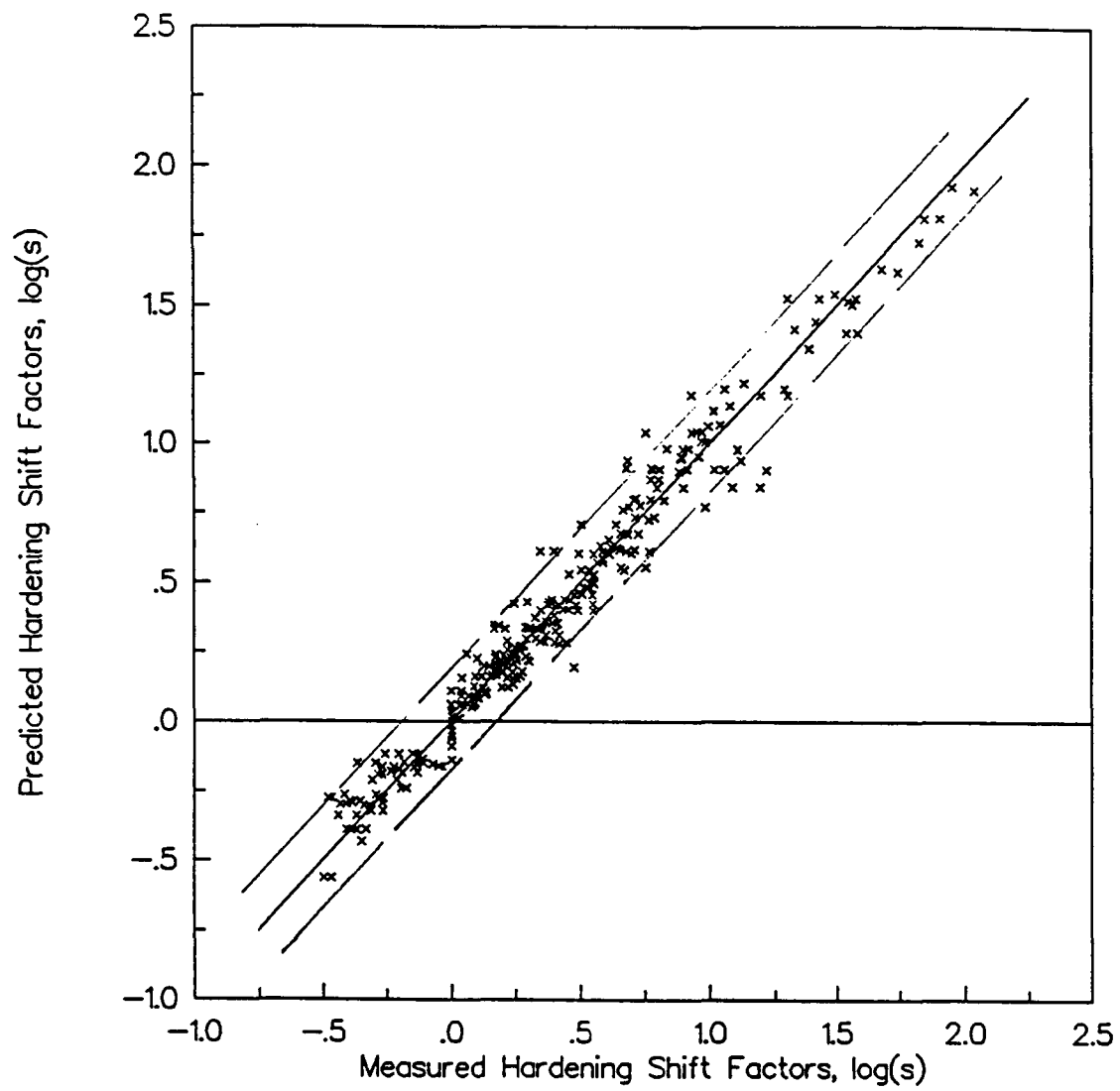
Figure 3.20 Equilibrium (Vertical) Shift Factors, β_E, for Hardening Curves of the Eight Study Asphalts

Reference Temperature: −15 °C
Reference Isothermal Age: 2 hr
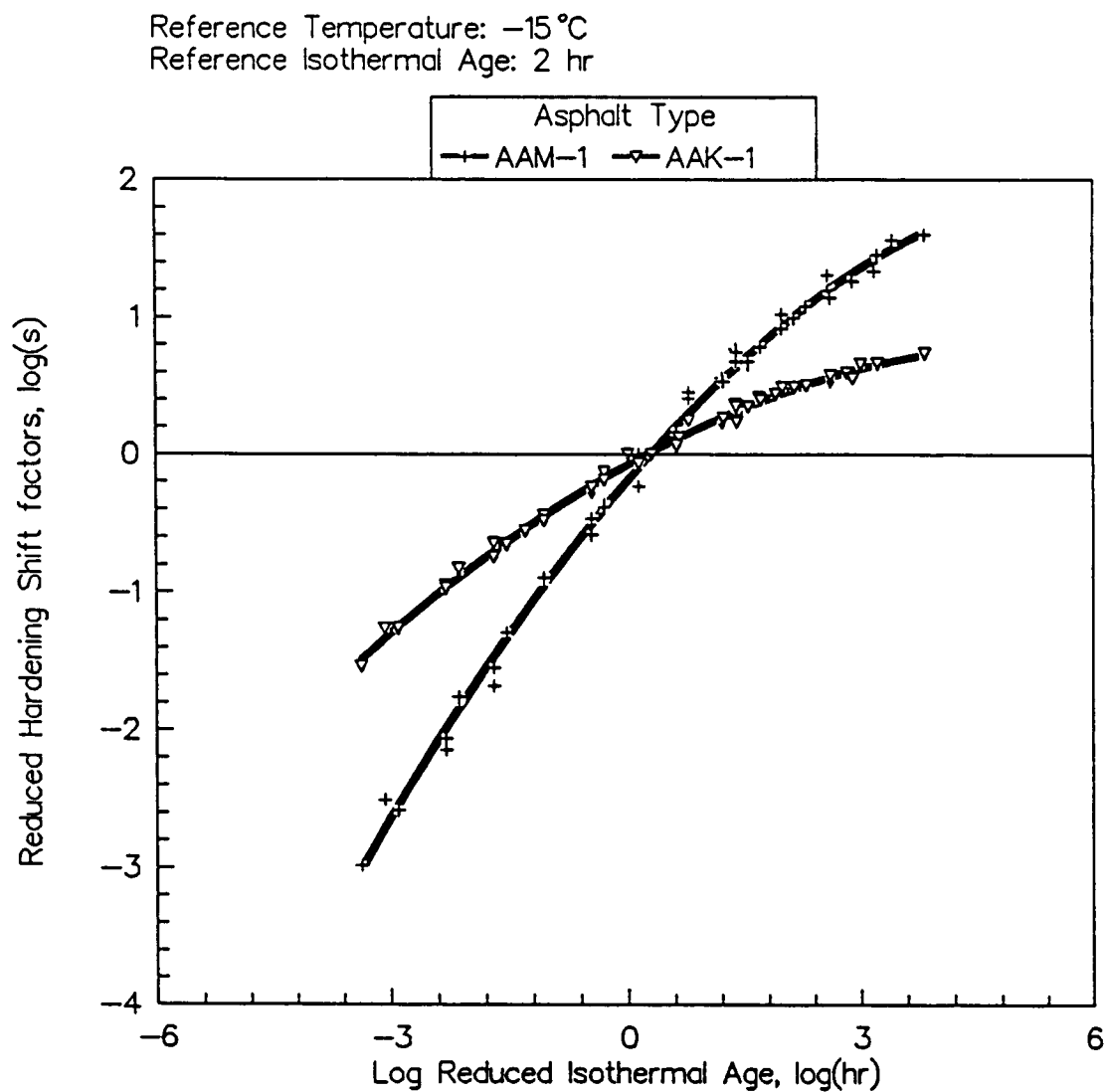
Figure 3.21   Hardening Shift Master Curves for Asphalts AAM-1 and AAK-1

171
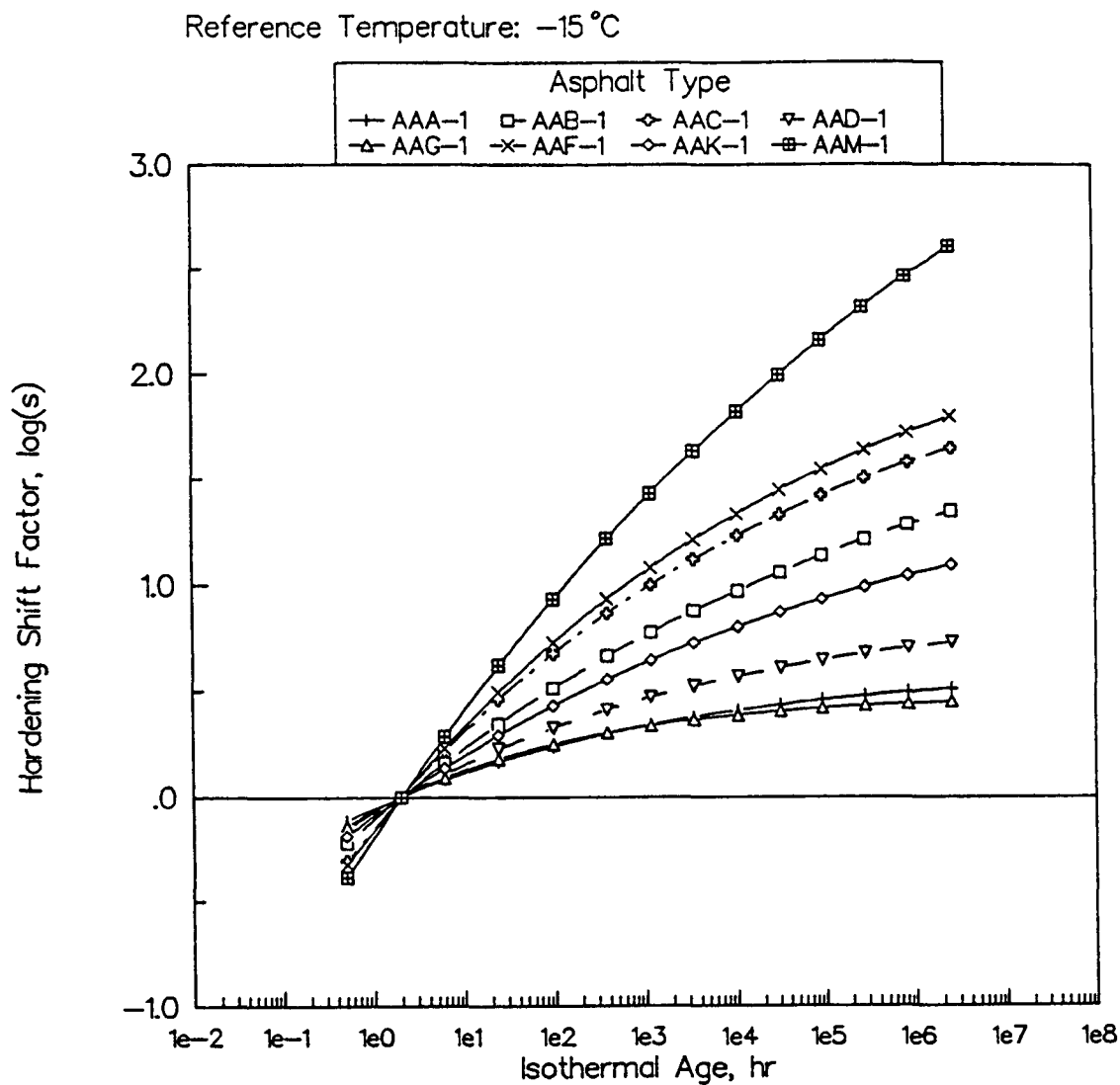
Figure 3.22 Fitted Hardening Master Curves for the Eight Study Asphalts Relative to Isothermal Time of 2 hrs at −15°C

172

Figure 3.23   Measured versus Predicted Values of Hardening Shift Factors
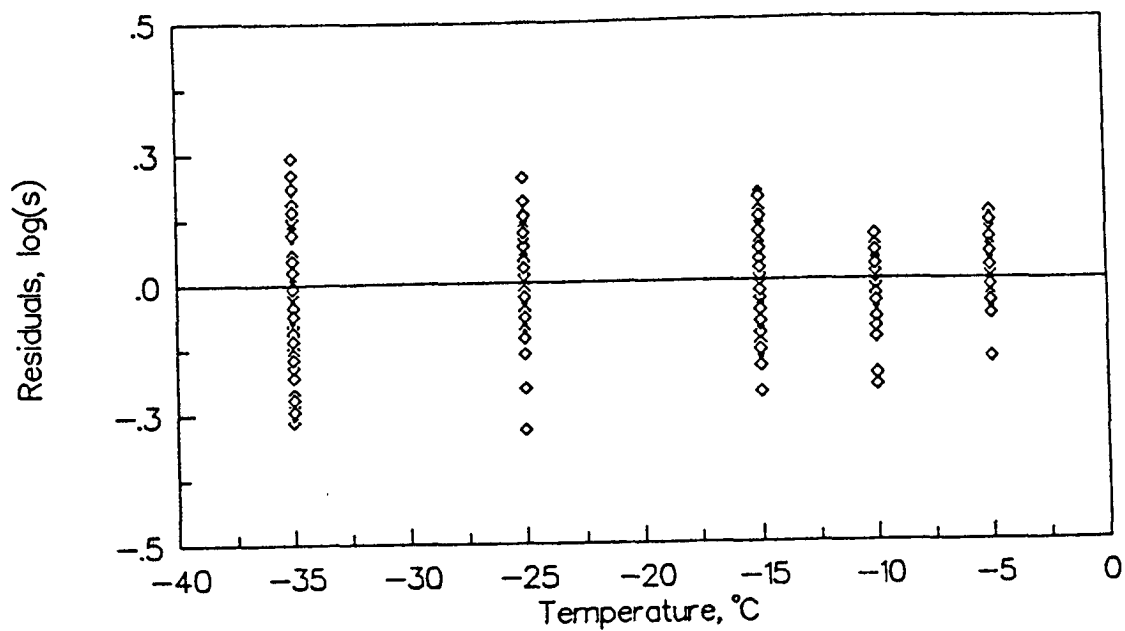
Figure 3.24   Residual Plot of Isothermal Shift Factors versus Temperature
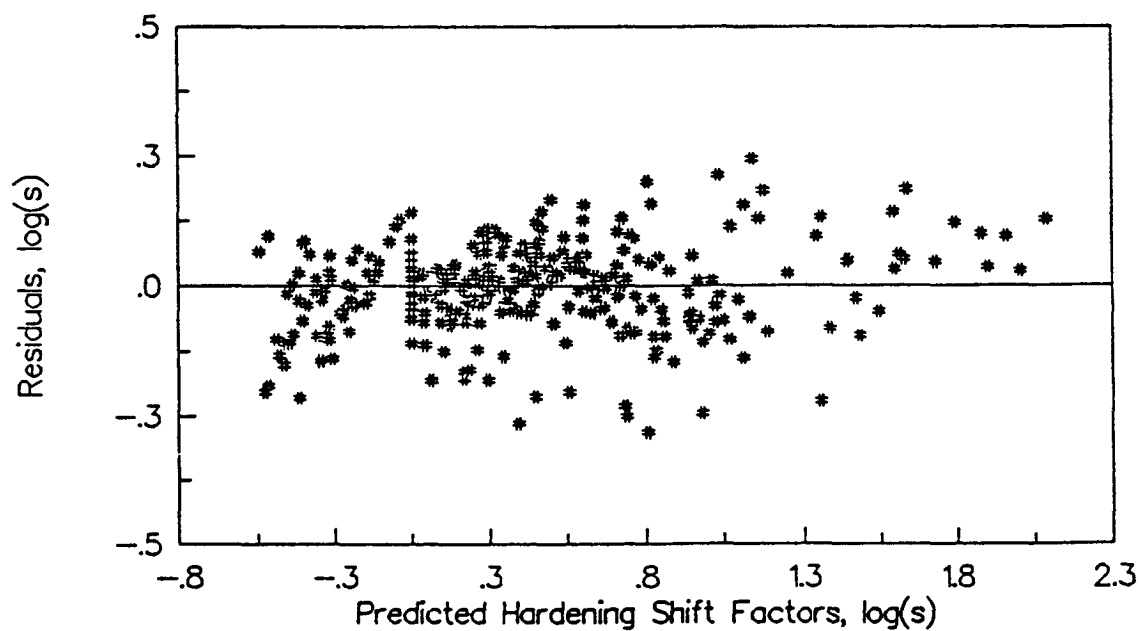
Figure 3.25   Residual Plot of Isothermal Shift Factors versus Asphalt Source

174
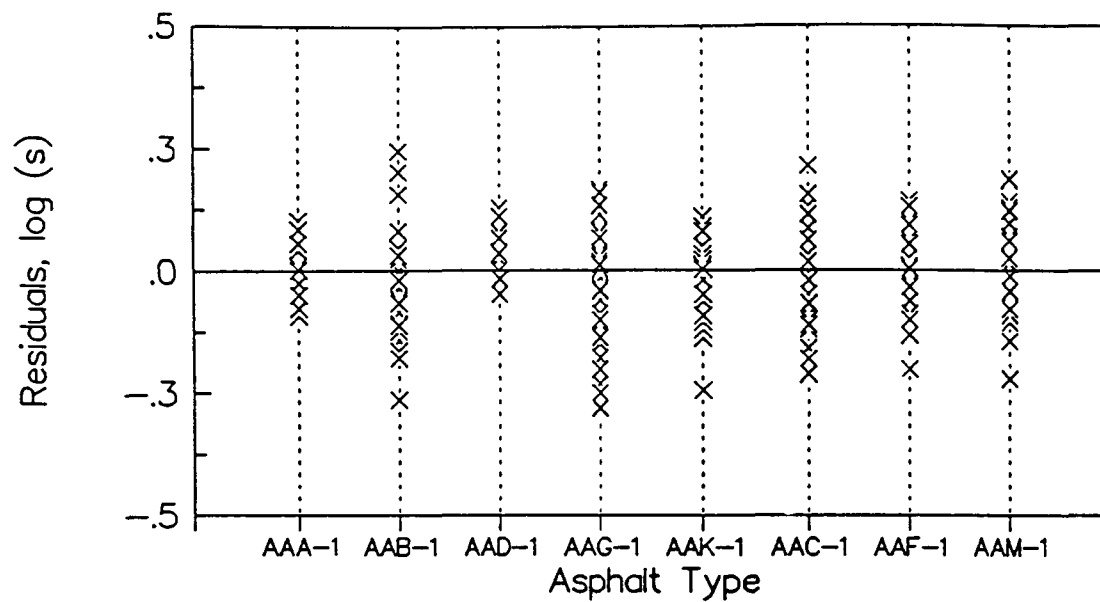
Figure 3.26   Residual Plot of Isothermal Shift Factors versus Isothermal Age
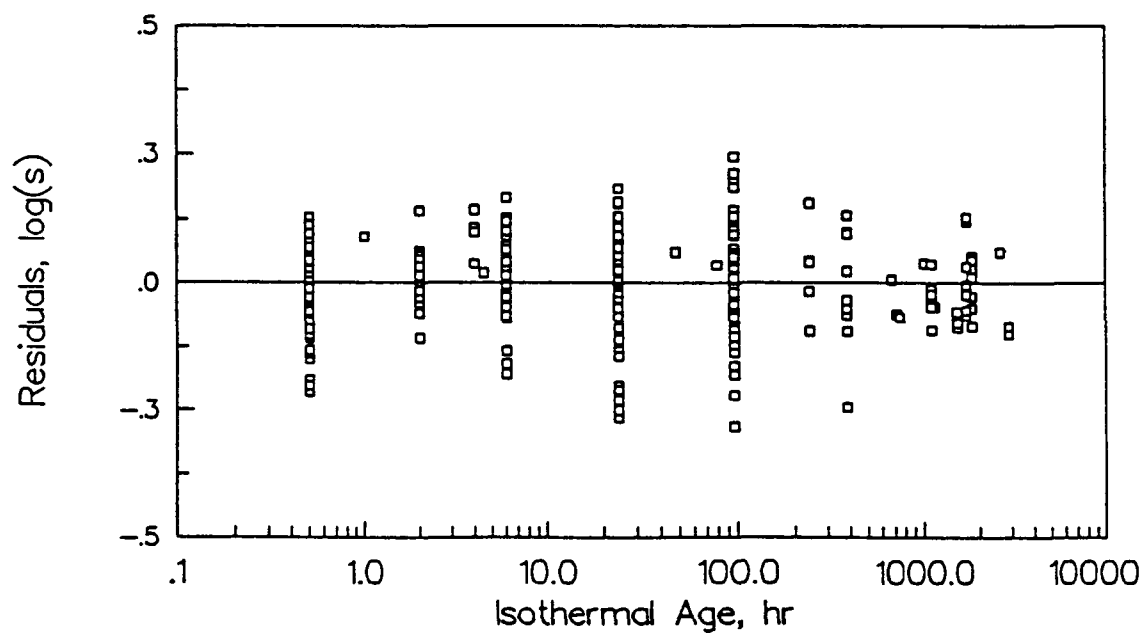
Figure 3.27   Residual Plot of Isothermal Shift Factors versus Predicted Values
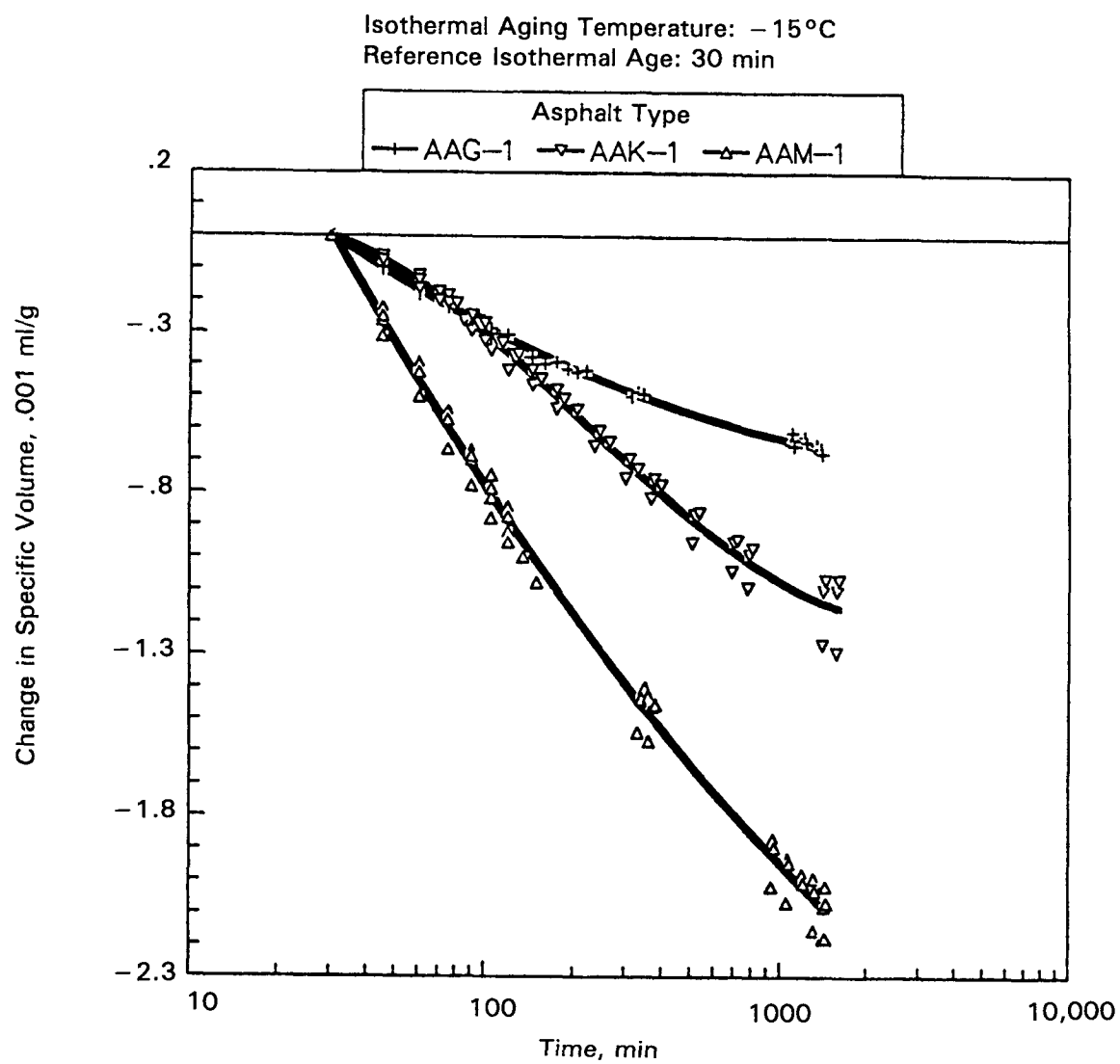
Figure 3.28   Measured Isothermal Volume Change for Three Asphalts at −15°C
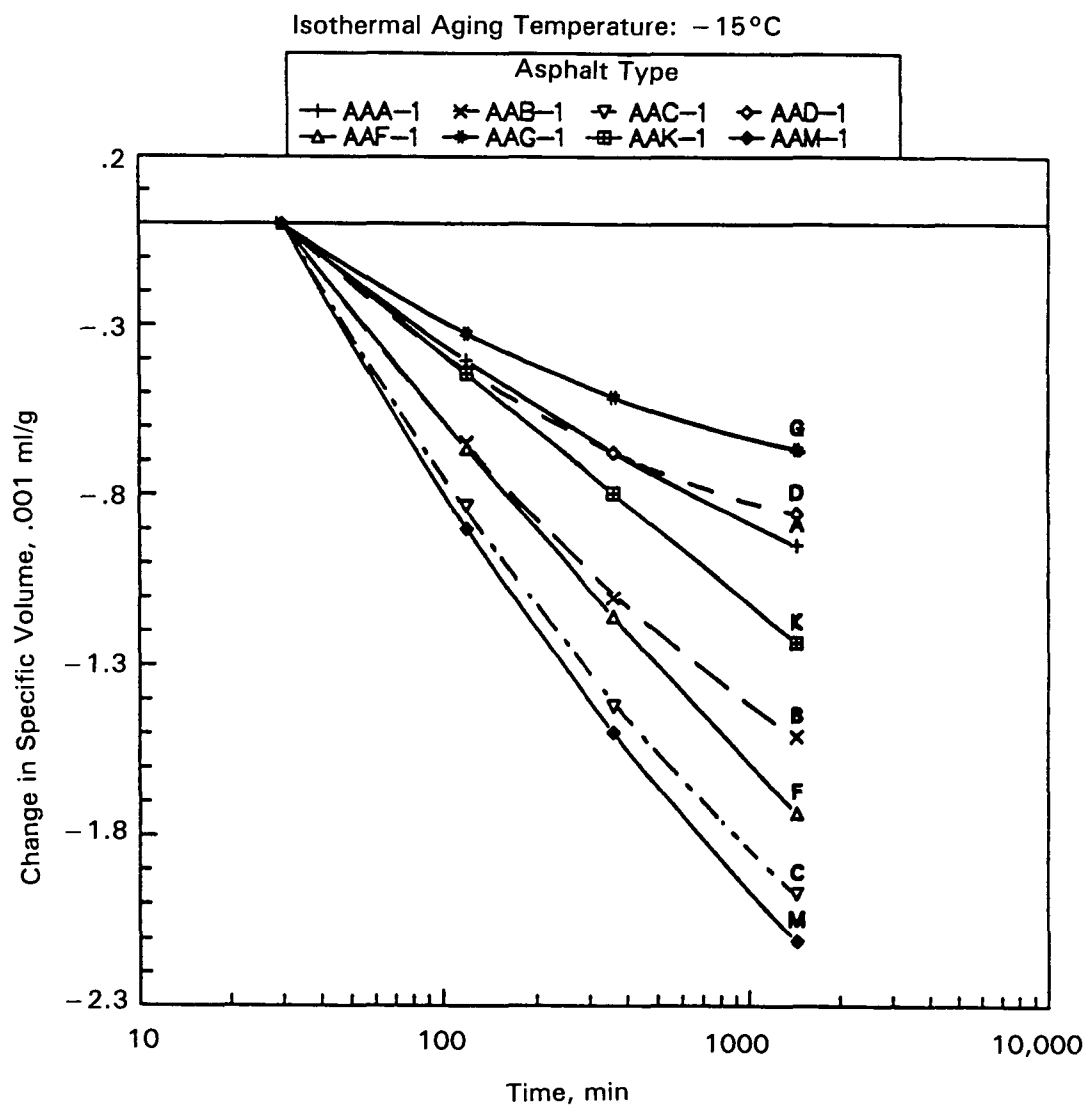
Figure 3.29 Fitted Relations for Isothermal Volume Changes of the Eight Study Asphalts
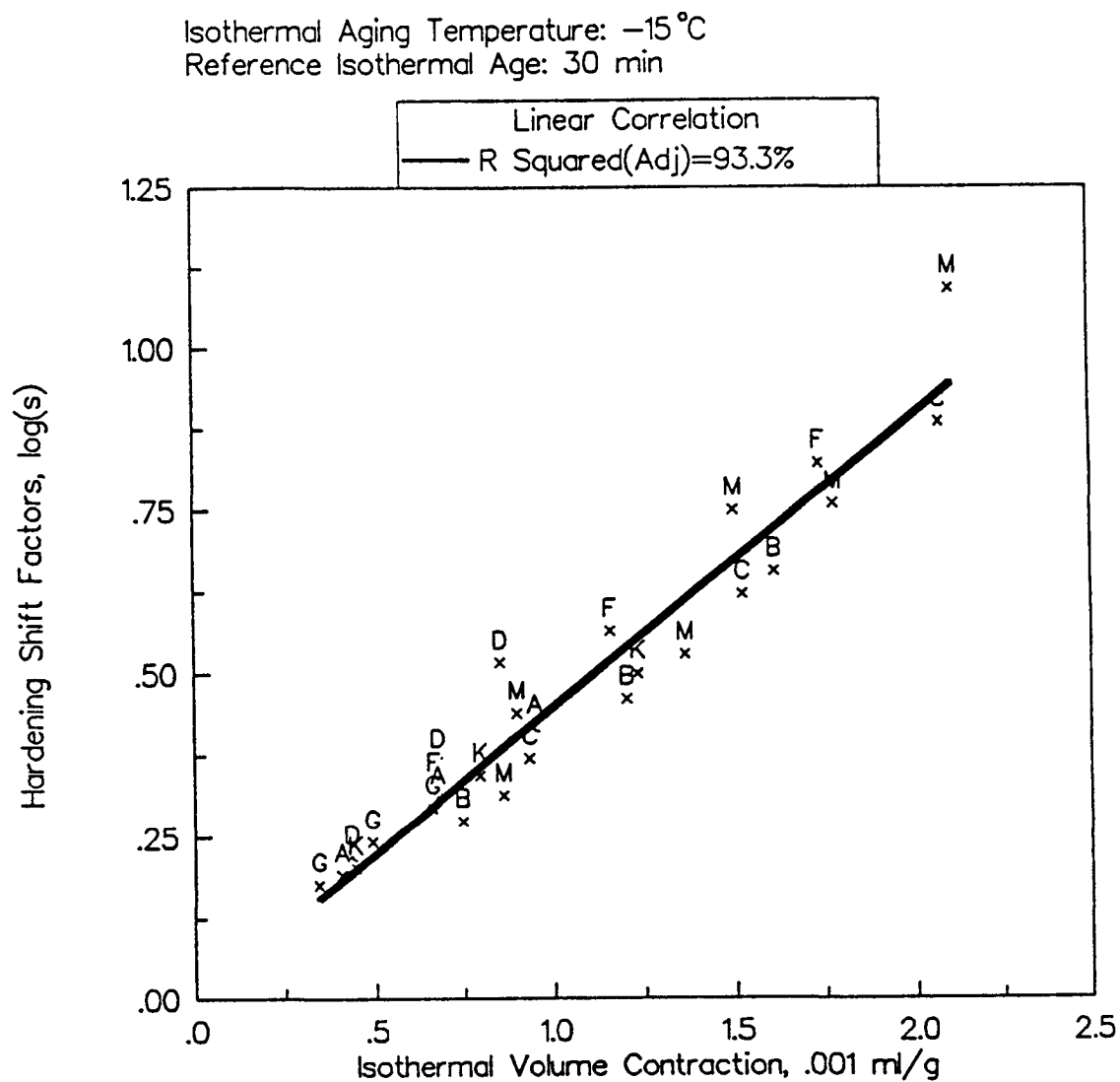
Figure 3.30   Correlation between Hardening Shift and Isothermal Volume Change at Common Isothermal Time
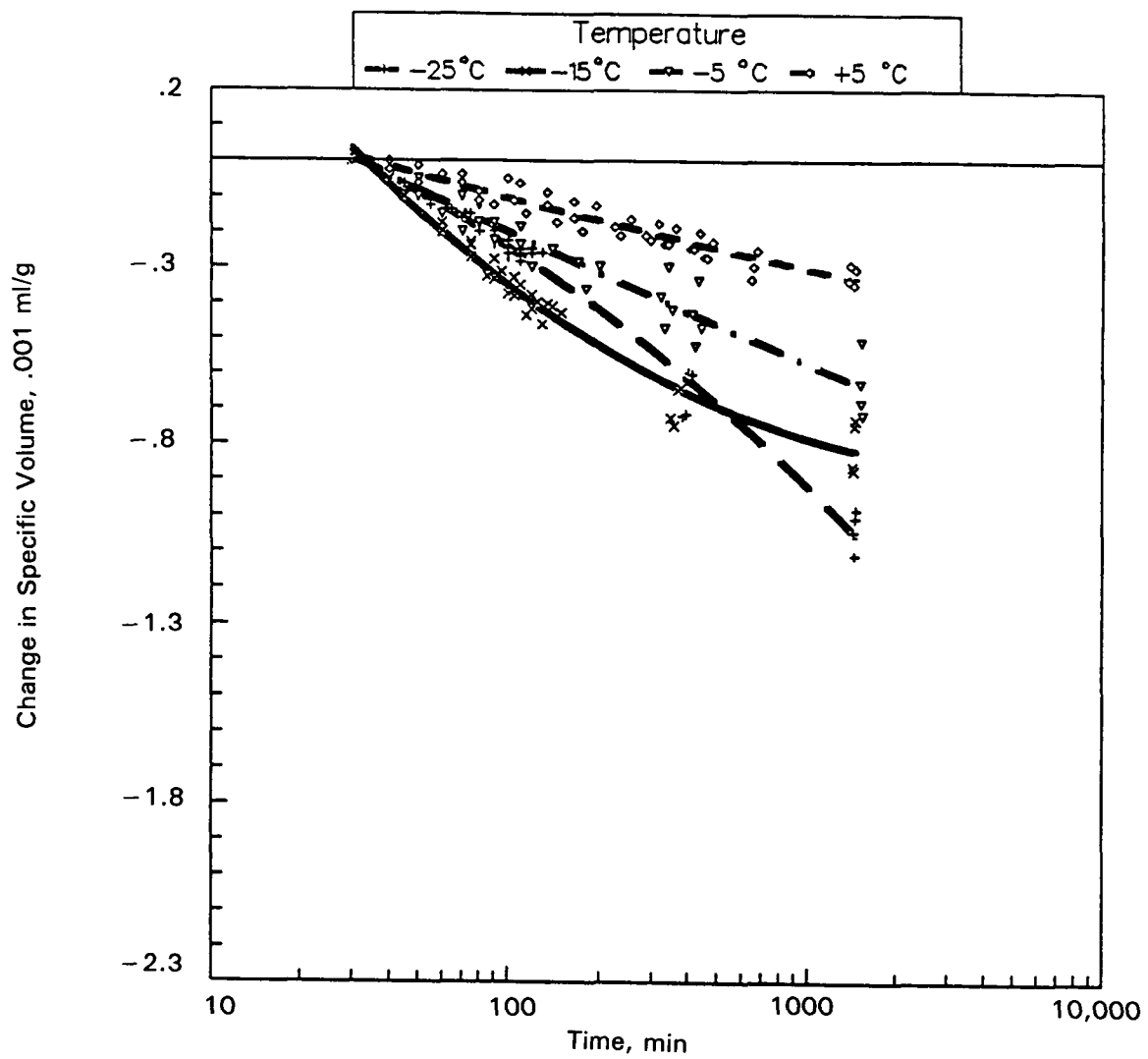
Figure 3.31 Isothermal Volume Contraction of Asphalt AAM-1 at Different Temperatures
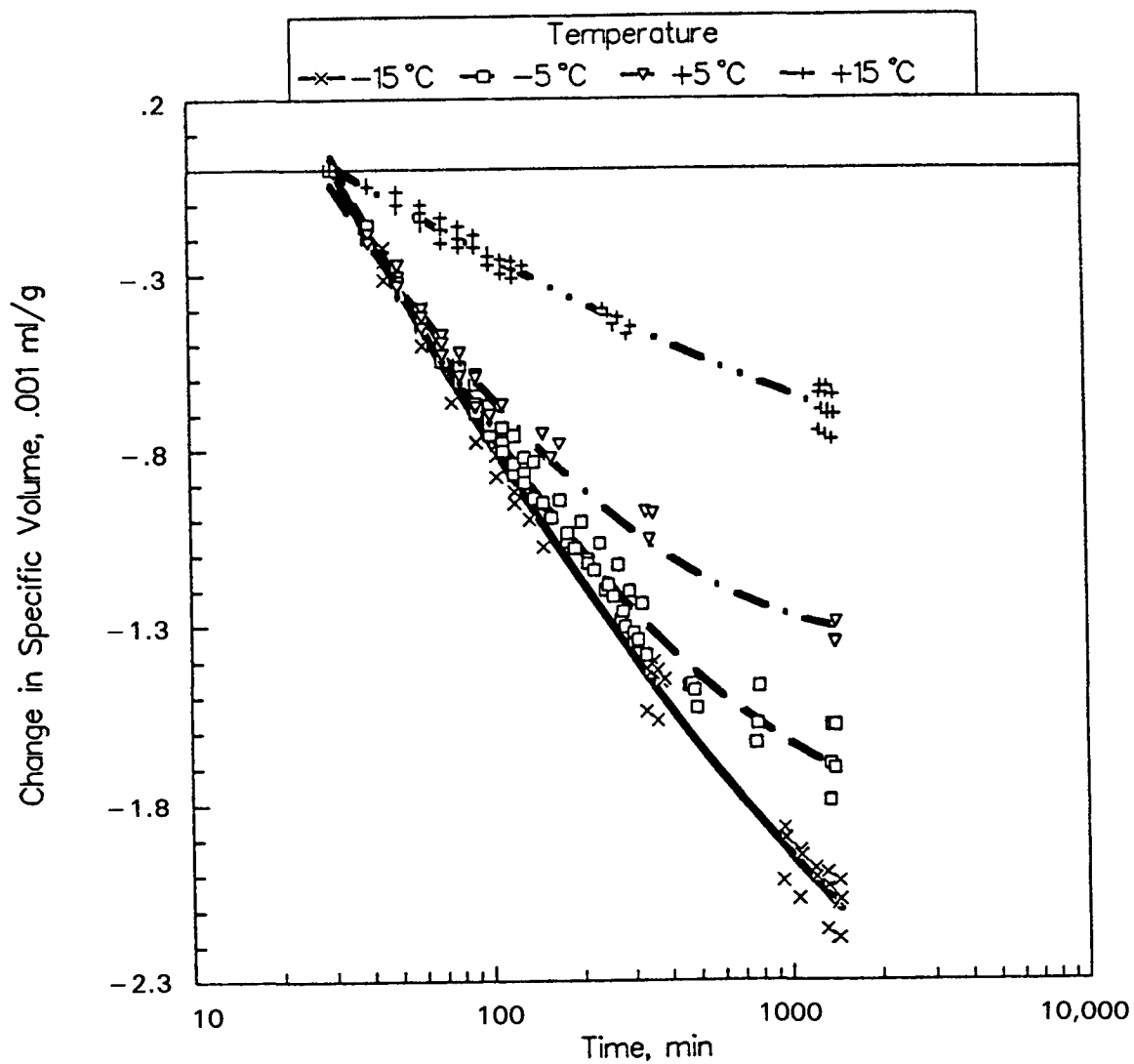
Figure 3.32   Isothermal Volume Contraction of Asphalt AAD-1 at Different Temperatures

180
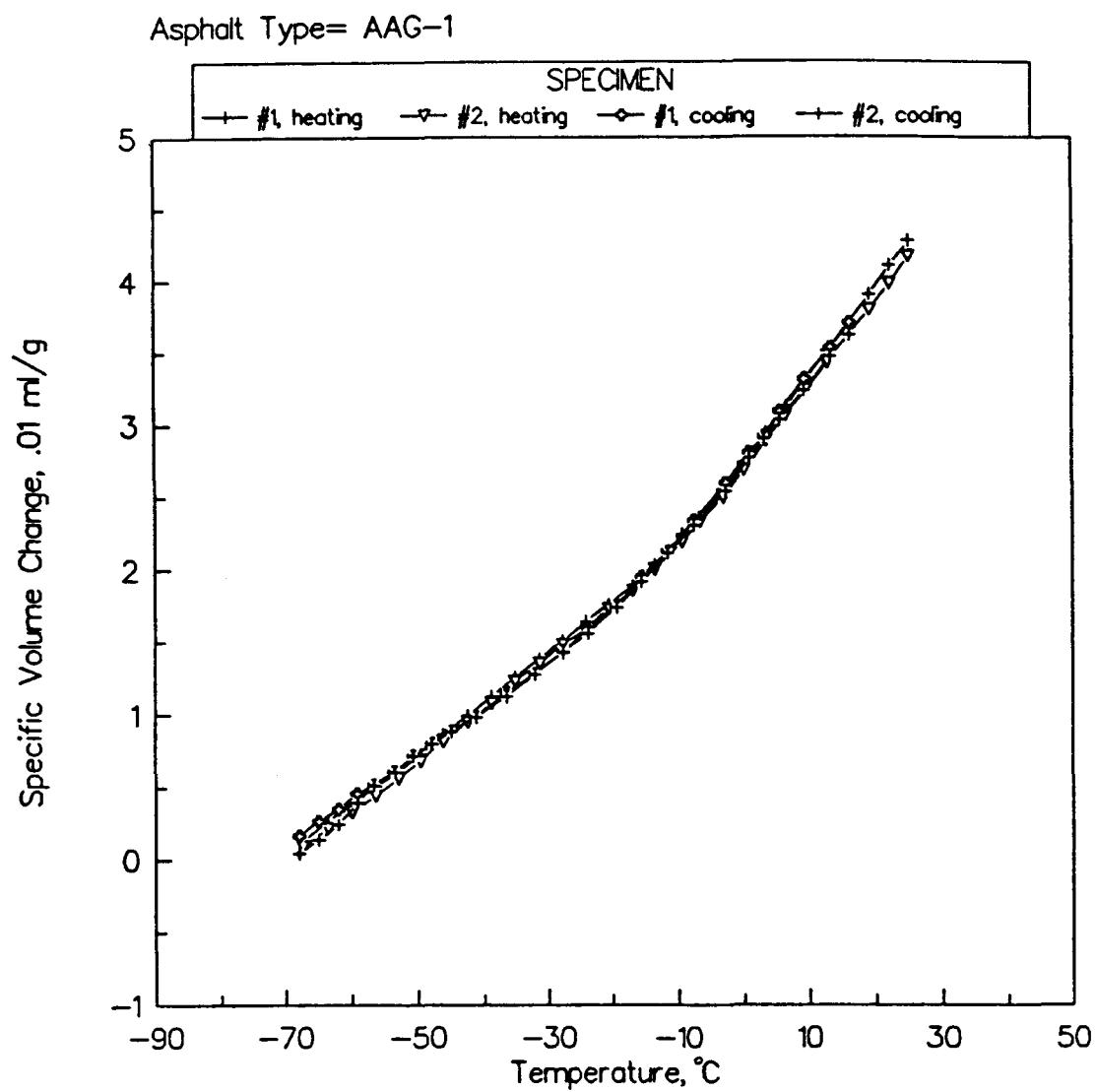
Figure 3.33 **Typical Example of Volume-Temperature Measurements in the Cooling and Heating Ramps**
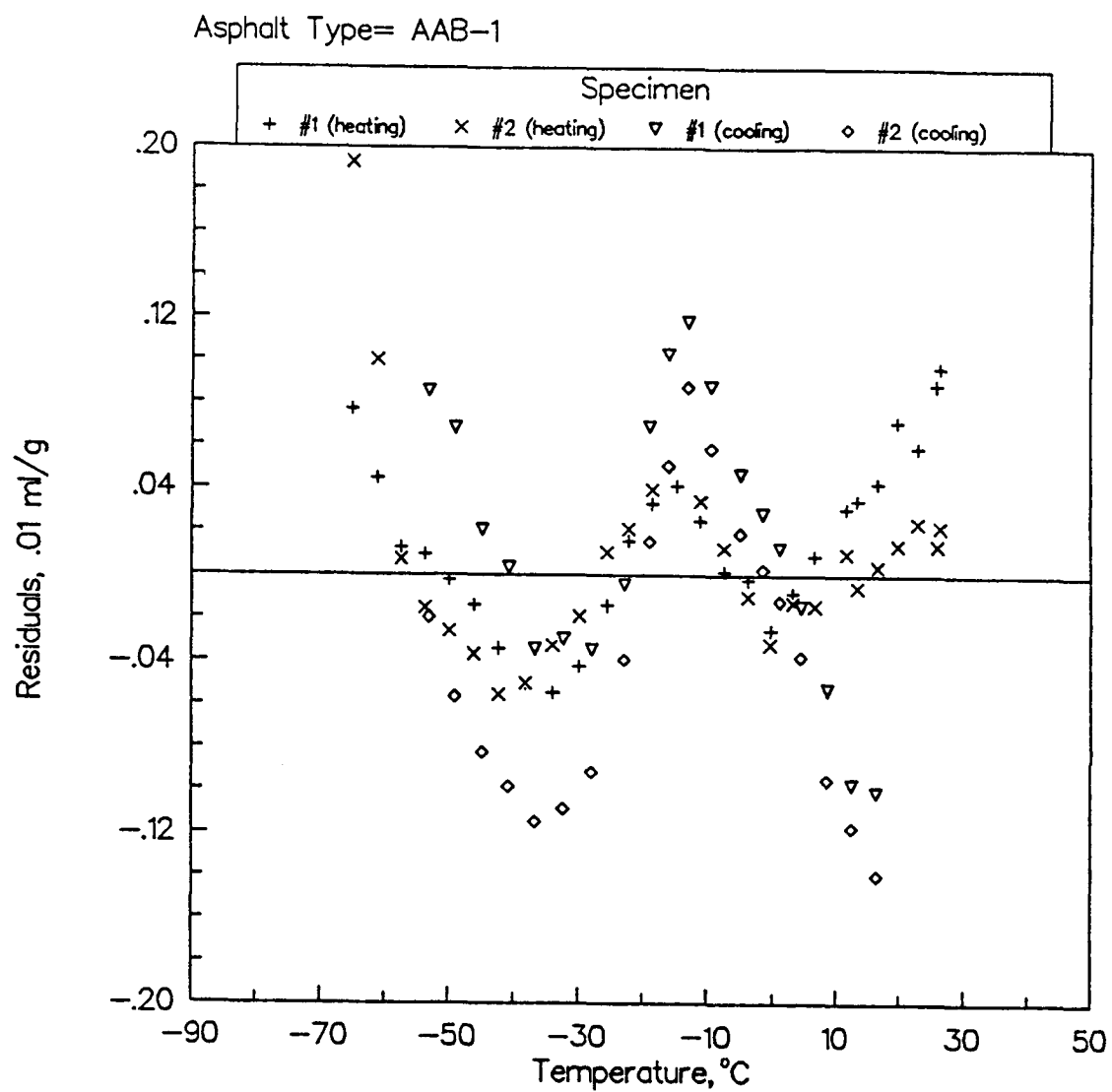
Figure 3.34 **Typical Example of Residual Plot versus Temperature Using the Bilinear Fit to Estimate** T_g

Asphalt Type= AAG−1
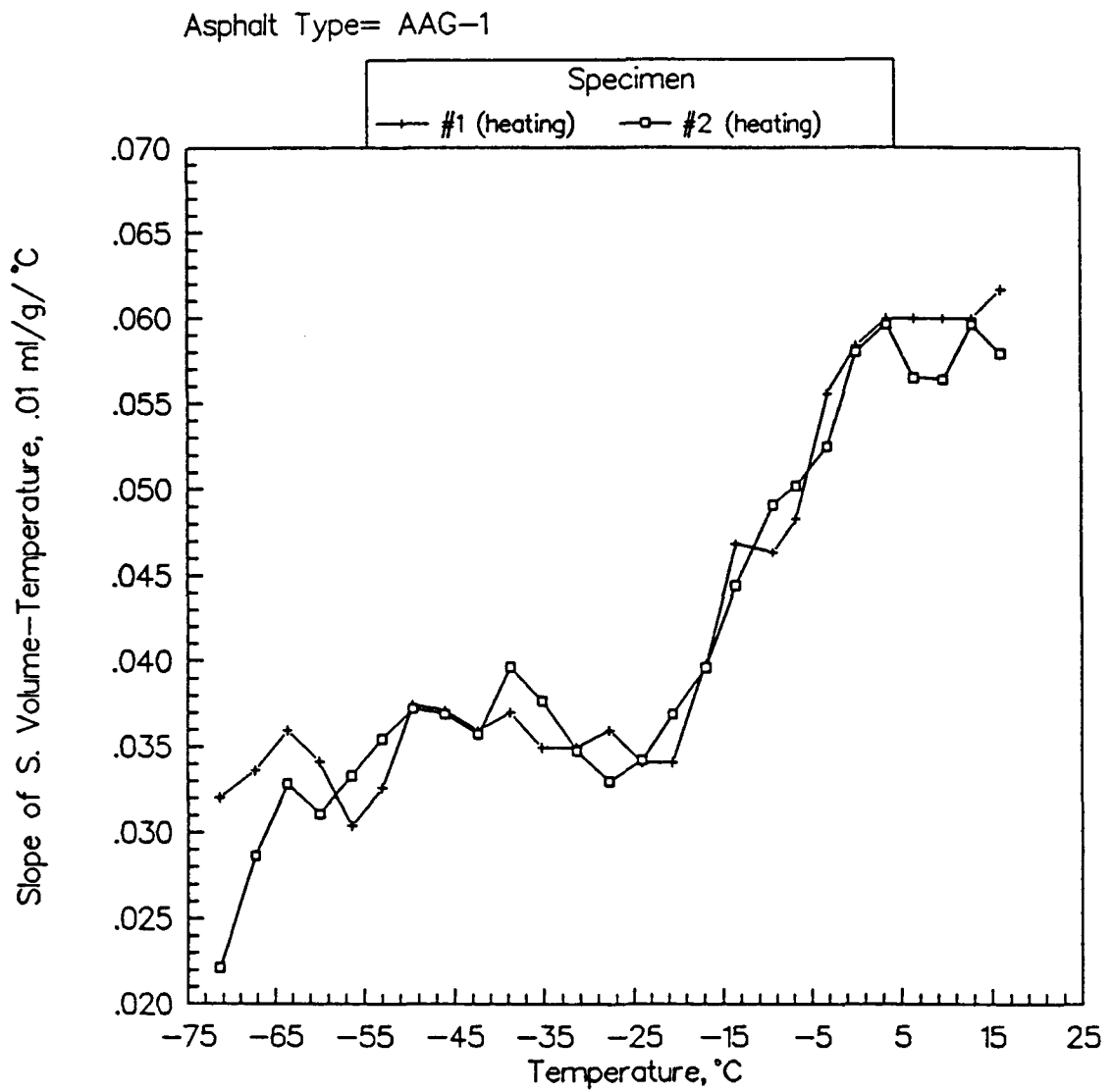
Figure 3.35 **Typical Example of Change with Temperature of Measured Specific Volume-Temperature Relation**
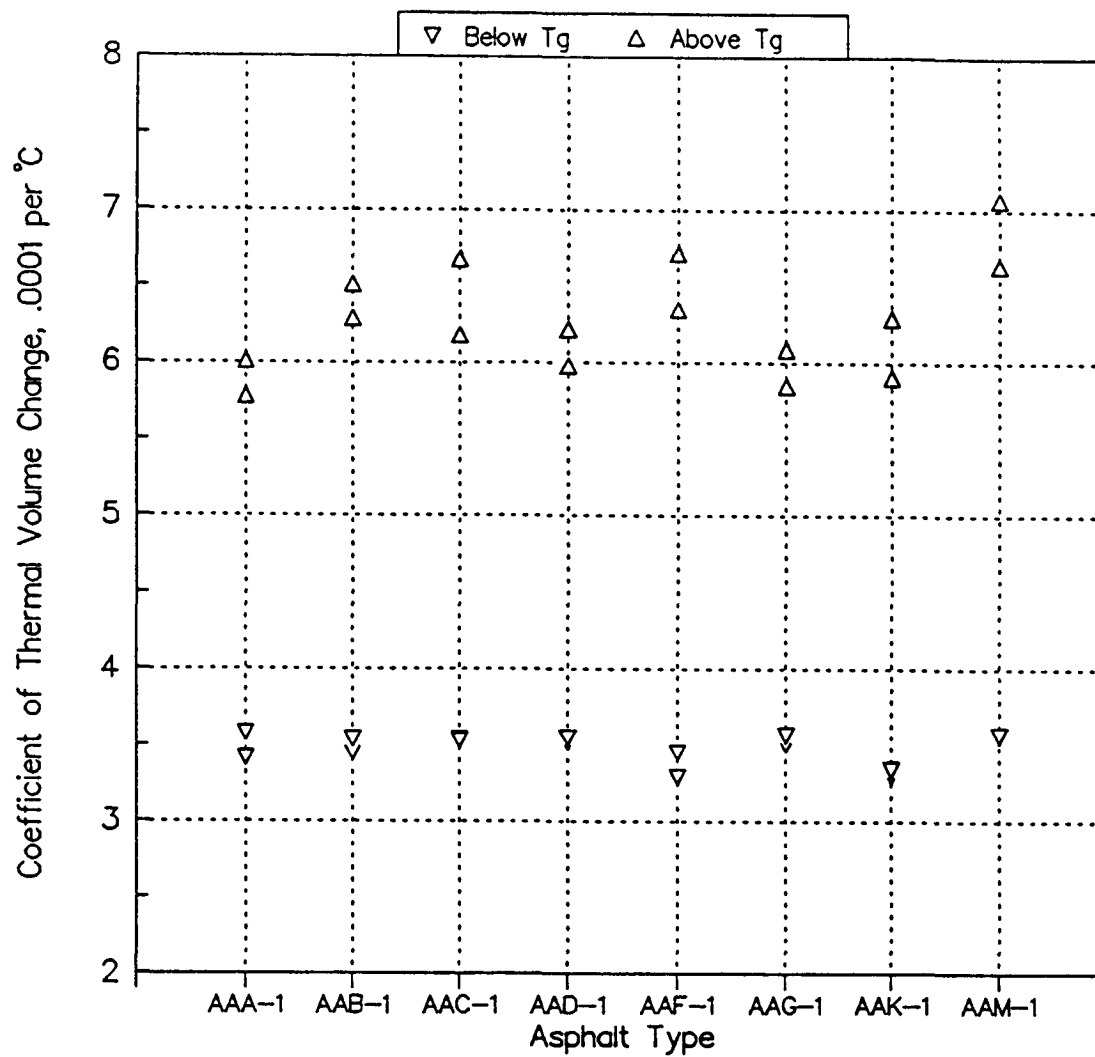
Figure 3.36   Coefficients of Volumetric Expansion for the Eight Study Asphalts
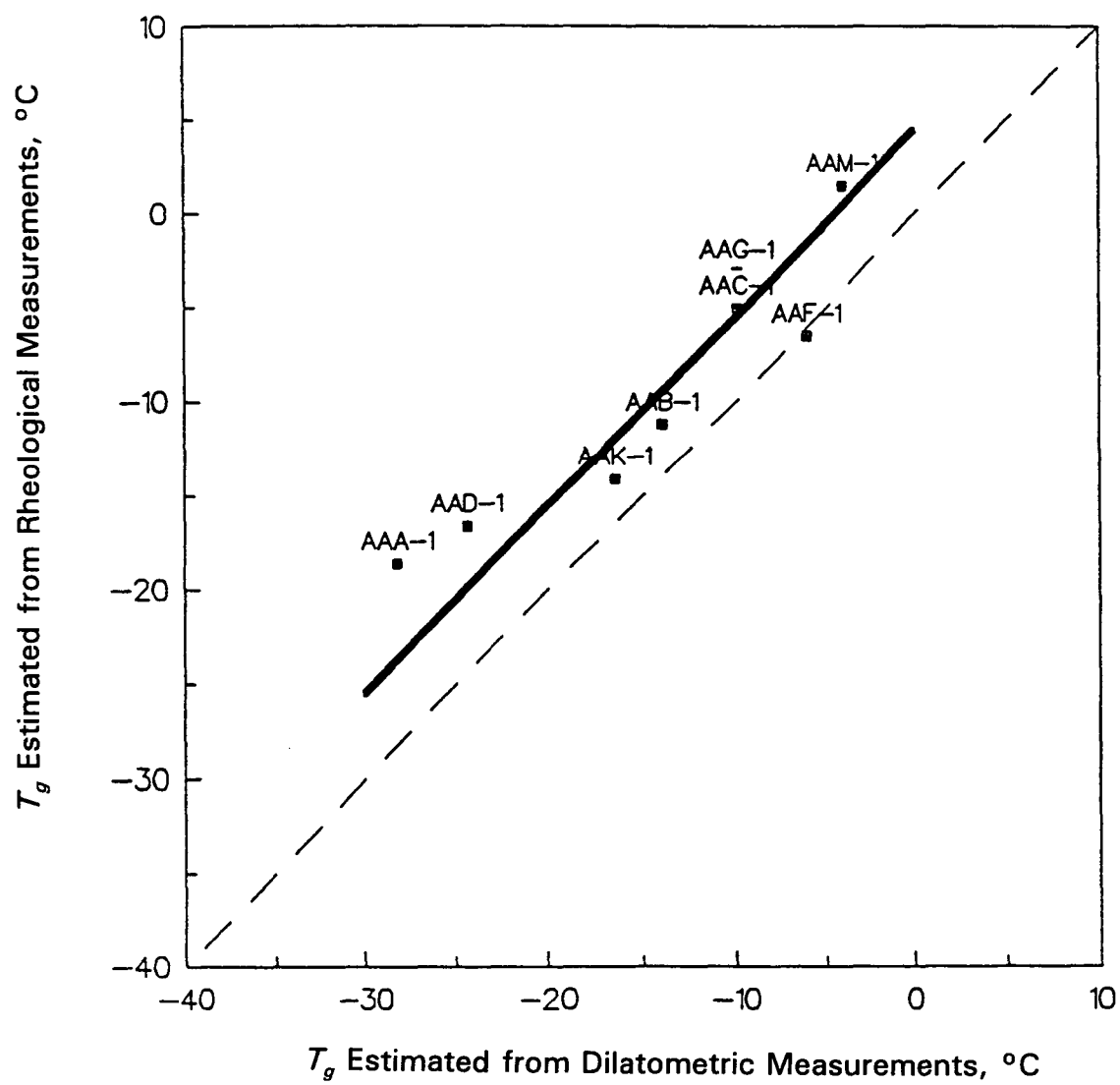
Figure 3.37   Correlation between Volumetric and Dynamic Glass Transition Temperatures
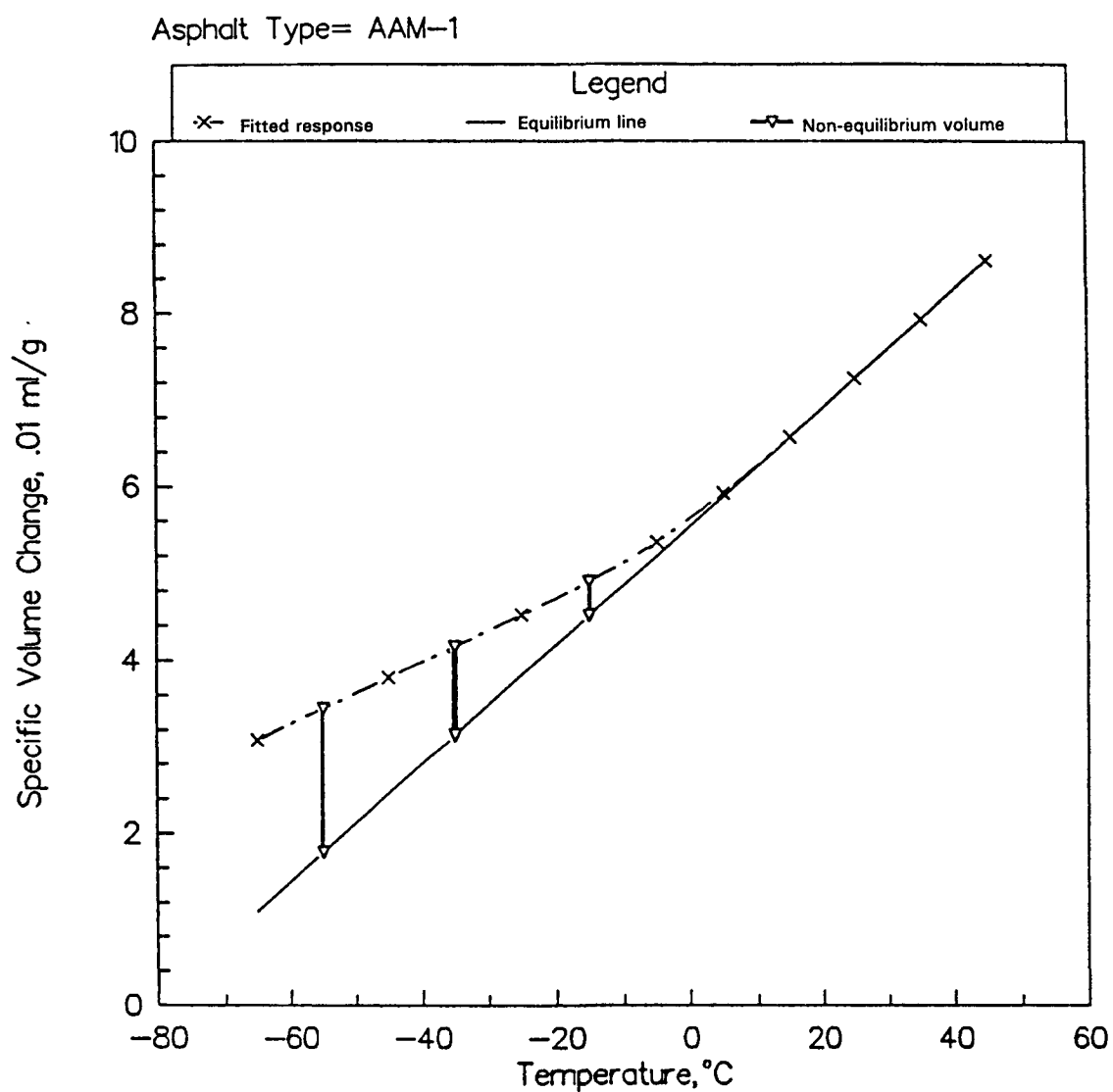
Figure 3.38 **Typical Plot of Volume-Temperature Relation Depicting the Method of Calculating the Nonequilibrium Volume**
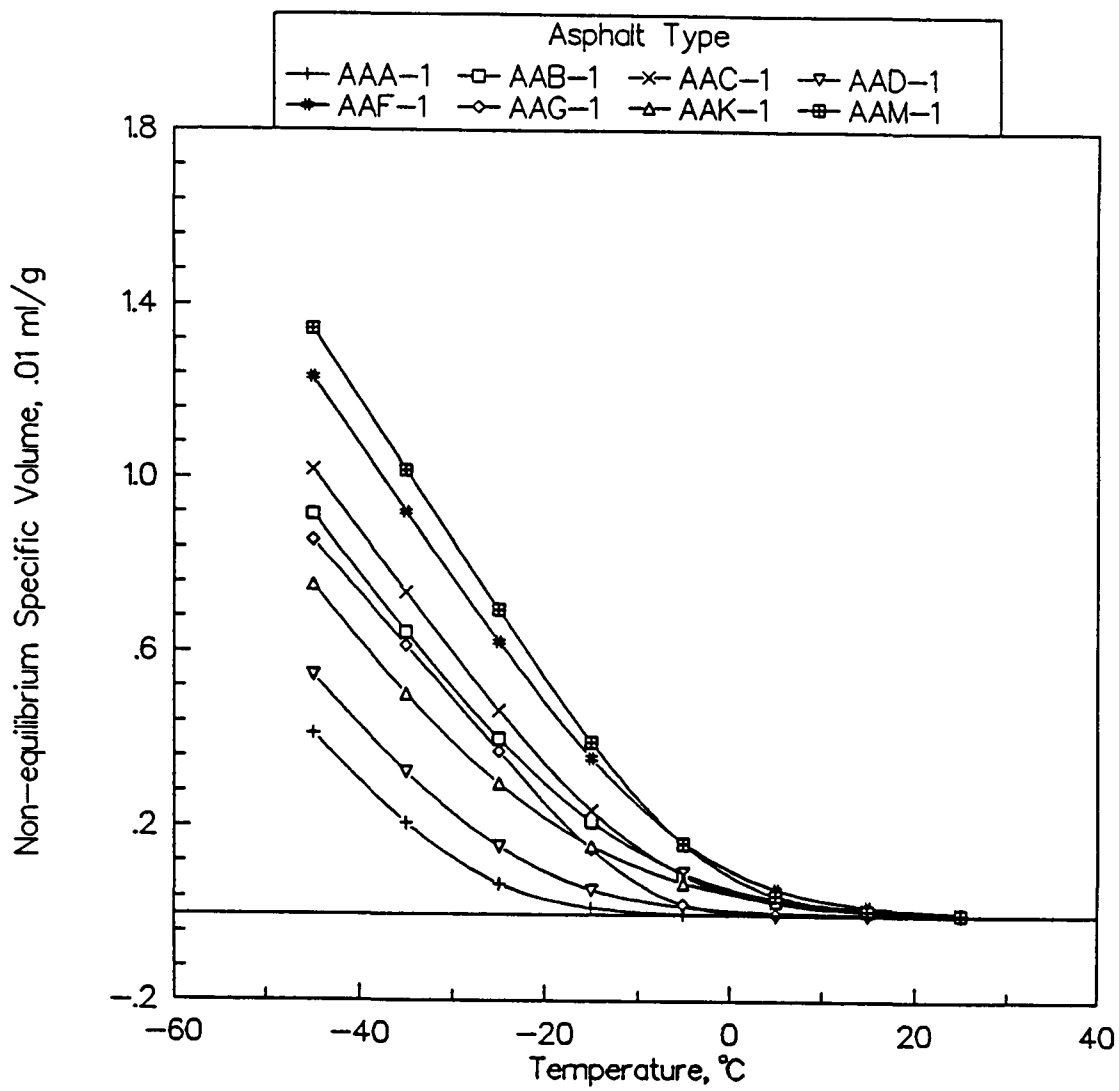
Figure 3.39 **Estimated Variation of Nonequilibrium Specific Volume with Temperature for the Eight Study Asphalts**
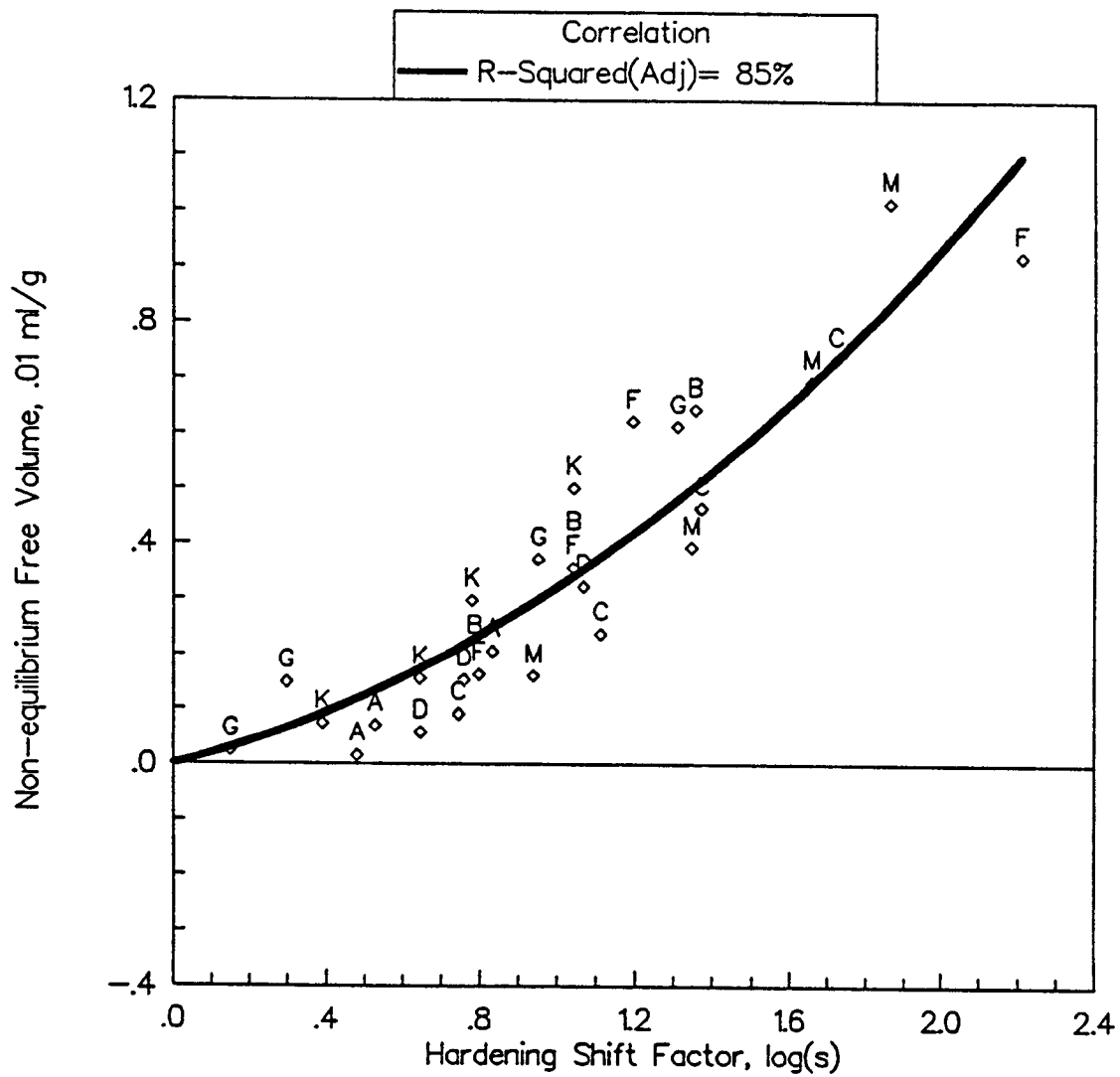
Figure 3.40   Correlation between Nonequilibrium Volume and Hardening Shift Factors
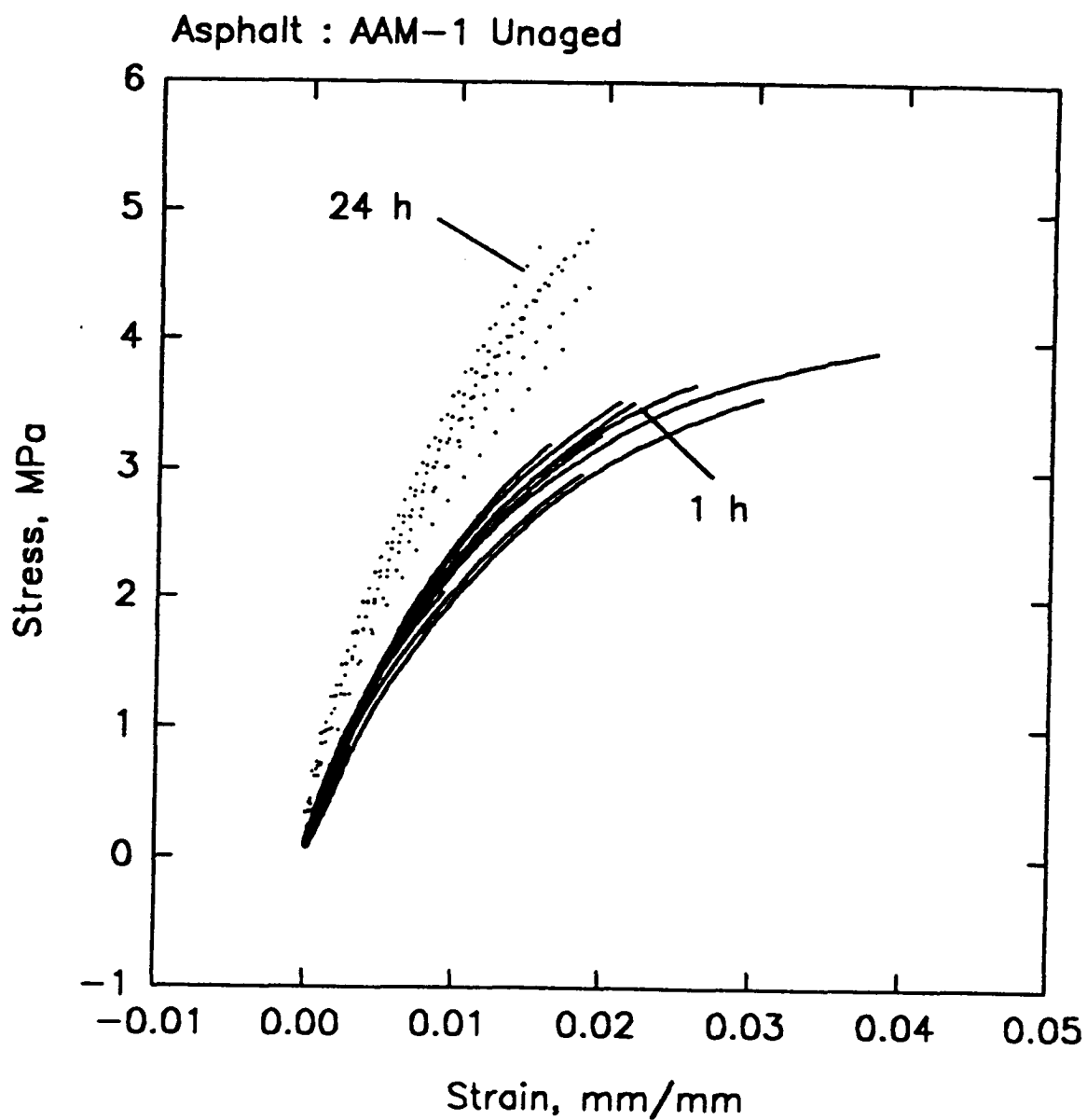
Figure 3.41   Effect of Physical Hardening on Stress-Strain Behavior to Failure of
Asphalt AAM-1
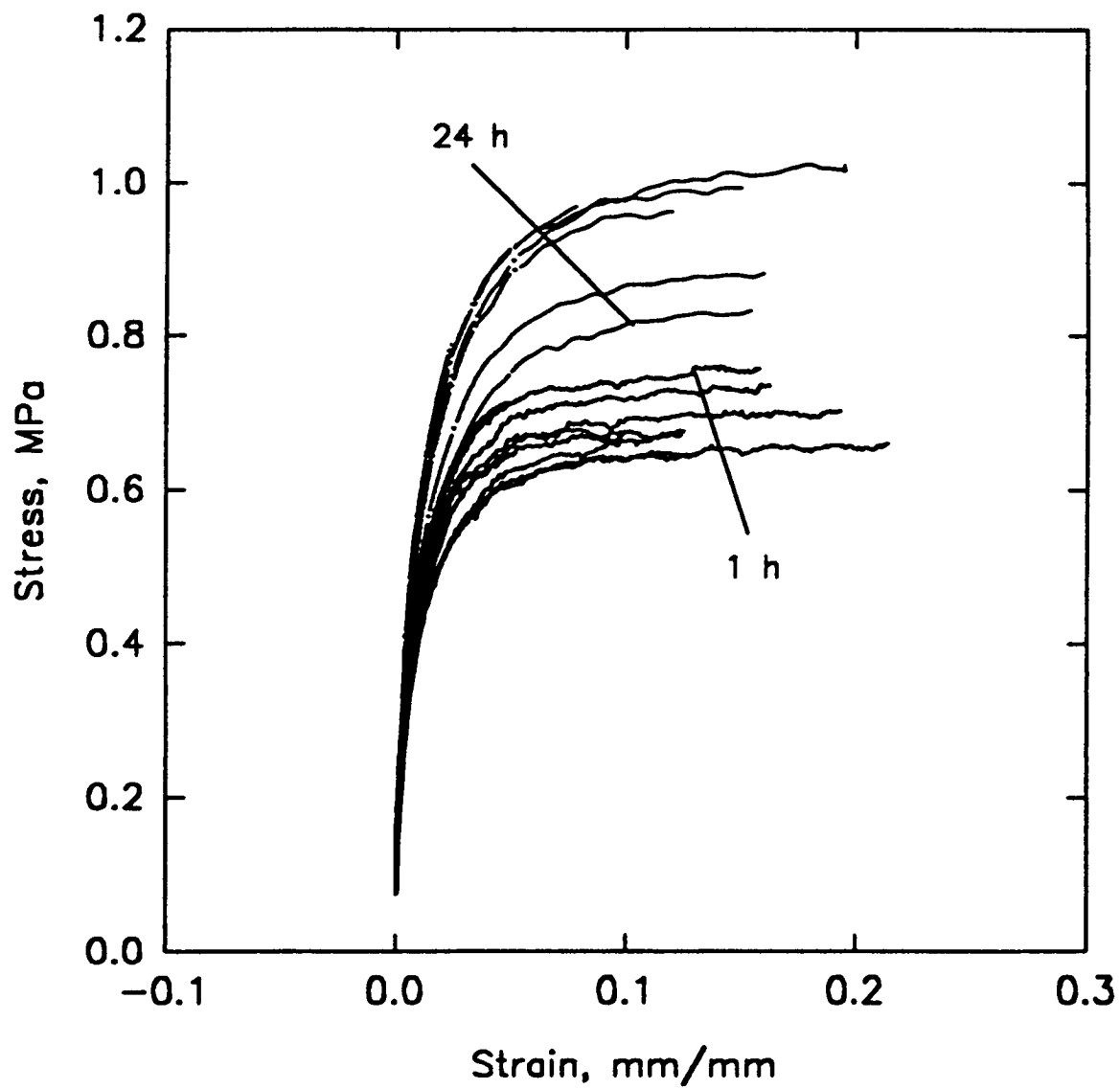
Figure 3.42   Effect of Physical Hardening on Stress-Strain Behavior to Failure of Asphalt AAA-1
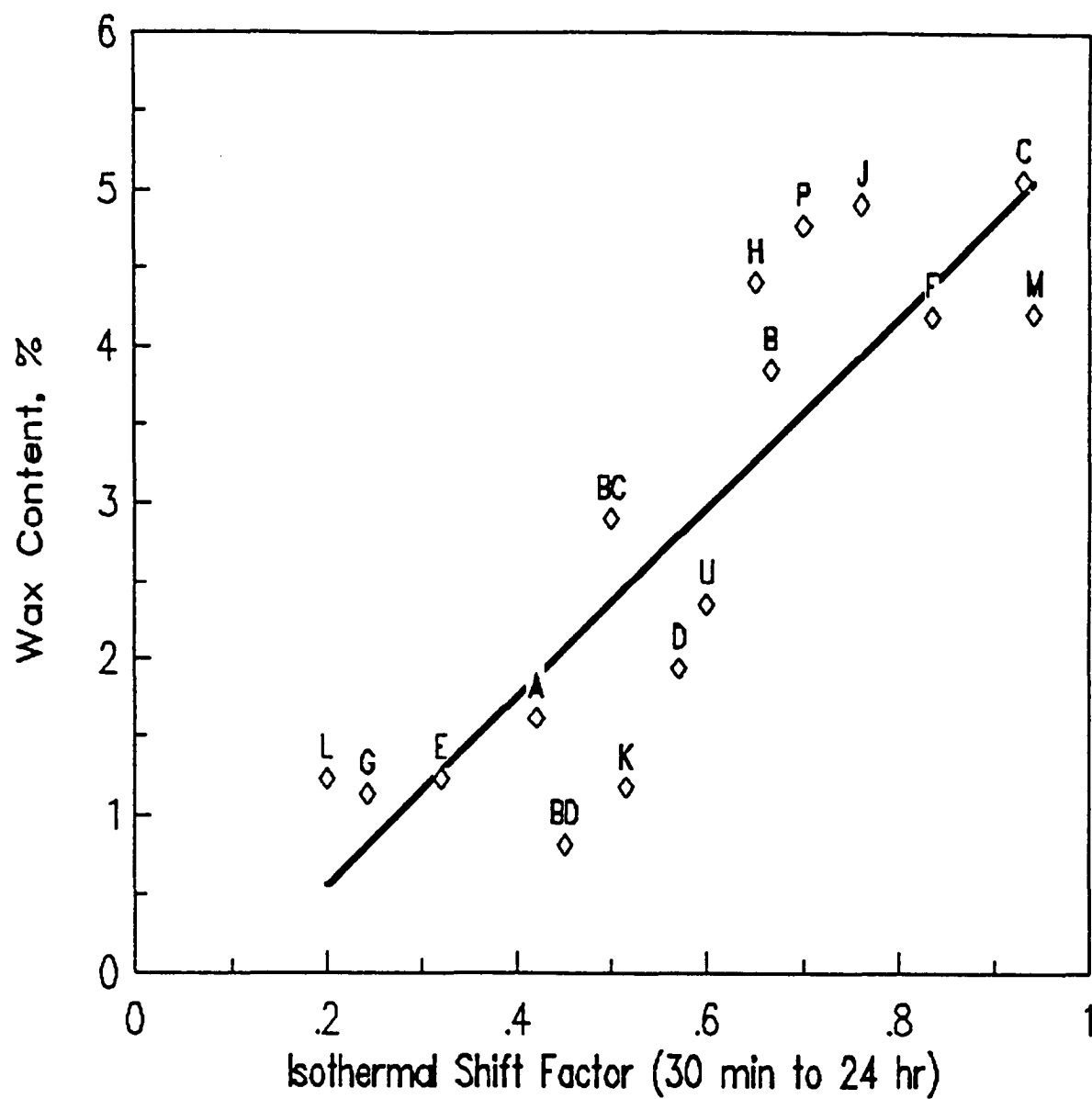
Figure 3.43   Correlation between Hardening Shift Factor at −15°C and Wax Content for 16 SHRP Asphalts
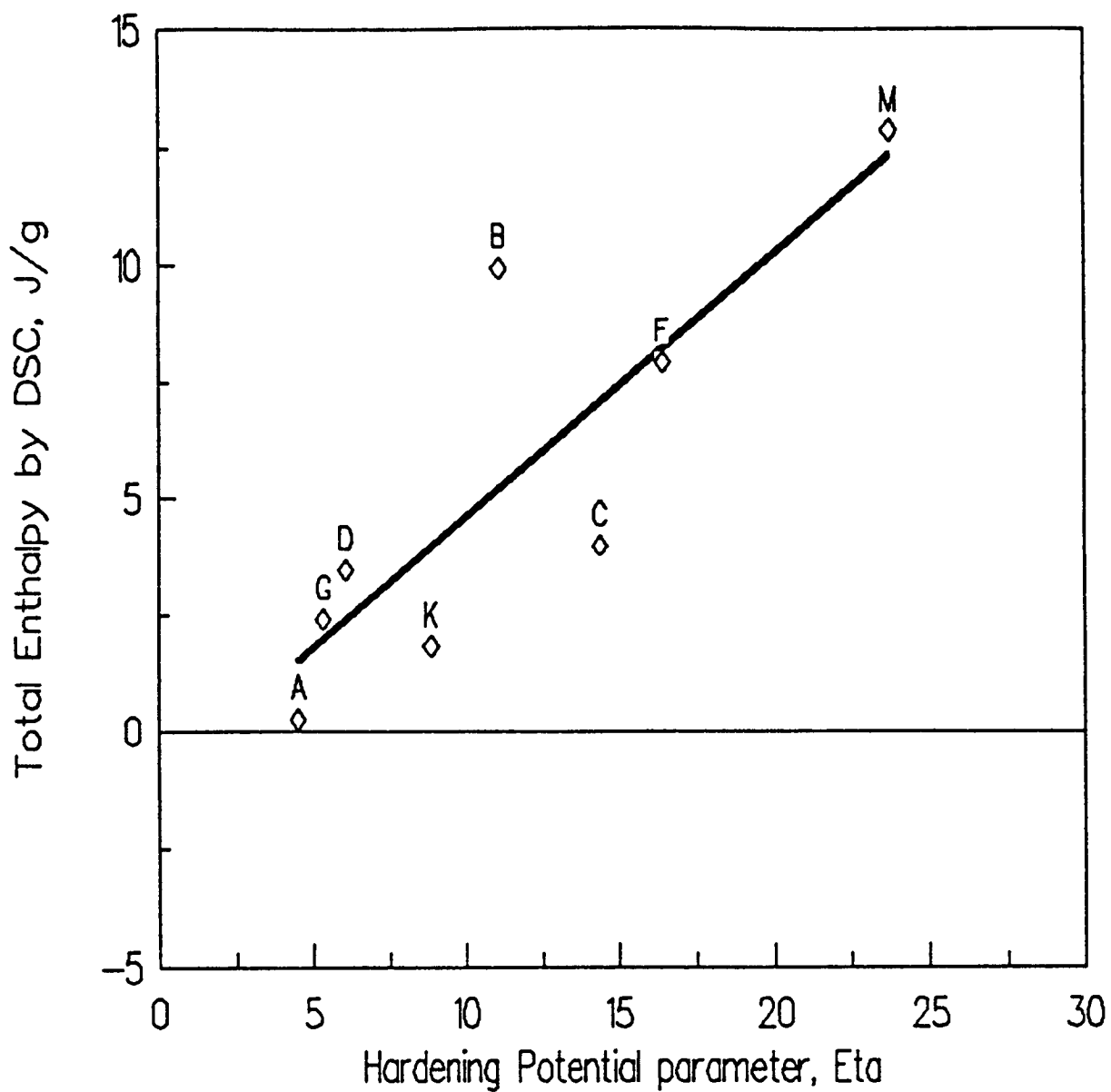
Figure 3.44 Correlation between Total Endothermic Enthalpy and Hardening Potential for Eight Core SHRP Asphalts

Table 3.1 Examples of Hardening Shift Factors Calculated Using Nonlinear Regression Procedure

Asphalt	Isothermal	Isothermal Time Shift Factors, log(s)								
AAA-1	6	.203	.044	.114	.027	.096	.013	.080	.017	.9978
Rep.#2	6	.173	.043	.155	.026	.107	.013	.080	.016	.9979
	24	.443	.046	.330	.027	.203	.013	.091	.016	
	96	.655	.048	.405	.027	.264	.014	.122	.016	
AAB-1	6	.246	.009	.236	.005	.254	.002	.127	.003	.9999
Rep.#1	24	.700	.010	.500	.005	.412	.002	.268	.003	
	96	1.22	.011	.681	.005	.539	.003	.349	.003	
Rep.#2	4	.269	.012	.254	.006	.241	.003	.127	.004	.9999
	24	.495	.012	.508	.006	.405	.003	.268	.004	
	96	.782	.013	.657	.006	.517	.003	.349	.004	
AAC-1	6	.296	.028	.356	.015	.221	.007	.139	.008	.9995
Rep.#1	24	.681	.031	.674	.016	.477	.007	.283	.008	
	96	1.39	.042	.899	.017	.661	.007	.388	.008	
Rep.#2	4	.420	.030	.339	.015	.305	.005	.108	.007	.9994
	24	.778	.034	.685	.016	.549	.007	.275	.007	
	96	1.39	.044	1.11	.017	.725	.007	.393	.007	
AAD-1	6	.218	.007	.180	.004	.134	.002	.094	.003	.9999
Rep.#1	24	.504	.008	.331	.004	.232	.002	.161	.003	
	96	.691	.008	.458	.005	.302	.003	.221	.003	
Rep.#2	4	.244	.008	.130	.005	.134	.003	.094	.003	.9999
	24	.673	.009	.325	.005	.252	.003	.161	.003	
	96	.982	.010	.556	.005	.328	.003	.221	.003	
AAF-1	6	.245	.021	.300	.010	.291	.004	.198	.004	.9998
Rep.#1	24	.688	.024	.505	.011	.556	.005	.369	.004	
	96	1.54	.036	.757	.011	.789	.005	.515	.004	
Rep.#2	4	.551	.025	.310	.012	.292	.004	.222	.005	.9996
	24	1.12	.040	.640	.013	.537	.005	.421	.005	
	96	2.19	.063	.933	.014	.715	.006	.532	.005	
AAG-1	6	.168	.005	.299	.014	.040	.005	.033	.004	.9998
Rep.#1	24	.346	.028	.553	.014	.101	.005	.070	.004	
	96	1.09	.048	.755	.015	.168	.005	.119	.004	
Rep.#2	4	.151	.011	.197	.039	.101	.012	.027	.010	.9985
	24	.699	.033	.491	.044	.171	.012	.041	.010	
	96	1.19	.102	.659	.047	.210	.012	.093	.010	

Continued

Table 3.1 Examples of Hardening Shift Factors Calculated Using Nonlinear Regression Procedure (continued)

Asphalt Type	Isothermal Age, hr	Isothermal Time Shift Factors, log(s) Temperature, °C								R-Squared
		-35		-25		-15		-5		
AAK-1	6	.280	.015	.211	.008	.242	.004	.045	.005	.9998
Rep.#1	24	.590	.017	.376	.009	.362	.004	.167	.005	
	96	.797	.018	.607	.009	.486	.004	.246	.005	
Rep.#2	4	.277	.017	.173	.009	.119	.004	.089	.005	.9997
	24	.569	.018	.419	.009	.347	.004	.176	.005	
	96	.899	.020	.587	.010	.413	.005	.250	.005	
AAM-1	6	.400	.017	.375	.011	.448	.005	.213	.005	.9997
Rep.#1	24	.920	.019	.707	.011	.767	.006	.447	.005	
	96	1.43	.021	1.06	.012	1.02	.006	.613	.005	
Rep.#2	4	.477	.023	.394	.014	.404	.005	.148	.007	.9995
	24	.837	.031	.824	.014	.679	.007	.461	.007	
	96	1.30	.028	1.29	.016	.915	.007	.612	.007	

Table 3.2 Hardening Model Parameters with Vertical Shift Factors

Asphalt Type	Model Constants		Vertical Shift Factors, log(s)					R^2,%
	Beta 1	Beta 2	-35	-25	-15	-10	-5	
AAA-1	0.67	3.44	1.08	0.42	0	-.17		97.9
AAB-1	2.28	6.27	1.62	0.69	0	-.30		95.9
AAC-1	2.46	4.88	2.38	1.03	0	-.42	-.75	98.1
AAD-1	0.99	3.84	1.37	0.51	0	-.21		96.3
AAG-1	0.55	2.35	1.51	0.62	0	-.19	-.25	90.5
AAF-1	2.74	5.10	2.56	1.04	0	-.40	-.74	97.7
AAK-1	1.74	5.59	1.47	0.62	0	-.26	-.47	98.5
AAM-1	5.02	7.85	2.69	1.23	0	-.54	-1.01	98.7

Table 3.3 Final Hardening Model Parameters with Statistical Data

Asphalt	T_g, °C	Model Parameters R	C	R^2	α_g	α_l
AAA-1	-28.2	6.210	1.474	99.85	3.49	5.89
	(.30)	(1.03)	(.015)		(.08)	(.11)
AAB-1	-13.9	9.594	1.694	99.65	3.50	6.40
	(.49)	(.82)	(.025)		(.05)	(.001)
AAC-1	-9.9	7.386	2.161	99.70	3.54	6.43
	(.48)	(.82)	(.022)		(.001)	(.031)
AAD-1	-24.3	8.239	1.313	99.66	3.54	6.10
	(.60)	(1.03)	(.032)		(.016)	(.12)
AAF-1	-6.1	8.103	1.836	99.71	3.37	6.53
	(.51)	(.854)	(.023)		(.08)	(.187)
AAG-1	-9.9	3.561	2.131	99.23	3.54	5.97
	(.44)	(.993)	(.020)		(.03)	(.12)
AAK-1	-16.5	11.008	1.419	99.86	3.31	6.10
	(.47)	(.855)	(.023)		(.105)	(.193)
AAM-1	-4.1	6.263	2.246	99.58	3.57	6.85
	(.62)	(.84)	(.024)		(.005)	(.217)

(....) = Standard error of parameter estimate
α_g = Coefficient of volumetric expansion below T_g, $*10^{-4}$ per °C
α_l = Coefficient of volumetric expansion above T_g, $*10^{-4}$ per °C
R and C = Hyperbolic model parameters, see text
R^2 = R squared of the model fit

Table 3.4   Constants for Best Fit Second Order Polynomials for Isothermal Volume Measurements at −15°C

Asphalt	C-0	C-1	C-2	DF	R^2	Y(std)
AAA-1	1.334	-1.03	.1012	41	.9771	.0488
AAB-1	2.671	-2.17	.2626	65	.9551	.1041
AAC-1	3.242	-2.60	.2956	57	.9647	.1193
AAD-1	1.706	-1.42	.1978	39	.9706	.0418
AAF-1	1.880	-1.34	.0677	54	.9751	.0716
AAG-1	1.213	-1.02	.1338	43	.9956	.0149
AAK-1	1.164	-0.755	.0046	60	.9802	.0522
AAM-1	2.908	-2.29	.2235	54	.9940	.0556

$\Delta V_{sp} = C_0 + C_1 \log(t_i) + C_2 [\log(t_i)]^2$
t_i = Isothermal time elapsed minus 30 minutes
Y(std) = Standard error of predicted value

Table 3.5   Volume-Temperature Fitted Model Parameters for the Eight Study Asphalts

Asphalt Type	Model Constants Beta 1	Beta 2	Adjusted R^2, %	Degrees of Freedom	Residuals, log(s) Average	STD
AAA-1	0.941	4.82	97.1	44	-.0139	.0422
AAB-1	1.976	5.625	95.6	43	.0009	.0837
AAC-1	2.667	5.397	97.9	57	-.0131	.0787
AAD-1	1.237	4.929	95.1	44	-.0212	.0709
AAF-1	2.966	5.551	97.4	57	.0115	.0915
AAG-1	1.161	4.623	82.4	48	-.0165	.1201
AAK-1	1.651	5.368	98.4	55	.0129	.0385
AAM-1	3.924	6.048	98.1	55	.0184	.0846

196

Table 3.6 Effect of Physical Hardening on Failure Properties of Unaged (Tank) Asphalts AAA-1 and AAM-1

Tank Asphalt	Physical Age, h	Temperature, °C	Failure Stress, MPa	Failure Strain, percent	Failure Energy, MN-m/m³
AAA-1	1	-15	0.69 (5)	14.9 (23)	0.095 (25)
AAA-1	24	-15	0.87 (17)	12.9 (57)	0.104 (60)
AAM-1	1	-15	3.16 (19)	2.0 (39)	0.045 (60)
AAM-1	24	-15	4.46 (8)	1.7 (15)	0.046 (22)

Note: The numbers in parentheses represent the coefficient of variation in percentage points.

Table 3.7 Properties Measured in This Study and Previous Studies of Selected SHRP Asphalts

Asphalt Source	Creep Compliance at −15°C, 120s 1/GPa	Isothermal Shift, log (a$_u$)	Wax Content % after	Melting Point, °C after	Total Enthalpy j/g after	Temp. of 2nd Endothermic Peak, °C after
AAA-1	43.48	0.42	1.62	35.8	0.27	83.5
AAB-1	14.29	0.67	3.85	62.1	9.94	41.9
AAC-1	7.67	0.93	5.06	65.7	4.00	53.9
AAD-1	35.71	0.57	1.94	50.6	3.48	46.1
AAE	20.80	0.32	1.23	42.5		
AAF-1	4.98	0.83	4.19	59.6	7.93	44.8
AAG-1	2.05	0.24	1.13	33.0	2.42	82.9
AAH	13.5	0.65	4.41	52.8		
AAJ	7.69	0.76	4.91	43.2		
AAK-1	13.89	0.52	1.17	56.1	1.83	47.2
AAL	40.32	0.21	1.23	43.9		
AAM-1	5.71	0.94	4.21	32.9	7.69	42.7
AAP	13.69	0.70	4.77	51.3		
AAU	3.52	0.60	2.35	58.6		
ABC	21.20	0.50	2.90	56.6		
ABD	1.58	0.45	0.81	38.2		

References

Anderson, D.A., Christensen, D.W., and Bahia, H. 1992. "Physical Properties of Asphalt Cement and the Development of Performance-Related Specification," Preprint of the 204th American Chemical Society National Meeting, Division of Fuel Chemistry, vol. 37, nos. 3 and 4.

Anderson, D.A., and Goetz, W.H. 1973. "Mechanical Behavior and Reinforcement of Mineral Filler-Asphalt Mixtures," *Proceedings of the Association of Asphalt Paving Technologists*, vol. 43, pp. 37–66.

Barrall, E.M., Schmidt, R.J., and Johnson, J.F. 1966. "Asphalt Transitions at Low Temperatures: Measurement Using Thermal Expansion Apparatus," Preprints, Division of Petroleum Chemistry, *American Chemical Society*.

Barth, E.J. 1962. *Asphalt Science and Technology*. New York: Gorden and Breach.

Brown, A.B., and Sparks, F.M. 1958. "Viscoelastic Properties of a Penetration Grade Paving Asphalt at Winter Temperatures," *Proceedings of the Association of Asphalt Paving Technologists*, vol. 27, pp. 35–51.

Brown, A.B., Sparks, J.W., and Smith, F.M. 1955. "Steric Hardening of Asphalts," *Proceedings of the Association of Asphalt Paving Technologists*, vol. 24, pp. 486–494.

Brule, B., Planche, J.P., King, G., Claudy, P., and Letoffe, J.M. 1990. "Relationship between Characterization of Asphalt Cements by Differential Scanning Calorimetry and Their Physical Properties," *American Chemical Society*, Division of Fuel Chemistry, vol. 35, no. 3, p. 330.

Claudy, P., Planche, J.P., King, G., and Letoffe, J.M. 1992. "Characterization of Asphalt Cements by Thermomicroscopy and Differential Scanning Calorimetry: Correlation to Classic Physical Properties," Preprint of the 204th American Chemical Society National Meeting, Division of Fuel Chemistry, vol. 37, no. 3 and 4.

Cohen, M.H., and Turnbull, D. 1959. "Molecular Transport in Liquids and Glasses," *Journal of Chemical Physics*, vol. 31, p. 1164.

Doolittle, A.K. 1951a. "Studies in Newtonian Flow. I The Dependence of Viscosity of Liquids on Temperature," *Journal of Applied Physics*, vol. 22, no. 12, p. 1031.

Doolittle, A.K. 1951b. "Studies in Newtonian Flow. II The Dependence of Viscosity of Liquids on Free-Space," *Journal of Applied Physics*, vol. 22, no. 12, p. 1471.

Doolittle, A.K., and Doolittle, D.B. 1957. "Studies in Newtonian Flow. V Further Verification of the Free Space Viscosity Equation," *Journal of Applied Physics*, vol. 28, no. 8, p. 901-905.

Ferry, J.D. 1980. *Viscoelastic Properties of Polymers*, 3d ed. New York: Wiley.

Harrison, I., Wang, G., and Hsu, T.C. 1992. *A Differential Scanning Calorimetry Study of Asphalt Binders*. Report no. SHRP-A/UFR-92-612. Washington, D.C.: Strategic Highway Research Program, National Research Council.

Jones, G.M., Darter, M.I., and Littlefield, G. 1968. "Thermal Expansion-Contraction of Asphaltic Concrete," *Proceedings of the Association of Asphalt Paving Technologists*, vol. 37, p. 56.

Jongepier, R., and Kuilman, B. 1969. "Characterization of the Rheology of Bitumens," *Proceedings of the Association of Asphalt Paving Technologists*, vol. 38, p. 98.

Jongepier, R., and Kuilman, B. 1970. "The Dynamic Shear Modulus of Bitumens as a Function of Frequency and Temperature," *Rheological Acta*, Band 7, Heft 1, p. 102.

Kauzmann, W. 1948. "Nature of the Glassy State and the Behavior of Liquids at Low Temperature," *Chemical Reviews*, vol. 43, p. 219.

Kovacs, A.J. 1958. "The Isothermal Volume Contraction of Amorphous Polymers," *Journal of Polymer Science*, vol. 30, p. 131-147.

Kovacs, A.J., Aklonis, J.J., Hutchinson, J.M., and Ramos, A.R. 1979. "Isobaric Volume and Enthalpy Recovery of Glasses. II. A Transparent Multiparameter Theory," *Journal of Polymer Science*, Polymer Physics Edition, vol. 17, p. 1097.

Kovacs, A.J., Straton, R.A., and Ferry, J.D. 1963. "Dynamic Mechanical Properties of Polyvinyl Acetate in Shear in the Glass Transition Temperature Range," *Journal of Physical Chemistry*, vol. 67, p. 152.

Krom, C.J. 1968. "Determination of the Wax Content of Bitumens," *Journal of the Institute of Petroleum*, vol. 54, no. 239.

McKenna, G.B. 1988. "Glass Formation and Glassy Behavior," in *Comprehensive Polymer Science, vol. 2, Polymer Properties*, edited by C. Booth, and C. Price. Oxford: Pergamon, p. 311.

Noel, F., and Corbett, L.W. 1970. "A Study of Crystalline Phases in Asphalts," *Journal of the Institute of Petroleum*, vol. 56, no. 261, pp. 261-268.

Petersen, J.C. 1984. "Chemical Composition of Asphalts as Related to Asphalt Durability: State of the Art," *Transportation Research Record No. 999*. Washington, D.C.: National Research Council, p. 13.

Schmidt, R.J., and Santucci, L.E. 1966. "A Practical Method for Determining the Glass Transition Temperature of Asphalts and Calculation of Their Low Temperature Viscosities," *Proceedings of the Association of Asphalt Paving Technologists*, vol. 35, p. 61.

Schmidt, R.J., Boynton, R.F., and Santucci, L.E. 1965. "Dilatometric Determination of the Glass Transition Temperature of Asphalts and Amorphous Polymers," *American Chemical Society*, Petroleum Division preprint, vol. 10, no. 3, p. 17.

Schweyer, H.E. 1974. "Glass Transition of Asphalts under Pressure," *Journal of Testing and Evaluation*, vol. 2, no. 1, p. 50.

Struik, L.C.E. 1986. Chapter 11 in *Failure of Plastic*, ed. by Brostwow and R.D. Corneliussen. New York: Hanser, p. 209.

Traxler, R.N., and Coombs, C.E. 1937. "Development of Internal Structure in Asphalts with Time," *American Society for Testing and Materials*, vol. 37, part II, pp. 549–555.

Traxler, R.N., and Schweyer, H.E. 1936. "Increase in Viscosity of Asphalts with Time," *Proceedings of the American Society for Testing and Materials*, vol. 36, part II, pp. 544–551.

Wada, Y., and Hirose, H. 1960. "Glass Transition Phenomena and Rheological Properties of Petroleum Asphalt," *Journal of the Physical Society of Japan*, vol. 15, no. 10, p. 1885.

Williams, M.L., Landel, R.F., and Ferry, J.D. 1955. "The Temperature Dependence of Relaxation Mechanisms in Amorphous Polymers and Other Glass-Forming Liquids," *Journal of the American Chemical Society*, vol. 77, p. 3701.

4

Fracture and Fatigue

Introduction

Many flexible-pavement designers and researchers have expressed concern over the premature cracking of pavements under various loading conditions. One frequently observed type of distress appears in the form of transverse cracking: nearly straight transverse cracks across the pavement, perpendicular to the direction of traffic. Transverse cracks are caused by stresses produced by temperature excursions (thermal stresses). One of the causes for temperature-induced transverse cracking in asphalt pavements is believed to be a single low-temperature excursion causing the tensile strength of the asphalt concrete to be exceeded by thermally induced shrinkage stresses—a mechanism called "low-temperature cracking or fracture." Temperature-induced transverse cracking can also result from thermal cycling that eventually initiates and propagates transverse cracks. This type of thermal shrinkage cracking has been referred to as thermal fatigue cracking.

The failure mechanism for both fracture and fatigue can be postulated in two ways. One mechanism is a single excursion of stress, with the pavement flaw size remaining constant, that rises to a critical value and results in failure. The other mechanism is the propagation of a starter or initial flaw into a critical flaw size, which, stress remaining constant, results in failure. The critical stress beyond which a flawed material fails is related to its fracture toughness. Fracture toughness is a material property generally used to characterize linear elastic materials. There is yet another method of characterizing materials, which applies to all materials regardless of their linearity or elasticity. In this method, the critical strain energy release rate, J_{Ic}, beyond which the flawed material fails represents its fracture resistance. To effectively design against fracture and fatigue failure, an accurate and reliable determination of fracture toughness or fracture resistance is required. Once these fracture resistance parameters are determined, they can be used in a mechanistic distress model to predict pavement performance as demonstrated by Lytton et al. (1983) in the THERM model. Ideally, it is necessary to determine the fracture mechanics parameters for neat asphalt cement as well for as hot-mix asphalt concrete.

203

Fracture Mechanics Concepts

Griffith (1920) postulated that the relatively low strengths of linear elastic brittle solids (glass, in his case), compared their expected theoretical strength based on atomic considerations, resulted from flaws or cracks inherent to the material. Griffith's theory states that the most critical crack (flaw with the largest stress concentration at its tip) will grow only when elastic energy released during crack growth exceeds the energy needed to create the new surface area. For example, using Griffith's approach, the fracture stress, σ_f, in a large plate containing an elliptical flaw or crack of length 2a subjected to uniaxial tension is given by

$$\sigma_f = \sqrt{\frac{2E\gamma_s}{\pi a}} \tag{4.1}$$

where

$$\begin{aligned}
\sigma_f &= \quad \text{fracture stress} \\
E &= \quad \text{Young's Modulus} \\
\gamma_s &= \quad \text{surface energy per unit area} \\
a &= \quad \text{crack length}
\end{aligned}$$

Irwin (1957) and Williams (1957) examined the stress distribution around the tip of a crack (the near-field stresses) in a linear elastic solid (glass, for example) and defined what they called the "stress intensity factor," relating the near-field stresses to the far-field stresses (stresses caused by applied loads). The stress intensity factor, denoted by K, defines the near-field stresses for any of the three possible deformation modes at a crack tip shown in figure 4.1.[1] The stress intensity factor for mode I (extension) loading is defined by the following equation:

$$\sigma_{ij} = \left[\frac{K_I}{\sqrt{2\pi r}}\right] f_{ij}(\theta) \tag{4.2}$$

where

---

[1] All figures and tables referenced in this chapter appear at the end of the chapter.

204

σ_{ij} = far-field stress (applied load)

K_I = stress intensity factor (I = 1, 2, 3 for mode = 1, 2, 3)

r, θ = polar coordinates for the near-field stress

$f_{ij}(\theta)$ = geometry-dependent function

Similar equations are possible for the mode II (shear) loading and mode III (antiplane shear or tearing) loading. K_I gives the severity of the stress singularity and is dependent on both the load (far-field stress) and crack geometry. The value of K_I at which the fracture occurs, K_{Ic}, is a material property. K_{Ic}, which measures fracture resistance in mode I loading, is called mode I fracture toughness.

When materials exhibit nonlinear elastic behavior, the K_I approach may not be used. Rice (1968) developed the J integral to analyze nonlinear problems. The J integral is defined as follows:

$$J = \int_{\Gamma} [Zdy - T(\frac{\delta u}{\delta x})ds] \tag{4.3}$$

where

J = J integral (critical strain energy release rate)

Z = strain energy density

T = stress vector

u = displacement vector

ds = element of arc length

Γ = any closed contour followed counterclockwise around the crack tip

J becomes equal to K_I^2/E if the material is linear elastic. J can hence be thought of as a general strain energy release rate parameter for analyzing crack propagation. When the J integral at fracture is determined for mode I loading it is called J_{Ic}. J_{Ic}, like K_{Ic}, is a measure of the resistance of a material to fracture and can be thought of as a fracture toughness parameter. Many metals have been successfully characterized using this approach. A standard test method is given for this procedure in ASTM E813. More information on fracture mechanics of linear and nonlinear elastic materials can be found in Hertzberg (1989).

Since neat asphalt cement or binder as well as hot-mix asphalt exhibits viscoelastic behavior, the concepts developed above have to be modified. In the case of elastic materials, a very small area surrounding the crack tip behaves inelastically. This response is usually negligible relative to the overall load deformation response of the elastic body and is, therefore, ignored. In the case of viscoelastic materials, however, the energy dissipation caused by time dependence is not restricted to the crack tip and influences the load deformation

behavior of the entire system. We cannot assume that all deformations result from elastic responses. However, it should be noted that while neat asphalt cement and hot-mix asphalt can be considered linear (for "short-term" loading), when tested in its glassy or brittle state, only negligible time dependence exists. When time dependence is significant, i.e., when asphalt binder and hot-mix asphalt are tested in their brittle-ductile transition region, the fracture process must be separated to consider (1) the crack initiation phase, in which the crack becomes critical as time passes while remaining stationary (no growth) and (2) the viscoelastic, or slow crack growth, phase, in which the crack grows slowly, thus leading to failure. The *J*-integral approach described above can then be modified and used as follows:

$$J = -\frac{1}{B}\frac{d}{da}\Big|\int_0^u P\,du\Big|_{u=constant} \tag{4.4}$$

where

$J =$ J integral
$B =$ thickness,
$a =$ crack length
$P =$ load
$u =$ deformation

Schapery (1983) advanced the application of the *J* integral to viscoelastic materials and gave a comprehensive treatment of this subject in his paper. Little and Mahboub (1985) studied the fracture mechanics properties of first-generation plasticized sulfur binders and recommend using J_{1c} as a fracture mechanics characterization parameter for sulphur binders. Abdulshafi and Majidzadeh (1985) successfully applied J_{1c} criteria to hot-mix asphalt Marshall specimens. Dongre et al. (1989) studied the effect of asphalt source on mixture behavior, using the J_{1c} parameter. Although these studies on hot-mix asphalts were successful, the tests required to develop the fracture parameters are difficult to perform and are therefore not recommended as routine design or specification tests. To date no literature is available on fracture mechanics studies conducted on neat asphalt cement or binders. However, the complexity of fracture mechanics testing and characterization dictates the use of surrogate methods of characterization for specification purposes.

Fatigue Concepts

Engineering materials have been observed to fail as a result of the repeated application of stresses that are of considerably less than their single cycle or static load fracture stress. The repeated stresses that are insufficient in magnitude to produce failure in one cycle nonetheless induce damage in the material with every cycle. This damage accumulates and ultimately leads to failure. Such failure in a material is known as fatigue failure. Traditionally, engineers have designed against fatigue by using S-N diagrams in which the magnitude of the

alternating stresses is plotted versus the logarithm of the number (N) of cycles to failure, as shown in figure 4.2. An engineering structure may be designed to resist fatigue by limiting the magnitude of the stress applied to the structure to values less than those described by the S-N curve. In case of some materials, the S-N diagram identifies a stress amplitude threshold below which fatigue failure would not occur even after an infinite number of load applications. Thus, using this information, design stresses can be limited to a value below the failure threshold.

Although a simple concept, the S-N diagram approach has two drawbacks: (1) large numbers of time-consuming tests are required to prepare the S-N diagrams, and (2) the concept does not address the mechanics of the fatigue process. Recognizing this need, Paris (1962) used concepts of fracture mechanics to demonstrate that the rate of change of crack length with the number of applied stress cycles was proportional to the difference in stress intensity factors, ΔK_I, computed at applied stress levels. Paris and Erdogan (1963) later proposed the following equation:

$$\frac{da}{dN} = A(\Delta K_I)^m \tag{4.5}$$

where

da/dN = rate of change of crack growth with number of applied cycles
A, m = material constants
ΔK_I = change in stress intensity factor

Equation 4.5 suggests that the fatigue process is controlled through ΔK_I by the near-field stresses at the crack tip. As was the case in fracture, the area around the crack tip should be small enough so that it has a negligible effect on the total elastic deformations. However, because of the viscoelastic nature of asphalt binders, the approach described above must be modified. All viscoelastic materials undergo some form of time-dependent flow or, as in the case of some polymers, even yield at some stress levels. These deformations are irreversible and therefore dissipate energy. Among the various approaches used by researchers to analyze fatigue in viscoelastic materials, the energy dissipation model appears to be the most promising. A summary of theoretical considerations necessary to apply these fatigue concepts to asphalt binder follows.

Fatigue Life Relation

The fatigue properties of asphalt cement and asphalt concrete can be calculated from log-log plots of cycles to failure against the inverse of the maximum fiber strain and by obtaining the slope K_2 and the intercept K_1 of the resulting straight line, which indicates that the fatigue behavior of asphalts can be represented by the following empirical power law relationship:

$$N_f = K_1 \left(\frac{1}{\epsilon}\right)^{K_2}$$ (4.6)

where

ϵ = strain amplitude
N_f = number of cycles to failure
K_1 and K_2 = fatigue parameters

In equation 4.6, K_1 represents the number of cycles to failure corresponding to unit strain, which is found to be a function of loading rate and temperature. The parameter K_2 represents the rate of change of fatigue life with strain amplitude.

The analysis of asphalt concrete fatigue data has also indicated that fatigue can be represented by the following relationship that reflects the effects of both temperature and strain amplitude:

$$N_f = K \left(\frac{1}{T}\right)^{n_o} \exp\left(-\frac{m}{T}\right)\left(\frac{1}{\epsilon}\right)^{K_2}$$ (4.7)

where

K, n_o, m, and K_2 = constants
T = temperature
ϵ = strain amplitude

Comparing equation 4.7 with equation 4.6,

$$K_1 = K \left(\frac{1}{T}\right)^{n_o} \exp\left(-\frac{m}{T}\right)$$ (4.8)

Equation 4.8 indicates that K_1 is a function of temperature and is influenced by the rheological properties of asphalts, whereas K_2 is independent of temperature.

Energy Dissipation Model

Under the repeated loading that is used in fatigue testing, energy is designated with each loading cycle. In materials such as asphalt cement and asphalt concrete, the energy dissipation results from viscoelastic and plastic flow mechanisms. In the energy dissipation criterion for fatigue developed here, it is hypothesized that failure under cyclic loading occurs when the energy absorbed in each cycle in excess of a certain nondamaging amount accumulates to a critical value. The total dissipated energy obtained by summing the areas of hysteresis loops under cyclic loading is assumed to be a measure of fatigue damage. In order to develop the energy dissipation model for fatigue, it is necessary to determine the energy dissipated per cycle, which can be mathematically represented by the following equation:

$$\Delta W = \sigma_t d \, \epsilon_t \tag{4.9}$$

where

$$\Delta W = \text{energy dissipated per cycle}$$
$$\sigma_t = \text{true stress}$$
$$\epsilon_t = \text{natural strain}$$

Equation 4.9 can be rewritten as

$$\Delta W = 4\sigma_{ta}\epsilon_{ta} - 2\int_0^{2\sigma_a} \epsilon_t d\sigma_t \tag{4.10}$$

where

σ_{ta} and ϵ_{ta} = true stress and strain amplitude, respectively

Equation 4.10 can be integrated by obtaining the cyclic stress-strain curve from fatigue tests and curve-fitting it to a power law relationship as given by

$$\sigma_t = \frac{2\sigma_{ta}}{(2\epsilon_{ta})} n^1 \, \epsilon_t^{n^1} \tag{4.11}$$

where

n^1 = the cyclic hardening coefficient

Substituting equation 4.11 into equation 4.10 and integrating,

$$\Delta W = 4 \left(\frac{1-n^1}{1+n^1} \right) \sigma_{ta} \epsilon_{ta} \qquad (4.12)$$

noting that

$$\sigma_{ta} = \sigma_{tf}(N_f)^m \qquad (4.13)$$

$$\epsilon_{ta} = \epsilon_{tf}(N_f)^q \qquad (4.14)$$

where

σ_{tf} and ϵ_{tf} = true failure stress and failure strain under monotonic loading
m and q = constants

Equation 4.12 reduces to

$$\Delta W = 4\sigma_{tf}\epsilon_{tf} \left(\frac{1-n^1}{1+n^1} \right) (N_f)^{(m+q)} \qquad (4.15)$$

Assuming the energy dissipated per cycle remains constant, the total plastic energy at failure can be shown to be

210

$$W_f = 4\sigma_{tf}\epsilon_{tf}\left(\frac{1-n^1}{1+n^1}\right)(N_f)^s \qquad (4.16)$$

where

$$s = (m + q + 1)$$

Equation 4.16 indicates that the total dissipated energy to failure is a power law function of the number of cycles to failure.

Need for Fracture and Fatigue Characterization

A summary of literature to date on low-temperature cracking is given by Vinson et al. (1990). They report that of the properties available, asphalt binder stiffness was cited as the single most important factor governing the incidence of low-temperature cracking and that, based on a number of field studies, the frequency of low-temperature thermal cracking is well correlated with the stiffness of the binder. None of the literature reviewed reported fracture properties for the binder. Consequently, relationships between fracture properties of the binder and low-temperature cracking are not available. One of the reasons for the lack of correlations between the fracture properties of binders and field performance is simply that no standard method is available to characterize the fracture properties of asphalt binders.

Considerable research has been conducted to date on the fatigue properties of hot-mix asphalt. In their literature review Finn et al. (1990) reported that to date only viscosity, penetration, and ductility have been used to predict fatigue cracking in pavements. Little information on the fatigue properties of binders has been published. Consequently, as with fracture properties, relationships between binder fatigue properties and pavement performance do not exist. Again, one of the reasons for the lack of such relationships is the lack of a convenient fatigue test for asphalt binders.

Given that no test methods exist for characterizing the fatigue or the fracture properties of asphalt binders, the following priorities were established for developing new test methods:

- An easy-to-use fracture (direct tension) test that can be used as a specification test

- An easy-to-use fatigue test that can be used as a specification test

- A test method for determining the fracture mechanics properties of asphalt binders

Project resources allowed the full development of the fracture (direct tension) test and the preliminary investigation of a fatigue test. Resources did not allow for the development of test methods for characterizing the properties of fracture mechanics.

Direct Tension—Test Development

Current performance prediction tests such as ductility, force ductility, and penetration reflect the viscoelastic behavior of asphalt but do not describe its brittle behavior (Anderson and Wiley, 1976). The Fraass test characterizes asphalt in its brittle state at temperatures as low as −30°C (−22°F) from which a brittle point temperature is obtained; however, it does not provide fundamental material properties (IP80/53, Fraass Method).

Rationale for Test Selection

For specification purposes, a standard test is needed that will characterize the failure behavior of asphalt binders in both the viscoelastic and the brittle state. Such a test must additionally provide fundamental material properties such as failure stress, failure strain, or failure energy in the brittle behavior region. A literature review revealed limited work pertaining to fracture testing of neat asphalt cements. Therefore, literature on fracture testing of similar nonmetallic materials was reviewed. The specimen geometries and testing methods used for these materials were evaluated by considering the feasibility of adapting them for fracture testing of neat asphalt cements. Based on the literature review, the direct tension mode of testing and the dogbone specimen geometry (ASTM D638) were selected. The following advantages were gained by selecting the dogbone specimen geometry:

- Specimen preparation is relatively easy, so a large number of specimens can be easily fabricated at one time.

- Stress distribution in the test specimen is uniaxial and uniform, so no detailed stress analysis or back-calculation procedure is needed to determine stresses.

- A standard experimental setup may be used to test the specimen.

- A large number of tests can be performed in a relatively short time.

- The effect of various parameters, such as strain rate, temperature, etc., on fracture properties can be evaluated.

Tensile failure properties of asphalts are highly dependent upon temperature and loading (elongation) rate. In order to determine the low-temperature thermal fracture resistance of asphalts, it is therefore necessary to select proper ranges of temperature and elongation rate during testing.

Original Test Procedure

The original dogbone specimen geometry was 127 mm (5.0 in.) long (overall length) by 6.35 mm (0.25 in.) thick. The gage portion was 38.1 mm (1.5 in.) long by 19.0 mm (0.75 in.) wide (see figure 4.3).

A traditional gripping system in which compressive clamping forces are used to grip the specimen is unsuitable for asphalt cement because the asphalt will flow under the compressive force at moderate temperatures. At low temperatures, where the asphalt is brittle, the clamping forces will break the specimen. Therefore, specially designed grips are needed to test asphalt cement. The gripping system used during the initial portion of this study is shown in figure 4.4. Plexiglas™ (polymethylmethacrylate) was used to manufacture these grips.

A screw-driven universal testing machine made by Instron (Model 4201) was used to load the specimens. This machine is capable of measuring loads as small as 0.048 N (0.01 lb) for the 500-N (100-lb) load cell used. Because temperature control is critical, a controlled temperature chamber was mounted on the testing machine to control the test temperature. Because the thermal history of asphalt cement affects its properties, the chamber was fitted with an access port so that the test specimens could be inserted in the chamber, held at the test temperature for a specified time, and mounted in the grips without opening the door of the test chamber. This chamber is capable of producing temperatures between −40°C (−40°F) to ambient temperature with a resolution of 1°C (1.8°F). Liquid nitrogen coolant with appropriate temperature-controlling equipment was used for the environment control. More recently, commercially developed adaptations of this equipment use mechanical refrigeration.

A computer-controlled data acquisition system was used to digitize signals from the load cell in the testing machine. The screw-driven testing machine provides a constant rate of platen movement. By recording the load cell readings as a function of time and noting the platen speed, it was possible to generate load-elongation data and to subsequently convert this data to a stress-strain plot.

Specimen Preparation and Testing

The specimen preparation and testing procedure involved three major steps: mold preparation, specimen preparation, and actual testing. The test specimens were cast in silicone rubber molds by pouring asphalt heated to 135°C (275°F) according to Strategic Highway Research Program (SHRP) protocol. They were then allowed to come to room temperature, cooled in a freezer only long enough to stiffen the specimens, and demolded from the silicone rubber by bending the rubber away from the test material. A fabric reinforcement was used in the end section of the test specimen to eliminate cracking at the ends and to force the failure into the necked-down portion of the dogbone. The demolded specimens were placed in the test chamber and tested after 60 ± 5 minutes. Careful control of the thermal history was maintained to avoid errors from physical hardening.

213

Experiment Design

After the equipment was constructed, an experiment design was developed with the intent of characterizing in detail the direct tension failure properties of the eight core asphalts in the unaged (tank) condition. The following controlled variables and levels were included in the experimental design:

- *Temperatures at five levels*— $-30°$, $-20°$, $-10°$, $-5°$, and $0°C$ ($-22°$, $-4°$, $14°$, $23°$, and $32°F$)

- *Deformation rates*—2.54, 7.62, 15.24, 25.4, and 50.8 mm/min (0.1, 0.3, 0.6, 1.0, and 2.0 in./min).

Details of the testing program are given in table 4.1.

Stress-Strain Curves

Nominal stress was computed by dividing the measured tensile force by the original cross-sectional area. Similarly, nominal strain was computed using elongation divided by the original gage length, 38.1 mm (1.5 in.). Figures 4.5 and 4.6 show the typical stress-strain curves at a fixed temperature of 0°C (32°F) at various elongation rates for a soft asphalt, (AAA-1) and a hard asphalt (AAG-1). Figures 4.7 and 4.8 show the same but for a fixed elongation rate of 2.54 mm/min (0.1 in./min) at various temperatures. These curves show that for softer asphalts, tensile stress and strain show a more pronounced deformation rate and temperature dependence than harder asphalts. These curves also show that tensile strength decreases with temperature for the hard asphalt (AAG-1). Similar observations were made by Rigden and Lee (1959) in their tensile strength tests on tars and pitches. This decrease in strength may be due to the brittle nature of failure for the harder asphalt or may be the result of thermally induced flaws. Similar trends would most likely be seen for the softer asphalt (AAA-1) if further data were obtained at temperatures lower than used in this study; i.e., below $-30°C$ ($-22°F$).

Statistical Analysis of Failure Data—Original Geometry

Failure measurements typically display large variation, even when test conditions such as deformation rates and temperatures are maintained as nearly constant as possible. It is important to make every effort to keep this variation as low as possible by maintaining a very careful experimental protocol with regard to the fabrication, thermal history, and handling of the test specimen. Nevertheless, important failure properties must be estimated in the presence of this variation.

As a first step in determining this variability, an exploratory experiment was carried out using core asphalts AAD-1 and AAG-1 at selected deformation rates and temperatures, given

214

in table 4.2. The resulting data from each combination were adequate for evaluating the variability in terms of the estimated standard deviation of the measurements and the coefficient of variation. These are given for asphalt AAD-1 in table 4.3 and AAG-1 in table 4.4 for failure stress, failure strain, and failure energy.

Because of the random distribution of inherent flaws in the asphalt test specimens, stress-to-failure is a random variable whose distribution is of interest and importance. An example of such data from some early testing is given in table 4.5 for asphalt AAD-1 in unaged (tank) condition tested at $-5°C$ ($23°F$) and elongation rate of 7.62 mm/min (0.3 in./min). The histogram of these data would suggest that a Weibull or lognormal distribution may be appropriate. Weibull (1952) has demonstrated that the strength of any material that can be modeled according to the weakest link theory can be appropriately represented by the Weibull distribution.

The Weibull (or lognormal) distribution requires estimation of location, scale and shape parameters. By employing the above data the location parameter for the Weibull was estimated to be A = 77.52 using a combination of maximum likelihood and method of moments procedure. The scale parameter, B, was estimated to be 74.5 and the shape parameter, C, was 3 (for other stress data the estimated values of C are often around 2). The form of the Weibull cumulative distribution considered is

$$F(x) = 1.0 - \exp(-((\frac{x-A}{B})^C)) \qquad x \geq A$$
$$F(x) = 0 \qquad \text{elsewhere}$$

(4.17)

where

A = location parameter
B = scale parameter
C = shape parameter

A reasonable procedure for choosing between the Weibull and lognormal models based only on the data available is to choose the model with the largest maximized likelihood. Dumonceaux and Antle (1973) have shown that in cases where the location parameter, A, is assumed to be known, this method for choosing between these models is a powerful test. For the value of $A = 77.52$, the ratio of maximized likelihood was found to be 3.2 in favor of the Weibull distribution and thus the Weibull should be chosen (over the lognormal) for these data.

The data from the exploratory experiment described before were also used in evaluating the two statistical models, and, in all cases, the Weibull model with a location parameter provided much better agreement with the observations than the lognormal model. A fitted Weibull cumulative distribution with the sample cumulative distribution is shown in figures 4.9 and 4.10 for a typical stress at failure data set for asphalts AAD-1 and AAG-1,

respectively. As a result of these experiments, we decided to use the Weibull model for the analyses of the failure data. We recommend that the 3-parameter Weibull be used as the appropriate distribution for the stress to failure of asphalt specimens tested in uniaxial (direct) tension.

Generation of Master Curves and Application of Shift Factors

Bueche (1955) has shown that, in the case of polymers, failure stress (tensile strength) can be expressed as a universal function of reduced time or strain rate (master curve), using the shift factors obtained from the rheological data for small deformations (linear viscoelasticity). Thor L. Smith (1958) later verified this finding to be true for GR-S rubber. He also showed that similar master curves can be created for failure strain. In other words, the temperature dependence of the failure properties of polymers and GR-S rubber can be expressed by the Williams, Landel, and Ferry equation, which describes the shift factor versus temperature relationship in the temperature range $T_g < T < (T_g+100)$. Christensen and Anderson (1992) have recently shown through the use of dynamic mechanical analysis data that the temperature dependence of asphalt can be similarly expressed. It appears from the failure data that shift factors determined from rheological data may be used to generate failure master curves. Figures 4.11 to 4.13 show the dependence of tensile strength, failure strain, and failure energy on physical time for asphalt AAD-1. The other asphalt binders all show similar trends. Figure 4.11 shows plots of log $\sigma(T_o/T)$ versus log t, where T_o is the standard reference temperature 263.15°K (-10°C (14°F)), T the measurement temperature in °K, and t the physical time in seconds. Figures 4.12 and 4.13 show the same for failure strain and failure energy. (Ordinate values are shifted arbitrarily for clarity.) The multiplication factor T_o/T is used to account for the temperature dependence of the elastic retractive forces on the asphalt molecules. According to the statistical theory of rubber elasticity, this factor should be included before failure properties at different temperatures are compared (Smith 1958).

The data in figures 4.11 to 4.13 suggest that failure stress, failure strain, and failure energy can be combined to produce master curves (composite curves). Direct-tension failure studies done on polymers and rubber indicate that the tensile strength and failure strain for a given material is a universal function of a reduced time or a reduced strain rate, except at very short times or high strain rates (Brostow and Corneliussen 1986). The same studies have shown that shift factors needed for superposing failure data measured at different temperatures are the same as those used to superpose viscoelastic data in small deformations (linear range). Figures 4.14 to 4.16 show failure stress (tensile strength), failure strain, and failure energy master curves, respectively, for asphalts AAA-1 and AAM-1. Figures 4.17 to 4.19 show the same for asphalts AAK-1 and AAG-1.

Characterization of Failure Master Curves

It was found that failure strain and failure energy are related to reduced time, at a reference temperature of -10°C (14°F) by equation 4.18:

$$F(\xi) = A + \beta 1 [(Z)^{(\beta_4 - 1)}][\exp(-(Z)^{\beta_4})] \qquad (4.18)$$

where

$F(\xi)$ = failure strain or failure energy
A = constant
β_1 = magnitude parameter
Z = $(\log(\xi) - \beta_2)/\beta_3$
β_2 = location parameter
    = $0.5392\beta_3$ for failure strain master curve
    = $0.5011\beta_3$ for failure energy master curve
β_3 = scale parameter
β_4 = shape parameter, fixed (constant) at 10
$\log(\xi)$ = common log of reduced time, $\xi = t/a(T)$
$a(T)$ = shift factor obtained from rheological measurements

Equation 4.18 is similar in form to the Weibull probability distribution.

The parameters β_1, β_2, β_3, and β_4 in equation 4.18 were determined as follows. Initially, all parameters were allowed to vary without any constraints. It was observed that β_4 was always around 10 for all cases. β_4 was fixed at 10 and other parameters were allowed to vary freely. When this combination was chosen a relationship between β_2 and β_3 was noticed. Then this relationship between β_2 and β_3 was fixed to the values shown above while keeping β_4 fixed at 10. It was also observed that after fixing the three parameters, the coefficient of determination, R^2, improved in all cases and the standard deviation on the remaining two parameters decreased.

Failure strain and failure energy plotted against reduced time are called failure strain and failure energy master curves. The reduced time is obtained by shifting physical time according to shift factors obtained from rheological measurements as explained earlier.

Equation 4.18 was found to be valid for the eight core asphalts and possibly valid for all asphalts. The regression coefficient, R^2, was estimated to be 0.98 in all but two cases, where it was 0.95. It was also determined that these parameters can be estimated with reasonable accuracy by selecting 6 points out of 25 and fitting the given expression. The regression coefficient, R^2, between the fitted data obtained from 6 points and the original 25 points was found to be more than 0.95 for all core asphalts.

Based on the above results, a reduced protocol was developed for use with the extended set of asphalts in the unaged (tank) condition. The reduced protocol is shown in table 4.6. Figure 4.20 shows master curves obtained using 6 points (reduced protocol, table 4.6) overlaid with the measured 27 points (full protocol, table 4.1) for asphalts AAD-1 and AAG-1.

Determination of Confidence Intervals for Master Curves

To determine the testing error associated with the direct tension test method, 0.95 confidence bands were determined for the master curves. The addition of the 0.95 confidence bands about their respective master curves provides the best possible means for evaluating the uncertainty in these curves. A computer program was developed to produce the confidence bands. This program provides an approximate variance-covariance matrix for the estimated parameters. This matrix is all that is needed to provide confidence bands for the expected values of the points on the master curve. In general, if the nonlinear model is of the form

$$Y = f(t, \beta_1, \dots, \beta_p) + e \tag{4.19}$$

where

Y = response variable, strain, energy, etc.
t = time, s
$\beta_1, \dots, \beta_p$ = regression coefficients

and the first order approximation of equation 4.19 is given by

$$
f(t, \beta_1, \dots, \beta_p) = f(t, \beta_1^o, \dots, \beta_p^o) +
$$
$$
[\frac{\delta f}{\delta \beta_1}(t, \beta_1^o, \dots, \beta_p^o)] (\beta_1 - \beta_1^o) + \dots,
$$
$$
+ [\frac{\delta f}{\delta \beta_p}(t, \beta_1^o, \dots, \beta_p^o)] \qquad (\beta_p - \beta_p^o) \tag{4.20}
$$

where

$\delta f / \delta \beta_1$ = partial derivative of the function f, with respect to β_1
$\delta f / \delta \beta_p$ = partial derivative of the function f, with respect to β_p

then the variance of $f(t, \beta 1, \dots \beta p)$ is approximated by

$$[\delta f/\delta \beta_1, \dots, \delta f/\delta \beta_p] \times [\text{estimated var-covar matrix}] \times [\delta f/\delta \beta_1, \dots, \delta f/\delta \beta_p]^T \tag{4.21}$$

where

T = transpose of matrix

218

and the partial derivatives have been evaluated at t, β_1, β_2, ...β_p.

These approximate estimates for the variance of the fitted values are exact when the function is linear in the betas and are generally quite good for nonlinear models. They provide the basis for the construction of confidence intervals for the failure strain and energy master curves. The failure strain and failure energy master curves, along with their 95 percent confidence limits, are shown in tables 4.7 and 4.8 and in figures 4.13 to 4.18.

Direct Tension—Specification Test

Rationale for Specification-Type Specimen Geometry

Based on the initial portion of the direct tension study a new specimen geometry and gripping system were developed for the specification test. From the rheological properties and failure properties (determined during the developmental phase of the study) it was determined that for specification purposes only failure strains in the range 0.5 to 10 percent were essential. As explained in detail in the data analysis part of the study, the proposed specification requires that an asphalt must be used at temperatures where the strains are larger than the brittle-ductile transition limit. This limit was found to be within 0.5 to 10 percent strain to failure, specifically at or near 1 percent for most asphalts. Therefore, only failure properties relevant to the development of specifications were measured using this new method. The failure properties were obtained at three temperatures and one elongation rate. The temperatures were selected to produce failure strains between 0.5 and 10 percent. A single elongation rate, 1.27 mm/min (0.05 in./min), was used for initial specification testing. Later this rate was modified to 1 mm/min (0.0394 in./min) to use hard SI units. This elongation rate was chosen based on three considerations. First and foremost was the fact that thermal stresses in the flexible pavement develop slowly. The second consideration the slowest elongation rate capability of the commercial testing machines. The third consideration was the time needed to produce a failure strain of 1 percent (brittle-ductile limit for most asphalts) at the chosen elongation rate.

For example, the lowest elongation rate available on the Instron Model 4201 universal testing machine is 0.508 mm/min (0.02 in./min), which produces a strain rate of 1.3 percent strain per minute for a 39.01-mm (1.536-in.)-long specimen. At this strain rate it would take approximately 50 seconds to produce a failure strain of 1 percent for a given asphalt. From rheological data, however, a loading time of between 20 to 30 seconds was found to be appropriate. Therefore, an elongation rate of 1 mm/min (0.0394 in./min) giving a 2.6 percent strain per minute was chosen.

The development of the new specification-type, direct-tension test resulted from the improvement and fine-tuning of the original specimen geometry and test method. The original specimen geometry was devised as an exploratory attempt to characterize fracture properties of asphalt cement since no other suitable method was available from the literature. Overall, the test procedure was reasonably successful, although the test specimen

geometry contained several shortcomings as described below. As a consequence, a revised specimen geometry was developed, which was adopted for specification use. The remaining testing was conducted with the specification geometry using a reduced testing protocol similar to that recommended for the specification.

The original direct tension specimen geometry and gripping method was not deemed suitable for specification-type testing because of the following:

- It required approximately 20 g of material per specimen, which made it impractical for use with aged residue, given that three to four replicate test specimens were needed for each test.

- The specimen preparation was too complicated for specification-type testing.

- The gripping arrangement introduced unacceptable errors in deformation measurements at strains less than 2 to 3 percent

- Repeatability was inadequate for specification-type testing

After a thorough evaluation of the various possible tension test geometries and a review of the literature, the preferred tension testing method continued to be the dogbone specimen geometry. The redesign of the test dictated a simpler gripping arrangement and a smaller specimen that consumed less test material.

The salient features of the new specification-type, direct-tension test method are listed below:

- Dogbone specimen geometry

- Requirement of only 3 g of asphalt per specimen

- Specially designed loading pin to ensure noneccentric loading

- Noncontact elongation measurement

- Unaged, aged, and modified binders and mastics able to be tested

- Results compare well with dynamic mechanical and bending beam measurements

Specification-Type Specimen Geometry

The new specimen geometry is shown in figure 4.21. Like the original, the new specimen geometry is dogbone-shaped except that it has plastic inserts at either ends that connect to specially designed pins, figure 4.22. The new specimen requires approximately 2 g of asphalt as opposed to the 20 g required by the original version. The new specimen is 100 mm (3.9 in.) in overall length including the end inserts. The end inserts are each 30-mm

220

(1.18 in.) long by 20-mm (0.79 – in.) wide. The asphalt portion of the specimen is 40 mm (1.57 in.) long with a gage length of 18 mm (0.71 in) and 6 mm-by-6 mm (0.24 in. by 0.24 in.) square cross-section. The gage portion widens at each end with a radius of 12 (twice its thickness) to provide a gradual transition with the end inserts.

In the initial trials, polypropylene was used to make the end inserts because it has a linear thermal coefficient of expansion, 6.8×10^{-4} mm/mm/°C (3.8×10^{-4} in./in./°F), relatively close to that of asphalt cement, 0.6×10^{-4} mm/mm/°C (0.33×10^{-4} in./in./°F). Matching the expansion coefficients of the asphalt binder and the inserts reduces thermal shrinkage stresses at the interface that otherwise could cause bond failures at the interface.

Polypropylene is difficult to machine and therefore plexiglass, with a linear thermal coefficient of expansion, 5.04×10^{-5} mm/mm/°C (2.8×10^{-5} in./in./°F), was selected for the end inserts. The end inserts have precision-machined holes through which they are mounted on specially designed pins that provide a freely rotating connection that is self-centering with the longitudinal axis of the specimen, figure 4.23. The design of the pins allows loads to be applied with minimal eccentricity, thereby reducing bending moments and concomitant testing variability. The equipment details, specification preparation, and testing protocol are explained in further detail in volume 4 of this report.

Details for conducting the test are similar to those for the original geometry except that the specimen elongation is measured with a plane of laser light as illustrated in figure 4.24. The laser provides a noncontact measurement with the high degree of resolution needed at strain levels approaching 1 percent or less. Silicone rubber molds are also used to prepare the test specimens for the specification-type geometry, figure 4.25, except that the plastic inserts are placed in the mold before the asphalt is poured.

Validation of Strain Values Determined with New Test Geometry

A series of specimens were prepared and tested to compare strain measurements based on platen movement with measurements based on laser-based extensometer measurements. The strains based on platen movement were calculated by multiplying the rate of platen movement (mm/min) by the time of testing (min) and then dividing by the gage length (mm) of the specimen. The laser-based strains were calculated by dividing the change in position of the spots of laser light, figure 4.26, by the specimen gage length. As shown in figure 4.27, where the two measurements are compared, there is good agreement between the two measurements for strains greater than approximately 2 percent, but at smaller strains the two measurements diverge significantly. The platen movement-based strains include grip and machine distortion as part of the strain calculation, leading to unacceptably inaccurate values. This experiment verified the hypothesis of the researchers that machine, load cell, and grip deformation were contributing to inaccurate measurements when the strains were small.

In order to validate the accuracy of the strains measured with the noncontact laser-based extensometer, an aluminum specimen (with the same geometry) having a modulus of elasticity, E, equal to 9.9×10^6 lb/in.^{2} was tested in direct tension. A series of tests were

conducted in which the aluminum specimen was displaced at a predetermined amount while the load and laser-measured elongation of the test specimen were recorded. The measured strains were then predicted from the known modulus of the aluminum and the stress on the specimen. It was found that the laser extensometer measured the strains accurately with a coefficient of variation of 1.18 percent between measurements (figure 4.27).

Comparison of Failure Master Curves—Original Versus Specification-Type Geometry

Two unaged asphalts, AAA-1 and AAG-1, were tested in direct tension using the new specimen geometry. The reduced testing protocol (see reduced experimental layout table 4.10) was followed for these tests. The test results were then compared with the results from earlier testing that was done using the original (larger) specimen geometry. Figures 4.28 to 4.30 show the failure stress, strain, and energy master curves superimposed with data points obtained from the new specimen for asphalt AAA-1 (tank condition). Figures 4.31 to 4.33 show the same data for asphalt AAG-1.

Figures 4.28 and 4.30 show that failure stresses are slightly higher for the new specification-type geometry. This result can be attributed to the fact that the new specification-type specimen has a cross-sectional area of 36.0 mm^2 (0.06 in.^{2}) compared to 121.0 mm^2 (0.19 in.^{2}) for the original specimen. It is well known from other materials data that a smaller cross-sectional area produces higher failure stresses (Brostow and Corneliussen 1986). The stress level should not otherwise be affected by the new specimen geometry, and the shape of the two master curves should be similar. This finding is verified in figures 4.28 and 4.33.

Figures 4.29 and 4.32 show the failure strain master curves. From these curves, it appears that the failure strains below approximately 2 percent are much larger for the original specimen geometry than for the new specification-type geometry, although the gage lengths are approximately the same. This result occurs because the failure strains for the new specimen were computed from deformations measured using the more representative laser-based extensometer, as opposed to computations based on the movement of the testing machine platen. Below approximately a 2 percent strain, the original specimen geometry and gripping arrangement produced errors because of slippage and flow in the grips. At low deformations these errors can sometimes be much larger than the actual deformations being measured, making it impossible to recover actual deformations.

Figures 4.30 and 4.33 show the failure energy master curves for the original and the specification-type geometries. These curves show that with the new geometry, the failure energy curves appear to shift to the left on the time scale, which would mean that the effect of reducing the specimen size is equivalent to a softening of the material. This effect is only an apparent one. The smaller specimen cross-section causes the brittle-ductile transition of the material to be shifted to shorter times (to the left). Such an apparent softening because of reduction in specimen size has been observed in other materials (Sih and Kiefer 1979).

Based on the results obtained with the aluminum test specimen and the comparison of the test results obtained with the two test geometries, it was concluded that the new geometry produced more reliable and accurate test results. Therefore, it was selected for all the remaining testing. Recognizing that it was impractical as part of specification testing to obtain sufficient data to fully describe the master curve, it was decided that only sufficient data would be obtained to determine the temperature where the strain to failure is 1 percent. Further, a single rate of elongation, 1.27 mm/min (0.05 in./min) was selected as the rate of elongation. The rate was chosen as the best compromise between the need to produce relatively linear stress-strain curves (not too slow) and also allow sufficient test time so that the stress-strain curve could be well defined (not too fast). The specification version of the test was converted to hard SI units so that the specified rate is 1 mm/min (0.04 in./min).

Experiment Designs—Specification Test

Experiments were designed, using the new test specimen geometry, to characterize the core, extended, and additional asphalt binders. The experiment for the core asphalts contains four replications of an 8 (core asphalts) by 3 (age condition) factorial experiment, Table 4.9. However, it should be noted that within each of these 96 primary cells three completely independent experiments were carried out in order to produce one value of the response variable of interest (the estimated failure strain, stress, or energy for that asphalt at its limiting stiffness condition). Thus, a total of 288 specimens were tested to failure in the experiment for characterizing the core asphalts. Experiments were also developed to characterize the extended and additional asphalts in the three aging conditions—unaged (tank), after thin film aging, and after thin film plus pressure aging.

Characterization of the extended and additional asphalts was done using the single rate of elongation. A sufficient number of test temperatures were used to define the temperature below which the strain to failure is 1 percent in accordance with the SHRP binder specification that was published at the time the experiment was designed. This protocol allows the determination of the brittle to brittle-ductile transition temperature. Time-temperature superposition can be used to predict this transition at different strain rates.

The transition from brittle to brittle-ductile failure occurs over a small temperature range. Because the temperature range cannot be predicted before the tension testing is conducted, some means of predicting the temperature range at which the failure strain is 1 to 10 percent was required. Because the failure strain of 1 percent corresponds to a modulus of 400 MPa (30,000 lb/in.²), a nomograph that relates modulus and the temperature at which the failure strain is 1.0 percent was constructed, figure 4.34.

The nomograph was constructed as follows: The strain rate of approximately 500 microstrain/s, corresponding to a rate of elongation of 1.27 mm/min (0.05 in./min), was selected as a fixed value. This value was chosen as a compromise to give the slowest strain rate that produces reasonably linear stress-strain curves and that produces failure within a reasonable test time. Faster strain rates made it difficult to acquire the data, especially when the strain to failure is less than 1 percent. Because the nomograph gives an approximation of

223

the failure strain, the initial direct-tension test was conducted at a temperature estimated from the stiffness of the asphalt as determined from the nomograph.

With the use of this nomograph, three temperatures that would produce failure strains between 0.5 and 10 percent were selected. Because of the approximate nature of the nomograph, the first test was conducted at an intermediate temperature. Then, based on the strain to failure results obtained at the first temperature, two other test temperatures chosen to produce strain to failure within the desired range of 0.5 percent to 10 percent. Thus, there may be no common temperatures over the 96 cells, but the desired (or estimated) response for a cell is independent of these temperatures. The accuracy of this estimated response, however, depends on the experimenter's ability to choose these levels for each asphalt. In the specification-testing mode this selection process will not be necessary. The direct-tension test will be conducted at the temperature specified for the given grade, and the measured value of strain to failure must simply be greater than 1 percent.

Failure properties obtained from the core experiment (average of four replicates) are given in tables 4.10 to 4.12. Failure stress is the stress at the point of instability (as manifested by a distinct peak in the stress-strain curve), and failure strain is the strain at that point. In the brittle region the failure is by fracture (i.e., physical separation), whereas in the ductile region failure is by flow (i.e., the specimen is unable to carry further load and elongates but does not break or fracture). Failure energy was computed by numerically integrating the stress-strain curve up to the point of instability. The secant modulus is obtained by taking the ratio of failure stress to failure strain. The tangent modulus (relaxation modulus) was estimated by computing the slope of the stress-strain curve where failure strain was arbitrarily chosen to be 0.25 percent. Also shown in table 4.12 are values of the coefficient of variation percentage. These values are enclosed in parentheses beside each average value.

Figures 4.35 and 4.36 show stress-versus-strain curves for a fixed deformation rate of 1.27 mm/min (0.05 in./min) at various temperatures for asphalts AAA-1 and AAG-1, respectively. These curves show trends similar to those shown by the curves from the original specimen geometry.

Statistical Analysis of Failure Data—Specification Geometry

Because of a lack of time and resources, detailed statistical modeling and experimentation were not undertaken. Instead, it was assumed, based on the findings of the developmental portion of the study (i.e., the original specimen geometry), that the Weibull distribution is applicable to the failure properties determined through the use of the new specimen geometry. However, for the failure properties obtained using the new method, the variability introduced due to such uncontrollable effects, such as the specimen flaw distribution, the basic precision of the testing equipment must be determined.

In order to determine this variability, data obtained from the 72 cells (8 asphalts by 3 aging conditions by 3 temperatures) of the experiment design matrix for core asphalts were used. In each of these cells, four specimens were tested to give a mean, standard deviation, and

coefficient of variation for the failure properties in each cell. The sampling variability in the standard deviations and thus the coefficients of variation would be appreciable, however, and some means of smoothing the data would be helpful. It was decided to rank the 72 cells by their averages and then place them into seven groups. Within each group, the within-asphalt variances were pooled and the cell averages (means) for each group were averaged. Thus, each group provided sufficient data for estimating the standard deviations for the failure response variables in the range of the means in that group.

It is clear from figures 4.37 to 4.39 that the coefficients of variation for these groups presented no trend for failure stress and failure energy, which, of course, is the desired effect when using the coefficient of variation to summarize the precision obtained in a testing process. Failure strain, however, shows a downward trend in the higher strains (above 5 percent strain). This phenomenon could be an artifact of the measurement process by which, as the measurements become larger, the repeatability improves. For specification purposes, the region of interest is between 0.5 and 10 percent, and within that region the trend is not as well defined. Thus, the best overall assessment of the precision of the new specimen geometry and test method is given by the average of these coefficients of variation, which are shown in table 4.13 for failure stress, strain, and energy. While they may appear large compared with other measured properties (e.g., modulus), and efforts should continue to reduce them, it must be emphasized that they are obtained from fracture, which is an inherently noisy process.

Fatigue

Rationale for Test Selection

Since asphalts under service conditions experience cyclic variation of temperature and loading, there is a need to obtain fatigue properties of these materials. A knowledge of fatigue properties is also important for specification purposes. However, because the number of tests must be limited for specification purposes, and because fatigue tests are very time-consuming, it is necessary to select surrogate test properties, such as tensile properties, for fatigue properties. Therefore, fatigue tests were conducted to determine if a correlation exists between fatigue and tensile fracture properties.

Experimental Design

The fatigue properties of asphalts were evaluated by using a specially fabricated apparatus, a schematic of which is given in figure 4.40. A composite beam specimen—an aluminum strip with a thin film of asphalt bonded to the undersurface (see figure 4.41)—is subjected to a four-point pulse loading. The deflection of the beam is controlled by the resistance of the aluminum beam; thus, the strain in the asphalt is relatively constant throughout the test. Therefore, the test procedure may be considered a controlled strain test. The test is conducted in an environmental chamber that can be controlled to ±0.1°C (±0.2°F). The pulse loading is imposed on the sample pneumatically by a Bellofram air cylinder (see figure

4.42). The compressed air supply line (see figure 4.40) is connected to the inlet port of the accumulator. The compressed air in the accumulator is fed into the Bellofram air cylinder through a pressure regulator and the solenoid valve. The duration of the load pulse is controlled by a pulser. The magnitude of the load pulse is measured by a load cell that is connected to the stem of the Bellofram cylinder. A counter indicates the accumulated cycles of loading on the specimen. The entire assembly is enclosed in a thermal chamber, the temperature of which can be maintained within a temperature range of −40° to 60°C (−40° to 140°F) using a digital temperature controller. The vertical midpoint deflection of the beam specimen is measured by a Linear Variable Differential Transformer (LVDT).

Fatigue tests on eight core asphalts were conducted by subjecting composite aluminum/ asphalt beams to a pulse loading of 0.1-second loading and 0.9-second unloading times. The tests were terminated when a hairline crack appeared on the surface of each of the specimens tested, and the cycles of loading corresponding to this point were noted. The fatigue properties were measured at four amplitudes of strain and at temperatures −30°, −20°, −10°, and 0°C (−22°, −4°, 14°, and 32°F). The tests were replicated three times. In addition, fatigue tests on three aged core asphalts—AAK-1, AAD-1, and AAG-1—were conducted at −30°C (−22°F).

Experimental Results

Fatigue Coefficients

Figures 4.43 and 4.44 show the plots of the number of cycles to failure versus the inverse of maximum strain for the eight core asphalts at −30°, −20°, −10°, and 0°C (−22°, −4°, 14°, and 32°F). Figures 4.45 to 4.47 show cycles to failure versus the inverse of maximum fiber strain curves for aged core asphalts AAD-1, AAG-1, and AAK-1 at −30°C (−22°F). In the same figures similar plots are shown for neat core asphalts AAD-1, AAG-1, and AAK-1 for comparison. In table 4.14 are the fatigue coefficients K_1 and K_2 representing the slope and intercept, respectively, of the lines in figures 4.43 and 4.44.

Energy Dissipation Criterion

Figure 4.48 shows the ratio of energy dissipated per cycle to the total input energy per cycle against the number of cycles for core asphalt AAA-1 obtained from fatigue tests at −30°C (−22°F) and four strain amplitudes. It is interesting to note that the ratio remains fairly constant for most of the fatigue life of the material and inverts rapidly just before failure. Using equation 4.16, the total energy dissipated was calculated for asphalts AAA-1 and AAB-1. The results are shown in figure 4.49. The plot was found to be linear. The fatigue testing conducted on the asphalt cements reported in this study reinforces the selection of dissipated energy as a fatigue interior.

Summary of Fatigue and Fracture Results

Direct Tension–Rheology Relationship

Tangent modulus values were compared with approximate relaxation moduli computed from rheological measurements as follows (see figure 4.50). An empirical model developed by the A-002A team was used to obtain shear storage and loss moduli at a given time (or frequency) and temperature for the eight core asphalts (Christensen and Anderson 1992). This model was developed using an extensive number of dynamic mechanical measurements made during the project. Using this model and the approximate conversion formulas given by Ninomiya and Ferry, the relaxation moduli were obtained at 4.6 seconds for all eight core asphalts (see Ferry 1980). The value of 4.6 seconds was used because it corresponds to the 0.25 percent strain level at which tangent moduli from the direct tension stress-strain curves were obtained.

From figure 4.50 it appears that the agreement between the two moduli determinations is reasonably good for moduli values above 400 MPa. At moduli values between 100 to 400 MPa there seems to be a deviation from the close agreement. This deviation may be caused due to the assumption of incompressibility. Another possible explanation is that at these stiffnesses the Poisson's ratio is not the same as that at higher stiffnesses.

Direct Tension–Fatigue Relationship

Assuming that the critical dissipated energy associated with fatigue failure corresponds to the dissipated energy at failure under monotonic loading fatigue-life curves were obtained by using the following relationship that is derived from equation 4.16.

$$N_f = \frac{U_f}{K}\left(\frac{1+n^1}{1-n^1}\right)\left(\frac{1}{\epsilon}\right)^n + 1 \tag{4.22}$$

where

U_f = energy for tensile failure
K = strengthening coefficient
n = strain hardening coefficient

Substituting tensile failure energy and the tensile true-stress–true-strain properties in equation 4.18, fatigue life curves were obtained and are compared with the experimental data for all the eight core asphalts in figures 4.51 to 4.54. These results substantiate the selection of direct tension as a surrogate for directly determined fatigue parameters.

Direct Tension Results—Use in Specification

Heukelom (1966) pointed out that there appeared to be a unique relationship for all paving-grade asphalts between the strain at failure and the creep stiffness. This relationship was verified by the research team. Figure 4.55 is a plot of strain at failure versus secant modulus at failure for direct tension data on a number of conventional asphalt cements. It can be shown through various approximate relationships described by Ferry (1980) that the secant modulus in a constant-rate-of-strain test is approximately equal to the creep stiffness at the identical loading time for data at short loading times and/or low temperatures. Additionally, both of these quantities will be approximately equal to three times the complex modulus in shear at a frequency equal to the inverse of the loading time (Van der Poel 1954). Thus, the relationship shown in figure 4.55 is essentially the same as that described by Heukelom. Additionally, since the secant modulus at failure is a unique function of ultimate stress and strain, it can be concluded that failure stress for conventional asphalts is also closely related to the creep stiffness. Thus, the creep stiffness for conventional asphalts seems to uniquely and accurately define, not only the stress-strain behavior under given loading conditions, but also the failure properties. These relationships explain why the use of the empirical limiting stiffness concept appears to predict low-temperature thermal shrinkage cracking so reliably.

Although limiting stiffness appears to be a valid tool for specification purposes, eliminating the need for the direct tension test, application of this principle to modified asphalts may result in significant errors in predicting the occurrence of low-temperature cracking. These errors occur because modification of asphalt cements may change the nature of the relationship between creep stiffness (or secant modulus) and the failure properties. This phenomenon is demonstrated in figure 4.56, which is identical to figure 4.55 except that data for several modified binders have been included. It is clear that the failure properties of modified asphalts might in some cases render the use of the limiting stiffness concept invalid, which then requires the direct inclusion of failure properties in the specification.

The relationship between secant stiffness in a constant-rate-of-strain test and failure stress, failure strain, and stiffness would at first suggest that a failure test alone is adequate to control low-temperature cracking. However, thermoviscoelastic analyses done by both the authors suggest that the use of failure properties alone is insufficient to fully characterize the resistance of a binder to low-temperature, in-service thermal cracking. The reason is that although two binders may have identical cracking temperatures when subjected to a rapid drop in temperature, the rate at which the stresses develop may be quite different. In actual paving applications, it is likely that the thermal stresses to which a binder is subjected will often be less than that required to cause immediate cracking, but, with repeated thermal excursions, the stresses would be sufficient to cause damage to the pavement system, which, when accumulated over time, can damage the pavement. This type of failure is called thermal fatigue.

As an example, figure 4.57 shows predicted stresses for two binders subjected to cooling at 10°C (50°F). This analysis is based on the binder properties without any consideration of

the amelioration of damage that may result from the aggregate. The properties of these binders (the defining temperature, crossover frequency, etc.) were selected so that they would have identical cracking temperatures at a stress of 2 kPa. However, one of the binders has a low rheological index ($R = 1$), while the other has a very high value ($R = 3$). It is clear that the binder with the high rheological index will develop stresses more gradually, and thus, under repeated subcritical thermal stressing be more prone to thermal fatigue. Thus, it was desirable to establish a maximum value for the rheological index in order to minimize thermal fatigue cracking. This step was done in the proposed SHRP binder specification by controlling both the creep stiffness and the log-log slope of the creep curve (m). At a given level of creep stiffness lower values of m are associated with higher values of the rheological index. Thus, by requiring a minimum m value of 0.35 at the minimum pavement temperature, the rheological index is indirectly limited to reasonable values.

Some comments are in order concerning the effect of the cooling rate on thermal cracking in the field and in the laboratory. In performing laboratory tests that directly determine cracking temperature, such as the thermal restrained tension test performed on mixes, relatively high cooling rates are used—typically, 5° to 10°C/hr (41° to 50°F/hr). Since at very high cooling rates, the cracking temperature becomes insensitive to the cooling rate a more or less rate independent, worst case value is established. Admittedly, a fast cooling rate allows for greater production in the laboratory. However, in light of the comments above, it seems possible that the effect of the cooling rate may be different for different asphalts. The current testing program to evaluate thermal cracking of asphalt mixtures does not consider this possibility. Therefore, an evaluation of the relationship between rheological type and cracking temperature should be developed for mixes.

The specification value for strain at failure, requiring a minimum failure strain of 1 percent, was selected to provide a reasonable degree of control over the failure property while still being consistent with the requirement for maximum flexural stiffness. Returning to figures 4.55 and 4.56, it is apparent from inspection that the failure strain associated with a stiffness of 200 MPa ranges from about 0.5 to 2 percent. This relationship is independent of loading time and temperature. In the current version of binder specification, both the bending beam test and the direct tension test are conducted at T_{min} + 10°C (T_{min} + 18°F). The specified loading time for reporting the creep stiffness and m value is 1 minute, and the loading rate for direct tension is given as 1 mm/min (0.0394 in./min). Under these conditions, an evaluation of data obtained for the MRL asphalts led to the final specification value for the direct tension test: *at T_{min} + 10°C (T_{min} + 18°F) and an elongation rate of 1 mm/min (0.0394 in./min), the failure strain should be greater than 1 percent.*

Mode I
Opening Mode

Mode II
Sliding Mode

Mode III
Tearing Mode
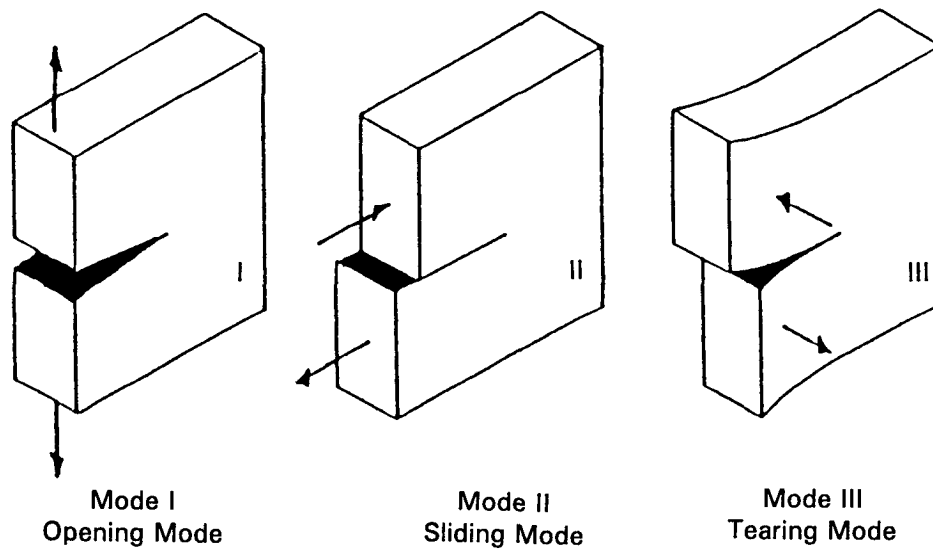
Figure 4.1   **Three Possible Deformation Modes at a Crack Tip**
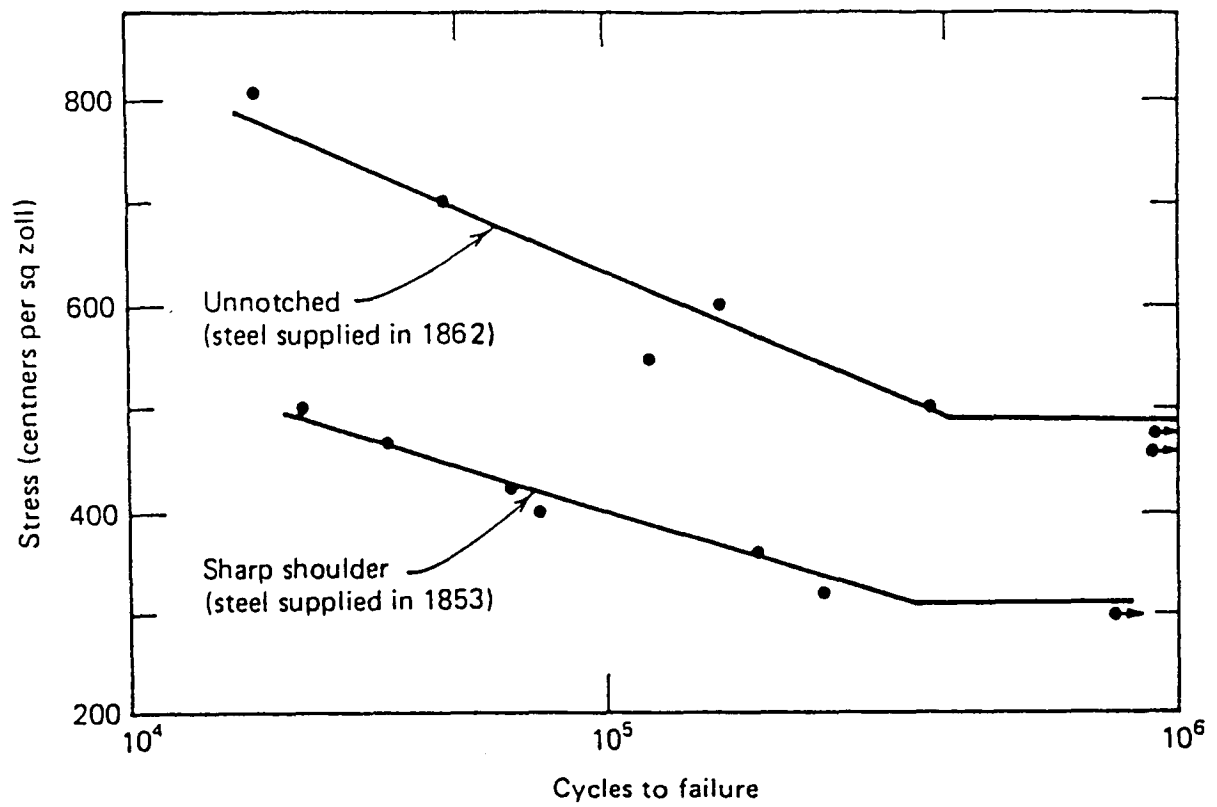
Figure 4.2   Wohler's S-N Curves for Krupp Axle Steel (Taken from Hertzberg 1989)
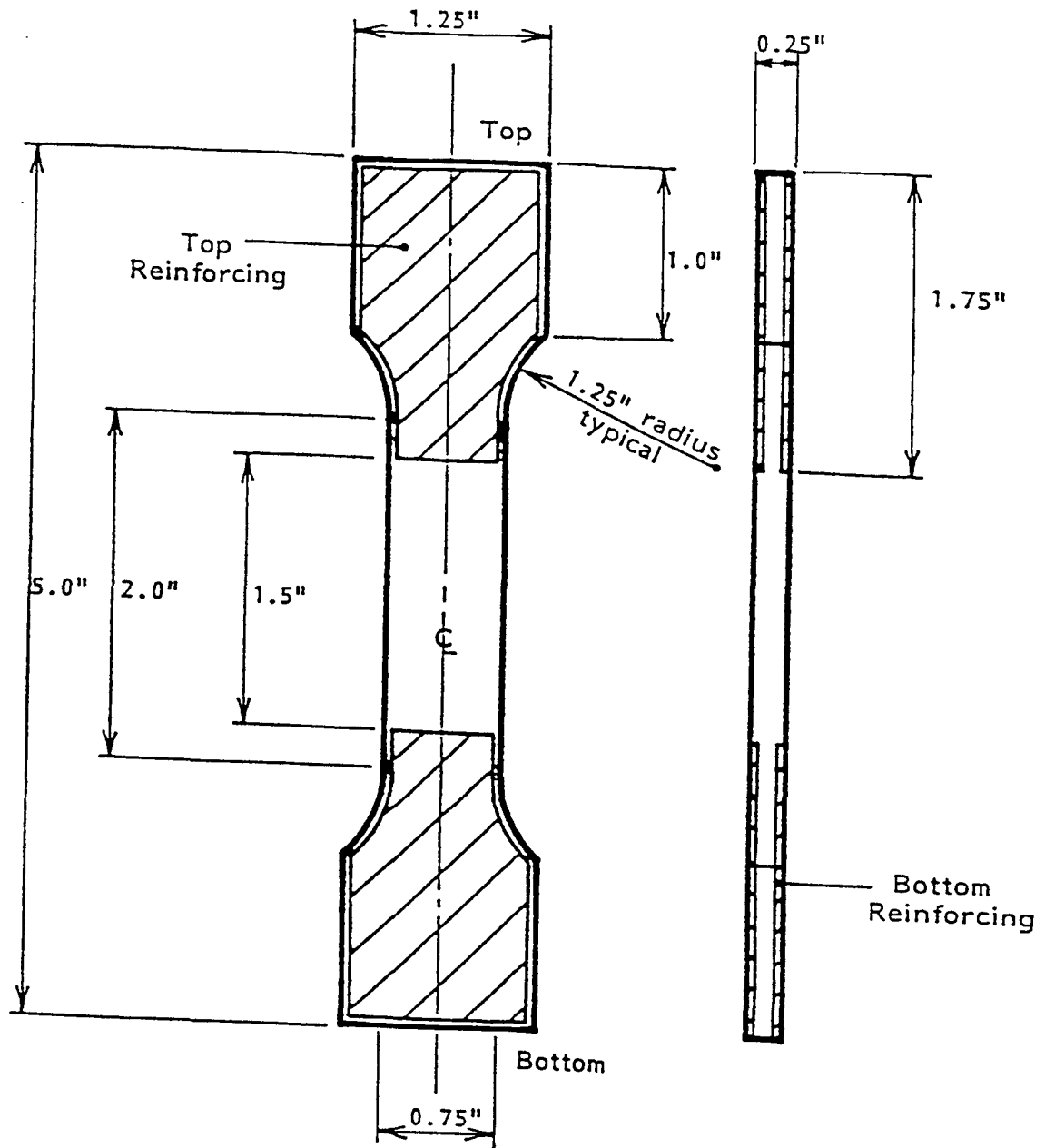
Figure 4.3   Direct Tension Original Specimen Geometry and Reinforcement Details

To INSTRON (need universal joint on top)

This should be adapted to fit into your INSTRON top and bottom

Material 1

Clamp locking screw

1.25" radius, typical

Clamp locking screw

Hinge

0.25" 0.5"

0.5"

1.0"

1.95"

Hinge

0.125" silicone sponge rubber padding

0.0625" silicone sponge rubber padding

0.75"

1.25"

TOP & BOTTOM GRIPS
(Direct Tension)
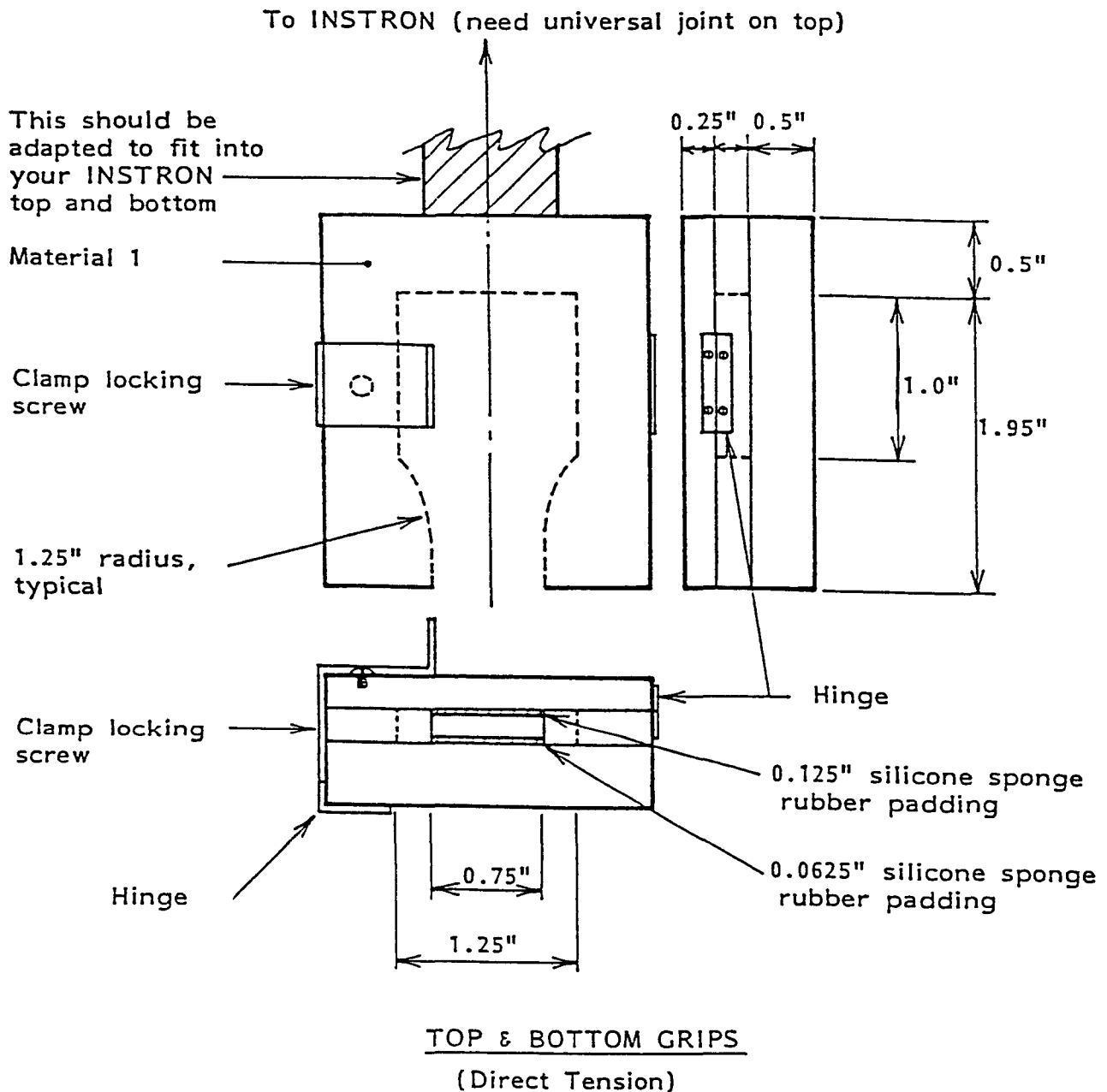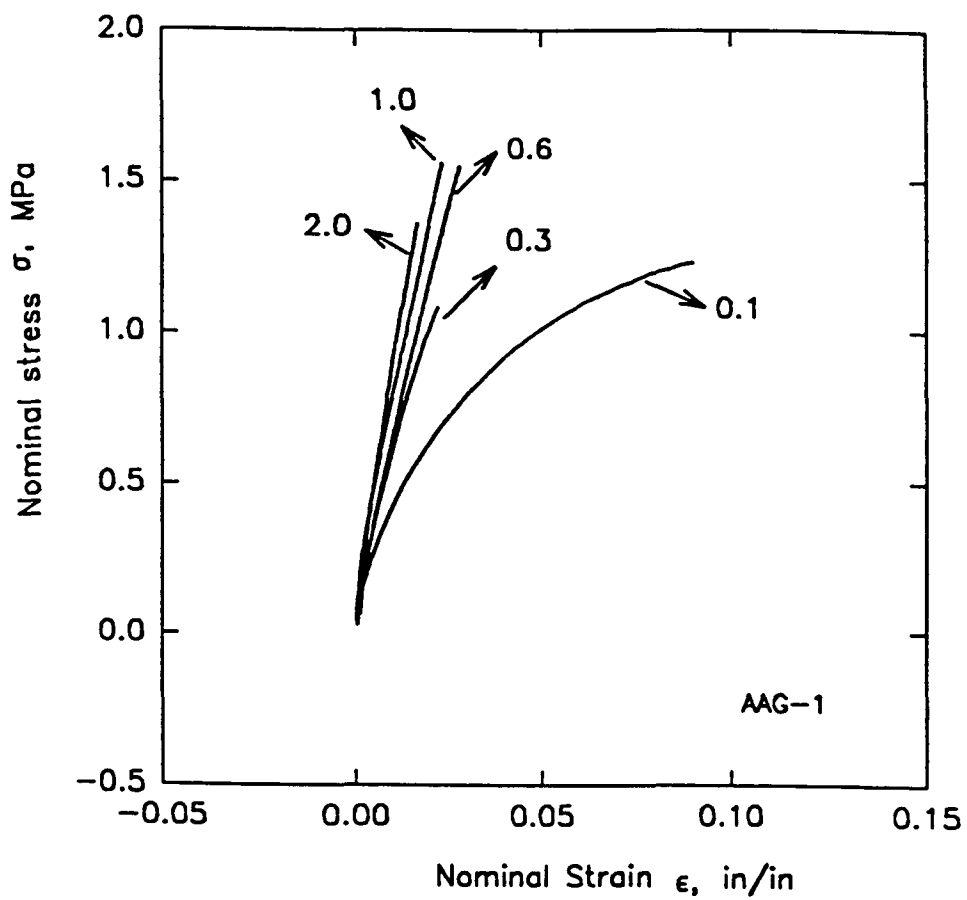
Material 1 = Plexiglass
Silicone sponge rubber: 1990 McMaster-Carr Catalog
0.125"--Item no. 8608K12, pg. 2164
0.0625"--Item no. 8608K11, pg. 2164

Figure 4.4   **Specially Designed Grip Used for Direct Tension Original Specimen Testing**
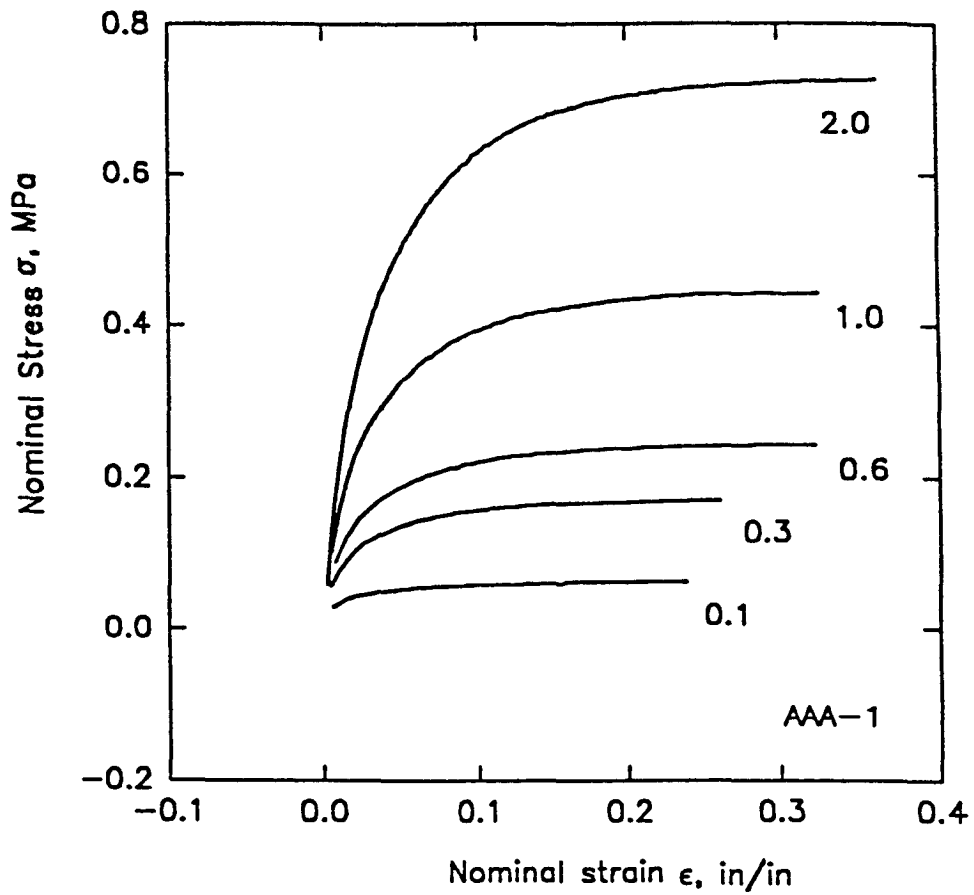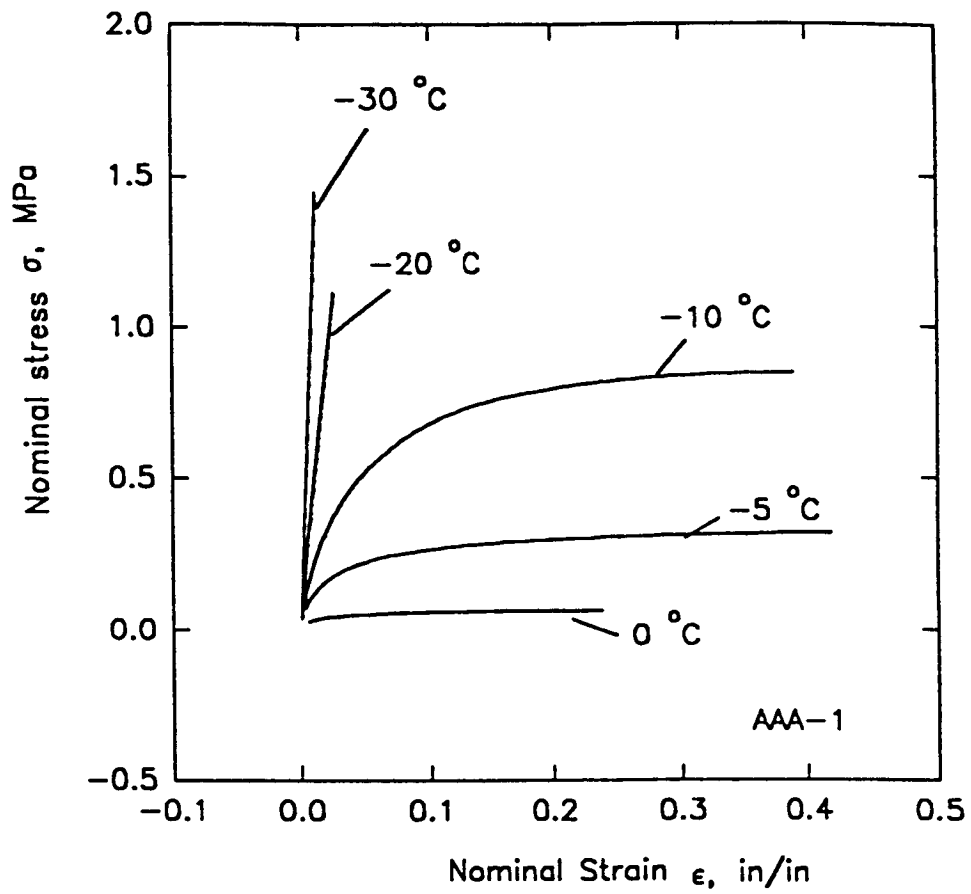
Figure 4.5 Nominal Stress versus Nominal Strain Curve for Asphalt AAA-1 at 0°C Showing Effect of Deformation Rate

Figure 4.6 Nominal Stress versus Nominal Strain Curve for Asphalt AAG-1 at 0°C Showing Effect of Deformation Rate

Figure 4.7 Nominal Stress versus Nominal Strain Curve for Asphalt AAA-1 at 0.1 in/min (Deformation Rate) Showing Effect of Temperature

236
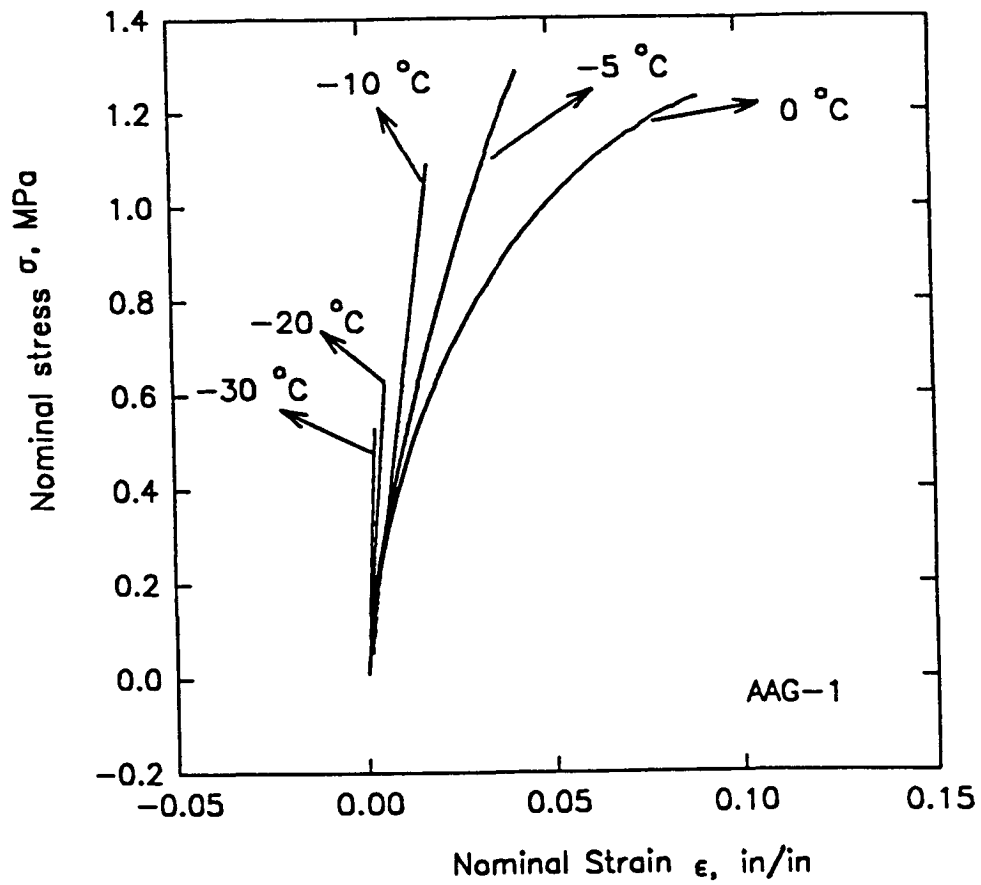
Figure 4.8   Nominal Stress versus Nominal Strain Curve for Asphalt AAG-1 at 0.1 in/min (Deformation Rate) Showing Effect of Temperature
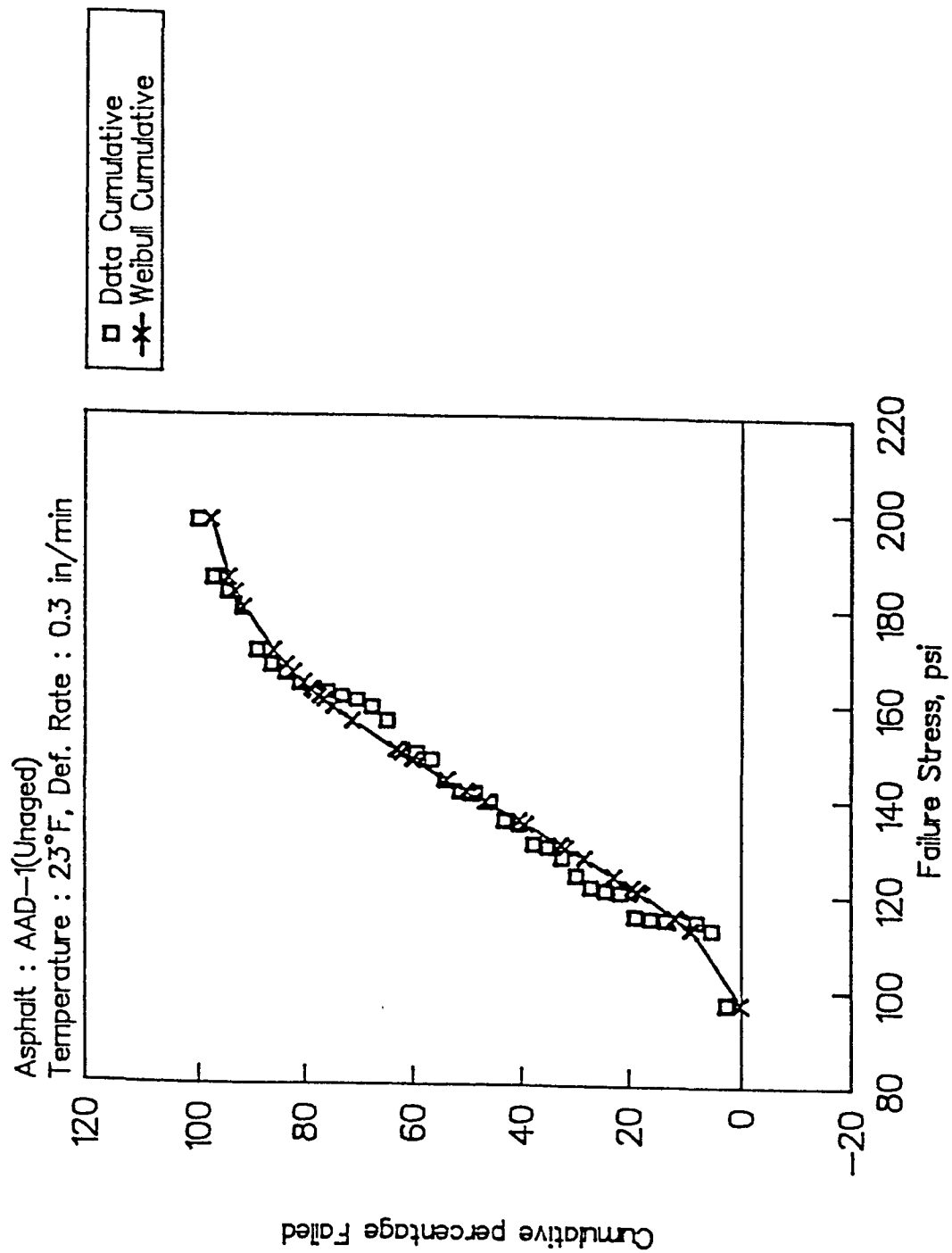
Figure 4.9 Weibull Cumulative versus Data Cumulative for Asphalt AAD-1

238
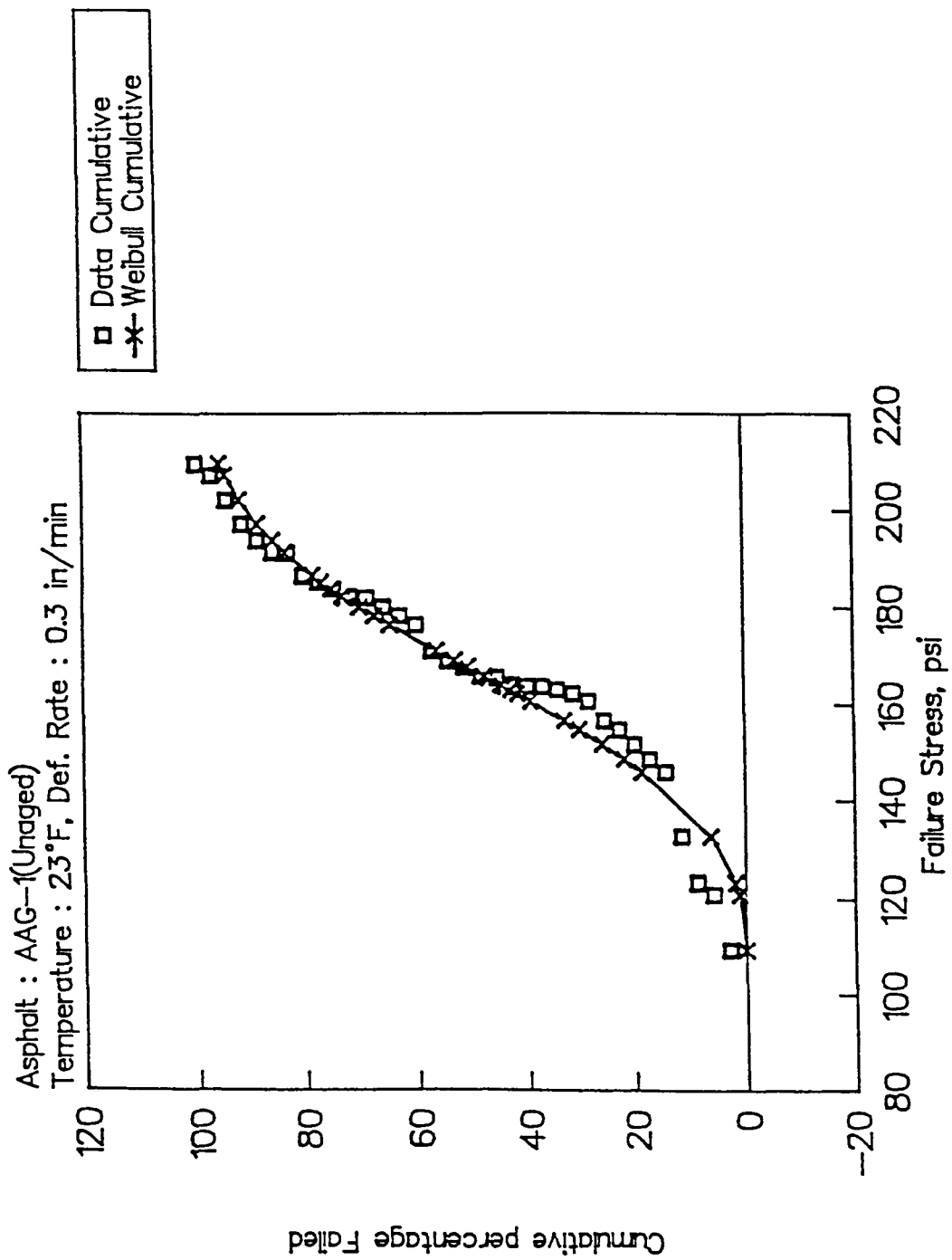
Figure 4.10 Weibull Cumulative versus Data Cumulative for Asphalt AAG-1

239
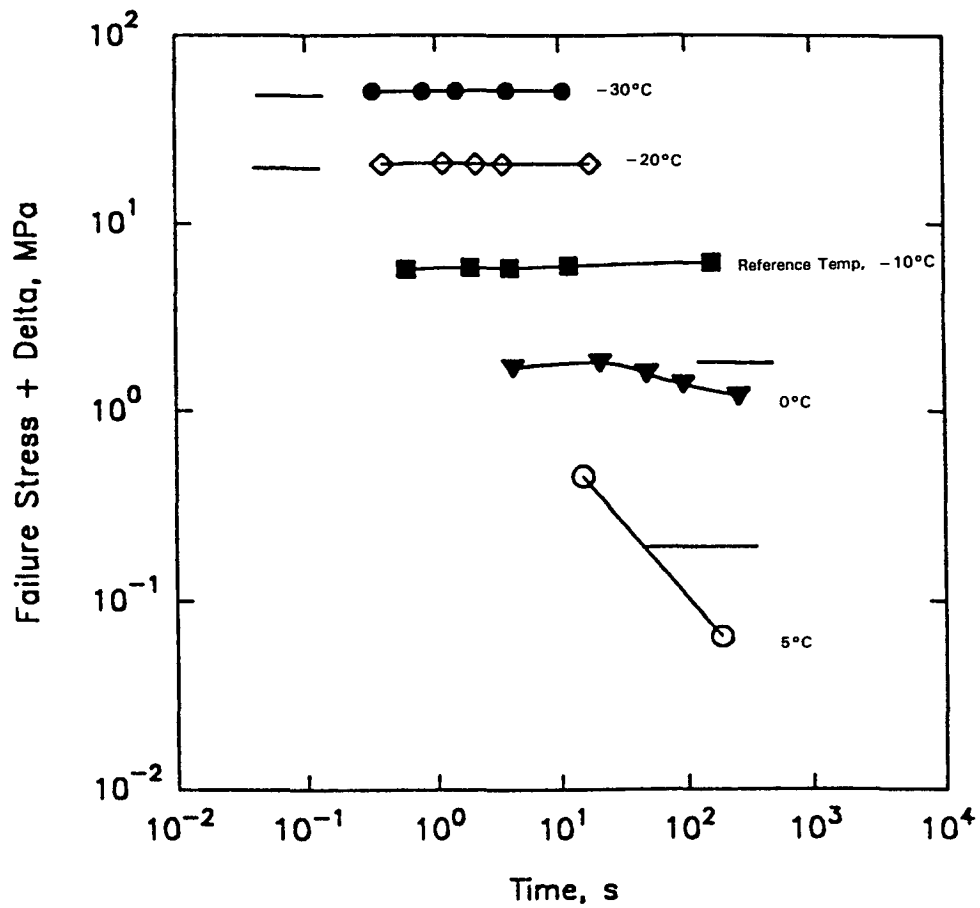
Note: Delta = arbitrary shift for clarity.

Figure 4.11   Failure Stress (Tensile Strength) versus Physical Time for Asphalt AAD-1
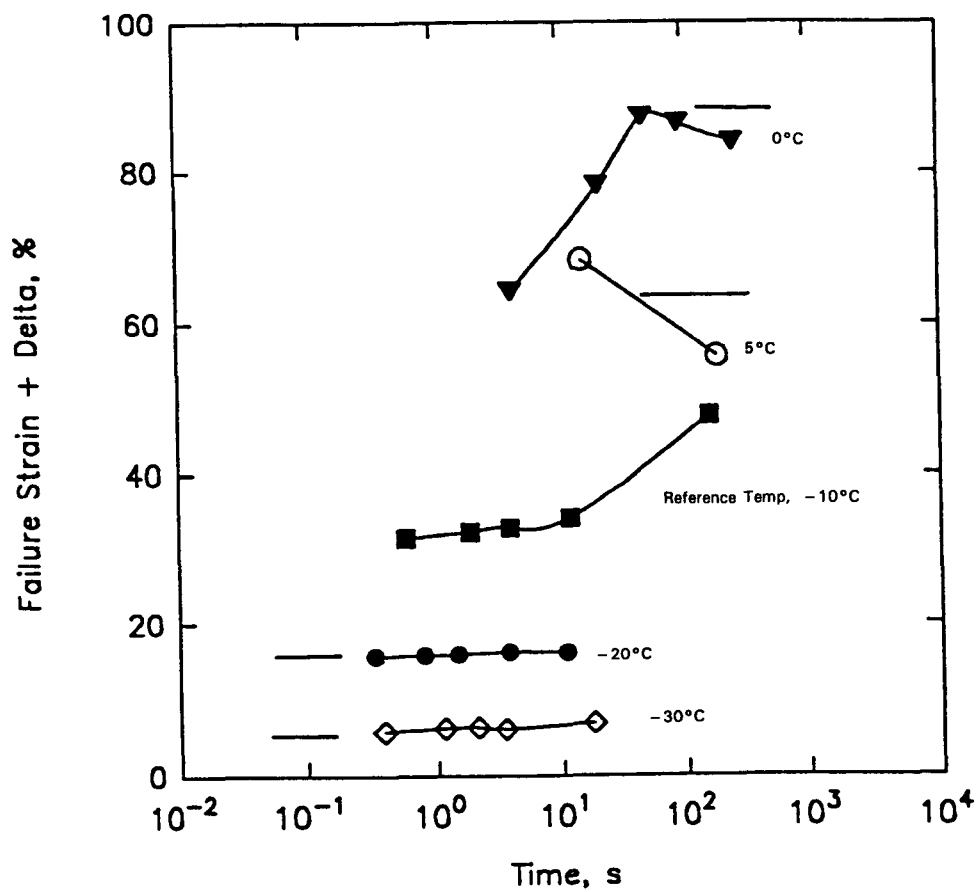
Note: Delta = arbitrary shift for clarity.
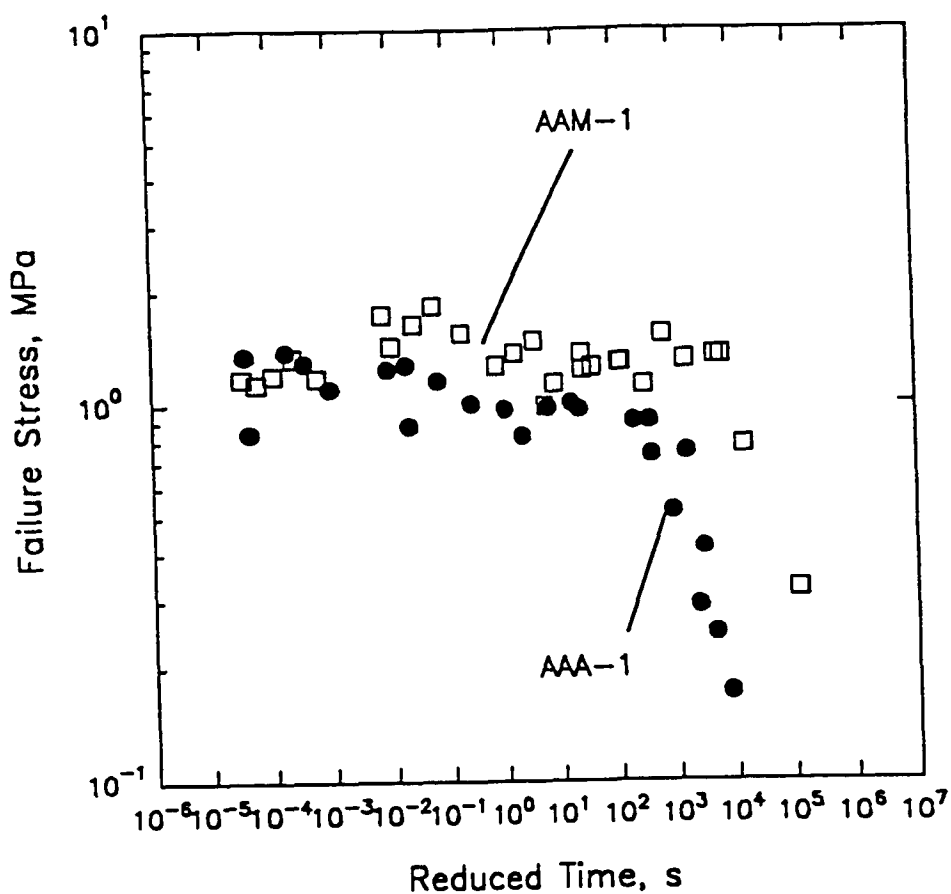
Figure 4.12   Failure Strain versus Physical Time for Asphalt AAD-1
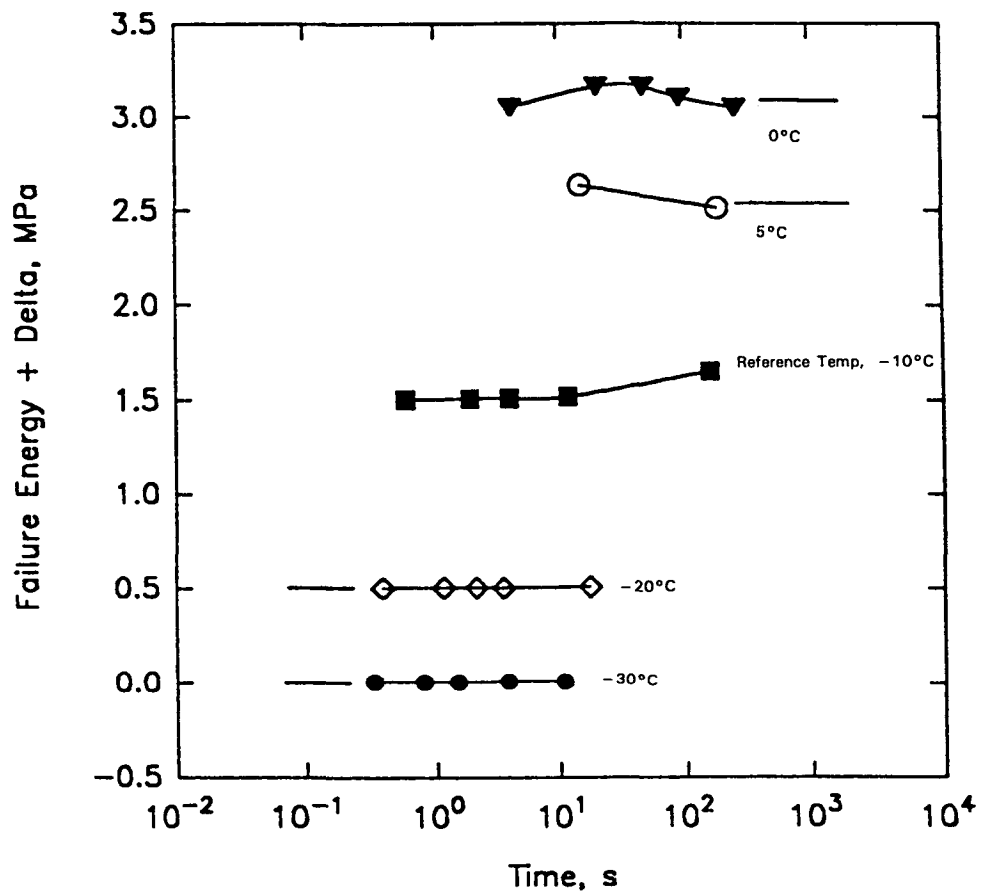
Note: Delta = arbitrary shift for clarity.
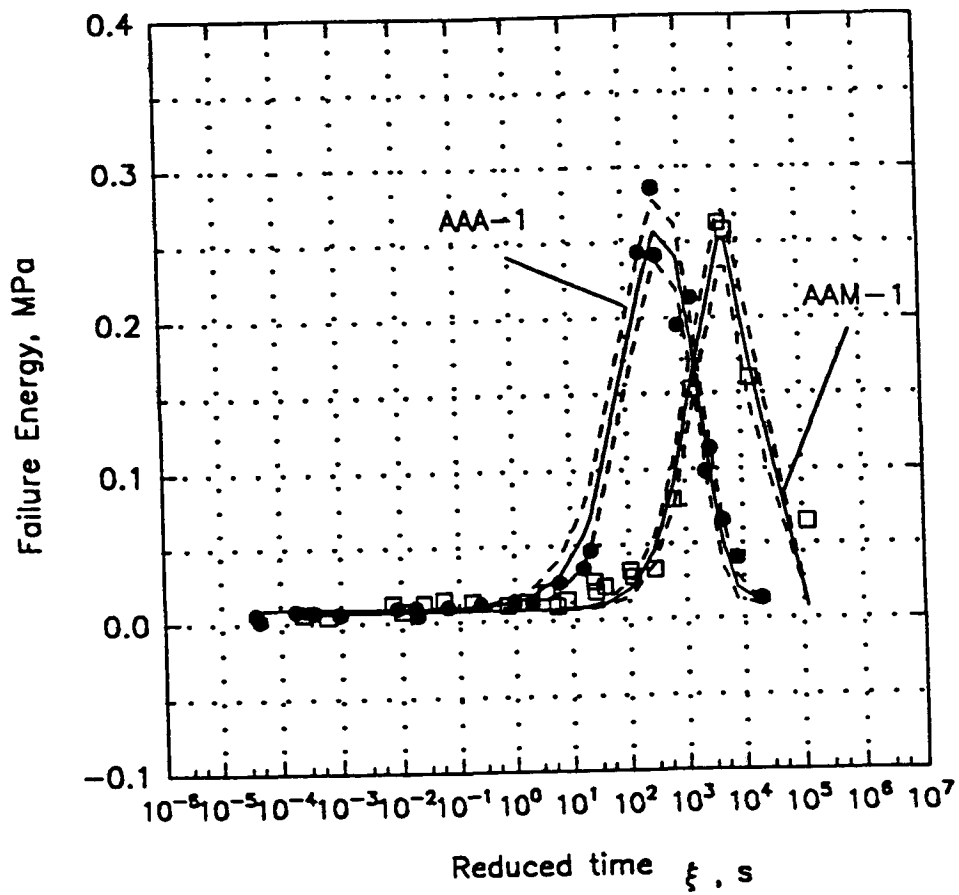
Figure 4.13   Failure Energy versus Physical Time for Asphalt AAD-1

Figure 4.14 Failure Stress (Tensile Strength) versus Reduced Time (Master Curve) for Asphalts AAA-1 and AAM-1

243
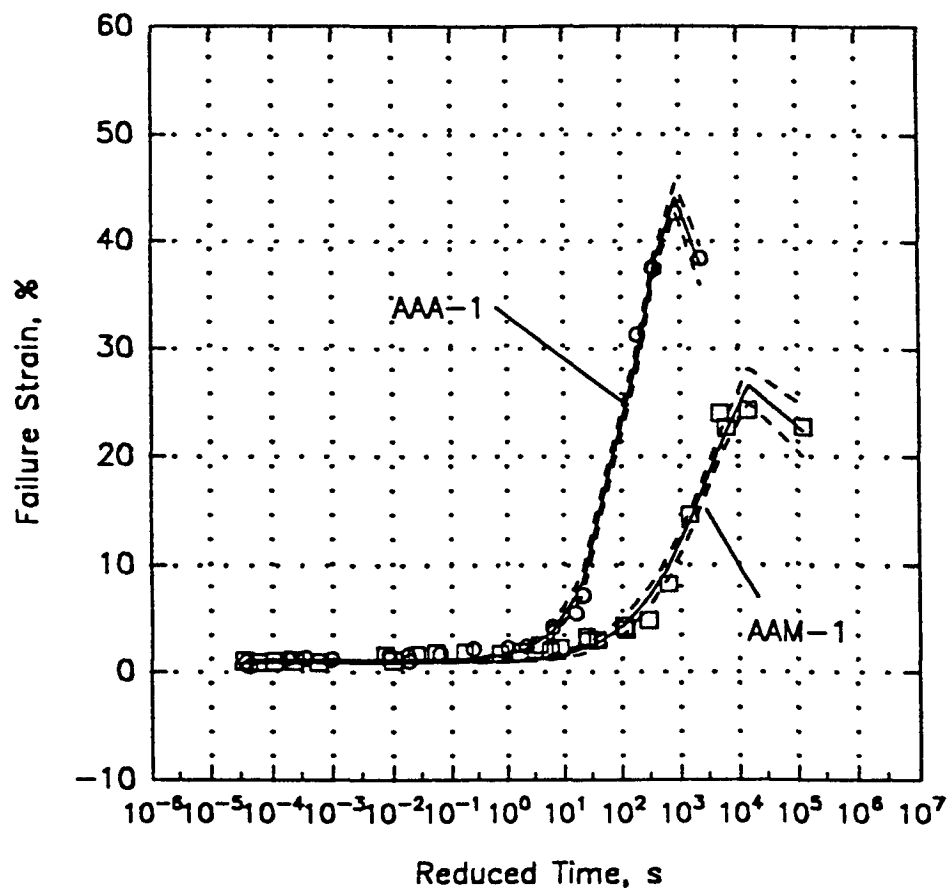
Figure 4.15 **Failure Strain versus Reduced Time (Master Curve) for Asphalts AAA-1 and AAM-1**

Figure 4.16 Failure Energy versus Reduced Time (Master Curve) for Asphalts AAA-1 and AAM-1
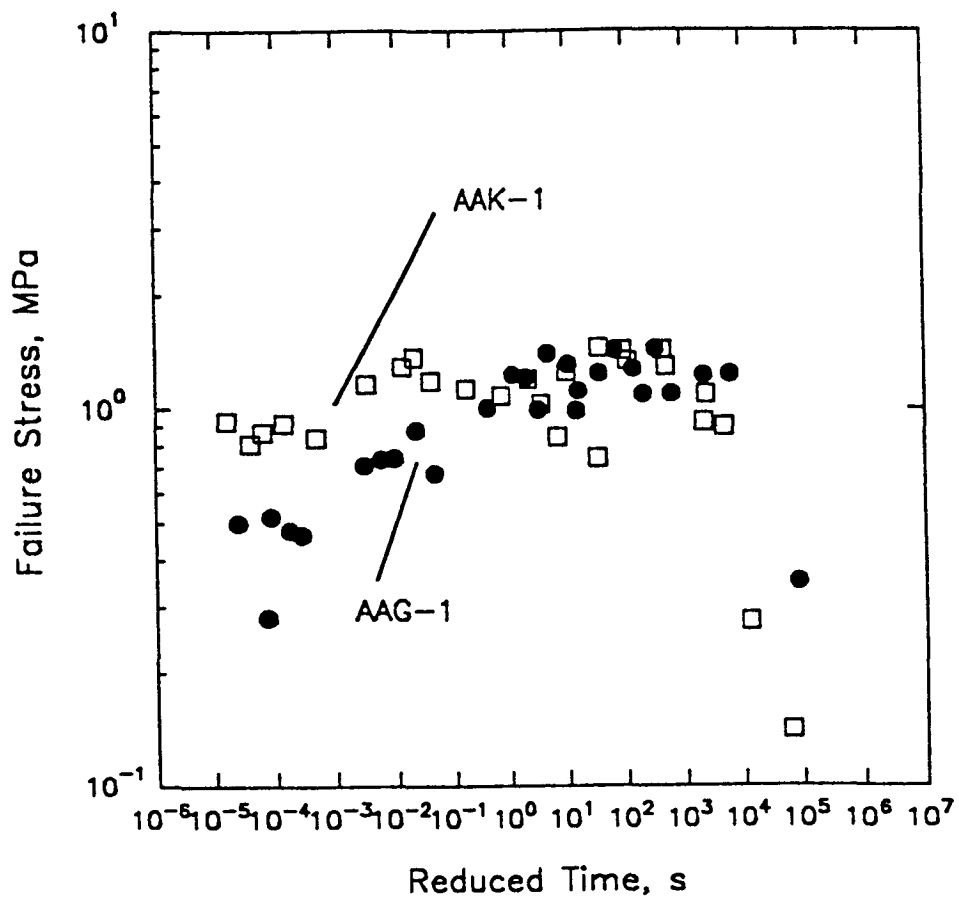
Figure 4.17   Failure Stress (Tensile Strength) versus Reduced Time (Master Curve) for Asphalts AAK-1 andAAG-1

246
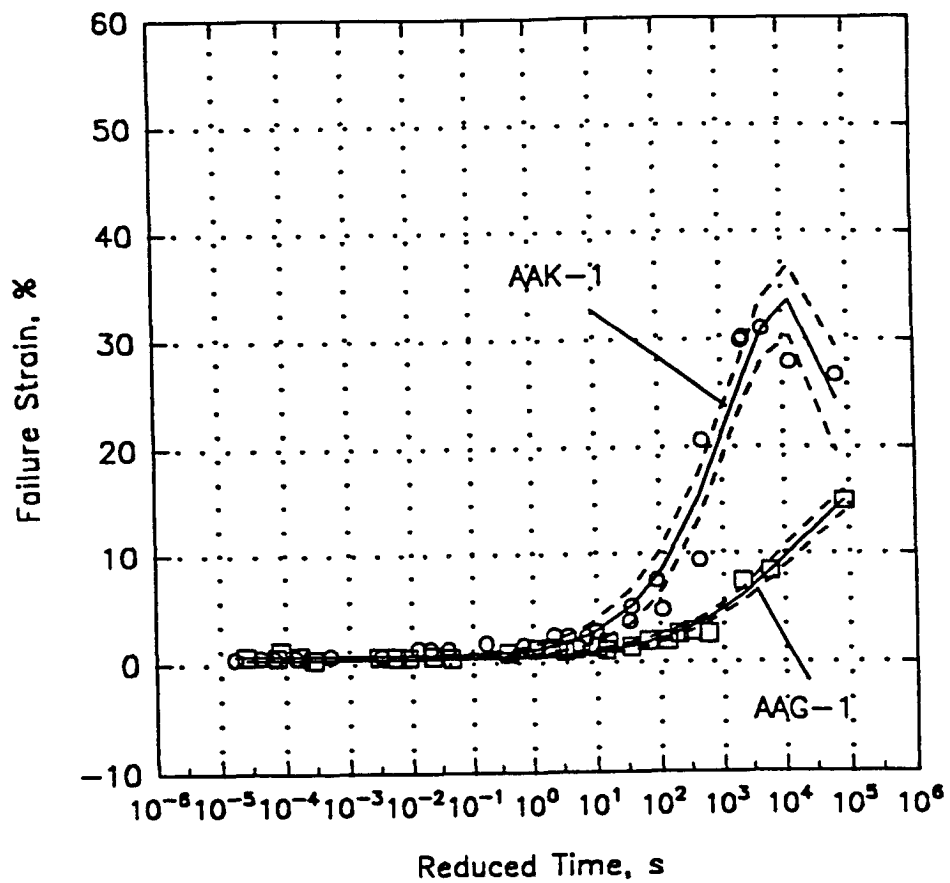
Figure 4.18 Failure Strain versus Reduced Time (Master Curve) for Asphalts AAK-1 and AAG-1
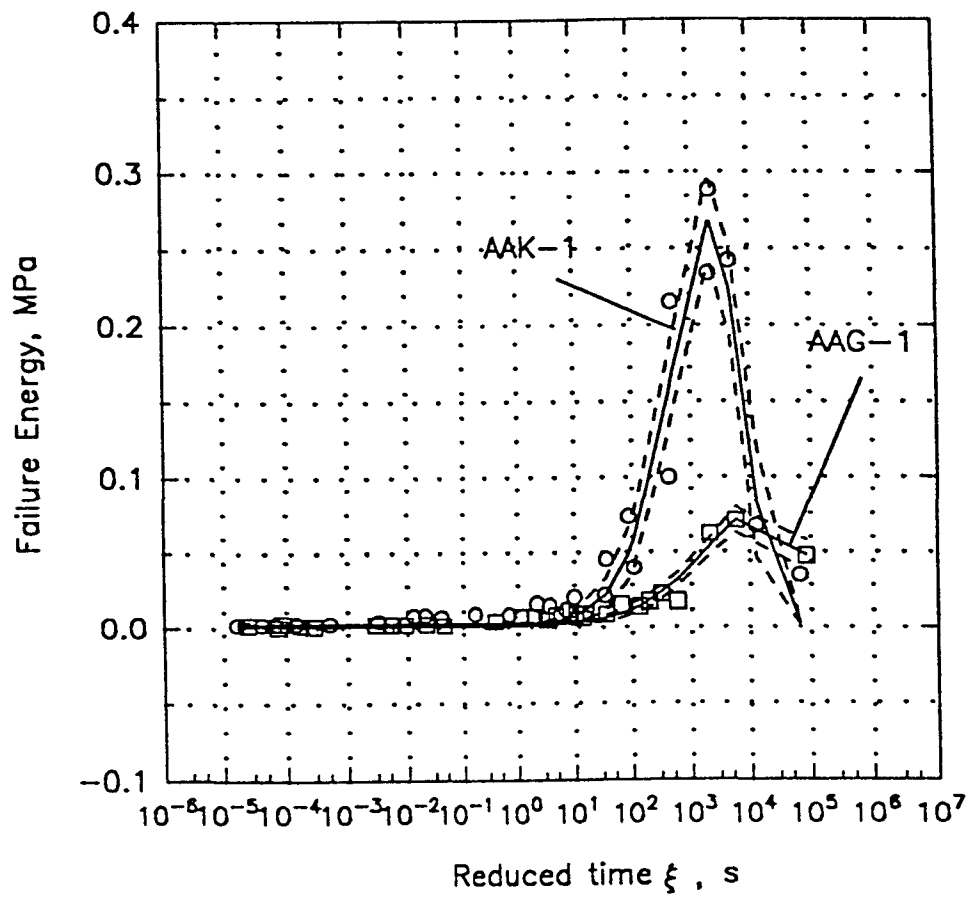
Figure 4.19   Failure Energy versus Reduced Time (Master Curve) for Asphalts AAK-1 and AAG-1
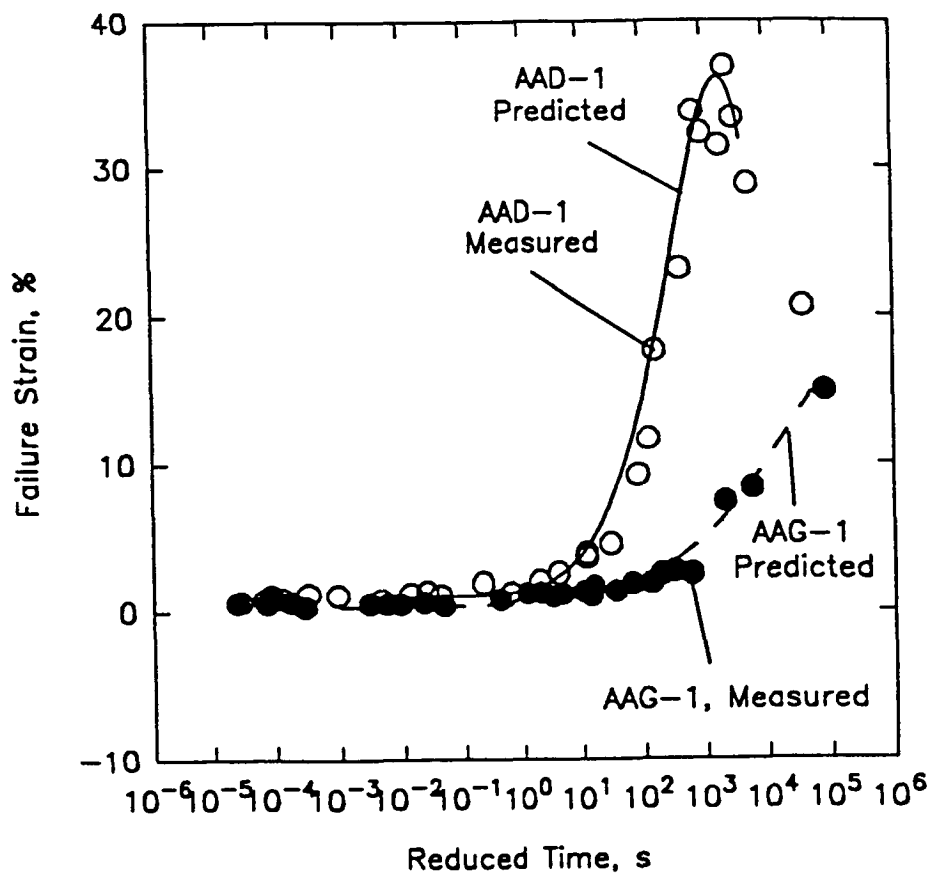
Figure 4.20 **Measured 27 Points (Full Matrix) Overlayed on Curve Obtained from Fitting 6 Points (Reduced Protocol) to Equation 4.18 for Asphalts AAD-1 and AAG-1**

R=5.0

R=2.5

R = 12.0

ASPHALT
SECTION

R = 12.0

END
INSERT

30.0

18.0

30.0

6.0

6.0

20.0
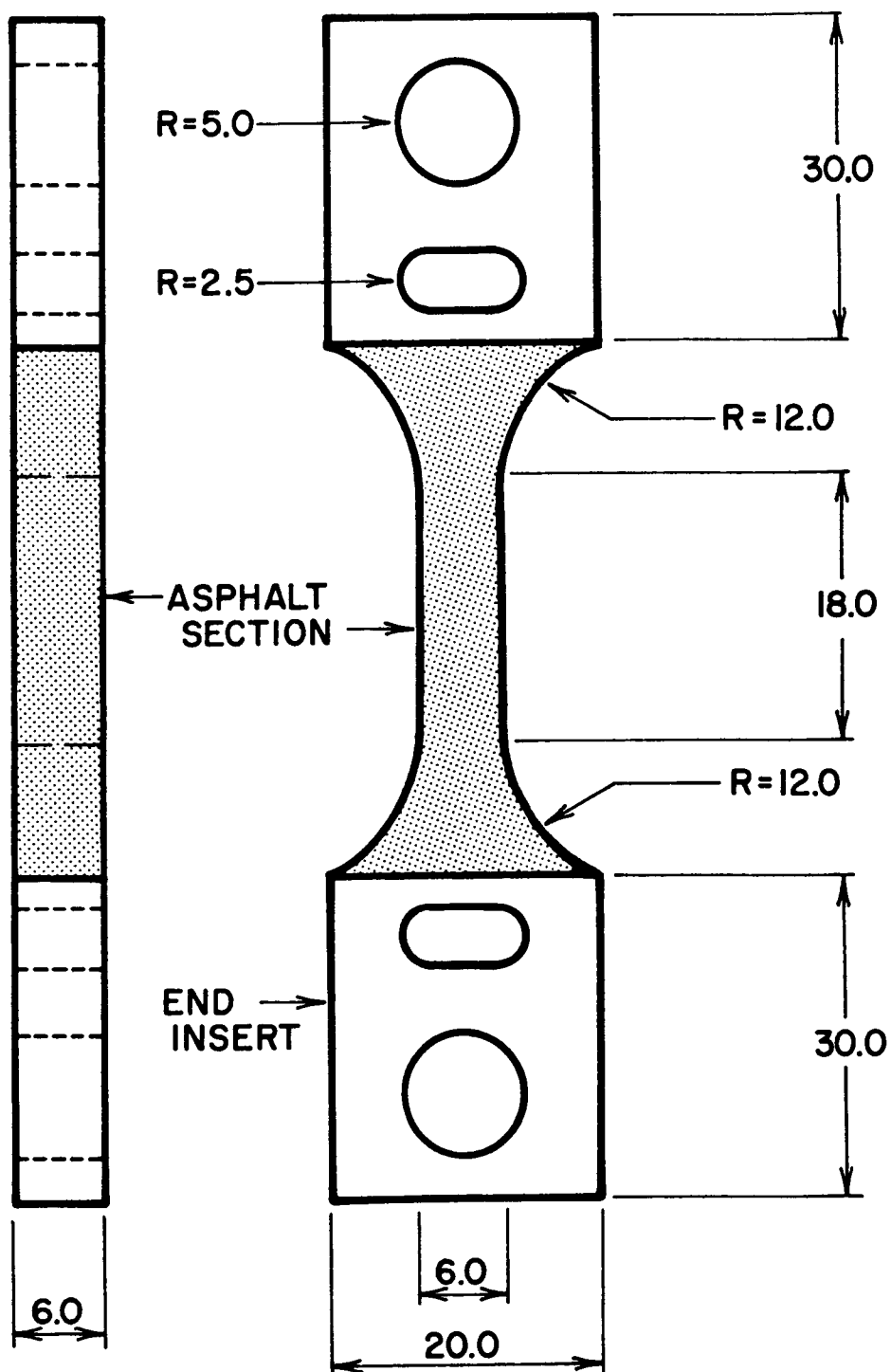
All Dimensions in Millimeters
Not to Scale

Figure 4.21   New Specification-Type Direct Tension Specimen Geometry

250

R=5.0

R=2.5

10.0

20.0

10.0

15.0

5.0

30.0

6.0
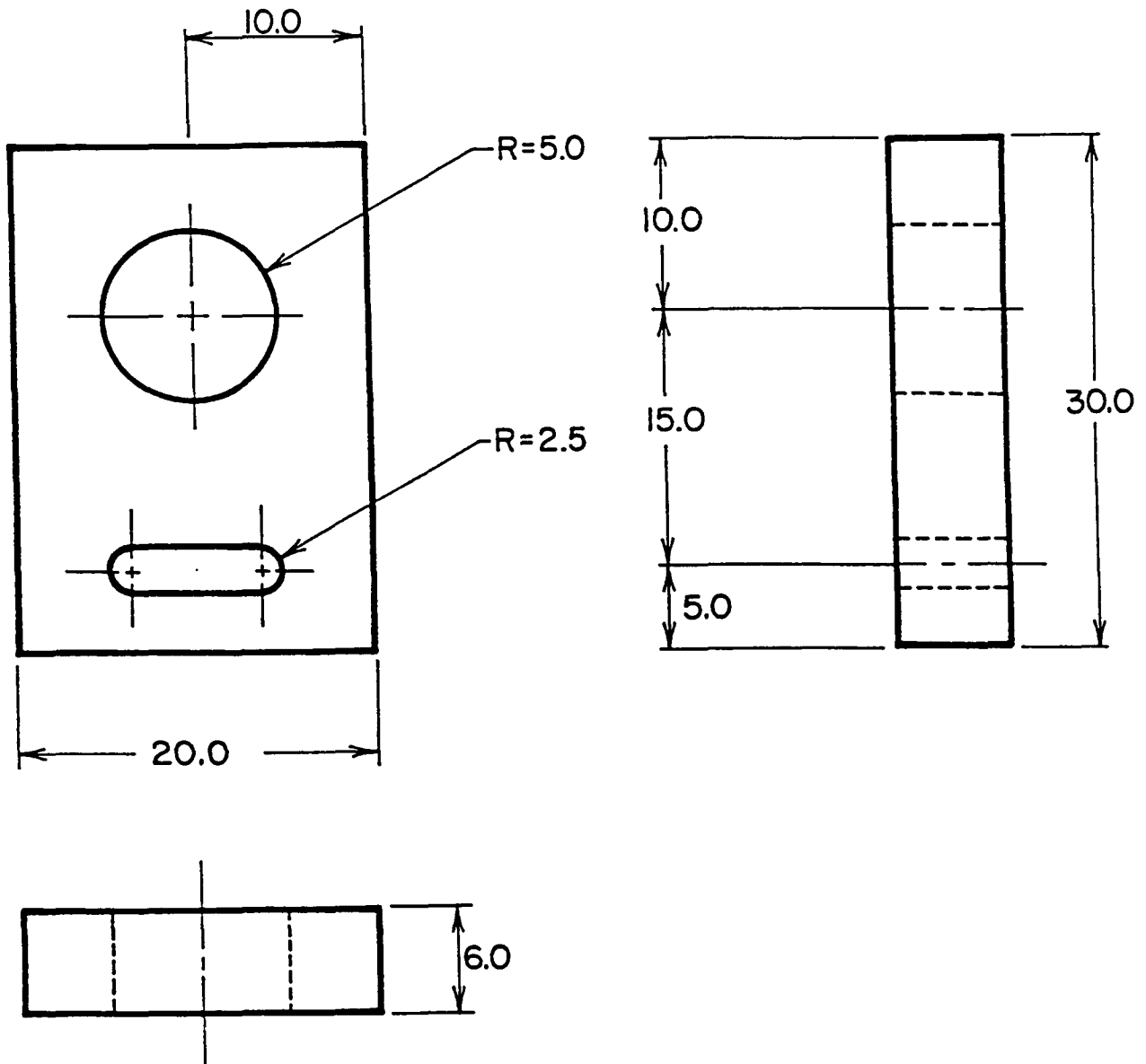
All Dimensions in Millimeters
Not to Scale

Figure 4.22 Plexiglas™ End Insert for Specification-Type, Direct Tension Test

5.0

9.5

SECTION A-A

R = 3.0

A   A

FILLET O.K.

6.0   26.0

10.0

5.0

All Dimensions in Millimeters
Not to Scale
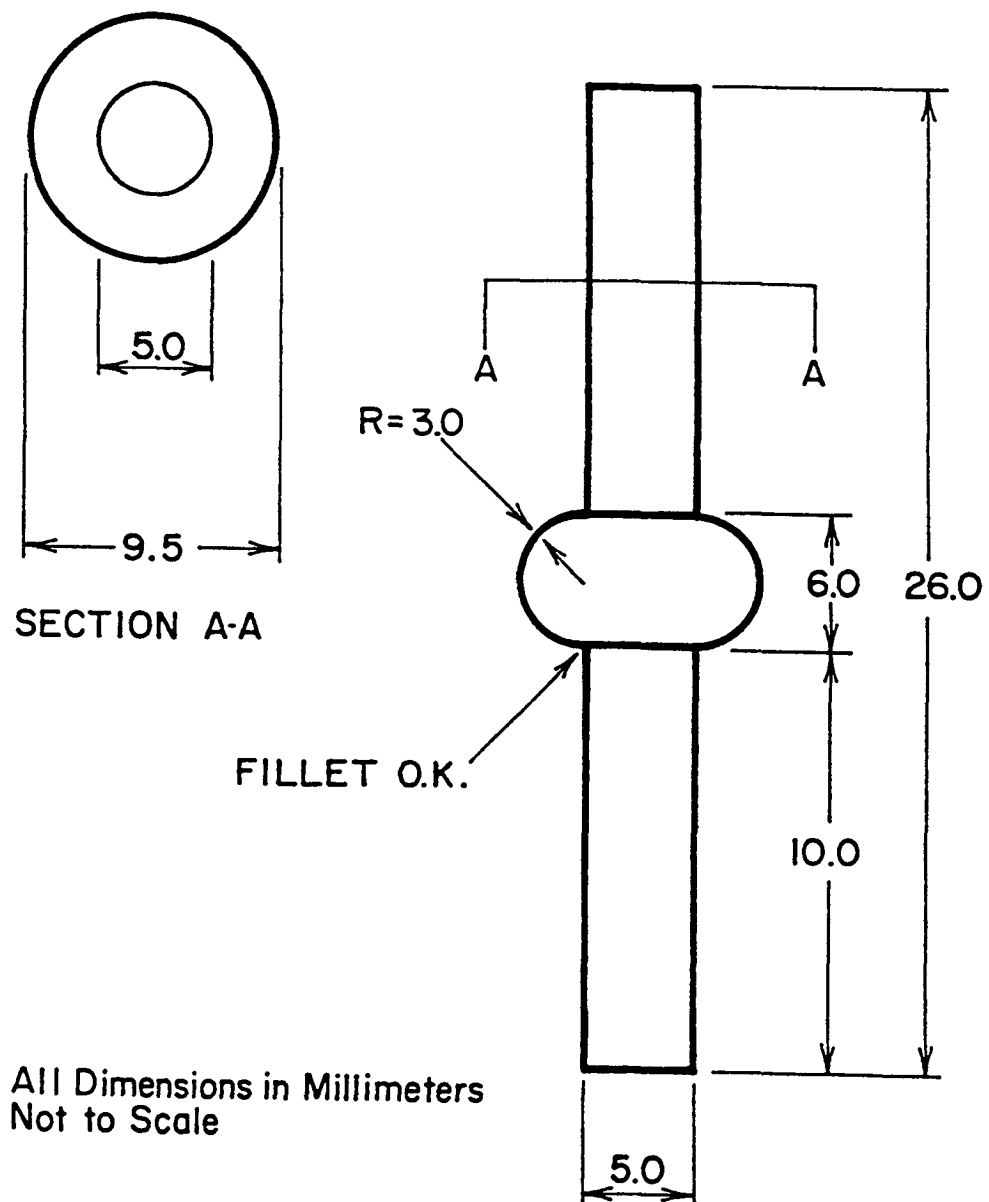
Figure 4.23   Specially Designed Pins for Specification-Type, Direct Tension Test

EDGE I

EDGE 2

LASER
RECEIVER

EDGE 3

EDGE 4

LASER
TRANSMITTER

Not to Scale
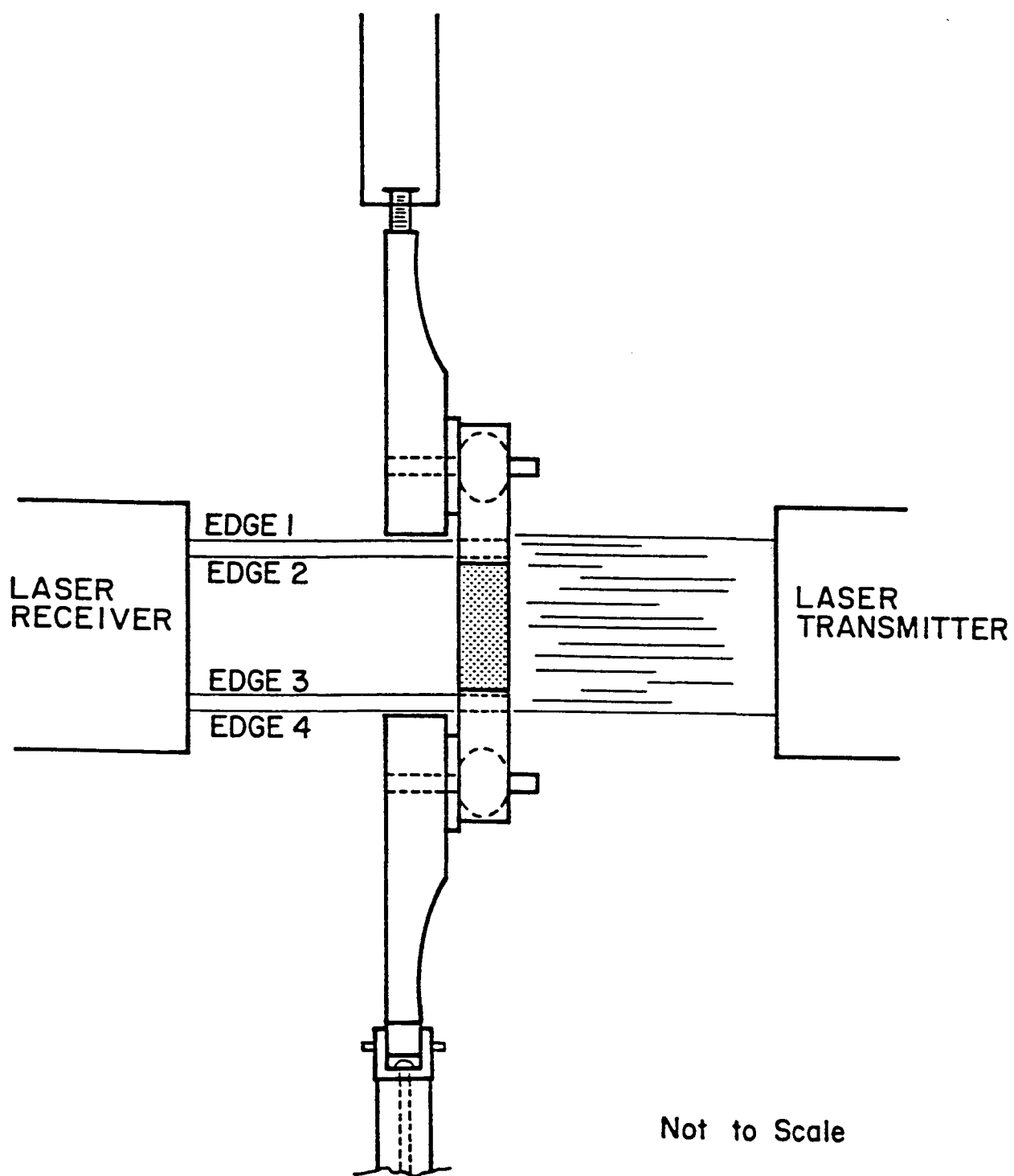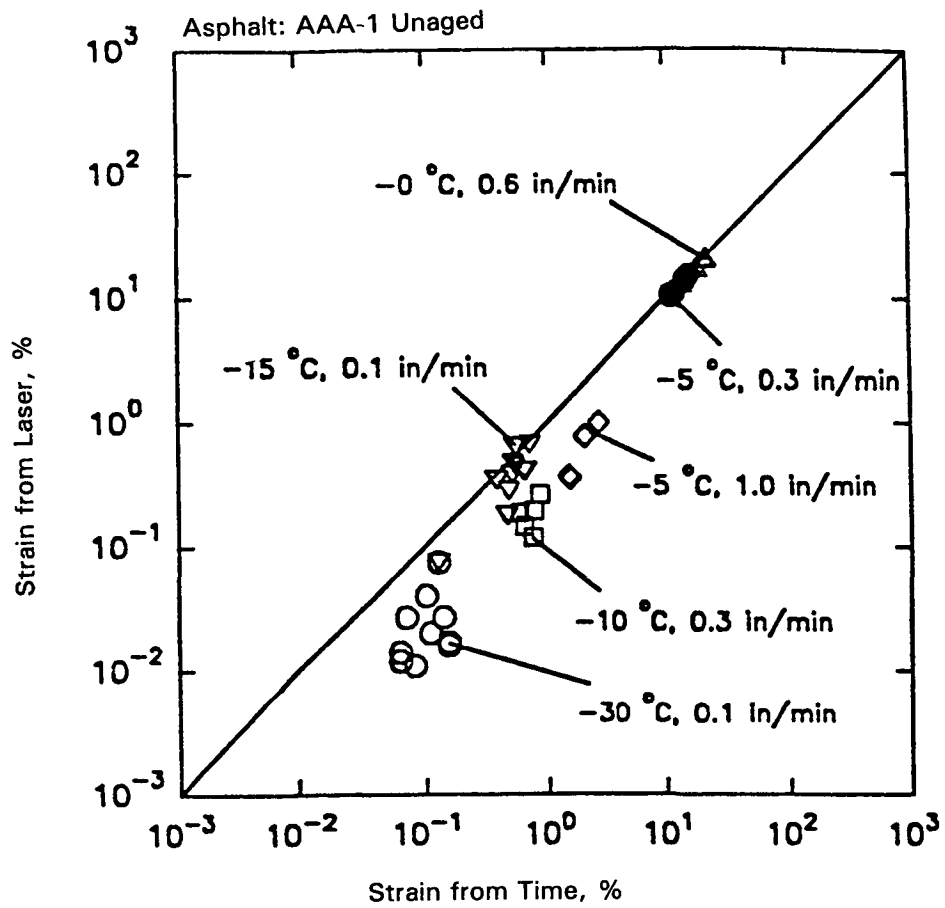
Figure 4.24   Specification-Type, Direct Tension Test, Illustrating the Laser-Based
Extensometer
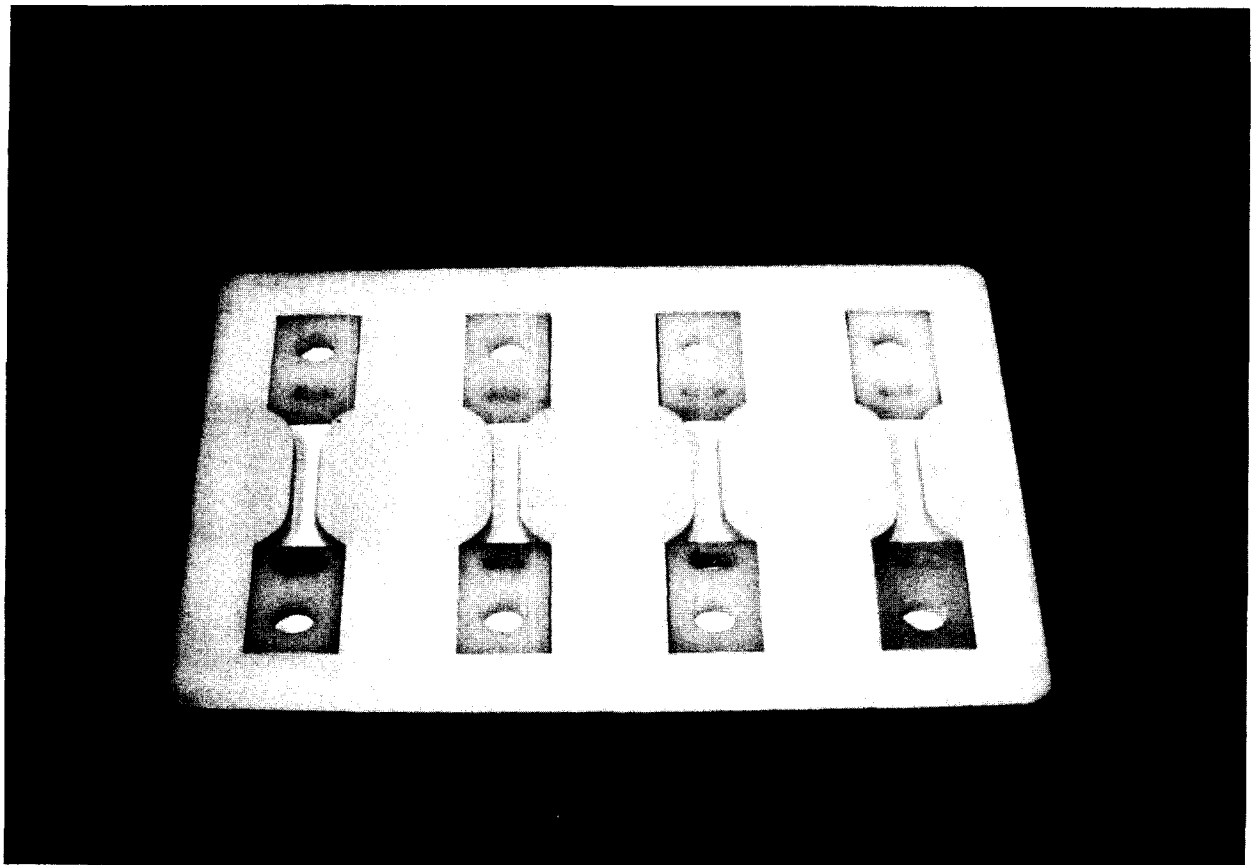
Figure 4.25   Silicone Rubber Molds Used to Fabricate Test Specimens for Specification-Type Test Specimens
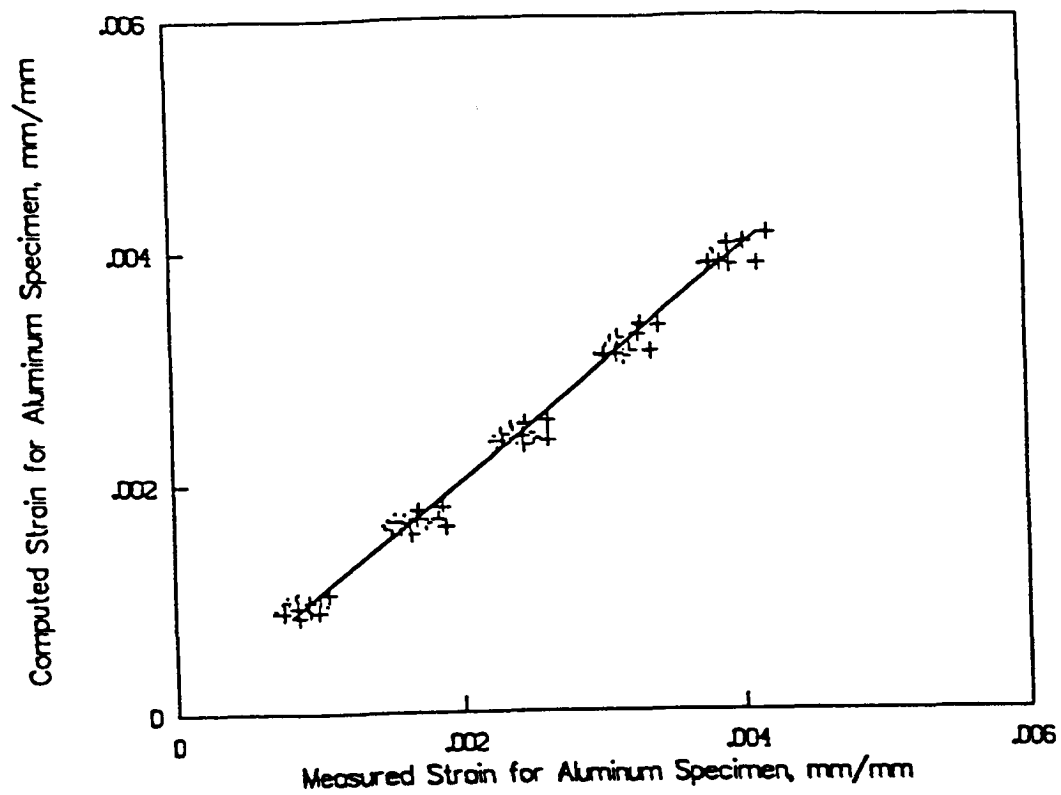
Figure 4.26 Comparison of Measured and Predicted Strains for Aluminum Specimen and Specification-Type Geometry

Figure 4.27   Platen-Measured Strain versus Laser (Noncontact)-Measured Strain
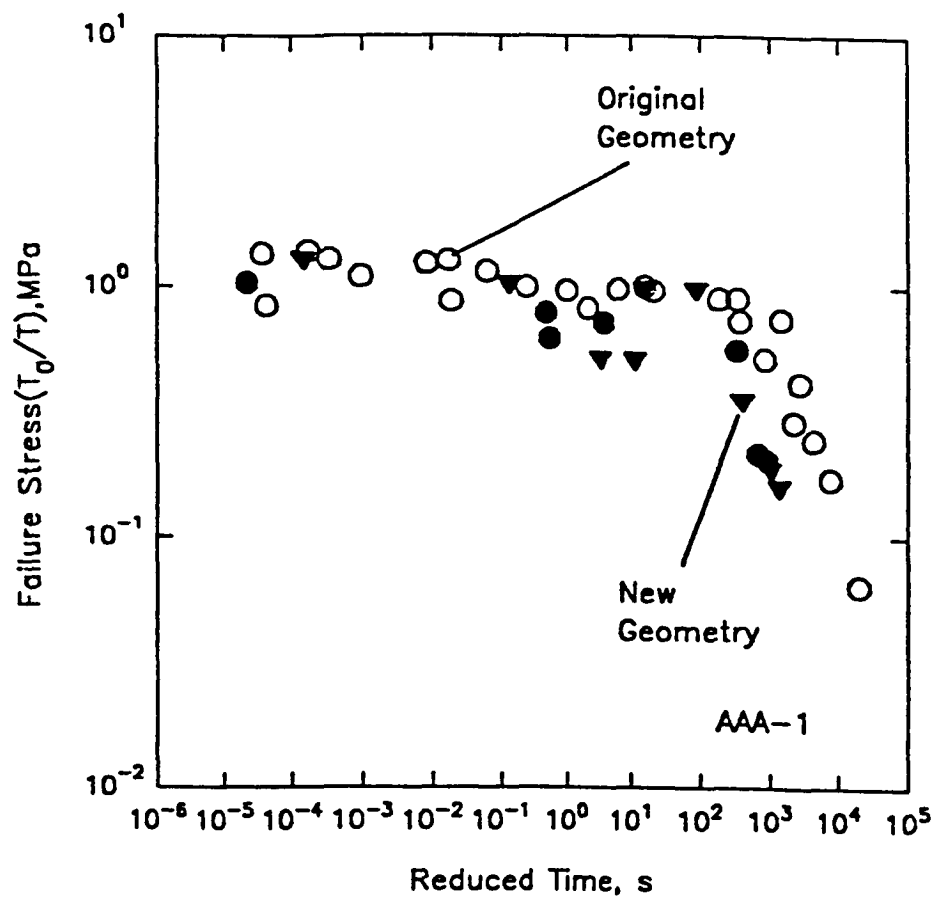
Figure 4.28 Failure Stress Master Curve Comparing Original and Specification-Type Geometry, Asphalt AAA-1 (Tank)
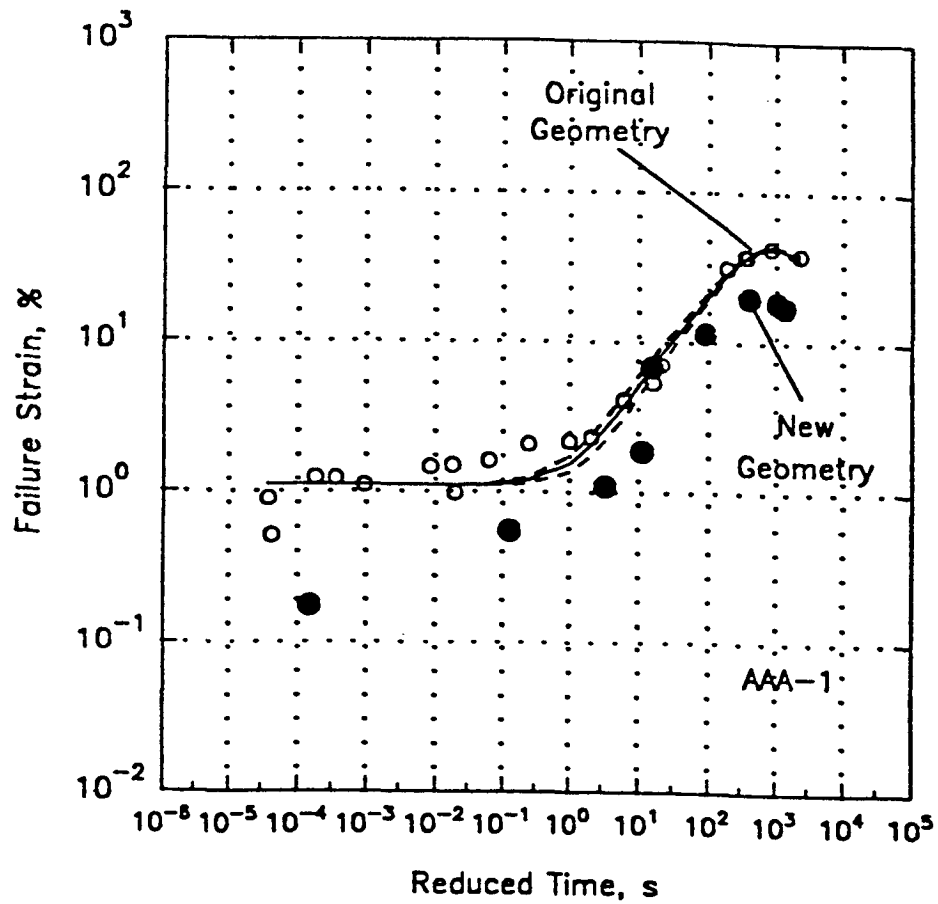
Figure 4.29 Failure Strain Master Curve Comparing Original and Specification-Type Geometry, Asphalt AAA-1 (Tank)
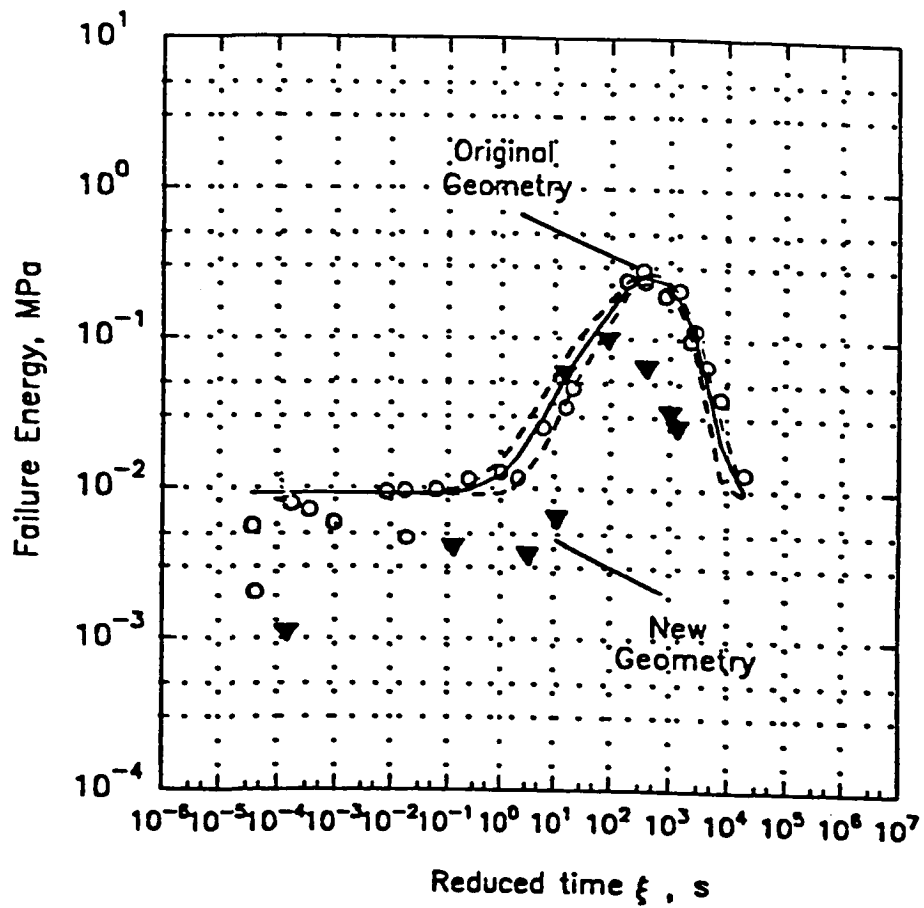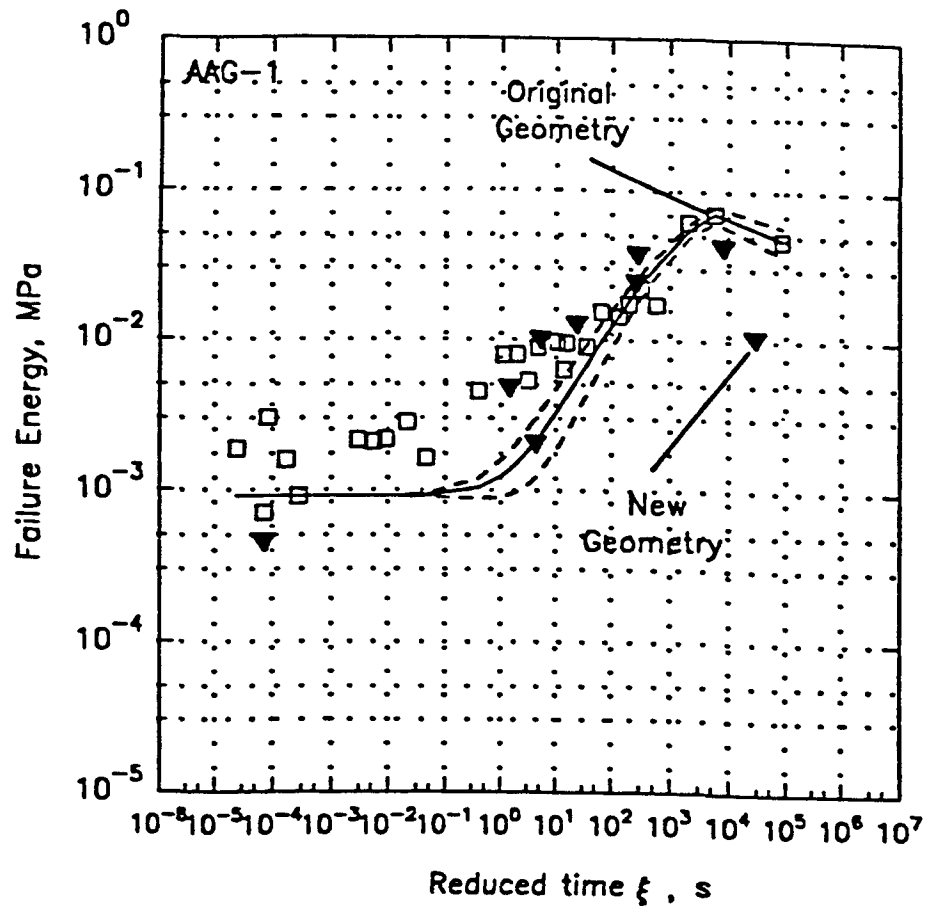
Figure 4.30 Failure Energy Master Curve Comparing Original and Specification-Type Geometry, Asphalt AAA-1 (Tank)
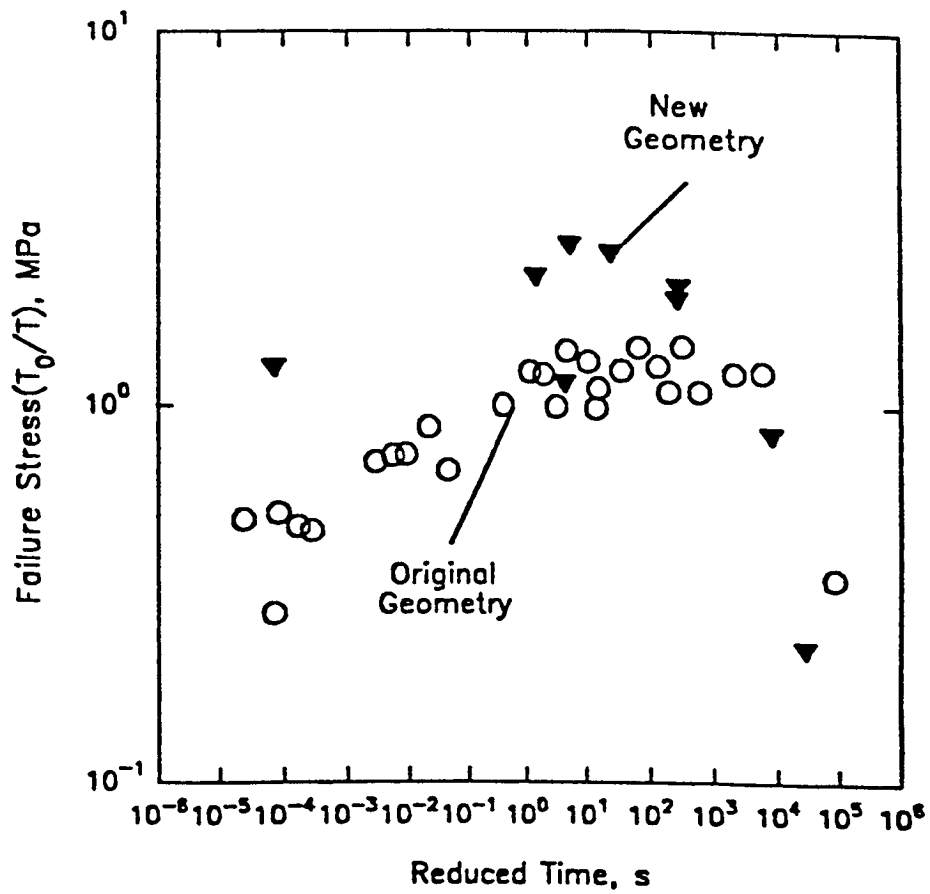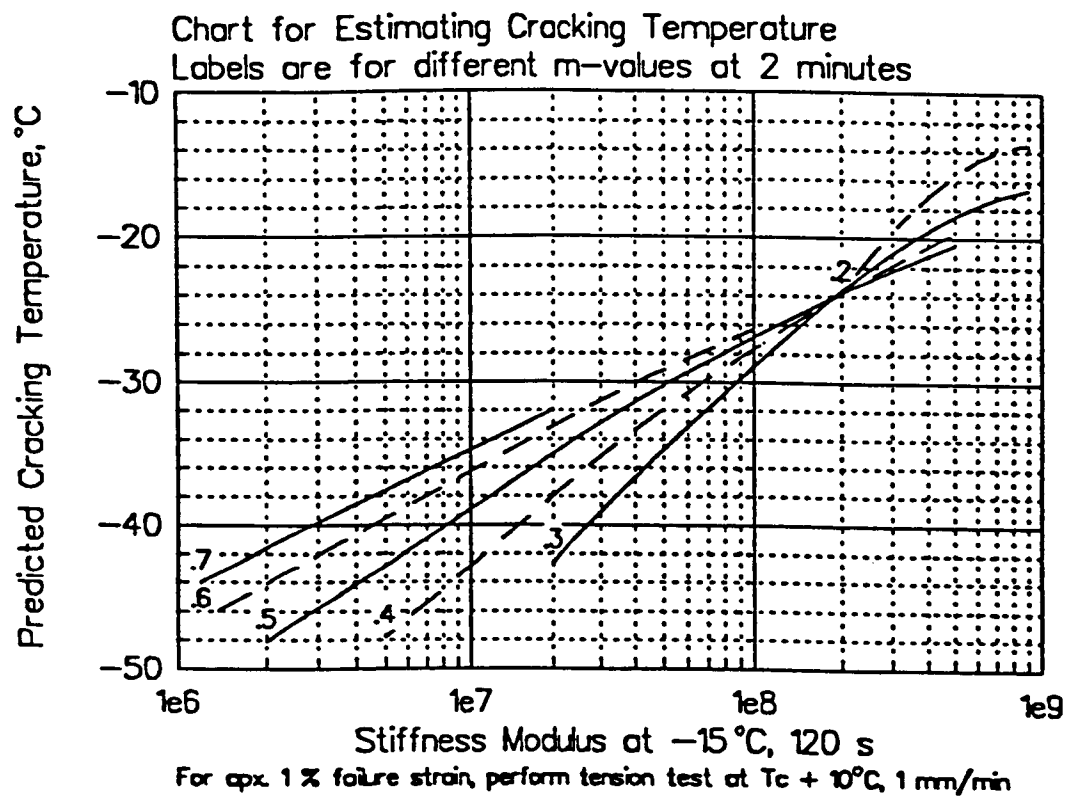
Figure 4.31 Failure Stress Master Curve Comparing Original and Specification-Type Geometry, Asphalt AAG-1 (Tank)
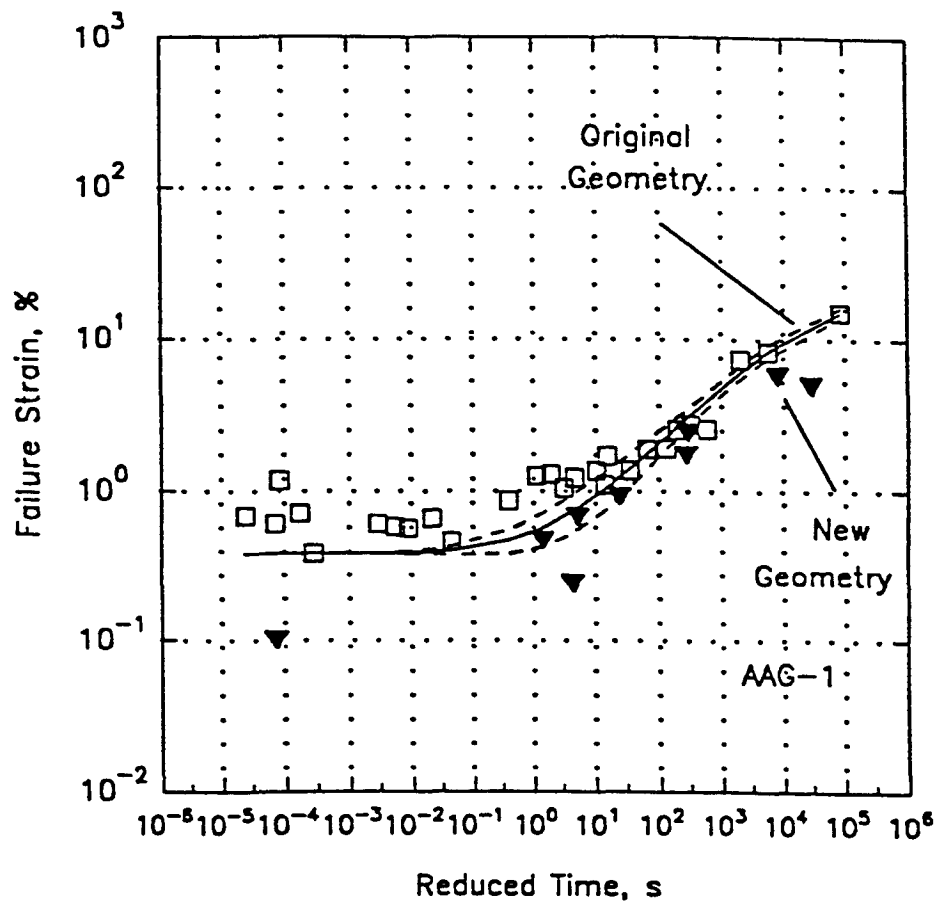
Figure 4.32 Failure Strain Master Curve Comparing Original and Specification-Type Geometry, Asphalt AAG-1

Figure 4.33 **Failure Energy Master Curve Comparing Original and Specification-Type Geometry, Asphalt AAG-1 (Tank)**

Figure 4.34 Nomograph for Estimating the Temperature at Which the Strain to Failure Is 1 Percent with a 540 $\mu\epsilon/s$ Strain Rate
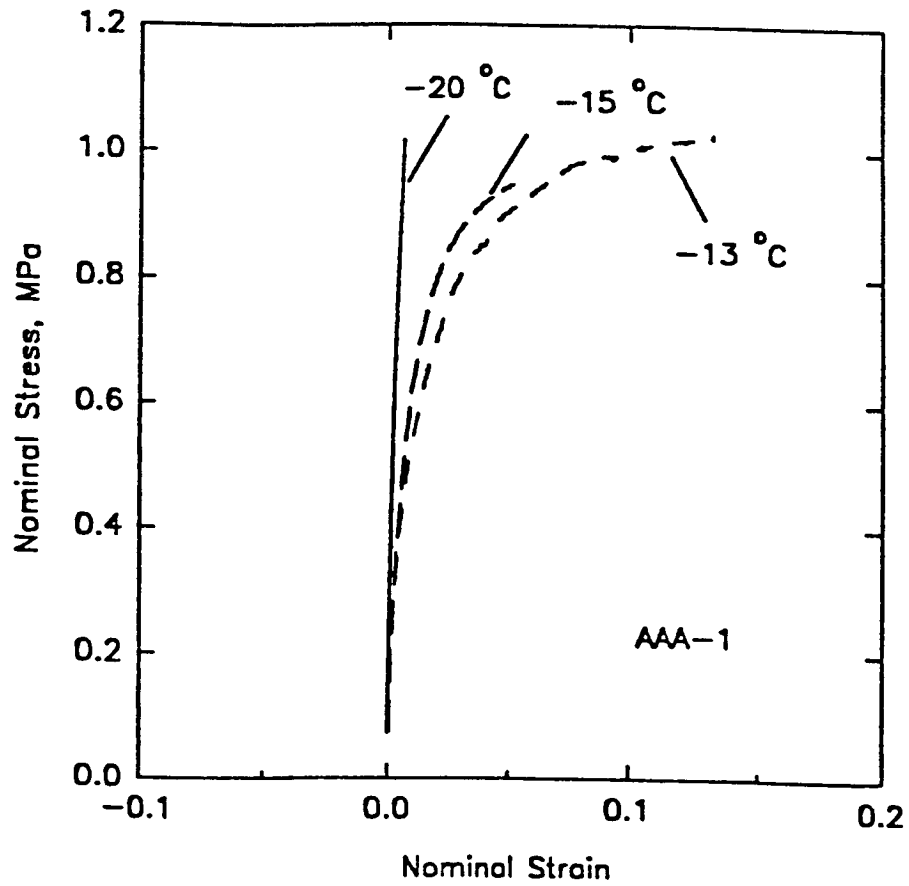
Figure 4.35 Nominal Stress versus Nominal Strain, Asphalt AAA-1 at 0.05 in/min Elongation Rate at Various Temperatures
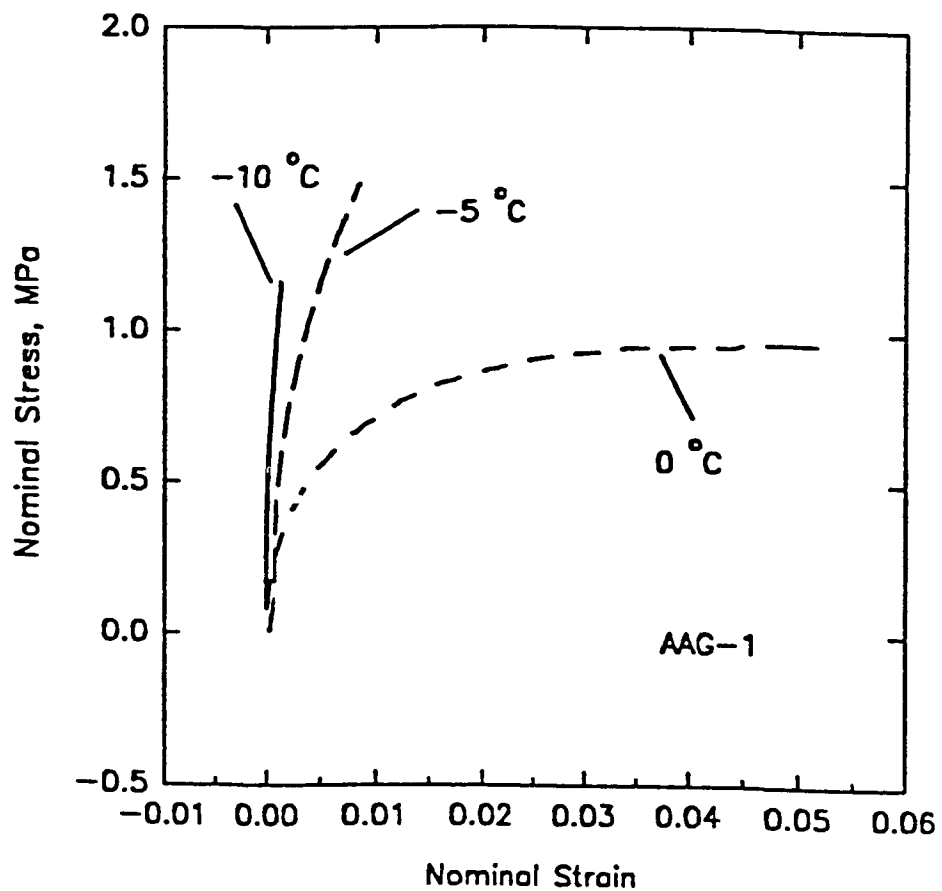
Figure 4.36 Nominal Stress versus Nominal Strain, Asphalt AAG-1 at 0.05 in/min Elongation Rate at Various Temperatures
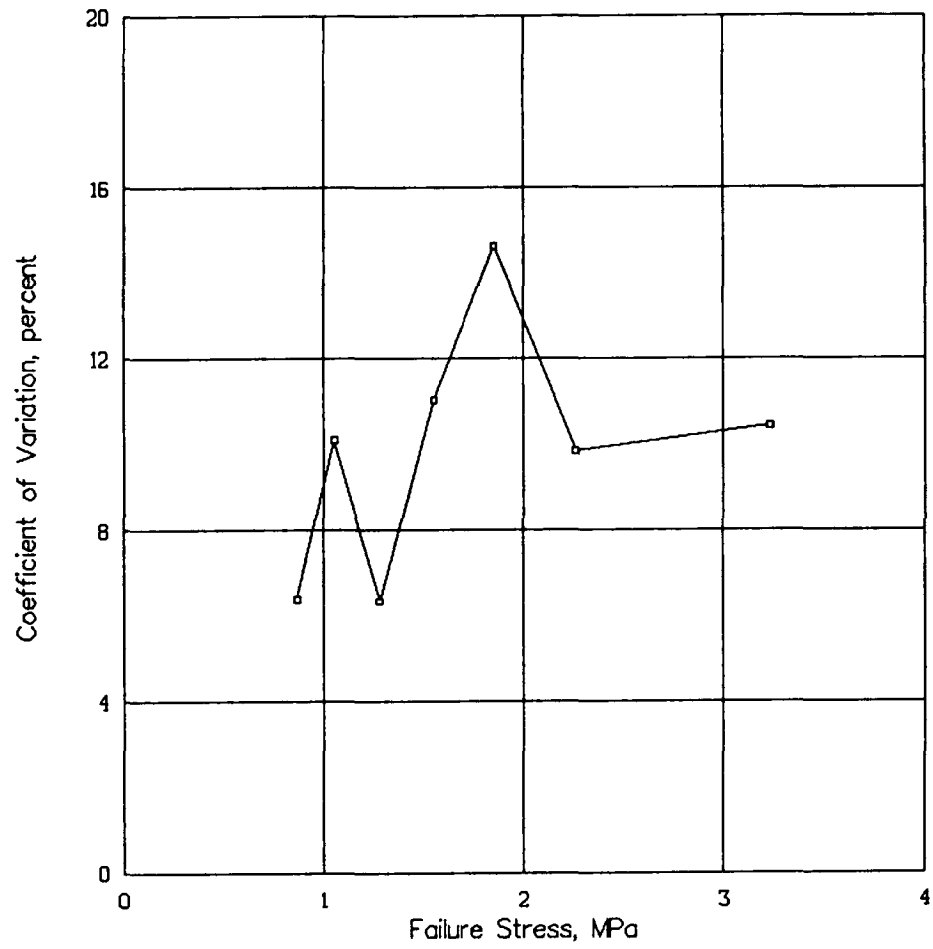
Figure 4.37   Failure Stress versus Coefficient of Variation for Core Asphalts

266
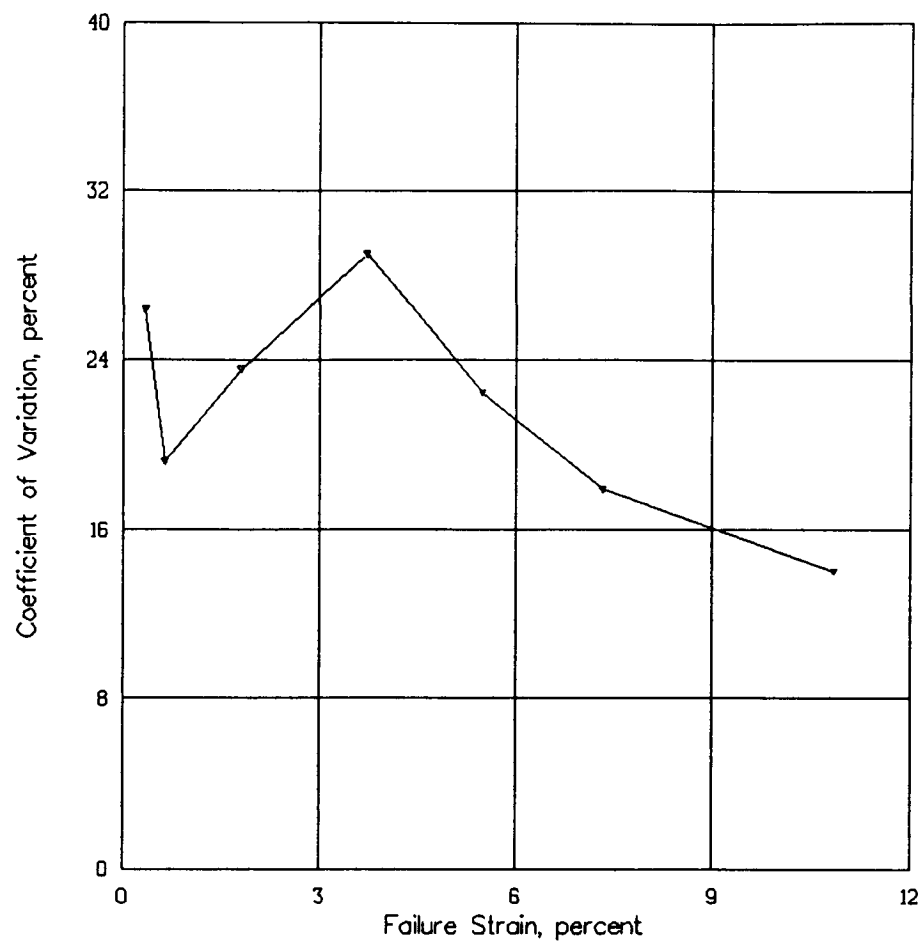
Figure 4.38   Failure Strain versus Coefficient of Variation for Core Asphalts
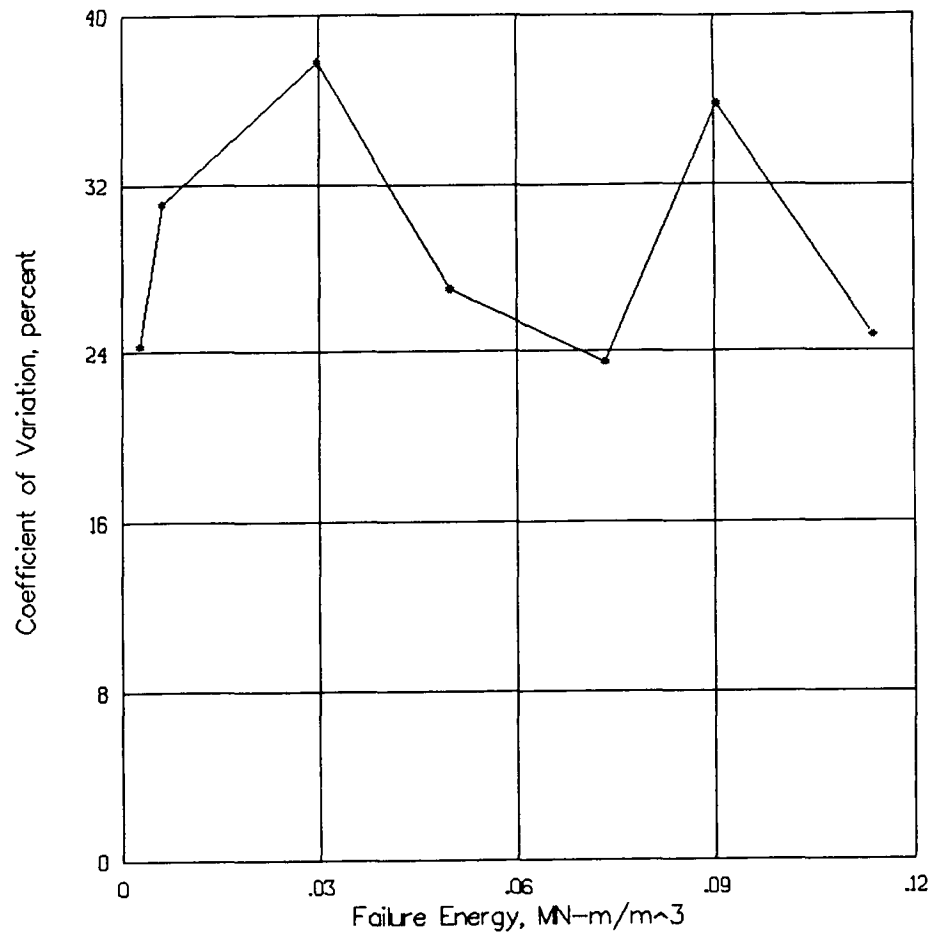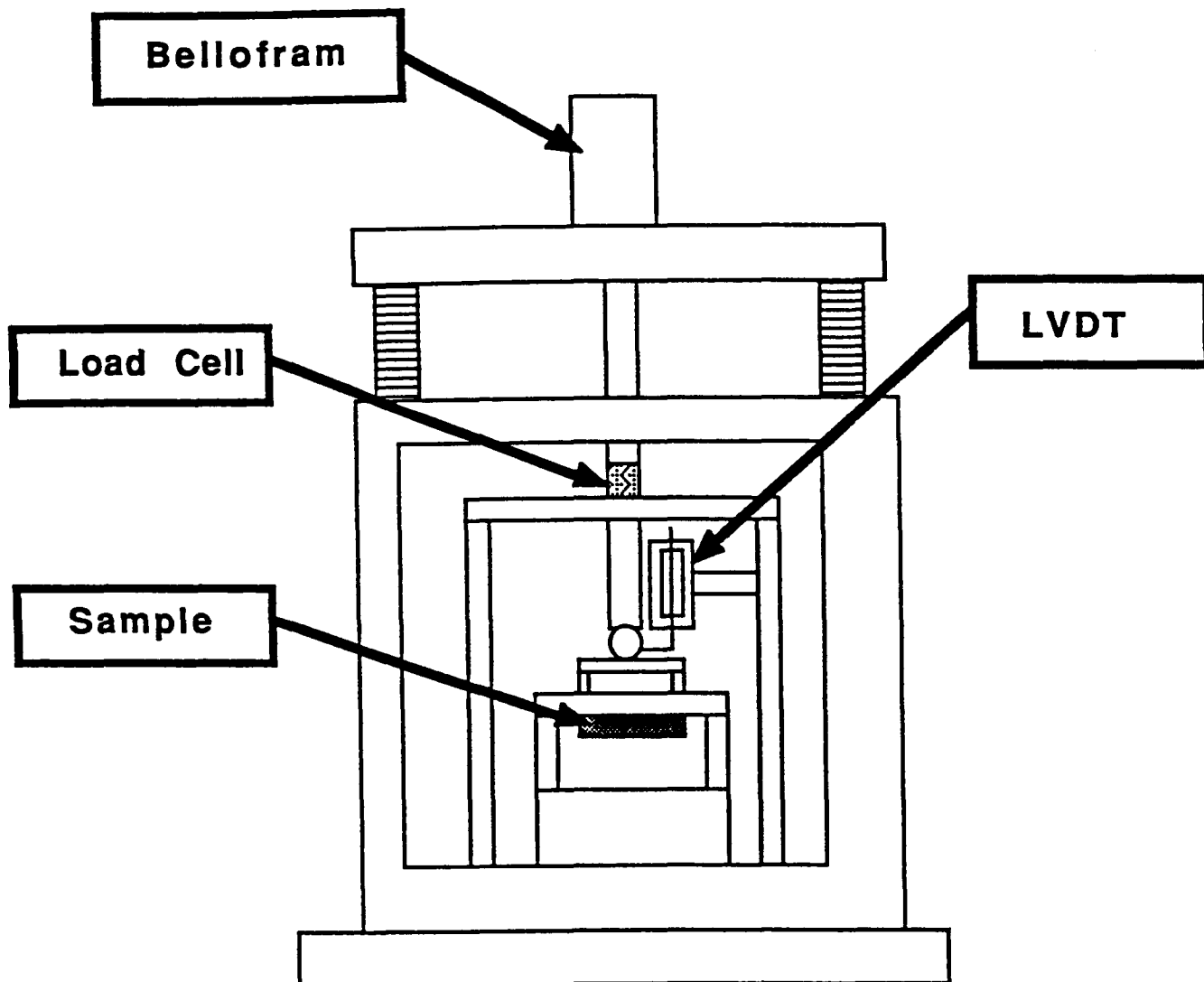
Figure 4.39   Failure Energy versus Coefficient of Variation for Core Asphalts
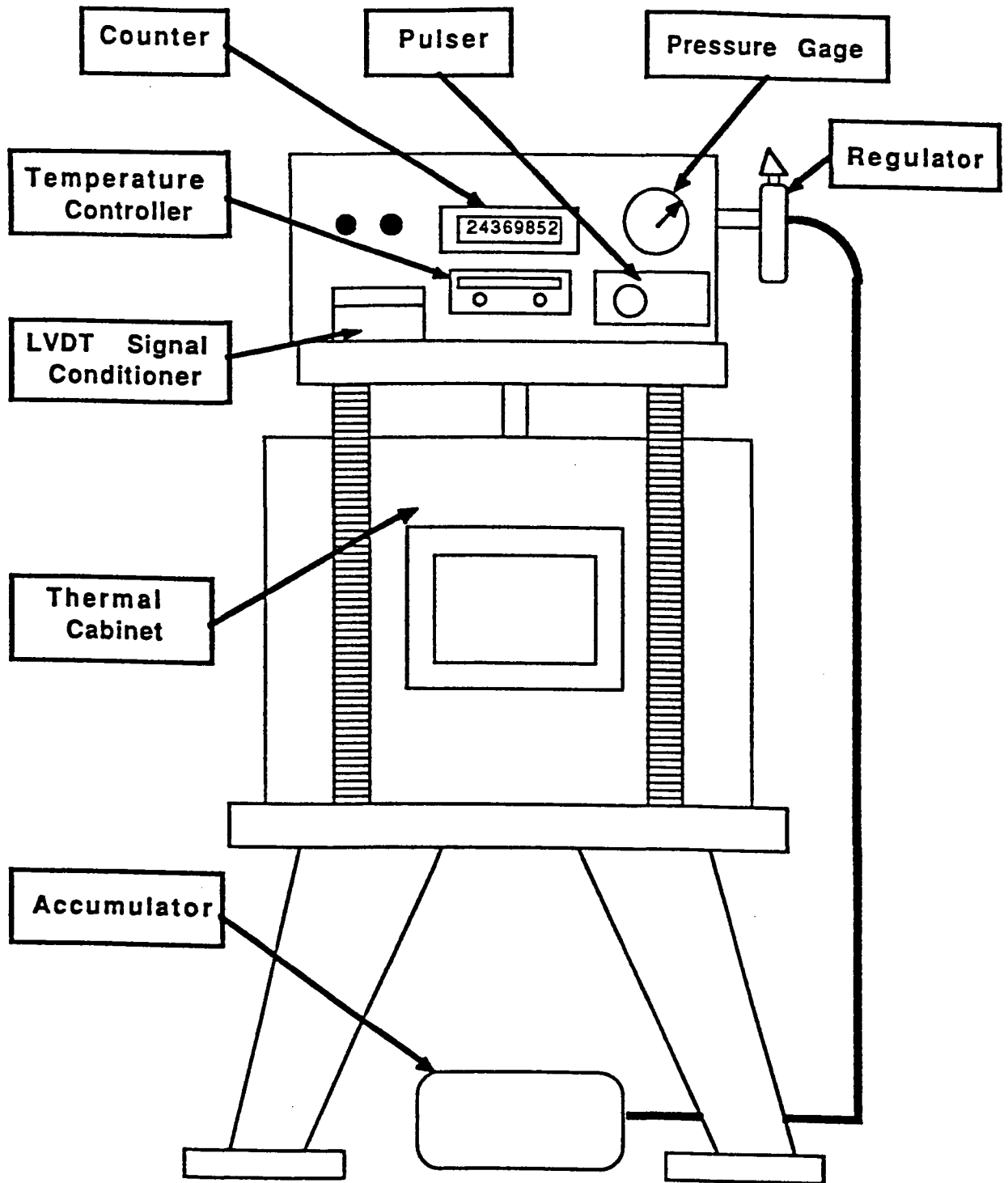
Figure 4.40 Fatigue Testing Apparatus
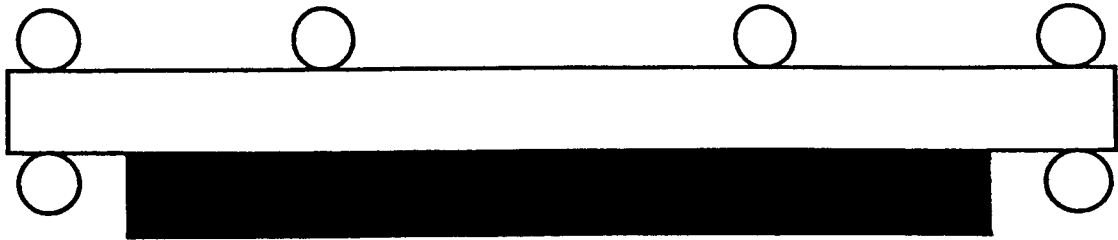
Figure 4.41 Composite Beam Specimen

Figure 4.42   Fatigue Testing Configuration
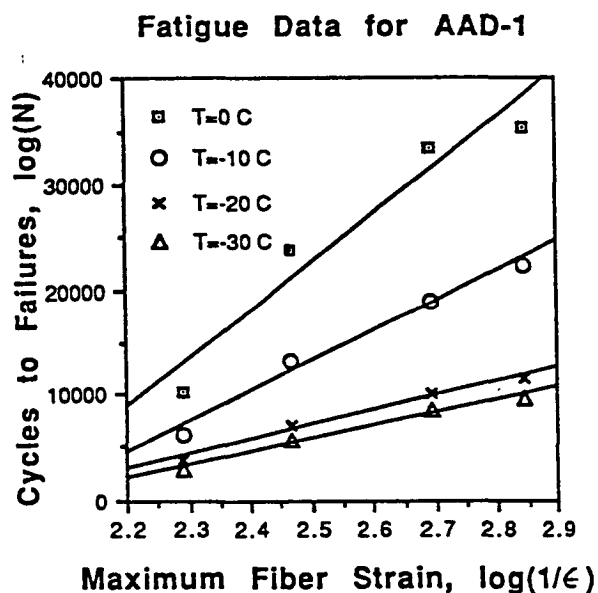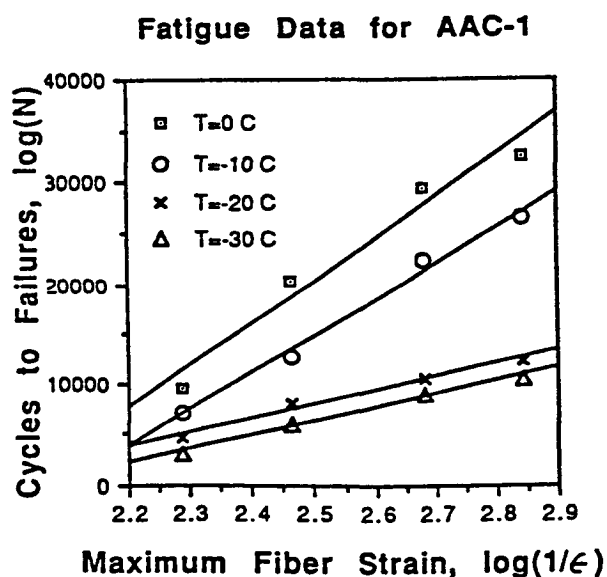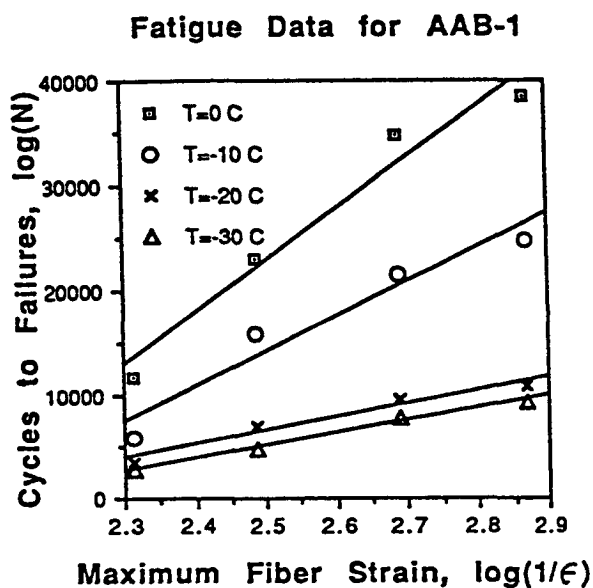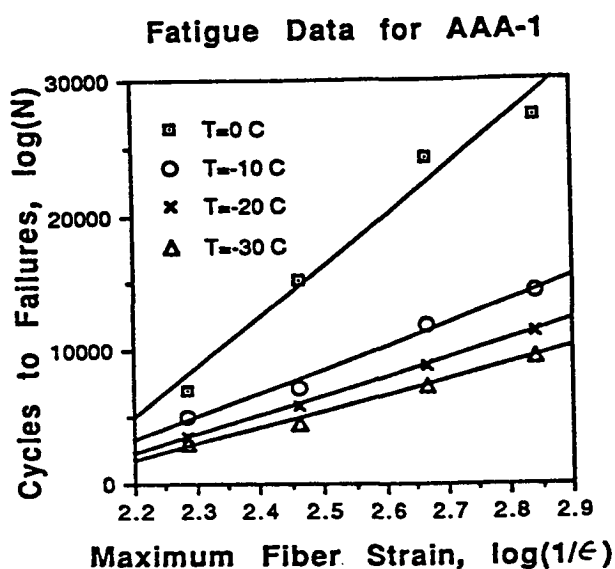
Figure 4.43 Cycles to Failure versus Inverse of Maximum Fiber Strain, Asphalts AAA-1, AAB-1, AAC-1, and AAD-1
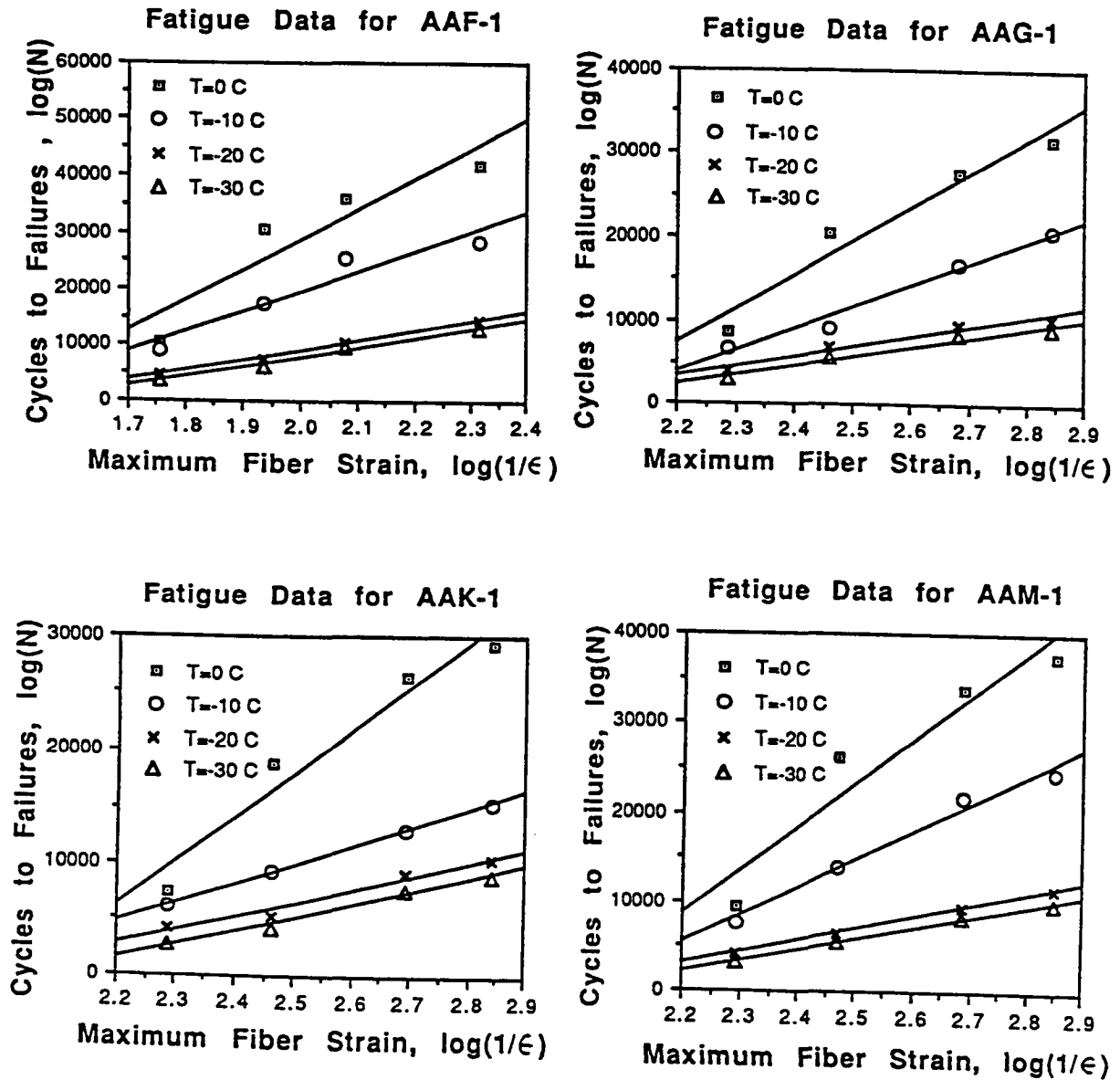
Figure 4.44 Cycles to Failure versus Inverse of Maximum Fiber Strain, Asphalts AAF-1, AAG-1, AAK-1, and AAM-1

Figure 4.45 Cycles to Failure versus Maximum Fiber Strain, Asphalt AAD-1 Aged and Unaged
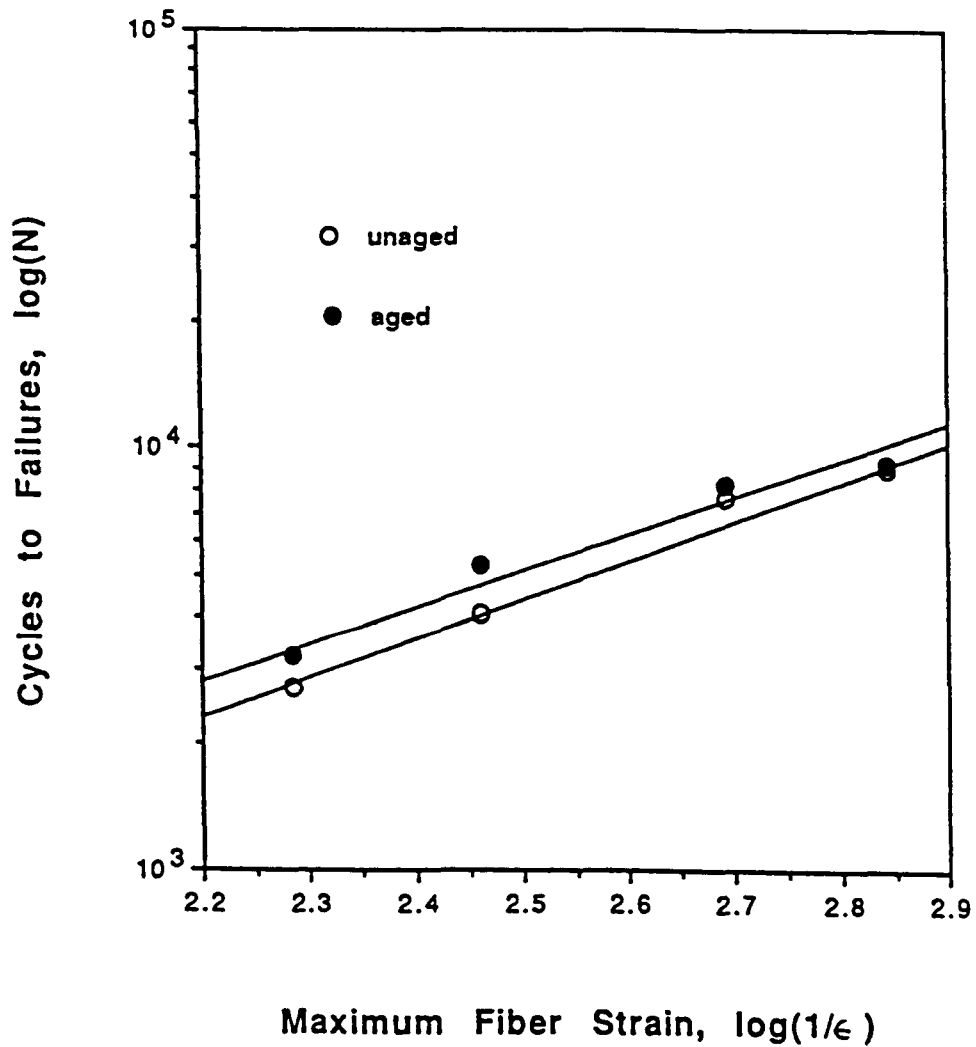
Figure 4.46   Cycles to Failure versus Maximum Fiber Strain, Asphalt AAK-1 Aged and
Unaged

Figure 4.47   Energy Loss versus Number of Cycles to Failure for Asphalt AAG-1

276

Energy Loss from Fatigue Test (AAA-1,Temp=-30 °C)
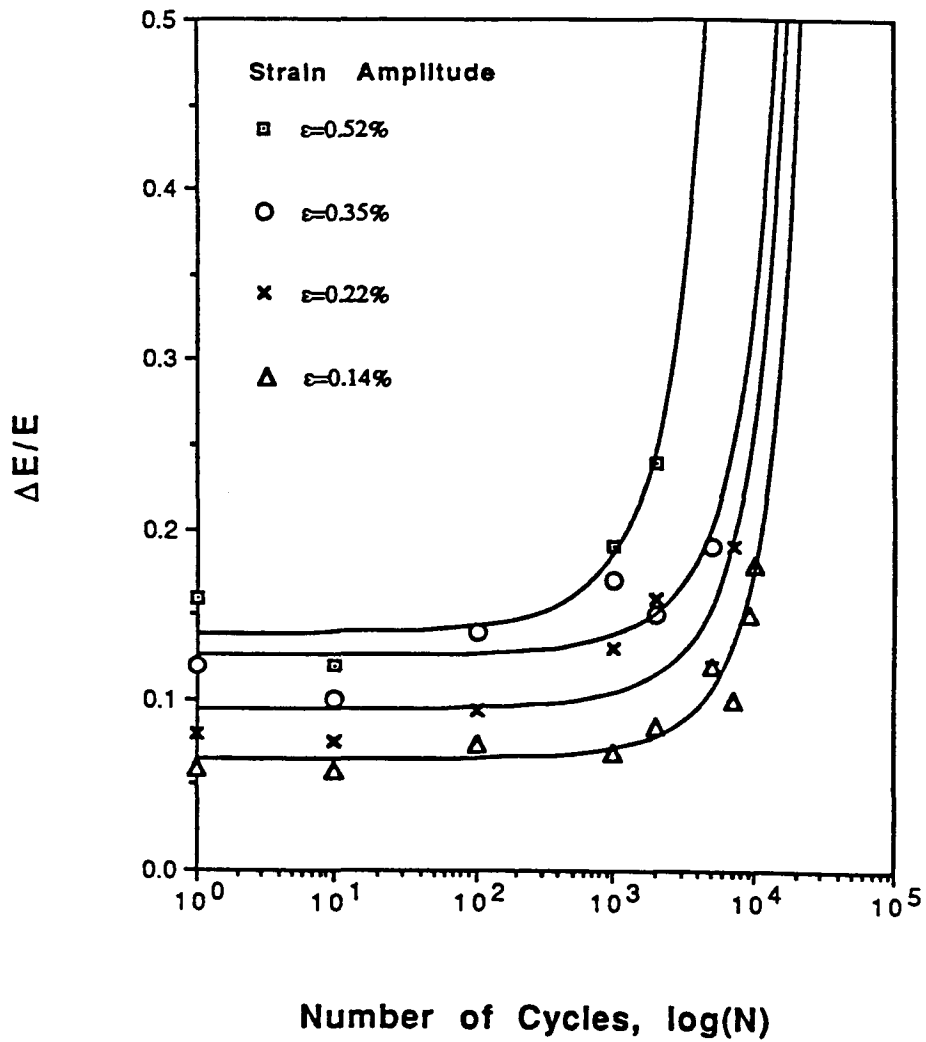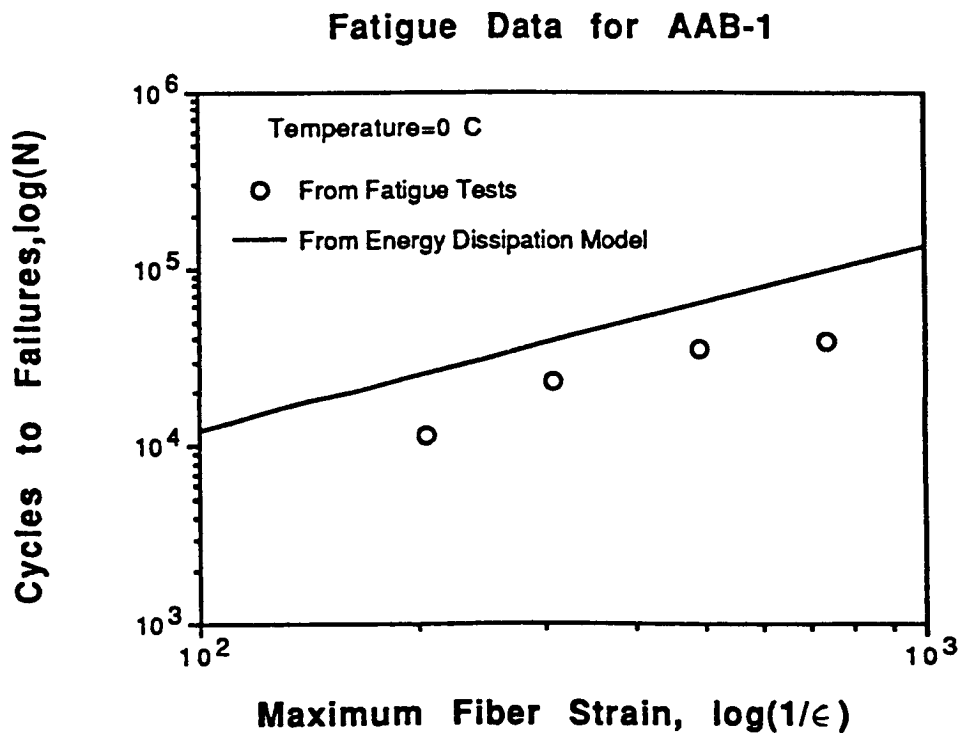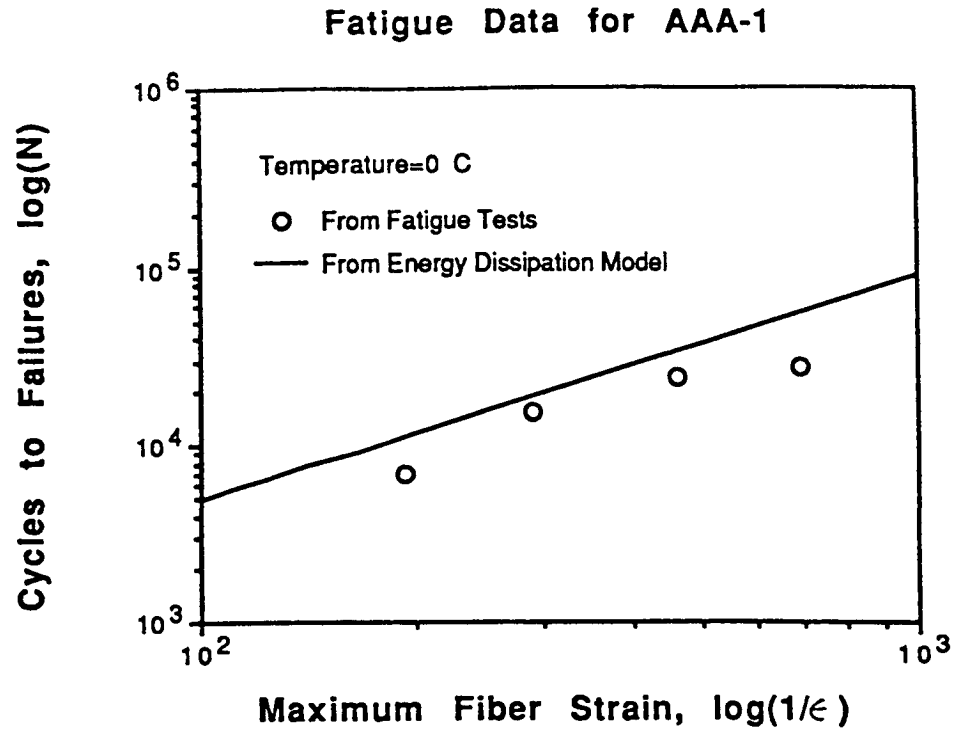
Figure 4.48   Energy Loss versus Number of Cycles at Different Strain Amplitudes

Figure 4.49 Cycles to Failure Predicted from Energy Dissipation Model Compared with Measured Fatigue Data, Asphalts AAA-1 and AAB-1
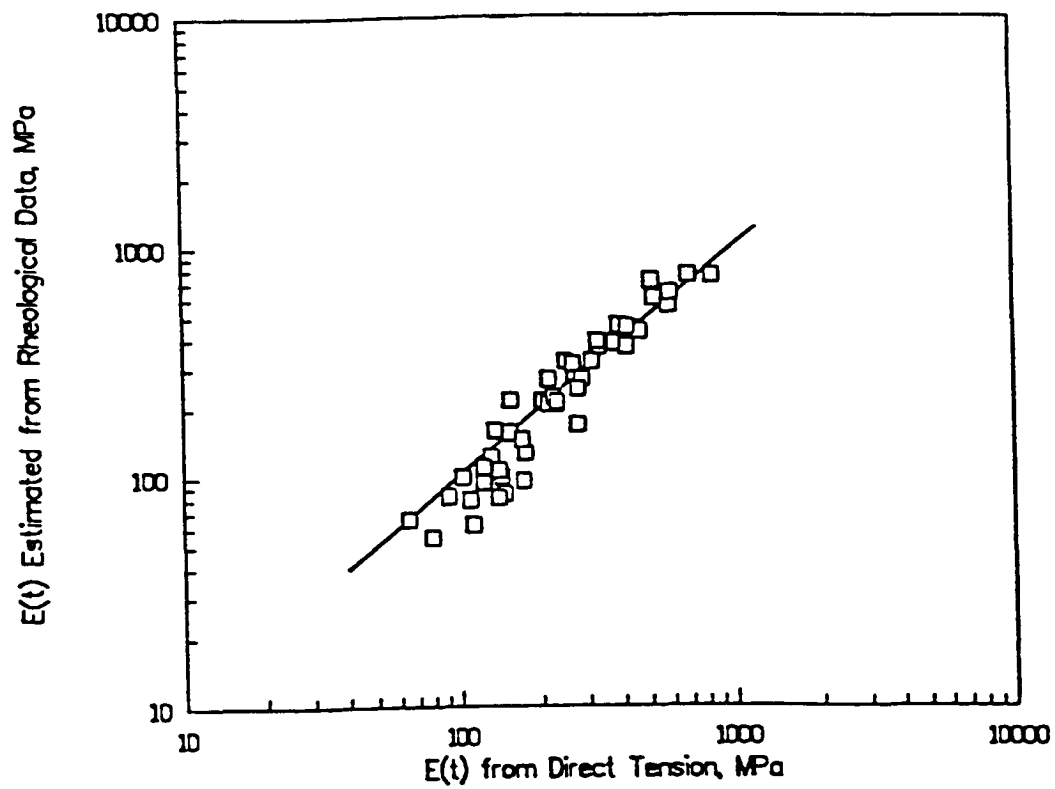
Figure 4.50   Tangent Modulus versus Approximate Relaxation Moduli Computed from Rheological Measurement
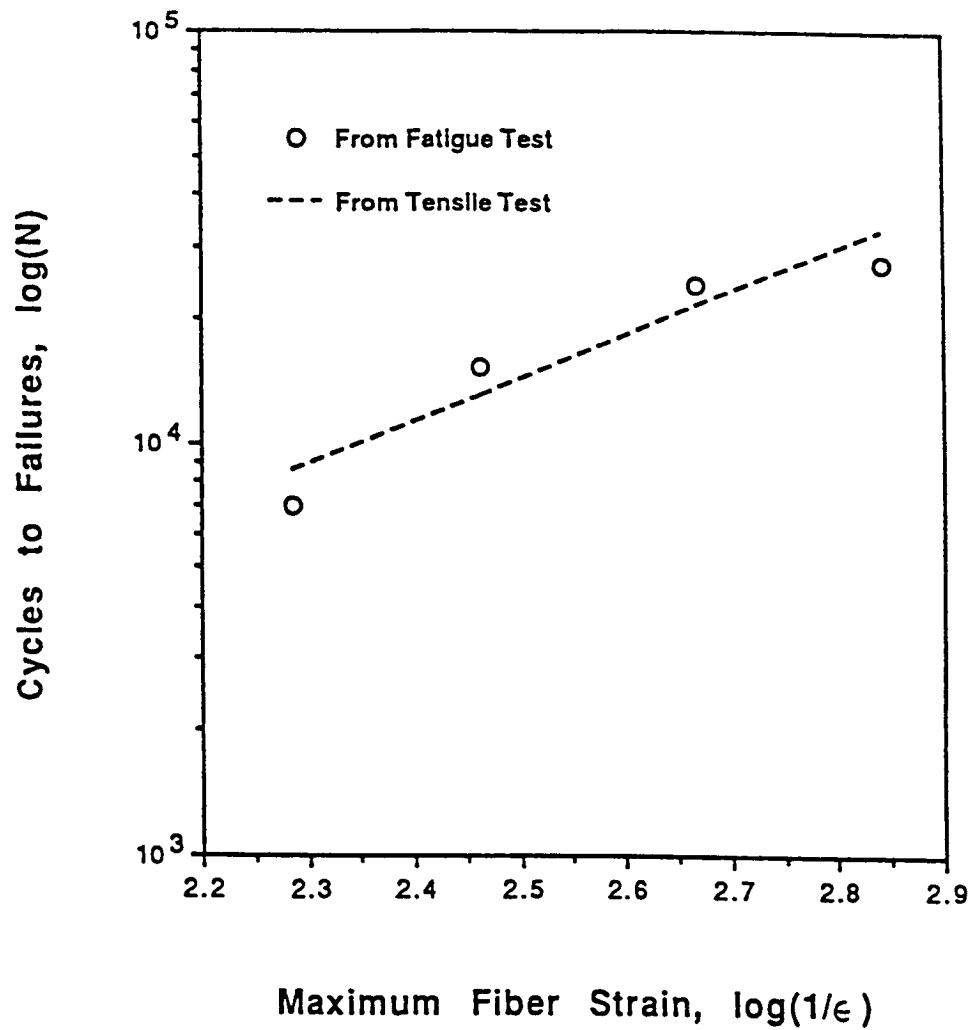
Figure 4.51   Cycles to Failure Predicted from Tensile Test Data Compared with Measured Fatigue Data

Fatigue Data for AAC-1

Temperature=0°C

○ From Fatigue Tests

—— From Energy Dissipation Model

Cycels to Failures, log(N)

Maximum Fiber Strain, log(1/ε)

Fatigue Data for AAD-1

Temperature=0°C

○ From Fatigue Tests

—— From Energy Dissipation Model

Cycles to Failures, log(N)

Maximum Fiber Strain, log(1/ε)
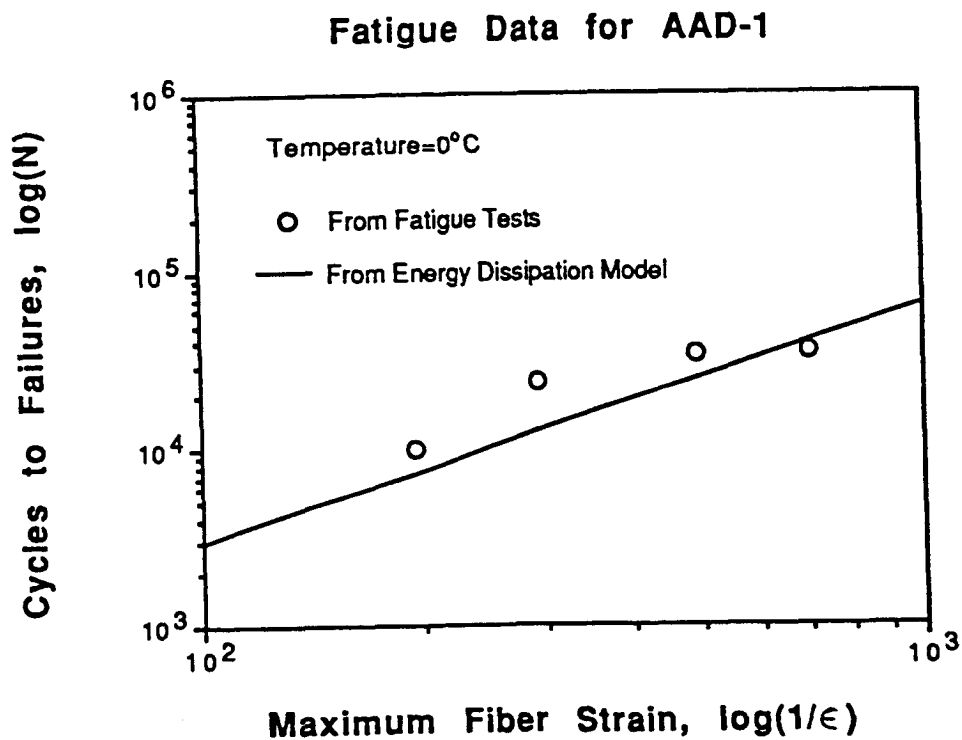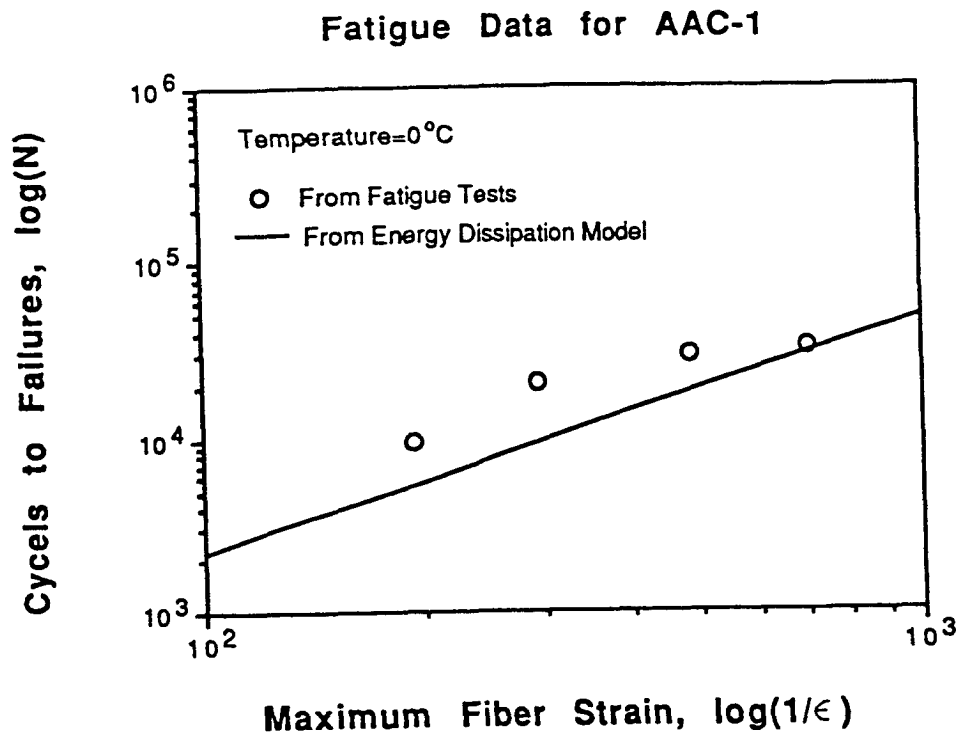
Figure 4.52   Cycles to Failure Predicted from Energy Dissipation Model Compared with Measured Fatigue Data, Asphalts AAC-1 and AAD-1

Fatigue Data for AAF-1

Temperature=0°C

O From Fatigue Tests
— From Energy Dissipation Model

Maximum Fiber Strain, $\log(1/\epsilon)$

Fatigue Data for AAG-1

Temperature=0°C

O From Fatigue Tests
— From Energy Dissipation Model

Maximum Fiber Strain, $\log(1/\epsilon)$
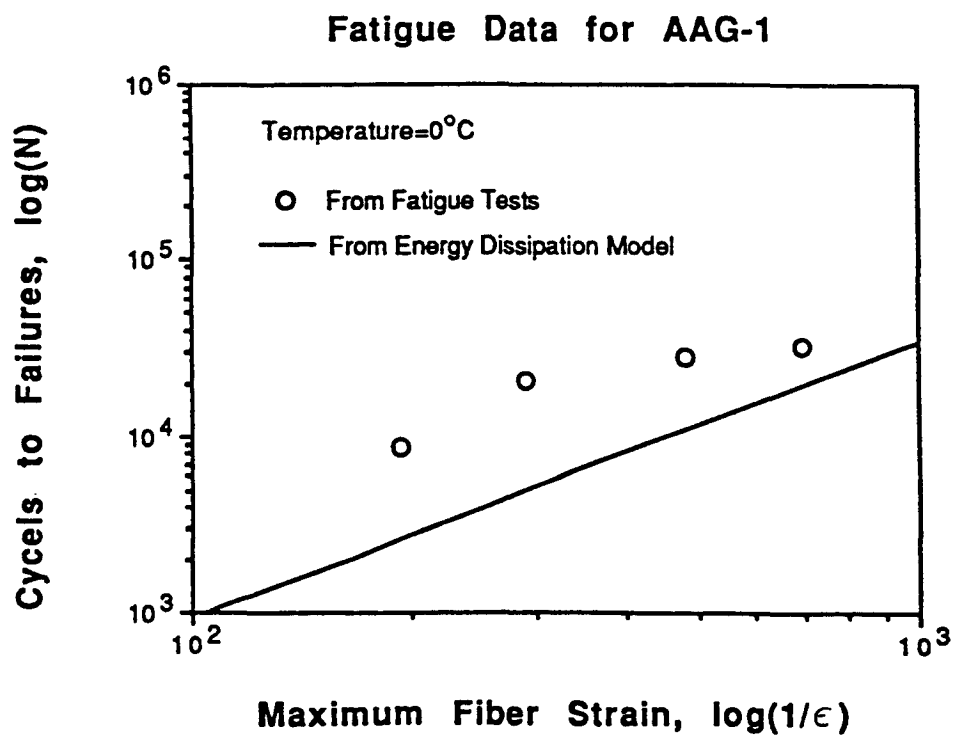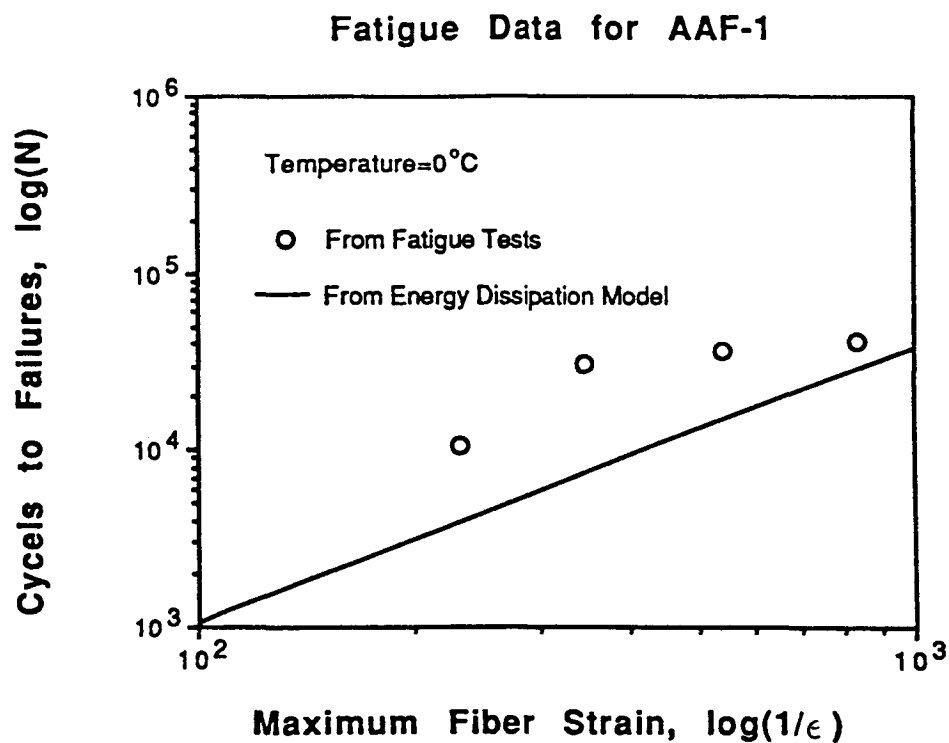
Figure 4.53 Cycles to Failure Predicted from Energy Dissipation Model Compared with Measured Fatigue Data, Asphalt AAF-1 and AAG-1
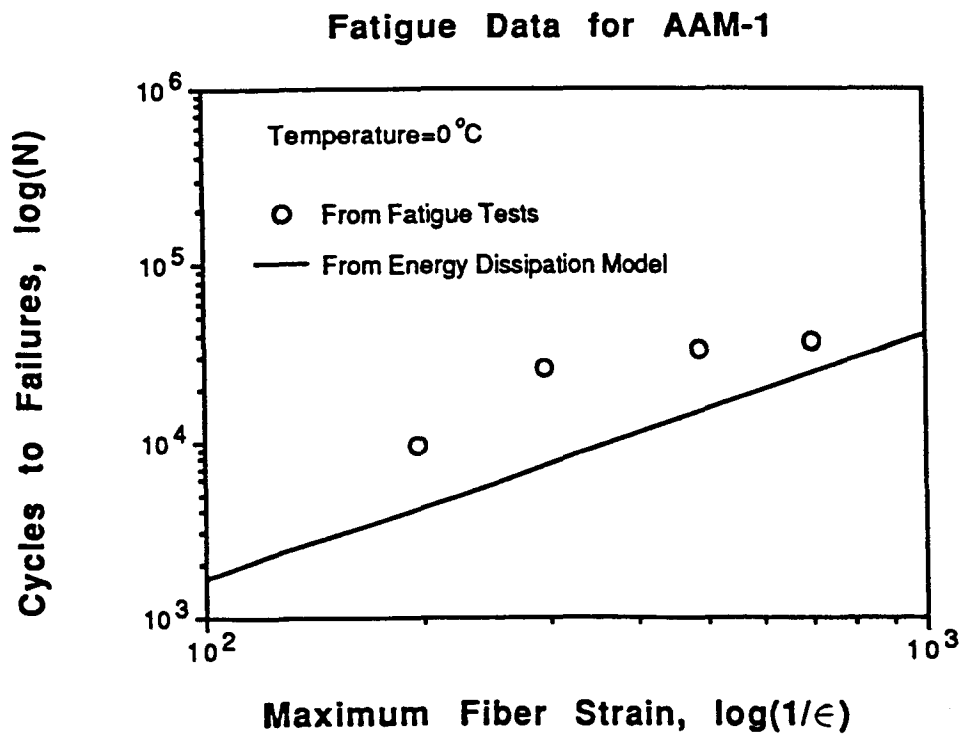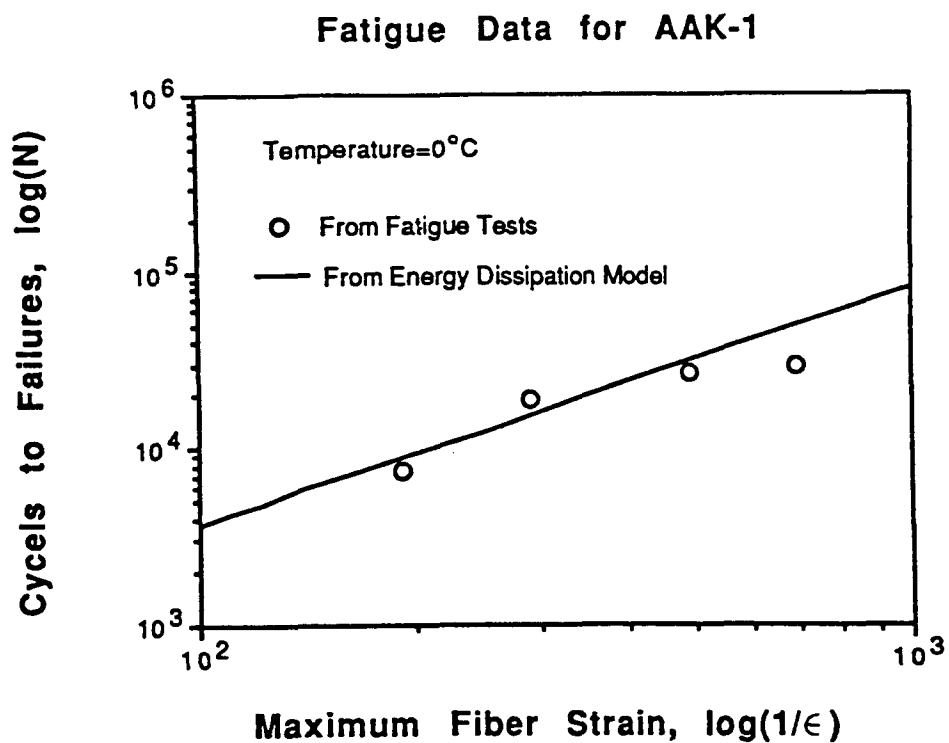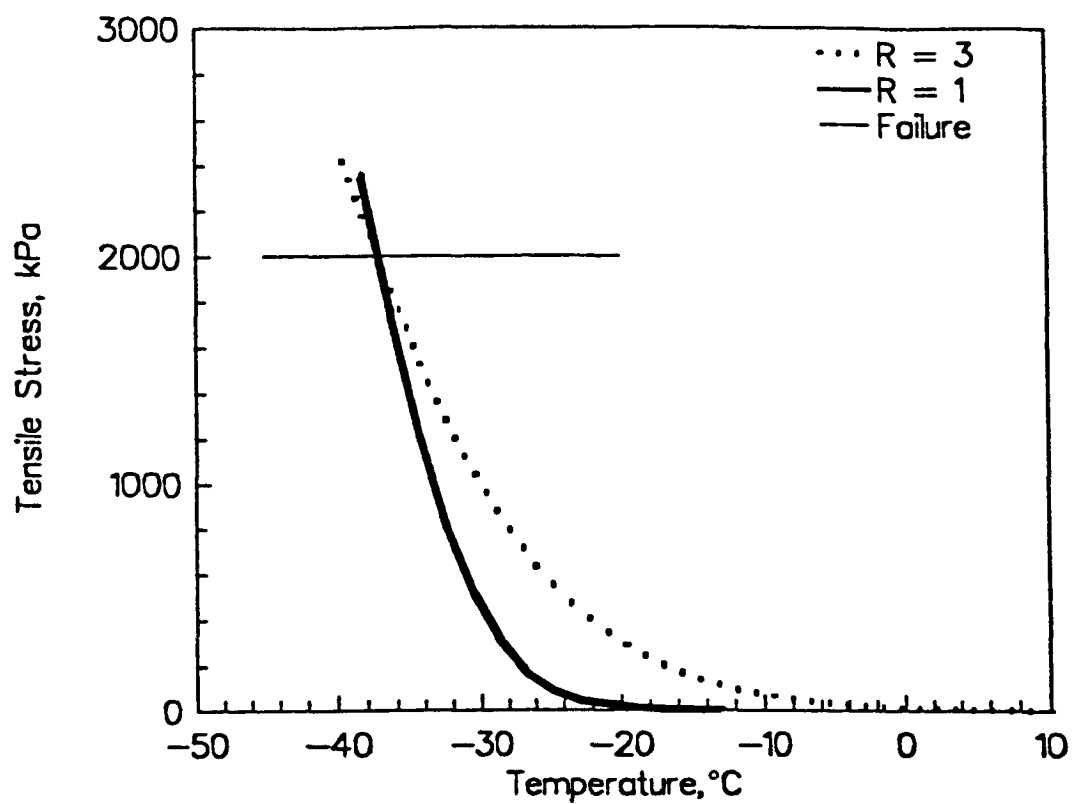
Figure 4.54 Cycles to Failure Predicted from Energy Dissipation Model Compared with Measured Fatigue Data, Asphalts AAK-1 and AAM-1
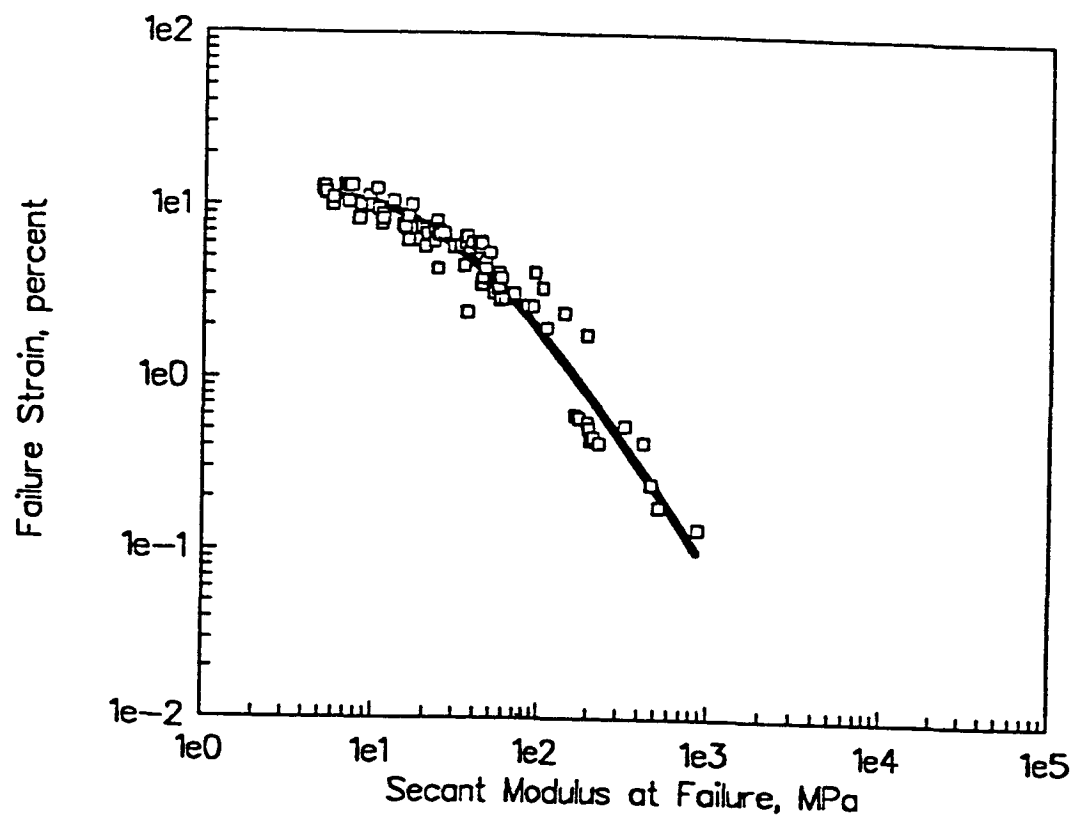
Figure 4.55   Failure Strain as a Function of Secant Modulus, Core Asphalts (Tank)
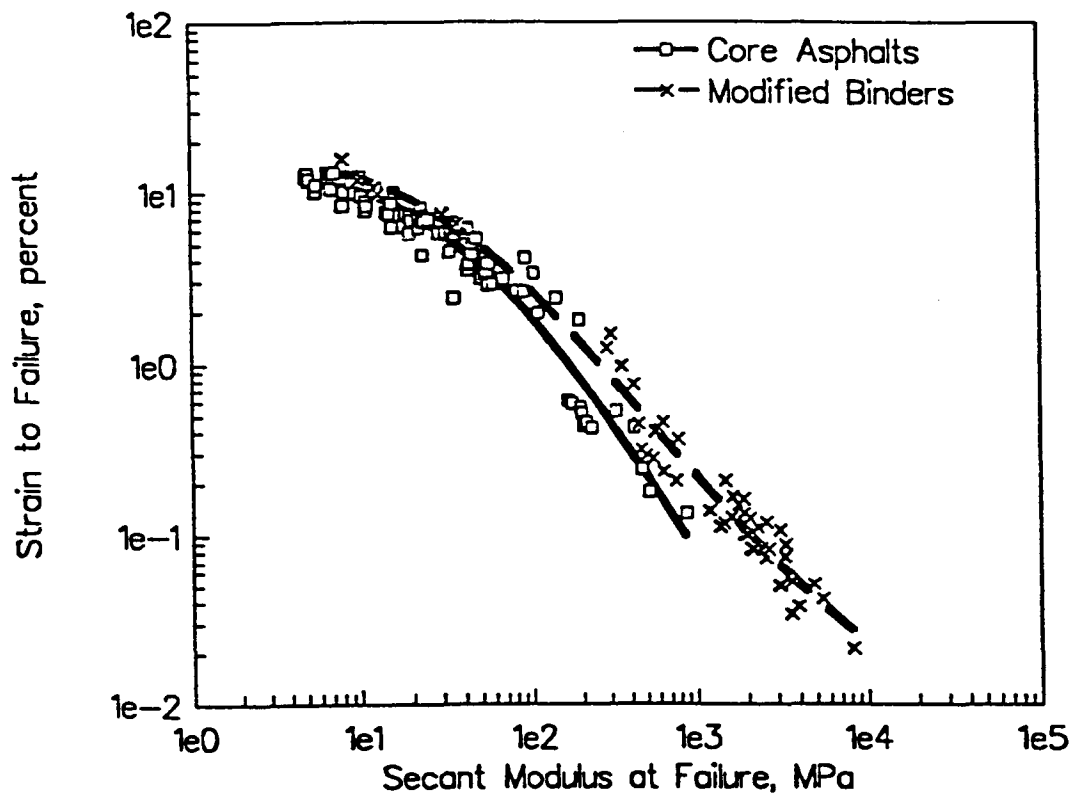
Figure 4.56 **Failure Strain as a Function of Secant Modulus, Core Asphalts, and Four Modified Binders (Tank)**

Figure 4.57 Calculated Stress Developed during 10°C/hr Cooling for Asphalts of Different Rheological Type

Table 4.1   Experimental Layout of Replicate 1 for Unaged Core Asphalts

Temperature Levels, °C	Deformation Rate Levels, in./min				
	0.1	0.3	0.6	1.0	2.0
-30	X	X	X	X	X
-20	X	X	X	X	X
-10	X	X	X	X	X
-5	X	X	X	X	X
0	X	X	X	X	X
+5	X				X

Table 4.2   Experimental Layout of Exploratory Experiment for Statistical Analysis of the Failure Properties of Asphalts AAD-1 and AAG-1

Temperature Levels, °C	Deformation Rate Levels, in./min				
	0.1	0.3	0.6	1.0	2.0
-30	19				18
-20		34		34	
-10					
-5		35		33	
0	19				17

Table 4.3 Estimated Standard Deviation and Coefficient of Variation of Measurements of Failure Data for Asphalt AAD-1

Variable	Temperature °C	Deformation Rate in./min	Sample Size	Sample Mean	Sample Standard Deviation	Coefficient of Variation Percentage
Stress, lb/in.^{2}	-30	0.1	19	164.0	40.0	25
Strain, percent	-30	0.1	19	1.6	0.4	26
Energy, lb-in./in.^{3}	-30	0.1	19	1.5	0.7	45
Stress, lb/in.^{2}	-30	2.0	18	136.0	29.0	21
Strain, percent	-30	2.0	18	1.2	0.3	23
Energy, lb-in./in.^{3}	-30	2.0	18	0.9	0.4	50
Stress, lb/in.^{2}	-20	0.3	34	159.0	30.0	19
Strain, percent	-20	0.3	34	1.8	0.5	25
Energy, lb-in./in.^{3}	-20	0.3	34	1.6	0.7	41
Stress, lb/in.^{2}	-20	1.0	34	185.0	25.0	14
Strain, percent	-20	1.0	34	2.1	0.4	18
Energy, lb-in./in.^{3}	-20	1.0	34	2.0	0.6	29
Stress, lb/in.^{2}	-5	0.3	37	144.0	25.0	17
Strain, percent	-5	0.3	37	27.0	13.0	50
Energy, lb-in./in.^{3}	-5	0.3	37	31.0	16.0	51
Stress, lb/in.^{2}	-5	1.0	33	138.0	16.0	12
Strain, percent	-5	1.0	33	4.5	1.0	22
Energy, lb-in./in.^{3}	-5	1.0	33	3.6	1.0	30
Stress, lb/in.^{2}	0	0.1	19	32.0	5.0	16
Strain, percent	0	0.1	19	30.0	3.5	12
Energy, lb-in./in.^{3}	0	0.1	19	7.3	1.0	14
Stress, lb/in.^{2}	0	2.0	17	154.0	33.0	21
Strain, percent	0	2.0	17	19.0	11.0	57
Energy, lb-in./in.^{3}	0	2.0	17	23.0	16.0	69

Table 4.4 Estimated Standard Deviation and Coefficient of Variation of Measurements of Failure Data for Asphalt AAG-1

Variable	Temperature °C	Deformation Rate in/min	Sample Size	Sample Mean	Sample Standard Deviation	Coefficient of Variation Percentage
Stress, lb/in.^{2}	-30	0.1	22	71.0	20.0	28
Strain, percent	-30	0.1	22	0.8	0.3	41
Energy, lb-in./in.^{3}	-30	0.1	22	0.3	0.2	56
Stress, lb/in.^{2}	-30	2.0	19	73.0	19.0	26
Strain, percent	-30	2.0	19	1.0	0.3	29
Energy, lb-in./in.^{3}	-30	2.0	19	0.3	0.2	50
Stress, lb/in.^{2}	-20	0.3	34	128.0	56.0	44
Strain, percent	-20	0.3	34	0.9	0.3	33
Energy, lb-in./in.^{3}	-20	0.3	34	0.7	0.5	70
Stress, lb/in.^{2}	-20	1.0	34	104.0	19.0	18
Strain, percent	-20	1.0	34	1.0	0.2	23
Energy, lb-in./in.^{3}	-20	1.0	34	0.6	0.2	41
Stress, lb/in.^{2}	-5	0.3	35	169.0	24.0	14
Strain, percent	-5	0.3	35	2.0	0.4	18
Energy, lb-in./in.^{3}	-5	0.3	35	1.9	0.6	29
Stress, lb/in.^{2}	-5	1.0	35	201.0	23.0	11
Strain, percent	-5	1.0	35	2.3	0.4	15
Energy, lb-in./in.^{3}	-5	1.0	35	2.4	0.6	23
Stress, lb/in.^{2}	0	0.1	22	158.0	19.0	12
Strain, percent	0	0.1	22	4.7	2.5	52
Energy, lb-in./in.^{3}	0	0.1	22	4.7	3.2	68
Stress, lb/in.^{2}	0	2.0	20	194.0	29.0	15
Strain, percent	0	2.0	20	2.7	0.5	19
Energy, lb-in./in.^{3}	0	2.0	20	2.7	0.9	32

Table 4.5 **Example Failure Stress Frequency Distribution Data for Asphalt AAD-1 in Unaged (Tank) Condition Tested at 23°F Using a Deformation Rate of 0.3 in./min (7.62 mm/min)**

Specimen Number	Failure Stress MPa	Specimen Number	Failure Stress MPa
1	0.8	20	0.9
2	1.0	21	1.1
3	1.1	22	1.1
4	1.1	23	1.1
5	0.9	24	1.0
6	1.4	25	1.1
7	0.8	26	1.0
8	1.0	27	0.8
9	1.3	28	1.1
10	0.8	29	1.0
11	0.9	30	1.2
12	1.3	31	0.9
13	0.8	32	1.2
14	0.8	33	1.2
15	1.0	34	0.7
16	0.8	35	0.9
17	0.8	36	1.0
18	0.9	37	1.1
19	0.8		

Table 4.6   Reduced Experimental Layout of Replicate 1 for Unaged Extended Set Asphalts

Temperature Levels, °C	Deformation Rate Levels, in./min				
	0.1	0.3	0.6	1.0	2.0
-30	X				
-20					
-10		X			
-5		X		X	
0			X		
+5					X

Table 4.7 **Failure Strain (%) Master Curve Parameters for All SHRP Asphalts in Unaged (Tank) Condition at Reference Temperature of −10°C (14°F)**

Asphalt	A	B1	95% Confidence Intervals for B1		B3	95% Confidence Intervals for B3	
AAA-1	5895	267518	246834	288203	5.55	5.45	5.66
AAB-1	3909	184091	170302	197881	6.86	6.66	7.05
AAC-1	3316	145480	132380	158580	7.58	7.33	7.83
AAD-1	8136	193744	169612	217876	5.88	5.68	6.07
AAE-1	2558	286824	237181	335777	6.83	6.47	7.20
AAF-1	2041	103422	94459	112385	9.41	9.08	9.75
AAG-1	910	76532	69637	83427	8.50	8.29	8.72
AAH-1	6233	137896	99285	175817	6.62	6.02	7.25
AAJ-1	2441	201328	178575	224770	7.45	7.17	7.73
AAK-1	2848	247523	222702	272345	6.80	6.57	7.04
AAL-1	7308	191675	126864	256487	5.37	4.96	5.80
AAM-1	4468	217876	194433	241318	8.02	7.68	8.37
AAN-1	1441	245455	195812	294408	6.99	6.52	7.48
AAO-1	6164	282687	186160	379214	6.05	5.61	6.52
AAP-1	6964	224770	196502	252350	6.91	6.68	7.14
AAQ-1	1455	167544	99975	234423	7.43	6.41	8.52
AAR-1	2220	208223	178575	237871	7.80	7.41	8.19
AAS-1	4378	211670	172370	250971	7.97	7.46	8.50
AAT-1	1420	301303	276481	325435	12.10	11.80	12.50
AAU-1	2130	172370	157201	188228	8.38	7.98	8.79
AAV-1	2103	155822	86874	224081	5.93	5.30	6.59
AAW-1	945	222013	155822	287513	9.18	7.62	10.90
AAX-1	800	268897	230286	306819	10.90	10.40	11.40
AAY-1	2206	268897	213739	324056	6.67	6.32	7.03
AAZ-1	1386	315782	273034	358530	12.50	11.50	13.70
ABA-1	8067	189607	122727	256487	6.59	6.02	7.18
ABC-1	5412	289582	177196	401967	6.04	5.49	6.62
ABD-1	1117	25097	20822	29441	6.29	5.71	6.91

292

Table 4.10   Failure Properties of Unaged (Tank) Core Set Asphalts Obtained Using the Specification Testing Method

Tank Asphalts	Temp °C	Failure Stress MPa	Failure Strain percent	Failure Energy MPa	Tangent Modulus MPa
AAA-1	-20	1.02 (5)	0.55 (12)	0.004 (8)	268 (10)
	-15	0.97 (4)	6.85 (30)	0.057 (35)	123 (12)
	-13	0.97 (6)	11.55 (20)	0.097 (21)	112 (4)
AAB-1	-20	1.57 (6)	0.42 (11)	0.004 (10)	435 (21)
	-15	1.90 (7)	5.26 (37)	0.082 (35)	202 (7)
	-10	1.43 (8)	8.93 (22)	0.108 (22)	146 (12)
AAC-1	-20	1.95 (16)	0.41 (22)	0.004 (21)	513 (14)
	-15	3.54 (4)	2.93 (30)	0.074 (27)	376 (11)
	-10	2.46 (9)	4.56 (29)	0.089 (28)	275 (9)
AAD-1	-20	0.97 (5)	0.46 (8)	0.003 (6)	248 (7)
	-17	N/A	N/A	N/A	N/A
	-15	1.19 (6)	10.31 (13)	0.108 (13)	131 (13)
AAF-1	-17	1.99 (2)	0.25 (23)	0.003 (3)	838 (22)
	-10	2.26 (4)	2.30 (14)	0.036 (15)	266 (12)
	-5	1.36 (3)	5.64 (7)	0.064 (7)	175 (5)
AAG-1	-10	1.14 (11)	0.24 (15)	0.002 (16)	523 (36)
	-5	1.91 (14)	1.74 (32)	0.024 (24)	286 (6)
	0	0.84 (13)	5.77 (16)	0.042 (16)	139 (15)
AAK-1	-20	1.48 (10)	0.27 (19)	0.002 (12)	588 (7)
	-15	2.22 (4)	4.95 (30)	0.086 (30)	215 (13)
	-10	1.30 (6)	12.66 (3)	0.145 (2)	143 (5)
AAM-1	-20	3.23 (11)	0.62 (30)	0.011 (17)	595 (25)
	-10	2.48 (7)	5.07 (28)	0.101 (27)	231 (13)
	-5	2.00 (6)	7.34 (12)	0.120 (11)	172 (8)

Table 4.11   Failure Properties of TFOT-Aged Core Set Asphalts Obtained Using the Specification Testing Method

TFOT Asphalts	Temperature °C	Failure Stress MPa	Failure Strain percent	Failure Energy MPa	Tangent Modulus MPa
AAA-1	-20	1.12 (3)	0.38 (8)	0.002 (9)	330 (12)
	-13	1.25 (16)	8.74 (13)	0.098 (24)	140 (20)
	-10	0.70 (4)	10.68 (19)	0.065 (17)	79 (14)
AAB-1	-15	2.55 (9)	1.93 (21)	0.033 (19)	311 (7)
	-10	1.49 (24)	7.23 (39)	0.090 (18)	153 (11)
	-5	0.62 (2)	11.40 (7)	0.062 (17)	65 (17)
AAC-1	-15	3.54 (25)	2.11 (38)	0.050 (18)	391 (6)
	-10	2.44 (15)	4.07 (31)	0.077 (20)	276 (14)
	-5	1.13 (4)	6.88 (28)	0.065 (20)	122 (11)
AAD-1	-15	0.97 (29)	0.78 (20)	0.005 (19)	213 (6)
	-13	0.80 (2)	0.77 (5)	0.004 (6)	170 (16)
	-10	0.93 (1)	10.51 (1)	0.085 (6)	109 (11)
AAF-1	-10	1.71 (12)	0.45 (18)	0.005 (9)	459 (16)
	-5	1.86 (3)	2.36 (11)	0.031 (12)	223 (14)
	0	0.96 (1)	10.04 (5)	0.085 (8)	122 (11)
AAG-1	-10	2.07 (7)	0.32 (22)	0.004 (12)	692 (15)
	-5	2.68 (5)	2.09 (24)	0.040 (29)	327 (5)
	0	0.93 (2)	5.23 (9)	0.042 (13)	135 (6)
AAK-1	-15	1.30 (22)	0.34 (20)	0.003 (18)	416 (26)
	-10	1.54 (2)	3.48 (9)	0.045 (12)	155 (25)
	-5	0.94 (1)	13.21 (13)	0.109 (14)	91 (16)
AAM-1	-15	4.16 (16)	1.67 (25)	0.043 (4)	414 (21)
	-10	3.08 (4)	5.23 (31)	0.122 (31)	231 (15)
	-5	1.67 (3)	7.16 (17)	0.097 (22)	123 (19)

296

Table 4.12   Failure Properties of PAV-Aged Core Set Asphalts Obtained Using the Specification Testing Method

PAV Asphalts	Temperature °C	Failure Stress MPa	Failure Strain percent	Failure Energy MPa	Tangent Modulus MPa
AAA-1	-15	1.18 (3)	0.67 (8)	0.005 (9)	189 (29)
	-13	1.14 (16)	0.84 (13)	0.005 (24)	263 (4)
	-10	1.35 (4)	9.90 (19)	0.111 (17)	119 (9)
AAB-1	-15	1.44 (9)	0.36 (21)	0.003 (27)	440 (10)
	-10	1.93 (24)	2.26 (39)	0.033 (20)	219 (11)
	-5	1.41 (2)	7.00 (7)	0.081 (11)	119 (17)
AAC-1	-15	2.28 (25)	0.55 (38)	0.008 (20)	527 (7)
	-10	2.60 (15)	3.69 (31)	0.073 (21)	227 (28)
	-5	1.62 (4)	7.13 (28)	0.095 (34)	136 (12)
AAD-1	-15	1.71 (29)	1.43 (20)	0.017 (10)	187 (17)
	-10	1.85 (2)	3.54 (5)	0.046 (7)	165 (18)
	-5	1.21 (1)	7.62 (1)	0.075 (2)	111 (12)
AAF-1	-5	1.72 (12)	0.96 (18)	0.010 (35)	268 (10)
	0	1.57 (3)	3.33 (11)	0.037 (16)	156 (10)
	5	1.24 (1)	5.35 (5)	0.052 (6)	125 (6)
AAG-1	-5	2.55 (7)	0.72 (22)	0.011 (25)	505 (16)
	0	2.06 (5)	4.76 (24)	0.077 (28)	198 (9)
	5	0.98 (2)	7.33 (9)	0.062 910)	121 (13)
AAK-1	-10	0.99 (22)	0.42 (20)	0.003 (20)	296 (15)
	-5	1.71 (2)	6.74 (9)	0.090 (12)	150 (2)
	0	1.06 (1)	10.06 (13)	0.090 (15)	110 (13)
AAM-1	-15	3.84 (16)	1.44 (25)	0.034 (21)	448 (4)
	-10	3.80 (4)	4.48 (31)	0.128 (20)	270 (17)
	-5	2.34 (3)	5.62 (17)	0.102 (21)	175 (12)

Table 4.13 Coefficient of Variation for Failure Data Obtained Using the New Specification Type Specimen Geometry

Group Number	Mean Failure Stress MPa	Coefficient of Variation percent	Mean Failure Strain percent	Coefficient of Variation percent	Mean Failure Energy MN-m/m^3	Coefficient of Variation percent
1	0.87	6	0.34	26	0.003	24
2	1.05	10	0.64	19	0.006	31
3	1.28	6	1.79	24	0.030	38
4	1.55	11	3.72	29	0.050	27
5	1.85	15	5.49	22	0.073	24
6	2.26	10	7.33	18	0.090	36
7	3.23	10	10.84	14	0.114	25
Average[1]		10		22		31

[1] Note : Only groups with failure strains between 0.5 percent and 10 percent (i. e. groups 2 - 6) are averaged

Table 4.14 Fatigue Coefficients K_1 and K_2 for All Unaged Core Asphalts

Asphalt	Load lbs	Fiber Strain (10^{-5})	Number of Cycles to Failure	Fatigue Parameters K_1	K_2
AAA-1	25	144	9612		
	43	215	7324	23.1	0.93
	60	345	4517		
	90	518	2986		
AAB-1	25	135	9413		
	43	204	7932	18.7	0.96
	60	325	4816		
	90	488	2814		
AAC-1	25	143	10413		
	43	208	8794	26.2	0.93
	60	344	5921		
	90	516	3096		
AAD-1	25	142	9653		
	43	204	8432	37.4	0.86
	60	342	5803		
	90	513	2976		
AAF-1	25	120	12935		
	43	184	9847	16.2	1.01
	60	288	6329		
	90	432	3547		
AAG-1	25	144	9125		
	43	208	8276	31.9	0.88
	60	345	5563		
	90	517	2912		
AAK-1	25	144	8947		
	43	204	7635	16.8	0.97
	60	345	4092		
	90	518	2714		
AAM-1	25	142	9846		
	43	206	8312	32.3	0.89
	60	341	5603		
	90	511	3127		

References

Abdulshafi, A., and Majidzadeh, K. 1985. "J-Integral and Cyclic Plasticity Approach to Fatigue and Fracture of Asphaltic Mixtures," *Transportation Research Record 1034*. Washington, D.C.: TRB, National Research Council, pp. 112–123.

Anderson, D.I., and Wiley, M.L. 1976. "Force Ductility: An Asphalt Performance Indication," *Proceedings of the Association of Asphalt Paving Technologists*, vol. 45, pp. 25–38.

Antle, C.E., and Dumonceaux, R. 1973. "Discrimination Between the Log-Normal and the Weibull Distributions," *Technometrics*, vol. 15 (Nov.), p. 923.

ASTM. "Standard Test Method for Ductility of Bituminous Materials," *Annual Book of ASTM Standards*, Designation: D 113-86, section 4, volume 04.03. Philadelphia: American Society for Testing and Materials.

ASTM. "Standard Test Method for Penetration of Bituminous Materials," *Annual Book of ASTM Standards*, Designation: D 5-86, section 4, volume 04.03. Philadelphia: American Society for Testing and Materials.

ASTM Standard. 1982. "Standard Test Method for J_{1c}, A Measure of Fracture Toughness," *Annual Book of ASTM Standards. Part 10*, Designation E 813-81. Philadelphia: American Society for Testing and Materials, pp. 822–840.

Breaking Point of Bitumen, Fraass Method, IP 80/53, The Institute of Petroleum.

Brostow, W., and Corneuliussen, R.D., eds. 1986. *Failure of Plastics*. New York: Hanser Publishers.

Bueche, F. 1955. "Tensile Strength of Plastics above the Glass Temperature," *Journal of Applied Physics*, vol. 26, pp. 1133–1140.

Dongre, R., Sharma, M.G., and Anderson, D.A. 1989. "Development of Fracture Criterion for Asphalt Mixes at Low Temperatures," *Transportation Research Record 1228*. Washington, D.C.: TRB, National Research Council, pp. 103–111.

Ferry, J.D. 1980. *Viscoelastic Properties of Polymers*. New York: John Wiley & Sons.

Finn, F.N., Yapp, M.T., Coplantz, J.S., and Durrani, A.Z. 1990. *Asphalt Properties and Relationship to Pavement Performance: Literature Review*, Report no. SHRP-A-314. Washington, D.C.: Strategic Highway Research Program, National Research Council.

300

Griffith, A.A. 1920. "The Phenomena of Rupture and Flow in Solids," *Philosophical Transactions*, vol. 221, pp. 163-198.

Hertzberg, Richard W. 1989. *Deformation and Fracture Mechanics of Engineering Materials*, 3d ed. New York: John Wiley & Sons.

Heukolom, W. 1966. *Proceedings of the Association of Asphaltic Paving Technologists*, vol. 36, pp. 359-397.

Irwin, G.R. 1957. "Analysis of Stresses and Strains near the End of a Crack Traversing a Plate," *Journal of Applied Mechanics*, vol. 24, pp. 361-364.

Kim, Y.R., and Little, D.N. 1989. "Evaluation of Healing in Asphalt Concrete by Means of the Theory of Nonlinear Viscoelasticity," *Transportation Research Record 1228*. Washington, D.C.: TRB, National Research Council, pp. 198-210.

Little, D.N., and Mahboub, K. 1985. "Engineering Properties of First Generation Plasticized Sulfur Binders and Low Temperature Fracture Evaluation of Plasticized Sulfur Paving Mixtures." *Transportation Research Record 1034*. Washington, D.C.: TRB, National Research Council, pp. 112-123.

Lytton, R.L., Shanmugham, U., and Garret, B.D. 1983. *Design of Flexible Pavements for Thermal Fatigue Cracking*, Report no. FHWA/TX-83/06+284-4. College Station: Texas Transportation Institute, Texas A & M University.

Paris, P.C. 1962. Ph.D. dissertation. Bethlehem, PA: Lehigh University.

Paris, P.C., and Erdogan, F. 1963. "A Critical Analysis of Crack Propagation Laws," *Journal of Basic Engineering*, vol. 85, pp. 528-534.

Rice, J.R. 1968. "A Path Independent Integral and the Approximate Analysis of Strain Concentration by Notches and Cracks," *Journal of Applied Mechanics*, vol. 35, pp. 379-386.

Rigden, P.J., and Lee, A.R. 1959. "Brittle Fracture of Tars and Bitumens," *Journal of Applied Chemistry*, vol. 3, no. 2, pp. 62-70.

Schapery, R.A. 1983. *Correspondence Principles and a Generalized J Integral for Large Deformation and Fracture Analysis of Viscoelastic Media*. Report no. MM 4665-83-7. College Station: Texas A & M University.

Sih, G.C., and Kiefer, B.V. 1979. "Nonlinear Response of Solids Due to Crack Growth and Plastic Deformation," *Nonlinear and Dynamic Fracture Mechanics*, The Winter

Annual Meeting of The American Society of Mechanical Engineers, New York, December 2-7, 1979, pp. 135-156.

Smith, T.L. 1958. "Dependence of the Ultimate Properties of a GR-S Rubber on Strain Rate and Temperature," *Journal of Polymer Science*, vol. 32, pp. 99-113.

Van der Poel, C. 1954. "A General System Describing the Visco-Elastic Properties of Bitumen and Its Relation to Routine Test Data," *Journal of Applied Chemistry*, vol. 4, pp. 221-236.

Vinson, T.S., Janoo, V.C., and Haas, R.C.G. 1990. *Summary Report on Low Temperature and Thermal Fatigue Cracking*, Report no. SHRP-A/IR-90-001. Washington, D.C.: Strategic Highway Research Program, National Research Council.

Weibull, W. 1952. "A Statistical Distribution Function of Wide Applicability," *Journal of Applied Mechanics*, vol. 19, pp. 293-297.

Williams, M. L. 1957. "On the Stress Distribution at the Base of a Stationary Crack," *Journal of Applied Mechanics*, vol. 24, pp. 109-114.

5

Oxidative Aging Studies

Introduction

Durability describes the resistance of a material to changes caused by environmental exposure. The durability of asphalt binders used in road pavements has been an important subject of investigation since the beginning of this century. By the late 1930s, it became apparent that asphalt binders harden as a result of two different aging phenomena: (1) irreversible oxidative aging and (2) reversible steric hardening. The first is mainly a chemical phenomenon in which the oxygen from the environment diffuses into and reacts chemically with the asphalt, changing its chemical properties. The asphalt becomes stiffer and more brittle. Oxidative aging was found to be asphalt specific; some asphalts were observed to age faster and become harder than others. This fact led to the need to characterize the aging behavior or performance of different asphalts so that aging is considered when selecting asphalts or attempting to predict the performance of pavements.

Asphalt cements harden during mixing and lay-down operations as well as during the service life of the pavements. The general understanding has been that during mixing and lay down, because of the high temperatures, asphalts age not only because of the loss of volatiles but also because of oxidation at these high temperatures. During the asphalt's service life temperatures are much lower and oxidation is considered to be the main aging mechanism.

In this project, the main emphasis was placed on the aging during the pavement life at relatively low in-service temperatures. The main objective was to develop a laboratory aging procedure to simulate in an accelerated fashion the aging in the field. Such a procedure was to predict the propensity of an asphalt to oxidative aging during the designed pavement life and thus be used for specification and quality control of binders. The approach that was taken by the research team assumed that the existing thin film oven test (TFOT), as described by the ASTM Standard Method D1754, or the rolling thin film oven test (RTFOT), as described by the ASTM Standard Method D2872, reliably simulates the aging that occurs during the mixing and lay down operations. Therefore, the new aging procedure is performed on TFOT or RTFOT residue and is intended to simulate the in-service aging.

In this chapter the results of the experiments conducted in the area of oxidative aging are presented. The scope of work for this subtask included four major experiments. These experiments were conducted to study the influence of oxidative aging on the physical properties of asphalt binders. The main topics covered included the effect of aging on rheological properties, the effect of aging on failure properties, the effect of mineral surfaces on the aging of binders, and field validation of the pressure aging vessel (PAV) procedure. In addition, a significant effort was spent on studying the oxidation kinetics in the PAV and evaluating the testing variables affecting the aging levels. The testing was conducted mainly on the eight core asphalts at different temperatures and frequencies or strain rates. The field validation included asphalts recovered from a number of test sections from around the United States and from sections as as old as 12 years.

The rest of this chapter is divided into five sections. The section that follows is a brief review of literature intended to give a background of and explain the rationale behind test methods for the PAV that simulate the aging phenomenon. The second section describes the steps needed to develop the test procedure and describes the process by which it was selected. The third section discusses the effect of oxidative aging on the rheological and failure properties followed by a summary of the field validation experiment and the relationship to changes in chemistry. The fourth section summarizes the results of testing with asphalt mastics and shows the effect of mineral surfaces on aging. The fifth section presents the summary of findings and conclusions. The results presented in the last section include only selected data that reflect the trends observed to justify the stated findings.

Current State of Knowledge

The research teams conducted an extensive review of the literature related to the oxidative aging of asphalts. The findings from the review are published in a separate topical report. The following sections summarize that review and describe how the findings were used to design the experiments in order to meet the research objectives.

Implication of Asphalt Aging and the Need for Long-Term Prediction

It is generally agreed that one of the most important factors that causes asphalt pavements to crack and disintegrate is asphalt oxidative hardening. Because oxidative hardening is a chemical process, the hardening that results from oxidation may be a strong function of the source or the chemical composition of the original asphalts. This fact was proven by the early studies on asphalt aging. A considerable number of laboratory and field studies have attempted to develop aging tests and models to predict asphalt aging and thus predict its effect on pavement performance. The field studies showed that aging depends not only on the source of the asphalt but also on the temperature, void content of the asphalt-aggregate mixture, and depth from the surface. Several models were developed to predict asphalt hardening. Some of these models were based on laboratory data; others, on field data. Most of these models do not consider the effect of environment or mixture type, nor do they show the relationship between laboratory aging and the equivalent aging in the field. The other

problem concerns the variety of laboratory procedures used in aging studies. Many studies use oven aging in which temperature is the main accelerating factor; others simulate field aging by using and a relatively low temperature combined with thin films and extended aging times.

The ideal aging test should provide enough information to allow the prediction of the change in properties of an asphalt at any time in the field during the designed life of the pavement. In a worst condition design, a test should result in aging that simulates the end of the designed pavement life. The objective in both cases is to prevent the use of an asphalt whose aging will adversely affect pavement performance. To understand the implications of asphalt aging on pavement performance, one must recognize the changes that occur in asphalt properties during aging. Aging is known to result in harder and more brittle asphalts. Different measures of consistency have been used to show the effect of aging on asphalts. It is known that as viscosity of asphalt increases, penetration and ductility decrease. As viscosity of asphalt increases, stiffness at any combination of temperature and loading time also increase. At high pavement temperatures, pavements fail by rutting and plastic deformations under load; therefore, aging of asphalt is not a detrimental phenomenon-harder asphalts will be more resistant to deformation. At intermediate and low pavement temperatures, however, harder asphalts will be more susceptible to fatigue. Thermal cracking and aging of the binders is detrimental. This effect of asphalt aging on pavements is well documented. Aging studies confirm that cracking is the major implication that asphalt aging has on pavement performance.

Magnitude of Aging in the Field

Aging of asphalts has been found to affect high-temperature properties differently than low-temperature properties. Therefore, researchers have used different properties to measure aging. In some studies only high-temperature properties, such as absolute and kinematic viscosity at 60°C (140°F) and 135°C (275°F) and softening point, have been measured. In others, properties at intermediate temperatures, such as penetration, ductility, and apparent viscosity at temperatures between 4° and 25°C (39° and −77°F) were used. In other studies, however, properties that are more fundamental in nature, such as stiffness and complex modulus, were measured over a wider spectrum of temperatures including very low temperatures that correspond to field cracking temperatures. The indices used to report field aging, therefore, varied with the type of measurement being considered. In addition, because of the role of environment and mixture type, the indices also varied with the location, pavement structure, and mixture type. To give a general idea of these indices, figures 5.1 and 5.2[1] depict aging indices in terms of viscosity at 60°C (140°F) and penetration at 25°C (77°F), respectively, as a function of pavement age. The indices were calculated from a number of studies done on pavement sections constructed in different states.

The plots show clearly that a number of factors affect aging in the field. There are more than 45 different asphalts in the plots. The fact that asphalts age differently is clearly

---

[1]All figures and tables referenced in this chapter appear at the end of the chapter.

depicted when each location is considered separately. For example, in the study conducted in Texas, the retained penetration ranged between 30 and 70 percent of the original value after only 24 months; viscosity aging indices in the California desert after 4 years ranged between 22 and 55, depending on the type of asphalt. The asphalt source and location (environment) were also shown to be important. In one instance, an asphalt used in Pennsylvania aged more in 30 months than an asphalt in service in Michigan for more than 96 months. An asphalt used in Nebraska showed an aging index of less than 5 after 120 months (10 years) in service. These findings show the importance of characterizing the aging susceptibility of an asphalt as well as considering the climate in which the asphalt will be used. An example of the importance of climate is shown in figure 5.3. Data taken from a study in California (Kemp and Predoehl 1981) indicated that the same asphalts aged in the field for 48 months showed a great difference in aging indices because of the effect of the area temperature.

In only a few studies have researchers attempted to establish the relationship between aging levels and pavement cracking. Since the findings are not very definitive, they cannot be generalized, although some general criteria were established by some researchers. For example, penetrations of less than 10 and ductilities of less than 20, measured at 25°C (77°F), were established to be the limits at which pavements start to show cracking. Such numbers are sometimes misleading because pavement cracking, whether it is due to fatigue or temperature, will only begin when the stiffness of the asphalt or the hardness reaches the strength of the material. The strength and stiffness of the asphalts depend not only on age but also on temperature and loading time. Even in a pavement made of hard asphalt that ages significantly and rapidly, if the temperature of the pavement does not reach low levels such that the binder reaches its strength limits, the pavement may not show any cracking. A similar situation occurs in fatigue cracking: If the traffic level is not very high, a harder and more aging asphalt may perform well for a long time. Therefore, to study the implication of aging on pavement performance and to look at aging levels in the field, the properties of the asphalt, as well as environmental conditions and traffic types, must be considered. Environmental conditions, such as seasonal and daily pavement temperatures, also strongly affect the aging rate of the binders. Regions with high temperatures will have faster aging rates although they may not reach the low temperature levels at which asphalt becomes so stiff that it cracks. The other complication arises from the fact that sensitivity of aging rate to aging temperature is asphalt specific; that is, the strength and stiffness dependency on temperature is not the same for all asphalts.

In this project, the strategy for developing an aging test was to design a test for the binder that simulates the aging in the field, takes into consideration the influence of other factors, and can be completed in a reasonably short time. The test for the binder should produce enough material to characterize rheological and failure properties of binders.

Previous Work Done to Simulate Long-Term Aging

Research efforts to develop simple, practical, and reliable aging tests go back to the beginning of the 20th century (Dow 1903). Among the more important techniques for

306

accelerating oxidation reaction are (1) increasing temperature, (2) decreasing asphalt film thickness, (3) increasing asphalt surface exposed to oxygen, (4) increasing air flow, and (5) increasing pressure. Existing aging tests combine the above techniques to accelerate oxidation. However, in general, they can be classified into two major groups: (1) oven tests of neat asphalts, and (2) pressure oxidation tests. Table 5.1 a list of the aging tests or procedures that have been used frequently in asphalt durability studies during the past 50 years.

The literature review at the beginning of this study indicated that the main obstacle asphalt researchers face is the lack of a practical laboratory aging procedure that simulates long-term aging of asphalts at in-service temperatures. The common procedure of using high temperatures and thin films to accelerate aging was observed to be unsuccessful because asphalt ages differently at high temperatures than it ages at in-service temperatures. The main problems are the loss of volatiles at high temperatures and the change in the nature of the chemical reaction of oxygen with asphalt components at high temperatures. Aging studies done on asphalts recovered from the field indicated that even after long periods, no significant loss of volatiles could be detected. Although cited in a number of studies was the fact that the temperatures at which changes in the nature of chemical reactions are significant were not reported or even carefully investigated. The general consensus among asphalt researchers, however, was that in order to successfully simulate long-term aging, aging in the laboratory has to be done at temperatures similar to pavement temperature.

To find an alternative to temperature, the nature of the aging phenomenon and the reason why temperature was such a powerful accelerating factor were investigated. Oxidative aging of asphalts is a physicochemical process. In a simplified description, oxygen from the environment has to diffuse physically into the asphalt before it reacts with the asphalt components to result in hardening. Temperature serves two purposes: (1) it softens the asphalt and increases the diffusion rate, and (2) it accelerates the chemical reaction. Based on this vision of the aging phenomenon, two alternatives were used: (1) decreasing the film thickness and increasing the amount of asphalt surface exposed to oxygen, and (2) using pure oxygen and accelerating its diffusion by pressure. The microdurability tests and the pressure oxygen bomb were among the tests introduced to age asphalts at in-service temperatures. In the microdurability test, asphalt film thickness was reduced to microns in an attempt to expose more surface and reduce the diffusion path. The pressure oxygen bombs were used at different pressures, temperatures, and film thicknesses to accelerate aging.

Using thin films in microdurability tests had some disadvantages: the limited quantity of material that could be aged during the test, the difficulty of producing uniform thin films, the difficulty of recovering thin films from the surfaces, and the possibility of excessive volatile loss during the test. Pressure oxygen bombs, on the other hand, are not limited by the quantity of residue that can be produced; the residue can be readily recovered; and thin films are possible. Their major problem is one of safety. The pressure-aging technique, however, had the important advantage of providing the means to control the volatilization process and separate the aging caused by oxidation from the aging caused by the loss of volatiles.

The advantage of controlling volatilization by using pressure was overlooked by many researchers. Most of the aging studies done with the pressure oxygen bombs (table 5.1b)

used temperatures that corresponded to the maximum pavement temperature. The majority of studies used temperatures between 50° and 60°C (122 and 140°F). Safety was also cited as a reason the pressure-aging procedure should not be run at a higher temperature. Factors affecting the aging rate in the pressure vessels were investigated in limited experiments. Pressure was not found to be very important; temperature and film thickness, on the other hand, were found to be significant factors. For practical reasons, most recent studies have been conducted with a temperature of 60°C (140°F) and a pressure of 2.07 MPa (300 lb/in.^{2}).

Influence of Interaction with Mineral Surfaces

Mineral aggregates have the potential to absorb and/or adsorb asphalt components on their surfaces. Although aggregates may have different absorption properties, the differences in aging performance of the same asphalts mixed with different aggregates is believed to be caused mainly by different adsorption properties. Aggregate surfaces also have the potential to orient the polar molecules in the asphalt in the vicinity of the asphalt-mineral surface interface. This effect has received almost no attention in the literature, but was studied in the SHRP A-003B contract, as well as in several AIIR contracts conducted within the SHRP. Studies addressing the adsorption and/or surface catalysis phenomenon and its influence on oxidation of asphalts have basically been conducted using two different techniques. The first is to spread relatively thin films of asphalts or asphalt generic fractions on aggregate surfaces and oxidize them. The second is to mix asphalts with mineral fillers and oxidize the resulting mastic.

Davis and Petersen (1966), Peterson (1974), and Barbour et al. (1970) and their co-workers pioneered a technique called Inverse Gas-Liquid Chromatography to study oxidation of asphalts in columns of aggregates coated by asphalt films. Their findings were extremely important in evaluating the adsorption phenomenon and its consequences. They showed that, depending on their mineral composition, aggregates may have a dual role in asphalt oxidation: they may work as catalysts promoting the formation of the oxidation products in the low polar generic fractions (saturates and naphthalene aromatics), or they may adsorb the highly polar fractions. Adsorption of the highly polar fractions makes them less oxidizable, isolates them at the mineral surface inhibiting their reaction with oxygen, and, at the same time, reduces their catalytic effect in promoting the oxidation of the saturates and naphthalene aromatics.

The adsorption of the highly polar fractions may have another effect: coating the mineral surfaces makes them inaccessible to the low polar fractions and thus reduces the catalytic action of the surfaces. Peterson and co-workers (1974), experimenting with four different asphalts and four different aggregates, indicated that those aggregates showing the least adsorption of highly polar fractions (e.g., quartzite) exhibited the greatest catalytic effect in asphalt oxidation; those showing the largest adsorption (e.g., limestone) exhibited the smallest catalytic effect. In conclusion, the authors indicated that the main catalytic effect is the internal one played by the highly polar fractions. Thus, the role of the aggregates comes mainly from inactivation, either physically or chemically, of these internal catalysts. In fact,

Plancher and co-workers (1976), indicated that certain types of limestone aggregates may reduce the asphalt oxidation as a result of their high adsorption activity.

The second technique, begun in the late 1930s, involves mixing mineral fillers with asphalts and aging them. It is interesting that this appropach was first used, not for paving asphalts, but for researchers of roofing asphalt who incorporated various types of natural fillers in an attempt to prolong the life of asphalt shingles. Oliensis (1947), who was one the first to use this technique, reported a study in which filled asphalt coatings were exposed outdoors on asphalt-saturated felts for approximately 10 years. In 1949 a symposium on accelerated weathering of roofing asphaltic materials was organized by ASTM. Several papers were presented that indicated the benefits of using mineral fillers (called, at that time, mineral stabilizers) to prolong the lives of roofing asphalts. Those early works did not address the chemical nature of the interaction of the asphalts with the mineral fillers; instead, the influence was studied in terms of the physical properties of the filled asphalts and the general performance. In general, the findings indicated that fillers have two effects: (1) they decrease the temperature susceptibility of the asphalts, and (2) they increase resistance to cracking by retarding the asphalt atmospheric oxidation (Fair et al. 1949).

After the 1949 symposium, several studies were conducted that measured the effect of different geometrical properties of filler on the aging of roofing asphalts (Greenfield 1959; Zapta and Hazmburg 1949). Other studies determined the degree of improvement that different fillers have on different asphalts (Mertens 1959; Greenfield 1956; Martin 1966). The findings of these studies provided more insight in to the relationship between asphalt-fillers interaction and the oxidation of asphalt. No correlation could be found between any single geometrical property of the fillers and its influence on the aging of asphalts. The degree of improvement in resistance to oxidation varied widely depending on filler type and geometry, and on asphalt composition or source. These findings are in full agreement with those of the more recent and more sophisticated studies (cited previously in this section) that address the chemical aspects of asphalt-aggregate interaction and that are presented here.

Studies using the mastic technique for aging paving asphalts are, unfortunately, very scarce. Schmidt (1973) was probably the first to try this approach in a study on the durability of paving asphalts. Schmidt used the rolling thin film oven test to oxidize the asphalts for half an hour at 149°C (300°F) followed by 48 hours at 82°C (180°F). He indicated that the lack of agreement between laboratory aging tests and field hardening may be partly due to the absence of aggregate surfaces in the laboratory aging tests. Therefore, he included fillers in a small part of his experiment and tried to study their effects. The results were inconclusive. There were changes in degree of hardening, but the author indicated that subjectively the results did not match field performance.

Geitz (1980) studied the effect of three different baghouse fines on the oxidation of two types of asphalts in the rolling thin film oven. He concluded that there is significant variation between different asphalt-fines combinations when aged in the thin film oven. He observed that fines having the largest surface area aged the most. Peterson and co-workers (1987) have also used the technique of aging filler-asphalt mixtures. Although their primary objective was to study the effect of high-calcium lime treatment on reducing oxidative aging, they included several types of lime and a limestone filler. They used a newly developed thin

film oven test to study the influence of mineralogically different fillers on the oxidative aging of four different asphalts. Wide variations were observed; the limestone filler was found to increase the oxidative aging as measured by the relative dynamic viscosity by 37 to 80 percent, depending on the type of asphalt. High-calcium lime, on the other hand, reduced the aging by 40 to 75 percent depending on both the type of asphalt and the type of the hydrated lime. Also, the improvement rate was observed to be related to the amount or volume concentration of the lime. A 10 percent volume concentration was found to cause approximately the same improvement as 20 percent of the most effective lime. Unfortunately, these studies are severely limited in value because the researchers did not isolate the physical volume-filling effect of the fillers from the stiffening resulting from physicochemical interactions between the surface and the asphalt cement.

Pressure Aging as Conducted in this Project

The aging studies in this project started by evaluating a procedure used by other research groups (Lee 1968; Kim et al. 1987). The procedure utilized pure oxygen under 2.07 MPa at 60°C (140°F) for 144 hours (6 days). Additional details regarding the development of the pressure-aging procedure are also described in volume II of this report. The emphasis during the early stages was on the amount of aging being done as a function of aging time in the pressure oxygen vessel (POV). Aging times were varied between a few hours and 1,000 hours. Aging was measured in terms of changes in chemical properties as well as complex viscosity at 60°C (140°F). Aging curves as functions of time were characterized for several asphalts and were compared in general with field-aging levels. The procedure, however, had several disadvantages that the research team thought needed to be evaluated and modified. Therefore, the procedure was changed during the course of the project as more data were collected and additional conditions were evaluated. In the following sections, the selection of the final procedure is summarized and results from the experiments conducted to evaluate the factors affecting the pressure-aging procedure are briefly described.

Selection of A-002A Final Aging Procedure—Summary of Changes

Since the beginning of the experiments, the safety issue of using pure oxygen in the aging procedure was one of the main concerns that the research team had with the POV. Therefore, a decision was made to substitute air for oxygen while keeping the other conditions unchanged. This new procedure was called the pressure aging vessel (PAV). The procedure of aging asphalts, after running the thin film oven test, using air under 2.07 MPa pressure at 60°C (140°F) for 144 hours, was initially recommended. The detailed evaluation of the changes in physical properties was then started for the eight core asphalts. As the rheological testing of the eight core asphalts was completed, a comparison with aging levels encountered in the field revealed that the aging levels resulting from the recommended procedures are not high enough and they do not represent field-aging levels after the targeted pavement lives of 10 to 15 years. The viscosity aging indices for the eight core asphalts after the TFOT and the TFOT followed by the PAV at 60°C (140°F) are shown in figure 5.4. Comparing these aging indices (range of 4.27 to 10.40) with those shown in figure 5.1,

it is clear that, although aging is asphalt-source dependent, on the average, more aging is needed to simulate field aging after 10 to 15 years.

In an effort to modify the PAV procedure to more closely simulate the aging levels in the field, the testing conditions were evaluated and temperature was selected as the most effective and practical choice. In trying to keep the temperature close to the in-service temperatures, a limited number of experiments were conducted on a subset of the core asphalts to look at the aging levels when increased by 5.6° and 11.1°C (10° and 20°F). After evaluating the results, a temperature of 71°C (160°F) was selected. The aging indices for the eight core asphalts aged in the PAV at 71°C (160°F) are shown in figure 5.4. Although the levels were felt to be adequate, there was still a concern about the length of the test procedure and the difficulty of keeping the conditions constant for 144 hours (6 days). As more data were collected, it became apparent that the aging time could be significantly shortened by changing two factors: (1) increasing the temperature of aging and (2) decreasing the film thickness.

This solution, however, required changing some of the hardware and introducing new factors to the aging procedure. In the original procedure the vessel was kept in a water bath maintained at 60° or 71°C (140° or 160°F); going to higher temperatures resulted in excessive water evaporation from the bath and the need for a different technique for controlling the temperature of the vessel. Also, reducing the film thickness meant that the uniformity of the asphalt film had to be more stringently controlled. A forced draft oven with precise temperature control was selected to maintain the temperature at the required level, and a rigid horizontally level surface was provided to support the vessel. The aging time was preselected to be 24 hours and the temperatures were to be around 100°C (212°F). A subset of four asphalts were used in an experiment to evaluate the aging at 100° and 113°C (212° and 235°F) using two film thicknesses: 1.59 and 3.18 mm (0.0626 and 0.125 in.). Later, the aging time was reduced to 20 hours to allow for the time required to prepare and clean the pressure vessel while keeping the total time at 24 hours. The temperatures included in the latter experiment were 90°, 100°, and 110°C. (194°, 212°, and 230°F).

The results from the high-temperature experiments were evaluated and compared with the aging indices measured with the PAV aging at 71°C (160°F) for 6 days, which was considered as producing acceptable levels of aging. The effect of the film thickness was looked at and the 3.18-mm (0.125-in.) film thickness was considered more practical for two reasons: (1) the same pans used for the TFOT procedure could be put directly in the PAV without the need to pour the asphalts and prepare new pans for the PAV, and (2) increasing the film thickness reduced the sensitivity of the aging to the uniformity of the film thickness in the asphalt pans. If a film thickness of 1.59 mm (0.0626 in.) was used, leveling of the pans inside the vessel and also the volume of asphalt (not the mass) would be critical or a high level of experimental error could be expected. Comparing the aging levels for the 3.18-mm (0.125-in.) film thickness, the 100°C (212°F) temperature was observed to give levels of aging similar to 6 days at 71°C (160°F). Figure 5.5 depicts a comparison of aging indices obtained from aging at 100°C (212°F) for 20 hours with those from aging at 71°C (160°F) for 6 days. The results reflect the significant effect of the temperature in reducing the aging time. The temperature of 100°C (212°F) was selected for use in the final PAV

recommended procedure of 20 hours. Ultimately, 90° and 110°C (194° and 230°F) were also selected for cool and desert climates, respectively.

Variables Affecting Oxidation Levels in the PAV

During the third year of the project, several experiments were conducted to evaluate the variables that influence the oxidation level in the PAV. The variables that were identified through the literature review and the preliminary testing included: (1) oxygen replenishment, (2) commingling, (3) position in the PAV, (4) film thickness, and (5) temperature level. In this section a brief review of previous findings is presented. The results presented here include data collected at the Texas Transportation Institute (TTI), Western Research Institute (WRI), and the Pennsylvania Transportation Institute (PTI) and were reported in the progress reports. The results represent only summaries of the data collected in the different experiments.

Oxygen Replenishment

Two experiments were conducted to study the effect of oxygen abundance in oxidizing the asphalt samples in the PAV. In the first experiment the amount of asphalt in the PAV was changed to see if that would influence the level of hardening or the amount of mass gain. In the second experiment the influence of replenishment of air in the PAV was studied.

In the first experiment two PAVs were placed in a well-controlled oven and each vessel was charged with a different quantity of material. In the first vessel, 50 g of asphalts AAF-1 and AAC-1 were placed on single TFOT pans, resulting in 100 g of material in the vessel. In the second vessel, nine TFOT pans were filled with 50 g of asphalt AAG-1 and one pan was filled with 50 g asphalt AAC-1 to the bring the total amount of asphalt in the second vessel to 500 g. Table 5.2 compares the results in terms of viscosity measurements at 60°C (140°F) and in terms of percentage mass gain. The differences shown are very small and depend on the type of asphalt. When compared with the estimated experimental variation for the PAV within the laboratory (coefficient of variation of 10 percent), the differences were found to be within the experimental error and therefore did not indicate any important effects resulting from the quantity of material aged in the vessel.

For the second experiment—effect of the amount of air replenishment—five asphalts were aged in two vessels under identical conditions except that one PAV was kept tightly sealed while the other was fitted with an opening that allowed air flow at the rate of approximately 0.5 liter per minute (30.5 in.³/min). For four of the asphalts the experiment was run in two independent replicates. Table 5.3 compares the viscosities and mass gain of these asphalts after the two different treatments. The table indicates that the percentage change taken with respect to the PAV without flow (standard condition) depends on property measured and on asphalt types. For three of the asphalts (AAK-1, AAM-1, and AAA-1), the change was in the negative direction, which means that permitting the continuous replenishment of air results in less hardening and less oxygen uptake than when the PAV is sealed. This result

runs counter to the hypothesis that oxygen is depleted sufficiently in a closed vessel that the oxidation level is affected. Apparently, the quantity of oxygen in the initial pressurization is sufficient to satisfy the oxidation potential at 100°C (212°F) for 20 hours. For asphalt AAG-1, however, the results were mixed; while a positive change in viscosity was observed, a negative change in mass gain was measured. For asphalt AAD-1, the changes in viscosity were small and opposite changes were measured for the two replicates. The fifth asphalt, AAA-1, showed a very small negative change in viscosity and a positive change in mass.

To evaluate the statistical significance of the changes, a statistical analysis of the results was carried out. To normalize the effect of air flow with respect to the viscosity and degree of hardening of the different asphalts, the analysis was run on the percentage change in viscosity and the percentage change in mass gain rather than the viscosities or the mass gain values. This analysis was provided in the experiment by taking the asphalts in each replicate for both the flow and the no-flow conditions from the same sample that was taken from the same TFOT run. In other words, the effects measured are purely related to the effect of flow. Also, in both conditions the asphalts were placed in the same location in the PAV, and measurements were made in the same period. All these precautions were taken to ensure that the measured effects truly reflect the flow effect.

The analysis indicates that the average of change in the viscosities for the asphalts under the no-flow conditions are higher than those under the flow conditions for the same asphalts by 2.57 percent. The average of change in mass gain, on the other hand, was 6.48 percent in favor of the no-flow condition, which agrees with the trend in change of viscosity. The 95 percent confidence limits calculated, considering the split plot experiment design, for changes in viscosity and changes in mass gain are as follows:

Change in viscosity relative to the no-flow condition = (−9.72% to +4.65%)

Change in mass gain relative to the no-flow condition = (−11.1% to −1.87%)

The results of the two experiments and the statistical analysis clearly indicated that, within the scope of the experiments conducted, oxygen replenishment was not an important factor affecting oxidative hardening of asphalts.

Commingling in the PAV

Previous studies on the high-temperature oxidation of asphalts have proven that aging different asphalts simultaneously at elevated temperatures may result in important complications. As the volatilization occurs, possible contamination results from different volatile materials coming from different asphalts. In the PAV, however, two factors are implemented to prevent such contamination: (1) the aging is done at moderate temperatures, and (2) it is done under high pressure, which tends to strongly limit any effect of volatilization. However, there is still a possibility of some contamination, particularly when the temperature of the test is raised to 71°C (160°F). To investigate the effect of

commingling, four of the core asphalts were aged simultaneously with different sets of asphalts, and the viscosity and penetration changes were measured and compared to study the effects. An example of the results for asphalts AAC-1 and AAD-1 are shown in figure 5.6. Table 5.4 compares the viscosity and penetration after aging asphalts AAC-1 and AAD-1 in the PAV under three different conditions: aged with asphalt AAF-1, aged with AAG-1, and aged individually. The analysis of previous results shows that no important influence can be detected. The variability between the results of aging with different sets is still within the limits of variability measured for the individually aged asphalts, and no specific trends can be detected.

However, the possible influence of commingling can be easily avoided by requiring that asphalts be run individually in the case of TFOT standard procedure. Aging several asphalts simultaneously in a single PAV run is of practical significance because it dramatically increases the productivity of the PAV.

Effect of Location in the PAV

Typically, there are 10 pans in the PAV positioned vertically in a rack. The objective of the location experiment was to investigate whether the asphalts in the different pans are oxidized differently, and whether the standard PAV procedure should call for mixing all pans before testing the aged material. Figure 5.7 shows an example of the location effect for three different asphalts. Table 5.5 lists the viscosity and penetration measured for three asphalts aged at different positions in the PAV. Two experiments were run: one at 71°C (160°F) and the other at 60°C (140°F).

Statistical analysis supported what can readily be observed in the results: no important effects can be detected because of the location of the pan. The results are not surprising for two reasons: (1) there is no circulation in the PAV, and (2) aging is done under high pressure.

Effect of Film Thickness

From the literature review of pressure oxidation, it became apparent that oxidation of asphalts involves a diffusion mechanism. Therefore, film thickness is expected to play a major role and must be controlled when studying the relative aging of the different asphalts. The objective of this experiment was to investigate whether the 2.07 MPa (300 lb/in.^{2}) used was sufficient to overcome the effect of the diffusion rate and whether the diffusion effect is asphalt specific. As presented in the literature review in this report, the interpretation of previous studies led to the conclusion that the diffusion mechanism may be very complicated. Temperature and pressure levels definitely affect the diffusion rate; since the permeability of asphalts is a function of consistency, then consistency, which varies significantly between asphalts, may be an influencing factor. Also, when the asphalt becomes harder because of oxidation, does that change the diffusion rate? In other words, is the continuous reduction in

314

aging rate due to physical reduction in permeability because of oxidative hardening or is it due to other chemical factors?

Figure 5.8 depicts the change in viscosity of the aged material with film thickness for three of the core asphalts. The results confirm the important effect of film thickness and also confirm that the influence is highly asphalt specific. The results presented are for aging at 71°C (160°F), under 2.07 MPa (300 lb/in.^{2}) of air for 144 hours. It is expected that these effects will change for different temperatures, pressures, and aging times. Resources did not allow this experiment to be conducted using the 100°C (212°F), 20-hour protocol.

Several analyses were done to study the effect of film thickness. It was observed that there is a linear relationship between log viscosity and the square of the film thickness. Based on the limited analysis, it was estimated that for the original protocol—71°C (160°F), 2.07 MPa (300 lb/in.^{2}), 144 hours)—a film thickness of 1.59-mm (.06261-in.) is appropriate because the decrease in viscosity is within 5 percent of the estimated zero film thickness value. Figure 5.9 represents the linear relation found and the concept of extrapolation to zero film thickness. Caution, however, should be exercised in generalizing the results to other conditions or other asphalts. More work in this area is needed before a decision on the optimum film thickness, as well other conditions, can be selected. Resources did not allow these studies to be conducted with the 3.18-mm (0.125-in.), 100°C (212°F) protocol that is now used for the binder specification.

Effect of Temperature

Two separate experiments were conducted to study the effect of temperature on asphalt aging in the PAV. In the first experiment, the procedure used was to last for 144 hours (6 days), the temperatures were varied between 55° to 77°C (130° to 170°F) and a water bath was used to control the temperature. In the second experiment, the aging time ranged between 20 and 24 hours, and the temperature ranged between 90° and 113°C (194° and 235°F), and an oven was used to control the temperature.

The Results of the 144-Hour Experiment

The initial experiments on the PAV were all conducted at 60°C (140°F) because this temperature represented the higher temperatures commonly encountered in the field, and because it was the most widely used temperature for pressure oxidation testing in previous works. As mentioned earlier, aging at 60°C (140°F) did not result in hardening similar to hardening in the field after 10 to 15 years. To study the effect of temperature in the PAV and to evaluate the feasibility of increasing temperature to increase aging, different combinations of asphalts were aged at four temperatures: 54°, 60°, 71°, and 77°C (129°, 140°, 160°, and 171°F). Aging indices using the viscosity at 60°C (140°F) were obtained. Figure 5.10 shows the change in these aging indices for the three asphalts with PAV temperature. The limited data indicate that first the effect of PAV temperature is asphalt specific. For example, asphalt AAD-1 showed an increase of aging index from 9 to 30 when

the temperature was changed from 60°C (140°F) to 77°C (171°F), while asphalt AAG-1 showed an increase from 4 to 7 for the same change in the PAV temperature. The other observation concerns the nonproportionality of the temperature effect. Asphalt AAD-1, for example, showed an increase in the aging index from 8 to 9 because of the increase in PAV temperature from 54° to 60°C (129° to 140°F); the increase from 71° to 77°C (160° to 171°F) resulted in an increase of 17 to 30 for the same asphalt.

The results of this experiment, although limited in scope, indicated that aging in the PAV can be accelerated significantly by increasing the aging temperature. They also indicated that the PAV procedure may be used effectively to measure the dependency of the aging rate of different asphalts on aging temperature. Such measurements can probably be used to predict how asphalts will age in the field under different temperature regimes. The results of the experiment pointed out the importance of further investigating the oxidation kinetics in the PAV in an attempt to calibrate the aging protocol to simulate field aging under different environments.

The Results of the High-Temperature, Short-Time Experiment

The second experiment was designed to evaluate the feasibility of running the PAV at high temperatures to shorten the aging time. The experiment was conducted in two steps. In the first step, four asphalts were aged in the PAV under 2.07 MPa (300 psi) of air pressure at two temperatures, 100° and 113°C (212° and 235°F), for 24 hours. Aged material was tested for viscosity at 60°C (140°F) and for rheological properties using the dynamic shear rheometer. The asphalt film thickness was also varied between 1.59 mm (0.0626 in.) and 3.18 mm (0.125 in.).

Figure 5.11 depicts the aging indices for the four asphalts aged in the PAV at two temperatures, 100° and 113°C (212° and 235°F), for 24 hours. For comparison, the figure also shows the aging index for the 71°C (100°F) aging for 144 hours. The results reflect the effectiveness of increasing the aging temperature in increasing the hardening levels. At 113°C (235°F), aging the asphalts with 1.59-mm (0.0626-in.) film resulted in severe hardening. For three of the asphalts, viscosity could not be measured and was estimated to be in excess of 50,000 Pa·s (5×10^5 poise). Even at 100°C (212°F) with a film thickness of 1.59 mm (0.0626 in.), an aging index of 305 is calculated for asphalt AAD-1. The asphalt-aging specificity was also clearly revealed in these measurements. While for three of the asphalts, hardening at 113°C (235°F) was too severe to be measured, asphalt AAG-1 showed an aging index of only 13 for the thinner film. The following findings were concluded from the first step of this experiment:

- Running the PAV at high temperatures is very effective in decreasing the time required to reach high levels of hardening. The hardening, as measured by relative change in capillary viscosity at 60°C (140°F) because of aging at 100°C (212°F) for 24 hours, is approximately equal to the hardening resulting from aging at 71°C (160°F) for 144 hours. This result is equivalent to approximately a 50 percent reduction in time for each 10°C (18°F) increase of aging temperature.

- Film thickness effect is very significant even at high temperatures. The expectation was that the high temperature and pressure would eliminate the film thickness effect and normalize aging with respect to the diffusion rate. The results clearly show that this is not the case. While the aging indices ranged between 5 and 20 for the 3.18-mm (0.125-in.) film, they ranged between 8 and 50 for the 1.59-mm (0.0626-in.) film. The film thickness effect was highly asphalt specific. The results of the film thickness illustrate the importance of considering the diffusion phenomenon.

- Increasing the temperature to 113°C (235°F) for 24 hours resulted in extreme oxidation. For three of the asphalts, with the 1.59-mm (0.0625-in.) film aging, the hardening was so severe that the viscosity was beyond the limits of the viscometer used, which is estimated at 50,000 Pa • s (5 x 10^5 poise). For asphalt AAG-1, the aging index was 13. Also, the 3.18-mm (0.125-in.) film aging also results were extreme. For AAK-1 the aging index was 80.7; for asphalt AAD-1, the aging index was 304.9; and for AAM-1, the aging index was 108.

- Mass gains were also very different. They ranged between 1.14 and 1.59 percent when asphalts were aged at 113°C (235°F) at 1.59-mm (0.0626-in.) film thickness. The mass gains during a PAV test do not reflect the aging of the asphalt in a direct manner and mass gain is not reported in the specification. Mass gain measurements depend on the level of outgassing at the end of the PAV test and are difficult to reproduce.

- The effect of temperature confirms previous results that indicate that the temperature effect is highly asphalt specific. The aging index of AAD-1 increased from 29 to 305 when the temperature of aging was changed from 100° to 113°C (212° to 235°F). AAG-1, on the other hand, changed only from 5 to 7.

The results of the dynamic rheological measurements were evaluated to study the effect of high-temperature PAV aging on rheological changes. The changes in the rheological type of two of these asphalts with aging, as reflected by the estimates of the rheological parameters, are shown in table 5.6. The table includes only the values for the 1.59-mm (0.0626-in.) film thickness aging. The changes in the values reflect the significant effect of the aging temperature on the rheological type for a given aging time, and show the importance of considering the changes in the whole spectrum of rheological properties, as opposed to considering only viscosity. A sample of the rheological measurements compared with the other aging procedures used is shown in figures 5.12 and 5.13 for asphalts AAK-1 and AAG-1, respectively. The plots depict changes in the rheological master curve that resemble changes caused by field aging, as reported in several previous studies. The plots also depict a clear trend of shift to the lower frequencies (decrease in log ω_0), and the significant flattening (increase in R value) with increasing temperature of aging. For both asphalts, the master curve for the 100°C (212°F), 1-day aging is above that for the 60°C (140°F), 6-day aging. The results were very encouraging because of the resemblance to the known field aging.

The second step of the high-temperature PAV experiment included testing four of the core asphalts at three aging temperatures for one aging period of 20 hours. This time period was

selected to allow enough time for preparation of the sample and vessel setup. To evaluate the effect of time, however, two other aging times of 10 and 40 hours were included, but at only the 100°C (212°F) temperature. The data collected were used to look at the sensitivity of aging levels to the variation in either of the two factors temperature and time of aging.

Figure 5.14 shows the sensitivity of aging in the PAV to the aging temperature. The temperatures selected for this study were 90°, 100°, and 110°C (194°, 212°, and 230°F) in order to investigate the effect of variability of temperature on the proposed standard temperature of 100°C (212°F). The figure indicates that temperature effect is asphalt specific and that it is not linear with temperature. To calculate the sensitivity of hardening level to aging temperature, the complex modulus at 45°C (113°F) and 10 rad/s was selected to reflect the hardening and a linear relation between the value of modulus. Aging temperature was assumed between the three aging temperatures. Relative to the modulus value after aging at 100°C (212°F), the sensitivity to per °C ranged between 3.0 and 16.5 percent. The sensitivity increased as the frequency at which the modulus is calculated decreased or as the temperature at which the modulus is calculated increased.

Time of aging effects is shown in figure 5.15. Again, the effect is asphalt specific. Using the same procedure and taking the modulus value for 20-hour aging as the reference, the sensitivity varied between 0.4 and 8.3 percent per 1 hour of aging. This aging sensitivity is much lower than that of temperature. It is therefore recommended that a ± 10-minute control on aging at the pressure of 2.07 MPa (300 psi) is adequate.

Film thickness has been shown to be important. Evaluating the effect at 100°C (212°F) at 20 hours indicated that for some asphalts an increase in modulus value of as much as 60 percent results by decreasing the film thickness from 3.18 mm to 1.59 mm (0.125 to 0.0626 in.). Assuming that the effect of film thickness is proportional to the square of the film thickness, a maximum increase in modulus of approximately 1.5 percent for each 1.0-percent decrease in film thickness is estimated. Since TFOT aging is required prior to PAV aging, control of the amount of material in each pan in the PAV is not a problem as long as the ASTM requirements for the TFOT are met. The important point is the leveling of the PAV and the requirement that the film thickness in the PAV pans remains uniform during aging.

As mentioned earlier, the 71°C (160°F), 144-hour protocol was found to give aging levels that fairly simulate the targeted aging in the field at moderate climates. Therefore, the equivalency of the high-temperature PAV protocol to previous aging done at 71°C (160°F) was evaluated. Figures 5.16 and 5.17 depict equality plots for the different aging temperatures and aging times. The figures include modulus and phase angle values at 15° and 45°C (59° and 113°F). The 100°C (212°F), 20-hour, 1.59-mm (0.0626-in.) protocol gives the best results considering the equivalency to the 71°C (160°F), 144-hour, 1.59-mm (0.0626-in.) protocol. This protocol is not practical because it requires changing the amount of the material after the TFOT aging procedure from the 3.18-mm (0.125-in.) film thickness to the 1.59-mm (0.0626-in.) required film thickness. Therefore, the 100°C (212°F), 20-hour, 3.18-mm (0.125-in.) protocol was selected as the standard test. This protocol, as shown in figure 5.16, still gives comparable aging levels, eliminates the need to change the TFOT pans, and potentially reduces the variability owing to uniformity of film thickness.

318

TFOT Volatilization Experiment

The TFOT volatilization experiment was initiated because of the need to evaluate the effect of volatile loss on aging of asphalts. Four asphalts were aged in a standard TFOT test oven that was modified so that an inert gas could be introduced at a constant rate of flow. Air and nitrogen gas were first used to compare the volatile loss and the resulting hardening. Argon gas was used later to replace nitrogen because of possible of oxygen presence in the nitrogen supply. Mass change, capillary viscosity at 60°C (140°F), and dynamic shear measurements at four temperatures were measured to reflect changes in physical properties.

Figures 5.18 and 5.19 show the change in viscosity at 60°C (140°F) and the mass change under the different aging environments. The modified oven, when operated with air results in mass change and viscosity increase similarly to the standard TFOT. Under a nitrogen and argon environment the mass change is almost the same but somewhat greater in the negative direction, when compared with an air environment. The viscosity increase, however, is significantly different when nitrogen is compared with argon. It is assumed that this result is due to the very small amounts of oxygen present in commercially bottled nitrogen. Therefore, the argon environment was considered more representative of an inert environment.

The results of this experiment led to the following findings:

- Aging asphalts in the standard TFOT oven under an inert environment harden significantly. Therefore, volatilization or the loss of volatile constituents contributes greatly to the hardening of asphalts at high temperatures.

- The mass change under an air environment is only marginally less than the mass change under an inert environment. This finding reflects the fact that during aging in the TFOT the mass gain because of oxidation is very small. This small mass gain, however, results in significant hardening.

- The more polar asphalts (AAD-1 and AAK-1) showed more mass loss in both air and argon environments than the less polar asphalts (AAG-1 and AAM-1). The relative difference in mass is not a good indicator of the relative hardening.

- Asphalts that showed maximum mass loss during the volatilization experiment under inert environment showed the maximum mass gain during the PAV high-temperature aging. This behavior may need further analysis and investigation.

The results from dynamic shear testing at lower temperatures using the dynamic shear rheometer are shown in figures 5.20 and 5.21 for two asphalts. The loss of volatiles was found to be a major contributor to the hardening in the TFOT treatment. An analysis of variance was made to determine whether treatment with air versus argon gas is important with regard to changes in physical properties. The response parameters used included the crossover frequency, the rheological index, and the defining temperature. The results,

summarized in table 5.7, indicate that treatment is an important factor and that there are significant differences between the effects of aging on the rheological properties because of the different treatments.

To evaluate the effect on chemical properties, infrared (IR) analysis was performed on the asphalts at WRI. The results are listed in table 5.8 for the four asphalts. The results confirm the findings drawn from the physical properties measurements that the loss of volatiles (as reflected by aging in argon) contributes a major part to changes in properties because of aging in the TFOT.

Effect of Aging on Rheology and Fracture of Binders

Aging is not a physical property that can be measured numerically. To define aging, a property or set of properties that is important to the specific application of the material is selected first, then the change in that set of properties resulting from aging is measured by the proper means. In the following section, the methods used to measure aging of asphalt binders in the past are first reviewed and critiqued. The changes in fundamental rheological and failure properties as measured in this project are then presented for a number of the SHRP asphalts.

Literature Review

Researchers studying asphalt have used different means to measure different flow properties. In general, the physical properties measured can be classified into three major groups: single-point measurements, susceptibility parameters, and linear viscoelastic (LVE) measurements.

Single-Point Measurements

One or several independent consistency measurements are used to evaluate asphalt hardening. Penetration, ductility, softening point, and various types of viscosity measurements are among the most commonly used. The first three are empirical in nature, while the fourth is a fundamental material property. A major part of the early asphalt durability studies relied completely on the empirical measures to evaluate asphalt hardening caused by natural aging in the field or accelerated aging in the laboratory (HRB Bibliography No. 35). A decrease in penetration and ductility values, and an increase in softening point temperature were considered good indicators of hardening. Penetration and ductility were measured at various temperatures, and critical limiting values were proposed to indicate the level of hardening at which cracking of the pavement is expected. The problem with these three measures is twofold: (1) they are one-point measurements that cannot possibly give an adequate representation of the original nature, or the change after aging, of asphalt complex viscoelastic properties, and (2) they are empirical in nature, which indicates that they cannot accurately, nor simply, be related to any fundamental rheological property of the material.

The coefficient of viscosity is an absolute fundamental measure for Newtonian fluids whose properties are independent of the rate of loading or stress level. Asphalts exhibit Newtonian behavior only at high temperatures (above the softening point), or at very low shear rates. At low temperatures, or short loading times, asphalts are not Newtonian and cannot be described by an absolute value of coefficient of viscosity. To solve this problem and salvage the use of viscosity, measurements were restricted to high temperatures above 60°C (140°F) where the behavior of asphalt is generally Newtonian or can be approximated as Newtonian. The other approach was to supplement the measure with the rate of loading and/or load level to make it meaningful. The new measure, "apparent viscosity," was dependent on shear rate, stress level, and temperature. There was a question as to where the apparent value should be measured within the time, stress, and temperature domains. Because of the lack of any valid reason for selecting a specific set of conditions, the selection varied among researchers and became a matter of experimental convenience. Traxler and his co-workers (Traxler and Schweyer 1936, Romberg and Traxler 1947, Traxler 1947) selected a temperature level of 25°C (77°F) because of experimental convenience and proximity to average in-service temperatures and a constant power input of 1,000 ergs. The authors clearly indicate that the choice was made because aged and unaged asphalts could be measured at that value of power input with the viscometers they used without any extrapolation (Romberg and Traxler 1947). Besides Traxler's group, several other researchers used this approach in asphalt-aging studies (Moavenzadeh and Stander 1966, Majidzadeh 1969, Page et al. 1985).

With the introduction of the Shell sliding plate viscometer (Griffin et al. 1955), a new proposal came about. The authors suggested measuring apparent viscosity at 25°C (77°F) with a constant shear rate of 0.05 sec^{-1}, again because of experimental convenience and suitability of the device for this measurement. A great number of research groups followed this approach; apparent viscosity at 25°C (77°F) and 0.05 sec^{-1} became the most common method for evaluating asphalt hardening with aging. Early as well as recent studies have used this measure (Heithus and Johnson 1958, Gallaway 1957, Kemp and Predoehl 1981, Button and Epps 1985).

Despite the wide acceptance of the constant strain rate viscosity measure, there were still other researchers who criticized the approach and chose another. These researchers indicated that the measure is completely misleading and indicated that stress level is as important as shear rate (Chipperfield and Welch 1967, Mack 1965). Based on an extensive field study, Chipperfield and Welch indicated that a constant stress-apparent viscosity, although not the ultimate choice, is a much better indicator of asphalt hardening caused by aging than the constant strain rate apparent viscosity.

The review of studies that used viscosity measurements indicates that viscosity and apparent viscosity have been widely used to measure asphalt-original properties and their changes with aging. Although to some extent these measures may be considered fundamental properties, they do not solve the whole problem. They are still one-point measurements that cannot tell much about the complex rheological nature of asphalts; the steady-state viscosity at high temperatures cannot be extrapolated to low temperatures; and apparent viscosity is a function of loading time, stress level, and temperature.

The Susceptibility Parameters

Recognizing the complexity of asphalt rheological properties and the drawbacks of single-point measurements led many researchers to propose viscoelastic parameters that may in some ways describe a range of properties within the time-temperature domain. These parameters may be divided into two types: temperature susceptibility parameters and shear susceptibility parameters. Their use resulted in better evaluation of rheological properties. However, many of the problems associated with the single-point measurements were carried over to these measures.

Temperature Susceptibility Parameters

A change in consistency with temperature is the general definition of temperature susceptibility. Several types of such parameters have been proposed and used. They basically vary in two ways: the type of consistency measurement used and the range of temperature covered. The early studies used penetration as the consistency measure. To define temperature susceptibility, the penetration at different temperatures was measured and the ratio of penetrations, the difference in penetration, the temperature required to increase the penetration by a certain number, or the slope of log penetration versus temperature have been used (Pfieffer and van Doormaal 1936, van der Poel 1954, Neppe 1952, Barth 1962).

More fundamental approaches used viscosity as the consistency measure for characterizing temperature susceptibility and to define a temperature susceptibility parameter. Again several types of relations have been used, such as slope of log viscosity versus temperature (Traxler and Schweyer 1936); log viscosity versus log temperature (Lee et al. 1940); log viscosity versus reciprocal of temperature (Lewis and Halstead 1940); log viscosity versus reciprocal of temperature raised to a variable power (Traxler and Schweyer 1936, Cornelissen and Waterman 1955), and log-log viscosity versus log temperature (Fair and Volkmann 1943, Nevitt and Krachma 1937). The latter is probably the most widely accepted and is referred to as Viscosity-Temperature Susceptibility (VTS).

A third approach is to use consistency indices: penetration and softening point are used for the well-known penetration index (PI) (Van der Poel 1954), and penetration and viscosity are employed for the widely used penetration viscosity number (PVN) (McLeod 1972). For evaluating asphalt hardening caused by aging, several of these parameters have been used. The conclusions about the effect of aging on temperature susceptibility are quite controversial. Pfieffer (1950) and Blokker and van Hoorn (1959), using the penetration index, reported a decrease in temperature susceptibility upon oxidative aging. Halstead and Zenewitz (1961), using plots of log-log viscosity versus temperature in the range of 60° to 95°C (140° and 203°F), indicated that some asphalts show a decrease in temperature susceptibility while others show an increase upon aging. McLeod (1972) used the PI and his PVN and observed that after 9 years of service, asphalts showed either no change or a significant increase in temperature susceptibility. Puzinauskas (1979) used the VTS and concluded that the majority of asphalts show an increase in temperature susceptibility. Anderson and co-workers (1983) used three different parameters (PI, PVN, and VTS) and concluded that PI and VTS show a general increase in temperature susceptibility, while PVN

does not show significant changes with aging. Anderson and co-workers, experimenting on a very large number of asphalts, indicated that these indices do not measure the same property, and that no simple explanation can justify the difference in the effect of oxidative aging on the values of these parameters. Button and co-workers (1983) confirmed Anderson's findings. The authors found that using the PVN (77-140) shows strange results; asphalts that were originally highly temperature susceptible became more susceptible with oven aging, while those that were less temperature susceptible became less susceptible with aging.

Besides those who used these parameters, there were other researchers who used apparent viscosity as the measure of consistency. Movenzadeh and Stander (1967) measured apparent viscosity at a constant power input (1,000 ergs) at a large number of temperatures ranging between 10° and 160°C (50° and 320°F), and concluded that aged asphalts are less temperature susceptible in the lower temperature range than in the higher temperature range. Kandhal et al. (1973) and Kandhal and Wenger (1975) confirmed the Moavenzadeh and Stander findings. They measured apparent viscosity at 4°, 25°, 60°, and 130°C (39°, 77°, 140°, and 266°F) and observed that temperature susceptibility, measured in terms of log-log viscosity versus log temperature, decreases in the lower temperature range with age hardening, while it increases in the higher temperature range. Culley (1972), however, did not agree; this author measured apparent viscosity at 15.6°, 60°, and 135°C (60°, 140°, and 275°F) and observed that a general decrease in temperature susceptibility across all that range was observed upon aging.

Fundamental reasons explain the problems with temperature susceptibility parameters and their use for measuring aging. Asphalt rheology, similar to many viscoelastic materials, depends on both time of loading and on temperature. Without separating these two factors, any temperature-dependency parameter will be arbitrary in nature and different at different loading times. Also, temperature susceptibility is not constant, and the effect of aging on that susceptibility is not necessarily the same at all temperature ranges. Furthermore, using the apparent viscosity is even more complicated. As the temperature decreases, or as the asphalt ages, the time required to reach the specified shear rate at which apparent viscosity is measured will be different, which results in using measures at different temperatures and two different times of loading. Such confounding of important factors may result in misleading indications. In summary, it is rather difficult to consider the temperature-susceptibility parameters discussed here as reliable measures to characterize asphalts or to determine the effect of oxidative hardening.

Shear Susceptibility Parameters

Two types of parameters have been used to represent the shear susceptibility of asphalt cements: the degree of complex flow, C, and the shear index. The degree of complex flow was introduced by Traxler and co-workers (1944) for use in characterizing paving asphalts. They indicated that measurements on different asphalts show that the slope of log shear stress versus log strain rate may be considered constant, and therefore asphalt rheological properties may be approximated by a complex flow equation that is usually used for power law fluids:

$$M = T/S^C \tag{5.1}$$

where M is a constant, T is the shear stress, S is the shear rate, and C is the degree of complex flow. C, therefore, is the slope of the curve generated by plotting the logarithm of shear stress versus the logarithm shear rate. For $C = 1$, the asphalt is a Newtonian fluid and M is the steady-state coefficient of viscosity. Therefore, C was considered a good measure of non-Newtonian behavior. A large number of researchers accepted the approximation, and the change in the C value was used as an indicator of the effect of oxidative aging on the properties of asphalts in many investigations (Gallaway 1957, Moavenzadeh and Stander 1967, Jimenez and Gallaway 1962).

The degree of complex flow, C, however, has been shown in several studies to be arbitrary. The relation between shear stress and shear rate is not constant, it is a continuously decreasing function of shear rate. At very low shear rates and at very small stress levels, most asphalts will show Newtonian behavior ($C = 1$). This behavior, depending on the type of asphalt, will start changing to non-Newtonian gradually, as the shear rate or stress level increases (Puzinauskas 1967). The parameter, being a measure of non-Newtonian behavior, will naturally depend on the stress history. Majidzadeh and Schweyer (1965) conducted an experiment where the C value was measured for the same asphalt under the same conditions, but the sequence of loading applications was changed. They compared "Cd" measured when the load increments were added in a decreasing sequence of load values with "Ci" measured with an increasing sequence of load step values. The results showed that the two measures are different and arbitrary in nature.

In addition to the above problems with the measurement of C, there is a fundamental problem with the procedure used to define C. Constructing the stress-shear rate relationship is subject to the same controversy associated with apparent viscosity. From a standard creep curve measured for a non-Newtonian material, the shear rate may not come to a steady state within a reasonable testing time or acceptable total deformation. Therefore, the value of the shear rate used to construct the log shear stress versus log shear strain plot must be chosen at an arbitrary time of loading with temperature.

The shear index is a different type of measure; it is obtained by plotting the apparent viscosity versus shear rate on a log-log scale. The slope of the relation between two different shear rates is determined and considered as the shear susceptibility parameter. Although early researchers tried to approximate the relation as linear (Jimenez and Gallaway 1961, Gallaway 1959), a large number of more recent studies showed clearly that this relation is not true.

The shear index has been used by many researchers to study aging. Zube (1969), Culley (1969), and Khandal et al. (1973) all compared the viscosity-shear rate plots of unaged asphalts with laboratory- or field-aged asphalts. However, since the plots are nonlinear and temperature dependent, they selected different ranges of shear rates and different temperatures. All agreed that an increase in the shear susceptibility is observed upon aging.

324

As with other susceptibility parameters, the shear index must be considered an arbitrary value. Its value depends to a great extent on the range of shear rate considered and the temperature at which it is measured. A single shear index may only indicate the type of behavior expected for an asphalt at the temperature and shear rate range at which it is measured; no simple extrapolation or even interpolation can be made. Moreover, it still uses the apparent viscosity, which is time-of-loading dependent; if this is not constant, then the plot is difficult to interpret.

To summarize, the review of shear-susceptibility parameters indicated that these parameters are not better than temperature-susceptibility parameters, they are arbitrary in nature, and they do not show high promise for use in asphalt-aging studies.

The Linear Viscoelastic Characterization

The use of LVE parameters is the most comprehensive approach to characterizing of changes that occur during aging. Stiffness modulus, compliance, or complex modulus is measured at different temperatures for certain ranges of time of loading or frequency. Then, using the time-temperature superposition principle, the master curves can be constructed. The effect of oxidative hardening is then followed through the shift and change in shapes of the master curves. The use of this approach requires that the asphalts, within the conditions of testing, be LVE and thermorheologically simple. Several research works have proved that asphalts can be well approximated as such materials (Jongpier and Kuilman 1969, Anderson and Goetz 1973, Pink et al. 1980). Since it is difficult, expensive, and time consuming, however, only few works have followed this approach for characterizing asphalts and measuring the effects of age hardening.

Majidzadeh (1969) and Majidzadeh and Schweyer (1968) used creep testing to construct master curves in terms of creep compliance over a wide range of loading times. They compared master curves for unaged and oven-aged asphalts and reported in detail about the change in the type of relation that is caused by different levels of oxidative hardening. The main findings were as follows: (1) the curves shift and at the same time distort (a change in shape), (2) at short loading times the aging has minimal effect while the effect increases with time or temperature, and (3) different aging conditions shift the curves differently.

Chipperfield and Welch (1967) used a vibration (dynamic) technique to measure the shear complex modulus of several unaged and field-aged asphalts. The authors, dealing with only limited data, suggested that the when depicting aging, asphalts' master curves may undergo a relatively small change in shape, but they are shifted at a certain angle when compared with the unaged response. The authors, however, did not try to generalize the trend, but indicated that this can only be considered an approximation for the data they collected.

Sisko and Burnstrum (1968, 1969) were the first to compare the effects of oxidative aging of asphalts in the laboratory with the effects of aging in the field using the LVE characterization technique. They used a vibrating cone-and-plate rheometer to measure the shear complex modulus over a wide range of temperatures and frequencies. The results agreed well with

Majidzadeh's findings. For the modulus-frequency relation the plot shows a shift and a change in the shape. It also shows minimum total change in the high-frequency region and more change in the low-frequency region. To study the effect of oxidative hardening on the temperature susceptibility of the tested asphalts, the authors used the plot of the shift factor, aT, versus temperature and found that aging changes the temperature dependency of the asphalts' properties. The change tends to be higher in the high-temperature range.

Few other works followed the Sisco and Burnstrum investigation and confirmed that the LVE characterization is necessary for characterizing the effects of oxidative hardening. However, those works reported different findings about the type of change in LVE properties that are due to aging. Dobson (1969), using dynamic testing to measure shear complex modulus, agreed with the earlier findings of Chipperfield and Welch. The author concluded that oxidative aging may have only small effects on the rheological type of the asphalt, and the main effect can be reasonably approximated by a shift of the rheological spectrum along the frequency scale—a shift similar to temperature effects. Dickinson and Witt (1970), on the other hand, reported differently. Also using a vibration technique, they reported that no such simple relation to aging could be found. The authors indicated that no reasonable shift can bring the aged and unaged response master curve to complete superposition and therefore the shape of the relation undergoes significant alteration. More recently Maccarrone (1987) reported on an extensive laboratory and field-aging study. His findings support what has been concluded in several other works; i.e., aging results in shifting and shape distortion of the linear-viscoelastic response master curve when compared with the unaged curve. Such changes depend on temperature and, more important, on the type of aging.

The review of the LVE characterization approach for studying the effect of oxidative hardening indicated that this approach has been used in many investigations and has been proven to be the only one that gives a comprehensive view about the changes in the rheological properties of asphalts that are due to oxidative aging. However, the investigations have also shown that the changes are not simple and they may depend on the type of oxidation carried out. The latter point is important because the changes caused by TFOT aging resulted in a rheological spectrum that does not mimic the shape of the extracted asphalt from the pavement. This result indicates that oxidation done in the laboratory at high temperatures may change the rheology differently from oxidation that occured in the field. Evidence in the literature indicates that this finding is true (Majidzadeh 1969, Maccarrone 1987). It has been proven that oxidation at high temperatures results in chemical changes that are different from changes that result from oxidation at low temperatures. It is quite plausible that such differences will be seen in the type of rheological changes in the material.

The above review covered only changes in consistency or rheological properties that are results of aging. Although it seems probable that aging will affect other properties such as fracture and fatigue, no published study has thoroughly addressed the effect of aging on these properties. Indirect measures of fracture properties such as the Frass Brittle point and the microductility measurements, although considered by some researchers to be good aging indicators, suffer from empiricism and inaccurate interpretation.

The Effect of Aging on Rheological Properties as Measured in this Project

An LVE characterization was selected by the research team to represent rheological properties of asphalts. Time dependency, hardness, and temperature dependency are factors that must be considered when evaluating the LVE behavior of asphalt cement. Time dependency is indicated by the rheological index, R; hardness by the crossover frequency at a given temperature, and temperature dependency by the defining temperature, T_d. In order to evaluate changes in rheology during aging, all three factors must be considered. The changes in R and crossover frequency will give the change and the shift in the rheological master curve. The change in T_d will give the change in the temperature shift function.

The conditions for the PAV-aging procedure used originally were 2.07 MPa 300 psi pressure at 60°C (140°F) for 144 hours. The eight SHRP core asphalts were aged using this method after treatment with the standard thin-film oven test. The dynamic shear rheometer was used to measure the complex shear modulus (G^*) and the phase angle as a function of frequency at 10 temperatures ranging between −35° and 60°C (−31° and 140°F). The time-temperature superposition principle was used to establish the rheological master curve and the temperature shift function. The rheological model developed by the research team was then fitted to the rheological curve and the model parameters were estimated using statistical regression.

An example of how aging changes the complex modulus master curve and the phase angle master curve is shown in figure 5.22. A change in shape (flattening) of the G^* master curve and a shift in the crossover point can be observed for both the TFOT and the PAV treatments. The flattening of the G^* master curve is also reflected in lower phase angles at the lower frequencies. The change in the temperature shift function is shown in figure 5.23. Because T_d is the parameter defining the shape of the temperature shift function, as it increases, a flattening of the curve can be seen. The flattening is a reflection of smaller shifts for a given temperature change. In other words, the properties become less sensitive to temperature. As will be shown later, the changes in T_d as a result of aging are rather small and tend to be even less within the low-temperature region.

The changes in the rheological parameters for the eight core asphalts after the TFOT and PAV treatments at −60°C (140°F) are shown in figures 5.24 to 5.26. As depicted, the trends for all asphalts increase in R, decrease in $\log(\omega_o)$, and increase in T_d. Because of the difficulty of interpreting the master curve and the shift function, it is much simpler to separate these factors and look at the changes of G^* and the phase angle as a function of temperature at a given frequency. Figures 5.27 and 5.28 are examples of such isochronal plots at a selected frequency of 10 rad/s for asphalt AAD-1. At this frequency the asphalt becomes harder at all temperatures while the phase angle becomes lower at all temperatures. The phase angle is a measure of the ratio between the loss modulus to the storage modulus (G''/G'). With aging, G'' increases because both $\cos(\delta)$ and G^* increase. However, G' is also increasing because the increase in G^* offsets the decrease in $\sin(\delta)$. In effect, the storage modulus, which reflect the elastic part of the binder deformation under load, increases more than the increase in the delayed-elastic and viscous part of that deformation. Looking at the plots in figure 5.28, it is important to note G^* is shown on a logarithmic

scale. The point is the change in G^* is much more significant than the changes in the phase angle. This reason is why a net change in G' is more than the increase in G". In general terms, with aging the asphalt becomes more elastic and its ability to recover or rebound increases.

The trend of changes in rheological properties described above was observed for all 30 asphalts tested in this project. The trend also agrees with the changes measured for asphalts recovered from pavements and reported in previous studies. Similar changes were also observed for other PAV-aging treatments including different aging temperatures and different aging times. Figure 5.28 depicts how the rheological master curve changes after asphalt is aged in the PAV at different temperatures, the higher the PAV temperature, the more the flattening and the shifting of the G^* master curve. The same was observed for the aging time in the PAV: Figure 5.29 depicts the change in the master curve for asphalt AAK-1 with aging time. The relative change is proportional to the aging time but is not as effective as the aging temperature.

Table 5.9 lists the changes in the rheological parameters that result from the different aging procedures in the PAV. The trend of increasing R, decreasing log (ω_o), and increasing T_d, with increasing temperature or aging time, is clear and consistent for all the tested asphalts.

The results of the investigation of oxidative aging on rheology emphasize two main points. First, that aging changes the rheological type of the asphalts is evident in the significant change in the rheological index (R) and the change in temperature dependency (T_d). Using a one-point measurement, even if it is a fundamental property, cannot give an adequate representation in which aging affects asphalt properties. Second, the change in R indicates that aging cannot be represented by a shift factor along the logarithmic time scale. Such a shift cannot take into consideration the change in shape of the G^* master curve and the phase angle master curve.

Effect of PAV Aging on Failure Properties

The direct tension test procedure employed two specimen configurations. Initially, a large specimen with an end reinforcement was used to test a number of different temperatures and strain rates. A master curve for failure properties was constructed and a model was fitted to the master curve from the collected data. Later in the project, a new testing technique using plastic inserts and a laser measuring system was used. The changes in failure properties because of TFOT and PAV aging were evaluated using both configurations.

Figures 5.29 and 5.30 depict the master curves for the failure properties as measured using the earlier testing technique for asphalts AAK-1 and AAG-1 in the PAV-aged and the unaged conditions. The PAV aging was done at 60°C (140°F) for 6 days. The details of constructing the master curves and estimating the model parameters were described in a previous chapter. The results shown in the figures indicate that aging affects the failure strain master curves in two ways. First, it shifts the failure strain master curves to the right, indicating higher stiffness. Second, it changes the shape of the master curves. The changes

328

are reflected in an increase in the model parameters B1, B2, and B3. The changes are given in table 5.10 for the strain-to-failure master curves and the energy-to-failure master curve. Note that the shape factor has been kept the same so that the change in shape is reflected in parameters B1 and B3.

Using the new sample configuration with the laser measuring system, further evaluation of the effect of aging on failure properties was done. The testing included all eight core asphalts in the unaged, TFOT-, and PAV-aged condition. With the new technique, a single deformation rate of 1.27 mm/min (0.05 in./min) was used and the testing was done at three temperatures for each asphalt. The temperatures were not the same for all asphalts, nor were the aging treatments. The temperatures were instead selected to achieve a strain level of 1.0 percent, because this strain level was selected as the critical failure strain that may indicate the propensity of the pavement mixture to cracking.

Figures 5.31 and 5.32 depict the effect of aging on the stress-strain response of asphalts AAK-1 and AAG-1, respectively. The PAV aging was done at 100°C (212°F) for 20 hours. The results indicate that within the prefailure zone the rate of increase in stress required to keep the deformation rate constant increases with aging. This increase is the consequence of the increase in stiffness of the asphalts as a result of aging. Within the failure zone, the results indicate that failure strain decreases as a result of aging while the stress at failure increases. The results correspond with the reports many asphalt researchers have made that aging results in more brittle asphalts. The decrease in strain at failure reflects the brittleness or the strain tolerance of a material. The results collected for the eight core asphalts are listed in table 5.11. The decrease in failure strain because of aging is consistent for all asphalts, but the relative change is highly asphalt specific and depends on the temperature. The change in failure stress because of aging, however, does not show a consistent trend. For some asphalts, a significant increase in the failure-stress with aging is observed, while, for others, stress decreases when the PAV-aged material is compared with the TFOT-aged material.

Figures 5.33 and 5.34 reveal how the PAV aging changes failure properties. Using the failure strains measured at the different temperatures, the temperature at which the failure strain is equal to 2 percent can be estimated. The bar chart in the figure 5.35 depicts that temperature for the eight asphalts in unaged, TFOT, and PAV conditions. The trend of increasing the critical temperature correlates with the trend observed when considering the strain at a selected temperature. The critical temperature increases with aging and indicates that the transition from brittle to ductile zone shifts to a higher temperature. The relative change in the critical temperature appears to be different for different asphalts. For example, the change is approximately 9°C (16.2°F) for AAK-1 and AAF-1, while it is less than 3°C (5.4°F) for AAM-1 and AAC-1.

The results collected to date indicate that changes in failure properties are complex. The asphalts in general become more brittle, but the specific changes in the failure envelopes, figures 5.33 and 5.34, vary widely from one asphalt to the other. The results lead to the conclusion that no single parameter can be used to describe the changes that are caused by aging. Similar to the rheological properties, failure parameters that describe failure master curves or failure envelopes are needed in an attempt to create a comprehensive picture about

329

changes that are caused by aging. The relation between rheology and failure properties as described in an earlier chapter does not seem to be affected significantly by aging. The linear-inverse relation between stiffness at failure time and failure strain appears valid for the PAV-aged material and to have a similar proportionality constant. The main conclusion that can be drawn from the limited investigation of the effect of aging on failure properties is that aging changes failure properties significantly and that the susceptibility of asphalts to the process of oxidative aging is an important factor to consider.

Field Validation Test Results

The first objective of this experiment was to verify that the changes in the physical and chemical properties of asphalts that occur during the PAV-aging procedure, are similar to the changes that occur during long-term aging in the field. The second objective was to establish the link between aging levels that occur in the PAV at different aging times and aging temperatures and the aging levels in the field in several different environments. The latter objective was considered an initial step for calibrating the PAV procedure to reflect the long-term aging in different environments. It was beyond the scope of this study to establish a quantitative relationship between laboratory-aging parameters (aging temperature-time) and field-aging parameters that include service temperature-time as well as mixture variables. Such relationships were the responsibility of the SHRP A-005 contractor.

The criteria for selecting the test sections included the availability of original material, age of test section, feasibility of getting cores from these sections, and environmental conditions. Fourteen sections were selected for the experiment. Original asphalts stored since the time of construction were located and collected for testing. Information about pavement structure and history was gathered. The selected test sections are listed in table 5.12 with grades and dates of construction. The experimental plan is summarized in the flowchart in figure 5.36. As shown in the figure, original asphalts were treated in the TFOT and PAV and the properties measured for the unaged, TFOT-aged, and PAV-aged asphalts were studied in conjunction with the asphalts recovered from the test sections. The rheological, failure, and chemical properties were evaluated to compare the TFOT- and PAV-aging effects with the field-aging effects.

Asphalts from 12 sections were tested in unaged, TFOT-aged, PAV-aged conditions. Also, asphalts recovered from eight sections were tested for their rheological properties. Figures 5.37 and 5.38 show the results of the rheological testing for the asphalt from a section in Florida. The unaged, the PAV-aged, and the recovered master curves and temperature shift functions for the three conditions are shown. The results shown in the first figure clearly indicate that the changes in rheology because of the PAV highly resemble those that occur during field aging. The age of the sections whose asphalt properties are shown is approximately 8 years, and the section is located in a relatively moderate climate. The time-temperature shift functions, shown in figure 5.38, indicate that aging, whether in the PAV or in the field, results in minimal changes in the time-temperature shift functions. Figure 5.38 also indicates that the aging levels caused by aging in the PAV at 100°C (212°F) for 20 hours are very close to the aging levels occurring in that Florida section after 8 years. This

similarity in the shape of the master curves for aging of the PAV and recovered asphalts was also seen for another asphalt used in another section. Figures 5.39 and 5.40 show master curves for asphalt aged in the PAV and recovered from the pavement section in Wyoming. The same similarity between PAV aging and field aging can be seen. This section, however, is only 4 years old.

The two previous examples indicate that PAV aging results in aging effects that are similar to aging in the field. The examples also indicate that the relation between aging conditions in the PAV and the conditions in the field is not very simple. The results for the Florida section give an equivalent of 8 years in the field, while for the Wyoming section, the equivalent is only 4 years. The data collected for the other sections confirm the latter point. Figure 5.41 shows the master curves for another section in Florida, while figure 5.42 shows the master curves for an asphalt used in a section in the California desert. For the section in California desert, the PAV aging falls short of simulating the aging level in the field after only 4 years. The results clearly depict the role of climate and how the equivalency of the PAV aging should be evaluated relative to local pavement climate.

Effect of Mineral Surfaces

The influence of the interaction of mineral surfaces on asphalt oxidative aging, as reported in the literature, has been summarized earlier in this chapter. The conclusion from the review is that a physicochemical interaction takes place at the interface between the asphalt and the mineral aggregate that may significantly alter the oxidation mechanism and thus change the aging progression. The review also revealed that one of the best techniques for studying this phenomenon is to use asphalt-filler mastics and to characterize the changes by measuring the fundamental properties.

Based on that conclusion, an initial limited experiment was designed to mix two types of fillers with four SHRP core asphalts and study the aging behavior of the eight mastics produced. The PAV was used to age the mastics, and rheological testing using the dynamic shear rheometer was conducted to study the changes in rheological properties at selected temperatures. The fillers selected were calcite and quartz, which represent two extremes in surface chemistry. The asphalts selected included AAD-1, AAG-1, AAK-1, and AAM-1, which have extremely different chemical compositions. To limit the factors in the experiment, only one filler-to-asphalt ratio of 0.5 (by volume) was used for all mastics. The ratio was selected to represent a typical hot-mix asphalt mixture used in conventional pavements. Examples of the results of the experiment are shown in figure 5.43 that depicts the master curves for the unfilled asphalt AAM-1 with the master curves for the calcite and quartz mastics. Figure 5.44 depicts the changes in the shape of the master curve after aging with the PAV procedure. After evaluating the influence of the filler type on PAV aging for all four asphalts, it was observed that the filler effects are not important and cannot be considered significant when compared with the differences in aging of asphalts from different sources. An example of the aging results is shown in figure 5.45 the ratio of $G*$ after aging to $G*$ before aging.

The results of the initial experiment contradict some of the reported results concerning the influence of asphalt-mineral surface interactions on the oxidative aging mechanism. Therefore, further evaluation was considered. In this experiment only two asphalts (AAK-1 and AAG-1) were included but five fillers, representing SHRP-selected aggregates, were included. The 10 mastics were then tested for their rheological properties before and after aging with the PAV. The fillers were mixed in this experiment at a constant free asphalt ratio as calculated by the dry compaction method discussed by Anderson (1986). Table 5.13 lists the mixing proportions for each of the fillers. The table also includes other properties of the different fillers. The testing included low- and high-temperature rheological measurements. The results in terms of G^* and G'' at three temperatures are listed in table 5.14. The measurements were used to calculate aging indices at 10 rad/s and to conduct statistical analyses in an effort to evaluate the effect of the different fillers. The statistical analysis for all temperatures indicated that the mineralogy of the filler did not have an important effect on oxidative aging. For some combinations of filler type and temperature, the influence cannot be characterized as statistically insignificant, but the effect is not totally unimportant when compared with the effect of the asphalt source.

Summary and Conclusions

This part of the research program addressed the important subject of the oxidative aging of asphalt binders. The main objective was to develop an aging test to best simulate the long-term aging of asphalt binders in the field. The pressure aging vessel was recommended by the A-002A contractor as the optimum procedure for simulating field aging. The factors affecting the operation and the results of the PAV-aging procedure were evaluated and a practical procedure was developed. The effect of oxidative aging on the rheological and failure properties of the binders was evaluated using the new testing procedures developed in the project. The bending beam, the dynamic shear rheometer, and the direct tension test were used to measure the change in properties that are related to performance. The effect of volatilization and its contribution to hardening were studied in a limited experiment. The aging that resulted from the PAV procedure was compared with field aging in a field validation study that included a large number of pavement sections varying in location, asphalt used, and age. Finally, an experiment to evaluate the role of mineral surfaces interaction in binder oxidative aging was conducted. The results collected led the research team to the following findings:

- The aging of asphalt cements is asphalt specific and a screening test to warrant the asphalt cement with respect to long-term aging is justified as a specification tool.

- The pressure aging vessel is a viable procedure for simulating the long-term aging of asphalt binders in the field. The procedure is simple, efficient, and practical for specification use.

- Temperature is the most influential factor that controls the rate of aging in the field and in the PAV. Therefore, the temperature in the PAV should be selected to reflect the climate under which the asphalt will be used. The equivalency of the PAV aging to the age in

the field should be established based on the pavement temperature. This equivalency will be affected by mixture variables, especially air voids.

- Asphalt cements develop more than a simple hardness shift during oxidative aging. The time and temperature dependency, as reflected in the shape of the master curve and the temperature shift function, changes significantly during aging.

- The changes in failure properties during aging are complicated. In general, strain to failure under a given temperature and deformation rate decreases with aging. Asphalts become more brittle and exhibit less strain tolerance with aging. The changes for the same aging procedures are highly specific to asphalt.

- The PAV procedure results in changes in rheological properties, which closely resemble changes due to aging in the field.

- Based on testing a limited number of asphalt-filler mastics, the interaction between asphalts and mineral surfaces does not appear to alter the oxidation process of the binder.

- Aging under inert environments indicates that the loss of volatiles is a major contributor to hardening resulting from short-term accelerated aging at high temperatures.

- A specimen's position in the PAV, the commingling of different binders, and the amount of air flow in the PAV were found to bear no important influence on oxidation in the PAV. Temperature, film thickness, and time were found to be important factors that control aging levels in the PAV procedure.
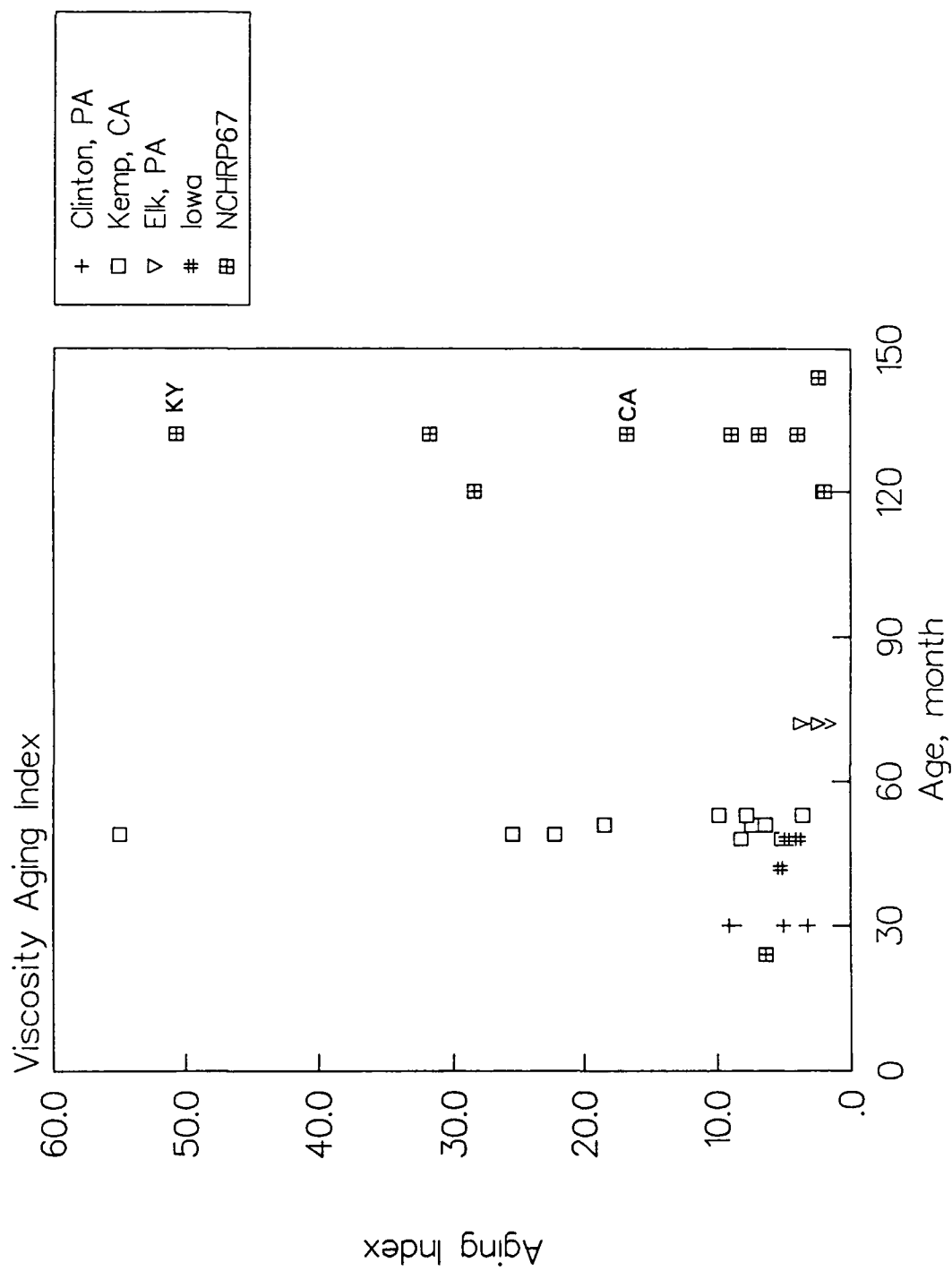
Figure 5.1 Viscosity Aging Indices at 60°C for Asphalts Recovered from Pavement Sections throughout the United States
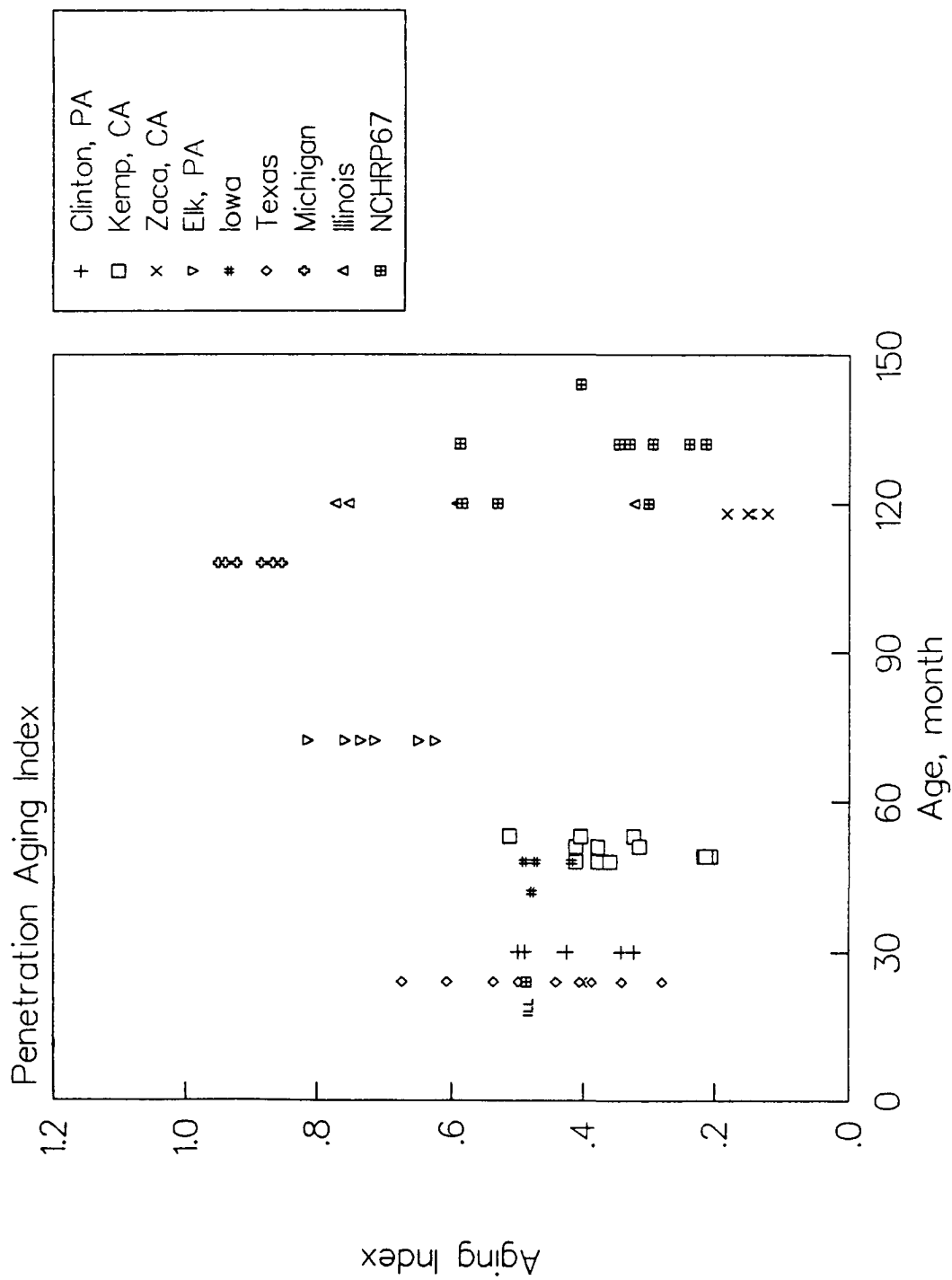
Figure 5.2 **Penetration Retention Ratio at 25°C for Asphalts Recovered from Pavement Sections throughout the United States**

335
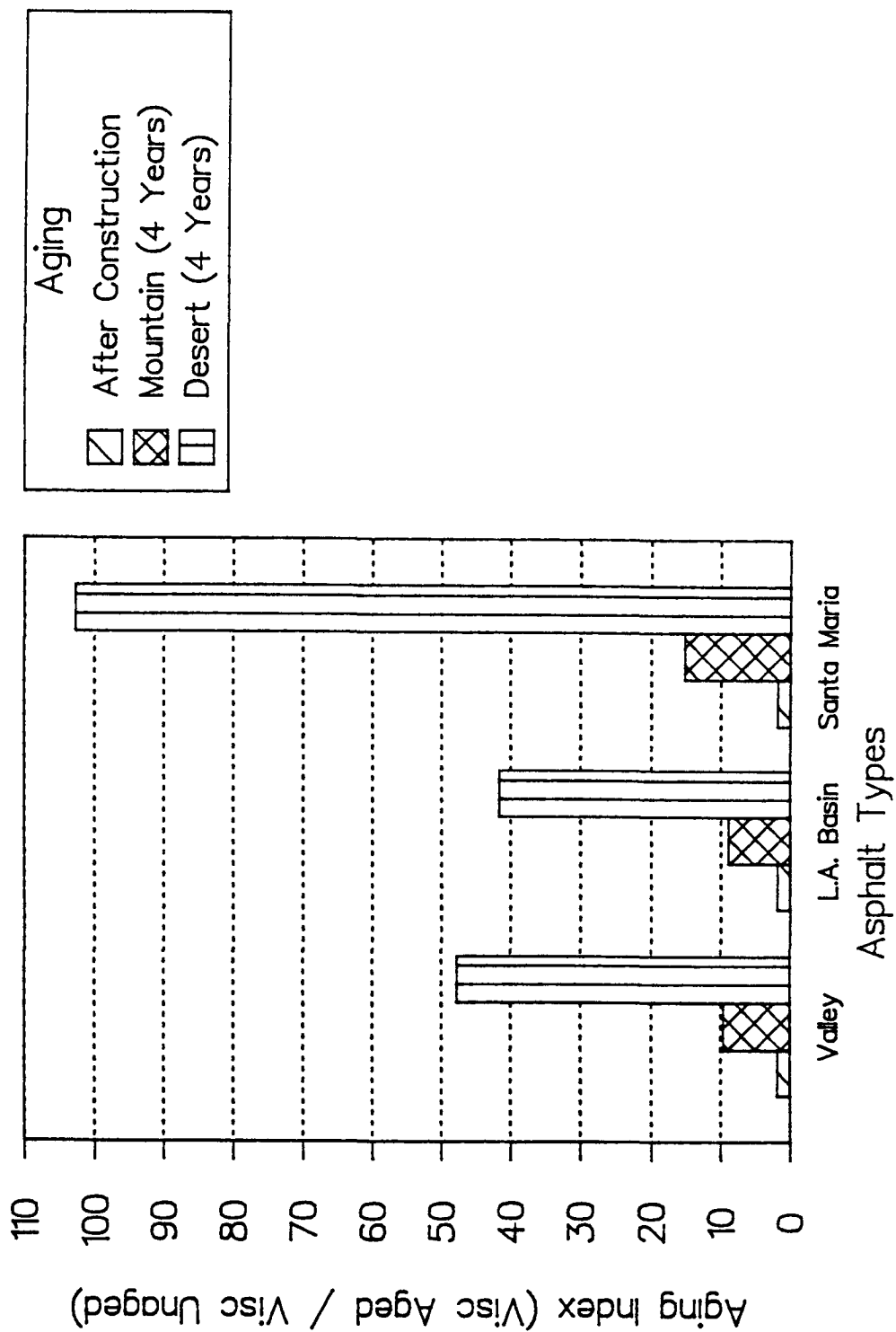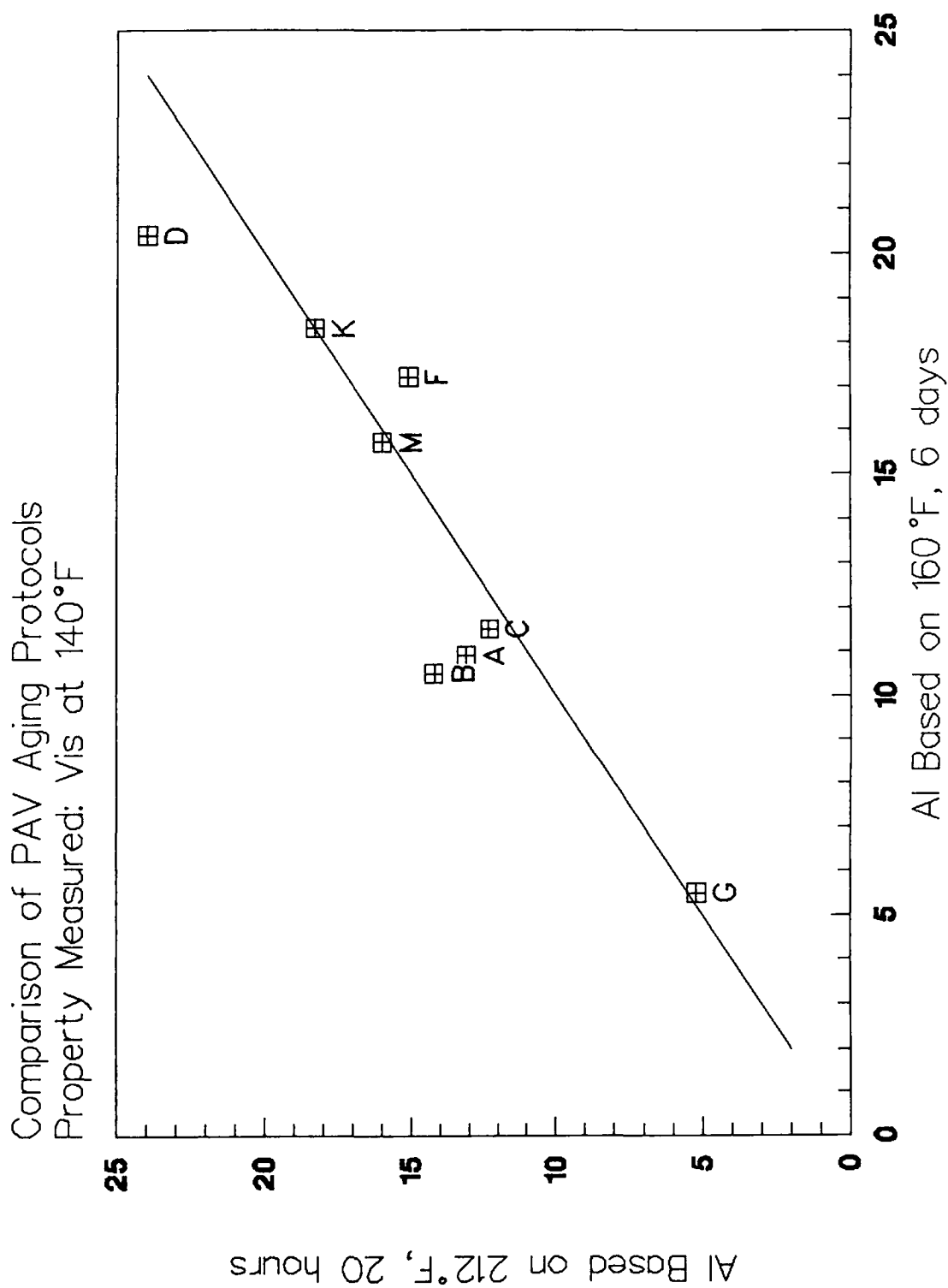
Figure 5.3 Effect of Climate on Aging Indices of Asphalts as Measured in Previous Study

336
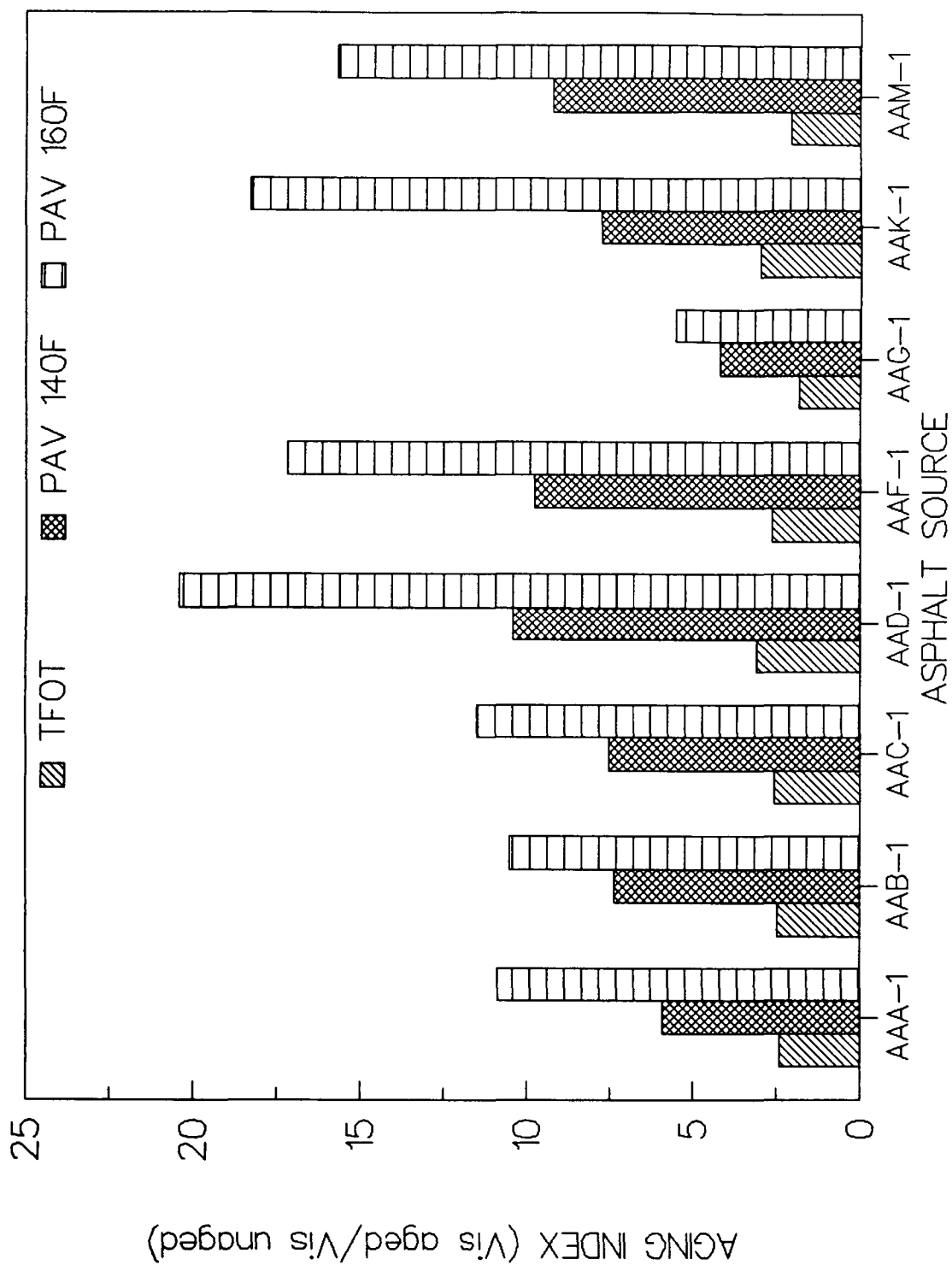
Figure 5.4 Comparison of the Aging Indices for the Core Asphalts after PAV Aging at 60°C and 71°C for 6 Days

337

Figure 5.5   Comparison of Aging Indices from Aging at 100°C for 20 hrs with Those Resulting from Aging at 71°C for 6 Days

338
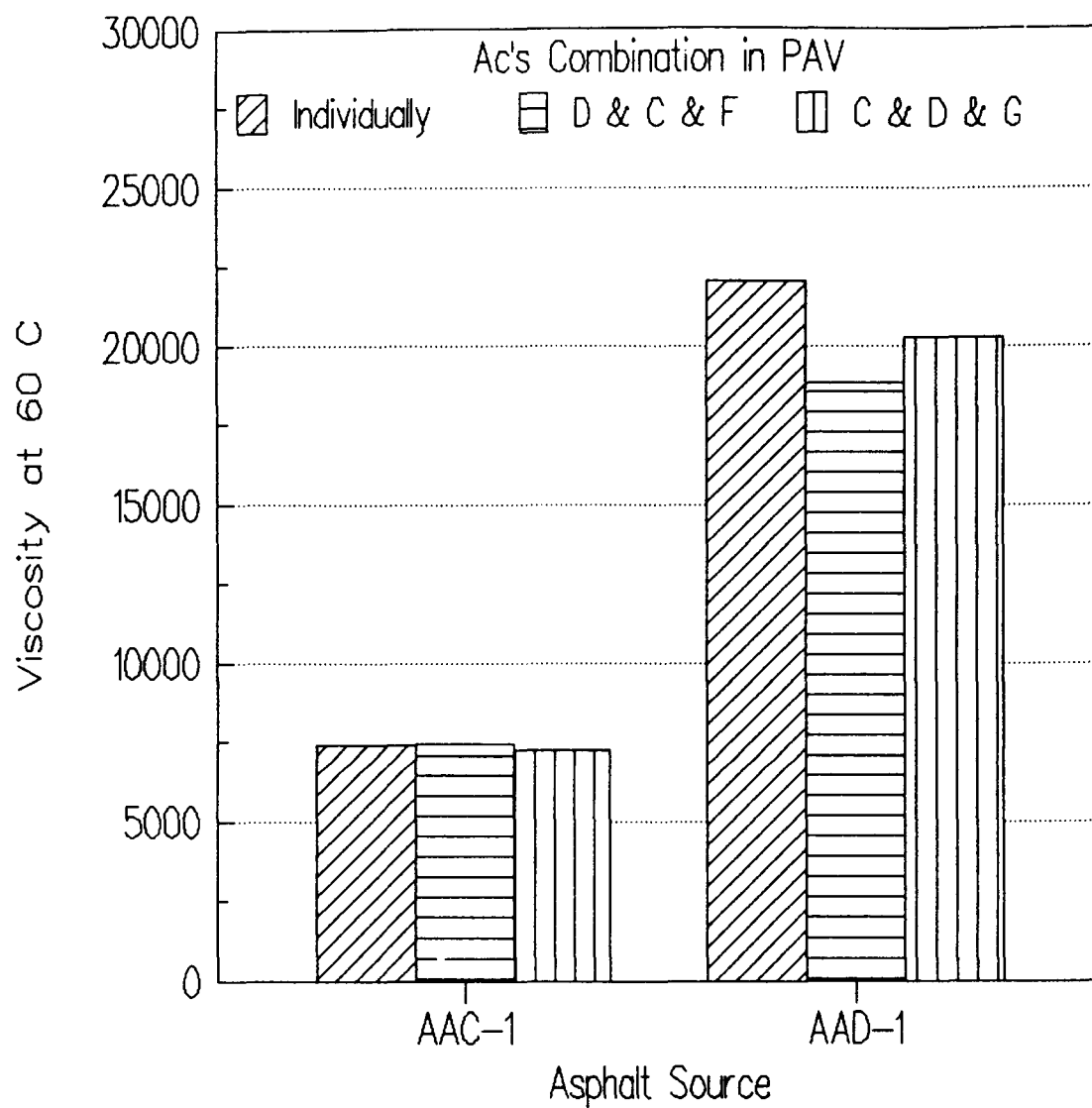
Figure 5.6   Results of the Asphalts Commingling Experiment in the PAV
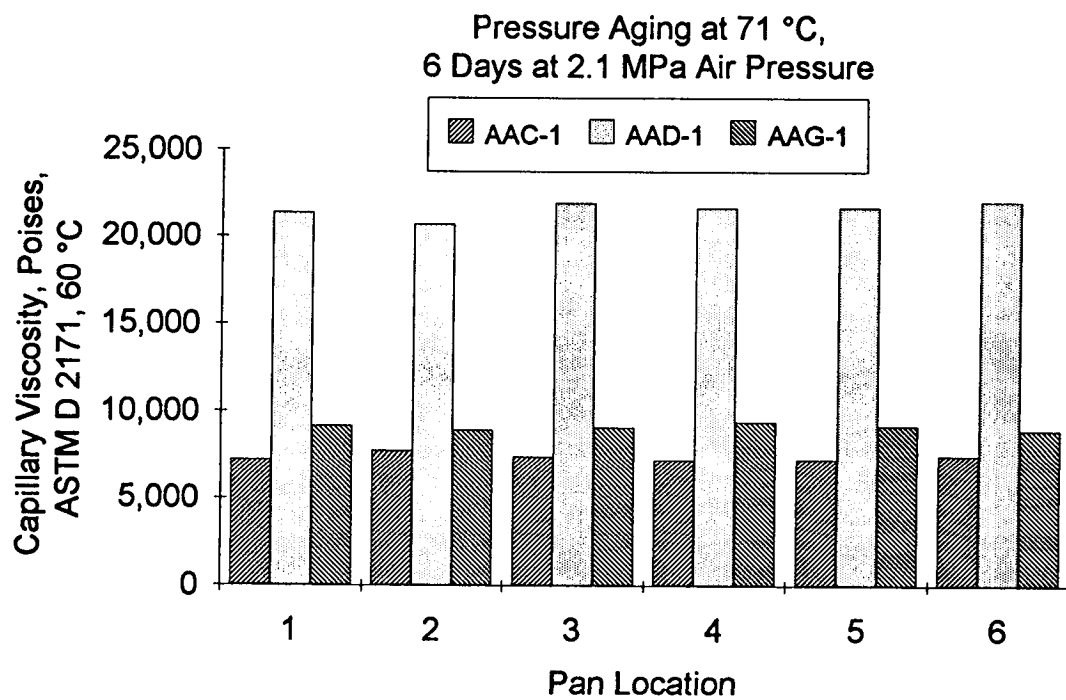
Figure 5.7 Effect of Location in the PAV on Asphalt Aging
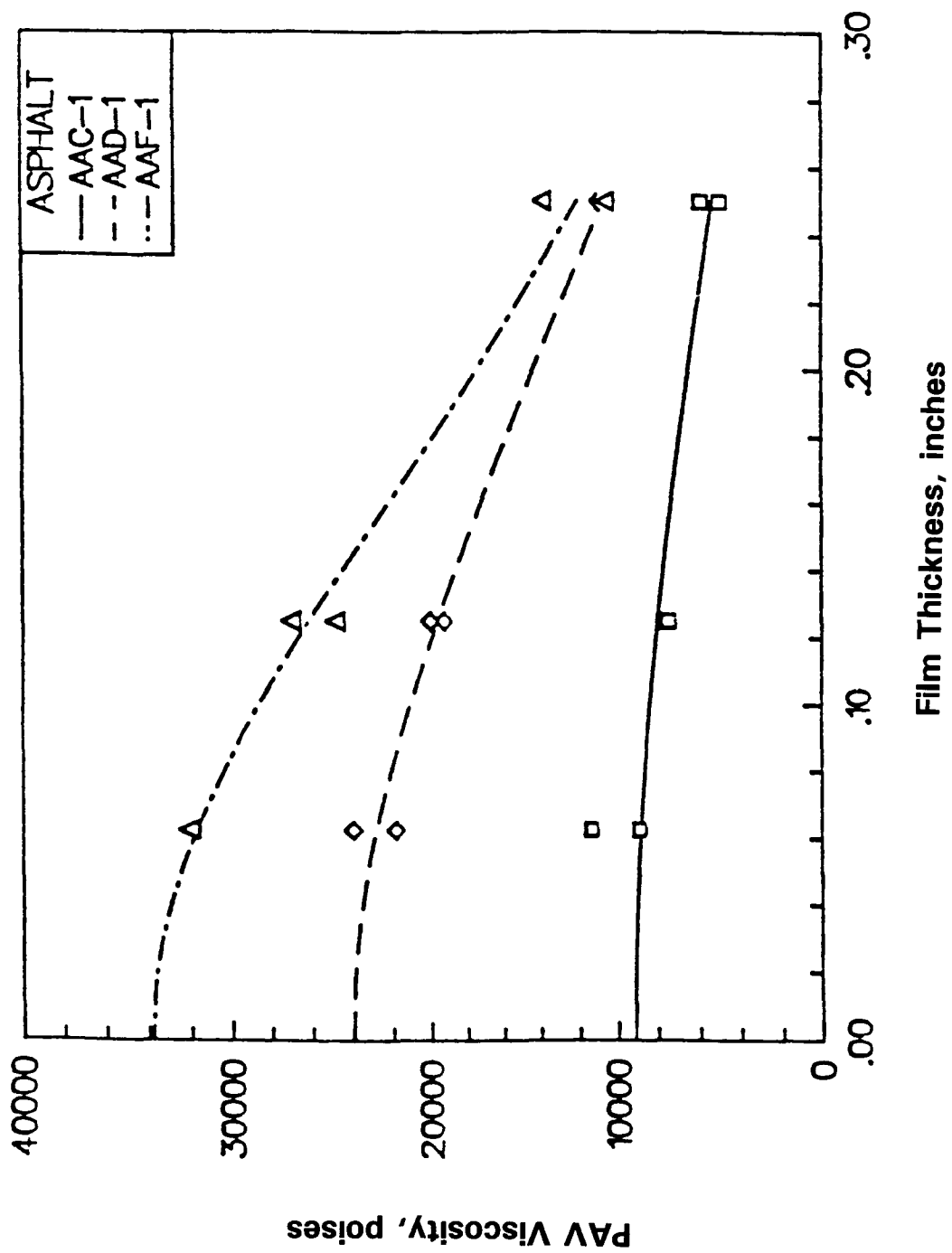
Figure 5.8   Effect of Film Thickness on Asphalt Aging in the PAV (144 hrs, 60°C), as Measured by Viscosity at 60°C

341
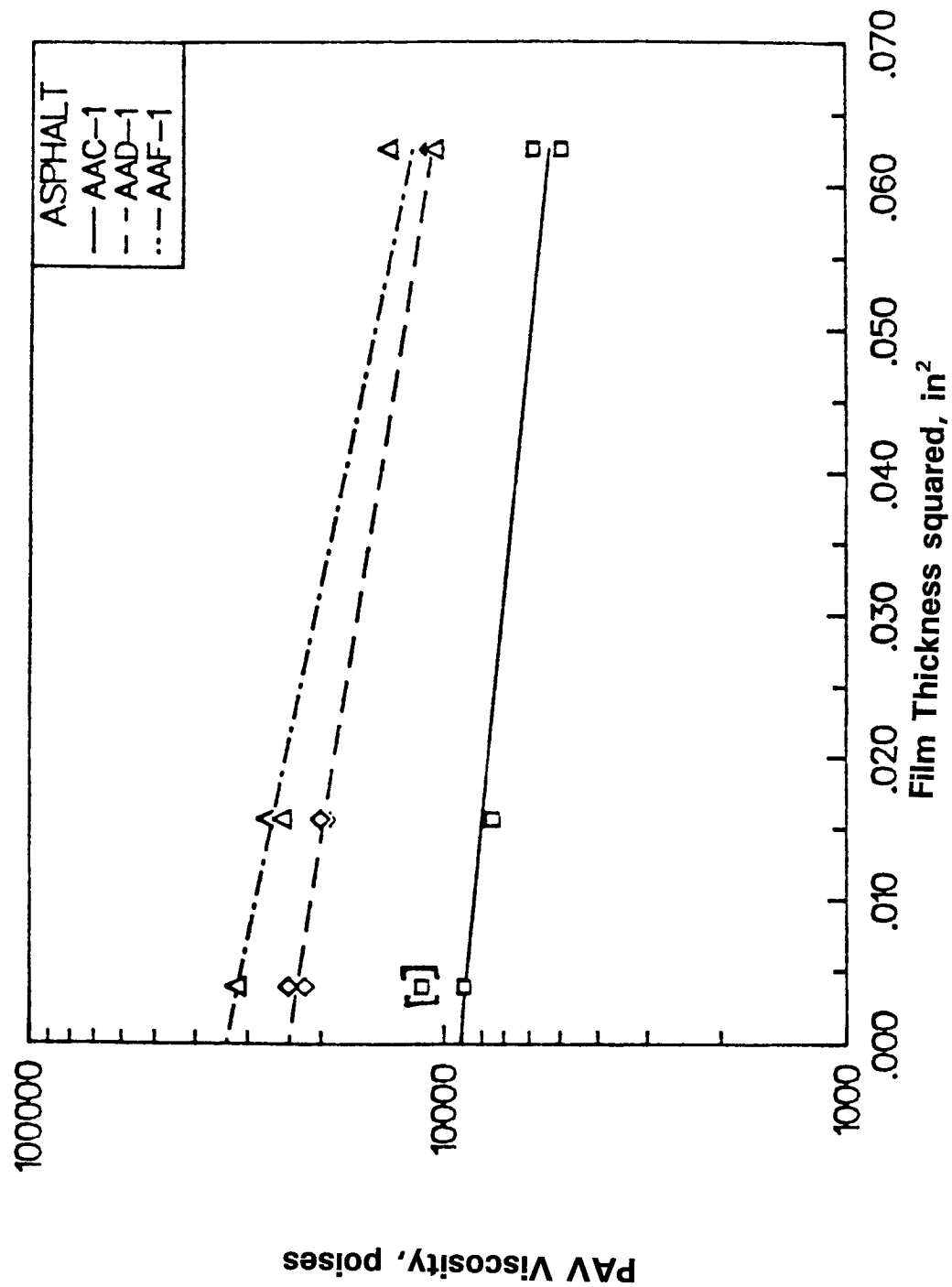
Figure 5.9 Relation Found for Effect of Film Thickness in the PAV on Increase in Aging Levels

342
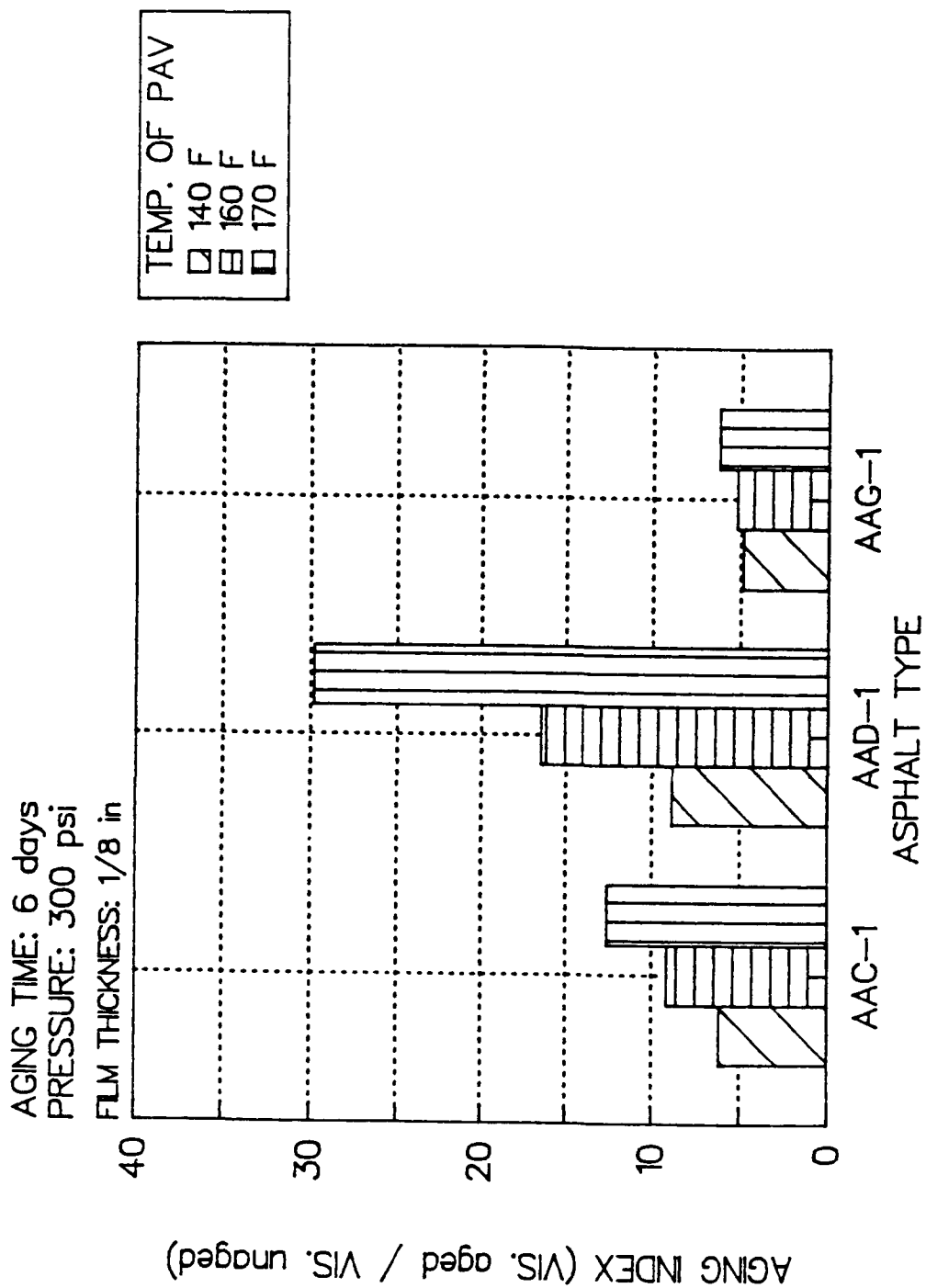
Figure 5.10 Effect of PAV Temperature on Asphalt Aging in the 144-hr Procedure
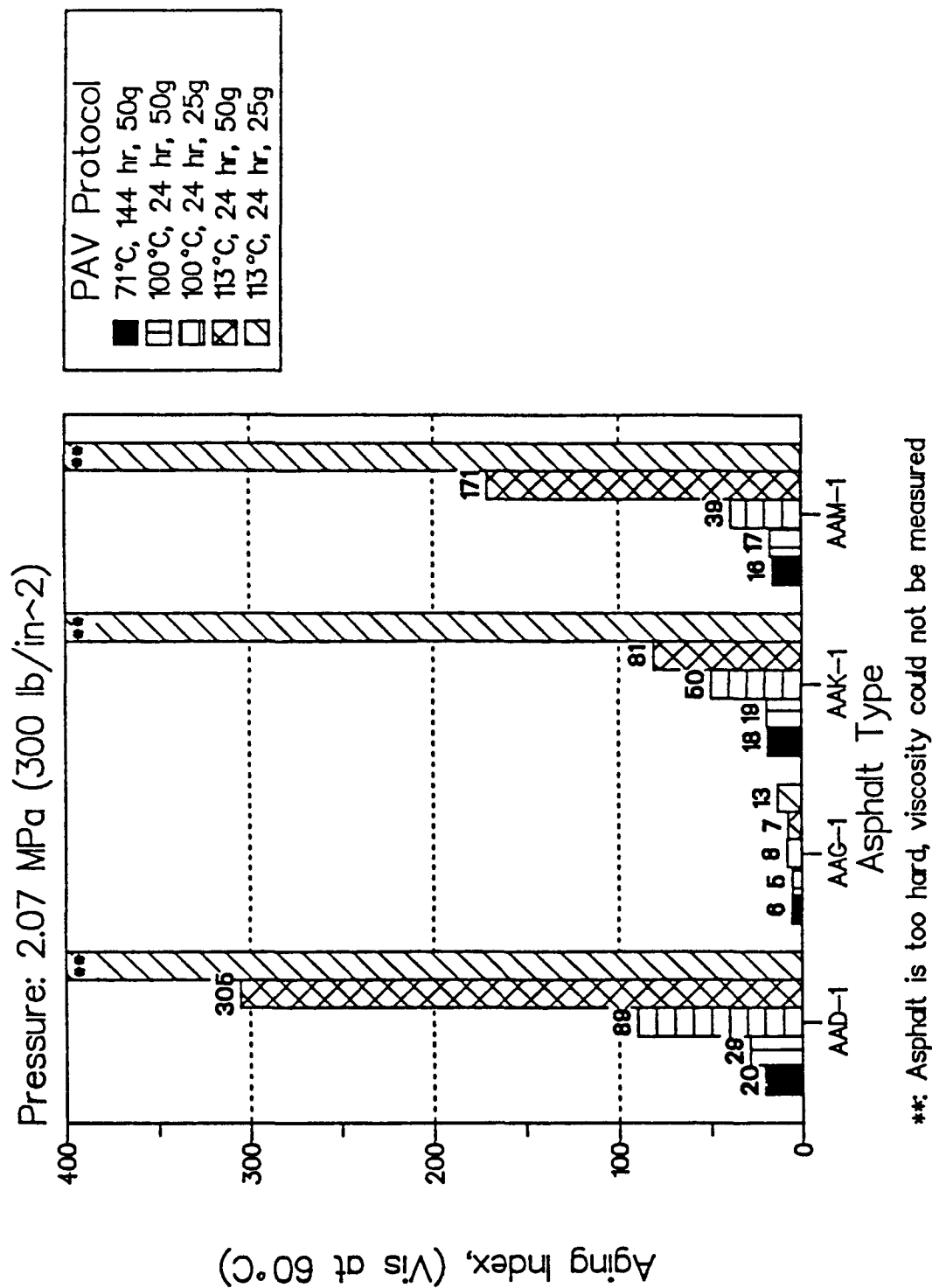
Figure 5.11 Effect of PAV Temperature and Film Thickness on Aging of Asphalts in the 24-hrs Procedure at High Temperatures
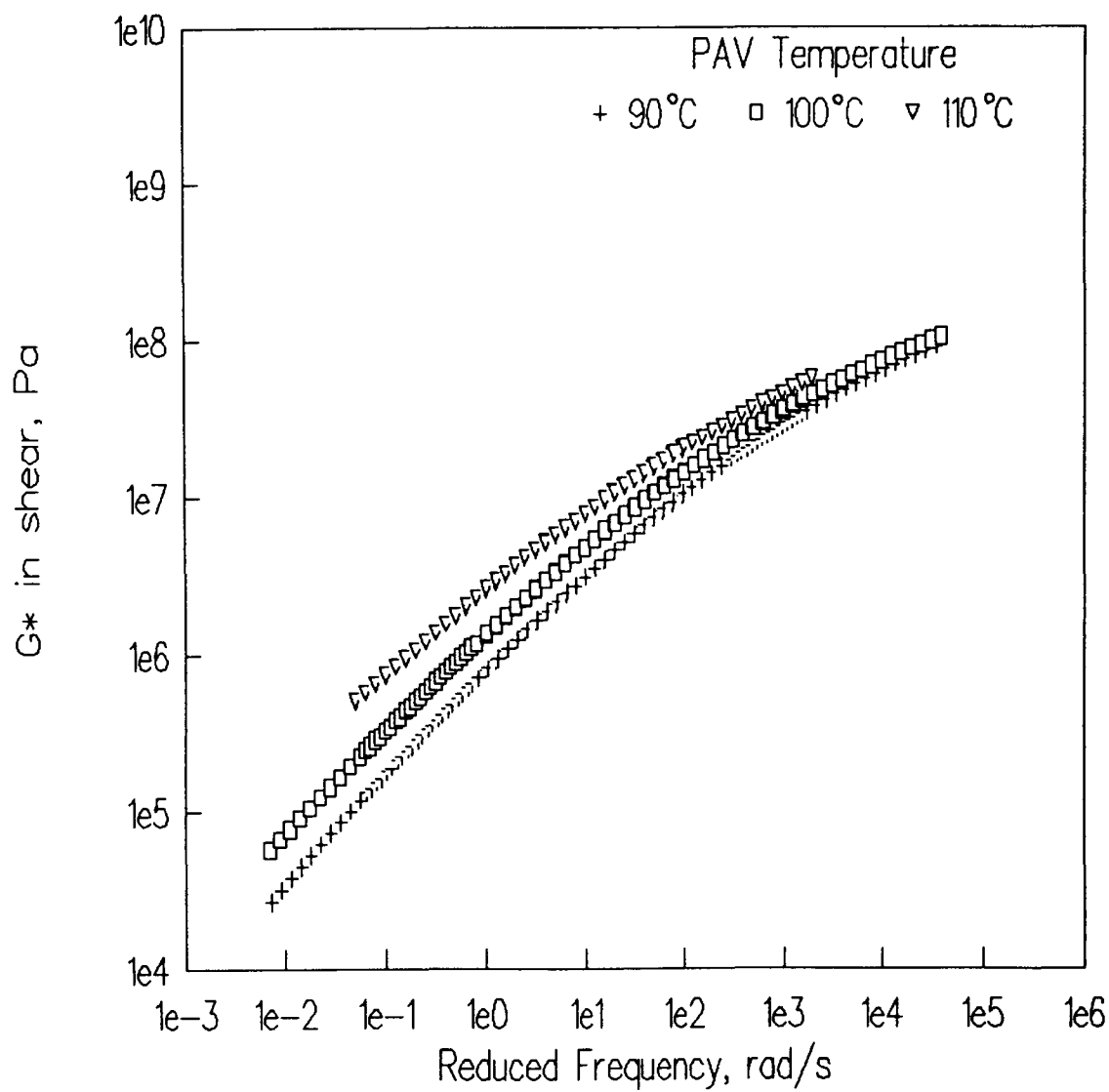
Figure 5.12   Changes in Rheological Master Curve of Asphalt AAK-1 upon Aging in the PAV at Different Temperatures
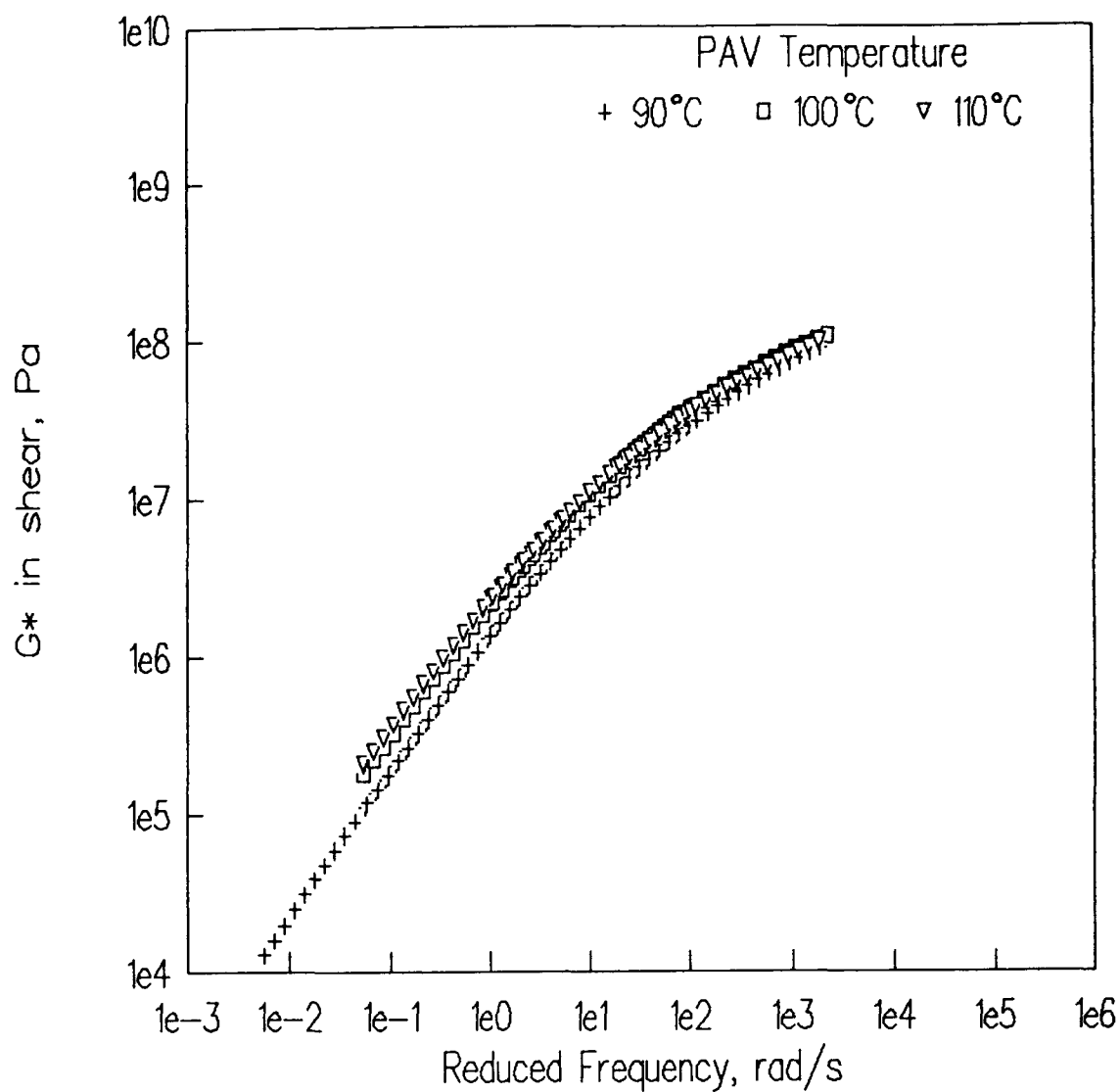
Figure 5.13   Changes in Rheological Master Curve of Asphalt AAG-1 upon Aging in the PAV at Different Temperatures
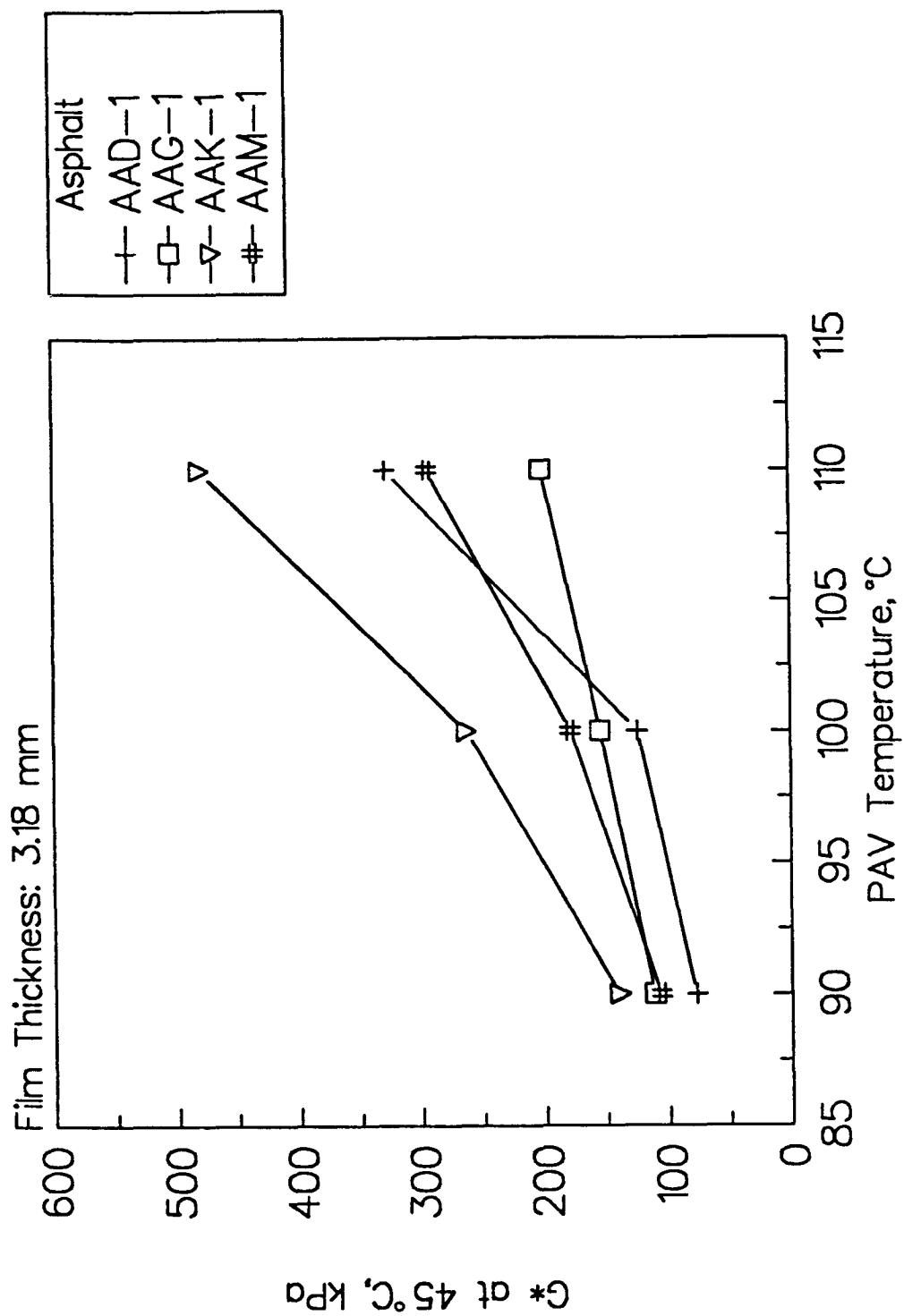
Figure 5.14   Effect of PAV Temperature on Aging of Asphalts for the 20-hr Procedure
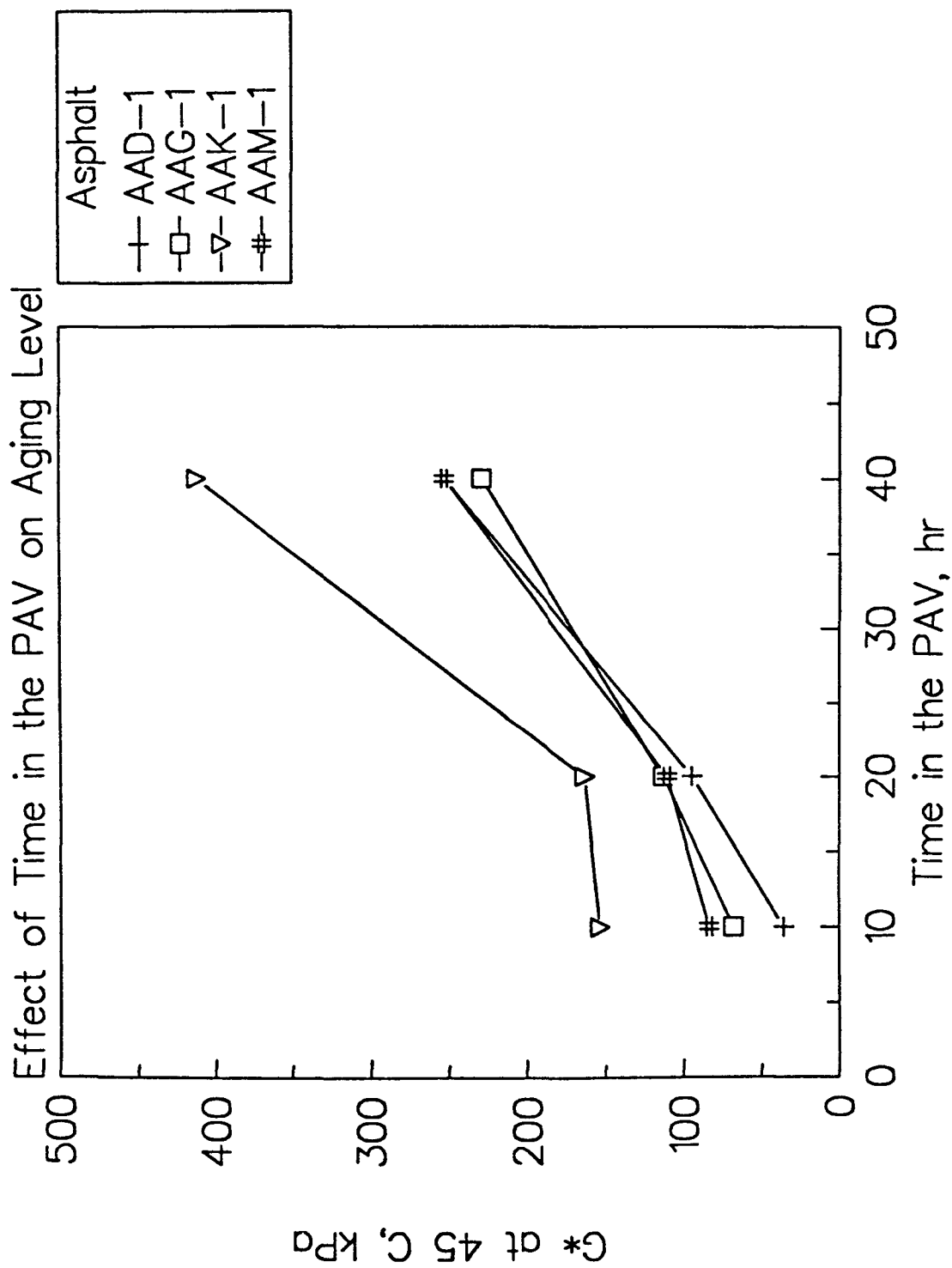
Figure 5.15 Effect of Aging Time in the PAV on Aging of Asphalts at the Aging Temperature of 110°C

348
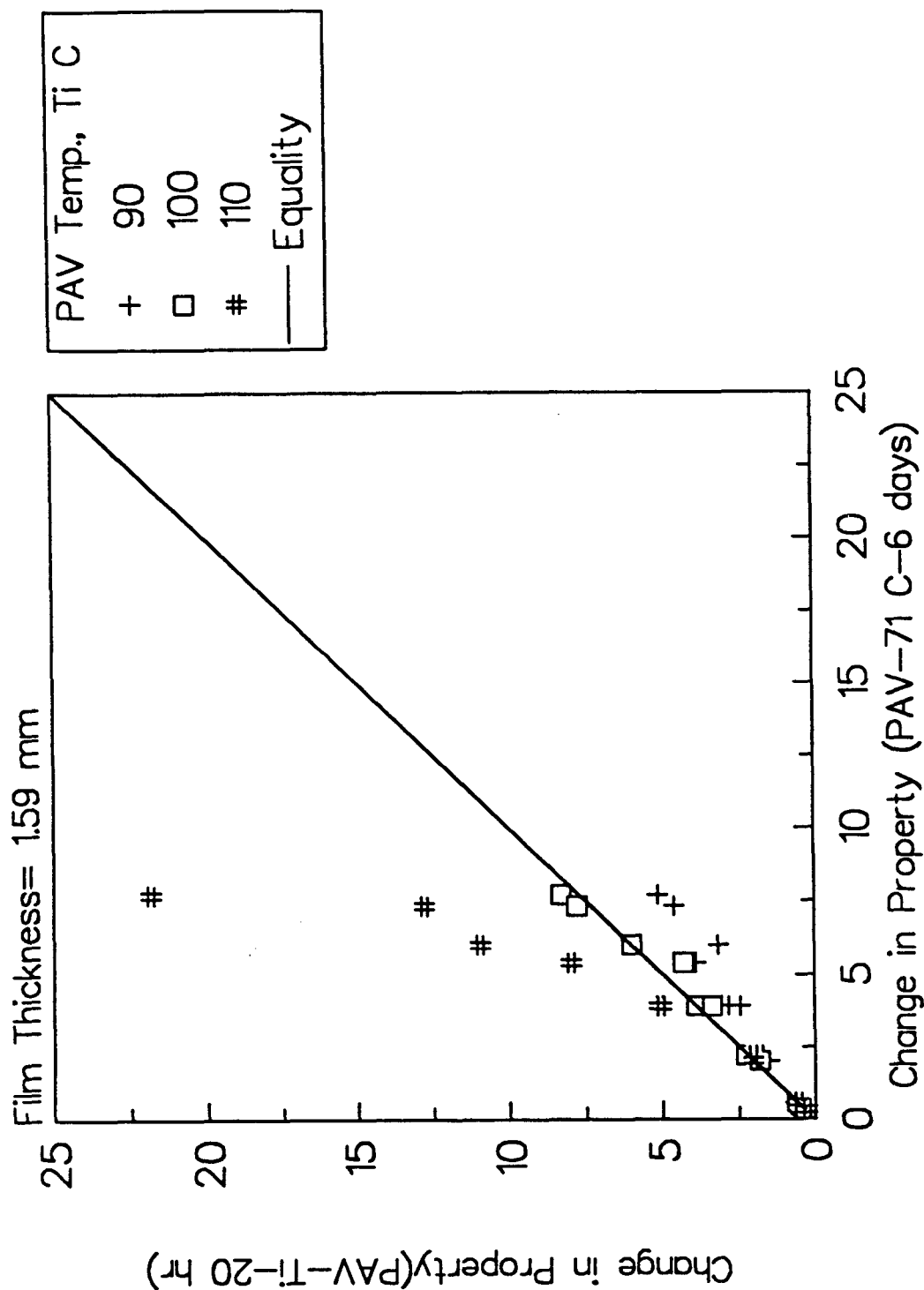
Figure 5.16 Equality Plot Depicting the Comparison between Hardening Because of PAV Aging Done at Different Aging Temperatures and the 71°C, 6-Day Hardening

349

Figure 5.17 Equality Plot Depicting the Comparison between Hardening Because of PAV Aging Done at Different Aging Times and the 71°C, 6-Day Hardening
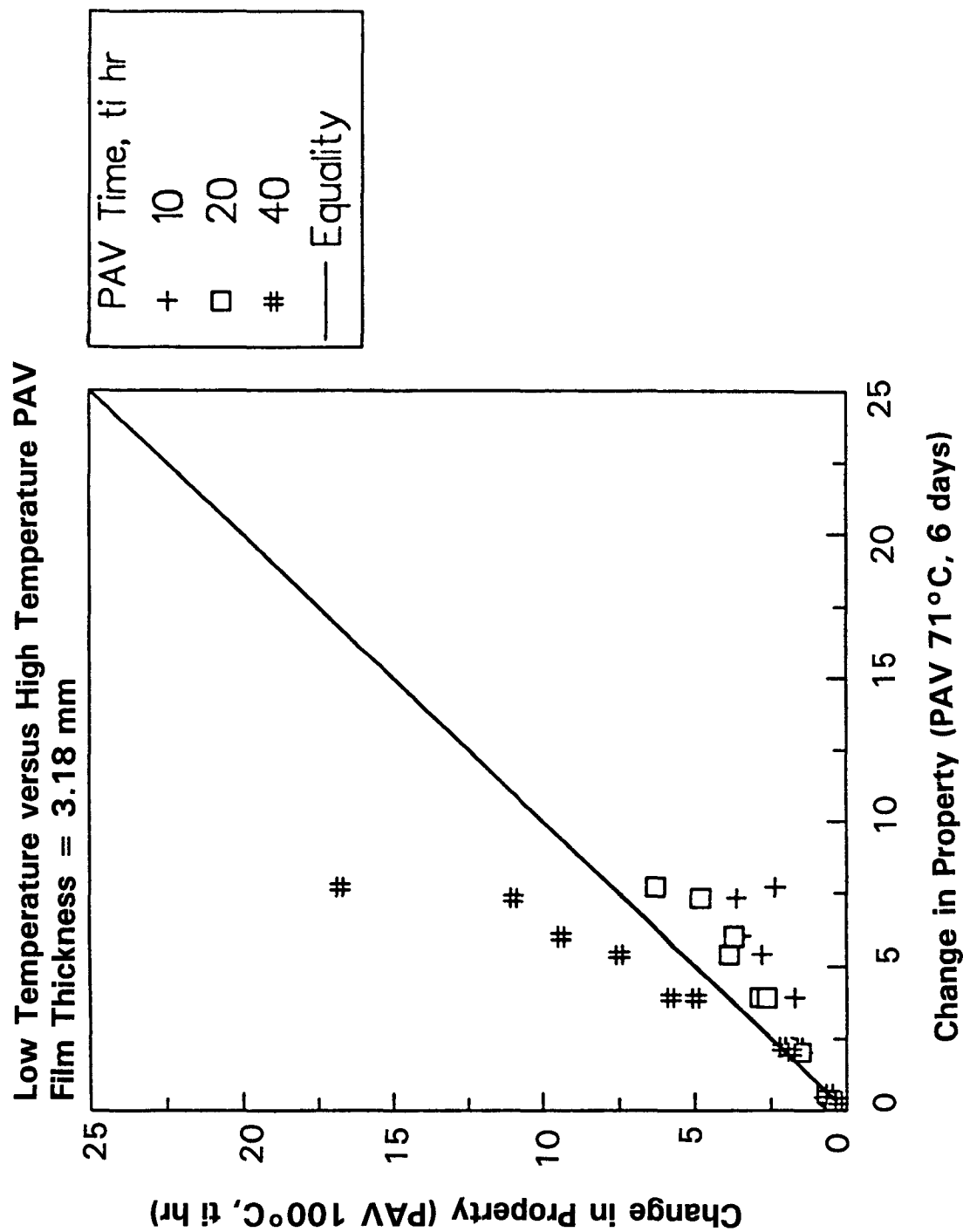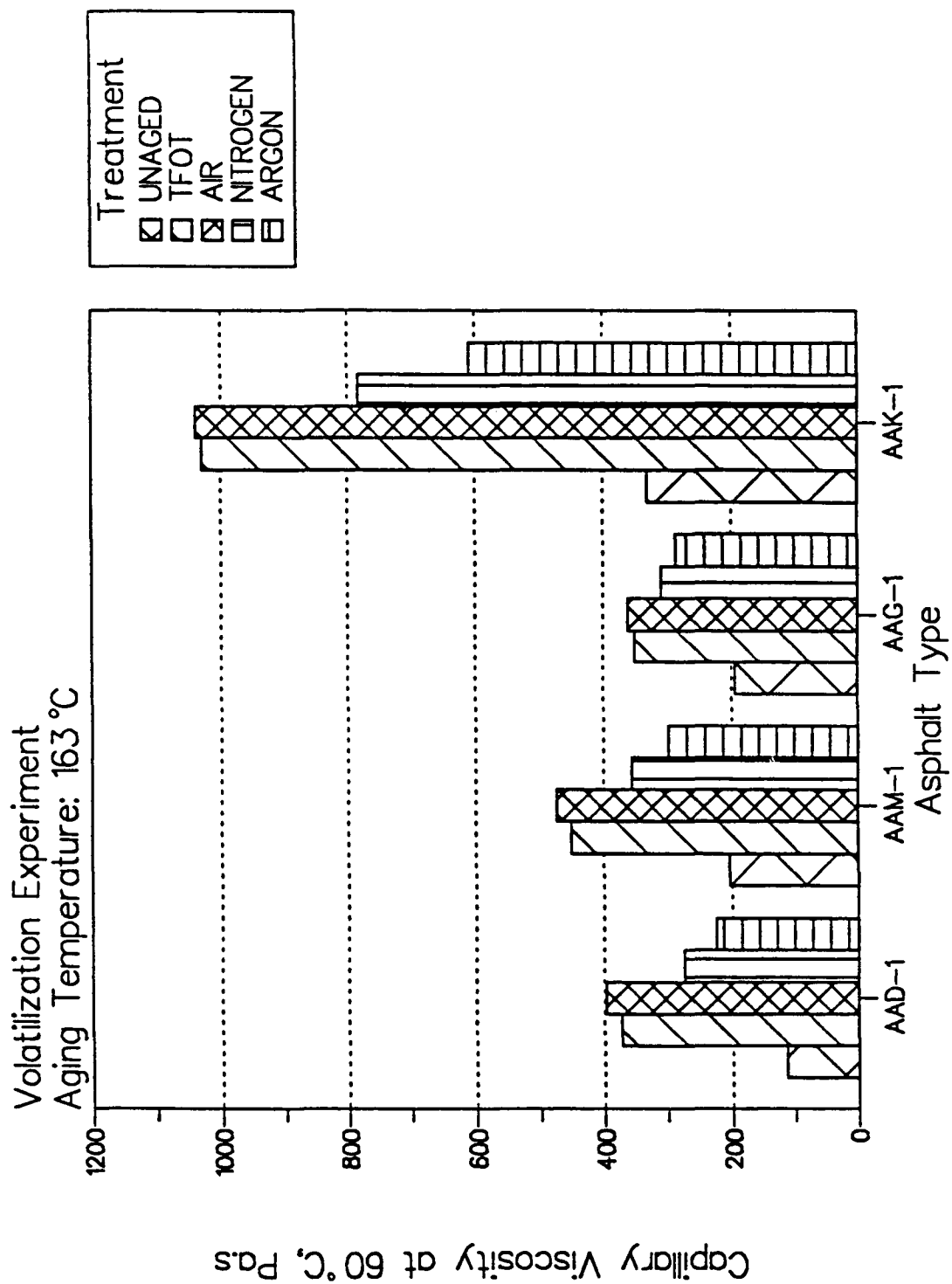
Figure 5.18 Change in Viscosity at 60° under Different Aging Environments in the Modified TFOT Oven
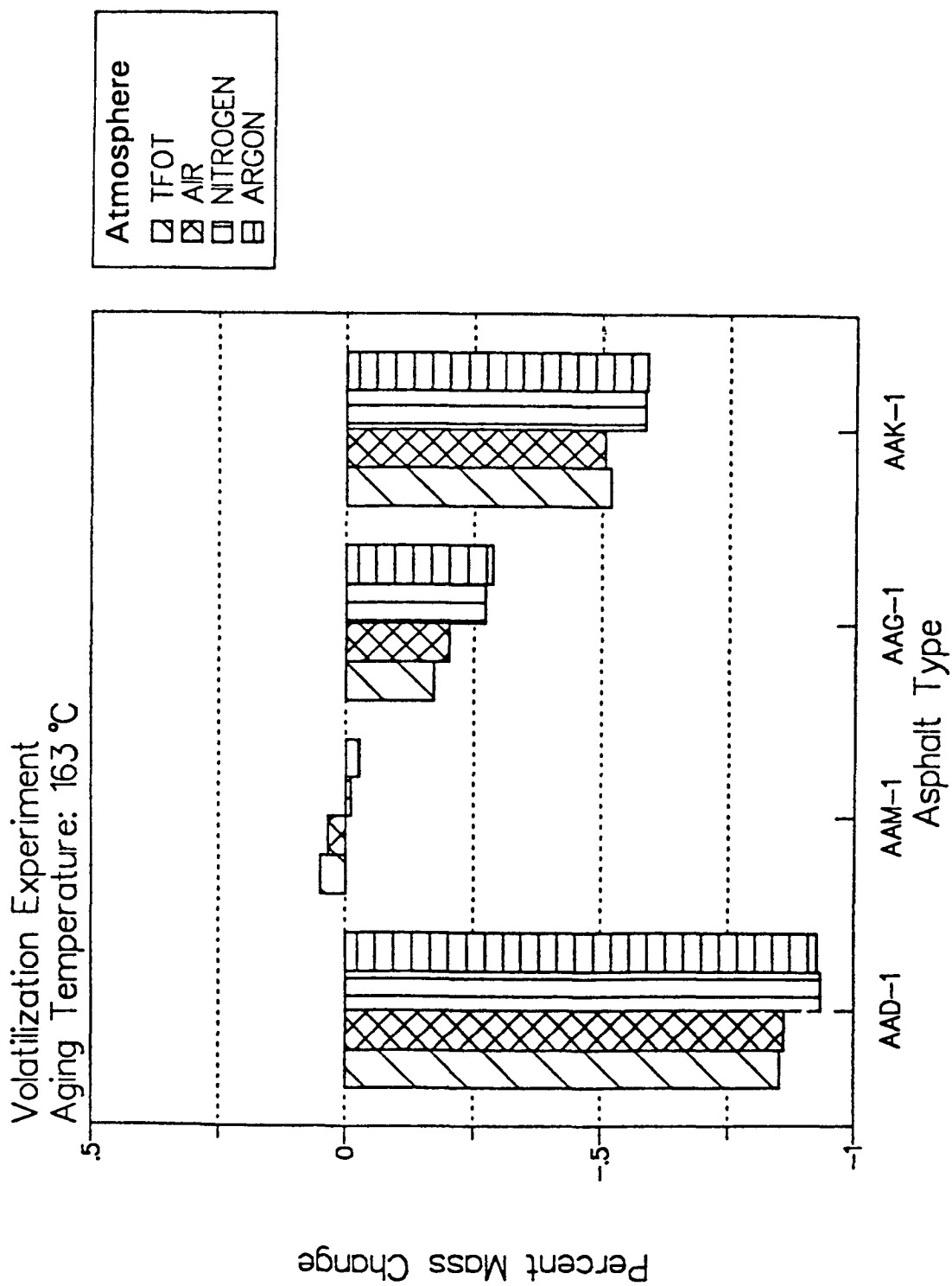
Figure 5.19 Change in Mass Change under Different Aging Environments in the Modified TFOT Oven
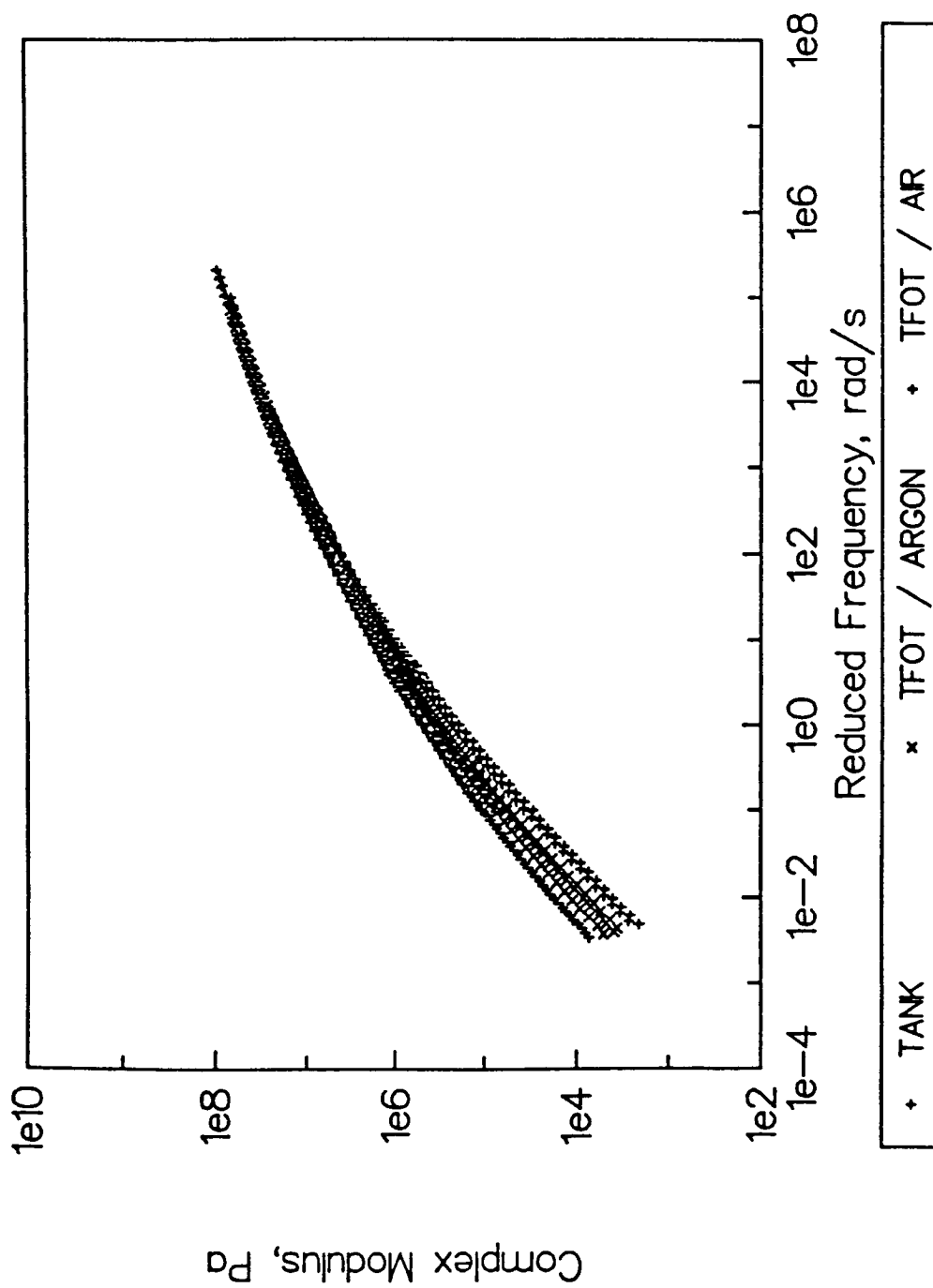
Figure 5.20 Master Curves for Asphalt AAM-1 before and after TFOT Treatment under Different Environments
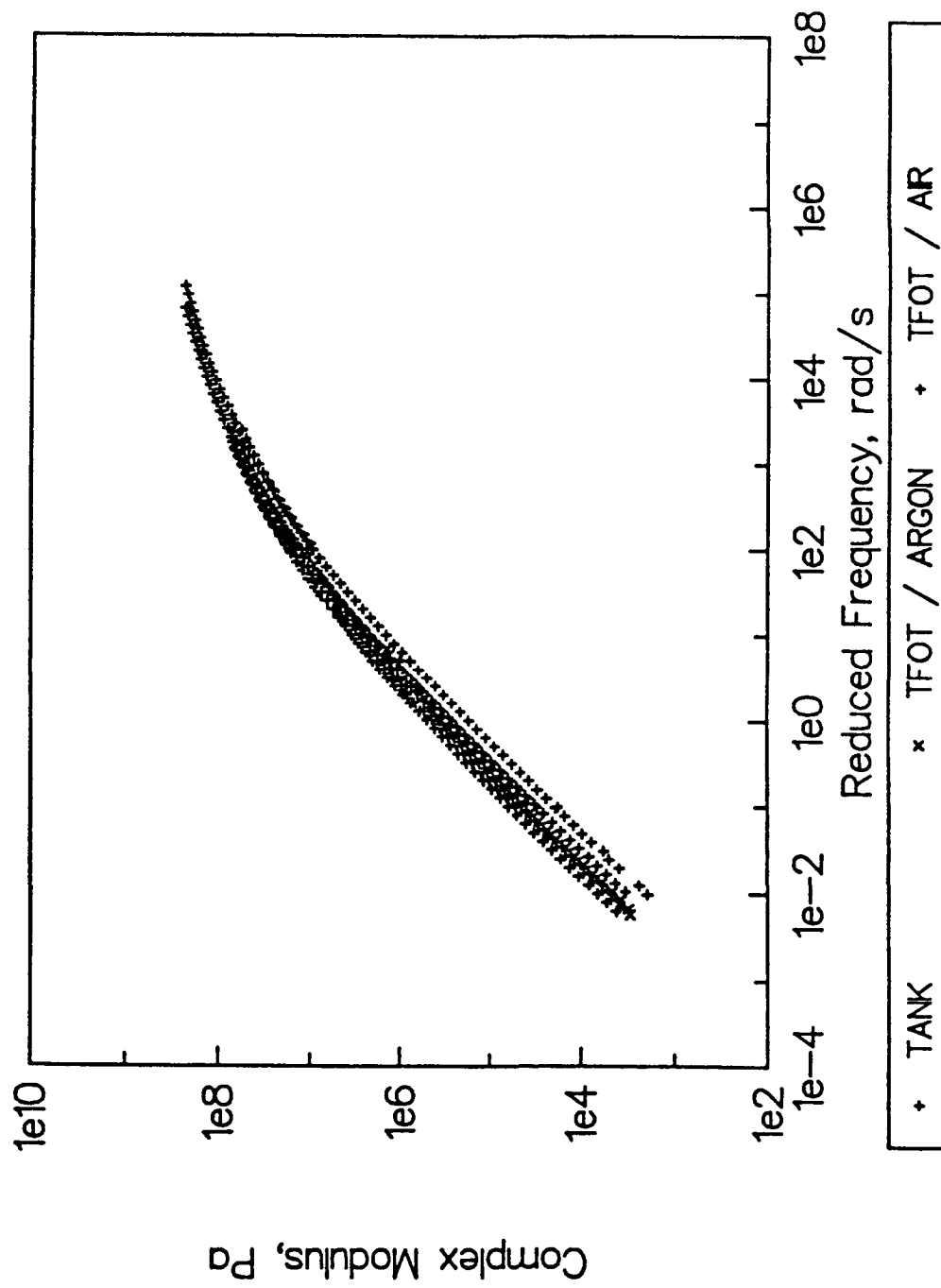
Figure 5.21 Master Curves for Asphalt AAG-1 before and after TFOT Treatment under Different Environments
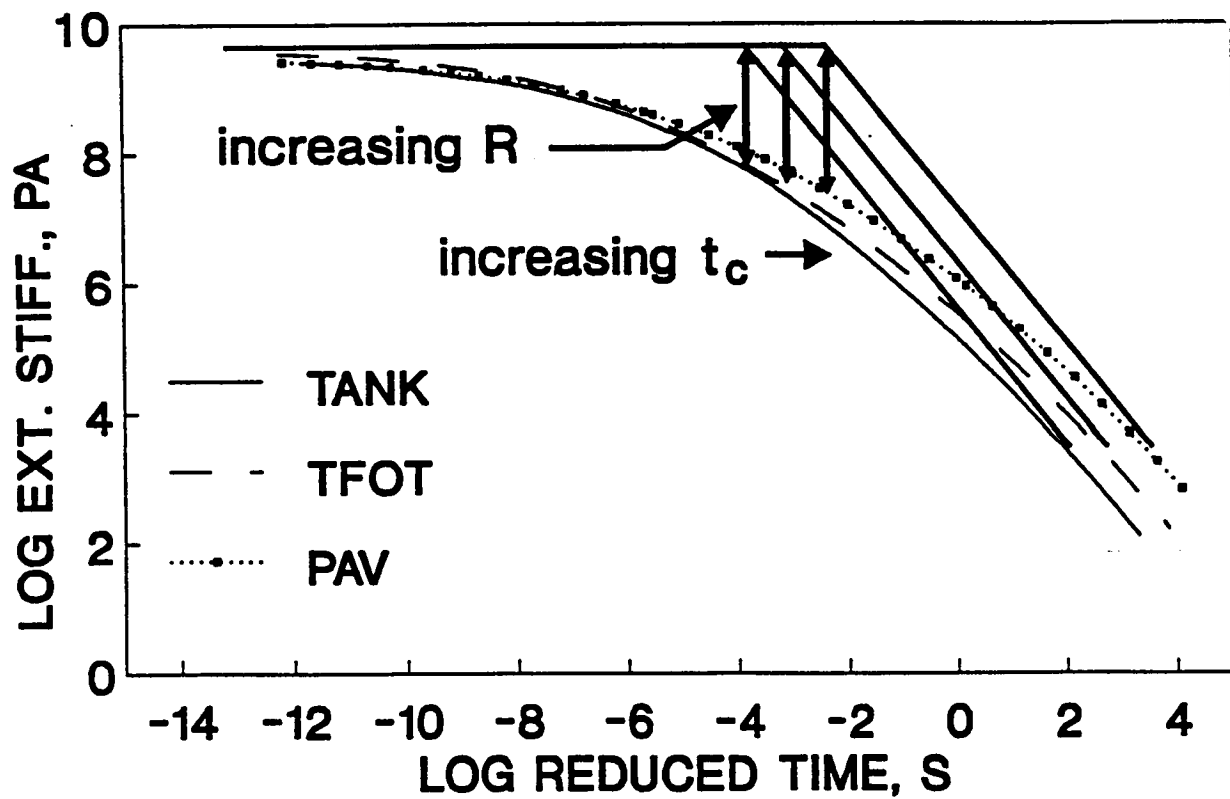
Figure 5.22 Changes in Rheological Master Curve of Asphalt AAD-1 after Aging with the PAV at 60°C for 144 Hours
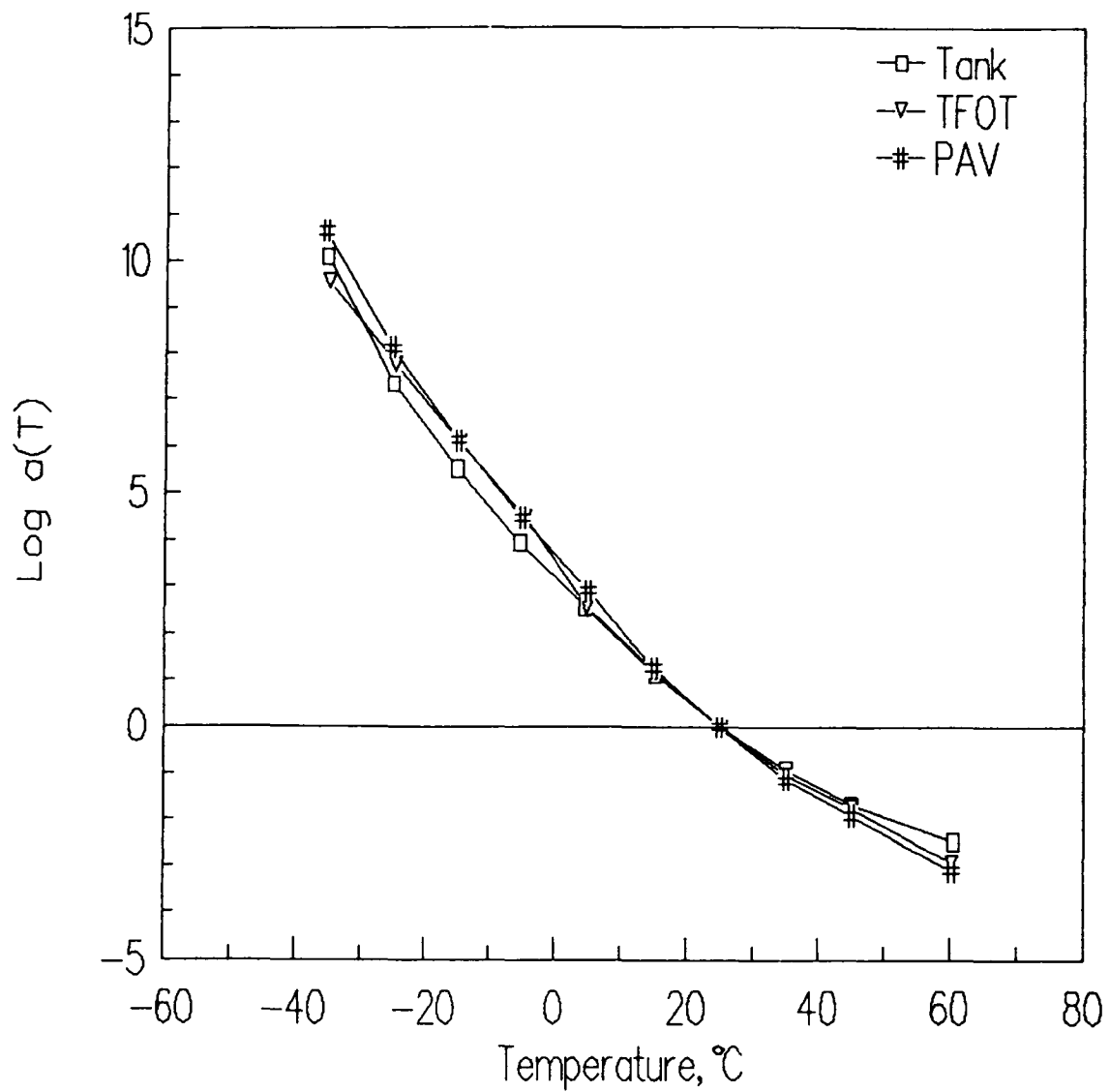
Figure 5.23 Change in Temperature Shift Function for Asphalt AAD-1 after Aging in the PAV
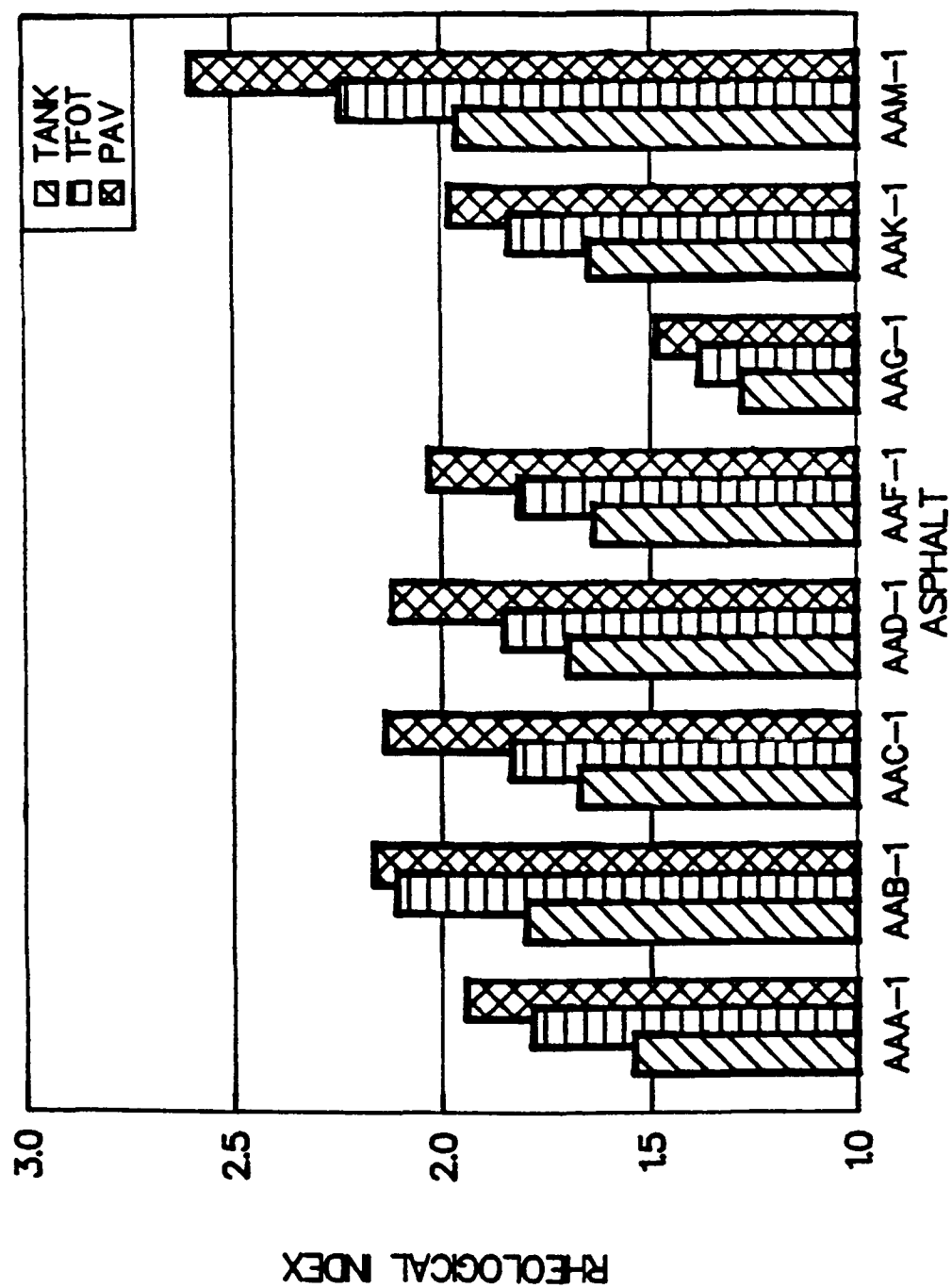
Figure 5.24 Changes in the Rheological Index (R) after Aging in the TFOT and the PAV for the Eight Core Asphalts

357
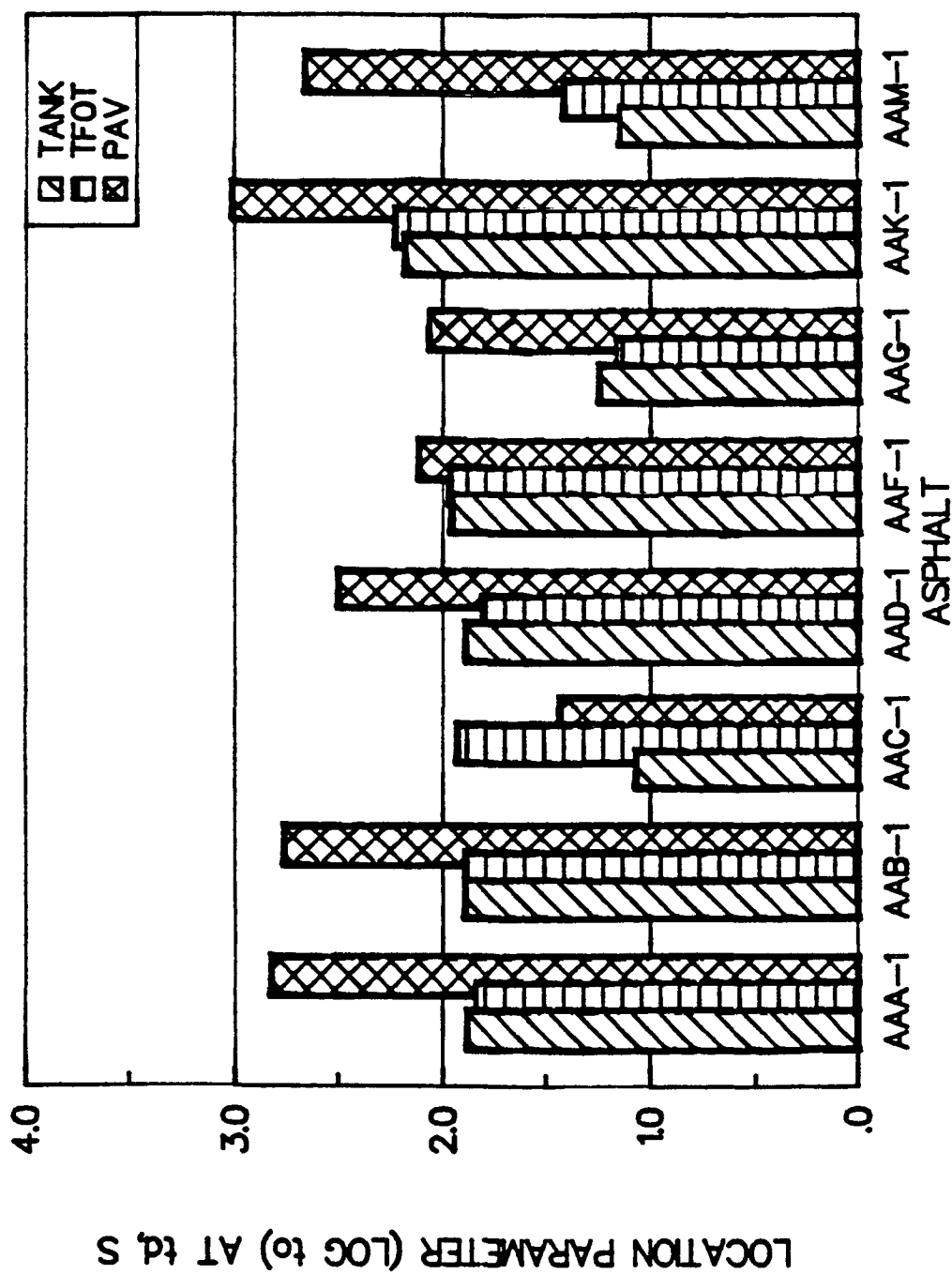
Figure 5.25 Changes in the Crossover Frequency (Log ω_o) after Aging in the TFOT and the PAV for the Eight Core Asphalts

358
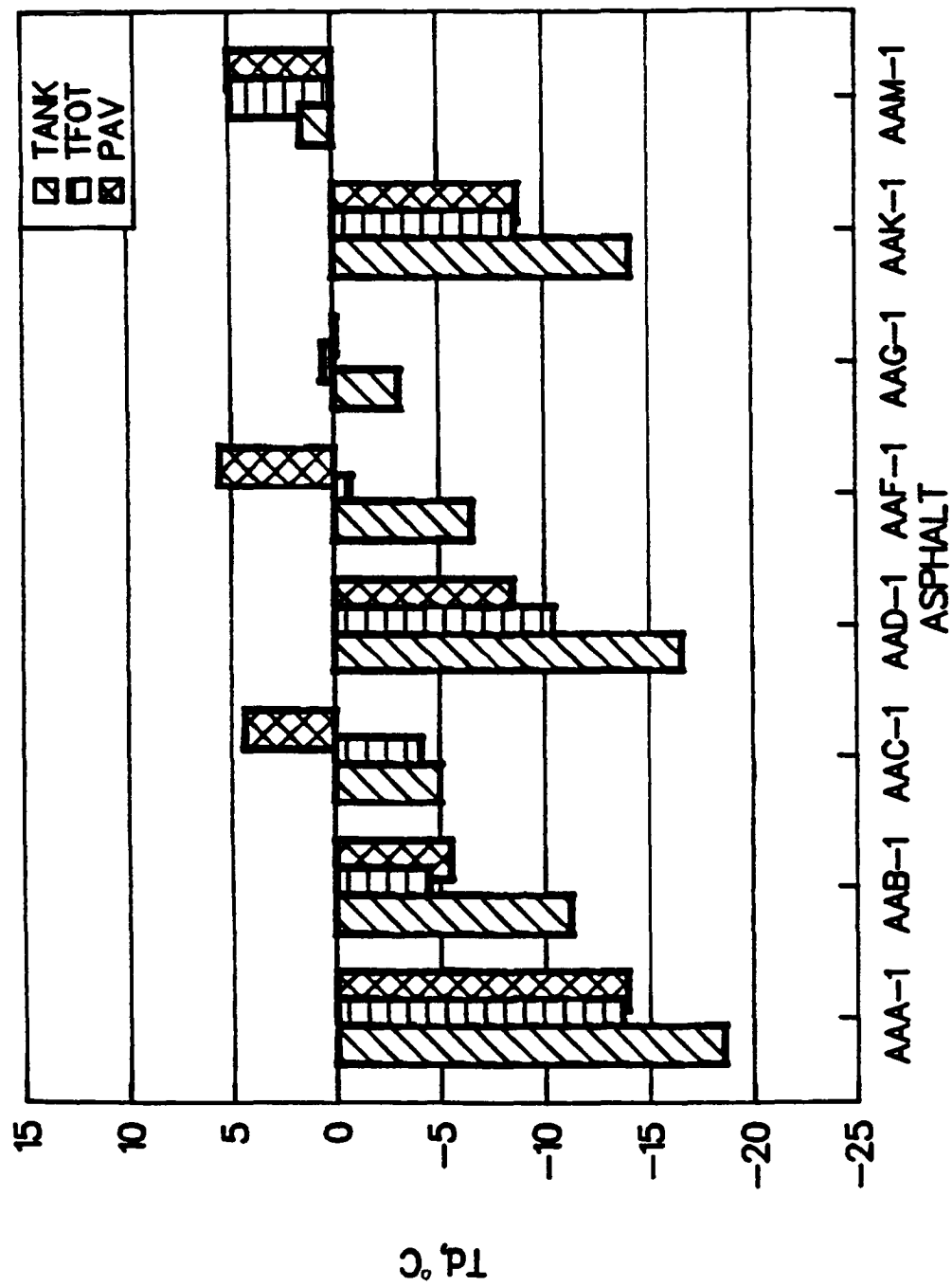
Figure 5.26 Changes in the Defining Temperature T_d after Aging in the TFOT and the PAV for the Eight Core Asphalts
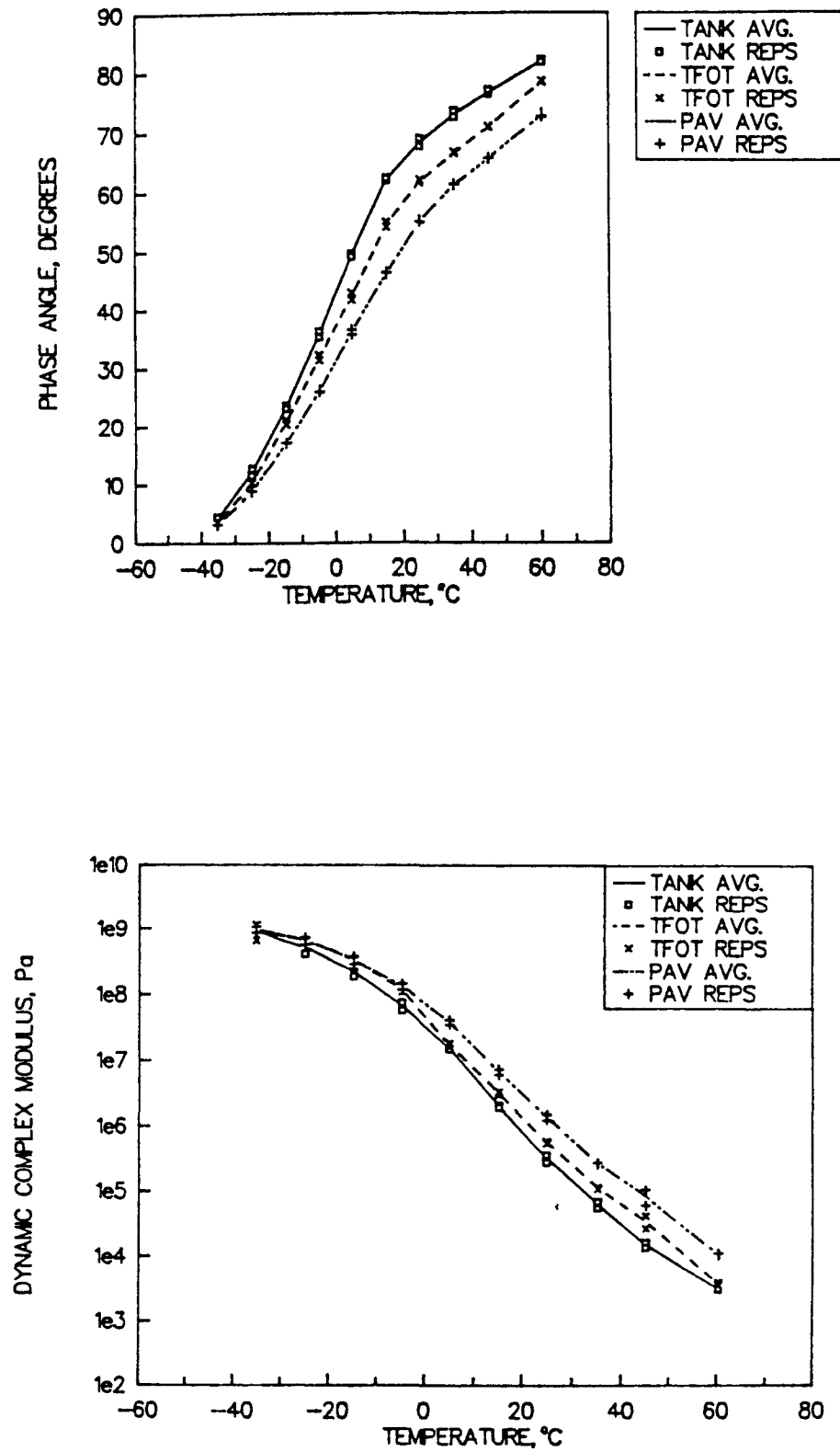
Figure 5.27   Example of Effect of Oxidative Aging on Complex Shear Modulus Isochronal Plots at 10 rad/s for Asphalt AAD-1

360
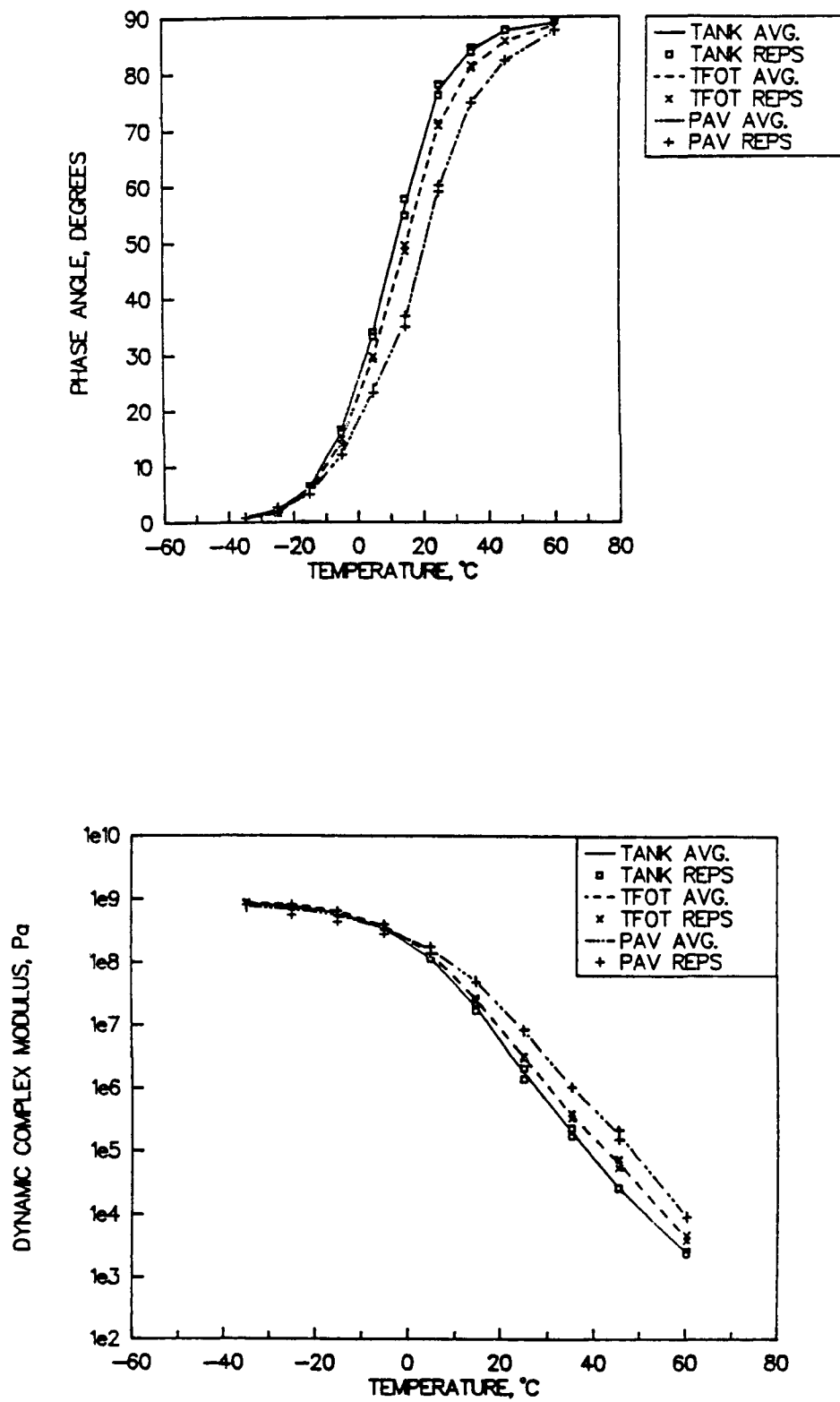
Figure 5.28 Example of Effect of Oxidative Aging on Phase Angle Isochronal Plots at 10 rad/s for Asphalt AAD-1
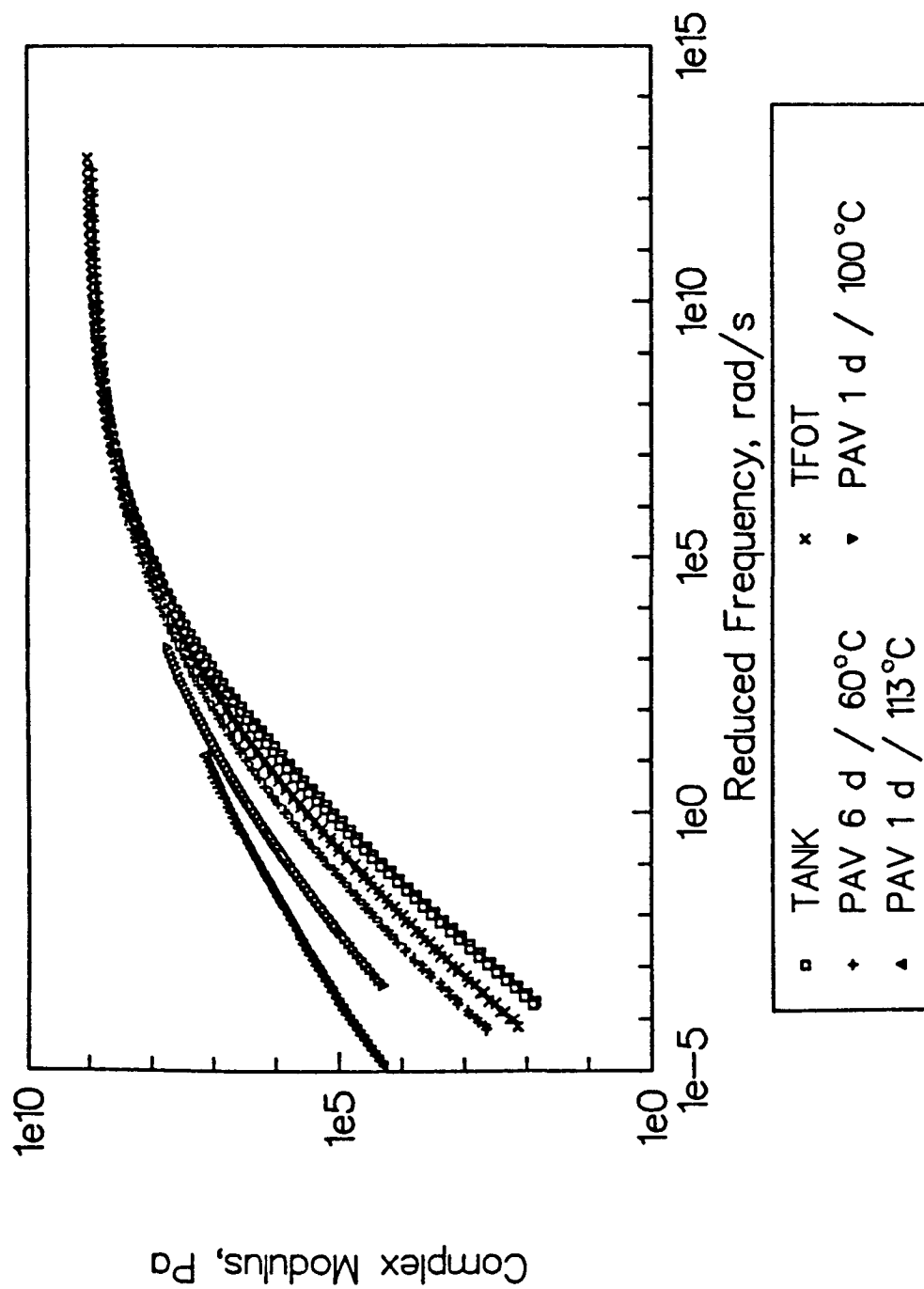
Figure 5.29 Master Rheological Curves for Asphalt AAK-1 Unaged and after Aging in the PAV at Different Temperatures
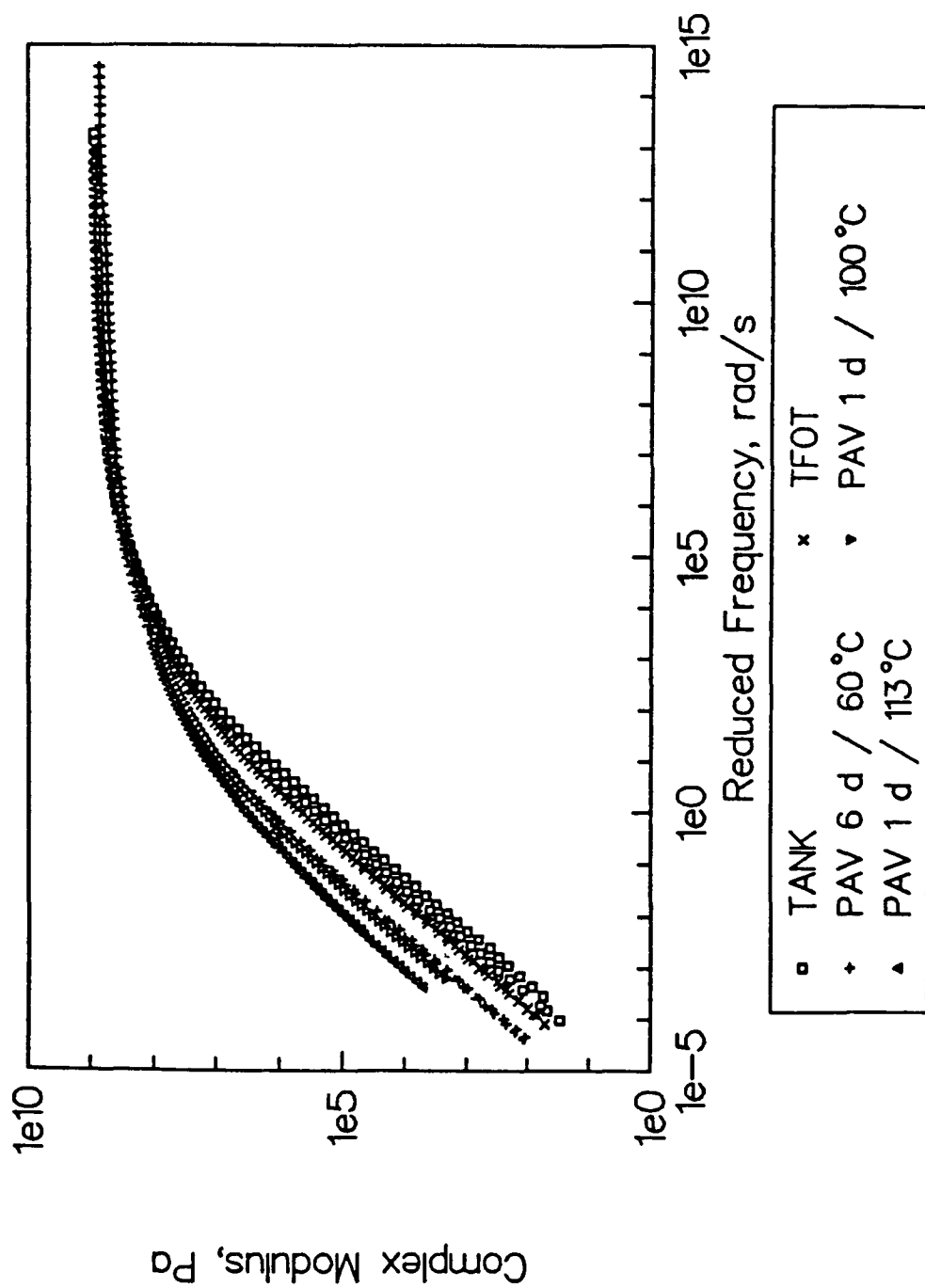
Figure 5.30 Master Rheological Curves for Asphalt AAG-1 Unaged and after Aging in the PAV at Different Temperatures
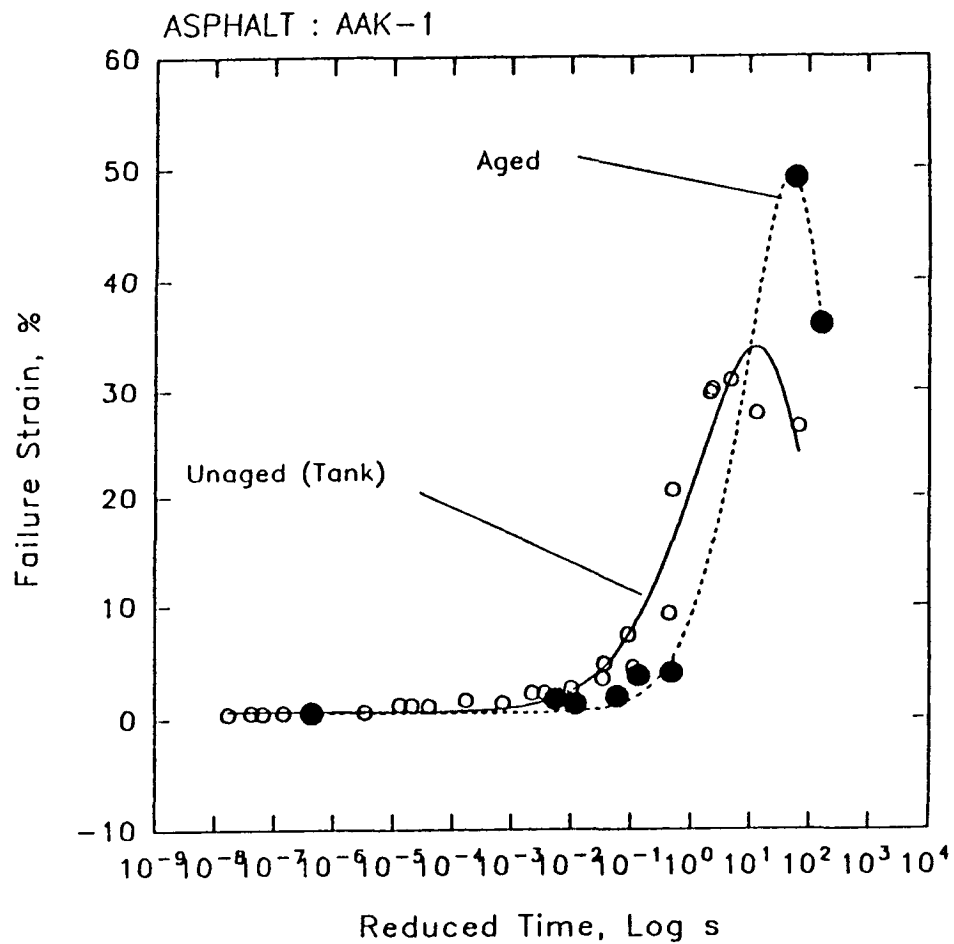
Figure 5.31 Master Failure Curves for Asphalt AAK-1 before and after Aging in the PAV for 6 Days at 60°C
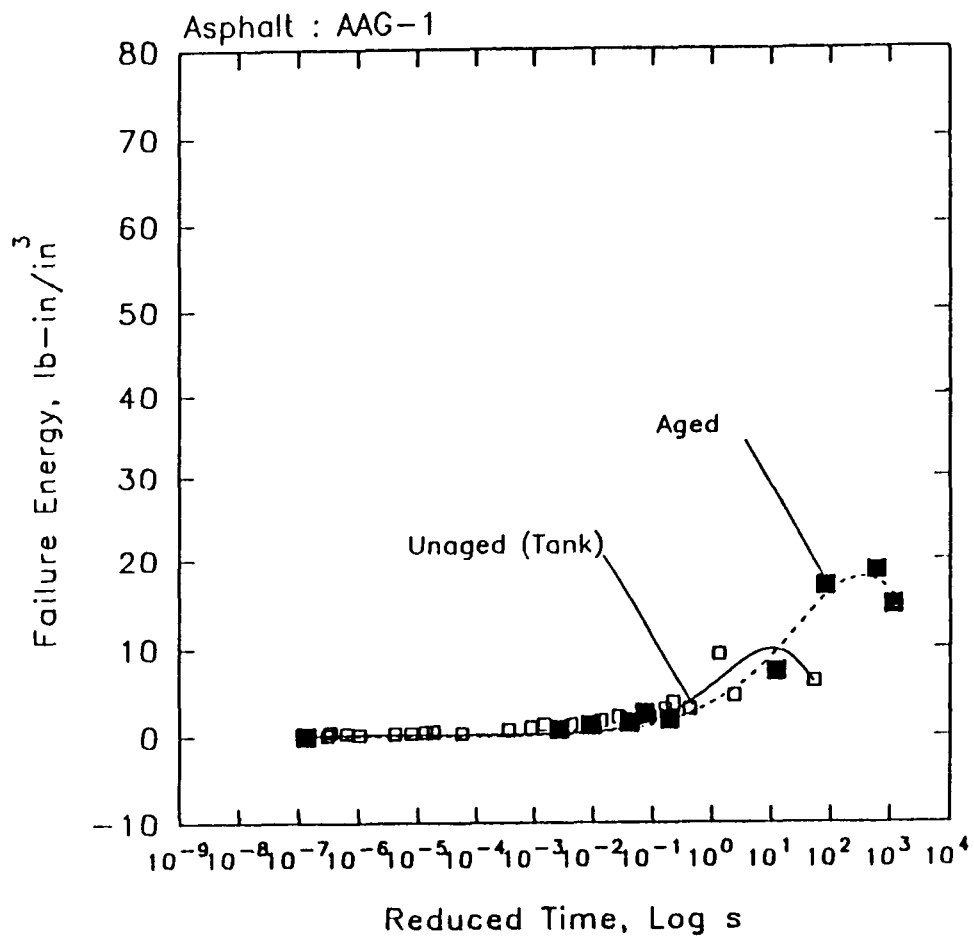
Figure 5.32 Master Failure Curves for Asphalt AAG-1 before and after Aging in the PAV for 6 Days at 60°C
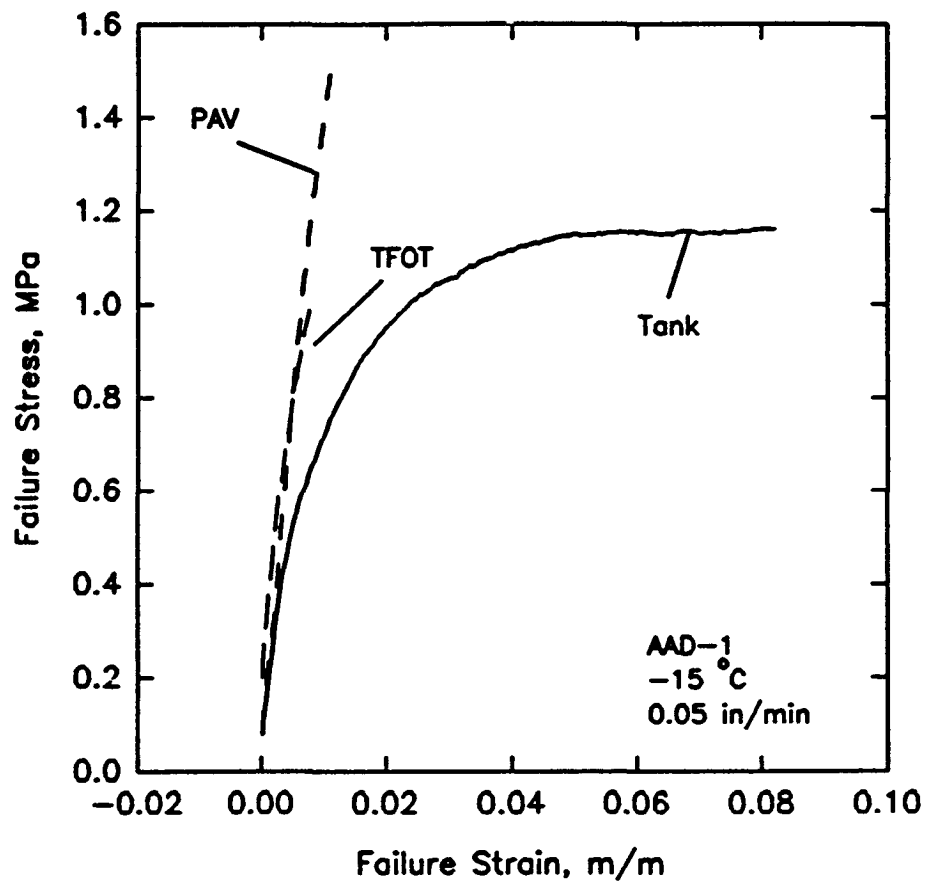
Figure 5.33 Effect of TFOT Aging and PAV Aging (20 Hours at 100°C)
on the Stress-Strain Curves for Asphalt AAD-1,
Measured Using the Plastic Inserts Technique

366
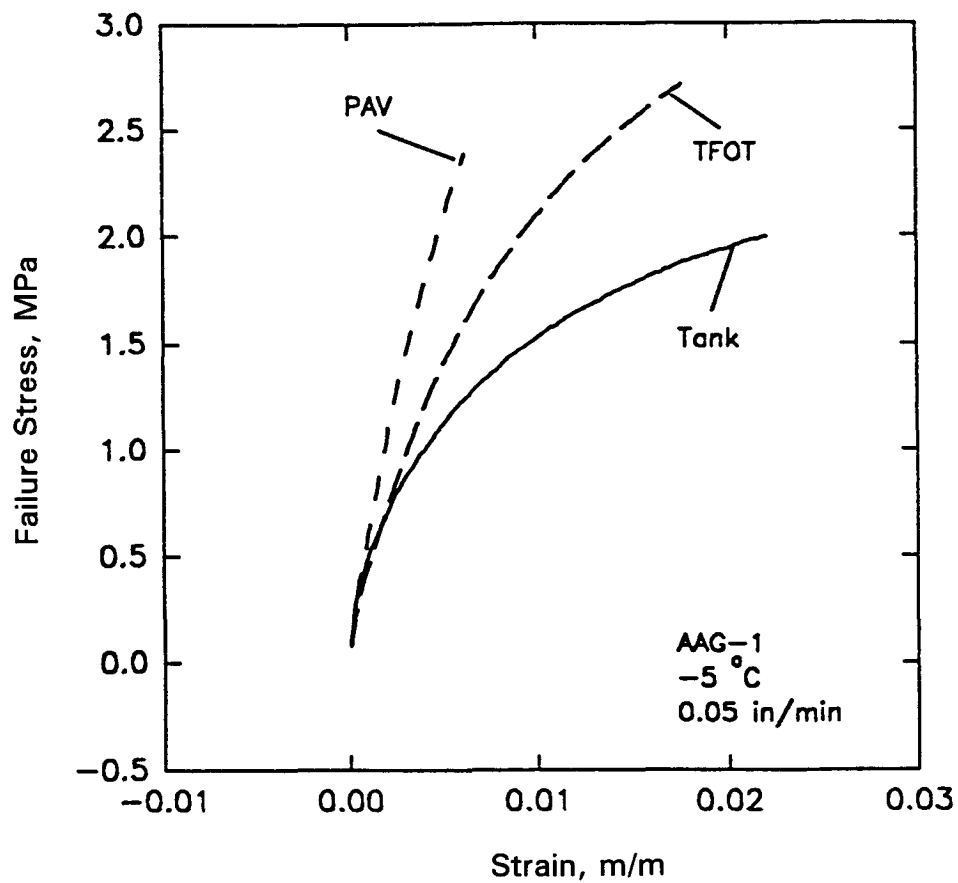
Figure 5.34 Effect of TFOT Aging and PAV Aging (20 Hours at 100°C) on the Stress-Strain Curves for Asphalt AAG-1, Measured Using the Plastic Inserts Technique
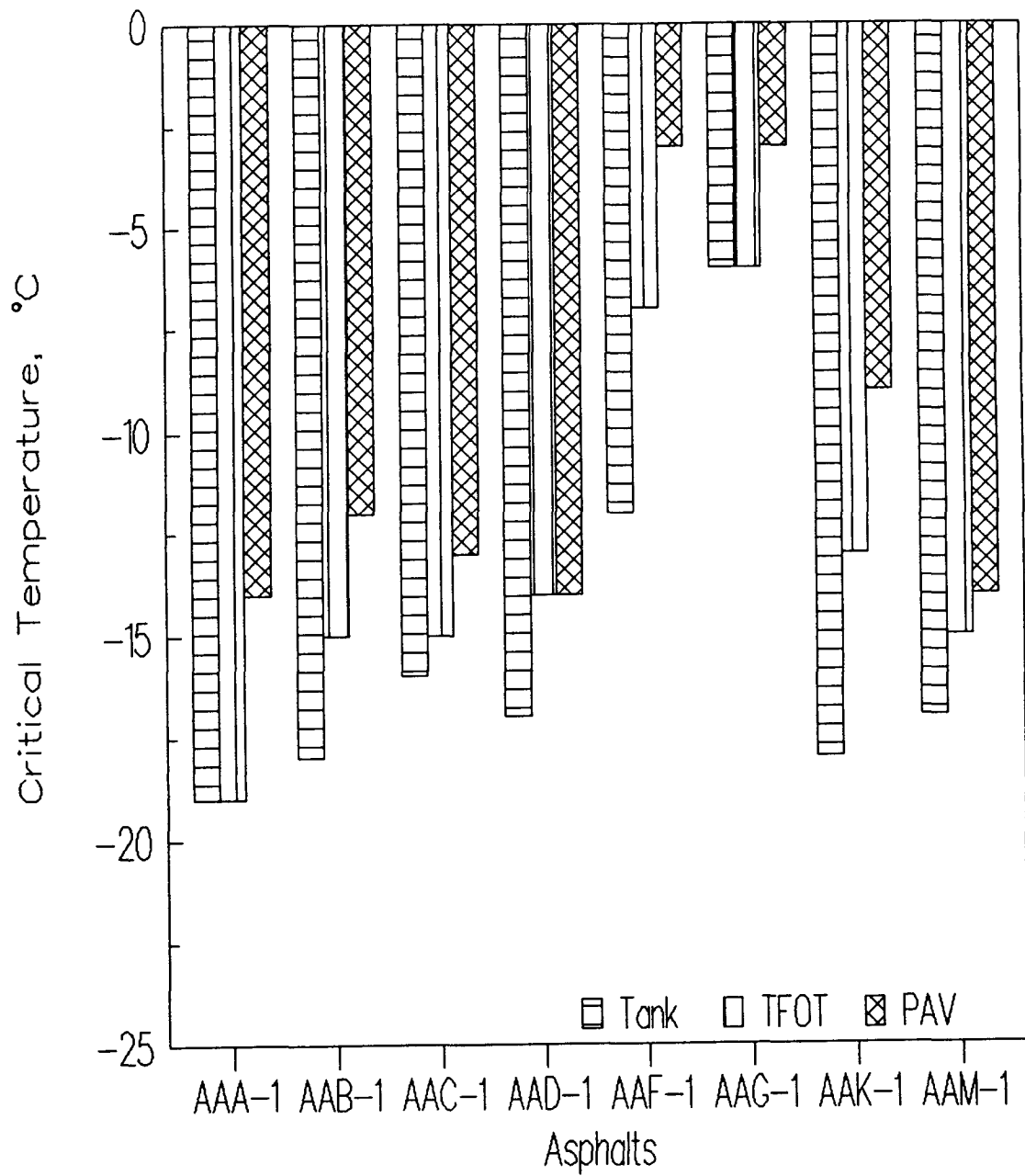
Figure 5.35   Effect of TFOT and PAV (20 Hours at 100°C) Aging on the Temperature at Which the Strain at Failure Equals 2% for the Eight Core Asphalts
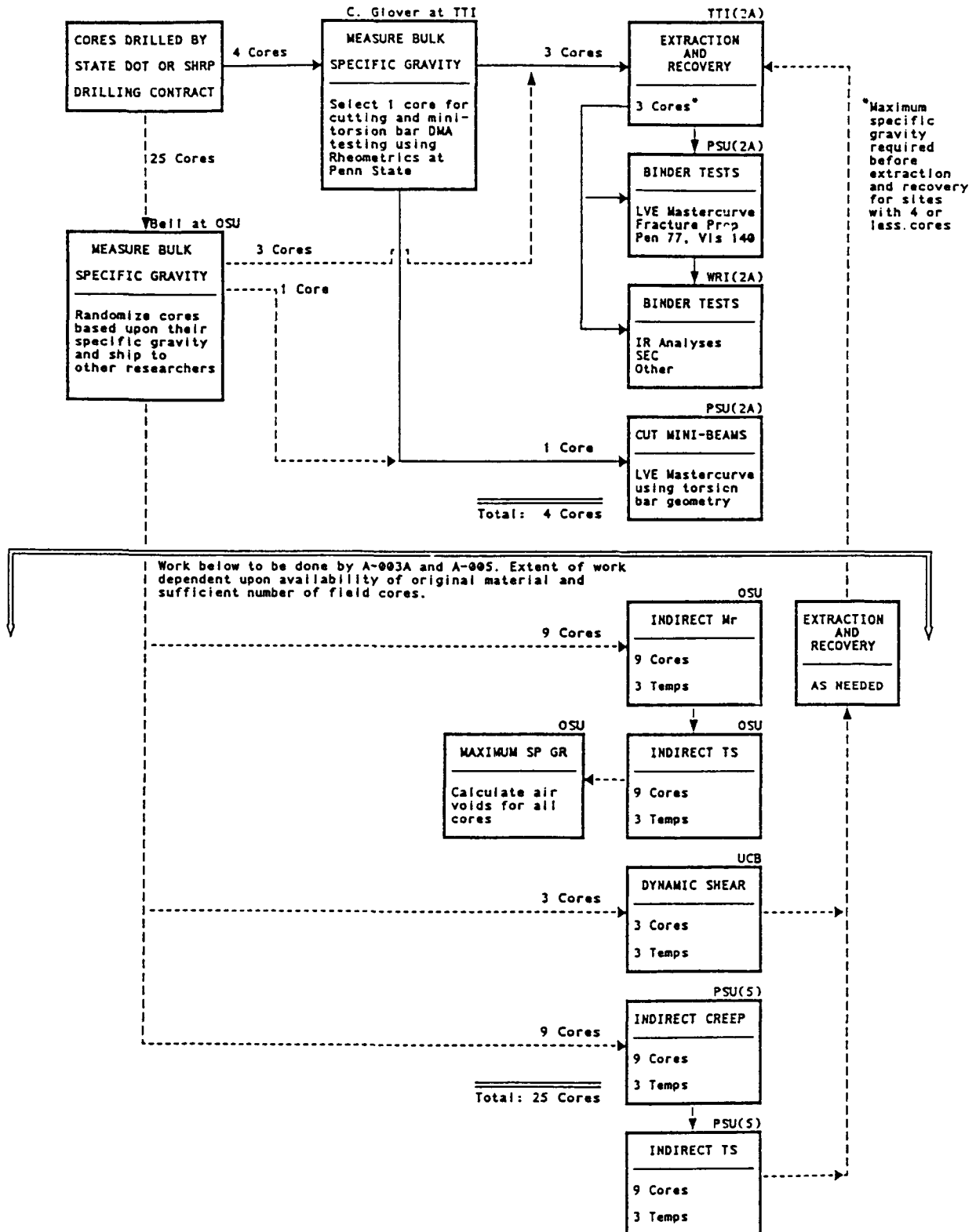
Figure 5.36   Experimental Plan for the Aging Field Validation Study Conducted for the A-002A Project

369

Figure 5.37 Rheological Master Curves for an Asphalt Used in a Florida Pavement Section in the Unaged Condition, PAV-Aged Condition, and after Recovering from Test Sections 8 Years after Construction

Field Validation Study
Section: Florida 1

+ · Unaged $-\Box-$ PAV aged $-\nabla-$ Recovered

Temperature, °C

Log (a_T)
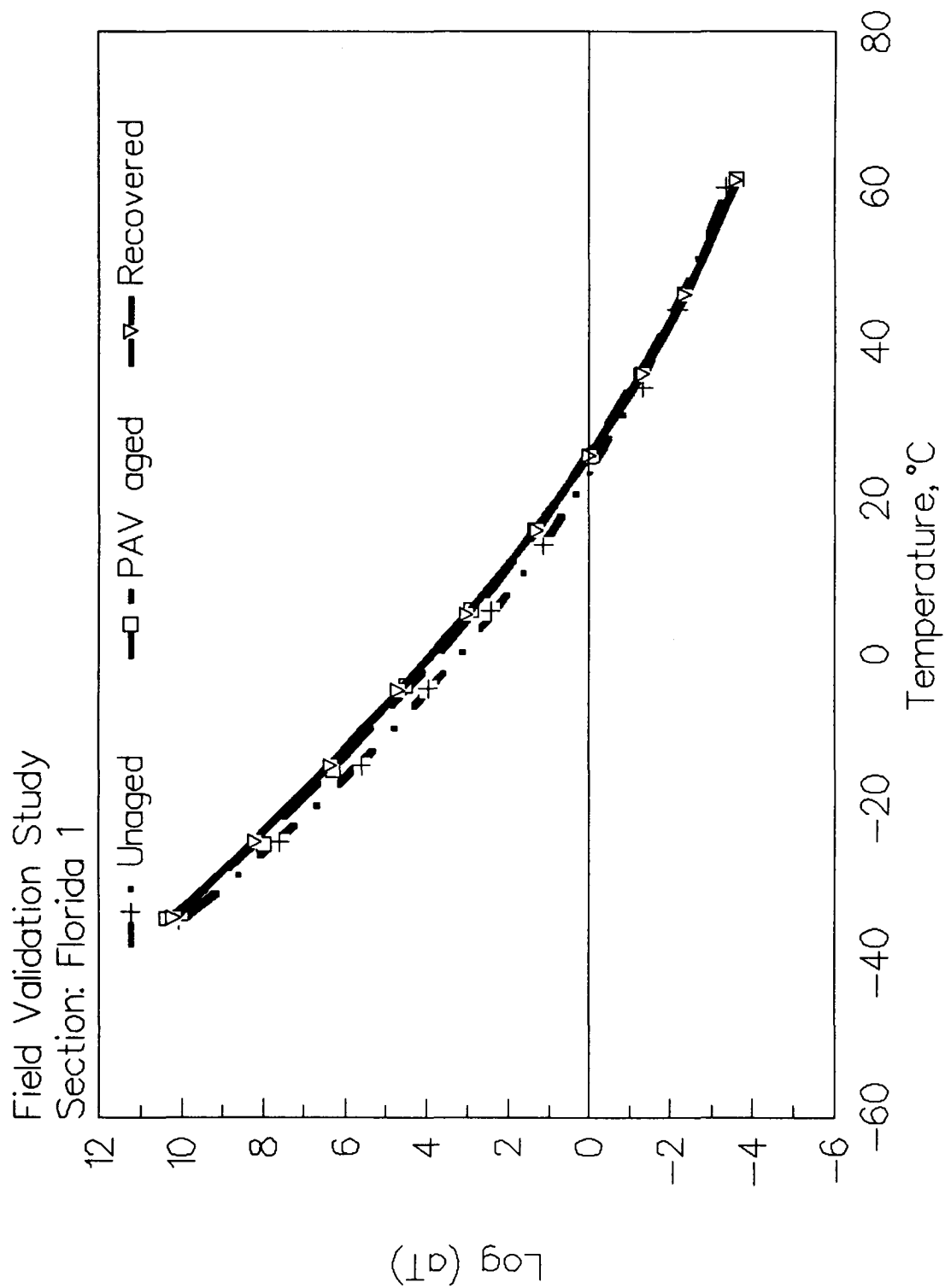
Figure 5.38 **Temperature Shift Functions for an Asphalt Used in a Florida Pavement Section in the Unaged Condition, PAV-Aged Condition, and after Recovery from Test Sections 8 Years after Construction**

371
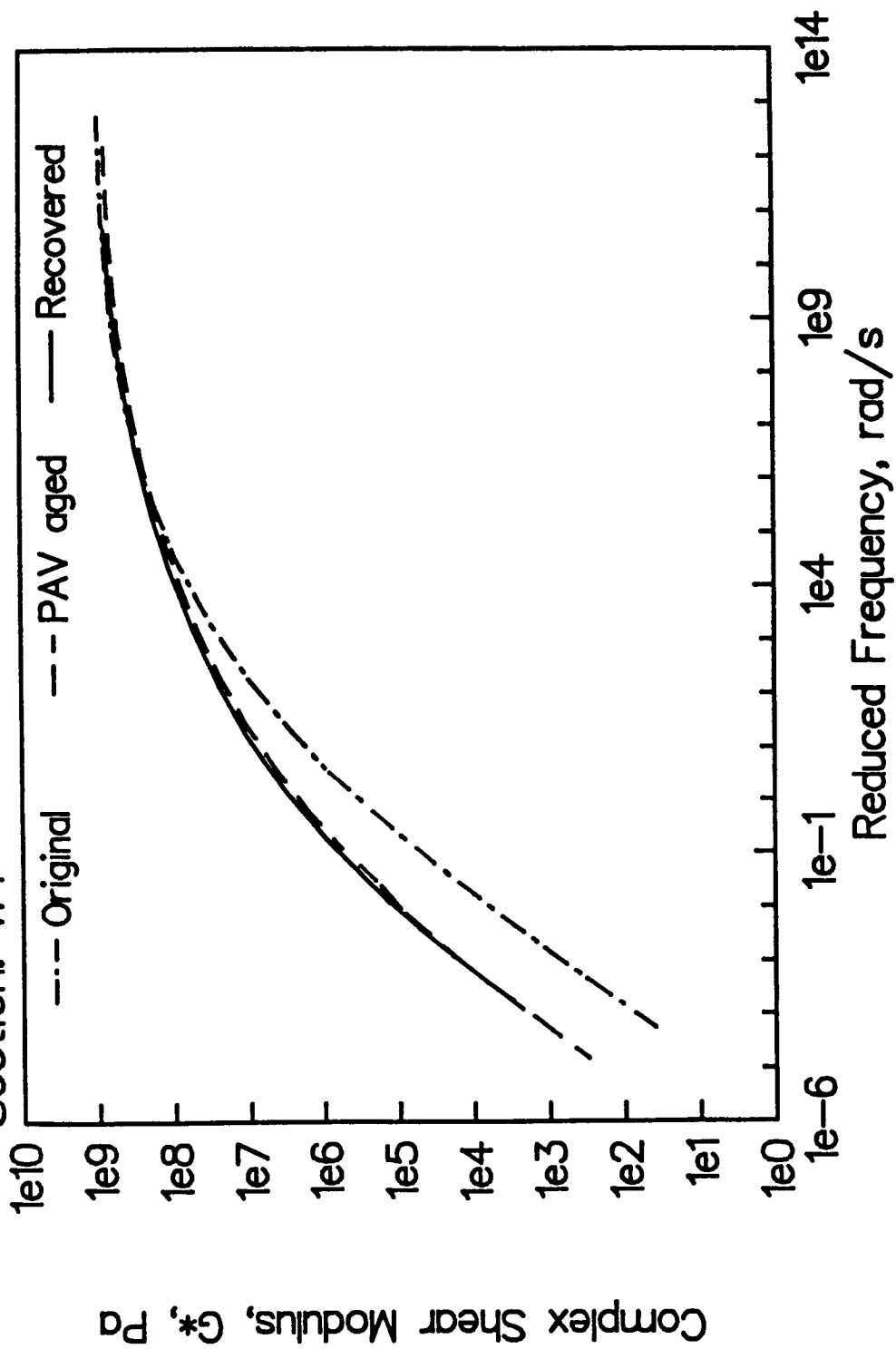
Figure 5.39 Rheological Master Curves for an Asphalt Used in a Wyoming Pavement Section in the Unaged Condition, PAV-Aged Condition, and after Recovery from Test Sections 4 Years after Construction

Figure 5.40 Temperature Shift Functions for an Asphalt Used in a Wyoming Pavement Section in the Unaged Condition, PAV-Aged Condition, and after Recovery from Test Sections 4 Years after Construction
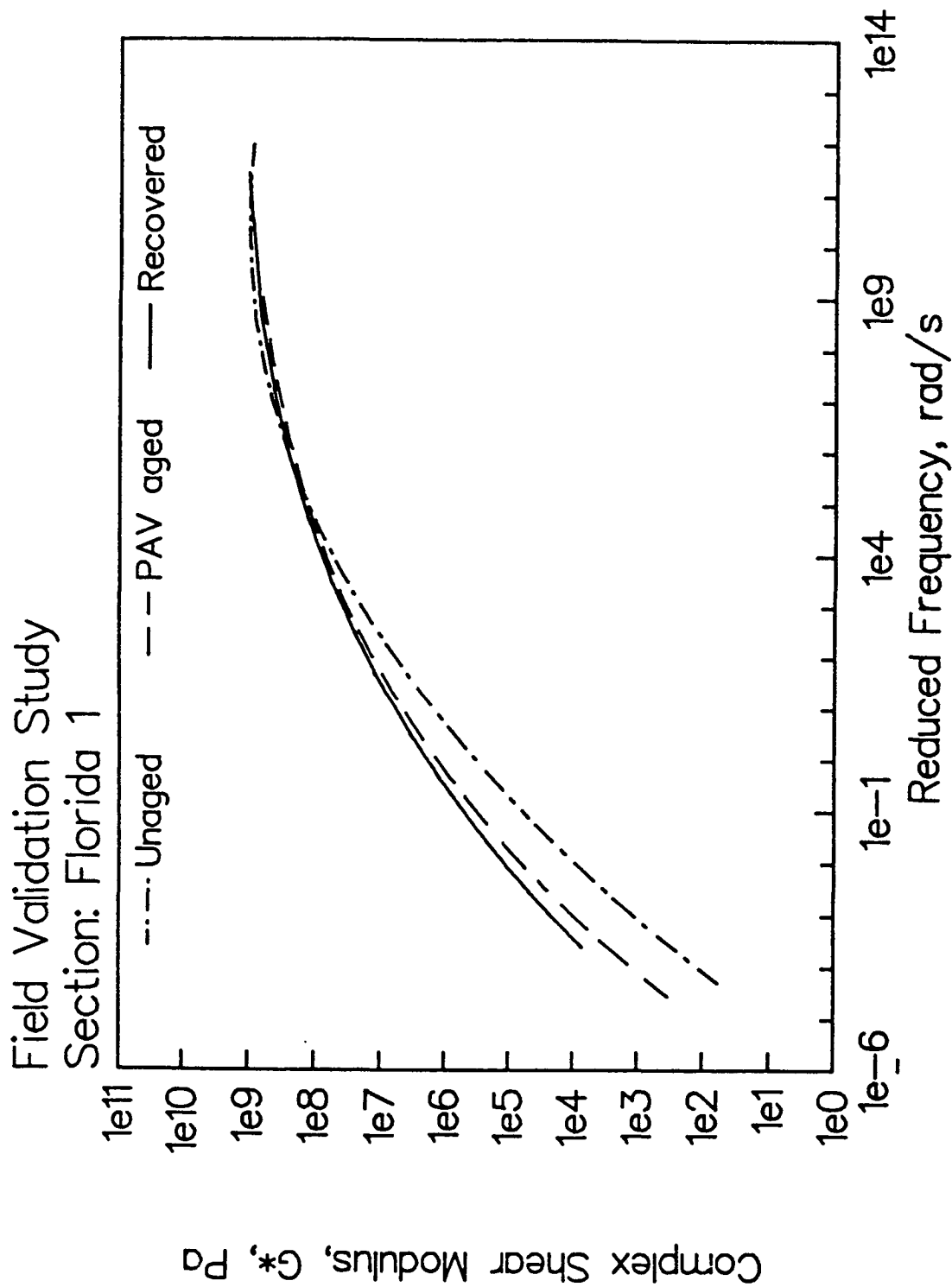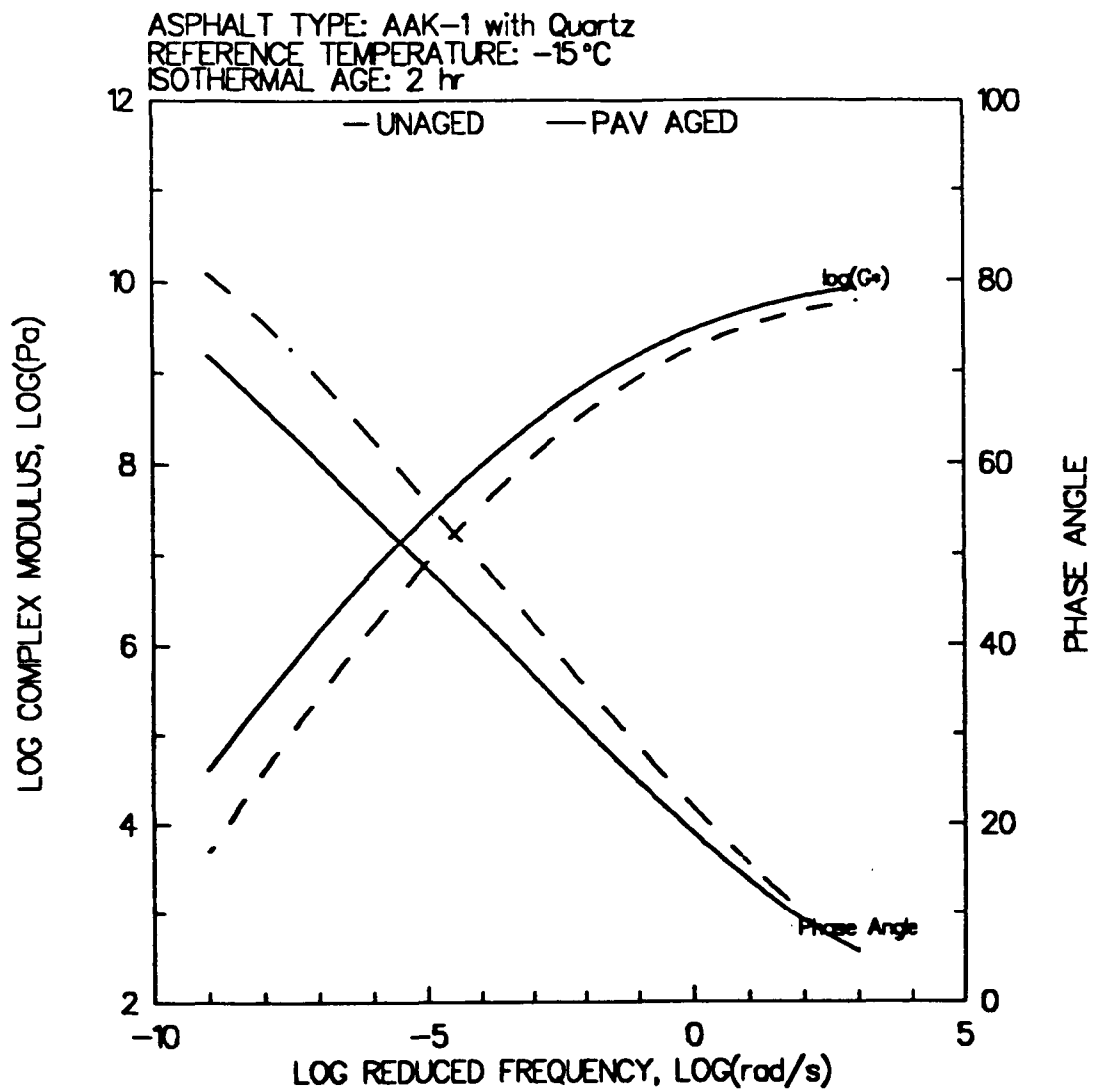
Figure 5.41 Rheological Master Curves for an Asphalt Used in Another Florida Pavement Section in the Unaged Condition, PAV-Aged Condition, and after Recovery from Test Sections 8 Years after Construction
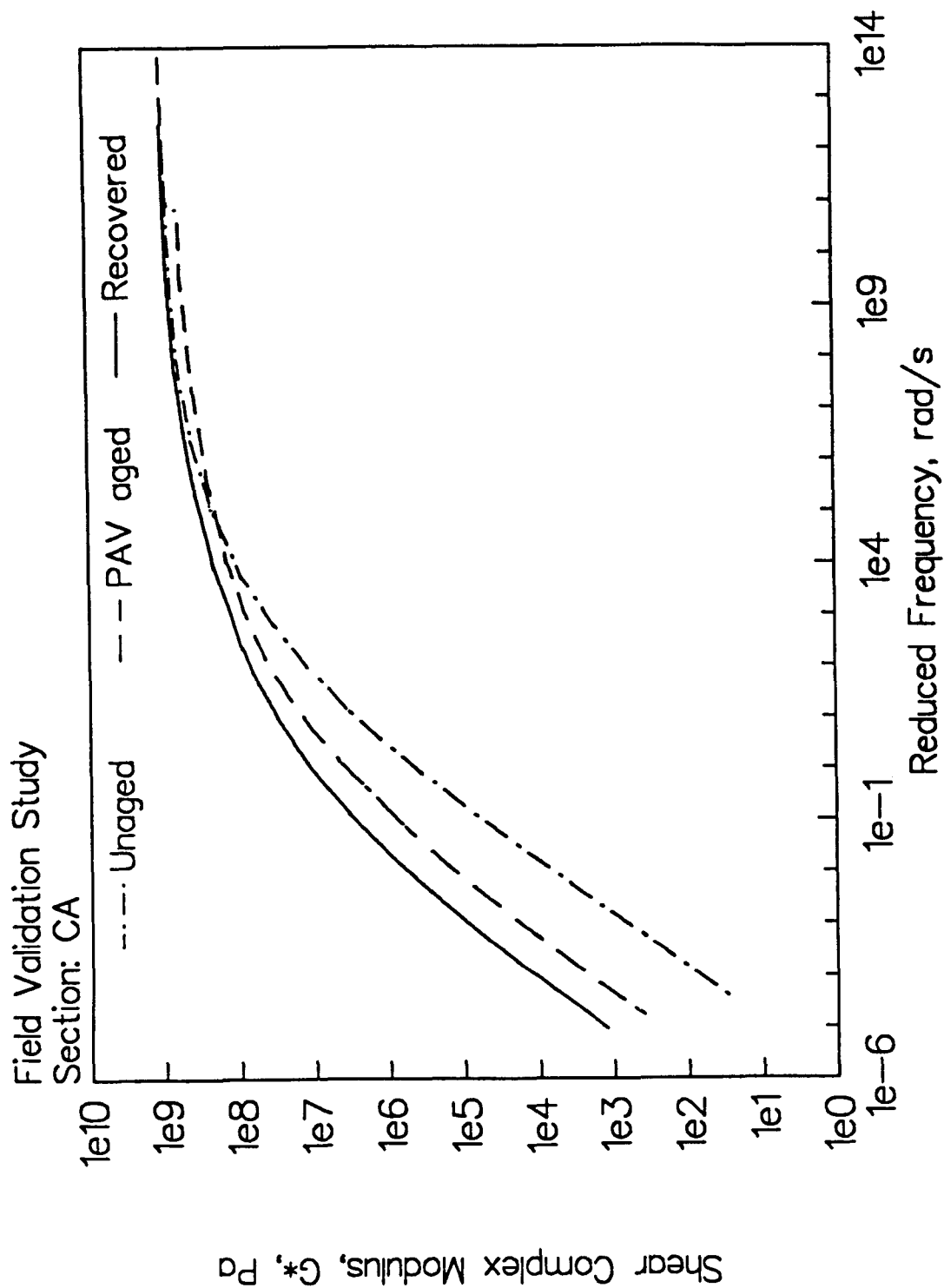
Figure 5.42 Rheological Master Curves for an Asphalt Used in a California Pavement Section in the Unaged Condition, PAV-Aged Condition, and after Recovery from Test Sections 4 Years after Construction
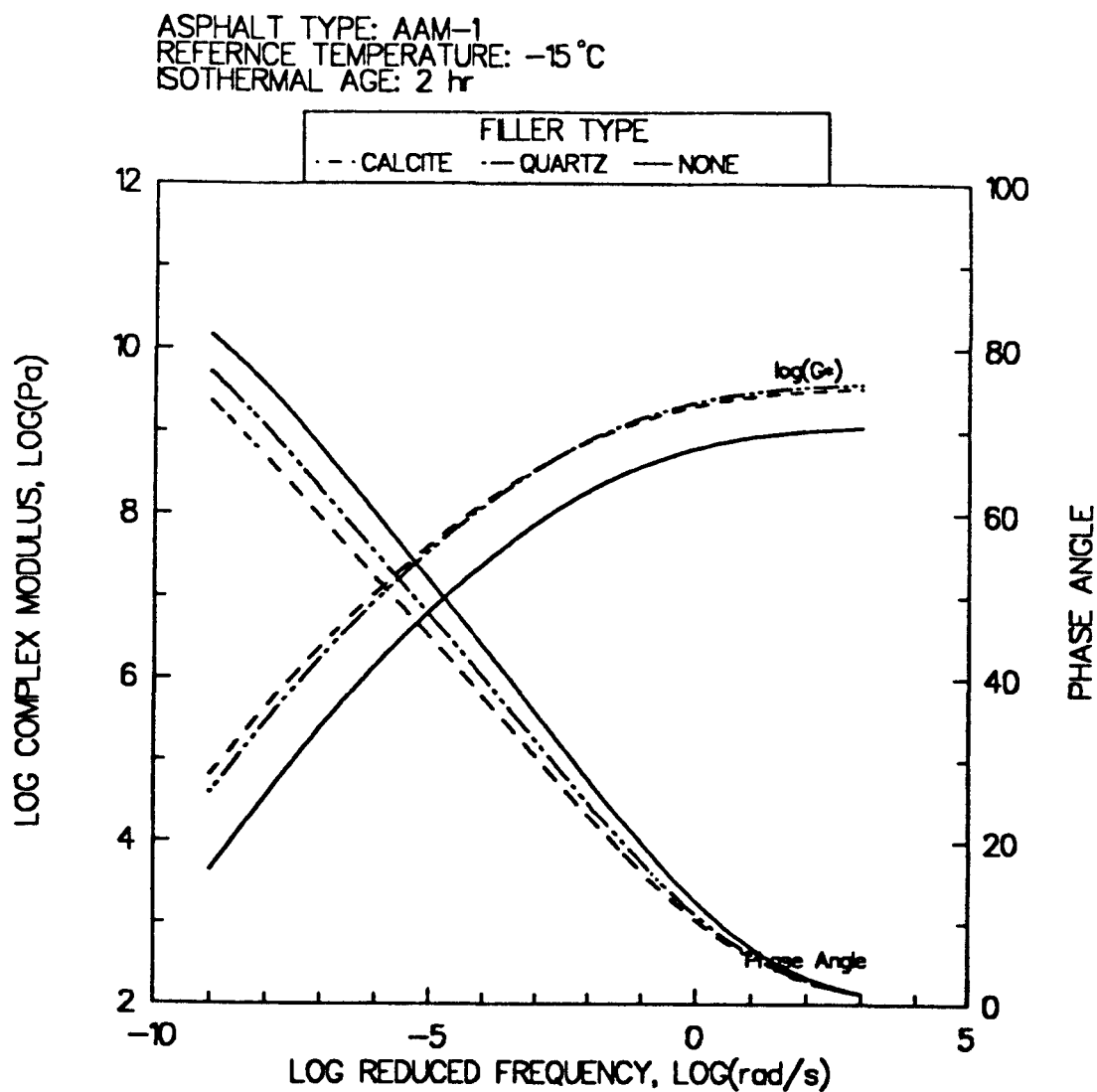
Figure 5.43 **Effect of Adding 50% by Volume Filler on the Shape of the Rheological Master Curve of Asphalt AAM-1**

Figure 5.44 Sample of Changes in the Rheological Master Curve of Asphalt Mastic (AAK-1 with Quartz) after Aging in the PAV (6 Days at 60°C)
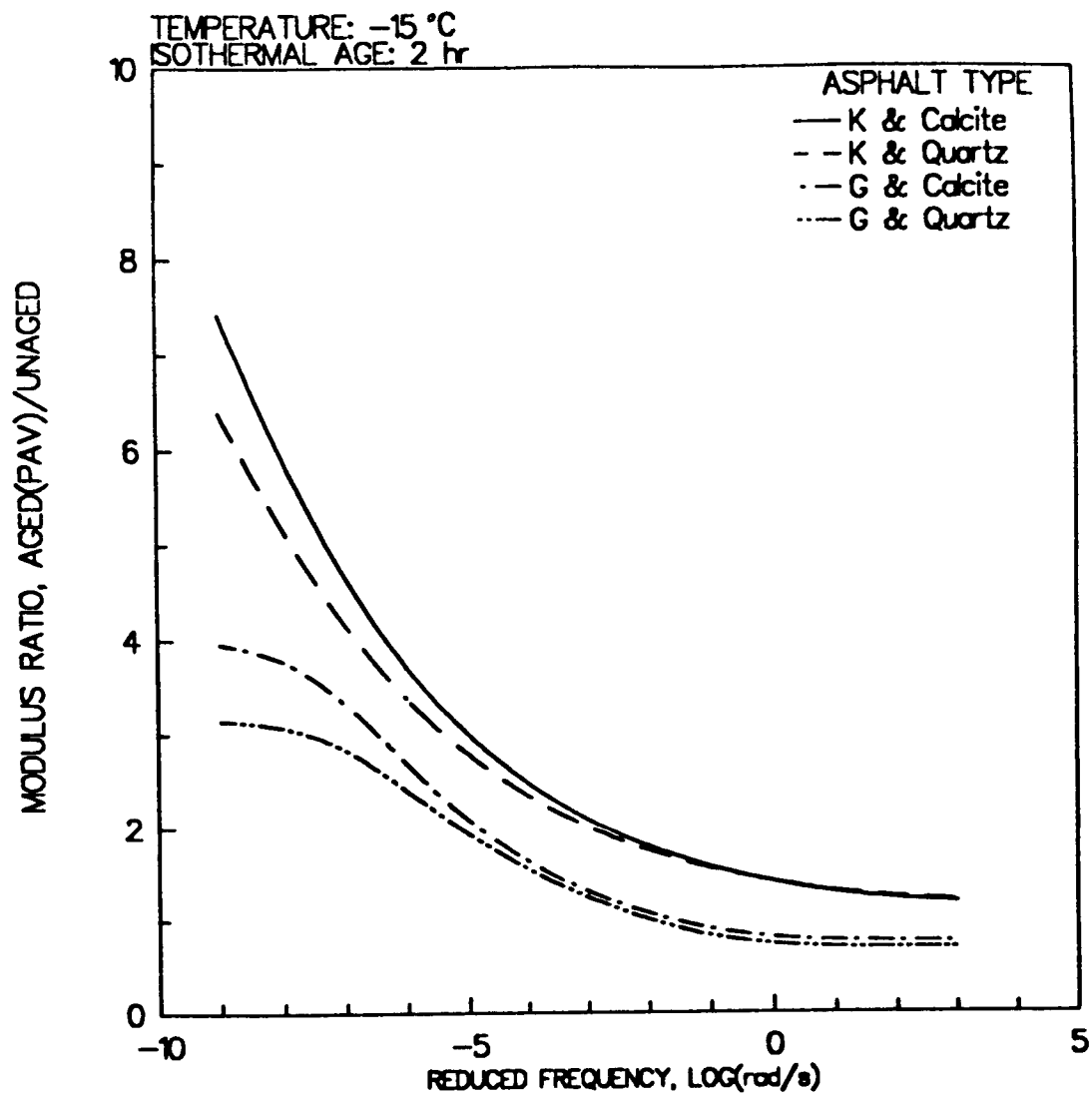
Figure 5.45   Comparison of Aging Effects on Modulus Ratio of Mastics Made of Two SHRP Asphalts and Two Fillers

378

Table 5.1a Summary of Laboratory Aging Tests Used in the Past

Test Type	Source
I. Oven Tests of Neat Asphalt:	
1. TFOT	ASTM D-1754
2. RTFOT	ASTM D-2872
3. Shattuck test	Shattuck (1940)
4. Tilted TFOT	Vallerga et al. (1957)
	Heithaus et al. (1958)
	Moavenzadeh & Stander (1967)
5. Microfilm Durability	Griffin et al. (1955)
Test (5 microns)	Halstead & Zenewitz (1961)
6. Accelerated Weathering	Paul et al. (1962)
Machine.	
7. IGLC Column Oxidation	Davis and Petersen (1966)
	Petersen et al. (1974)
8. RMFO	Schmidt & Santucci (1969)
9. Weathering Plates	Kemp (1973)
(CA test method 347)	
10. RMF-C (Chevron Method)	Schmidt (1973)
11. ARRB Durability Test	Witt (1976)
	Dickinson (1982)
	Oliver (1984)
12. Weatherometer (S. Africa)	Strauss et al. (1984)
13. Modified TFOT	Edler et al. (1985)
14. ERTFOT	Edler et al. (1985)
15. TFAAT	Petersen (1989)
II. Oven Aging of Mixtures:	
1. Air Blowing of Compacted	Garrity (1939)
Mixes at 200°C.	
2. Loose Mixes in at	Clark (1958)
150°F for 1 to 9 weeks.	
3. Loose Mixes in at	Mauppin (1972)
300°F for 2 hours.	
4. Storage of Loose Mixes at	Kandhal & Wegner (1973)
290°F for various periods.	
5. Compacted Mixes at	Goode & Lufsey (1965)
140°F for various periods.	Kumar & Goetz (1977)
	Goodrich & Dimpfl (1986)

Table 5.1b Pressure Oxidation Studies

Pressure Oxidation Conditions	Source
1. Pure oxygen at 50°C and 100 lb/in.² using asphalt-benzen mixtures	Anderson et al. 1942
2. Pure oxygen at 50°C under different pressures, using 7-micron films of asphalts.	Van Oort 1956
3. Air and Pure oxygen at temperatures of 20°C and 50°C under pressures ranging between 1 atm. and 20 atm.	Blokker & Van Hoorn 1959
4. Pure oxygen at temperatures of 140°C and 210°C under 300 lb/in.² using asphalt-saturated filter papers.	Krachma et al. 1960
5. Pure oxygen at 60°C and 300 lb/in.² using thin films of asphalt and asphalt-filler mixtures	Burch et al. 1962
6. Pure oxygen at 65°C and 300 lb/in.² for 64 hours using 0.27-in. film thickness (British standard aging procedure)	Lee & Dickinson 1962
7. Pure oxygen at 60°C and different pressure levels using 1/8-in.-thick films.	D. Lee 1967–1973
8. Pure oxygen at 65°C and 300 lb/in.² using 30-micron asphalt films	Elder et al. 1985
9. Pure oxygen at 60°C and 100 lb/in.² using 0.5-mm asphalt films and compacted mixtures.	Kim et al. 1987

380

Table 5.2 Summary of Results of Influence of Asphalt Amount in PAV on Viscosity and Mass Gain Changes During Aging at 160°F

Asphalt Type	Property Measured	1st PAV with 50 g	2nd PAV with 500 g	% Change of 2nd PAV
AAF-1	Visc. at 60°C	35586	33619	+ 5.9
AAF-1	% Mass gain	0.761	0.745	+ 2.1
AAC-1	Visc. at 60°C	8853	8975	- 1.4
AAC-1	% Mass gain	0.608	0.599	+ 1.5

Table 5.3 Summary of Results of Influence of Air Flow on Hardening and Mass Gain Changes in the PAV at 160°F

Asphalt Type	Property Measured	Rep. No.	1st PAV No Flow	2nd PAV With Flow	% Change of 1st PAV
AAK-1	Visc. at 60°C	1	58.8	52.1	- 11.4
	Visc. at 60°C	2	56.9	48.7	- 14.4
	% Mass gain	1	0.747	0.666	- 10.8
	% Mass gain	2	0.752	0.632	- 16.0
AAG-1	Visc. at 60°C	1	11.6	12.8	+ 10.3
	Visc. at 60°C	2	11.5	11.9	+ 3.5
	% Mass gain	1	0.894	0.848	- 5.1
	% Mass gain	2	0.921	0.814	- 11.6
AAM-1	Visc. at 60°C	1	33.7	32.0	- 5.1
	Visc. at 60°C	2	33.1	29.9	- 9.7
	% Mass gain	1	0.630	0.616	- 2.2
	% Mass gain	2	0.638	0.590	- 6.3
AAD-1	Visc. at 60°C	1	22.9	24.6	+ 7.4
	Visc. at 60°C	2	23.8	23.1	- 2.9
	% Mass gain	1	0.712	0.704	- 1.1
	% Mass gain	2	0.731	0.674	- 7.8
AAA-1	Visc. at 60°C	1	9.38	9.3	- 0.8
	% Mass gain	1	0.571	0.586	+ 2.6

Table 5.4 Summary of Influence of Aging Different Asphalts in One PAV on Viscosity and Penetration Changes During Aging at 160°C

Observation	Condition	Asphalt Type	Replicate	Viscosity @ 60°C, Poises	Penetration @ 25°C, 0.1 mm
1	DCF[1]	AAC-1	1	7291	34
2	DCF	AAC-1	2	7606	30
3	DCF	AAC-1	3	7455	27
4	DCF	AAD-1	1	17150	31
5	DCF	AAD-1	2	19357	29
6	CDG[2]	AAD-1	3	20012	27
7	CDG	AAC-1	1	8022	30
8	CDG	AAC-1	2	6419	30
9	CDG	AAD-1	1	22316	34
10	CDG	AAD-1	2	18217	29
11	I[3]	AAD-1	1	7027	32
12	I	AAC-1	2	7828	30
13	I	AAD-1	1	25195	29
14	I	AAD-1	2	18926	33

[1]DFG: Asphalts AAD-1, AAC-1, and AAF-1 were aged in one PAV.
[2]CDG: Asphalts AAC-1, AAD-1, and AAG-1 were aged in one PAV.
[3]I: Aged individually.

Table 5.5 Penetration Data for Asphalts Aged Individually in PAV at 160°F and 300 psig Air

Asphalt ID	AAC-1		AAD-1		AAG-1	
Run No.	E41	E37	E38	E40	E32	E31
Technician	2	2	2	2	2	2
Penetration						
Original Asphalt	109	111	138	142	56	52
TFOT Conditioned	62	63	75	80	39	19
PAV Pan 1	30	30	30	32	14	19
PAV Pan 2	32	28	27	31	16	19
PAV Pan 3	34	31	30	36	16	19
PAV Pan 4	33	28	28	34	18	18
PAV Pan 5	30	30	27	34	15	17
PAV Pan 6	33	31	30	31	17	17
PAV AVERAGE	32	30	29	33	16	18
Viscosity						
Original Asphalt	813	745	1,139	1,171	1,835	1,891
TFOT Conditioned	1,549	1,731	3,135	2,965	2,951	3,108
PAV Pan 1	6,668	7,913	24,684	18,057	8,825	9,494
PAV Pan 2	7,589	7,623	22,268	19,138	8,550	9,341
PAV Pan 3	7,177	7,760	25,266	18,559	8,544	9,584
PAV Pan 4	6,598	8,015	24,840	18,489	9,151	9,675
PAV Pan 5	7,042	7,650	24,318	19,065	9,008	9,398
PAV Pan 6	7,090	8,004	23,794	20,247	8,743	9,130
PAV AVERAGE	7,027	7,828	25,195	18,926	8,803	9,440

Table 5.6 Rheological Parameters for Oxidation Kinetics Experiment

Asphalt	Treatment	Log ω_o, rad/s	Rheological Index	T_d, °C
AAG-1	Tank	3.14	1.24	-4
	TFOT	2.75	1.35	1
	PAV, 6 d. @ 60°C	1.97	1.44	3
	PAV, 1 d. @ 100°C	1.99	1.65	2
	PAV, 1 d. @ 113°C	1.24	1.73	4
AAK-1	Tank	3.42	1.60	-15
	TFOT	2.78	1.80	-9
	PAV, 6 d. @ 60°C	2.05	1.94	-9
	PAV, 1 d. @ 100°C	0.57	2.47	2
	PAV, 1 d. @ 113°C	-2.01	3.15	6

Table 5.7 Rheological Parameters for Volatilization Study

Asphalt	Treatment	Rep. No.	Log ω_o rad/s	Rheological Index	T_d °C
AAD-1	Tank	1	4.07	1.60	−10
		2	3.97	1.57	−12
	TFOT/Argon	1	3.69	1.81	−9
		2	3.63	1.81	−13
	TFOT/Air	1	3.36	1.85	−9
		2	3.14	1.86	−5
AAG-1	Tank	1	3.17	1.34	−5
		2	2.99	1.31	−7
	TFOT/Argon	1	2.72	1.41	−2
		2	2.81	1.36	0
	TFOT/Air	1	2.62	1.45	0
		2	2.59	1.44	0
AAK-1	Tank	1	3.62	1.59	−8
		2	3.32	1.66	−12
	TFOT/Argon	1	3.05	1.82	−5
		2	3.07	1.80	−7
	TFOT/Air	1	2.81	1.92	−3
		2	2.69	1.92	−7
AAM-1	Tank	1	2.62	2.08	6
		2	2.52	2.12	5
	TFOT/Argon	1	1.84	2.34	2
		2	2.01	2.35	2
	TFOT/Air	1	1.36	2.56	5
		2	1.50	2.46	1

Table 5.8 Results from IR Analysis for the Volatilization Experiment

Asphalt	Atmosphere	Carbonyl Absorbance Units	Sulfoxide MOL/L
AAD-1	Air	0.045	0.061
	N_2	0.04	0.038
	Argon	0.03	0.032
AAG-1	Air	0.04	0.054
	N_2	0.02	0.050
	Argon	0.02	0.035
AAK-1	Air	0.04	0.043
	N_2	0.02	0.037
	Argon	0.02	0.022
AAM-1	Air	0.03	0.037
	N_2	0.02	0.033
	Argon	0.02	0.027

Table 5.9 Changes in the Rheological Parameters of the Core Asphalts Because of Aging in the PAV

AC	PAV Temp °C	T_d	log W_o	R
AAD	Unaged	−17.0	3.95	1.56
AAD	90	−3.7	1.91	2.24
AAD	100	−6.2	1.52	2.37
AAD	110	0.4	0.12	2.71
AAG	Unaged	−4.0	3.14	1.24
AAG	90	0.1	2.41	1.31
AAG	100	2.7	1.94	1.47
AAG	110	0.7	1.80	1.55
AAK	Unaged	−15.0	3.42	1.60
AAK	90	−5.0	1.63	2.16
AAK	100	−3.9	1.06	2.28
AAK	110	1.4	0.27	2.45
AAM	Unaged	1.0	2.05	1.93
AAM	90	3.9	0.71	2.69
AAM	100	4.9	−0.22	2.92
AAM	110	5.5	−0.99	3.19

Table 5.10 Weibull Parameters for Failure Master Curves

Asphalt Type	Unaged Strain Master Curve Parameters					PAV-Aged Strain Master Curve Parameters				
	A	B1	B2	B3	B4	A	B1	B2	B3	B4
AAG-1	0.38	44.6	−6.82	12.6	10	0.20	107.2	−9.8	18.0	10
AAK-1	0.72	90.1	−5.00	9.20	10	0.60	131.9	−4.7	15.6	10
	Unaged Energy Master Curve Parameters					PAV-Aged Energy Master Curve Parameters				
	A	B1	B2	B3	B4	A	B1	B2	B3	B4
AAG-1	0.21	26.1	−3.8	7.8	10	0.04	48.30	−5.20	10.9	10
AAK-1	0.75	94.4	−3.1	6.5	10	0.36	198.0	−1.98	12.4	10

Table 5.11   Changes in Temperature at Which Failure Strain Is 2 Percent upon Aging in the TFOT and the PAV for the Eight Core Asphalts

Asphalt	Treatment		
	Tank	TFOT	PAV
AAA-1	−19	−19	−14
AAB-1	−18	−15	−12
AAC-1	−16	−15	−13
AAD-1	−17	−14	−14
AAF-1	−12	−7	−3
AAG-1	−6	−6	−3
AAK-1	−18	−13	−9
AAM-1	−17	−15	−14

Table 5.12 Field Locations Used in Aging Study

State	Test Section	Quantity of AC Available	Cores—Total Number Available within A-002A	Cores—Extract/ Recover Complete by A-002A	Original Asphalt Rheo-logical Testing	TFOT	PAV	Recovered Asphalt
Florida	Location 1	1500 ml	9	3	Yes	Yes	Yes	Yes
	Location 2	1500 ml	9	3	Yes	Yes	Yes	Yes
California	Octillo	1000 ml	1	1	Yes	Yes	Yes	Yes
Pennsylvania Elk Co.	T-1	400 ml	4	3 at TTI	Yes	Yes	Yes	Yes
Pennsylvania Elk Co.	T-3	400 ml	4	3 at TTI	Yes	Yes	Yes	No
Pennsylvania Elk Co.	T-5	800 ml	4	3 at TTI	Yes	Yes	Yes	No
Pennsylvania Elk Co.	T-6	800 ml	4	3 at TTI	Yes	Yes	Yes	No
Wyoming— Point of Rocks	Section 13	300 ml	4	3	Yes	Yes	Yes	Yes

Table 5.13 Properties of Mineral Fillers Used in the Study

Source	Mineral Type	Sp. Gravity	Bulk Density of Compacted Dust g/cm^3	Void in Compacted Dust %	Surface Area m^2/g	Free Asphalt =50% Dust/Asphalt Ratio (Vol. Base)
RC	Limestone (H. Absorp.)	2.726	1.606	41.100	1.970	0.418
RD	Limestone (L. Absorp.)	2.727	1.730	36.600	1.830	0.465
RE	Gravel	2.750	1.417	48.500	1.550	0.347
RG	Sandstone	2.697	1.650	38.800	1.450	0.441
RH	Graywacke	2.663	1.349	49.400	3.230	0.339

Table 5.14 Results of Asphalt-Filler Aging Experiment

AC Source	Filler Source	Vol. Ratio F/AC	Temp. (°C)	Avg. Unaged G* (Pa)	Avg. PAV G*(Pa)	Aging Index	Variance	95% Confidence Interval	
AAG-1	RC	0.418	25	4.06e+06	1.94e+07	4.778	0.351	3.6	6.0
AAG-1	RD	0.465	25	4.96e+06	1.80e+07	3.629	0.160	2.8	4.4
AAG-1	RE	0.347	25	3.82e+06	1.60e+07	4.181	0.327	3.0	5.3
AAG-1	RG	0.441	25	5.52e+06	1.99e+07	3.608	0.128	2.9	4.3
AAG-1	RH	0.339	25	2.86e+06	1.68e+07	5.874	0.982	3.9	7.9
AAK-1	RC	0.418	25	1.66e+06	1.13e+07	6.807	3.741	2.9	10.7
AAK-1	RD	0.465	25	1.67e+06	9.13e+06	5.467	2.563	2.3	8.7
AAK-1	RE	0.347	25	1.36e+06	1.07e+07	7.857	7.173	2.5	13.2
AAK-1	RG	0.441	25	1.58e+06	1.08e+07	6.804	4.126	2.7	10.9
AAK-1	RH	0.339	25	1.56e+06	7.44e+06	4.766	2.371	1.7	7.8

Table 5.14 Results of Asphalt-Filler Aging Experiment (continued)

AC Source	Filler Source	Vol. Ratio F/AC	Temp. (°C)	Avg. Unaged G* (Pa)	Avg. PAV G*(Pa)	Aging Index	Variance	95% Confidence Interval	
AAG-1	RC	0.418	45	6.12e+04	3.49e+05	5.707	0.591	4.2	7.2
AAG-1	RD	0.465	45	7.38e+04	2.86e+05	3.869	0.308	2.8	5.0
AAG-1	RE	0.347	45	5.30e+04	2.94e+05	5.538	0.766	3.8	7.3
AAG-1	RG	0.441	45	7.91e+04	3.47e+05	4.383	0.289	3.3	5.5
AAG-1	RH	0.339	45	4.61e+04	2.98e+05	6.471	1.175	4.3	8.6
AAK-1	RC	0.418	45	8.77e+04	7.01e+05	7.993	0.410	6.7	9.3
AAK-1	RD	0.465	45	7.46e+04	4.99e+05	6.687	0.464	5.3	8.0
AAK-1	RE	0.347	45	6.12e+04	6.05e+05	9.886	1.118	7.8	12.0
AAK-1	RG	0.441	45	7.72e+04	5.84e+05	7.565	0.496	6.2	9.0
AAK-1	RH	0.339	45	6.55e+04	4.26e+05	6.509	0.585	5.0	8.0

Continued

Table 5.14 Results of Asphalt-Filler Aging Experiment (continued)

AC Source	Filler Source	Vol. Ratio F/AC	Temp. (°C)	Avg. Unaged G^* (Pa)	Avg. PAV G^* (Pa)	Aging Index	Variance	95% Confidence Interval	
AAG-1	RC	0.418	60	4.77e+03	2.25e+04	4.717	0.966	2.8	6.7
AAG-1	RD	0.465	60	5.90e+03	1.92e+04	3.249	0.465	1.9	4.6
AAG-1	RE	0.347	60	3.86e+03	1.81e+04	4.689	1.467	2.3	7.1
AAG-1	RG	0.441	60	6.89e+03	2.38e+04	3.457	0.356	2.3	4.6
AAG-1	RH	0.339	60	4.29e+03	1.99e+04	4.644	1.179	2.5	6.8
AAK-1	RC	0.418	60	1.09e+04	9.44e+04	8.661	0.406	7.4	9.9
AAK-1	RD	0.465	60	9.98e+03	6.62e+04	6.632	0.330	5.5	7.8
AAK-1	RE	0.347	60	7.54e+03	8.16e+04	10.82	1.216	8.6	13.0
AAK-1	RG	0.441	60	9.80e+03	7.92e+04	8.077	0.452	6.7	9.4
AAK-1	RH	0.339	60	9.03e+03	6.05e+04	6.704	0.409	5.4	8.0

393

References

Anderson, A.P., Struss, F.H., and Ellings, A. 1942. "Measurement of Oxidation Stability of Road Asphalts," *American Chemical Society*, vol. 147, pp. 45–49.

Anderson, D.A., Dukatz, E.L., and Rosenberger, J.L. 1983. "Properties of Asphalt Cement and Asphaltic Concrete," *Proceedings of the Association of Asphalt Paving Technologists*, vol. 52, pp. 291–324.

ASTM. 1991. *Annual Book of ASTM Standards*, vol. 4.03. Philadelphia: American Society for Testing and Materials.

Barbour, F.A., Dorrence, S.M., and Petersen, J.C. 1970. "Inverse Gas-Liquid Chromatographic Studies of Asphalts. Variation in Experimental Parameters," Preprints, Division of Petroleum Chemistry, *American Chemical Society*, vol. 2, no.6, pp. 668–670.

Barth, E.J. 1962. *Asphalt Science and Technology*. New York: Gorden and Breach.

Blokker, P.C., and Van Hoorn, H. 1959. "Durability of Bitumen in the Theory and Practice," *Proceedings of the 5th World Petroleum Congress*, vol. 6, pp. 417–432.

Burgh, A.J.P. Van Der, Boswman, J.P., and Steffelaar, G.M. 1962. *The Aging of Asphalt Bitumen*. Rijkswaterstaat Communications.

Button, J.W., and Epps, J.A. 1985. "Identifying Tender Asphalt Mixtures in the Laboratory," *Transportation Research Record 1034*, pp. 20–26.

Button, J.W., Little, D.N., Gallaway, B.M., and Epps, J.A. 1983. "Influence of Asphalt Temperature Susceptibility on Pavement Construction and Performance," *NCHRP Report 268*. Washington, D.C.: TRB, National Research Council.

Chipperfield, E.H., and Welch, T.R. 1967. "Studies on the Relationships between the Properties of Road Bitumens and Their Service Performance," *Proceedings of the Association of Asphalt Paving Technologists*, vol. 36, pp. 421–488.

Cullery, R.W. 1969. "Relationship between Hardening of Asphalt Cements and Transverse Cracking of Pavements in Saskatchewan," *Proceedings of the Association of Asphalt Paving Technologists*, vol. 38, pp. 1–15.

Davis, T.C., and Petersen, J.C. 1966. "Inverse Gas-Liquid Chromatography. A New Approach for Studying Petroleum Asphalts," Preprints, Division of Petroleum Chemistry, *American Chemical Society*, vol. 38, no. 2, pp. 241–243.

Dickinson, E.J., and Witt, H.P. 1974. "The Dynamic Shear Modulus of Paving Asphalts as a Function of Frequency," *Transaction of the Society of Rheology*, vol. 18, no. 4, pp. 591–606.

Dobson, G.R. 1969. "The Dynamic Mechanical Properties of Bitumen," *Proceedings of the Association of Asphalt Paving Technologists*, vol. 38, p. 123.

Dow, A.W. 1903. "The Testing of Bitumen for Paving Purposes," *Proceedings of the 6th Annual Meeting, American Society for Testing and Materials*. Philadelphia.

Edler, A.C., Hattingh, M.M., Servas, V.P., and Marais, C.P. 1985. "Use of Aging Tests to Determine the Efficacy of Hydrated Lime Additions to Asphalt in Retarding Its Oxidative Hardening," *Proceedings of the Association of Asphalt Paving Technologists*, vol. 54, pp. 118–139.

Fair, W.F., Beck, H.R., and McKee, B.K. 1949. "Accelerated Weathering of Pitches and Asphalts," *ASTM Standard Tests and Practices* 94, p. 109.

Gallaway, B.M. 1959. "Factors Relating Chemical Composition and Rheological Properties of Paving Asphalts with Durability," *Proceedings of the Association of Asphalt Paving Technologists*, vol. 28, pp. 280–293.

Gietz, R.H. 1980. "Mineral Fines Effect on Asphalt Viscosity," Washington State Department of Transportation, Materials Office, report no. 164.

Greenfeld, S.H. 1956. "The Effects of Mineral Additives on the Durability of Coating Grade Roofing Asphalts," *Bitumen Material Series*, p. 147.

Greenfeld, S.H. 1958. "Effect of Mineral Fillers on Weather Resistance of Composition Roofing Covering Masses," *Bitumen, Terre, Asphalte, Peche*, p. 112.

Griffin, R.L, Miles, T.K., and Penther, C.J. 1955. "Microfilm Durability Test for Asphalt," *Proceedings of the Association of Asphalt Paving Technologists*, vol. 24, pp. 31–62.

Halstead, W.J., and Zenewitz, J.A. 1961. "Changes in Asphalt Viscosities During the Thin Film Oven and Microfilm Durability Tests," *ASTM Standard Tests and Practices* 309, p. 133.

Heithaus, J.J., and Johnson, R.W. 1958. "A Microviscometer Study of Road Asphalt Hardening in Field and Laboratory," *Proceedings of the Association of Asphalt Paving Technologists*, vol. 27, pp. 17–34.

Jimenez, R.A., and Gallaway, B.M. 1961. "Laboratory Measurements of Service Connected Changes in Asphaltic Cement," *Proceedings of the Association of Asphalt Paving Technologists*, vol. 30, p. 328.

Jongepier, R., and Kuilman, B. 1969. "Characterization of the Rheology of Bitumens," *Proceedings of the Association of Asphalt Paving Technologists*, vol. 38, pp.98–122.

Kandhal, P.S., and Wenger, M.E. 1975. "Asphalt Properties in Relation to Pavement Performance," *Transportation Research Record 544*. Washington, D.C.: TRB, National Research Council, pp. 1–13.

Kandhal, P.S., Sandvig, L.D., and Wenger, M.E. 1973. "Shear Susceptibility of Asphalts in Relation to Pavement Performance," *Proceedings of the Association of Asphalt Paving Technologists*, vol. 42, pp. 99–111.

Kemp, G.R., and Predoehl, N.H. 1981. "A Comparison of Field and Laboratory Environments on Asphalt Durability," *Proceedings of the Association of Asphalt Paving Technologists*, vol. 50, pp. 492–533.

Kim, O., Bell, C.A., Wilson, J.E., and Boyle, G. 1987. "Development of Laboratory Oxidative Aging Procedures for Asphalt Cements and Asphalt Mixtures," *Transportation Research Record 1115*. Washington, D.C.: TRB, National Research Council, pp.101–112.

Lee, A.R., and Dickson, E.J. 1954. "The Durability of Road Tar," *Road Research Technical Paper no.31*. Department of Scientific and Industrial Research Road Research.

Lee, A.R., Warren, J.B., and Waters, D.B. 1940. "The Flow Properties of Bituminous Materials," *Journal of the Institute of Petroleum*, vol. 26, 1940, p. 101.

Lee, D. 1968. "Development of a Laboratory Durability Test for Asphalts," *Highway Research Record* 231, pp. 34–49.

Lewis, R.H., and Halstead, W.J. 1940. "Determination of the Kinematic Viscosity of Petroleum Asphalts with a Capillary Tube Viscometer," *Public Roads*, vol. 21, p. 127.

Maccarrone, S. 1987. "Flow and Deformation Properties of Bitumen Service Weathered to Near Distress Level," *Australian Road Research Board*, no. 28, p. 34.

Mack, C. 1958. "Physical Aspects of Hardening of Paving Asphalts," *Proceedings of the Association of Asphalt Paving Technologists*, vol. 27, pp. 183–185.

Mack, C. 1965. "An Appraisal of Failure in Bituminous Pavement," *Proceedings of the Association of Asphalt Paving Technologists*, vol. 34, pp. 234-247.

McLeod, N.W. 1972. "A 4 Year Survey of Low Temperature Transverse Pavement Cracking on Three Ontario Test Roads," *Proceedings of the Association of Asphalt Paving Technologists*, vol. 41, pp. 424-493.

Majidzadeh, K. 1969. "Rheological Aspects of Aging: Part II," *Highway Research Record no. 273*, pp. 28-41.

Majidzadeh, K., and Schweyer, H.E. 1965. "Non-Newtonian Behavior of Asphalt Cements," *Proceedings of the Association of Asphalt Paving Technologists*, vol. 34, p. 20.

Majidzadeh, K., and Schweyer, H.E. 1968. "Viscoelastic Response of Aged Asphalts Cements," *Highway Research Record no. 231*, pp. 50-61.

Martin, K.G. 1966. "Influence of Stabilizers on Bitumen Durability," *Journal of Applied Chemistry*, vol. 16, pp. 197-202.

Mertens, E.W., and Greenfield, S.H. 1959. "Some Qualitative Effects of Composition and Processing on the Weatherability of Coating Grade Asphalt," ASTM, 3d Pacific Area National Meeting, no. 2.

Moavenzadeh, F., and Stander, R.R. 1966. "Durability Characteristics of Asphaltic Materials," in *Research Report* EES-259. Columbus: Ohio State University Experiment Station, p. 236.

Neppe, S.L. 1952. "Durability of Asphaltic Bitumen as Related to Rheological Characteristics," *Transaction, South African Institute of Civil Engineers*, vol. 2, pp. 103.

Page, G.C., Murrphy, K.H., and Ruth, B.E. 1985. "Asphalt Binder Hardening—Causes and Effects," *Proceedings of the Association of Asphalt Paving Technologists*, vol. 54, pp. 140-167.

Petersen, J.C. 1974. *Effects of Chemical Composition on the Properties of Asphalt and Asphalt-Aggregate Mixtures*. Laramie, Wyoming: Western Research Institute.

Petersen, J.C., Barbour, F.A., and Dorrence, F.M. 1974. "Catalysis of Asphalt Oxidation by Mineral Aggregate Surface and Asphalt Composition," *Proceedings of the Association of Asphalt Paving Technologists*, vol. 43, pp. 162-177.

Petersen, J.C., Planchre, H., and Harnsberger, P.M. 1987. "Lime Treatment of Asphalt to Reduce Age Hardening and Improve Flow Properties," *Proceedings of the Association of Asphalt Paving Technologists*, vol. 55, pp. 632–653.

Pfeiffer, J.P.H. 1950. *The Properties of Asphaltic Bitumen*. New York: Elsevier.

Pfeiffer, J.P.H., and van Doormaal. 1936. "The Rheological Properties of Asphaltic Bitumen," *Journal of the Institute of Petroleum Technologists*, vol. 22, p. 414.

Pink, H.S., Merz, R.E., and Bosniak, D.S. 1980. "Asphalt Rheology: Experimental Determination of Dynamic Moduli at Low Temperature," *Proceedings of the Association of Asphalt Paving Technologists*, vol. 49, p. 64.

Plancher, H., Green, E.L., and Petersen, J.C. 1976. "Reduction of Oxidative Hardening of Asphalts by Treatement with Hydrated Lime—A Mechanistic Study," *Proceedings of the Association of Asphalt Paving Technologists*, vol. 45, pp. 1-24.

Puzinauskas, V.P. 1967. "Evaluation of Properties of Asphalt Cements with Emphasis on Consistencies at Low Temperature," *Proceedings of the Association of Asphalt Paving Technologists*, vol. 36, p. 489.

Puzinauskas, V.P. 1979. "Properties of Asphalt Cements," *Proceedings of the Association of Asphalt Paving Technologists*, vol. 48, pp. 646-710.

Romberg, J.W., and Traxler, R.N. 1947. "Rheology of Asphalt," *Journal of Colloid Science*, vol. 2, p. 33.

Schmidt, R.J. 1973. "Laboratory Measurement of the Durability of Paving Asphalts," *ASTM Standard Tests and Practices* 532, pp. 79-99.

Sisko, A.W., and Brunstrum, L.C. 1968. "The Rheological Properties of Asphalt in Relation to Durability and Pavement Performance," *Proceedings of the Association of Asphalt Paving Technologists*, vol. 37, pp. 448-475.

Sisko, A.W., and Brunstrum, L.C. 1969. "Relation of Asphalt Rheological Properties to Pavement Durability," *NCHRP Report 67*. Washington, D.C.: TRB, National Research Council.

Traxler, R.N. 1947. "Review of the Rheology of Bituminous Materials," *Journal of Colloid Science*, vol. 2, p. 49.

Traxler, R.N., and Schweyer, H.E. 1936. "Increase in Viscosity of Asphalts with Time," *Proceedings of the American Society for Testing and Materials*, vol. 36, part II, pp. 544-551.

Traxler, R.N., Schweyer, H.E., and Romberg, H.W. 1944. "Rheological Properties of Asphalt," *Industrial and Engineering Chemistry*, vol. 36, no. 9, p. 823.

Van Ort, W.P. 1956. "Durability of Asphalt: Its Aging in the Dark," *Industrial and Engineering Chemistry*, vol. 48, no. 7, pp. 1196-1201.

Van der Poel, C. 1954. "A General System Describing the Viscoelastic Properties of Bitumens and Its Relation to Routine Test Data," *Journal of Applied Chemistry*, vol. 4, pp. 221-236.

Zapata, J., and von Hazmburg, R.S. 1949. "The Effect of Fillers on the Durability of Asphalt," *Proceedings of the Association of Asphalt Paving Technologists*, vol. 18, p. 95.

Zube, E., and Skog, J. 1969. "Final Report on Zaca-Wigmore Asphalt Test Road," *Proceedings of the Association of Asphalt Paving Technologists*, vol. 38, pp. 1-39.

6

Miscellaneous Tests

The coefficient of viscosity has been traditionally used to determine mixing and compaction temperatures and to ensure that asphalt cement can be readily pumped at storage and mixing temperatures. Currently, capillary viscometers are used for this purpose but, for a number of reasons explained below, an alternative method for measuring viscosity at mixing and compaction temperatures is needed. As part of this study a rotational viscometer was evaluated for this purpose.

During the evaluation and development of test methods and procedures to characterize the physical properties of asphalt binders the main emphasis was placed on performance-related test methods that could be used for specification purposes. A number of test methods were investigated and found unsuitable for one or more reasons. These included

- The blow-off adherometer or "blister test" for measuring asphalt binder-aggregate adhesion in the presence of water,

- The dielectrics test as a method for determining rheological properties, and

- The ultrasound test as a method for determining rheological properties.

The results of these studies are described in this chapter.

Rotational Viscometer

Capillary tube viscometers are used in the current asphalt cement specifications to specify the coefficient of viscosity at 165°C (329°F). Measurements at this temperature, along with a second measurement at 60°C (140°F), can be used to generate a viscosity-temperature curve or profile. Capillary tube viscometers require considerable quantities of organic solvent, which is undesirable from an environmental standpoint. More important, capillary tube viscometers provide rather low rates of shear that are inappropriate for characterizing modified asphalts at the high rates of shear that occur during pumping and mixing operations.

Therefore, rotational viscometers were evaluated as a substitute for the capillary tube viscometers that are now widely used for asphalt cement. This work was done under the direction of J. Button at the Texas Transportation Institute (TTI).

An ASTM specification currently exists for rotational viscometers, ASTM Standard Method D4402, "Viscosity Determinations of Unfilled Asphalts Using the Brookfield Thermosel Apparatus." A Brookfield rotational viscometer, Model DVII, which meets the requirements of the ASTM standard, was evaluated for specification use. The evaluation centered around the development of a technique for rapidly developing a viscosity-temperature profile. The Brookfield is routinely used by many asphalt suppliers and is covered by an ASTM standard. Therefore, the purpose of this work was not to qualify the Brookfield viscometer but to establish a protocol for its use.

Viscometer Characteristics

Comparison of Available Viscometers

Several viscometer manufacturers were contacted and questioned regarding their products. Of particular interest were portable viscometers that would be suitable for measuring viscosity at a plant site or in a field laboratory. Literature was requested from the manufacturers and reviewed. Common methods used in determining viscosity include rotary, capillary, vibratory, falling ball, parallel plates, and timed flow from a container of known volume. Viscosity measurements may be provided in standard units or in relative units peculiar to a particular instrument or manufacturer.

Most commercially available portable viscometers are of the rotational type, as shown in table 6.1.[1] These devices afford simple operation and can be removed from their stands and hand held if the need arises. Some models provide a readout in nonstandard units that must be converted to viscosity units using a simple calculation, while others provide a direct readout in conventional viscosity units. Some more expensive models provide a direct readout of temperature, shear rate, rotational speed, shear stress, and torque. Hand-held, battery-operated models are available, which offer complete portability. Accessories are available that can maintain a sample of asphalt at a constant temperature.

For a rapid measurement in a field environment, where accuracy may be sacrificed for measurement rapidity, the coefficient of viscosity as a function of temperature could easily and rapidly be obtained from a can of hot asphalt as it cools. Of course, periodic stirring immediately before measuring viscosity and temperature would be necessary to avoid development of a temperature gradient within the can. This procedure could be used to "bracket" the viscosity at a temperature of interest and thus obtain a value with a relatively high level of confidence.

---

[1]All figures and tables referenced in this chapter appear at the end of the chapter.

During the study, it was found that in-line viscometers are also available and that they can be used to continuously monitor the viscosity of a material as it is transferred from one area of a plant to another. These devices respond instantly to viscosity changes and are designed to be mounted directly in pipelines and tanks, operating where flow is fast and turbulent. They resist high temperature and pressure, impact, and corrosion. Most of these devices employ the principle of vibration or oscillation at very low amplitudes (about 1 micron) and high frequencies. This type of instrument would allow one to directly measure viscosity of asphalt at any point in an asphalt plant and to monitor the viscosity of modified binders during blending operations. In-line viscometers are available from Automation Products Dynatrol, Nametre Company, and Bendix Corporation. The cost of these instruments ranges from $6,000 to $12,000. These instruments probably merit more widespread use and need to be investigated in more detail to determine their suitability and utility in the asphalt industry.

The applied shear rates for in-line viscometers may correlate reasonably well with those found in the nozzles of asphalt distributor trucks. Thus, binder viscosity could be controlled directly through temperature measurements. This direct measurement would eliminate the need for a viscosity-temperature curve for each different product used in distributor trucks. Asphalt viscosity could be precisely adjusted to optimize the performance of the spray nozzles on distributor trucks. This information needs to be conveyed to asphalt user agencies and paving contractors. Additional study on the applicability or evaluation of this equipment was beyond the scope of this project but is merited.

Consideration of Shear Rates Experienced in Practice

Experience from the field indicates that for some modified asphalts significant shear thinning occurs during pumping and that capillary viscometers do not give realistic measurements when pumpability is a concern. No reliable estimates for shear rates typical of transfer pumps were found, although they may be in excess of 10^3 to 10^4 s^{-1} (Shuler 1992). Simply duplicating these shear rates may not be sufficient to represent the flow behavior of asphalt binders during pumping. Because of the close tolerances in most pumps, very high energies are involved and energy transfer may be the primary cause of the shear thinning. Nonetheless, the shear rates afforded by rotational viscometers are much closer to those expected in pumps as illustrated by the data in tables 6.1 and 6.2. For example, the Nametre in-line viscometer applies a constant shear rate of 4,084 sec^{-1}.

Selection of a Viscometer for Detailed Study

This portion of the study was initiated to identify an "appropriate" device for measuring viscosity of asphalts at relatively high temperatures and to develop a test method for uniformly and consistently performing the measurement. "Appropriate" is defined, in this case, as reasonably accurate and precise, fast, convenient, rugged, economical, and not requiring a high degree of operator skill. The selected instrument will replace the capillary viscometer as a SHRP specification test for asphalt binders at binder storage and handling temperatures and at temperatures normally required for mixing and compacting paving

mixtures. Based on convenience of use, versatility, and cost, the researchers selected a rotational viscometer for further study. On the basis of the prior experience of other researchers and practitioners within the industry and the existence of an applicable ASTM standard, a Model DVII Brookfield viscometer was selected for evaluation.

Rotational viscometers measure the coefficient of viscosity by sensing the torque required to rotate a spindle at a constant speed while immersed in the test fluid. The torque is proportional to the viscous drag on the immersed spindle, and thus to the viscosity of the fluid. For the user, rotational viscometry is advantageous when measuring the coefficient of viscosity of asphalt binders:

- The rate of shear is high when compared with that of a capillary tube viscometer and, for this reason, the rotational viscometer better simulates the high shear rates associated with in-plant pumping and compaction of paving mixtures.

- The rate of shear to which the sample fluid is subjected during a given test is constant, so the instrument is suitable for measuring Newtonian and non-Newtonian fluids.

- By rotating the immersed spindle at several different speeds, shear dependent behavior of non-Newtonian fluids can be detected and characterized.

Rotational viscometers are rugged, mechanically simple instruments that are capable of measuring a wide range of viscosities. Multiple speeds and interchangeable spindles result in a large selection of viscosity (or temperature) ranges for optimum sensitivity and accuracy. Instrument setup is usually a relatively simple operation. Reasonably accurate and reproducible viscosity determinations can be made quickly without requiring a high degree of operator skill.

Existing ASTM Standards for Rotational Viscometers

Several ASTM standards currently exist for rotational viscometers. They are reviewed briefly below:

- *ASTM D4402-84*—This standard is titled "Viscosity Determinations of Unfilled Asphalts Using the Brookfield Thermosel Apparatus," outlines a procedure for measuring the apparent viscosity of asphalt from 38° to 260°C (100° to 500°F) using the Brookfield Thermosel apparatus.

  The Brookfield Viscometer Thermosel system described in this procedure can be used to measure the apparent viscosity of asphalt at elevated temperatures. The torque on a spindle rotating in a special thermostatically controlled sample holder (Thermosel) that contains a small sample of asphalt is used to measure the relative resistance to rotation. A factor is applied to the torque dial reading to yield the viscosity of the asphalt in mPa·s or a direct readout model viscometer

can be used. For most routine asphalt testing ASTM D4402 should be the preferred test procedure.

- *ASTM D2196-86*—This standard, "Rheological Properties of Non-Newtonian Materials by Rotational (Brookfield) Viscometer," calls for a Brookfield model LVF or LVT having four or eight rotational speeds, respectively. This test method covers the determination of the apparent viscosity and the shear thinning and thixotropic properties of non-Newtonian materials in the shear rate range from 0.1 to 50 s^{-1}.

Test method A consists of determining the apparent viscosity of coatings and related materials by measuring the torque on a spindle rotating at a constant speed in the material.

Test methods B and C consist of determining the shear thinning and thixotropic (time-dependent) rheological properties of the materials. The viscosities of these materials are determined by using a prescribed series of spindle speeds. The agitation of the material immediately proceeding the viscosity measurements is carefully controlled.

- *ASTM D3236-73*—This standard, "Apparent Viscosity of Hot Melt Adhesives," employs a rotating spindle-type viscometer. A Brookfield with Thermosel is depicted in the standard. This method covers the determination of the apparent viscosity of hot-melt adhesives and coating materials compounded with additives and having apparent viscosities as large as 200 mPa·s at temperatures up to 175°C (347°F).

A representative sample of the molten material is maintained in a thermally controlled sample chamber. Apparent viscosity is determined under constant temperature conditions using a precision rotating spindle-type viscometer. Data obtained at several temperatures can be plotted on appropriate semilogarithmic graph paper and apparent viscosity at intermediate temperatures can be estimated.

- *ASTM D2493-85*—The standard is titled "Viscosity-Temperature Charts for Asphalts." The viscosity-temperature chart covered by this standard is a convenient means of plotting data for estimating the viscosity of asphalts at any temperature within a limited range. Conversely, the chart may be used to ascertain the temperature at which a desired viscosity is attained.

The data are presented as the logarithm-logarithm of the viscosity in cSt versus the reciprocal of the absolute temperature in the Rankine scale. To be consistent with the SI units used in the SHRP binder specifications, the chart should be revised to show the units in Pa·s and the reciprocal of the absolute temperature in degrees Kelvin.

Description of Equipment

The operating principle of the DVII Brookfield viscometer is based on the measurement of torque generated as a spindle is rotated at a preselected speed. The torque is measured with a beryllium copper spring; the degree to which the spring is wound, detected by a rotational transducer, is proportional to the viscosity of the fluid. Consequently, the higher the rotating speed, the higher the drag or torque.

The temperature control system, or Thermosel, includes a digital proportional temperature controller with a platinum resistance thermometer (RTD) sensor. The controller has several programmable functions and can be set to display either Fahrenheit or Celsius temperature scales.

The spindle speed of the Brookfield DVII viscometer is controlled incrementally with a selector knob. Possible spindle speeds include 0.5, 1.0, 2.5, 5.0, 10.0, 20.0, 50.0, and 100.0 rpm. As the spindle speed increases the resistance to flow increases, thereby increasing the torque on the spring. The coefficient of viscosity is determined from the torque (stress) and spindle speed (shear rate).

The Brookfield DVII viscometer can be used with optional Brookfield DV-Gather software. This software facilitates testing procedures by preprogramming certain commonly used data-gathering techniques. It displays data to the computer screen, saves data to a diskette, prints and plots data, presents screen templates for easy input of test parameters, and programs preselected torque alarm settings to signal an out-of-range condition. The main *shortcoming of the DV-Gather software is that it does not acquire temperature data from the* Thermosel.

Three different testing modes are available with the software:

- The *manual mode* is convenient but not necessary. It prints out the coefficient of viscosity, torque, shear stress, and shear rate for each data point, which is difficult to accomplish without the software.

- The *timed mode* is extremely valuable in establishing the different parameters of the testing procedures, the timed mode enables the technician to automatically obtain multiple data points at as little as 2-second intervals. Although, the program allows a setting of 1-second, the buffer action does not really permit an actual 1-second interval. The 2-second interval, however, is reliable.

- The *varispeed mode* automatically obtains, through the software, a data point every time the speed is changed, as described in the testing procedure detailed above.

Temperature Control

A major concern with the design of the Thermosel is that it does not directly measure the temperature of the asphalt. The RTD sensor for the controller is mounted in the insulated portion of the Thermosel housing but outside the sample chamber. This design places the metal walls of the sample chamber and container between the RTD probe and the asphalt specimen. This placement results in considerable lag in the temperature recorded with the RTD and the temperature of the asphalt when the temperature of the heating medium is being changed.

Limited tests were conducted to verify the accuracy of temperature measurement in the Thermosel. The device appeared to measure temperature within less than $\pm 1°C$ ($\pm 1.8°F$) in the temperature range of interest in this study, 80° to 180°C (176° to 356°F), when ample time was allowed for equilibration.

Several tests were performed to establish the time required for an asphalt specimen to reach the set temperature or the temperature displayed on the temperature controller. Figure 6.1 shows results typical of several tests where the temperature controller was alternately set to hold a given temperature for 20 minutes and then increased by 25°C (45°F) and held for 15 minutes. The Brookfield DV-Gather software (discussed earlier) was set to collect and record data every 1.5 minutes. In figure 6.1, the viscosity reaches a constant value when the specimen temperature is no longer increasing. From these experiments, it was established that a 15-minute hold time is required to ensure that the specimen has reached the set temperature. Much more time is required when viscosity measurements are made with the temperature descending since the Thermosel is well insulated and has no mechanism for cooling the sample. Thus, without future modification, measurements should be made by increasing the temperature rather than by lowering the temperature.

Effect of Spindle Speed

Different asphalts were tested at a constant temperature with spindle SC4-27 while varying only the spindle speed. Typical results are depicted in figures 6.2 and 6.3. It can be seen that as the speed of the spindle increases there is initially a drop in viscosity. Then viscosity levels off at rotating speeds above 10 rpm. Viscosity readings in the level area of the plots compare well with the values obtained in previous testing and reasonably well with the capillary viscometer. Therefore, it was concluded that the Brookfield viscometer should not be operated below the 10-rpm range for routine testing of asphalt binders. Thus, it is recommended in the test procedure that the test be performed at a spindle speed of 20 rpm.

Shear Rate versus Time of Loading

The Brookfield viscometer inherently yields incorrect viscosity readings during the first few seconds after the device is turned on. The documentation provided by the manufacturer recommends that the viscometer be turned on and allowed to run until a constant reading is

obtained since momentum is gained by the spindle during the initial acceleration. The time required to reach that constant reading depends on the speed of the spindle and the viscosity of the material being tested. Thus, the incorrect readings are equipment and not material characteristics. Tests were performed at various temperatures with several different asphalts to determine the time required to obtain stable readings. Figures 6.4 and 6.5 show results typical of several of these tests. The data points were taken at 3-second intervals after the start of the viscometer motor, 3 seconds being the time for one full rotation of the spindle at 20 rpm.

As can be seen from the graphs, the time required to attain a constant viscosity reading varies significantly with temperature. The longer time required at lower temperatures is most likely because the binder is more viscous at the lower temperatures. Consequently, the test method should require continuous rotation of the spindle for at least 2 minutes before any reading is recorded when testing at 20 rpm.

Reproducibility

Viscosity as a function of temperature for a high-temperature viscosity standard oil is shown in figure 6.6. The standard values for the oil are 8.875 Pa·s at 93.3°C (200°F) and 4.39 Pa·s at 148.9°C (300°F). The instrument was capable of measuring viscosity within 2 percentage points of the standard value.

Statistical analyses were performed on an extensive series of tests to determine the repeatability of the Brookfield viscometer and test procedure. The data consist of two replicate viscosity measurements of eight different types of asphalt, with approximately five measurements, each at a different temperature. Occasionally, the viscosity measurements were not performed at exactly the same temperatures for both the test runs. In these cases, the needed values were interpolated between temperatures to obtain the viscosity values at the same temperature for both the test runs in a given pair. Repeatability for this paired data set was determined using the paired t test.

The t test involves proof by contradiction. To conduct the analyses, The two sets of the paired data are assumed to be no different from each other, i.e., their means are the same ($\mu_1 - \mu_2 = 0$, the null hypothesis). This hypothesis is checked to determine, for a given confidence level, if it can be rejected. If there is sufficient evidence to disprove the hypothesis, it is rejected; otherwise, it is accepted.

For the Brookfield viscosity data, Test 1 and Test 2 had mean values of 1.3842 and 1.3627, respectively. The difference in means, μ_D, was 0.0215 and the standard deviation of the differences, s_D, was 0.1455. Using the following relationship

$$t_{\text{paired}} = [\mu_D/s_D]\sqrt{n} \qquad (6.1)$$

where

n = number of pairs,

t_{paired} was calculated as 0.9091. For a 95 percent confidence level and 38 data points, the $t_{a/2,n-1}$ value is 2.025. According to the statistical procedure, for the hypothesis to be rejected, the necessary condition is $t_{paired} \geq t_{a/2,n-1}$. Since this condition was not satisfied, there was insufficient evidence to reject the null hypothesis. Hence it can be stated, with 95 percent confidence level, that the two test runs are not different from each other. In another test, samples of the same asphalt were performed by different technicians several months apart. The results of these tests are shown in figure 6.7. Repeatability for these tests was considered excellent, especially when the coefficient of viscosity was greater than 1 Pa·s.

Information provided by the manufacturer indicates that any viscosity data recorded at a torque lower than 10 percent is guaranteed to be accurate only to $\pm$ 10 percent. Correlation of data between the individual tests and comparison with data acquired by other testing procedures has indicated that precision better than ± 10 percent is attainable unless the torque falls below 1 percent.

Comparison with Capillary Viscometers

Results of selected Brookfield tests were compared with the kinematic viscosity from the existing standard procedure (ASTM D 2171), which uses the capillary viscometer. Figures 6.8 through 6.10 compare the results of the viscosity-temperature curve obtained using the Brookfield system with the curve obtained using a kinematic viscosity test. The kinematic data were converted from centistoke to Pa·s, and the Brookfield data were converted from centipoise to Pa·s. These graphs demonstrate a fairly good correlation between the established kinematic method of viscosity determination for asphalts and the Brookfield procedure developed in this study. Single-value viscosity determinations were normally within 15 percent of each other. The widest variations between the Brookfield and kinematic viscometers occur at viscosities less than 1 Pa·s.

If a viscosity measurement is required at a single temperature, the Brookfield can produce it in about 20 minutes after preparing the specimen, which is not a significant improvement over the time required for a capillary viscometer test (ASTM D 2170, "Kinematic Viscosity of Asphalts"). Time required for the capillary test depends on the oil bath temperature and whether it has been previously brought to the temperature required for the test. The Brookfield, however, can produce a measurement at a second temperature in an additional 20 minutes without any delay to adjust the temperature chamber.

Development of Recommended Test Procedure

Objective

The rotational viscometer provides an alternative test method to conventional capillary tube viscometers. Measurements at a single temperature with the rotational viscometer can be

made in approximately the same amount of time as with capillary tube viscometers, but the level of skill required by the operator is judged to be somewhat less. The main reason for evaluating the rotational viscometer, however, was to develop a rapid method for obtaining a viscosity-temperature profile as required to determine mixing and compaction temperatures. A test procedure capable of accurately quantifying the consistency of asphalt cement or modified asphalt binders within a viscosity range of approximately 0.1 to 20 Pa·s, or a temperature range of about 80° to 190°C (176°F to 374°F), was the objective of this part of the study. Three methods were developed by the TTI research team:

- *Method 1*—Raise the temperature of the system incrementally, allowing thermal equilibrium at each step. Obtain the coefficient of viscosity at each step and plot the data as a logarithm of viscosity versus temperature. Total testing time is approximately 2 hours.

- *Method 2*—Allow the Thermosel to heat incrementally, but do not obtain equilibrium at each heating increment. Apply a correction factor to the coefficient of viscosity to allow for the temperature lag between the temperature of the sample and the temperature of the Thermosel. Total testing time is approximately 30 minutes.

- *Method 3*—Measure the viscosity at two temperatures and determine viscosity values at intermediate temperatures by interpolation.

Method 1: Equilibrium Incremental Heating

Approximately 20 minutes are required to obtain each data point for method 1, and a complete curve with six data points can be completed in approximately 2 hours. To reproduce the same five points using the capillary viscometer would require more than 5 hours, primarily because of the time required to adjust the temperature of the oil bath.

Details for running the test can be found in ASTM D4402-84, "Viscosity Determinations of Unfilled Asphalts Using the Brookfield Thermosel Apparatus." Instead of conducting a single temperature measurement, the temperature is increased incrementally by 20°C (36°F) over the temperature range of interest. Six temperatures are sufficient to define a plot of the logarithm of the coefficient of viscosity versus temperature.

Method 2: Nonequilibrium Incremental Heating

At each heating increment, hold times of 0, 2, and 4 minutes were investigated. The reduced hold time did not produce thermal equilibrium and, as a consequence, the actual and reported temperatures differ by several degrees. A typical set of data with 0-, 2-, and 4-minute hold times is given in figure 6.11. To account for the thermal lag, a "correction factor" was developed as shown in table 6.3. The correction factors are asphalt

binder-source dependent. An average value, 0.472, was determined and recommended for use with this method.

To apply this method, the temperature in the Thermosel is raised in 20°C (36°F) increments and a 2-minute hold time is used at each temperature. The data are then corrected by applying a factor of 0.472 to the measured coefficients of viscosity. The procedure for conducting measurements in accordance with method 2 are the same as with method 1 except that the hold time is 2 minutes rather than 20 minutes.

Method 3: Two-Point Determination

Method 1 is time-consuming and Method 2 requires a "correction factor," which is somewhat unsettling and introduces an added degree of uncertainty in the results. The logarithm-logarithm of the coefficient of viscosity is reported to plot as a linear function of the reciprocal of the absolute temperature, and there are standard ASTM charts for this purpose. (Note: The charts are based on the log-log of viscosity in cST: ASTM is in the process of developing a chart in Pa·s units.) Data for a number of plain and polymer-modified asphalts are shown in figure 6.12. These data are very linear, suggesting that measurements could be made at two points and plotted as shown in figure 6.12. The SHRP binder specifications require a viscosity measurement at 135°C (275°F) to ensure pumpability. Assuming that a viscosity-temperature profile is needed over the range from approximately 120°C (248°F) to 135°C (275°F), a viscosity measurement at 120°C (248°F) and a second measurement at the specification temperature should provide sufficient data for a reliable plot of the logarithm-logarithm of viscosity versus reciprocal temperature.

Thus, after reviewing the TTI results, a two-point measurement is recommended in instances where a viscosity-temperature profile is required. With a 20-minute hold time at each temperature, approximately 45 minutes would be required to obtain the profile.

Summary and Recommendations for the Rotational Viscometer Study

- The Brookfield DVII viscometer and Thermosel system is a reliable instrument for efficient measurement of asphalt viscosity at typical paving application temperatures.

- Results from the Brookfield viscometer compare reasonably well with results from standard capillary viscometers.

- A two-point measurement method using a linear logarithm-logarithm coefficient of viscosity versus the reciprocal of the absolute temperature is recommended for field control of mixing and compaction temperatures when such control is desired.

- Based on the findings of this study, it is recommended that the ASTM D4402-84 be used as the standard test method for field laboratory measurements of asphalt viscosity and that the Brookfield viscometer Model DVII with Thermosel be adopted as the standard equipment.

- A temperature controller (Thermosel) should be developed that requires the temperature sensor to be in physical contact with the asphalt (as opposed to the bath medium) while the viscosity measurement is being made. Such a device may be more expensive than the current Thermosel but will eliminate thermal lag during a temperature sweep. This physical contact with asphalt would allow method 2 (continuous measurement) to be adopted for field control and as a specification procedure.

Blister Test

Selection of an Adhesion Test Method

A literature review was conducted to identify test methods that could be used to measure the strength of the bond between asphalt and aggregate surfaces. This review included traditional asphalt literature but was extended to include literature relating to structural adhesives. The literature related to the aerospace applications of structural adhesives was found to be useful for identifying new debonding tests. A great deal of work has been done to study the behavior of polymer-metal joints and the effect of moisture on the strength of the polymer-metal bond. Although most of the aerospace applications were for metal adherend, fracture mechanics concepts were identified that may ultimately prove useful in studying the debonding mechanism of asphalt-aggregate systems. In addition, during the review, several types of debonding tests were identified as described below.

Some important conclusions from the literature review of test methods were

- The parameters derived from physicochemical studies of water-aggregate-asphalt systems—such as surface energy, surface roughness, contact angle, and others related to composition of asphalt or the surface chemistry of aggregates—do not offer great promise. Although they are important in terms of understanding the cause of debonding, they are often difficult to evaluate experimentally, cannot be directly related to the moisture damage and pavement performance, and do not result in engineering terms that can be directly related to mixture properties.

- The debonding, film rupture, and pore water pressure concepts are of great promise and may potentially explain moisture damage failure mechanisms. However, there is a lack of reliable test procedures that are compatible with these concepts and that provide meaningful bond-strength parameters.

- The nature of the aggregate surface has a significant role in defining the bond strength. Aggregates, during asphalt concrete mixing operations, are exposed to

412

extreme heat, which may significantly change their surface conditions. Further, the performance of freshly crushed and stockpiled aggregates are often very different. These factors have not been well investigated in previous studies and are believed to be important. They must be included in any debonding test used for specification and design purposes.

- The rheological properties of asphalt binder have greatly influence the strength of the bond as well as the debonding mechanism. Displacement of the binder by water is opposed by high consistency of the asphalt. Asphalts with high coefficients of viscosity have been observed to resist displacement. This finding suggests that hardening of asphalts because of oxidative aging or steric aging plays an important role in the resistance of pavements to moisture damage. The effect of asphalt hardening on moisture damage has not been studied extensively.

- Fracture properties of the asphalt binder and the application of fracture mechanics techniques for predicting or measuring asphalt-aggregate bond performance were found to be of great promise. Several testing configurations and techniques are used to study the fracture properties of joints where polymeric adhesives are used with metal adherends. Several of these tests appear to be suitable for studying the asphalt aggregate bond. The tests also appear suitable for age conditioning.

Four potentially useful test procedures were identified for possible use in this work. Each of these tests offers a slightly different approach to the measurement of adhesion and disbonding:

- The blister blow-off adherometer (Liechti et al. 1987)—This test consists simply of a coating of asphalt binder (adhesive) over a flat aggregate surface (adherend). A hole, drilled through the aggregate under the coating, permits the application of steady or varying water pressure to the underside of the coating (see figure 6.13). Adhesion is measured by the force required to displace the film from the aggregate.

- Double cantilever beam (ASTM D3433)—This widely used test in the area of structural adhesives consists of two beams between which a film of asphalt cement is sandwiched (see figure 6.14). The force required to initiate a crack when the two beams are pulled apart is related to the strength of the bond, and fundamental fracture mechanics properties can be obtained from the test data.

- Spherical indenter (Barquins and Wehbi 1986)—In this method, the force and depth of the indentation of a solid ball into a free asphalt surface is measured. In this application, the solid ball would be an aggregate particle (see figure 6.15). The force-deformation diagram can then be related to adhesion/disbonding and to a fracture mechanics evaluation of disbonding and crack growth.

- Scarf test (Trantina 1972)—This test is merely a butt joint for which asphalt cement is the adhesive. The joint is constructed diagonally rather than at a 90-degree-angle, (see figure 6.16). By varying the angle of the scarf, an adhesive

413

failure can be induced in the joint. An extensive body of literature is available for analyzing the results of this test. For use with asphalt cement, the substrate could be two pieces of aggregate.

For the following reasons it was decided to develop the blow-off adherometer for measuring asphalt-aggregate bond strength:

- The test appeared to be one of the simplest to perform.

- Water can be used to force the asphalt from the aggregate surface, representative of in-service conditions.

- Water can be introduced at the asphalt-aggregate interface, which is essential if water-induced damage is to be measured.

Each of the above tests suffers from a major deficiency—the aggregate surface must be ground or sawn to produce a flat surface. A sawn face is probably not representative of a crushed or fractured face. This deficiency is further aggravated when it is necessary to polish the adherend surface.

Description of Test Method

Considerable effort was expended to develop a simple method for preparing test samples, conditioning the specimens, and conducting the test. Discussions regarding test specimens, testing protocol, and data analysis were held with Dr. Victor Chang, one of the A-002B researchers. The review of the literature showed that the analysis of the test data was much more complicated than originally thought. In order to fully characterize the failure mode, a nonlinear fracture mechanics analysis would be required along with a nonlinear viscoelastic constitutive equation for the asphalt binder. As a consequence, a more pragmatic approach was taken and the focus at Penn State University was placed on measuring the ultimate strength of the bond as opposed to obtaining fundamental material properties. Dr. Chang provided suggestions regarding the specimen geometry, which were adopted as follows:

- Specimen diameter, 25 mm (1 in.);

- Blister diameter (initial unbonded area), 5 mm (0.2 in.); and

- Film thickness, 1.0 to 2.0 mm (0.04 to 0.08 in.).

After considerable trial and error, the final test configuration included an aluminum film placed on top of the asphalt layer to prevent a "blow out" of the asphalt film during pressurization. Dr. Chang assured the A-002A researchers that a theoretical analysis can be generated for the case with a composite aluminum-asphalt layer. The device that was

414

ultimately developed as part of the study is shown in figure 6.17. The final specimen preparation and testing procedure was as follows:

- Imbed 25 mm (1 in)-size aggregate particles in a layer of epoxy. Cut a 25-mm (1-in.) diameter core from the epoxy-aggregate composite so that a core approximately 25-mm (1-in.) long, with epoxy on one end and aggregate on the other end, is obtained.

- Trim the core (with a fine diamond saw on the aggregate end) to give two flat faces: one epoxy and the other aggregate.

- Drill a 3-mm (1/8-in.) diameter hole from one face to the other through the axis of the trimmed core to give a cylinder with a concentric hole.

The aggregate surface is then coated with asphalt on one end. The difficult part of the preparation procedure is to provide an unbonded pocket above the hole in the aggregate face. A thin 5-mm (0.20-in.) Teflon™ disc placed over the hole was used for this purpose. The blister is then composed of a small Teflon™ disc above the hole, a layer of asphalt cement, and, on top of the asphalt, a sheet of aluminum foil to prevent a blow-out above the hole. The foil must be thin enough to allow the blister to deform when pressure is applied to the underside of the disc. It was found that pressures as large as 689.5 KPa (100 lb/in.^{2}) are necessary to dislodge the asphalt cement at the lower test temperatures when stripping is not present. In these conditions, the failure is cohesive, occurring within the asphalt film as opposed to the interface between the asphalt and the aggregate surface.

Test Results

A series of tests involving the eight core asphalts and two aggregates was completed using the blister test. The initial tests used a limestone aggregate that, based on extensive field experience, does not show evidence of stripping. This aggregate is used locally in the State College, Pennsylvania, area and consists primarily of calcium carbonate. When tested with each of the eight core asphalts, a cohesive failure was observed within the asphalt film. In other words, it was not possible to cause stripping with this aggregate.

Attention was then focused on the Texas chert aggregate (MRL designation RL) and, in a similar manner, only cohesive failure was observed. This experience contradicts the reputation of this aggregate—it is a notorious stripper. The conditioning procedure that had been used up to that point consisted of the following steps:

- Prestress the blister to cause a slight "bulge" in the blister.

- Place the specimen in a vacuum chamber and evacuate the air.

- Backflood the specimen with water while the vacuum was applied.

- Soak the specimen for 12 hours at 60°C (140°F).

- Cool the specimen to the test temperature, 0° or 25°C (32° or 77°F), and apply the air pressure to cause failure.

With this procedure, no adhesive failures were observed with either of the aggregates or any of the eight core asphalts.

In a second conditioning procedure, in which a freezing step was added after the 60°C (140°F) soaking, adhesive failures were produced. However, adhesive failures were produced in both the limestone and the Texas chert aggregate, and there was no significant difference in the behavior of the two aggregates. In other words, the test did not differentiate between two aggregates with radically different susceptibility to water damage. The results of this testing are described in table 6.4.

Recommendation for Implementation of Blister Test

Based on the test results reported in table 6.4, the A-002A research team recommended that the blister test be dropped as a SHRP specification-type test and that further research with this test be stopped. This recommendation was based on the following:

- To complete a single test, 1 to 2 person days are required, including sample preparation, the most lengthy step in the process.

- The surface of the aggregate does not represent an aggregate surface as it exists in the field, because the tested surface is sawn and free of surface contaminations, whereas in the field the aggregate is crushed and contaminated with dust and other naturally occurring material. Polishing the surface of the aggregate makes the sample even more unrepresentative of the in-service aggregate.

- The test does not reflect experience in the field—an aggregate known to strip did not show an adhesive failure unless a freezing cycle was added. Further, when the freezing cycle was added, an aggregate known to be resistant to stripping in the field did not show any evidence of disbonding in the blister test.

- The test procedure requires very sophisticated theoretical analysis and material characterization to generate fundamental material properties and to evaluate the results on a fundamental basis. Such analysis is not available at this time.

- The test cannot be used to evaluate particles smaller than approximately 25 mm (1 in.) in diameter.

No further testing was attempted with the blister test.

416

Dielectrics

Dielectric measurements were initially intended to measure the properties of asphalt binders in situ within mixtures or within the pavement structure. The extraction of asphalt cement from paving mixtures destroys molecular associations (steric hardening as well as any aggregate-asphalt interactions) that are developed during long-term service. Thus, dielectric measurements were initially intended as a means for estimating the in situ rheological properties of asphalt cement, especially for studies of steric hardening. Later in the project, after the SHRP management decided to eliminate steric hardening studies, dielectric measurements were directed toward the study of physical hardening and an explanation of the microstructural model.

In the first year of the project, Dr. Andrea Chow of Stanford Research International (SRI) was in charge of the dielectric studies. When she left SRI, this work was transferred to Penn State under the direction of Dr. V. J. Veradan. A great deal of effort was expended at both institutions to develop test equipment and test methodology, primarily to control the temperature of the test cells and to develop techniques for testing at lower frequencies.

Testing Conducted at Stanford Research International

A schematic of the test equipment used by Dr. Chow at SRI is shown in figure 6.18. A Solartron 1250 Frequency Analyzer was used in the frequency range from 1 to 10,000 kHz; a Hewlett-Packard 4192A Impedance Analyzer was used for the higher frequencies. By using various solvent/CO_2 baths, it was possible to obtain test data in the range from $-68°$ to 100°C ($-90°$ to 212°F).

Table 6.5 gives the dielectric constants of three core asphalts as initially measured by Dr. Chow in the frequency range of 10 kHz to 10 MHz. Because of the very small values measured for the loss tangent and the limited accuracy of the technique used for calibration, the loss tangent data could not be measured accurately. However, the measured dielectric constant values are in good agreement with those reported by Westphal and Sils (1972).

Dielectric permutivity, ϵ', and dielectric loss, ϵ'', measurements for unaged and aged AAG-1 are shown in figures 6.19 and 6.20. The loss measurements do not appear to be affected by the aging process, whereas the permutivity measurements show significant change with aging. These early measurements showed that the dielectric properties were sensitive to asphalt properties, and the initial results were considered encouraging.

Two asphalts were then tested over a wide temperature range, and master curves for the dielectric loss tangent, ϵ''/ϵ' loss, were generated as shown in figures 6.21 and 6.22. Figures 6.23 and 6.24 also show the time-temperature shift functions for the dielectric and rheological loss tangent master curves. There is excellent agreement between the two sets of time-temperature shift functions except at the low temperatures, where physical hardening was later shown to affect the shift factor.

In summary, the dielectric property measurements made at SRI were encouraging, and a decision was made to continue the work at Penn State.

Testing Conducted at Penn State

Improvements in the test cell and the addition of a controlled temperature bath to afford more convenient temperature control were completed at Penn State under the direction of Dr. Veradan. The cell used at Penn State is shown in figure 6.25. This cell allows the test temperature to be controlled so that dielectric properties can be measured over the temperature range from $-40°$ to $60°C$ ($-40°$ to $140°F$). The cell was later modified so that mixtures could also be tested. Mixture test specimens were prepared from laboratory-compacted cores by sawing thin slabs approximately 3 mm (1/8 in.) thick. The impedance of the binder and mixture samples was measured using a Hewlett-Packard Model 4192A Impedance Analyzer and Model 9836 computer. Using the open-circuit/short-circuit calibration technique developed at Penn State, the dielectric constant and loss tangent of the asphalt binder and mixture samples could be calculated.

As a result of improvements in calibration technique and refinements in the dielectric cell, it was ultimately possible to obtain measurements on asphalt or asphalt-concrete samples in the frequency range of 50 Hz to 50 MHz. Below 50 Hz, the asphalt samples gave susceptance or conductance values that were less than 5 times 10^{-9} mhos, which could not be measured accurately using the 4192A impedance analyzer. Provisions were also made to prevent moisture condensation on the dielectric cell at low temperatures.

Dielectric measurements were completed for the eight unaged core asphalts and for PAV residue from the eight core asphalts in the frequency range of 50 Hz to 1 MHz at 25°C (77°F). Four replicate specimens were measured for each asphalt. Figures 6.26 and 6.27 show the mean dielectric constant and loss tangent values for the eight unaged core asphalts, and figures 6.28 and 6.29 show the mean dielectric constant and loss tangent values for eight PAV-aged SHRP core asphalts. There are significant differences in dielectric constant values depending on the asphalt source, and the properties are also affected by PAV aging.

Larger differences were observed in the loss tangent values than in the dielectric constants for the eight core asphalts. For asphalts AAG-1, AAK-1, and AAD-1, the dielectric constant decreases appreciably with increasing frequency. In contrast, for asphalt AAM-1, there is little variation of the dielectric constant with frequency. The differences between core asphalts become significant at lower frequencies (e.g., 500 Hz). At the higher frequencies (e.g., 500 kHz), the difference between the asphalts is somewhat reduced.

Statistical Analysis of Penn State Data

The dielectric properties of the eight core asphalts were determined within the framework of a statistically designed experiment. This experiment was carried out as four complete replications of a split plot design in which the asphalts were assigned to the main plots and

the frequencies were assigned to the split plots. With the use of the four independent replications it is possible to select a frequency of interest and then analyze those data as if they were from a completely randomized design with the asphalts as the treatments.

Dielectric Data

To establish the significance of asphalt source, an analysis of variance was completed for the dielectric data obtained at 1,000 Hz and 5,000 Hz. The results are given in tables 6.6 and 6.7. It is clear from these analyses that the dielectric properties of these eight core asphalts can be measured with good precision (coefficient of variation of about 2 percent) and that there are differences among the asphalts (p value of 0.0001)

The Waller-Duncan procedure for the statistical evaluation of the observed differences among the dielectric measurements was used to place the asphalts into groups such that the observed differences for the asphalts within the same group were not statistically significant. The groups thus formed using the 1,000 Hz data for the dielectric measurements were

- Group 1: Asphalts D, K, A

- Group 2: Asphalts K, A, B, F

- Group 3: Asphalts F, C, G

- Group 4: Asphalts C, G, M

The groups formed by using the Waller-Duncan procedure with the 5,000 Hz data for the dielectric measurements were

- Group 1: Asphalts D, A

- Group 2: Asphalts A, K

- Group 3: Asphalts B, F

- Group 4: Asphalts G, C

- Group 5: Asphalts C, M

The measurements at 5,000 Hz were somewhat more precise than those at 1,000 Hz, which resulted in the smaller groups and thus better discrimination among the asphalts. It may be noted from tables 6.6 and 6.7 that the estimated standard deviations of the experimental errors are 0.05 for the 1,000 Hz data and 0.04 for the 5,000 Hz data, each with 24 degrees of freedom (the replications are not to be regarded as blocks). These estimates make it possible to provide 95 percent confidence intervals for the means. See table 6.8 for the 5,000-Hz data.

419

Loss Tangent Data

The determination of the loss tangent properties from the dielectric experiments was also carried out for the eight core asphalts for the 10,000 Hz and the 50,000 Hz data. The appropriate analysis of variance for these data are given in tables 6.9 and 6.10. It may be seen from these tables that the loss tangent has been determined with good precision (coefficient of variation of about 4 percent) and that there are differences among the asphalts (p value of 0.0001).

The Waller-Duncan procedure for the statistical evaluation of the observed differences among the asphalt loss tangents was also carried out. The groups thus formed at 10,000 Hz were

- Group 1:   Asphalt D

- Group 2:   Asphalt K

- Group 3:   Asphalts A, B

- Group 4:   Asphalt M

- Group 5:   Asphalt F

- Group 6:   Asphalt C

- Group 7:   Asphalt G

When the Waller-Duncan procedure is applied to the 50,000-Hz loss tangent data, each asphalt forms its own group so that all are declared to be significantly different. This finding is quite impressive and suggests strongly that these eight core asphalts have distinctive loss tangent properties when measured at this frequency. It remains to be seen, of course, as to just how useful this measured property may be. This determination will be based on the importance of these measured values in predicting the measured physical properties of these core asphalts.

The estimated standard deviations of the experimental error (sigma) are reported in tables 6.9 and 6.10 as 0.000719 at 10,000 Hz and 0.000465 at 50,000 Hz for the loss tangent data. These, again, are for 24 degrees of freedom. The resulting 95 percent confidence intervals for the means of such loss tangent measurements for the eight core asphalts are given in table 6.11 for the 50,000-Hz data.

Miscellaneous Test Results

In an attempt to provide insight into the physical hardening mechanism, dielectric measurements were obtained for two asphalts at −5°C (23°F) after 10 minutes and 1.33,

21.33, and 30.00 hours of isothermal storage time. Tables 6.12 and 6.13 show the measured dielectric constants for two core asphalts (AAD-1 and AAM-1) as a function of time at $-5\,^\circ$C ($23\,^\circ$F). No change in dielectric properties was observed as a function of time in the 500-Hz to 500-kHz range. The fact that the dielectric constant did not change with isothermal storage time is not surprising given that there is little change in the dielectric constant with frequency or asphalt source in the 500-Hz to 500-kHz range. This finding was one of the reasons why, at the end of this study, testing focused on the low-frequency range, from 5 Hz to 500 Hz. Because these low-frequency data were not obtained, little can be concluded regarding dielectric property changes during physical hardening.

Relationships should exist between the rheological properties and the dielectric properties if the polarity of the asphalt molecules plays a role in physical properties as postulated by the polar dispersed fluid (PDF) microstructural model. A plot of the defining temperature, T_d, versus the measured dielectric constants is given in figure 6.30 where it is seen that, except for aged asphalt AAC-1, there appears to be a relationship between these measured properties. The dielectric constants that appear in figure 6.30 were measured at 5,000 Hz. Additional relationships and further discussion of such relationships are given in volume I of this report.

Dielectric measurements were made in replicate at $25\,^\circ$C ($77\,^\circ$F) on mixes prepared with asphalts AAA-1, AAD-1, and AAG-1 in the frequency range of 200 Hz to 500 kHz. Figures 6.31 and 6.32 give dielectric constant and loss tangent data (average of two test specimens) for asphalt concrete samples with AAA-1, AAD-1, and AAG-1 asphalt cements as the binder, respectively. There is a considerable difference for the dielectric constant values as well as the loss tangent values for these three asphalt concrete samples. The dielectric constant and loss tangent values for the mixes are an order of magnitude larger than for the plain asphalt cement. The dielectric properties of the aggregate overwhelm those of the asphalt binders, making the dielectric properties of the mixtures primarily aggregate dependent. Because the dielectric properties of the mixtures appear to be dominated by the aggregate, the dielectric measurements of the mixture are very insensitive to those of the asphalt. As a consequence, the dielectric measurements obtained using the techniques available within this study offer little promise as measures of the in situ rheological properties of asphalt binder.

Conclusions

The dielectric measurements discriminated between asphalt sources, and the dielectric properties were significantly affected by aging. Measurements obtained at low frequencies were more discriminating than measurements obtained at the higher frequencies. In future research even lower frequencies should be investigated, although significant enhancements in the test equipment will be required for the lower frequencies.

The dielectric program was stopped when it became apparent that the method did not discriminate between different asphalts when in the presence of the aggregate. The dielectric constants for the aggregate are several orders of magnitude larger than for the asphalt

binders, and therefore the dielectric properties of the aggregate dominates the measured values for the mixes. Based on the data obtained in this study, the dielectric technique is useful for studying asphalt cement but not for studying asphalt-concrete mixtures. More research with the technique is warranted but the emphasis should be placed on frequencies less than 50 Hz.

Ultrasound

Ultrasonic measurements were investigated as a means for measuring the in situ properties of asphalt cement. Initially, it was envisioned that the method would be of value for measuring the properties of both neat asphalt cement and asphalt cement in situ within mixtures or within the pavement system. Therefore, studies were conducted with both plain asphalt and concrete mixtures.

Test Equipment

A system, shown in figure 6.33, was designed that allows a wide range of testing temperatures, from −20° to 55°C (−6° to 131°F). With this system it is possible and convenient to change transducers during a test, which allows the testing to be performed over a wide range of frequencies. A schematic of the testing arrangement is shown in figure 6.34. The arrangement provides full contact between transducer and asphalt cement. Two different thicknesses, 4.4 and 8.8 mm (0.17 and 0.35 in.), were used to measure the wave speed and attenuation.

Testing of Asphalt Cement

Four different asphalts (aged and unaged AAG-1 and AAK-1) were tested at 2.25 MHz. For this experiment, the temperature level was varied in increments from −20° to 40°C (−4° to 104°F). The change in acoustic impedance was assumed to be caused solely by a change in the wave speed through the asphalt. Figures 6.35 and 6.36 show average storage and average loss modulus based on two replicate measurements. Table 6.14 gives the numerical data.

Because the ultrasound equipment measures the longitudinal modulus, it was necessary to convert the longitudinal moduli to shear moduli in order to compare the ultrasonic and dynamic mechanical analysis (DMA) measurements. The equations for this conversion are as follows:

$$E = (1 - 3\mu^2 - 2\mu^3)/(1 - \mu^2)\, C \tag{6.2}$$

$$G = E/2(1 + \mu) \tag{6.3}$$

where

$$
\begin{aligned}
E &= \quad \text{Young's modulus} \\
C &= \quad \text{measured ultrasonic modulus} \\
G &= \quad \text{shear modulus} \\
\mu &= \quad \text{Poisson's ratio}
\end{aligned}
$$

For example, the measured storage modulus, 5.0 GPa at $-20°C$ ($-4°F$), is converted to a Young's modulus, $E = 3.12$ GPa (0.45×10^6 lb/in.^{2}), and a shear modulus, $G = 1.16$ GPa (0.17×10^6 lb/in.^{2}), if we assume Poisson's ratio to be 0.35 at $-20°C$ ($-4°F$). A comparison of the ultrasonic and dynamic shear moduli showed an order of magnitude agreement when the low-temperature glassy dynamic modulus was used for the comparison.

Testing of Asphalt Concrete

It was found that asphalt concrete requires the use of lower frequencies because of the high attenuation resulting from the inherent heterogeneity at the asphalt concrete. Two asphalt concretes (laboratory-compacted, dense-graded surface mixture specimens) were evaluated at 500 kHz. The wave speed and attenuation are shown in figures 6.37 and 6.38, respectively.

The Young's moduli of two asphalt concrete specimens were computed using the measured ultrasonic wave speeds. Assuming a Poisson's ratio of 0.3, the calculated moduli of the specimens were 21.53 and 26.97 GPa (3.1×10^6 and 3.9×10^6 lb/in.^{2}), respectively (see table 6.15). These moduli compare well with values reported in the literature.

Statistical Analysis of Plain Asphalt Data

Experiment Design

The ultrasonic experiments resulted in two reduced data sets: one for the loss and one for the storage modulus. The factors were asphalts (four levels) and temperatures (seven levels), and two independent replications were carried out at each combination. Since the measurements were nondestructive, only eight samples were used and each was studied at all seven temperatures. The experimental design can be regarded as two replications of a split plot with asphalts assigned to the main plots and temperatures assigned to the split plots. Alternatively, if there are temperatures of special interest, the effects of the asphalts (two replications of a completely randomized design) may be evaluated for this reduced experiment. Both approaches, as well as certain descriptive and graphical methods, are useful in the analysis of these experimental results.

Analysis

The results of the experiment are presented in figures 6.35 and 6.36. The temperature effect for both loss and storage is quite small for all asphalts, ranging from 2×10^9 to 5×10^9 Pa (2.9×10^6 to 7.3×10^6 lb/in.^{2}) over a 60°C (108°F) temperature range. As expected, the

loss moduli are significantly smaller than the storage moduli. The main plots were assigned to the asphalts and the temperatures were assigned at the split plot level. This assignment is typical of many such experiments when the measuring process is nondestructive and may be applied to a given sample at several levels (temperatures). With sufficient independent replications (new samples are required if the results are to be independent) the asphalt effect can be evaluated. The analysis of variance table for the storage response is given as table 6.16.

It is clear from table 6.16 that asphalt source affects the storage modulus depending on the temperature. A separate one-way analysis of variance (for asphalt effects) at each of the seven temperatures was conducted. For each temperature, the p value for the asphalt effect and an estimate of σ, the standard deviation of the experimental error, would be of interest. These results are given in table 6.17, where it can be seen that the asphalt effect is most significant for temperatures in the range of 0 to 20°C (32 to 69°F). A pure estimate of σ would be about 0.05. The storage modulus means and a 95 percent confidence interval for the four asphalts at 0°C (32°F) are given in table 6.18.

On the basis of the statistical analysis, the possible usefulness of the ultrasonic measurements for the storage properties of the asphalts at temperatures in the range of 0° to 20°C (32° to 68°F) cannot be ruled out completely. Clearly, the aged asphalts have storage values that are higher than when they are unaged. Asphalt source, temperature, and aging all have a statistically significant effect on the measured loss and storage modulus of asphalt cement. Although the differences can be demonstrated statistically, the actual differences are small from an engineering standpoint.

Split Plot Analysis of the Loss Modulus

The main plots are assigned to the asphalts and the temperatures are assigned to the subplots. The analysis of variance appropriate for this design is given in table 6.19. It is clear that the temperature effect is very large, but this finding is unexpected. It is also clear that the asphalt effect, averaged over the temperatures, is of no importance (p value = 0.97). However, since the asphalt-temperature interaction is significant, it is of interest to consider the one-way analysis of variance at each temperature level. When this step is done the resulting p values for the asphalt effect and the estimates of σ (the standard deviation of the experimental error) are as given in table 6.20.

Now the only temperature at which the asphalt effect would seem to be present is 30°C (86°F). However, with the lack of significance at so many other temperatures any significance at this temperature may simply be due to chance. Furthermore, if we examine the estimated mean loss for each of these asphalts, as given in table 6.21, we see an apparent increase in loss for the AAG-1 aging and an apparent decrease in loss for the AAK-1 because of aging.

It is clear from table 6.21, which was prepared for the loss data at 30°C (86°F), that loss data are most affected by asphalt source or aging treatment and that this property as measured by ultrasound does not show any promise of being useful in evaluating asphalts.

Conclusions

Although the statistical analysis indicates that ultrasonic measurements can differentiate between asphalts by the storage modulus, it must be asked whether the observed differences are in fact significant from a practical, rheological standpoint.

First, the storage moduli measured by the techniques used in this study varied from a low value of about 2 GPa (300,000 psi) to a high value of about 5 GPa (700,000 psi). These values represent moduli very close to the glassy limit and represent only a small portion of the region of interest in the rheological characterization of asphalt cement. A typical rheological characterization, for instance, covers 8 to 10 logarithm decades of modulus, a fraction of that covered with ultrasound.

Additionally, since the ultrasonic moduli are in the glassy or plateau region, all asphalts should show similar values. In fact, the observed differences in storage moduli, although statistically significant, represent a range of only about 8 percent, which is not a practically significant difference. In fact, many rheological measurements have precision rates higher than this value.

Although the ultrasonic measurements are in the plateau region, the reported loss moduli decrease with temperature, rather than increase as is normally the case. This phenomena is unexplained, but might be due to the very high frequency and low amplitude of excitation used in this study.

In conclusion, from a practical standpoint, the ultrasonic characterization seems to have two major drawbacks. First, the measured moduli are all in the plateau region where there are very small differences among the mechanical behaviors of asphalt cements. Second, the measurements are made at such a high frequency that analysis and comparison with other data, and with in situ loading conditions, is difficult or impossible. Further, the measurements with the equipment used in this study, result in very small differences according to source, temperature, and aging. From an engineering standpoint these differences are of questionable significance. Additional study using ultrasound as pursued in this project cannot be recommended.
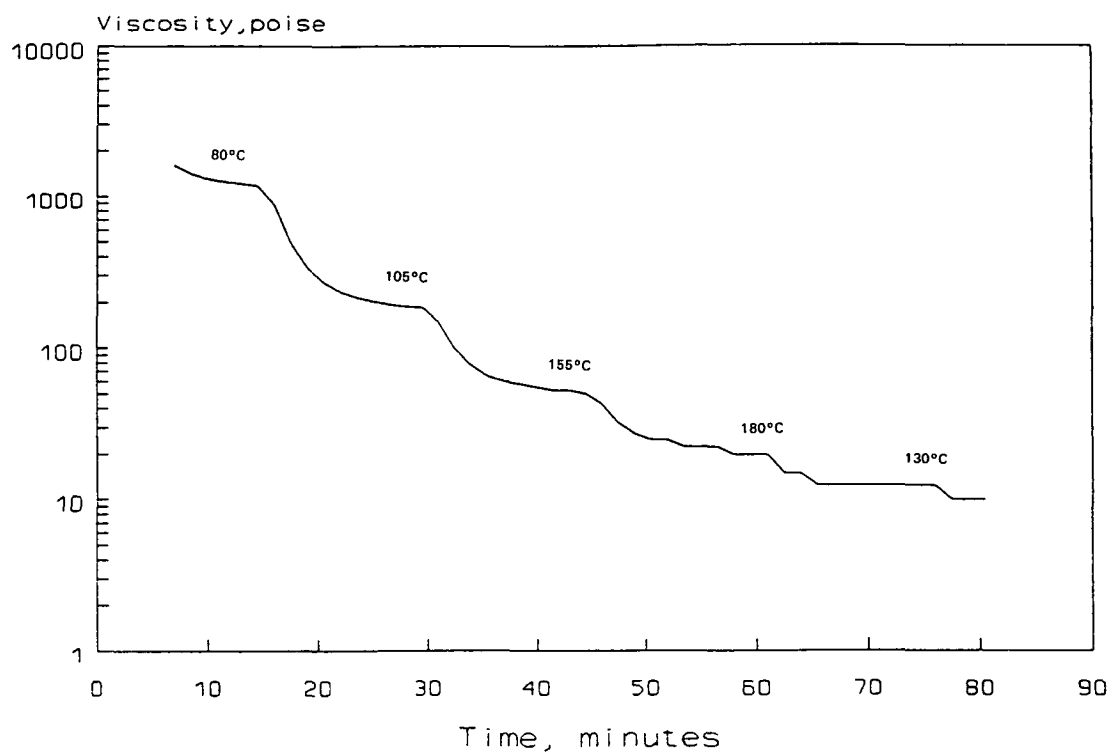
Figure 6.1 Coefficient of Viscosity versus Time with 15–20 Minute Equilibrium Period (Asphalt AAM-2, SC4-27 Spindle, 20 rpm)
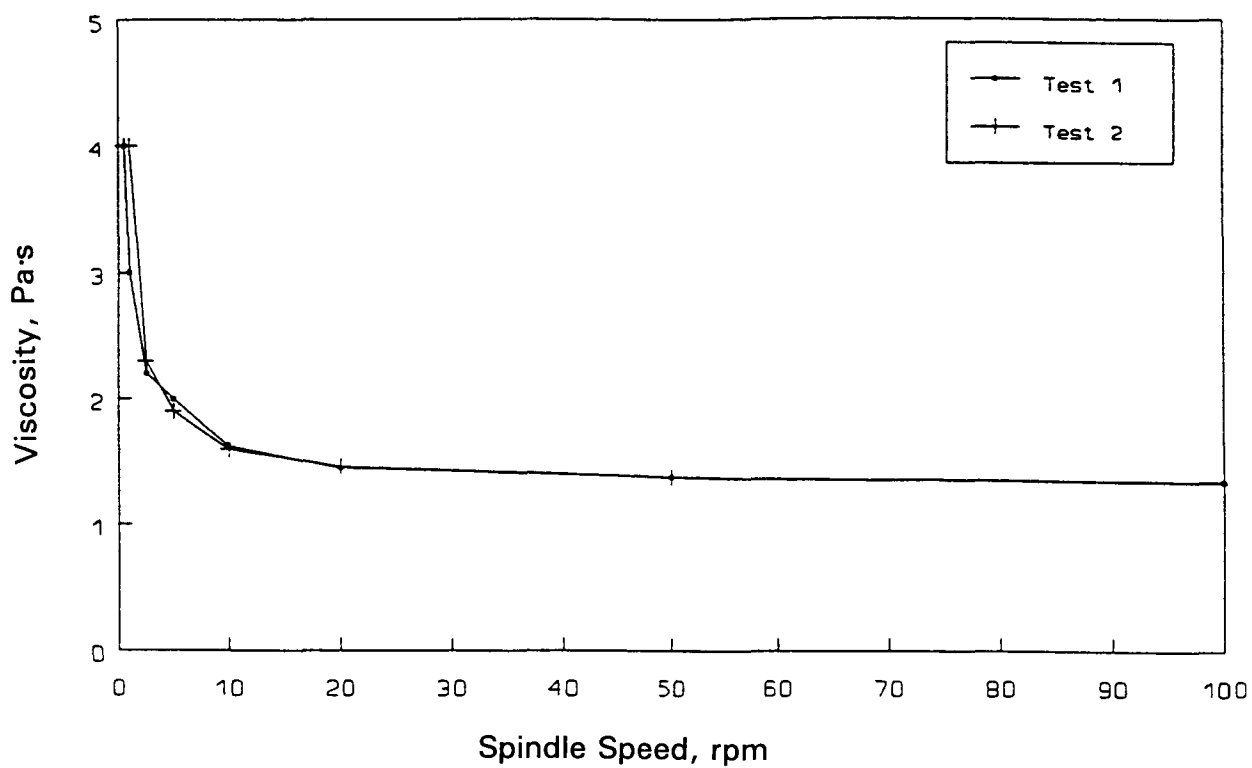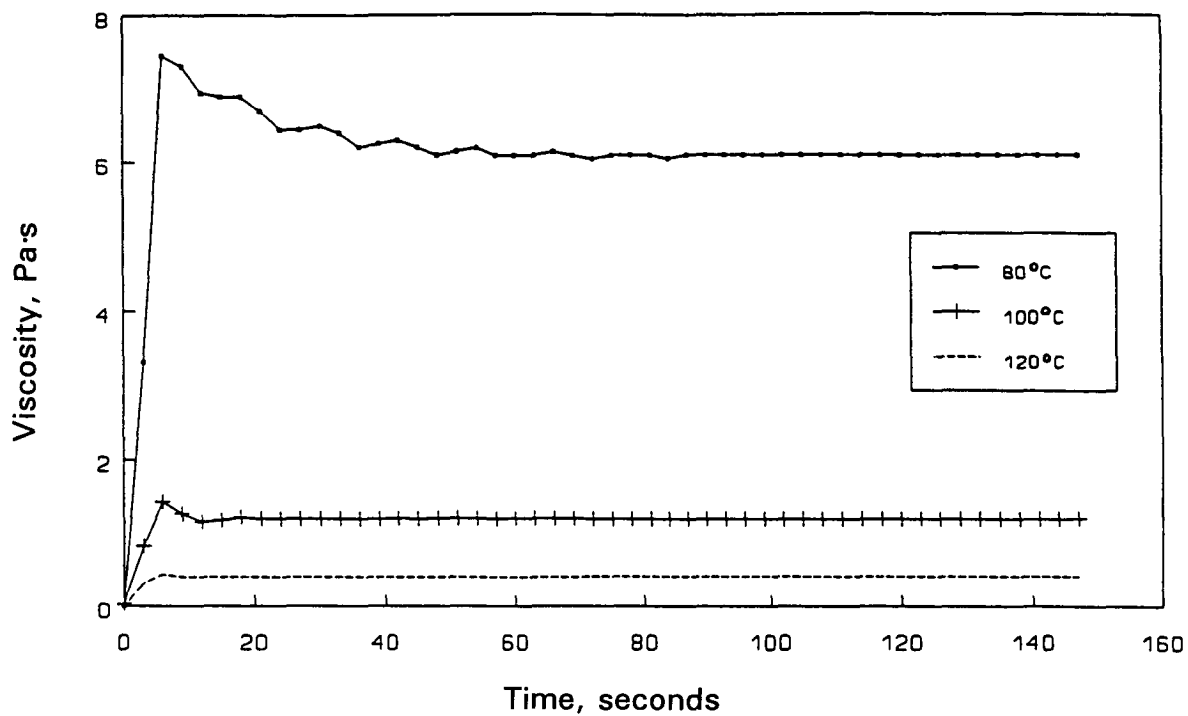
Figure 6.2 **Coefficient of Viscosity versus Spindle Speed (Asphalt AAM-2 Modified with 3% Latex, SC4-27 Spindle at 115°C)**
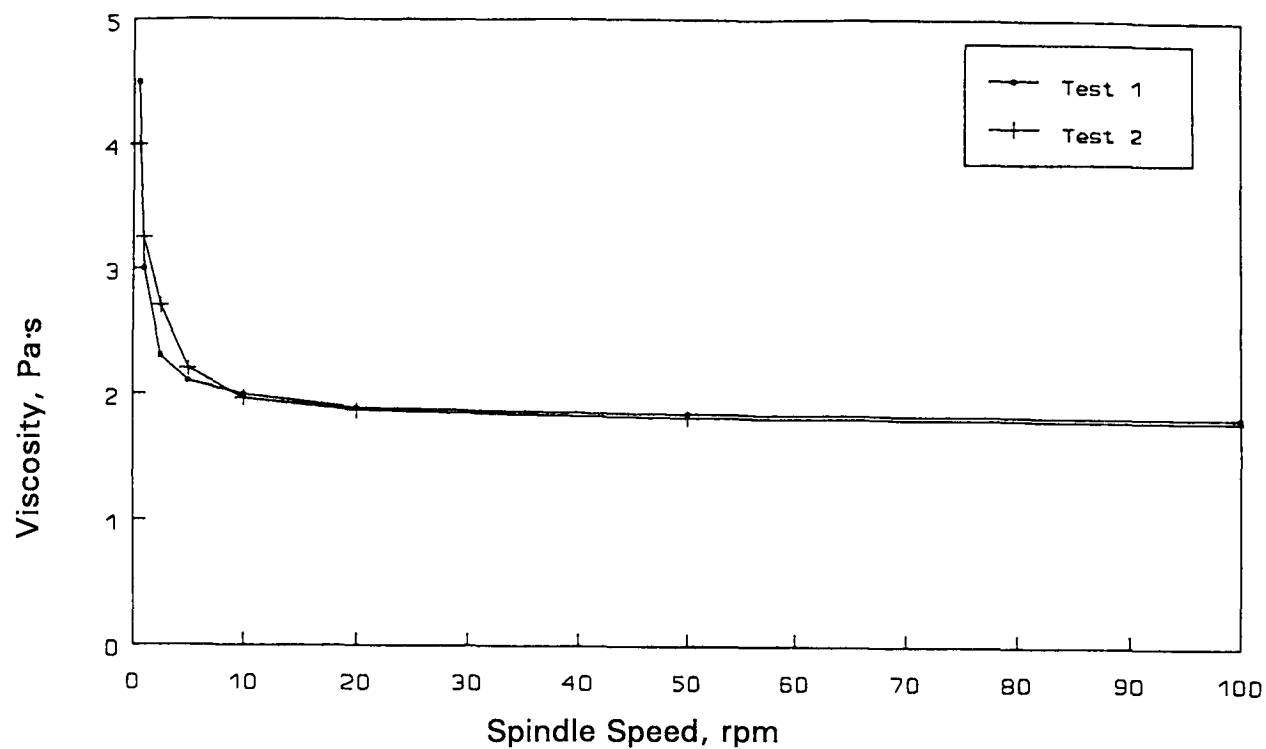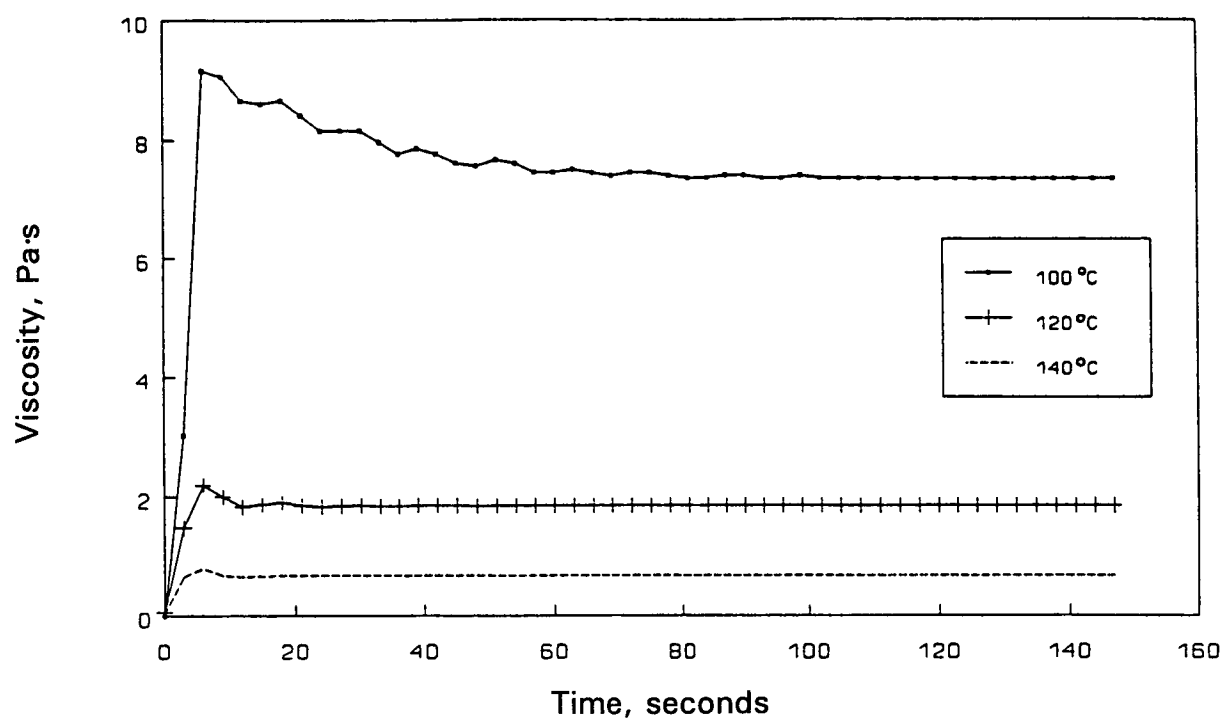
Figure 6.3 Coefficient of Viscosity of Asphalt AAC-2 versus Time after Initiating Spindle Rotation (SC4-27 Spindle at 20 rpm)
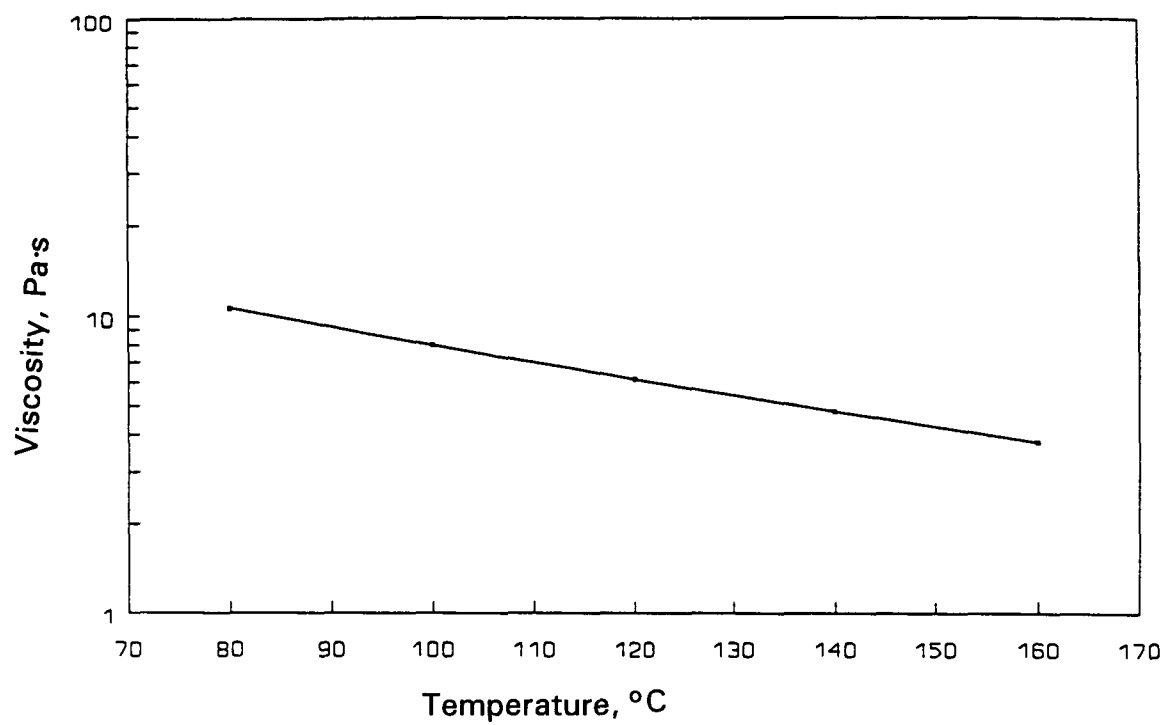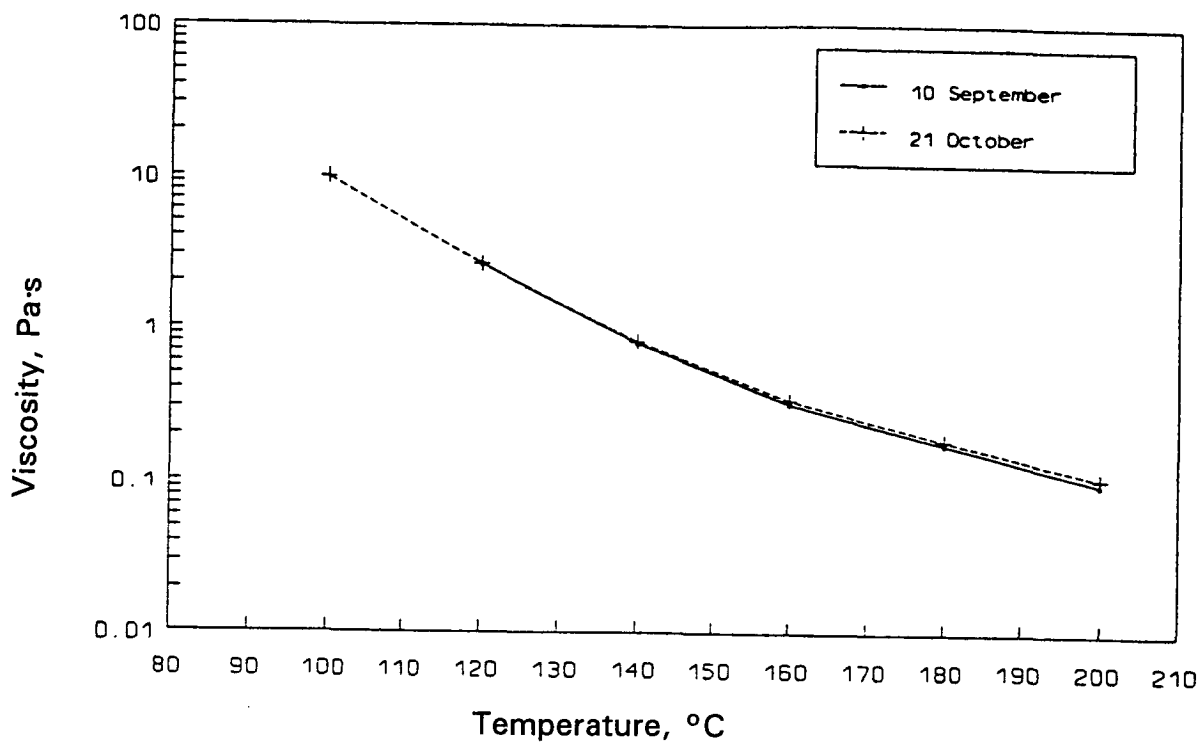
Figure 6.4   Coefficient of Viscosity versus Spindle Speed (Modified Asphalt, SC4-27 Spindle at 140°C)
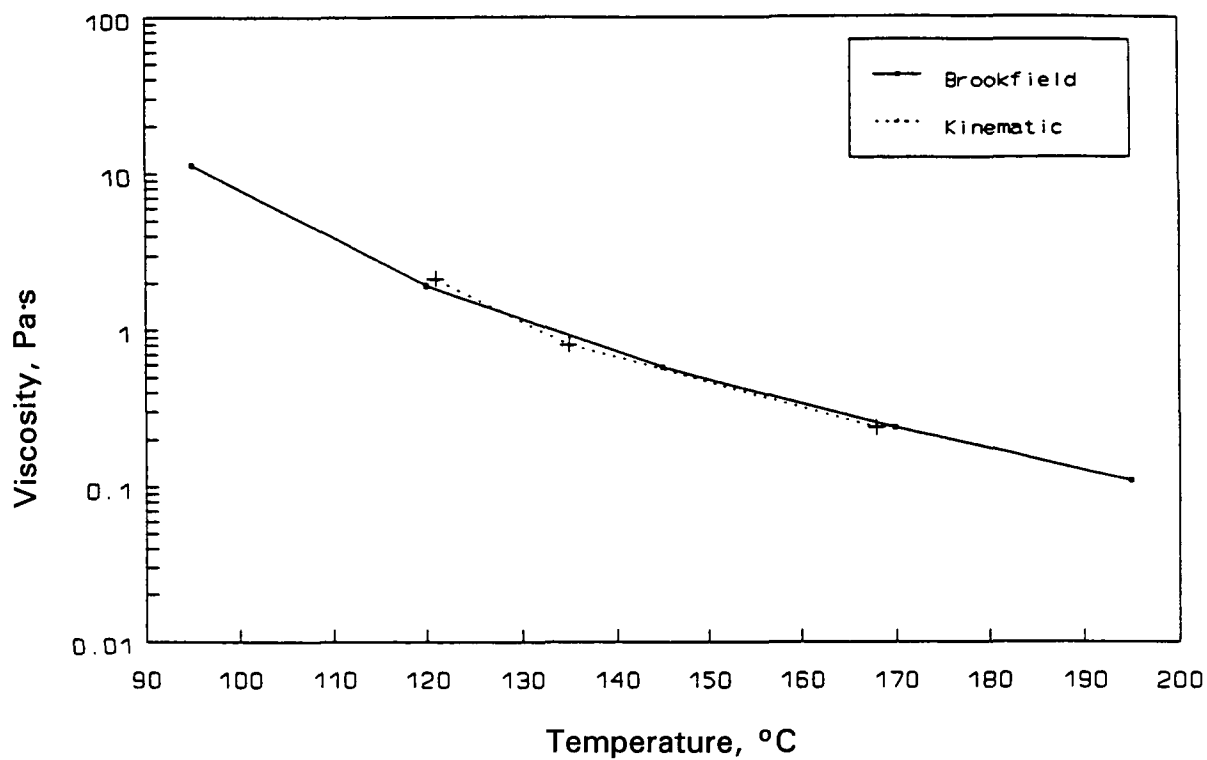
Figure 6.5   Coefficient of Viscosity versus Time after Initiating Spindle Rotation
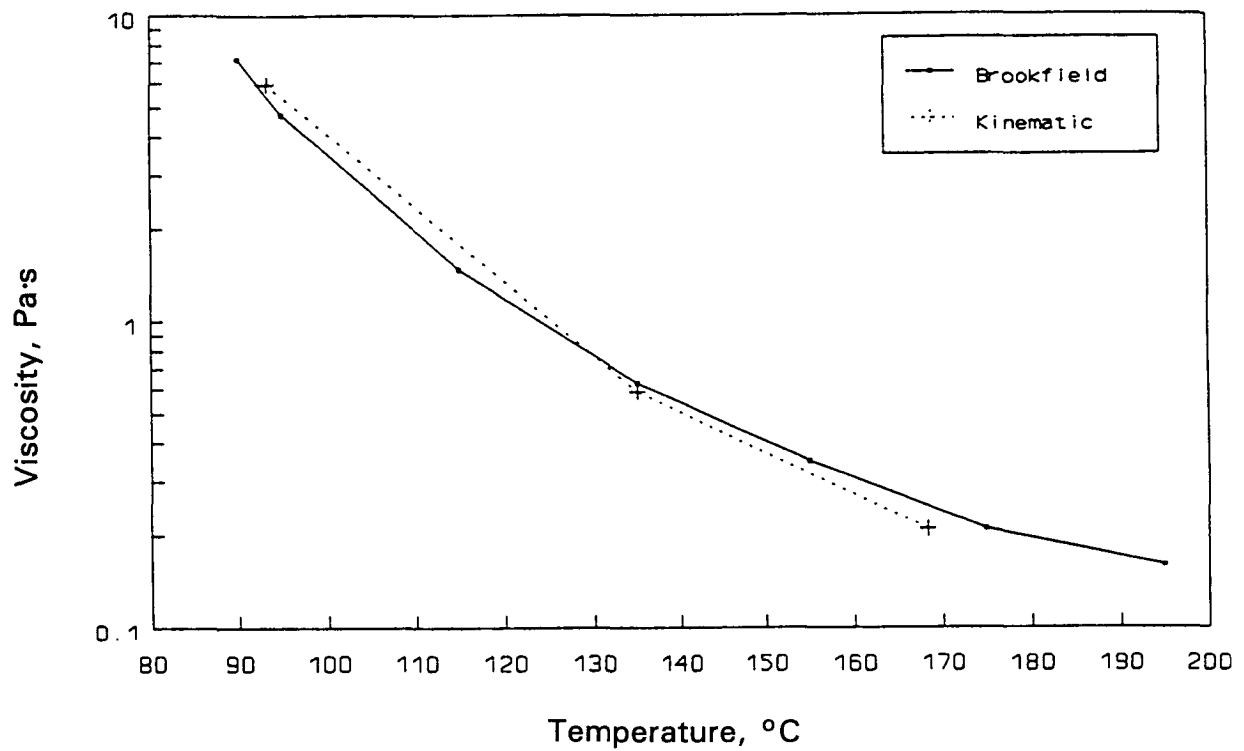(Modified Asphalt, Spindle at 20 rpm)

Figure 6.6 Coefficient of Viscosity versus Temperature for a Commercial High-Temperature Viscosity Standard Oil (SC4-27 Spindle at 20 rpm)

431

Figure 6.7 Coefficient of Viscosity versus Temperature for a Modified Asphalt
(Texaco AC-10 with a 4% Polypropylene) Measured Several Months Apart
by Two Different Technicians (SC4-27 Spindle at 20 rpm)

432

Figure 6.8   Coefficient of Viscosity Measured with Capillary and Brookfield Viscometers (Modified Asphalt, SC4-27 Spindle at 20 rpm)

Figure 6.9 Coefficient of Viscosity Measured with Capillary and Brookfield Viscometers (Asphalt AAM-2 with a Latex Modifier, SC4-27 Spindle at 20 rpm)
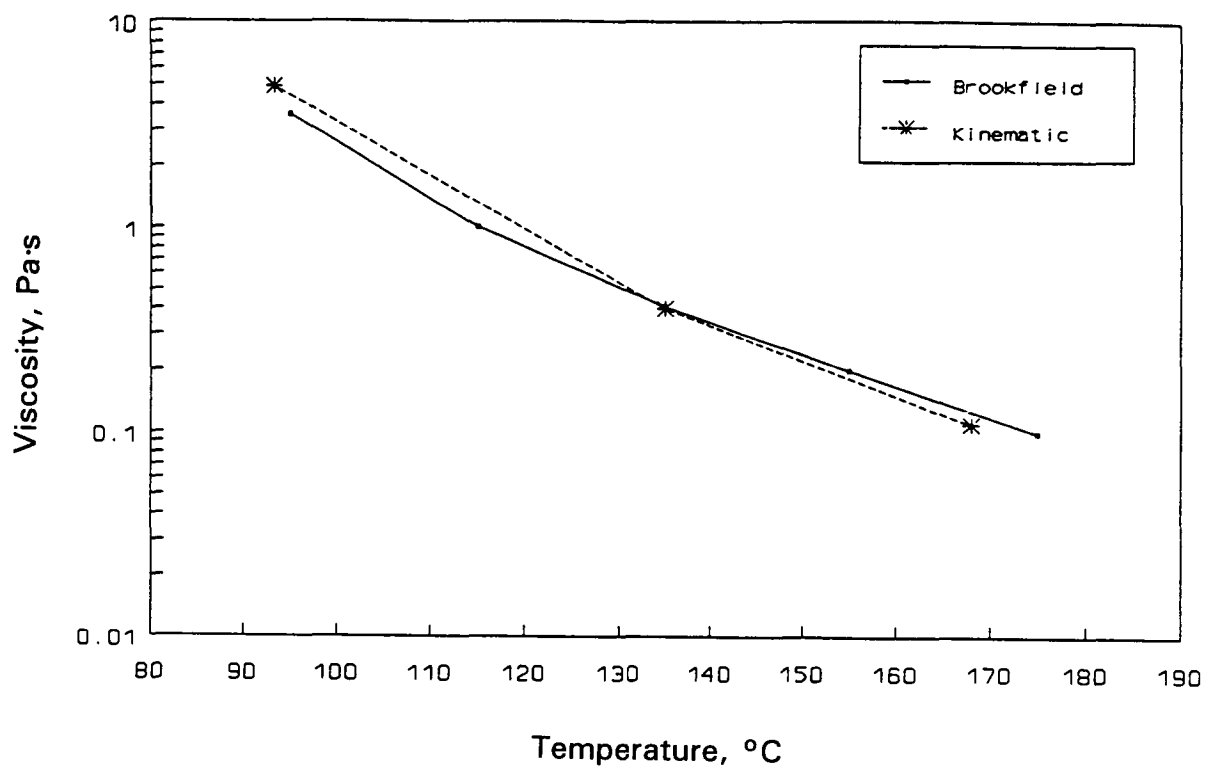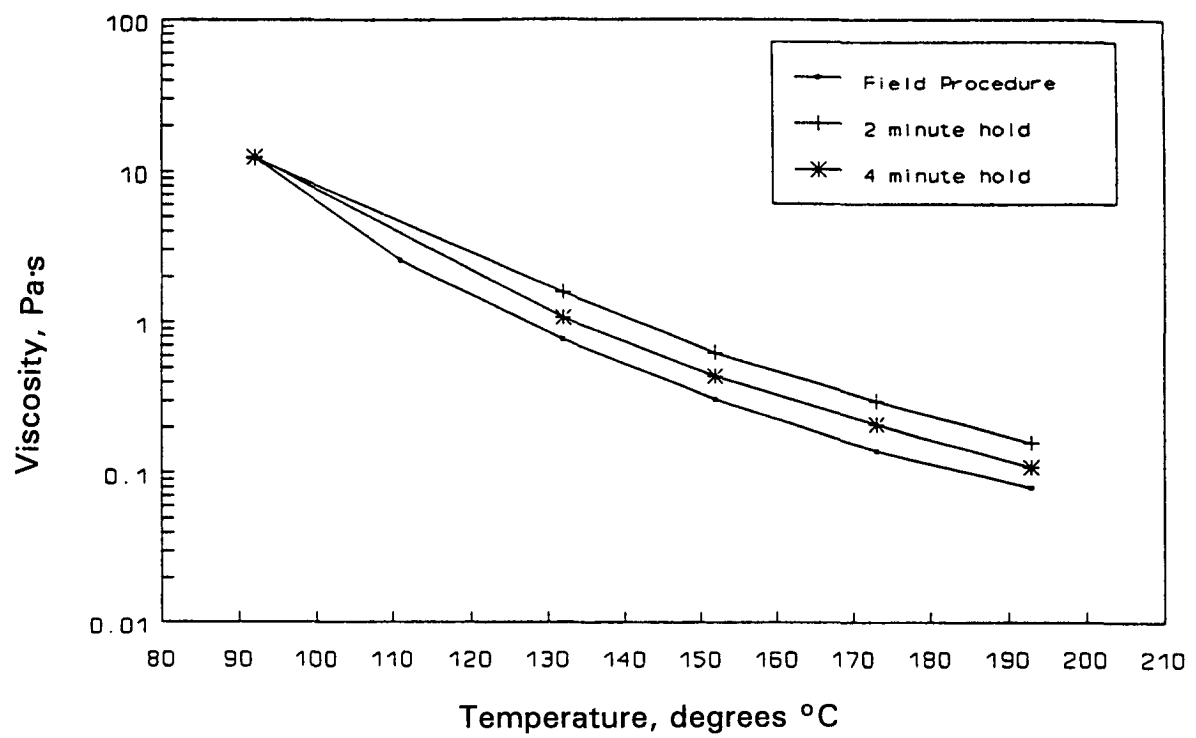
Figure 6.10 Coefficient of Viscosity Measured with Capillary and Brookfield Viscometers (Core Asphalt AAM-2 Unaged, SC4-27 Spindle at 20 rpm)
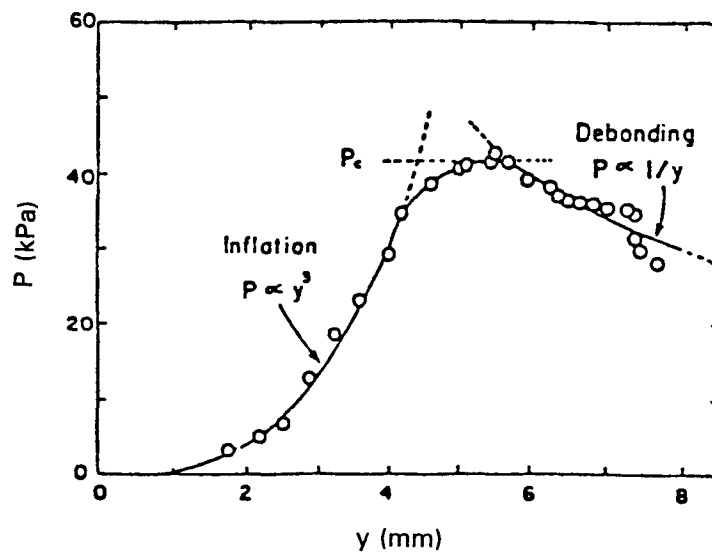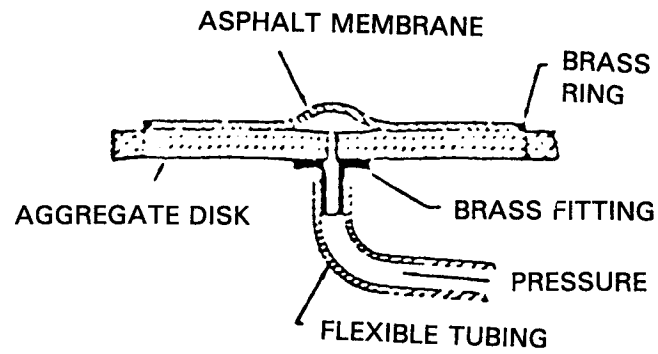
Figure 6.11   Coefficient of Viscosity versus Temperature with Different Hold Times (Asphalt AAK-1, SC4-27 Spindle at 20 rpm)
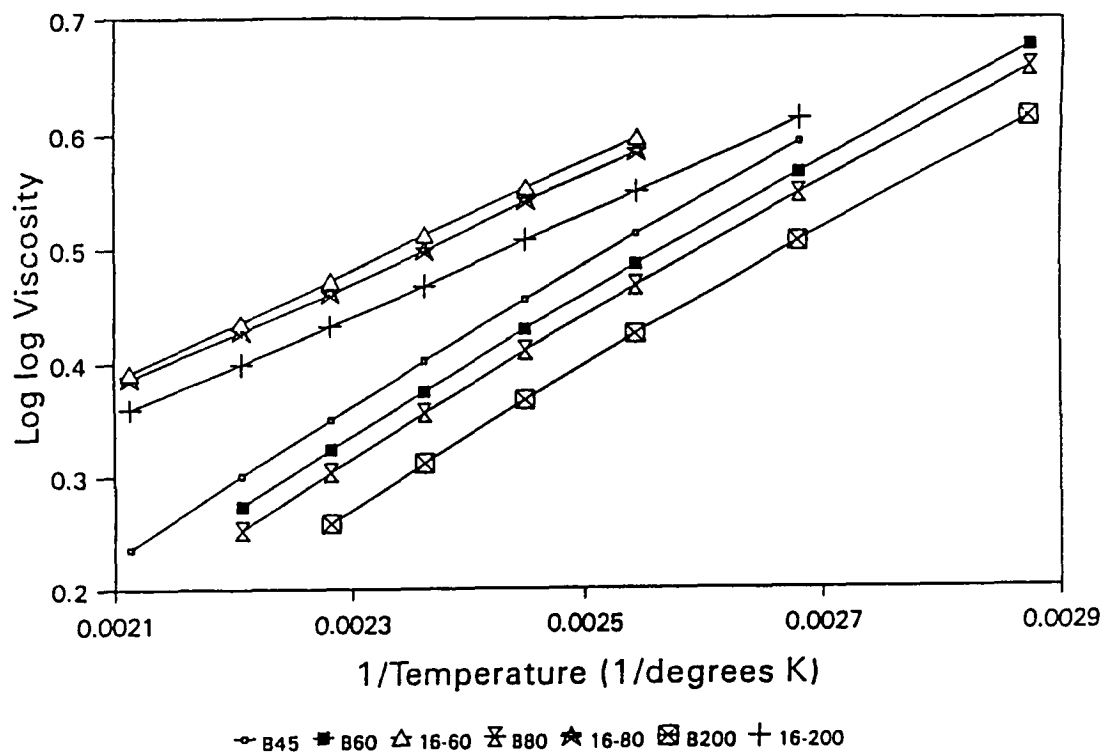
Figure 6.12 **Logarithm-Logarithm Coefficient of Viscosity versus Reciprocal of Absolute Temperature**

Figure 6.13 Blister Blow-Off Adherometer and Typical Data for Polypropylene-Backed
Packing Tape (Liechti et al. 1987)
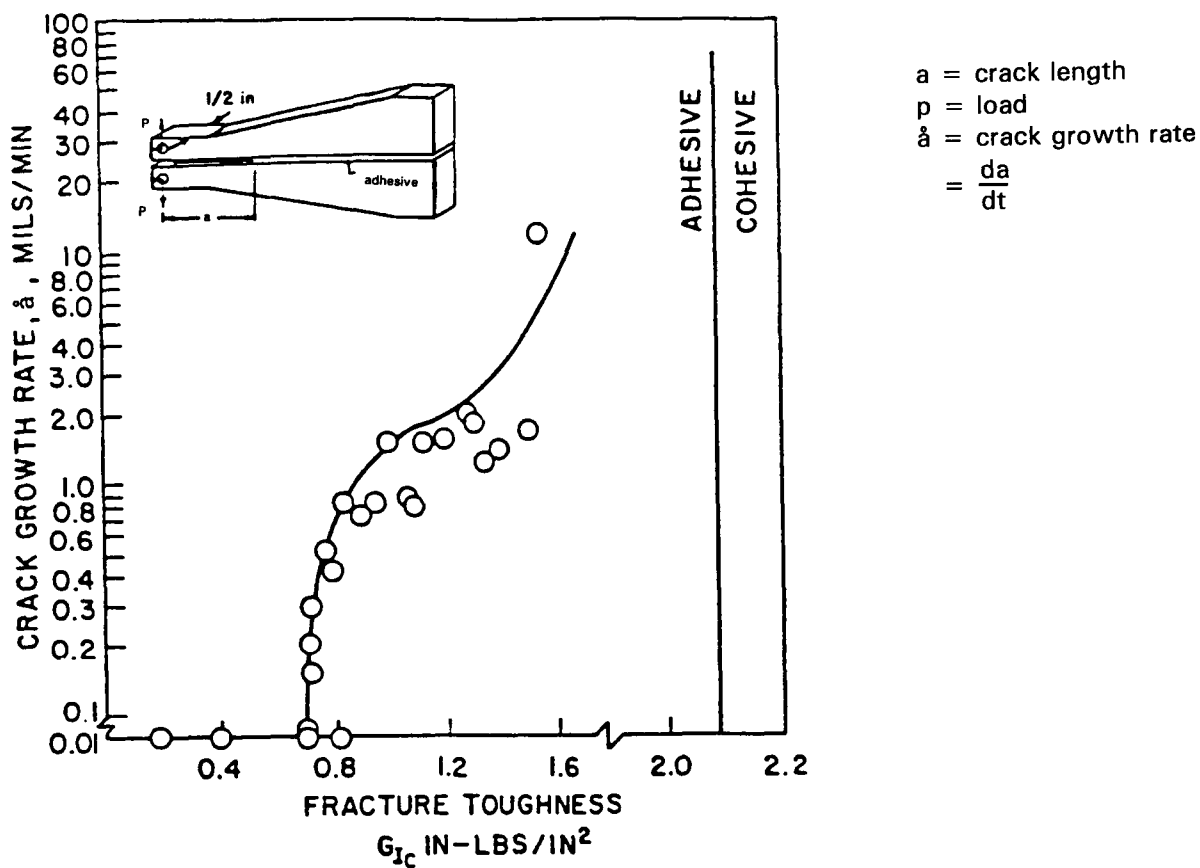
Figure 6.14 Cracking Rate versus Fracture Energy for a Commercial Adhesive-Aluminum Bond Immersed in Water at 25°C (Mostovoy and Ripling 1970)
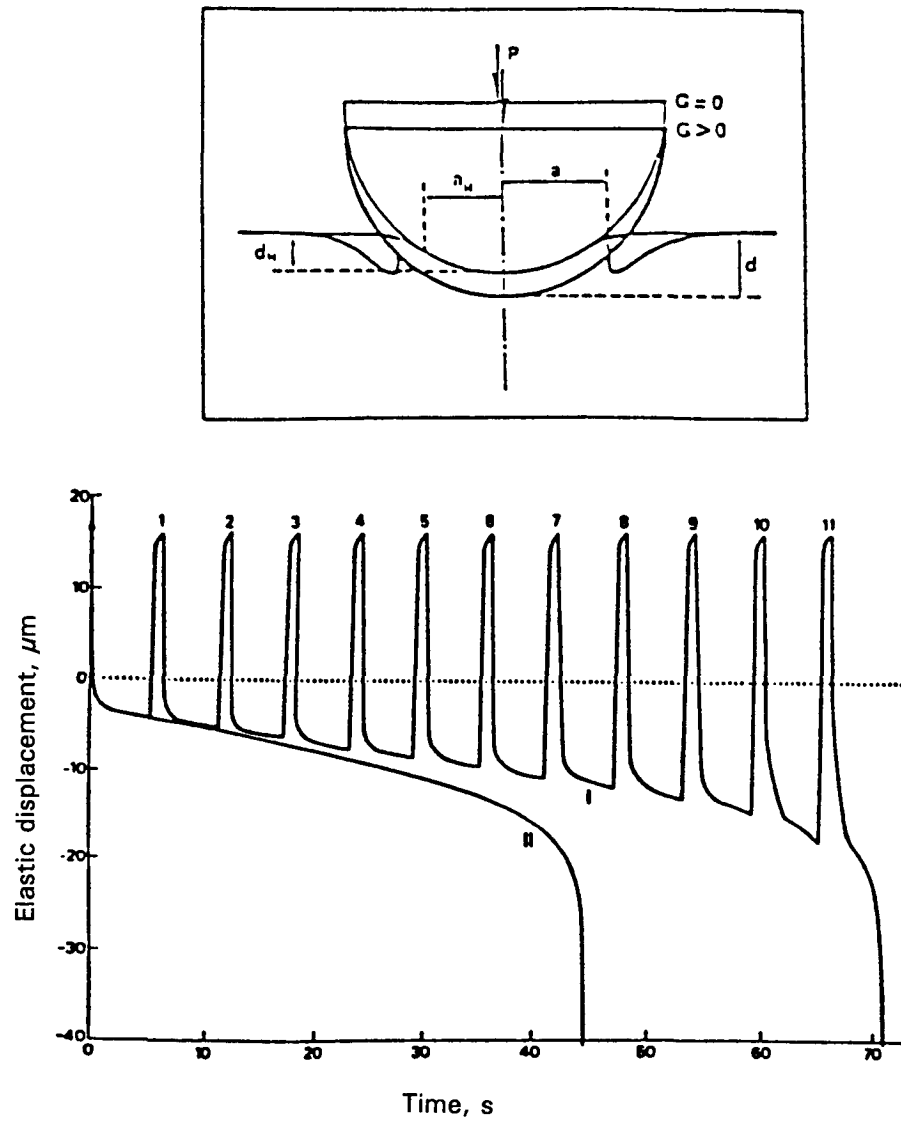
Figure 6.15   Geometry of Adhesive in Equilibrium for a Rigid Sphere on an Elastic
Half-Space
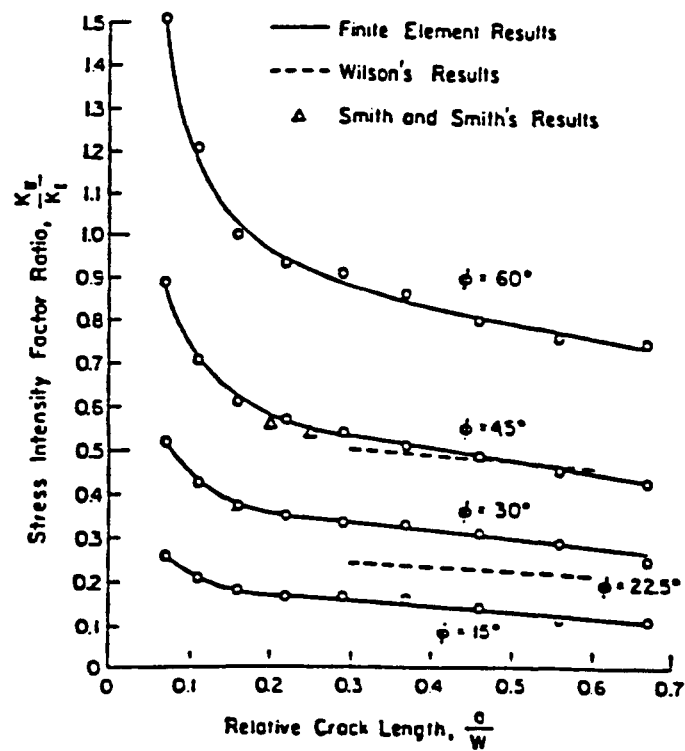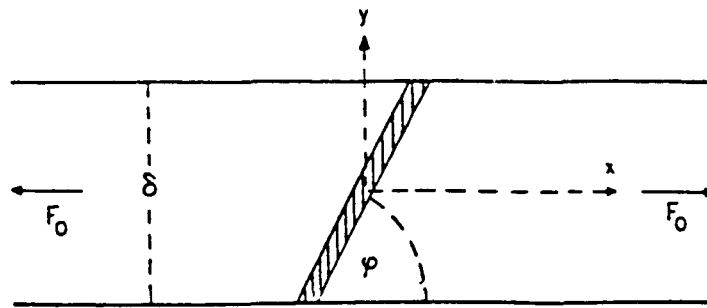
Figure 6.16   Scarf Test and Typical Data Showing Stress Intensity Factor Ratio versus Crack Length at Various Crack Orientations (Trantina 1972)

LVDT

WATER LEVEL INDICATOR

BLEED SYSTEM

ASPHALT FILM

AIR OVER WATER PRESSURE CHAMBER

SOLENOID VALVE

SOLENOID VALVE

PRESSURE TRANSDUCER

PRESSURE GAUGE

PRESSURIZED AIR INLET

SOLENOID VALVE

REGULATOR

BRASS SHIM STOCK
ASPHALT FILM
TEFLON
AGGREGATE
EPOXY
HOLE FOR WATER ACCESS
PIPE NIPPLE
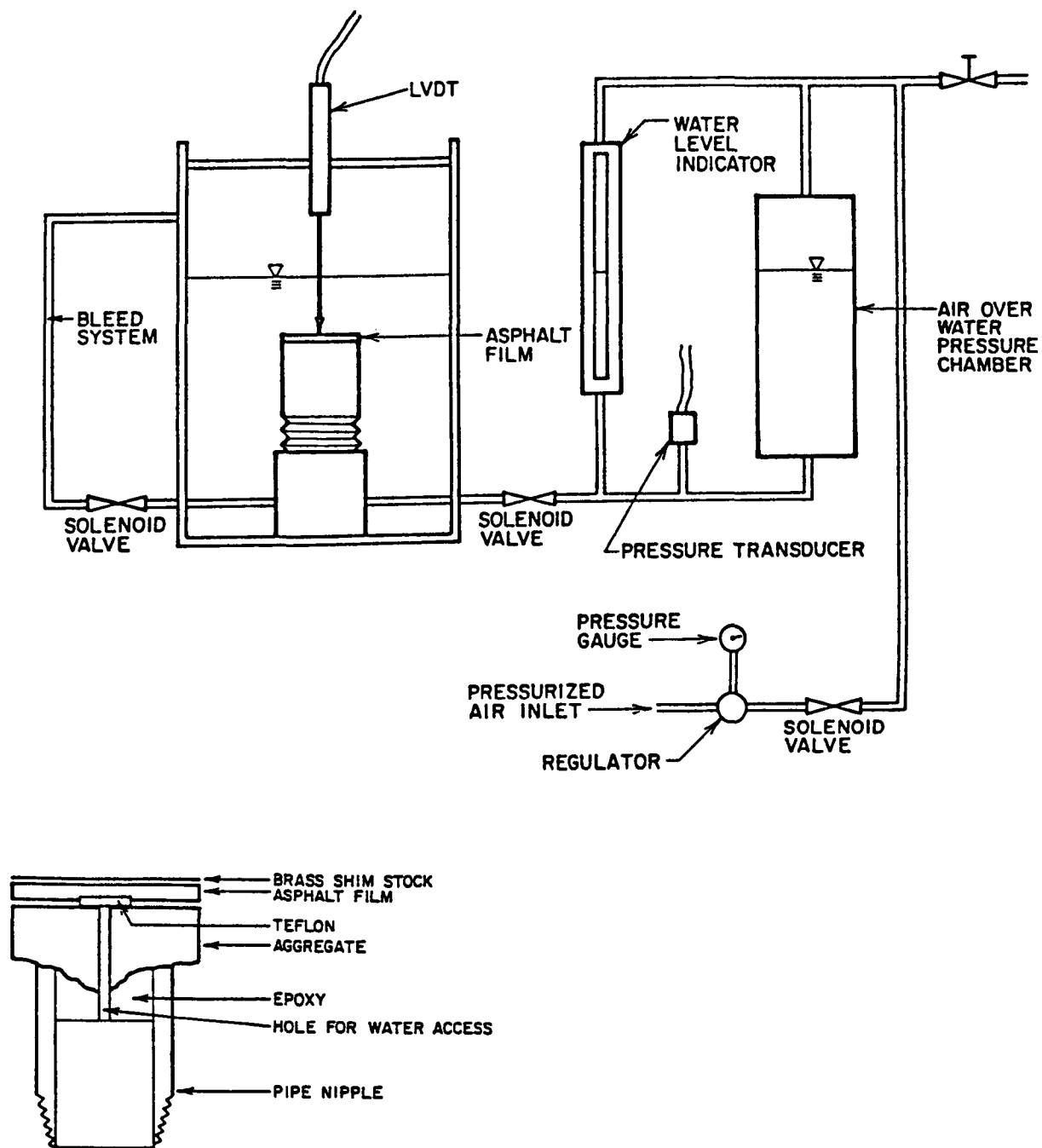
Figure 6.17   Blister Test Apparatus

442
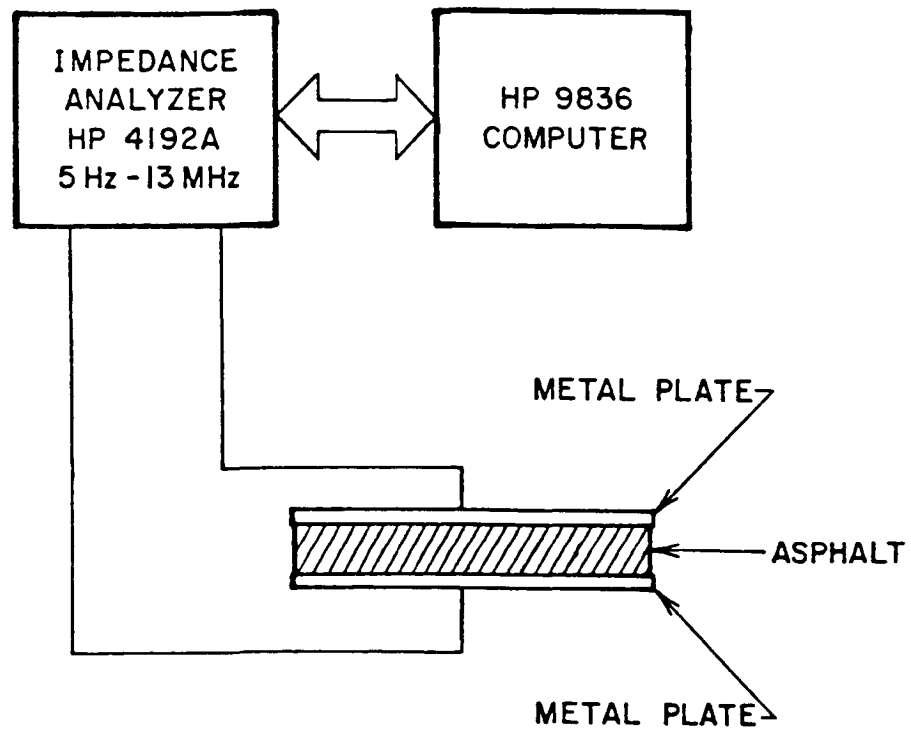
Figure 6.18   SRI Dielectric Test Apparatus
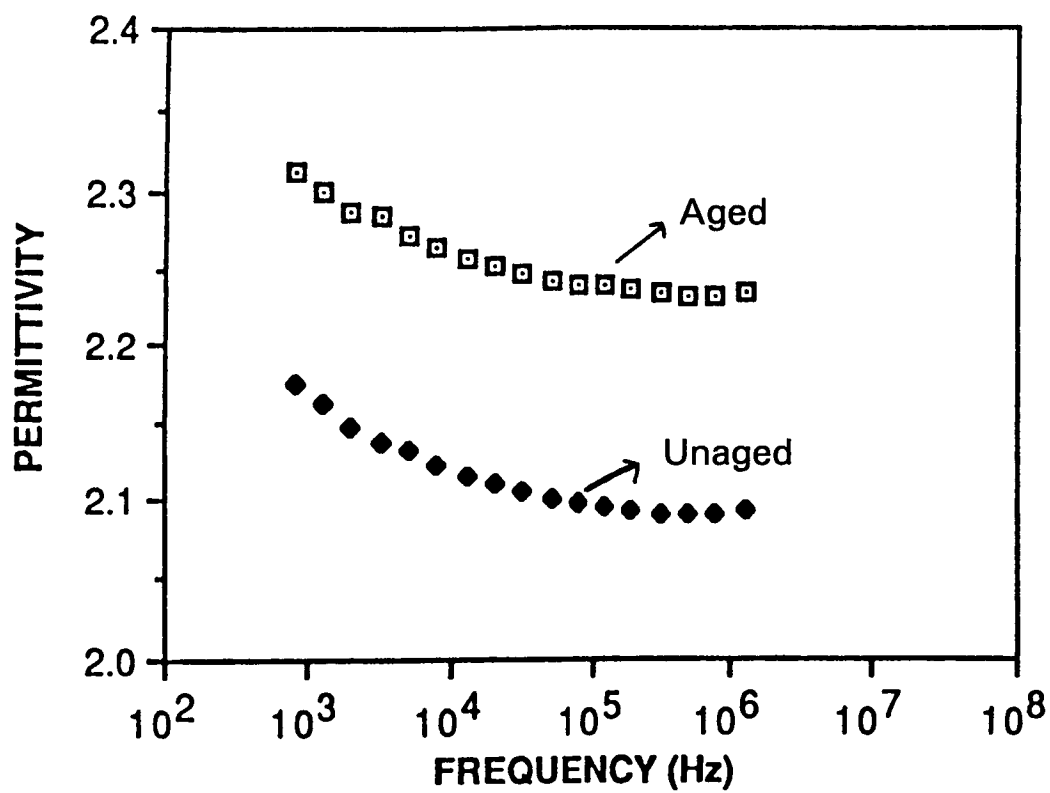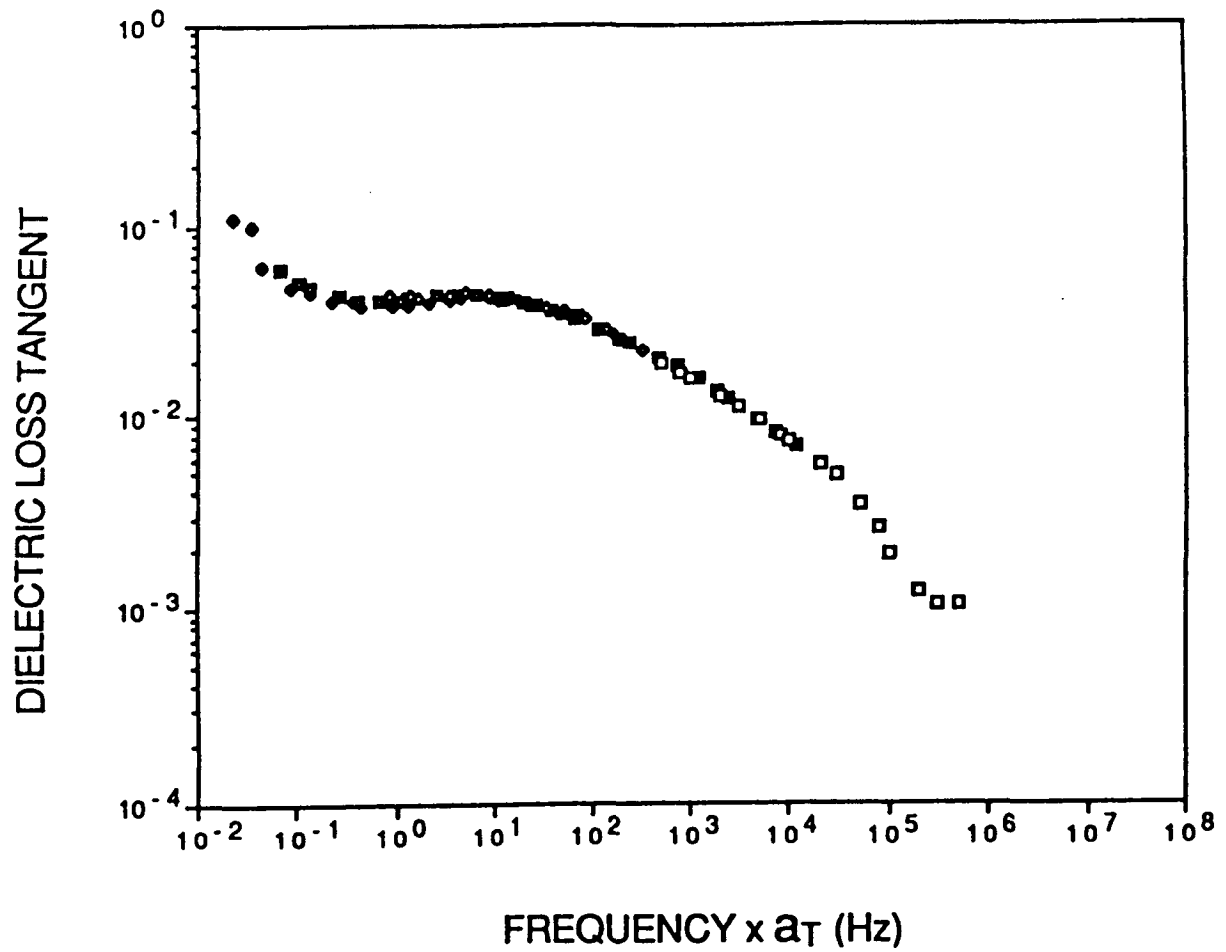
Figure 6.19   Dielectric Permutivity (ϵ') versus Frequency at 25°C for Asphalt AAG-1 in Unaged and PAV-Aged Condition
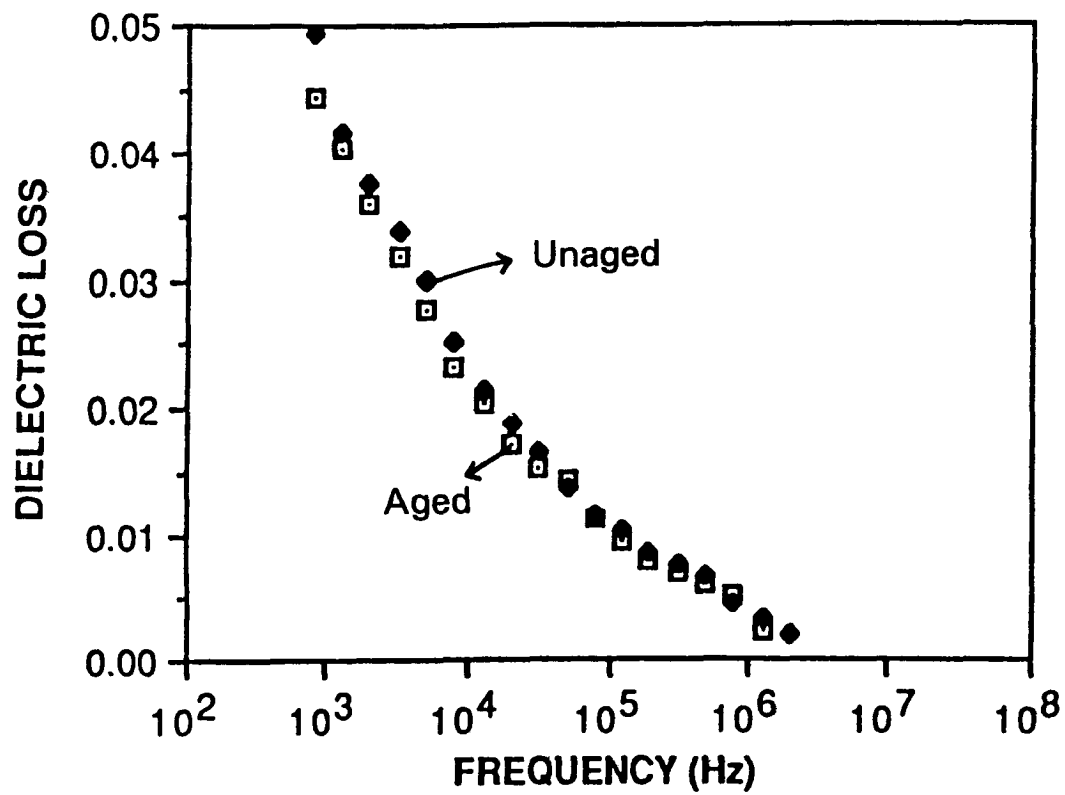
Figure 6.20 Dielectric Loss (ϵ'') versus Frequency at 25°C for Asphalt AAG-1 in Unaged and PAV-Aged Condition

Figure 6.21 Master Curve for Dielectric Loss Tangent versus Reduced Frequency, Asphalt AAG-1 at 24°C Reference Temperature

446
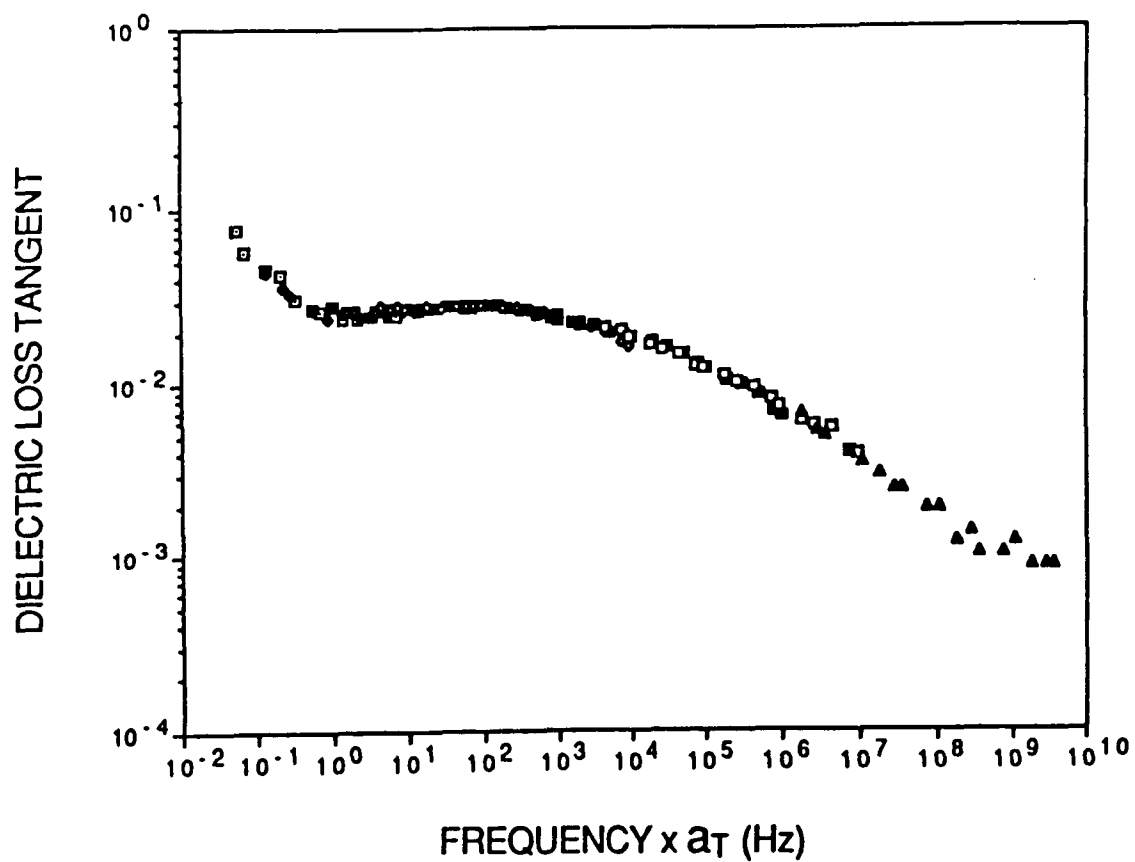
Figure 6.22 Master Curve for Dielectric Loss Tangent versus Reduced Frequency of Asphalt AAK-1 at Reference Temperature 24°C
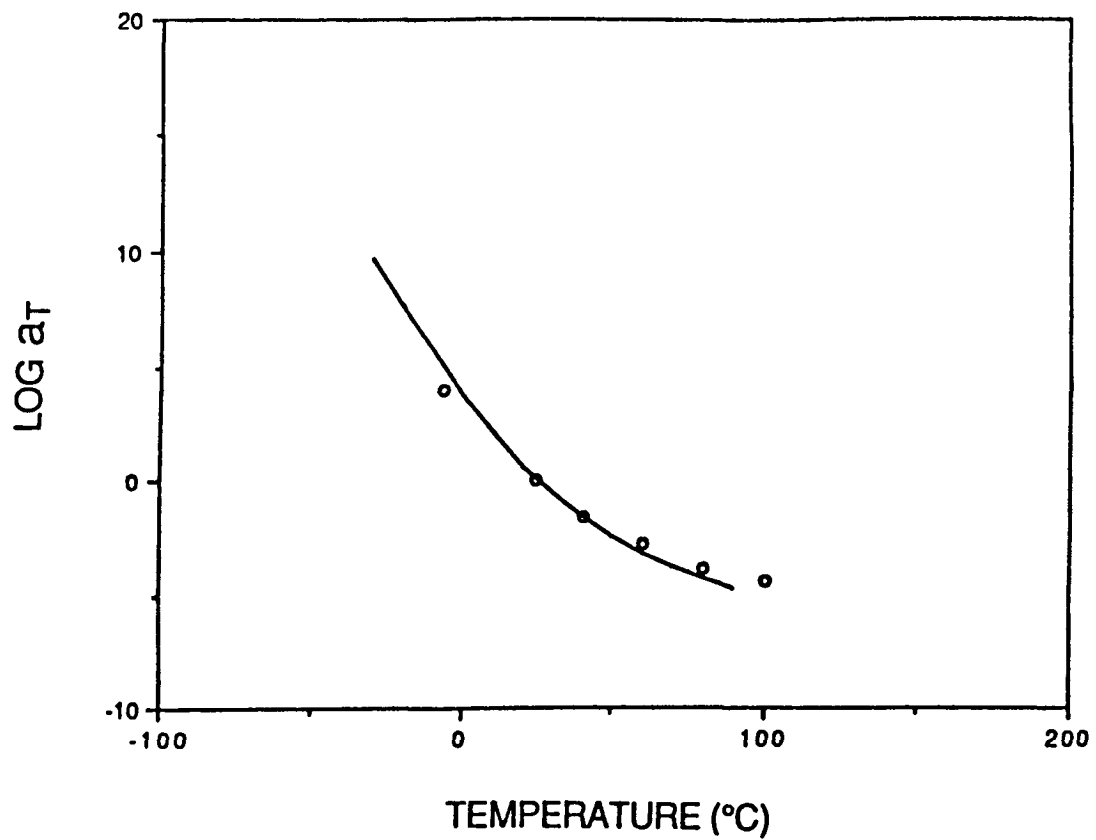
Figure 6.23 Shift Factor a_T versus Temperature for Asphalt AAG-1 (Open circles represent values from dielectric measurements and the solid line represents a_T determined from dynamic mechanical analysis measurements.)
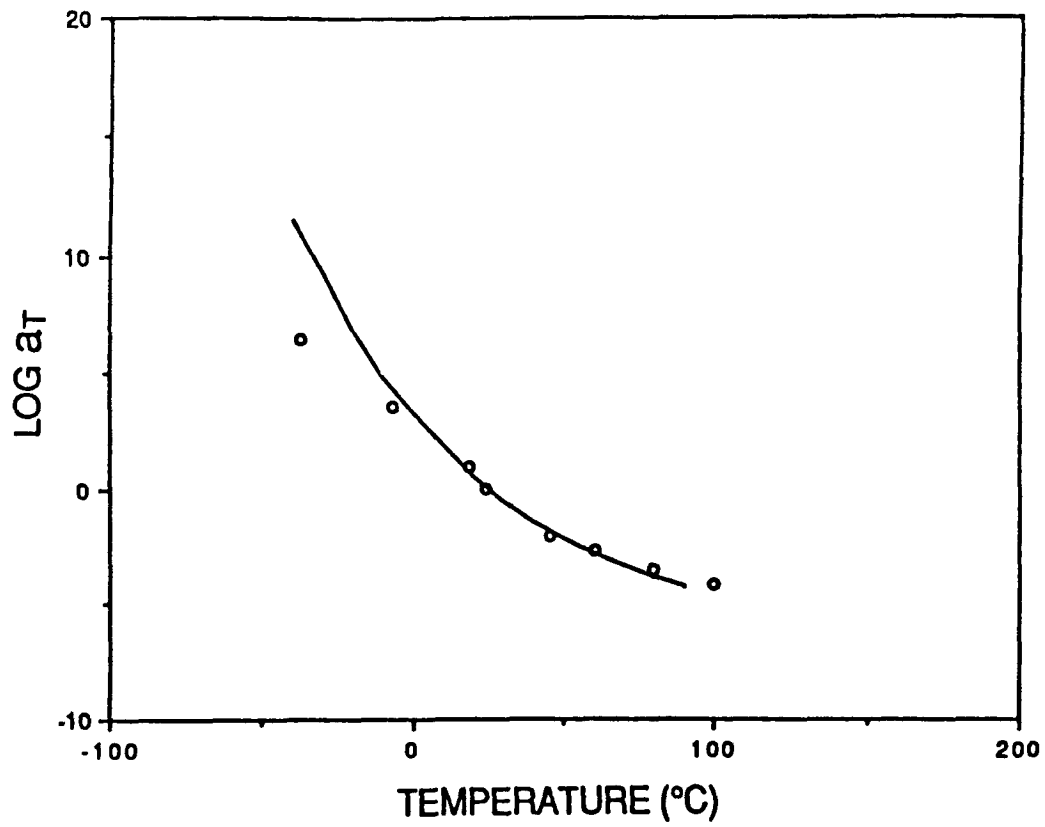
Figure 6.24   Shift Factor a_T versus Temperature for Asphalt AAK-1 (Open circles represent values from dielectric measurements and the solid line represents a_T determined from dynamic mechanical analysis measurements.)
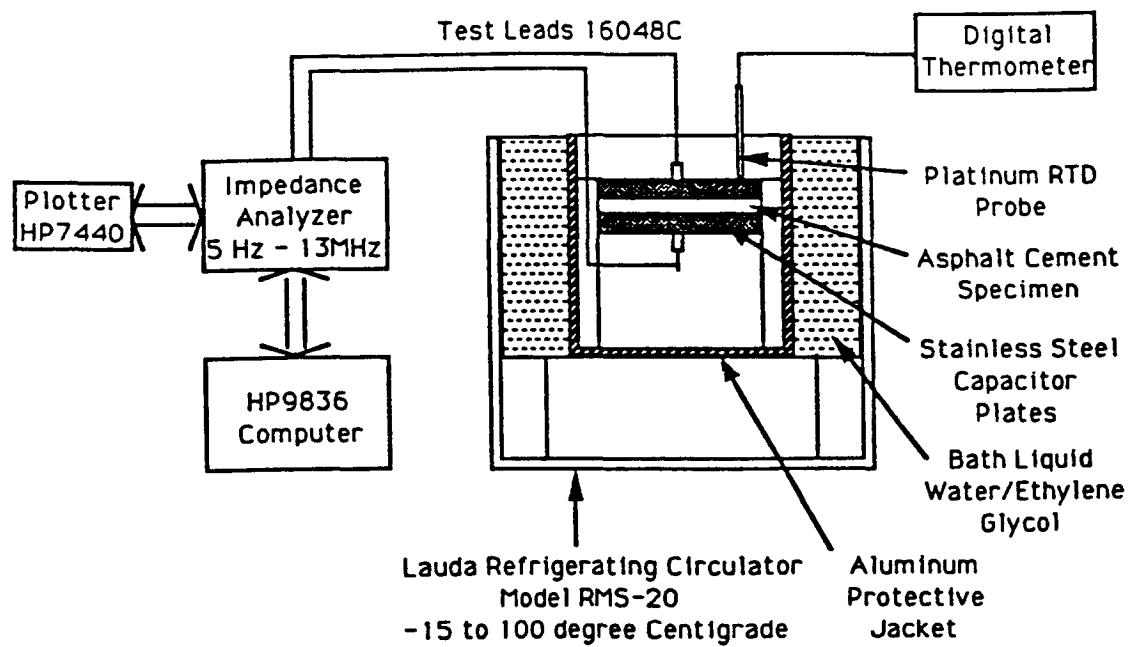
Figure 6.25   Penn State Dielectric Test Apparatus
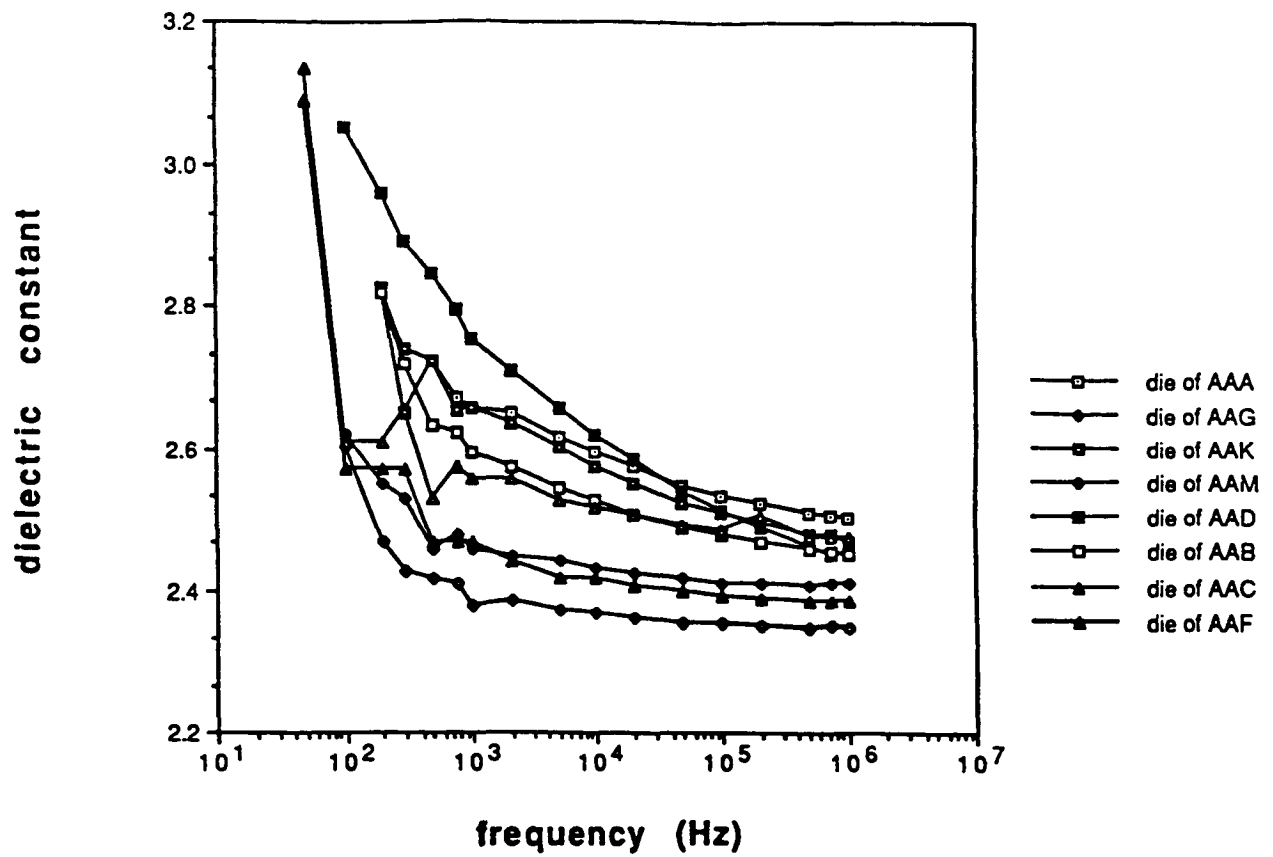
Figure 6.26 Mean Dielectric Constant Values for Eight Core Asphalts in Unaged Condition
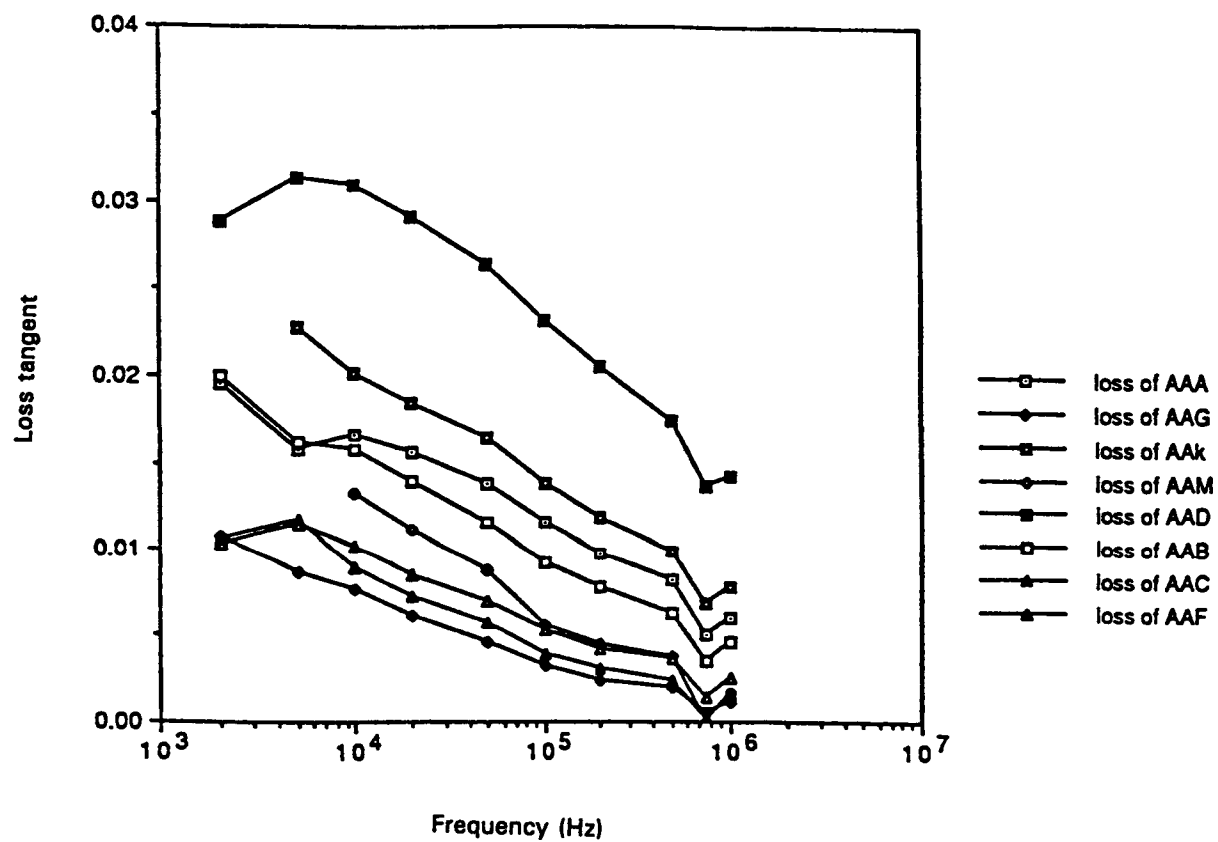
**Figure 6.27   Mean Dielectric Loss Tangent Values for Eight Core Asphalts in Unaged
Condition**
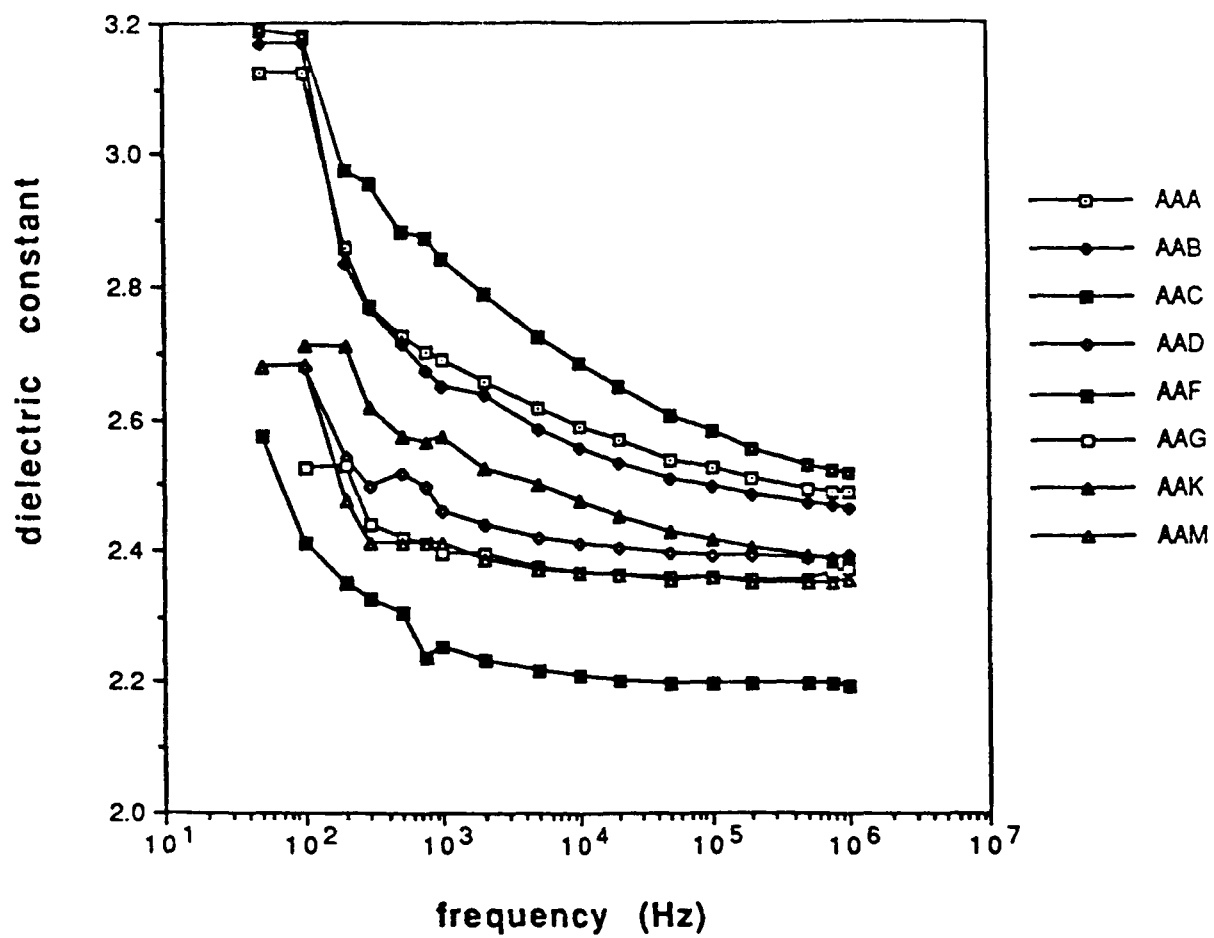
Figure 6.28 **Mean Dielectric Constant Values for Eight Core Asphalts in PAV-Aged Condition**
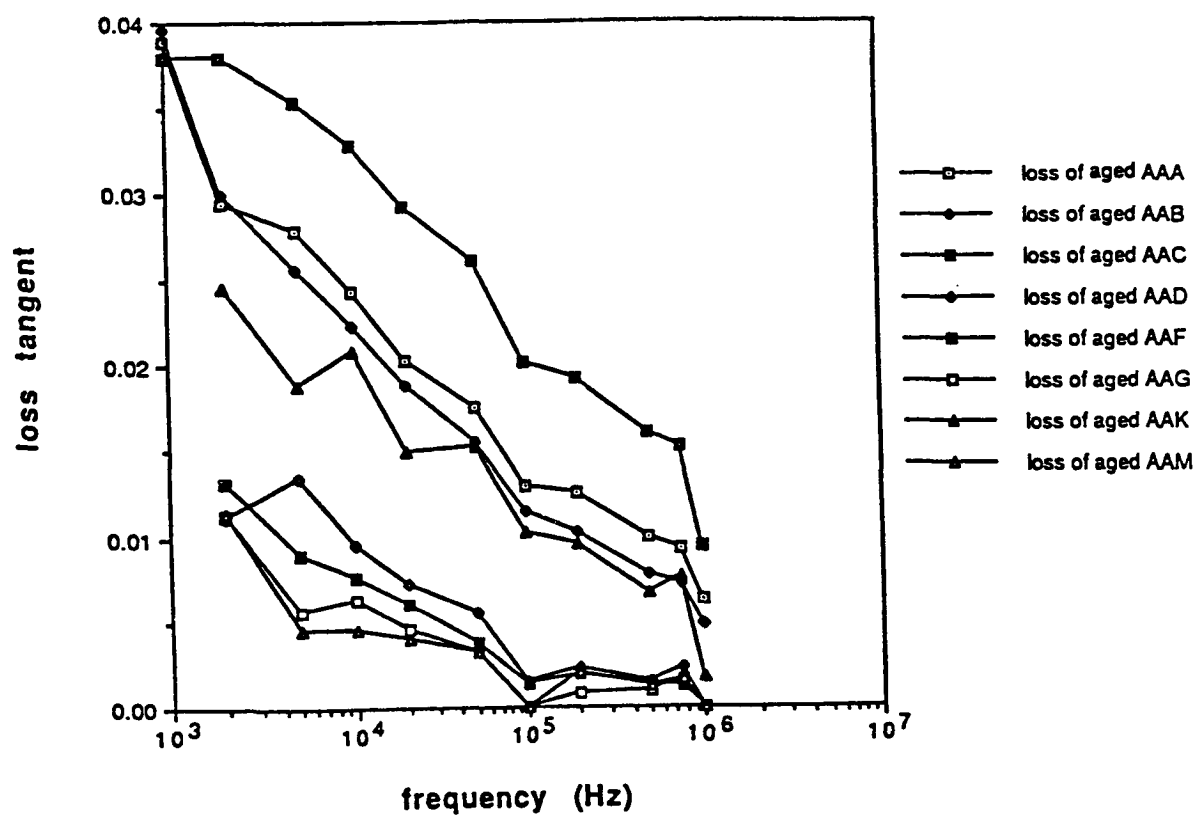
Figure 6.29 Mean Dielectric Loss Tangent Values for Eight Core Asphalts in PAV-Aged Condition

454
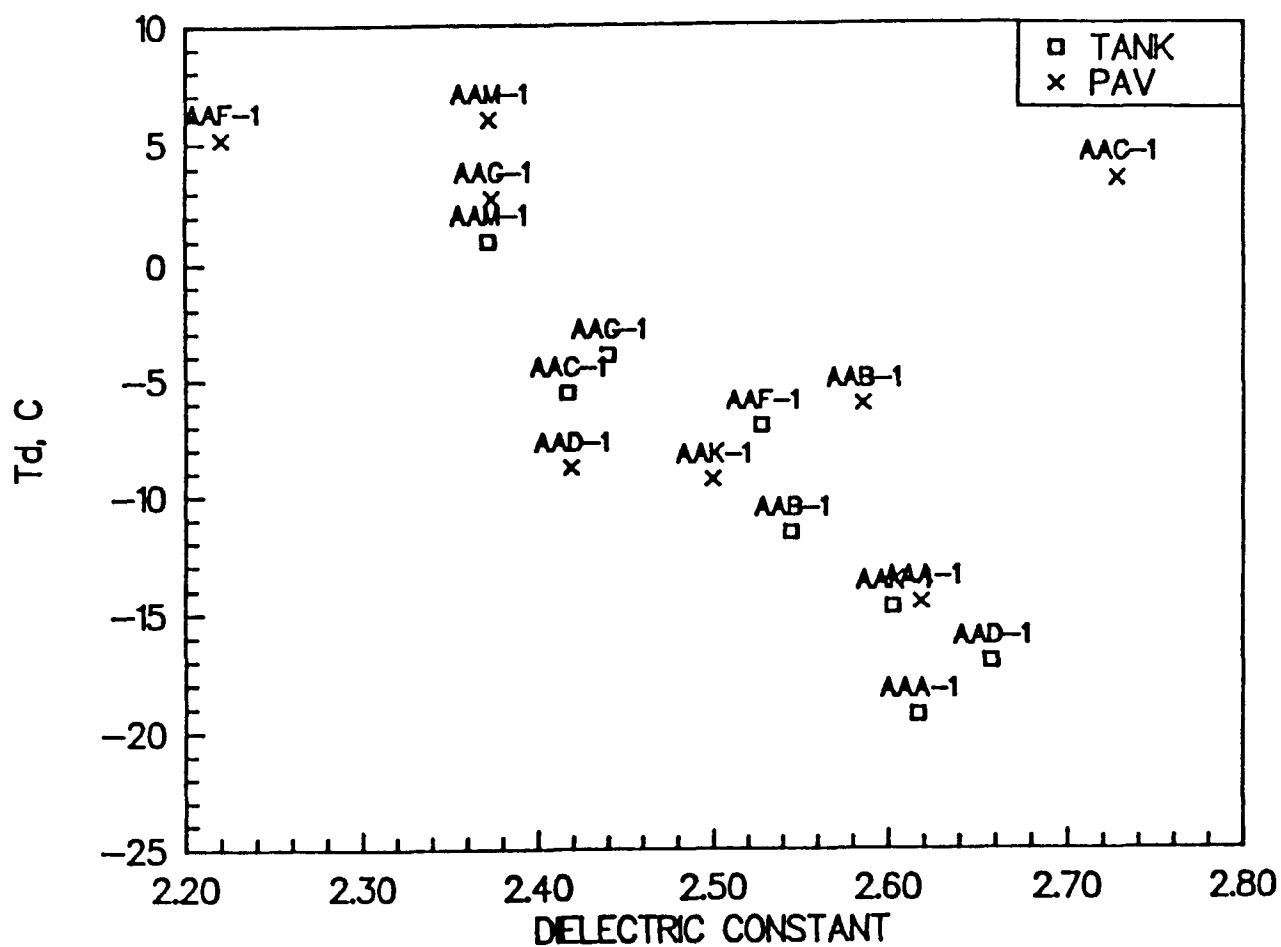
Figure 6.30   Plot of T_d (Defining Temperature) versus Dielectric Constants (5,000 Hz) for Eight Core Asphalts, Unaged and PAV-Aged
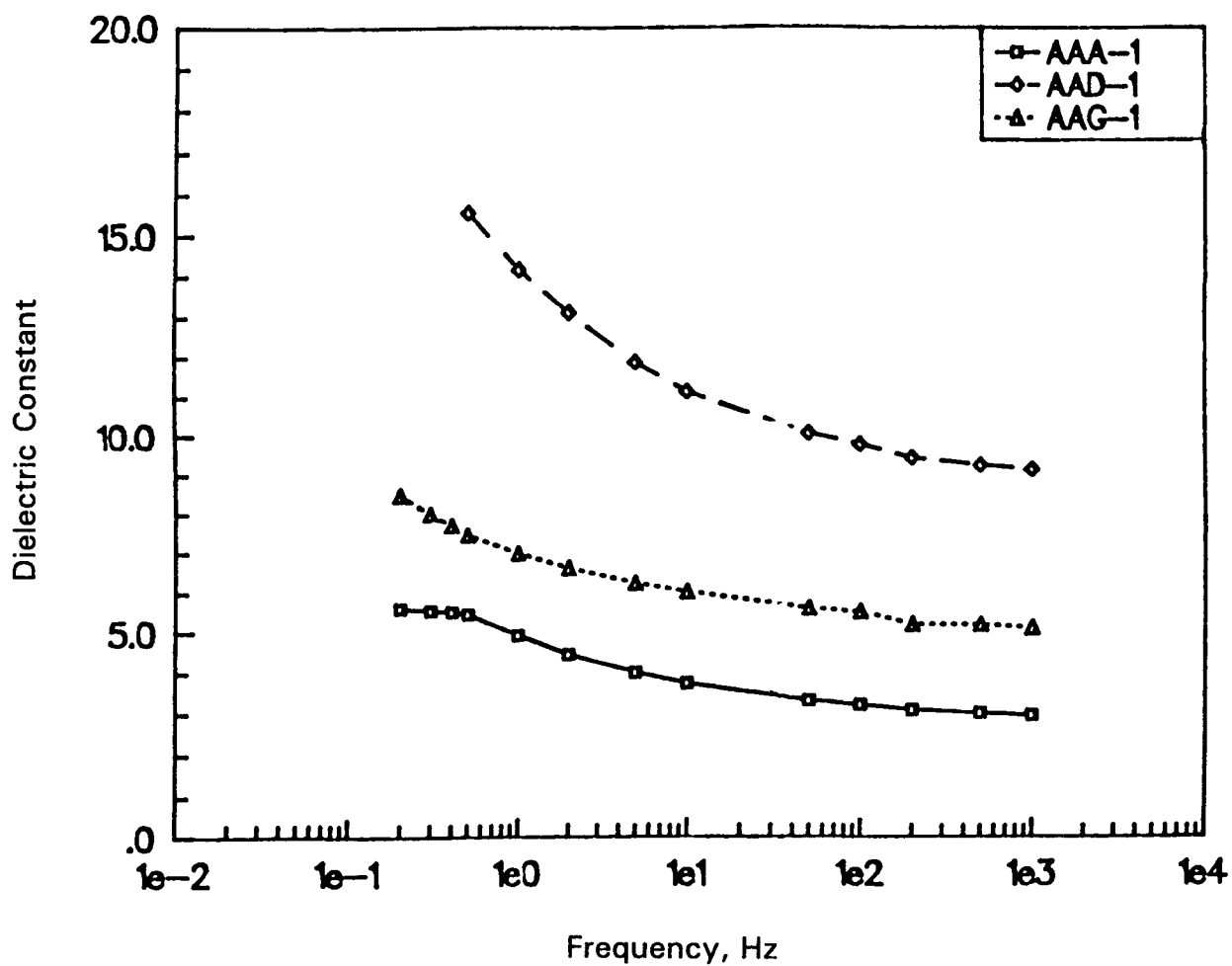
Figure 6.31   Dielectric Constants for Mixes Prepared with Core Asphalts AAA-1, AAD-1, and AAG-1
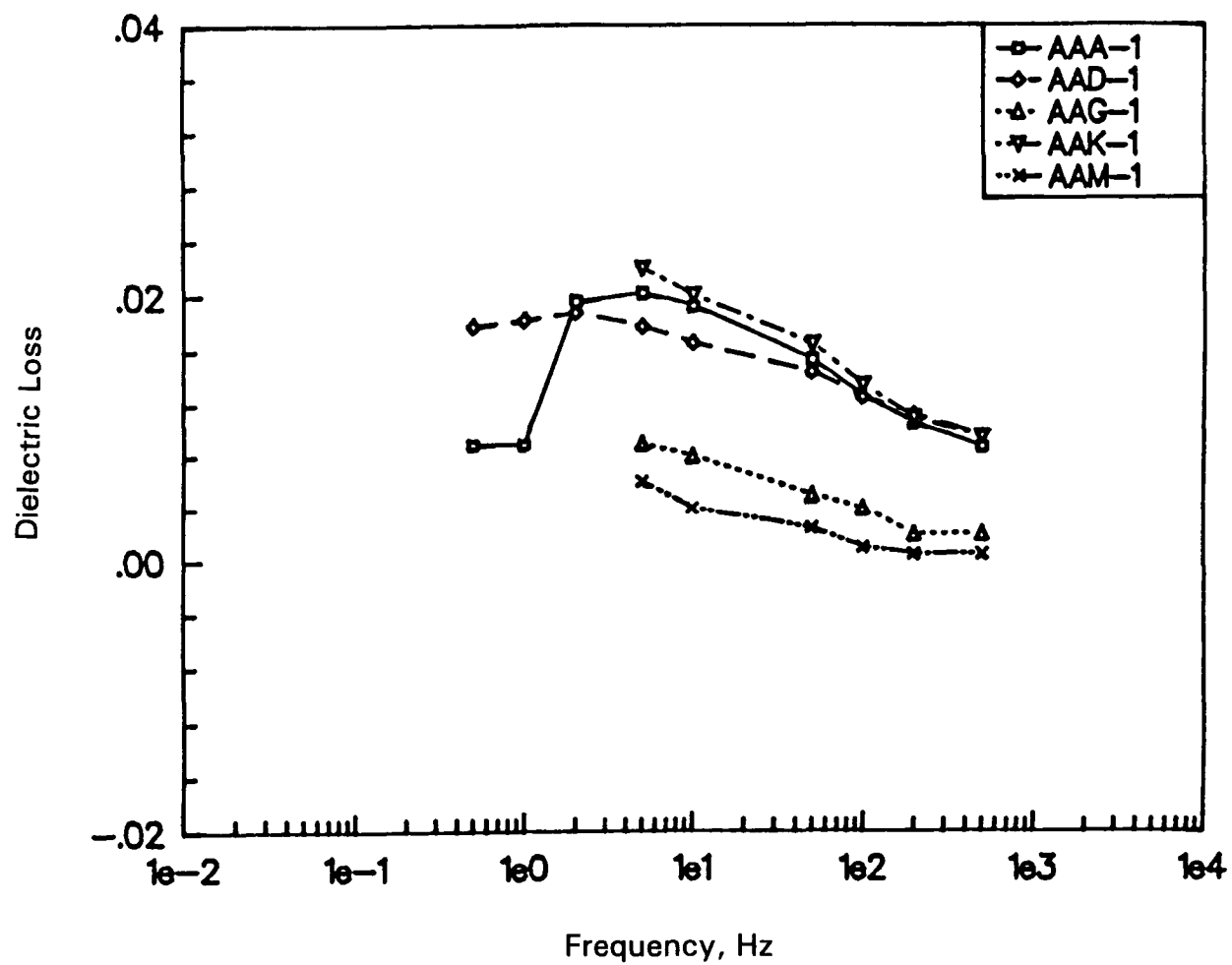
Figure 6.32 Dielectric Loss Tangent for Mixes Prepared with Core Asphalts AAA-1, AAD-1, and AAG-1

PUMP

cooled
air
environment

ultrasonic
tester

Liquid
Nitrogen

ultrasonics
analysis
equipment
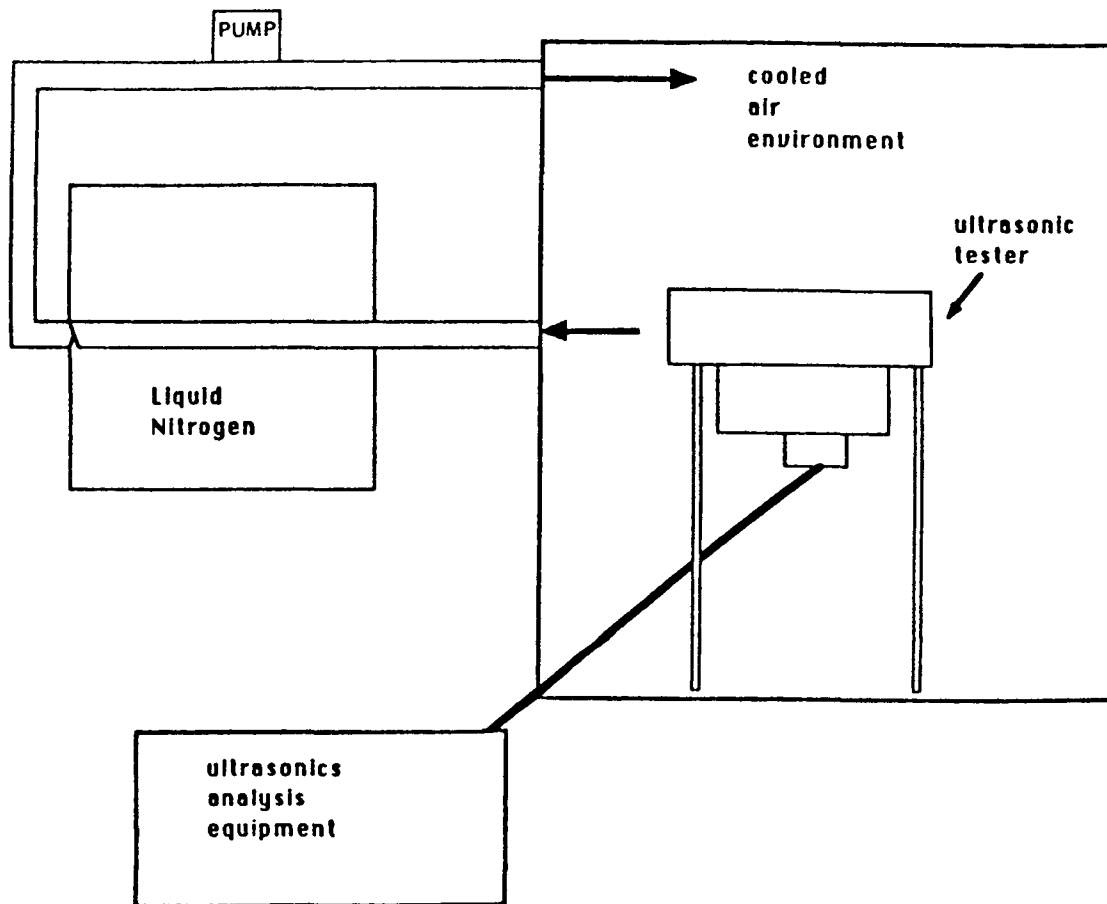
Figure 6.33 Low-Temperature Ultrasonic Measurement System

458
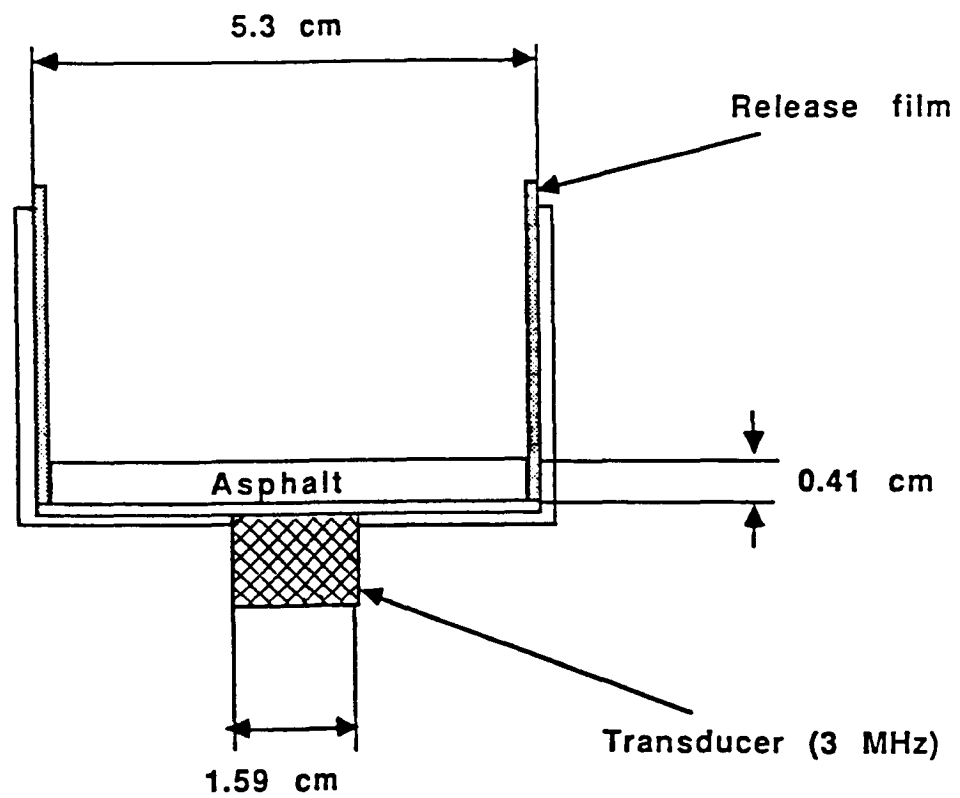
Figure 6.34 Ultrasonic Test Apparatus for Asphalt Cement
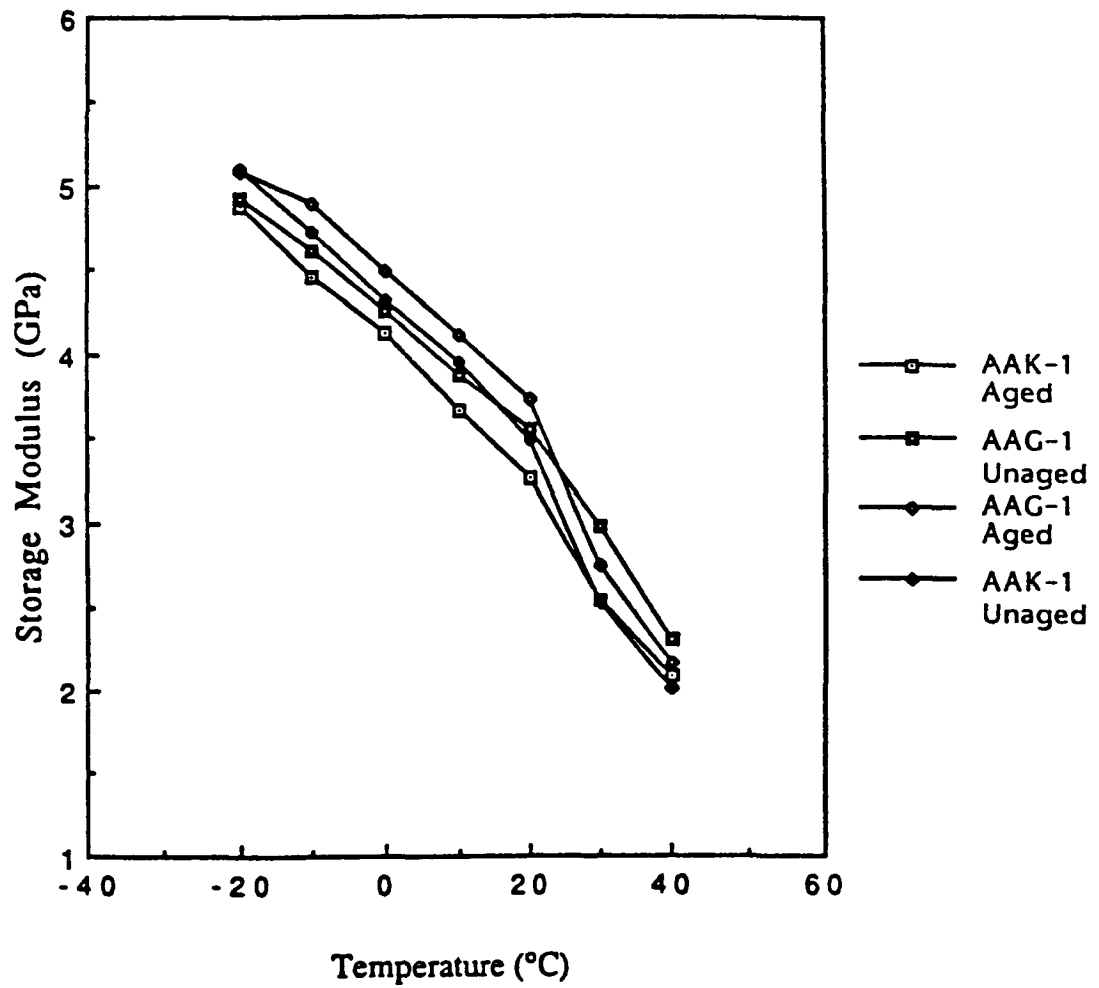
Figure 6.35   Ultrasonic Storage Modulus versus Temperature (Asphalts AAG-1 and
                AAK-1 in Unaged and PAV-Aged Condition, 2.25 MHz)
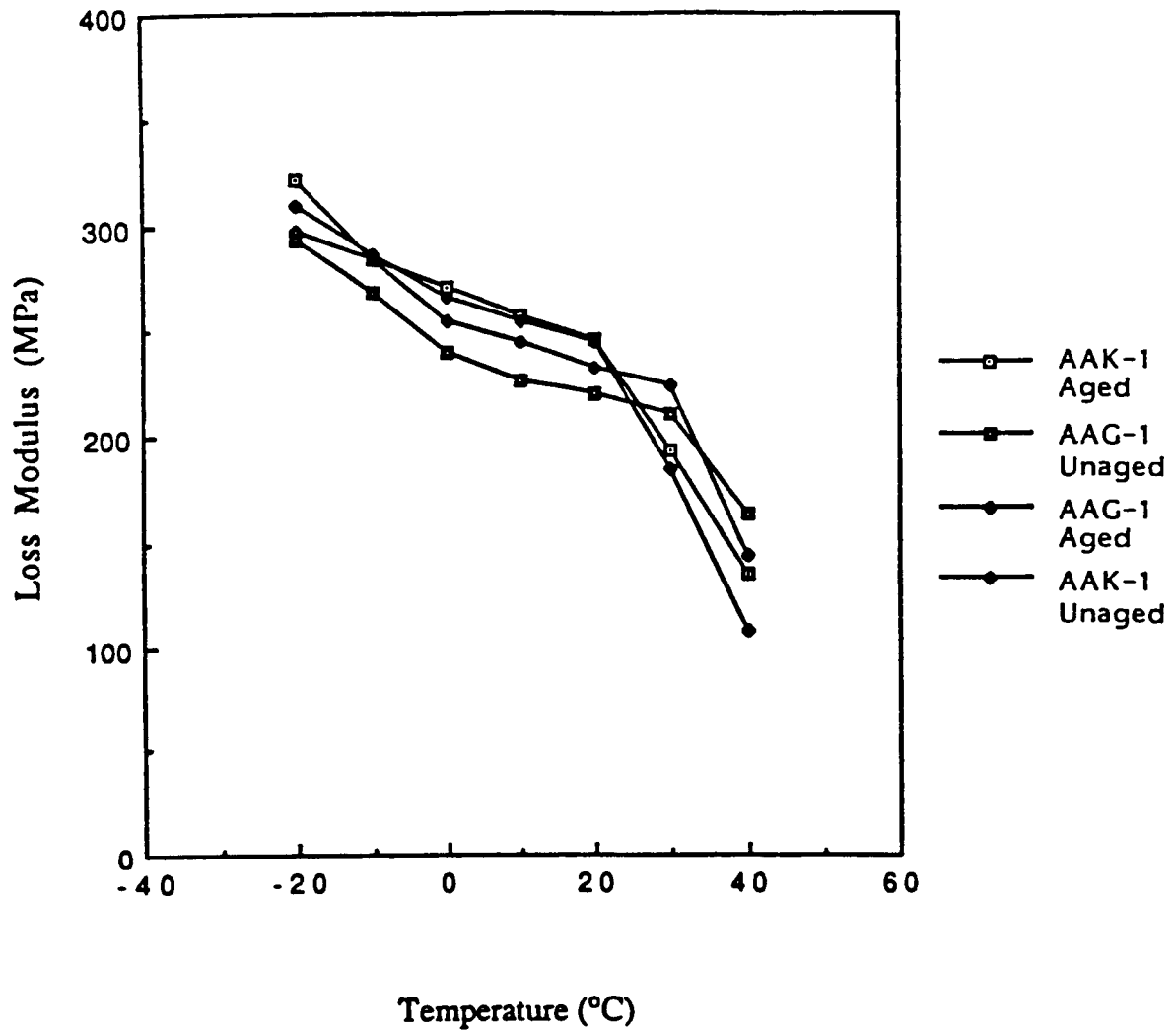
Figure 6.36 Ultrasonic Loss Modulus versus Temperature (Asphalts AAG-1 and AAK-1 in Unaged and PAV-Aged Condition, 2.25 MHz)

Table 6.1 Description of Portable Viscometers[1]

Brand Name	Model Number	Operating Principle	Viscosity Operating Range, Pa·s	Shear Rate Operating Range, 1/s	Reproducibility percent	Direct Readout of Shear Stress	Battery Operated	Approximate Cost, dollars
Bohlin	Visco 88	Rotational	$6.5 - 3.5 \times 10^2$	4 - 1,200	-	Yes	Yes	7,000 - 15,000
Brookfield	Dial Reading	Rotational	$5 - 10^4$	0.06 - 750	± 1.0	No	No	1,100
Brookfield	DV-I	Rotational	$5 - 10^4$	0.6 - 750	± 0.5	No	No	1,500
Brookfield	DV-II	Rotational	$5 - 10^4$	0.6 - 750	± 0.5	Yes	No	1,800
Haake	Viscotester VT500	Rotational	$0.5 - 10^4$	5 - 6,000	± 0.2	Yes	No	10,000
Haake	VT01	Rotational	0.0015 - 0.330	-	± 2.0	No	Yes	1,650
Haake	VT02	Rotational	$30 - 4 \times 10^2$	-	± 2.0	No	Yes	1,650
Nametre	N-1	Rotational	2 - 10	0 - 2,100	± 1.0	No	No	17,00
Nametre	AR706	Vibrating[2] Sphere	$0.1 - 2 \times 10^2$	4,084	± 1.0	No	No	10,000

[1] Hand held only
[2] Models are also available with vibrating collet, cylinder, rod, and plate geometries.

Table 6.2 Estimated Shear Rates for Various Testing and Service Conditions[1]

Testing or Service Condition	Estimated Shear Rate, sec^{-1}
Settlement	3×10^{-7}
Light loads (static)	2×10^{-5}
Heavy loads (static)	3×10^{-4}
Penetration test	2×10^{-1}
Moving traffic (slow)	1×10^{1}
Moving traffic (fast)	1×10^{3}
Capillary viscometer	1×10^{-3}
Sliding plate viscometer	5×10^{-2}
Transfer pump in hot-mix plant	1×10^{3} to 1×10^{4}

[1] These data were assembled from estimates of shear rates presented in ASTM STP 328.

Table 6.3 Thermal Lag Correction Factors

Asphalt	Grade	Test Temperature Range	Correction Factor
AAA-1	150/200	80-180	0.489
AAC-1	AC-8	80-165	0.461
AAC-2	AC-5	80-185	0.433
AAD-1	AR-4000	85-180	0.495
AAF-1	AC-20	85-185	0.487
AAG-1	AR-4000	85-190	0.434
AAK-1	AC-30	90-195	0.476
AAM-1	AC-20	90-190	0.495
AAM-2	AC-10	80-180	0.482
Average Correction Factor		0.472	

Table 6.4 Summary of Blister Test Results

Conditioning	Aggregate	Asphalts	Type of Failure
Unconditioned	PA Limestone	8 Core	Cohesive
Unconditioned	RL, Texas Chert	8 Core	Cohesive
Conditioning #1	RL, Texas Chert	8 Core	Cohesive
Conditioning #1	PA Limestone	8 Core	Cohesive
Conditioning #2	RL, Texas Chert	AAK-1, AAF-1, AAC-1	Adhesive
Conditioning #2	PA Limestone	AAF-1	Adhesive

Conditioning #1: Vacuum saturation, 30 minutes 140°F immersion, 18 hours test temperature: 0°C, 25°C.

Conditioning #2: Vacuum saturation, 30 minutes 140°F immersion, 18 hours frozen, 4 hours test temperature: 0°C.

Table 6.5 Dielectric Constants for Asphalts AAG-1, AAK-1, and AAM-1

Frequency (MHz)	AAG-1	AAK-1	AAM-1
0.01	2.54	2.59	2.32
0.05	2.54	2.58	2.36
0.10	2.51	2.54	2.34
0.50	2.60	2.61	2.44
1.00	2.56	2.57	2.38
5.00	2.61	2.60	2.44
10.00	2.61	2.54	2.44

Table 6.6 Analysis of Variance for Dielectric Constants at 1,000 Hz

Source	d.f.	Sum of Squares	Mean S.S.	F-Ratio	P-value
Asphalts	7	.43820785	.06260112	23.69	.0001
Error	24	.06342328	.00264264		

Rsquare = .87
Coefficient of Variation = 2.0%
Sigma = .0514

Table 6.7 Analysis of Variance for Dielectric Constants at 5,000 Hz

Source	d.f.	Sum of Squares	Mean S.S.	F-Ratio	P-value
Asphalts	7	.29915640	.04273663	28.08	.0001
Error	24	.03652397	.00152183		

Rsquare = .89
Coefficient of Variation = 1.5%
Sigma = .0390

Table 6.8 Confidence Intervals for Dielectric Constants at 5,000 Hz

Asphalt	.95 C.I. for Dielectric Constant (5,000 Hz)
A	2.617 ± .04
B	2.545 ± .04
C	2.417 ± .04
D	2.658 ± .04
F	2.528 ± .04
G	2.440 ± .04
K	2.603 ± .04

Table 6.9 Analysis of Variance for the Loss Tangent Data at 10,000 Hz

Source	d.f.	Sum of Squares	Mean S.S.	F-Ratio	P-value
Asphalts	7	.00157670	.00022524	435.84	.0001
Error	24	.00001240	.00000052		

Rsquare = .99
Coefficient of Variation = 4.7%
Sigma = .000719

Table 6.10 Analysis of Variance for the Loss Tangent Data at 50,000 Hz

Source	d.f.	Sum of Squares	Mean S.S.	F-Ratio	P-value
Asphalts	7	.00143482	.00020497	949.36	.0001
Error	24	.00000518	.00000022		

R^2 = 0.99 Coefficient of Variation = 3.9% Sigma = .000465

Table 6.11 Confidence Intervals for Loss Tangent at 50,000 Hz

Asphalt	.95 C.I. for the Loss Tangent
A	.01385 ± .00048
B	.01168 ± .00048
C	.00578 ± .00048
D	.02638 ± .00048
F	.00698 ± .00048
G	.00463 ± .00048
K	.01646 ± .00048

Table 6.12 Dielectric Constant of Core Asphalt AAD-1 at −5°C for Various Isothermal Storage Times

Frequency (kHz)	10 Minutes	1.33 Hours	21.33 Hours	30 Hours
0.5	2.84	2.76	2.76	2.76
1.0	2.76	2.68	2.65	2.65
5.0	2.75	2.71	2.69	2.69
10.0	2.73	2.70	2.70	2.69
50.0	2.70	2.68	2.67	2.67
100.0	2.69	2.67	2.67	2.67
500.0	2.67	2.66	2.66	2.67

Table 6.13 Dielectric Constant of Core Asphalt AAM-1 at −5°C for Various Storage Times

Frequency (KHz)	10 Minutes	1.33 hours	21.33 hours	30 hours
0.5	2.59	2.66	2.51	2.59
1.0	2.59	2.59	2.59	2.59
5.0	2.59	2.59	2.59	2.59
10.0	2.59	2.59	2.59	2.59
50.0	2.61	2.61	2.61	2.61

Table 6.14 Ultrasonic Test Results for Eight Core Asphalts

Specimen ID	Replicate No.	Freq. (MHz)	Temp. (°C)	Lo St M (GPa)	Lo Ls M (MPa)
AAK-1, Aged	1	2.25	-20	4.94	321.0
AAK-1, Aged	2	2.25	-20	4.79	321.4
AAK-1, Aged	1	2.25	-10	4.51	277.5
AAK-1, Aged	2	2.25	-10	4.40	288.9
AAK-1, Aged	1	2.25	0	4.13	255.7
AAK-1, Aged	2	2.25	0	4.11	284.0
AAK-1, Aged	1	2.25	10	3.68	243.0
AAK-1, Aged	2	2.25	10	3.65	270.2
AAK-1, Aged	1	2.25	20	3.26	227.1
AAK-1, Aged	2	2.25	20	3.27	263.7
AAK-1, Aged	1	2.25	30	2.65	196.1
AAK-1, Aged	2	2.25	30	2.45	190.3
AAK-1, Aged	1	2.25	40	2.20	143.2
AAK-1, Aged	2	2.25	40	2.01	125.7
AAG-1, Unaged	1	2.25	-20	4.87	278.8
AAG-1, Unaged	2	2.25	-20	4.98	307.4

Continued

Table 6.14 Ultrasonic Test Results for Eight Core Asphalts (continued)

Specimen ID	Replicate No.	Freq. (MHz)	Temp. (°C)	Lo St M (GPa)	Lo Ls M (MPa)
AAG-1, Unaged	1	2.25	-10	4.52	245.4
AAG-1, Unaged	2	2.25	-10	4.68	290.1
AAG-1, Unaged	1	2.25	0	4.21	224.4
AAG-1, Unaged	2	2.25	0	4.28	254.8
AAG-1, Unaged	1	2.25	10	3.82	212.8
AAG-1, Unaged	2	2.25	10	3.93	238.4
AAG-1, Unaged	1	2.25	20	3.48	196.9
AAG-1, Unaged	2	2.25	20	3.62	242.3
AAG-1, Unaged	1	2.25	30	2.90	194.8
AAG-1, Unaged	2	2.25	30	3.07	223.8
AAG-1, Unaged	1	2.25	40	2.25	147.1
AAG-1, Unaged	2	2.25	40	2.38	179.5
AAG-1, Aged	1	2.25	-20	5.15	340.3
AAG-1, Aged	2	2.25	-20	5.00	254.7
AAG-1, Aged	1	2.25	-10	4.92	310.9
AAG-1, Aged	2	2.25	-10	4.86	256.2
AAG-1, Aged	1	2.25	0	4.49	284.0
AAG-1, Aged	2	2.25	0	4.48	224.9

Table 6.14 Ultrasonic Test Results for Eight Core Asphalts (continued)

Specimen ID	Replicate No.	Freq. (MHz)	Temp. (°C)	Lo St M (GPa)	Lo Ls M (MPa)
AAG-1, Aged	1	2.25	10	4.11	270.3
AAG-1, Aged	2	2.25	10	4.09	217.0
AAG-1, Aged	1	2.25	20	3.73	258.9
AAG-1, Aged	2	2.25	20	3.72	204.5
AAG-1, Aged	1	2.25	30	2.82	225.5
AAG-1, Aged	2	2.25	30	3.69	221.4
AAG-1, Aged	1	2.25	40	2.25	177.7
AAG-1, Aged	2	2.25	40	2.09	108.6
AAK-1, Unaged	1	2.25	-20	5.01	303.2
AAK-1, Unaged	2	2.25	-20	5.17	316.0
AAK-1, Unaged	1	2.25	-10	4.66	278.0
AAK-1, Unaged	2	2.25	-10	4.77	294.0
AAK-1, Unaged	1	2.25	0	4.28	264.2
AAK-1, Unaged	2	2.25	0	4.35	266.3
AAK-1, Unaged	1	2.25	10	3.90	261.1
AAK-1, Unaged	2	2.25	10	3.99	247.7
AAK-1, Unaged	1	2.25	20	3.48	252.3
AAK-1, Unaged	2	2.25	20	3.51	236.2

Continued

470

Table 6.14 Ultrasonic Test Results for Eight Core Asphalts (continued)

Specimen ID	Replicate No.	Freq. (MHz)	Temp. (°C)	Lo St M (GPa)	Lo Ls M (MPa)
AAK-1, Unaged	1	2.25	30	2.50	178.7
AAK-1, Unaged	2	2.25	30	2.57	189.0
AAK-1, Unaged	1	2.25	40	2.07	119.3
AAK-1, Unaged	2	2.25	40	1.97	97.4

Note: AAK-1, Aged   = SHRP Designation
        AAG-1, Unaged = SHRP Designation
        AAG-1, Aged   = SHRP Designation
        AAK-1, Unaged = SHRP Designation

        Lo St M (GPa)   = Longitudinal Storage Modulus
        Lo Ls M (MPa)   = Longitudinal Loss Modulus

Table 6.15 Calculated Young's Moduli of Asphalt Concretes

Measured Property	Sample 8-10	Sample 16-6
Mean wave speed, m/s	3450	3830
Standard Deviation of wave speed, m/s	163	75
Density, g/cm^3	2.44	2.47
Calculated Young's Moduli, GPa	21.5	27.0

Table 6.16 Split Plot Analysis of Variance for the Storage Modulus

Source	df	SS	MSS	F-Ratio	P-Value
Asphalts	3	0.70702	0.236	5.688	0.11
Asphalts × Replicate (main plot error)	3	0.12447	0.04149		
Replicates	1	0.00145			
Temperature	6	51.084			
Asphalt × Temperature	18	0.4816	0.0268	10.83	0.0001
Split Plot Error	24	0.05933	0.00247		

Table 6.17 Results of One-Way Analysis of Variance by Temperatures

Asphalt Temperature, °C	P-Value	$\hat{\sigma}$ (4 df)
-20	0.20	0.10
-10	0.02	0.08
0	0.00	0.04
10	0.00	0.05
20	0.00	0.05
30	0.04	0.11
40	0.17	0.11

Table 6.18   Storage Means with .95 Confidence Intervals for Asphalts AAG-1 and AAK-1 in Unaged and Aged Conditions

Asphalt	Mean Storage
AAK-1 Unaged	4.12 (±.098)
AAG-1 Unaged	4.245 (±.098)
AAK-1 Aged	4.315 (±.098)
AAG-1 Aged	4.485 (±.098)

Table 6.19   Split Plot Analysis of Variance for the Loss Modulus

Source	df	SS	MSS	F-Ratio	P-Value
Asphalts	3	1,146	382	0.08	0.97
Asphalts × Replicates (main plot error)	3	14,686	4,895		
Replicates	1	97			
Temperature	6	145,123	24,187		
Asphalt × Temperature	18	8,354	464	2.79	0.01
Split Plot Error	24	3,991	166		

Table 6.20 Results of One-Way Analysis of Variance by Temperatures

Asphalt Temperature, °C	P-Value	$\hat{\sigma}$ (4 df)
-20	0.82	32
-10	0.89	26
0	0.67	26
10	0.59	23
20	0.79	29
30	0.08	11
40	0.40	29

Table 6.21 Loss Means with .95 Confidence Intervals for the Four Asphalts

Asphalt	Mean Loss
AAK-1 Unaged	193.0 ($\pm$ 21.6)
AAG-1 Unaged	209.3 ($\pm$ 21.6)
AAK-1 PAV Aged	183.9 ($\pm$ 21.6)
AAG-1 PAV Aged	223.5 ($\pm$ 21.6)

References

ASTM. 1985. "Standard Practice for Fracture Strength in Cleavage of Adhesives in Bonded Joints," *Annual Book of ASTM Standards*, designation D 3433-75. Philadelphia: American Society for Testing and Materials, vol. 15.06, pp. 241-247.

Barquins, M., and Wehbi, D. 1986. "Study of Adherence of Elastomers by Cyclic Unloading Experiments," *Journal of Adhesion*, vol. 20, pp. 55-74.

Liechti, K.M., Ginsburg, D., and Hanson, E.C. 1987. "A Comparison between Measurements and Finite Element Predictions of Crack Opening Displacements near the Front of an Interface Crack," *Journal of Adhesion*, vol. 23, pp. 123-146.

Mostovoy, S., and Ripling, E.J. 1971. "The Fracture Toughness and Stress Corrosion Cracking Characteristics of Anhydride-Hardened Epoxy Adhesive," *Journal of Applied Polymer Science*, vol. 15, pp. 641-659.

Trantina, G.G. 1972. "Combined Mode Crack Extension in Adhesive Joints," *Journal of Composite Materials*, vol. 66 (July), pp. 371-391.